

DEPARTMENT OF THE INTERIOR
GEOLOGICAL SURVEY

MINUTES OF THE
NATIONAL EARTHQUAKE PREDICTION EVALUATION COUNCIL
July 26-27, 1985
Menlo Park, California

by
Clement F. Shearer¹

Open File Report 85-754

This report is preliminary and has not been edited or reviewed for conformity with U.S. Geological Survey publication standards and stratigraphic nomenclature.

¹ U.S. Geological Survey, 106 National Center
Reston, Virginia 22092

REPRODUCED FROM BEST AVAILABLE COPY

TABLE OF CONTENTS

	<u>Page</u>
Preface	iv.
List of members, National Earthquake Prediction Evaluation Council	v.
Minutes of the July 1985 meeting	1
Appendices:	
A. Papers and summaries of presentations given at July 1985 meeting	
1. Parkfield Seismicity Review - W. H. Bakun, A. G. Lindh, K. Poley, and S. S. Schulz	19
2. The Parkfield, California, Earthquake Prediction Experiment - W. H. Bakun and A. G. Lindh	32
3. Foreshocks and Short-Term Earthquake Hazard Assessment at Parkfield - L. M. Jones	39
4. The Detection History of the Parkfield Segment of the San Andreas Fault: A Preliminary Assessment - R. E. Habermann	63
5. Review of Seismic Wave Monitoring in Central California - R. Clymer and T. V. McEvilly	78
6. Preliminary Results from Vertical Seismic Profiling of Oroville Microearthquake S-Waves - P. E. Malin and J. A. Waller	97
7. Summary of Geodetic Survey Measurements near Parkfield - P. Segall, W. Prescott, R. Stein, N. King, R. Harris, and A. G. Lindh	102
8. Two-Color Laser Strain Monitoring in the Parkfield Region - R. O. Burford and L. E. Slater	117
9. Strain, Creep, Magnetic, and Tilt Data - M. Johnston, S. Schulz, R. Mueller, and C. Mortensen	130
10. Water Level Monitoring - J. D. Bredehoeft	158

	<u>Page</u>
11. The Significance Expected of Near-Surface Tiltmeter Data from Parkfield, California - S. Morrissey	173
12. Seismicity Record, $M > 2.5$, for the Central Coast Region of California - R. A. Uhrhammer	198
13. Earthquakes of $M > 6$ in the South San Francisco Bay Area - T. Topozada	213
14. An Overview of the Distribution of Relative Plate Motion along the San Andreas Fault System from Hollister, California, to the Mendocino Triple Junction - W. H. Prescott	232
15. Seismic Slip on the Calaveras Fault, California - W. H. Bakun, G. C. P. King, and R. S. Cockerham	247
16. Potential for Future Damaging Shocks on the Calaveras Fault, California - W. H. Bakun and A. G. Lindh	265
17. The Detection History of the Calaveras Fault: A Preliminary Assessment - R. E. Habermann	280
18. Retardations in Aseismic Slip Rates Along the Calaveras and San Andreas Faults in the Monterey Bay Region, California - R. O. Burford and S. S. Schulz	294
19. Seismicity of the San Andreas Fault from Cienega Winery to the Golden Gate - J. Olson and A. G. Lindh	316
20. Seismic Hazard from the Southern Segment of the 1906 Rupture, California - C. H. Scholz	325
21. San Andreas Fault, Central California - K. McNally	335
22. Seismic Hazard Estimate for the San Jose-San Juan Segment of the San Andreas Fault: 1985-2005 - S. P. Nishenko and P. L. Williams	350
23. Current Episodes of Seismic Quiescence along the San Andreas Fault between San Juan Bautista and Stone Canyon, California: Possible Precursors to Local Moderate Mainshocks? - M. Wyss and R. O. Burford	367

Page

B. Evaluations of a prediction of an earthquake for the San Andreas Fault near San Juan Bautista, California	
1. Reviews of Wyss and Burford Paper "Current Episodes of Seismic Quiescence along the San Andreas Fault between San Juan Bautista and Stone Canyon, California: Possible Precursors to Local Moderate Mainshocks?"	427
2. Council letter to Director, USGS, regarding its review of a prediction for the San Andreas fault near San Juan Bautista, California	443

PREFACE

The National Earthquake Prediction Evaluation Council (NEPEC) was established in 1979 pursuant to the Earthquake Hazards Reduction Act of 1977 to advise the Director of the U.S. Geological Survey (USGS) in issuing any formal predictions or other information pertinent to the potential for the occurrence of a significant earthquake. It is the Director of the USGS who is responsible for the decision whether and when to issue such a prediction or information.

NEPEC, also referred to in this document as the Council, according to its charter, is comprised of a Chairman, Vice Chairman, and from 8 to 12 other members appointed by the Director of the USGS. The Chairman shall not be a USGS employee, and at least one-half of the membership shall be other than USGS employees.

The USGS recently has begun to publish the minutes of NEPEC meetings. This open-file report is the third in an anticipated series of routinely published proceedings of the Council.

NATIONAL EARTHQUAKE PREDICTION EVALUATION COUNCIL

Dr. Lynn R. Sykes
CHAIRMAN

Higgins Professor of Geological Sciences
Lamont-Doherty Geological Observatory
of Columbia University
Palisades, New York 10964
Office: 914/359-2900
Home: 914/359-7428

Dr. John R. Filson
VICE CHAIRMAN

Chief, Office of Earthquakes, Volcanoes,
and Engineering
U.S. Geological Survey
National Center, MS 905
Reston, Virginia 22092
Office: 703/860-6471
Home: 703/860-2807

Dr. Clement F. Shearer
EXECUTIVE SECRETARY

Hazards Information Coordinator
Office of the Director
U.S. Geological Survey
National Center, MS 106
Reston, Virginia 22092
Office: 703/860-6208
Home: 703/620-9422

Dr. Keiiti Aki

Department of Geological Sciences
University of Southern California
Los Angeles, California 90007
Office: 213/743/3510
Home: 213/559-1350

Dr. John N. Davies

State Seismologist, Alaska Department of
Natural Resources, Division of Geological
and Geophysical Surveys, and,
Adjunct Associate Professor, Geophysical
Institute, University of Alaska
794 University Avenue, Basement
Fairbanks, Alaska 99701
Office: 907/474-7190
Home: 907/455-6311

Dr. James F. Davis

State Geologist, California
Department of Conservation
California Division of Mines and Geology
1416 Ninth Street, Room 1341
Sacramento, California 95814
Office: 916/445-1923
Home: 916/487-6125

Dr. James H. Dieterich	Research Geophysicist Branch of Tectonophysics U.S. Geological Survey 345 Middlefield Road, MS 977 Menlo Park, California 94025 Office: 415/323-8111, ext. 2573 Home: 415/856-2025
Dr. William L. Ellsworth	Chief, Branch of Seismology U.S. Geological Survey 345 Middlefield Road, MS 977 Menlo Park, California 94025 Office: 415/323-8111, ext. 2782 Home: 415/322-9452
Dr. Hiroo Kanamori	Division of Geological & Planetary Science California Institute of Technology Pasadena, California 91125 Office: 818/356-6914 Home: 818/796-8452
Dr. Thomas V. McEvilly	Department of Geology and Geophysics University of California, Berkeley Berkeley, California 94720 Office: 415/642-4494 Home: 415/549-0967
Dr. I. Selwyn Sacks	Department of Terrestrial Magnetism Carnegie Institution of Washington 5241 Broad Branch Road, N.W. Washington, D.C. 20015 Office: 202/966-0863 Home: 301/657-3271
Dr. Wayne Thatcher	Chief, Branch of Tectonophysics U.S. Geological Survey 345 Middlefield Road, MS 977 Menlo Park, California 94025 Office: 415/323-8111, ext. 2120 Home: 415/326-4680
Dr. Robert E. Wallace	Chief Scientist, Office of Earthquakes, Volcanoes, and Engineering U.S. Geological Survey 345 Middlefield Road, MS 977 Menlo Park, California 94025 Office: 415/323-8111, ext. 2751 Home: 415/851-0249

Dr. Robert L. Wesson

Research Geophysicist
Branch of Seismology
U.S. Geological Survey
National Center, MS 922
Reston, Virginia 22092
Office: 703/860-7481
Home: 703/476-8815

Dr. Mark D. Zoback

Professor of Geophysics
Department of Geophysics
Stanford University
Stanford, California 94305
Office: 415/497-9438
Home: 415/322-9570

National Earthquake Prediction Evaluation Council
Minutes of the Meeting
July 26 & 27, 1985
Menlo Park, California

Council Members Present

Dr. Lynn R. Sykes, Chairman, Lamont-Doherty Geological Observatory
Dr. John N. Davies, Alaska Department of Natural Resources
Dr. Thomas McEvelly, University of California, Berkeley
Dr. Mark D. Zoback, Stanford University
Dr. Keiiti Aki, University of Southern California
Dr. James H. Dieterich, U.S. Geological Survey
Dr. William L. Ellsworth, U.S. Geological Survey
Dr. Wayne Thatcher, U.S. Geological Survey
Dr. Robert E. Wallace, U.S. Geological Survey
Dr. Robert L. Wesson, U.S. Geological Survey
Dr. James F. Davis, California Division of Mines and Geology
Dr. Hiroo Kanamori, California Institute of Technology
Dr. I. Selwyn Sacks, Carnegie Institution of Washington

Invited Speakers

W. H. Bakun, U.S. Geological Survey
Al Lindh, U.S. Geological Survey
Lucille Jones, U.S. Geological Survey
R. E. Habermann, Georgia Institute of Technology
R. Clymer, University of California, Berkeley
P. E. Malin, University of California, Santa Barbara
P. Segall, U.S. Geological Survey
L. E. Slater, CIRES, University of Colorado
Robert O. Burford, U.S. Geological Survey
M. Johnston, U.S. Geological Survey
J. Bredehoeft, U.S. Geological Survey
Sean-Thomas Morrissey, St. Louis University
Robert A. Uhrhammer, University of California, Berkeley
T. Toppozada, California Division of Mines and Geology
William H. Prescott, U.S. Geological Survey
Jean Olson, U.S. Geological Survey
C. H. Scholz, Lamont-Doherty Geological Observatory
Karen McNally, University of California, Santa Cruz
Max Wyss, CIRES, University of Colorado/NOAA
Doborah Ryan, Office of the Solicitor, Department of the Interior

JULY 26

PARKFIELD MONITORING EXPERIMENTS

In his introductory remarks, Chairman **Sykes** outlined the purposes of the meeting. The Council would continue its discussion of the Parkfield, California, situation for the first day. The Council would then begin a discussion of the San Francisco Bay area faults, principally the Calaveras fault and the section of the San Andreas fault from mid-Peninsula to Bear Valley on the second day. At its last meeting, the Council expressed the opinion that more research and thought is needed on intermediate-term earthquake precursors and recommended that work be done on several precursors--such as changes in the rate or occurrence of small earthquakes, b-values, and changes in the parameters of the coda of an earthquake. The Council also felt that it needed a review of what circumstances at Parkfield might constitute either short-term or intermediate-term alarms. Today's speakers were requested to address what would constitute an alarm--either a scientific alarm that would convene a scientific group or one that might cause the U.S. Geological Survey (USGS) to issue a public statement. Further, the discussants were asked to consider what procedures might be instituted quickly, in a short-term situation where there is insufficient time to convene the Council, enabling a timely warning to be issued.

Thatcher gave a brief description of the background and guidance for the first day's meeting on Parkfield. In addition, he requested a discussion of what would be an appropriate response to a given change in the situation at Parkfield. This discussion would help the Council in its efforts to construct a scenario of situations and responses regarding Parkfield. Thatcher noted that in discussions with the USGS Parkfield Working Group, it was concluded that they are not able thus far to construct such a series of scenarios. Today's session will include briefings on the kinds of monitoring that are being conducted and the background of activities that would allow us to make interpretations of the monitored observations at Parkfield. Each speaker will address signal-to-noise ratios, normal versus abnormal rates of observed parameters, and will give criteria for alarms that would indicate that unusual activity is occurring.

Seismic Monitoring at Parkfield

Bakun set the stage for the seismic observation programs, particularly those geared to detect precursory changes that might occur before the next characteristic Parkfield earthquake. The trend of the San Andreas fault to the northwest of Parkfield is characterized by fault creep and small to moderate earthquakes. Southeast of Parkfield is the rupture section that last broke in the Great Fort Tejon earthquake of 1857. In between is a transition zone between the creeping and locked sections. Researchers do not understand why nearly all Parkfield earthquakes are so repeatable and so well behaved. One explanation is that in the last 100 years, where

there is historical observation, the adjoining fault segments have been characterized by fairly steady behavior. The seismicity illustrates that this characterization may have changed in the past several years. Bakun discussed the effects of the nearby Coalinga earthquake on the Parkfield earthquake and how this earthquake might have affected the timing of the next Parkfield earthquake.

(Editors note: Interested readers can find a more thorough discussion of the Parkfield situation, including the influence of the Coalinga earthquake, in the report of the Council's March 1985 meeting, USGS Open-File Report 85-507).

Lindh discussed the rationale for linking some automatic alarms to seismicity data. Two foreshock criteria at Parkfield have been devised. Retrospective application of these criteria to the last 5 years of data to gauge implications and frequency of warnings was described. This analysis allowed determination of the probability gain that any foreshock will actually be followed by a larger earthquake. The frequency since 1983 of these empirical alarms has been approximately three per year, or about 25 by 1992. Spreading that probability gain over 2 to 3 days, and assuming a 50 percent chance that the next earthquake will have foreshocks, there is a 4 percent probability of each event actually being a foreshock of the predicted event; if the assumption is a 50 percent probability of no foreshock, the probability drops to 2 percent. Lindh expressed doubt that seismicity alone would justify a prediction but the percentages set up by this analysis, if they were to occur, would have serious implications. Should there be a satisfaction of the criteria, and if the creep meters, water wells, and two color lasers gave any believable support to the seismicity, then we would be reaching a probability of about 50 percent.

Foreshocks and Probability Gains at Parkfield

Jones described an analysis, using the Southern California Earthquake Catalogue and defining foreshocks as earthquakes followed within 5 days and 10 kilometers by larger earthquakes, to describe probability gains. In southern California the probability of an aftershock occurring is about 6 percent, independent of the magnitude of the initial event. With the assumption that two sets of main shocks with foreshocks and main shocks without foreshocks form a binomial distribution, the probability of a foreshock being followed by a main event is 1.6 for the first hour. Jones applied these general findings to Parkfield using both average southern California probabilities as well as probabilities derived solely for the Parkfield region. The time distribution for Parkfield is similar to that for southern California, but there is a large difference in the magnitude dependency; there may not be a statistically distributive sample at Parkfield as there is in southern California. The percentage of earthquakes that have been foreshocks to a characteristic Parkfield earthquake is the percentage that a future event will be a foreshock to a characteristic Parkfield earthquake. Using her analysis, the probability

that a magnitude 5 or greater earthquake will be followed by a characteristic Parkfield earthquake within 5 days is 80 percent; for a magnitude 2 earthquake, it is 5 percent; for a magnitude 3 earthquake, it is 18 percent; and for a magnitude 4 earthquake, it is 40 percent.

Seismic Quiescence at Parkfield

Habermann noted that while many people propose that a change in seismicity rate can occur as part of the process of preparation for large earthquakes, most of these changes are not followed by large earthquakes and therefore are not precursors. Habermann discussed how to distinguish real changes from manmade changes, either detection increases or magnitude decreases. Detection and reporting changes divide seismicity data into smaller events, which are affected by the change, and larger events, which are unaffected. The goal is to find a magnitude cutoff that eliminates the affected events from consideration. Habermann looked at seismicity changes as a function of magnitude band and used a z-test for a difference between the two means. For the Parkfield region, most of the major changes appear to be detection increases with some magnitude decreases and changes due to the installation of stations. Real seismicity changes in Parkfield were also detected, one was a rate increase associated with a swarm of events on April 23, 1975, and another real change was a decrease in activity in 1978. He noted a period of quiescence at Parkfield which concluded near the end of 1982, followed by a period of increased activity, at Parkfield, lasting up to the Coalinga earthquake, which in turn was followed by another quiescent period.

Velocity Monitoring with Vibroseis Methods

Clymer reviewed work in the Hollister, California, area designed to illustrate the capabilities of velocity monitoring and discussed expectations for work in the Parkfield area using new equipment. The research used 3 to 4 kilometer-source receiver offsets in three different locations: the Cienega Winery, Stone Canyon, and Bear Valley. The precision of the instruments appears good, but there has been a problem with accuracy; large seasonal variations in travel time and amplitude caused by near-surface changes in moisture. Procedures used for dealing with this included installation of borehole geophones and measurements of near-surface travel times which were then subtracted from the path measurements. A different procedure is planned for Parkfield. All receivers will be placed in boreholes to eliminate near-surface variations at that end of each path. Source-end variations will be reduced by simultaneously recording a number of paths and using as a reference one path where we do not expect near-surface variations. S-wave travel times and amplitudes are also being monitored. Work at the Geysers, California, geothermal area confirmed that an S-wave vibrator will radiate S_V or S_H waves toward the receiver depending on the orientation of the vibrator base plate, thereby permitting measurement of near-surface anisotropy. Clymer

and McEvilly think this has implications for earthquake prediction research at Parkfield since S-wave amplitude anisotropy may be more sensitive indicators of fault zone properties than P-wave parameters. Preliminary data revealed a high signal-to-noise ratio and complex S-wave arrivals that changed in character upon rotation of the vibrator base plate. They conclude that they can detect changes in wave form dissimilarity, indicating variations in fault zone properties.

Downhole Seismic Monitoring

Malin described experiments at Parkfield in which he is studying two earthquakes using seismograms recorded from instruments in boreholes. He compared S-wave forms from borehole receivers and surface-level receivers. The borehole data (spectra) contains much high frequency energy which is not recorded at the ground-level stations. The purpose of his experiments is to characterize the difference between seismic events recorded at downhole stations with how the events would be recorded on a ground array that would be used extensively to study the statistics and frequency characteristics of Parkfield earthquakes.

Trilateration and Leveling at Parkfield

Segall summarized geodetic survey measurements at Parkfield. While this data set is limited in ability to detect short-term changes, it is unique in another respect--it shows the long-term behavior of the fault over a whole earthquake cycle. Segall described trilateration data for the 1966 coseismic period. He used the coseismic line length changes to determine fault slip during the 1966 earthquake. A number of coseismic slip models were considered and those with slip between depths of 2 to 4 kilometers and 8 to 10 kilometers gave acceptable fits to the data. In the final analysis, though, it is the seismic moment, determined to be $4 \text{ to } 5.5 \times 10^{25}$ dyne-cm, that is best determined by the geodetic observations. Segall next described measurements of the interseismic period (1966-1985). Current configuration of the large aperture network has grown by an order of magnitude. The network is remeasured approximately every year by the Crustal Strain Project. Four small aperture geodetic networks were installed to determine surface slip rates; these networks will be monitored semiannually by the Crustal Strain Project. Segall compared the inferred slip rates from fault crossing lines in the small aperture arrays with long-term slip rates determined from creepmeters and alignment arrays. North of Middle Mountain the values are about 25 millimeters per year, values around Parkfield are about 12 millimeters per year, and the creep rate tapers off to zero to the south. For detecting precursors, only the monitor networks are measured frequently enough to warrant attention. Based on the distribution of monitor line residuals, it was determined that 14 cm of slip on the 1966 rupture surface produced line length changes that occur randomly only 10 percent of the time.

Segall next considered the question of how the fault slips at depth during the interseismic period. Two models were considered. In the first model, the 1966 rupture surface is locked between earthquakes. In the second model, surface creep rates are extrapolated through the seismogenic zone, producing a smooth transition zone between the creeping zone NW of Parkfield and the 1857 locked zone. Segall concluded that the data favor the locked 1966 rupture surface model as opposed to models with significant buried interseismic slip.

Two Color Geodolite Measurements

Slater and **Burford** outlined the past year's progress of a geodolite network at Parkfield. They described possible seasonal influence and found that most of the north-south lines have a flat or down trend; most of the east-west lines show an upward trend. Superimposed on this pattern is a large excursion, particularly on the east to west line, indicating a possible seasonal fault normal gravitational strain. The results of a simple fault slip strain model used to calculate average slip were given and strain histories were shown. Dextral simple shear accumulated at a nearly constant rate of 1 ppm per year until March 1985 when the rate dropped to nearly zero.

Low Frequency Measurements at Parkfield

Johnston discussed strain, tilt, creep, and magnetic measurements at Parkfield. The focus of his presentation was on short-term prediction. He also discussed the design concept for these arrays, which are within one-half to one fault depth of the fault.

Strain: Johnston discussed strain resolution of Parkfield dilatometer sites. Over weeks to months strains better than 0.1 microstrain can be resolved, particularly if the effects of earth tides and atmospheric loading are removed from the data. The main features of data from the two dilatometers at Gold Hill are long-term drift due to cement curing, earth tides, atmospheric pressure, and strain events. Efforts this year are focussed on constraining the source location, length scale, and some geometry of these events. Curious relations to local seismicity were noted as well. Several seismic events corresponded in time to the observed strain perturbations. No first order causal relationship has been found.

Creep: Creep measurements yielded two important results. One is changing slip rates moving north to south along the fault; verified by the alignment data and by comparison with geodetic data. And the second is apparent retardation effect associated with the Coalinga earthquake. The retardation effects may represent a precursor to the earthquake predicted to occur at Parkfield about 1988.

Magnetics: The purpose of this experiment is to detect magnetic perturbations that result from changes in the mean state of crustal stress since both magnetic remanence and magnetic susceptibility have a stress sensitivity of about 0.0001 per bar. Summary plots of the complete difference field records were discussed. In general these records are uneventful at the sub-nanotesla level. However, coherent changes of about 1 nT across the array would constitute anomalous behavior.

Tilt Meter: There is a limited tilt meter array at Parkfield. The results of tilt meter experiments show that long-term tilt trends from shallow borehole installations are not generally coherent between instruments and, therefore, reflect only the movement of the material immediately surrounding the instruments. Johnston was unable to identify signals of a period band greater than days to weeks and larger than one microradian. Johnston presented two anomaly detection algorithms. The first system is the use of amplitude detectors on creep meter data, and the second system is the use of rate detectors on continuous strain and tilt data. Both systems are scaled according to the level of background noise. Johnston concluded his discussion with a presentation of general alarm thresholds for Parkfield creepmeters.

Water Level Monitoring

Bredehoeft discussed earlier work on water well responses to earth tides. From this work 1) it is clear that water level responds to the volume strain, and 2) conditions under which water level responds to earth tides are not very restricted, suggesting the ability to use water wells as a volume strain meter. Bredehoeft experimented at Palmdale on the use of real time data and signal processing with the idea of using water wells as volume strain meters. More recently he moved his experiment to Parkfield. For his experiments he was careful to chose wells with good tidal signals located in confined aquifers. Bredehoeft discussed observations at the Hi Vista well at Palmdale. He noted tidal fluctuations of about 0.3 feet, and complications in the measured barometric pressure, showing diurnal, semi-diurnal, and higher harmonic peaks, which have to be removed from the records. While comparing other wells he noted that during several years of data collection, only a few of the observed events seem to be tectonic. Bredehoeft also computed the dilatational strain associated with a dislocation model and used this model as a guide both to where water wells would be sensitive to slip and to establishing a network in Parkfield. Both surface dislocation and buried faults were considered in his model.

Near-Surface Tilt Monitoring

Morrissey described a near-surface tilt network and gave some indication of the noise sources and what he intends to do about them. His program has essentially just begun and so he described data from Adak, Alaska, and the work he is proposing for Parkfield. The Adak network has 2-meter deep units and the Parkfield network will have 10-meter deep units. Morrissey discussed how he proposes to use the Adak data in establishing the Parkfield network. Morrissey redesigned the electronics to reduce noise from the instruments. One source of noise is the bubble sensor itself; as it is free to move within its housing. Other problems discussed were the installation of sensors and local thermal sensitivity. Morrissey briefed the Council on estimates of temperature change in the ground. Direct attenuation of surface temperature with depth can be estimated for temperature cycles of various periods. The diurnal signal is attenuated more at the 2-meter depth than the annual thermal cycle at the 30-meter depth. And, even at 30 meters a direct annual thermal effect on the sensor may be evident in the data. He described Adak data with the 2-meter deep instruments and suggested that with 10-meter deep instruments at Parkfield the data would be about an order of magnitude better. The attenuation of noise with depths is a $(\text{depth})^3$ factor. These variations can be removed if they are a linear function of temperature at the sensor. With 10-meter depth installations rough estimates of baseline stability, achievable after removing annual thermal effects, can be made. He concluded his discussion with implications of this work for prediction at Parkfield.

EXECUTIVE SESSION

Southern California Working Groups

As a followup to the Southern California Special Study Areas Workshop held in San Diego, California, in February and March 1985 and the Council's March 1985 meeting held in Pasadena, working group chairmen were appointed for three segments of the San Andreas fault - the Mohave segment, the San Jacinto segment, and the southernmost San Andreas segment. The chairmen are organizing working group meetings to be held in October and November of 1985 in order to consider what steps should be taken next in order to designate special study areas.

Short-Term Precursors

The Council debated the concept of holding a workshop, or future meetings, on short-term precursors. Although there is merit in holding a lengthy discussion of this issue, they questioned whether now is an appropriate time for such a meeting since, for example, we can't resolve yet what confidence should be placed on seismicity rate changes as a precursor to an earthquake.

Parkfield

Wesson stated that he is pleased with the progress at Parkfield as evidenced from the day's presentations; most observational aspects seem to be coming along and the Council is beginning to knit together an analysis of Parkfield data. He believes two areas need significantly more work: 1) the decision tree mentioned at the Council's March meeting, and 2) constructing physical models for prediction. He feels the Council should revisit and emphasize some of these issues in 6 months or so, design a strategy for bringing observations together with physical models, and present an opinion of its implications.

Dieterich was of the opinion that one of the most important problems facing the Parkfield experiment and earthquake prediction in general was that of developing rapid decisionmaking procedures. At the time information is in hand to make a prediction it is very likely the situation will be very complex with little or no time to discuss all the interpretations and issues. Therefore, everything possible should be done in advance to work through responses to likely scenarios. It has been Dieterich's experience that this type of exercise also helps focus attention on those weak points that need more thought or more work.

Wesson sees the following as a problem: it is difficult to present geophysical data to a USGS Director, have him rapidly sort through it as well as myriad other issues, and make an intelligent and confident decision regarding the Survey issuing a prediction. The point of a decision tree is to get a lot of the information sifting out of the way early. He asserted that much of the knowledge needed for a decision tree is already intuitively held by Council members. Wallace and some of the other Council members agreed that a decision tree is critical to make an effective prediction.

The Council then had considerable discussion regarding logistical problems of scientifically analyzing data, convening the Council, informing the USGS Director, etc., and completing the process before either the predicted event happens or the appropriate time window for its occurrence passes. And, they discussed how a decision tree might be designed and used.

Sykes offered the question as to whether or not the required turnaround time for making or confirming a prediction necessitates a need to consider intermediate-term precursors in addition to short-term precursors. It was noted that some consideration of intermediate-term precursors is being given at the periodic data review meetings within the USGS.

Sykes offered to arrange an appointment with Dallas Peck, Director, U.S. Geological Survey, to discuss these issues. He stated that the intention of this appointment would be to get guidance from the Director regarding what kind of a decision tree is needed. Additionally, he would hope an outcome would be a sense of both what the Director would accept regarding either a decision matrix or delegation of authority to make various predictions and statements about future earthquakes and what boundary conditions the Council might use in its own work.

JULY 27

INTRODUCTION TO SAN FRANCISCO BAY REGION

Ellsworth outlined the purposes of the second day's meeting as follows. The Council will discuss background information about earthquake activity in the southern San Francisco Bay area and background on geodetic research. The Council will take a concentrated look at the Calaveras fault followed by discussion of the earthquake potential of that section of the San Andreas fault from near Palo Alto (mid-Peninsula) to San Juan Bautista and thence into the northern part of the creeping zone as far as Bear Valley.

The southern one-third segment of the San Andreas fault that broke in the 1906 earthquake is at a substantially higher risk today than the segments to the north. This is largely so because the amount of slip fell off rather rapidly on the San Francisco Peninsular as one moves south to San Juan Bautista. Although there are differences among researchers regarding the detail of how the segments may fail, basically they agree upon the overall dimensions of the failure. The situation of the Calaveras fault is different. There is no clear evidence of an earthquake larger than magnitude 6 or 6.5 on the Calaveras fault system from its southern end up to where it merges with the Hayward fault system. It is clear that at least about 50 kilometers of that fault has ruptured in two recent earthquakes; a magnitude 6 earthquake at Coyote Lake in 1979, and a 6.2 earthquake at Morgan Hill in 1984. The seismic potential of those segments would be somewhat lower than the segments to either the south or the north.

Instrumental Seismic Record

Uhrhammer discussed the seismicity record in central California. The record extends back to 1887, but it is not complete. He considered two 150 km. by 20 km. regions, one along the San Andreas from San Francisco to the south, the other along the Calaveras fault. There is a considerable difference in the seismicity between these two regions. The Calaveras has about 40 percent higher seismicity than the San Andreas in these two areas. Both are more active at their southern ends. Uhrhammer looked at all earthquakes of magnitude 2.5 or greater and for future analysis removed all clustering of earthquakes in order to preserve the main shocks. He did this using a variable time and space window that was a function of magnitude. For both zones the seismicity follows the Gutenberg-Richter relation up to magnitude 6; and, the b-values (approximately .83) are typical for California. Uhrhammer discussed whether there are significant periodicities in the seismicity. Using a frequency spectrum for distribution of earthquakes as a function of time for the San Andreas and Calaveras faults with 1-week time bands, no hidden periodicities could be detected in the range of 10 weeks to 1000 weeks. He also looked for significant spatial distributions.

Uhrhammer identified about 25 foreshock sequences of magnitudes greater than or equal to 2.5 for the past 37 years for the San Andreas fault.

Foreshock probabilities are about 4.6 percent for magnitudes from 2.5 to 5.0. Also, at the magnitude 5 level one-third of the earthquakes on the San Andreas have foreshocks, which agrees with Jones' observations for other parts of California. For the Calaveras fault, 36 foreshocks at magnitude greater than or equal to 2.5 were found; and the probability of foreshocks there is about 4.5 percent.

He also looked at b-values and the rate of seismicity to help answer questions regarding the presence of seismic gaps in the record. Uhrhammer found no significant variation in b-value at magnitudes greater than or equal to 2.5 prior to the 1979 Coyote Lake earthquake or the 1984 Morgan Hill earthquake. However, the resolution at this magnitude level is poor.

Historic Earthquakes

Topozada gave a summary of the history of earthquakes in the southern San Francisco Bay area. Since 1850 there have been two earthquakes greater than magnitude 7; a magnitude 7 on the Hayward fault in 1868 and a magnitude 8 on the San Andreas in 1906. Before and after the Hayward earthquake most events occurred on the San Andreas fault, but before and after the San Andreas earthquake magnitude 6 or greater earthquakes were located on the Hayward-Calaveras faults.

The first report of earthquake damage was in 1800 from San Juan Bautista; and the aftershocks lasted for about 7 weeks suggesting a main shock of a magnitude in excess of 6.0. Before the 1849 gold rush the record for magnitude 6 earthquakes probably is not complete. After 1849 earthquake effects reported in newspapers made construction of isoseismal maps possible. The largest earthquakes, greater than magnitude 7, occurred on the San Andreas fault in 1838 and 1906, and on the Hayward fault in 1836 and 1868. Magnitude 6 or greater earthquakes generally occurred at intervals of 7 or fewer years in the southern San Francisco Bay area. The quiescent periods from 1870 to 1890 and 1911 to 1979 apparently resulted from large stress release in the magnitude 7 and magnitude 8 earthquakes of 1868 and 1906 respectively. Earthquakes of magnitude greater than 6 have occurred on the Hayward-Calaveras zone east of San Jose in 1858, 1897, 1903, 1911, 1979, and 1984, and on the San Andreas fault between San Juan Bautista and Los Gatos in 1864, 1865, 1870, and 1890. Hayward-Calaveras earthquakes occurred principally during the decades prior to the 1906 San Andreas earthquake. San Andreas earthquakes occurred from the decade prior to the 1868 Hayward earthquake and continued to 1890. This suggests that earthquakes of magnitudes greater than 6 on the Hayward-Calaveras zone precede and follow magnitude 7 or greater activity on the San Andreas, while magnitude 6 or greater activity on the San Andreas precedes and follows magnitude 7 or greater activity on the Hayward-Calaveras zone. Topozada discussed some of the inherent uncertainties in locating epicenters using early seismic records. For example, the difficulty of discriminating whether an event occurred on the Hayward or Calaveras fault, the possibility of earthquakes south of Hollister not being detected, and the difficulty of using records from the Spanish missions.

Geodetic Survey Measurements

Prescott presented an overview of the distribution of relative plate motion along the San Andreas Fault system from Hollister to the Mendocino triple junction. South of Hollister all the relative plate motion occurs as rigid block motion in a narrow zone on the fault. North of Hollister a major change occurs. First, the fault is not creeping aseismically. Also, the deformation is no longer associated solely with the San Andreas fault and a large part of the motion occurs to the east of the fault. Prescott places constraints on how much slip could occur on the San Gregonio fault. Prescott's work shows that at Hollister the motion partitions with about one-third of it on the San Andreas fault and with the rest of it distributed to the east. Further, the fault system behavior appears nearly constant north up to the Mendocino triple junction.

A large geodetic network covers the plate boundary between Hollister and the Mendocino triple junction. The line lengths have been measured many times and Prescott has calculated motions of the individual stations. Total displacement across the entire area is about 30 mm per year. Very little of this displacement is occurring on the San Andreas fault itself. There is some distributive shear east of the Calaveras fault produced by rotation of the block east of the fault.

In the northern San Francisco Bay area Prescott again constructed a profile of the component of displacement parallel to the fault system. There is no evidence of offset on any fault traces in the area and no deformation west of the San Andreas fault appears to be taking place. High rates of shear east of the San Andreas fault continue as far north as the triple junction.

Seismic Slip on the Calaveras Fault, California

Bakun discussed implementation of a model slip budget over active faults. Over a significantly long period of time there should be a match between potential slip rates inferred from geodetic data and observed deformation (either coseismic slip, fault creep, or off-fault deformation). Even for short periods of time, slip along fault surfaces can be used to identify sections of the fault which are likely to fail in future damaging earthquakes. Bakun looked specifically at the slip pattern on the Calaveras fault associated with the Morgan Hill earthquake and then made inferences for the area to the north.

He converted catalogue size-estimates to seismic moments and calculated the slip contributions from each earthquake. The advantages to this method are that all the major contributions to the seismic moment are from the big earthquakes and the catalogue is robust and stable for these larger earthquakes.

The distribution of seismic slip on the Calaveras fault suggests that (1) larger earthquakes tend to occur within regions of slip deficit left by earlier earthquakes; (2) since 1969 seismic slip on the Hollister section is significantly less than the seismic slip elsewhere on the Calaveras fault; (3) there is a considerable geodetic versus seismic slip rate discrepancy on the Calaveras fault northwest of the 1984 Morgan Hill earthquake rupture zone. Assuming that both 82- and 73-year recurrence times for the central sections can be extrapolated to the north and two magnitude 5.8 earthquakes occurred on the Calaveras reservoir section in 1903, Bakun's work concludes that it is prudent to anticipate a magnitude 6 earthquake on the Calaveras reservoir section in the next several years. More speculatively, the Calaveras-Sunol fault poses a lesser immediate threat.

Seismic Quiescence on the Calaveras Fault

Habermann found apparent seismicity rate decreases before the Coyote Lake and Morgan Hill earthquakes. He examined the relationship between possible seismicity rate changes and pre-earthquake seismicity patterns. He tried to recognize and account for effects of changes in network operation on seismicity rates. His results indicate the need for careful determination of detection and reporting histories. Habermann divides the earthquake catalogue into groups of smaller and larger events at some magnitude threshold, distinguishing events which are, from those which are not, affected by detection changes. Looking at increasingly larger events, the effects of detection decreases go away at about magnitude 0.9 and above, maximizing the record without the effect of detection changes. The effects of detection increases disappear at events below magnitudes equal to 1.3.

He also considered whether magnitude corrections calculated for the entire fault are applicable to any section of the fault. He divided the region into two segments; a southern segment of Coyote Lake and Morgan Hill, and a northern segment. For the southern segment the pattern looks like that of the entire fault. For northern segments he finds something completely different, a strong increase in detection and some indication of a magnitude change.

These results indicate that detection and reporting histories vary substantially for the Calaveras fault. Also, understanding the causes for the different ways the northern and southern segments behave may be helpful in seeing how the changes occurred.

Habermann's presentation generated considerable discussion about the need to improve earthquake catalogues, specifically, the establishment of a standard catalogue as free as possible of changes in instrumentation and methods of data analysis and its importance to earthquake prediction.

Creep Rate Variations on the Calaveras and San Andreas Faults

Burford discussed possible retardation in aseismic slip rates in the Monterey Bay region, California. His discussion was limited to the region around Hollister involving the Paicines, Calaveras, Sargeant, and Busch faults and nearby portions of the San Andreas fault. Despite the general lack of baseline data, there is a long-term record for the Cienega Winery site on the San Andreas fault south of Hollister. Possible retardations in creep prior to moderate shocks from 1971 to 1973 near Bear Valley and San Juan Bautista were followed by creep acceleration and afterslip. However, monitoring was started too late to distinguish possible creep rate retardations from the possibility that coseismic surface slip and accelerated afterslip effects were superimposed on steady lower rate backgrounds.

The duration of retardation in several cases may be approximately proportional to the seismic moment of the subsequent earthquake, perhaps modified by inverse proportionality of distance from the creep site to the epicenter; although such a quantitative relation has not been tested. He also noted possible fault interaction in the Hollister area that might have an important role in initiating creep rate retardations. Burford presented the hypothesis that local creep rate retardations associated with local seismic quiescences may relate to changes in combined seismic and aseismic slip processes for impending moderate earthquakes. And, from this hypothesis he suggested that retardation associated with evidence of seismic quiescence may reflect a period of rapid increase in shearing stress across an area of impending seismic rupture.

Seismicity of the San Andreas Fault from the Cienega Winery to the Golden Gate

In her presentation **Olson** reported that the San Andreas fault north of the San Juan Bautista transition area is seismically quiescent along the 1906 break except for recurrent low-level microearthquakes along the San Francisco Peninsula. The microseismicity along the fault is concentrated in three zones: a northernmost zone in the 1906 epicentral area; a zone in the mid-Peninsula area near Portola Valley; and a zone near the junction of the San Andreas and Sargeant faults. She also noted that many events occurred off the fault, including some in the mid-Peninsula area with thrust focal mechanism solutions.

The depth distribution of the events is such that those north of the San Juan Bautista area occurred at depths between 5 and 15 kilometers with peaks at 10 kilometers and those events in the San Juan Bautista area occurred at depths less than 10 kilometers with peaks at 4 kilometers. Also noted was an abrupt transition in the modes of slip at San Juan Bautista.

Earthquake Risk on the Southern End of the 1906 Earthquake Rupture

Scholz notes that the southern end of the 1906 break slipped only about 1 to 1.5 meters as opposed to 3 to 4 or more meters to the north. Therefore, the slip deficit region would be a region of increased risk. Some estimates of probabilities on the gaps have been made by other workers. From the standpoint of seismic risk, considering the region's demography, it is important to determine the northern end of this deficit region. Scholz concludes from his investigation that the slip deficit area begins abruptly near Black Mountain, stretching 75 kilometers to San Juan Bautista. If this area were to slip in a single event, it could produce an earthquake of about magnitude 6.9. He contends that the abrupt change, between Alpine and Page Mill roads, marks a major change in the physiographic expression of the San Andreas fault. Considering strain accumulation rates, he estimates that the period for reaccumulating the amount of strain drop for the 1906 earthquake would be about 60 to 110 years. In other words, we are presently midway through the time period estimated for a major shock to occur.

Structural Heterogeneities on the San Andreas Fault

McNally used data from 1975 to 1985 of earthquakes with magnitudes greater than or equal to 2.5 in the Stone Canyon-Bear Valley region in her study of structural heterogeneities. She noted that the largest earthquakes occurred in this region in 1972, 1961, 1951, and 1938. The largest earthquakes in the region occur at relatively equally spaced time intervals. McNally's study is to determine if this is representative of the long-term behavior of the region. A simple technique to analyze clustering or swarms is to separate the clustering from background activity based on a first order Poisson dispersion coefficient. The clustering of seismicity suggests that the next earthquake will be located between latitudes 36°36' and 36°41' north along the San Andreas. The last moderate earthquake there was a M_L 5.0 event in 1938. Her analysis also indicates that an 11-year interval for earthquakes of magnitude 5.0 or greater is representative for this region. This gives a date for a M_L 5.0 to 5.6 Parkfield earthquake as 1987 + 2.14 years; and a M_L 5.0 to 5.6 event for Bear Valley as May 1983. Applying confidence levels to the latter event gives a date of May 1984 at 1 standard deviation; May 1985 at 2 standard deviations; and May 1986 at 3 standard deviations.

Considering slip as a function of distance and the time-distance relation suggests that Bear Valley breaks slightly earlier than Parkfield, and the median time separation between them is 2 to 5 years with a range of 1 to 6 years. McNally also noted an increase in lateral wave refraction at the same location as the clustering since 1978, suggesting a time-dependent change in velocity contrast.

Seismic Hazard Estimate for the San Jose-San Juan Segment of the San Andreas Fault: 1985 to 2005

Sykes presented a paper written by Stewart Nishenko and Patrick Williams. The paper updated the probability map for the 1985 to 2005 time interval for the zone along the San Andreas fault from opposite San Jose to San Juan Bautista. Two data sets were used for this analysis:

1. a large earthquake in 1838 along a segment of the San Andreas fault that was broken again in 1906; and
2. direct calculation of occurrence time by dividing coseismic displacement in 1906 by the rate of fault motion.

The conditional probabilities for the two conditions are respectively 51 percent to 73 percent for a recurrence time of 68 years (i.e., 1906 minus 1838) and 27 percent to 37 percent for a recurrence time of 93 years. The study also looked at changes in the strike of the San Andreas fault between Bear Valley and San Francisco. The study also noted partitioning of fault zones into segments capable of breaking independently for earthquakes of magnitude 6.0 to 6.5; with other earthquakes (1906) breaking several segments. The authors point out that some of the previous earthquakes, for example, 1890 and 1865, have had sizeable areas of intensity VI and VII or greater shaking.

Seismic Quiescence on the San Andreas Fault

Wyss presented a prediction of an earthquake on the San Andreas fault near San Juan Bautista, California, based on a paper by Wyss and Burford that was circulated to NEPEC members. The prediction is based on the seismic quiescence of three sub-segments of the San Andreas fault from late 1973 to 1984. Within the 5 to 10 kilometer long segments the seismicity rates are lower than the average by about 70 percent. These segments are separated by volumes of more nearly constant rate. They also noted that two previous quiescent periods, of 1.3 to 1.6 years duration, were followed by main shocks of $M_L = 4.0$ and 4.2 within the quiet fault-segment. Based on these observations, Wyss and Burford proposed that the recent quiescent anomalies are likely precursors to one or several earthquakes. The short lengths of the anomalous segments suggest expected main shocks in the range of $M_L 4.0$ to 5.0 . They further suggest that should these three zones and their intervening segments rupture all at once, the result would be an earthquake of about magnitude 6.2. The magnitude estimates given by Wyss and Burford are based on the assumption that expected ruptures will happen within the next 12 months; larger magnitudes are postulated if the quiescent period persists for another year. This prediction was discussed by the Council in its July 27 executive session.

EXECUTIVE SESSION JULY 27

The Council had a lengthy debate on a number of aspects of the Wyss and Burford earthquake prediction. These aspects were (1) the significance to

public safety of either magnitude 4 to 5 shocks or a magnitude 6.2 earthquake; (2) the validity and persuasiveness of the analysis, including methodology; and (3) the false alarm rate.

The Council summarized the more important aspects of this debate in a letter to Dallas L. Peck, Director, U.S. Geological Survey, sent by Dr. Lynn R. Sykes, Chairman, National Earthquake Prediction Evaluation Council. This letter is reprinted in the appendix of this report. In essence, the Council finds the prediction of magnitude 4 to 5 earthquakes in the area specified by Wyss and Burford unconvincing. Such events have a moderate probability of occurring in the next 1 or 2 years solely by chance based on the historic record of moderate-size shocks; events of that size do not constitute a significant risk to public safety in any case. The Council is of the opinion that no public action about the prediction of a magnitude 6.2 earthquake is warranted at this time. The Council was not convinced of the validity of the methodology used to make these predictions and feels that more research is needed on seismic quiescence and false claim rates. Nevertheless, the reported quiescence appears to be real and bears close watching over the next 2 years.

Discussion of Legal Liability

In response to the Council's consistent concern about the liability of its members, particularly the non-Federal Government members, John Filson arranged for Deborah Ryan of the Department of the Interior's Solicitor's Office to give a presentation and lead a discussion on this issue.

It was pointed out that to her knowledge there are no cases involving liability suits against members of advisory committees in their personal capacities. Therefore, much of the presentation is the professional opinion of the presenter only. She stated that it is possible, although highly unlikely, that a member of the Council will be held personally liable for advising the Director, USGS, regarding earthquake prediction. The important distinction to draw is not between Governmental and non-Governmental members of the Council but between Governmental liability and personal liability. A Governmental liability suit is against the Government and/or its officials and if damages are awarded, it is the Government who pays. On the other hand, in a personal liability suit, the suit is against the individual and it is the individual who would pay if damages are awarded. Since individuals are unlikely to have enough resources to satisfy an award in a suit involving earthquake predictions, the Government would most likely be the target of a law suit.

It was suggested that if a Council member is sued the member should call the USGS who would coordinate the response to the suit with the Department of the Interior's Solicitor's Office who in turn would work with the Justice Department. If suit is against the Government, the Justice Department would defend the action. A central question is whether or not non-Government members of the Council are considered Government employees for purposes of Department of Justice representation. Her personal opinion

is that, yes, as members of a Federal advisory committee, one is carrying out Federal Government responsibilities and would be considered as a Federal employee for Justice Department representation. She next outlined some of the defenses that could be used in a liability suit against Council members. One category of defense is the threshold defense, by which one tries to get the case dismissed out of hand and there is no resolution or consideration of whether the member acted properly or improperly. An example of this is use of the Federal Tort Claims Act, which would prohibit suit against a Government employee on a claim for which the Government has already been held liable. Another example is a technical defense, such as jurisdictional considerations or whether the plaintiff has standing to sue. Another category of defense is the immunity defense. There are two types of immunity, an absolute immunity, which is likely to be raised in a negligence case, and a qualified immunity, which would be available to Government employees who are sued for constitutional torts. Constitutional torts are more commonly Fourth Amendment torts against peace officers. If a person performed a discretionary function within the scope of his or her official duties and did not violate a clearly established constitutional or statutory standard, he or she is likely to have qualified immunity.

The Council is most likely to experience common law negligence suits. In this case the plaintiff would have to prove questions of State law. To win this type of suit, the plaintiff would have to prove all of the following points:

- (1) the Council owed a legal duty of care to the plaintiff;
- (2) the Council acted negligently either by action taken or not taken and breached that duty of care; and
- (3) the plaintiffs were directly injured by the Council's action or inaction.

Her basic advice is that the Council members best defense is to continue to act prudently and in accordance with their best scientific judgment. Lastly, she noted that legislative amendments to provide general immunity for the USGS and the Council for earthquake prediction activities are unlikely because in the absence of any lawsuits it will be difficult to prove a need to the Congress. She recommends focusing any efforts on getting legislative amendments on the question of the personal liability of the Council members. An alternative is administrative action by the USGS or the Department of the Interior. This could include documenting that non-Government employees are in Government service during tenure and actual duty on the Committee.

The members of the Council asked that the USGS continue to pursue the question of legal liability, especially in the area of legislative amendments and administrative action, and seek to clarify whether all members are considered Governmental employees for legal purposes during their service on the Council.

APPENDIX A. 1.

Parkfield Seismicity Review

W. H. Bakun, A. G. Lindh, K. Poley, and S. S. Schulz

25-JUL-85

Report for NEPEC, (26 July 1985)

26 July 1985

Parkfield Seismicity Review
Bakun, Lindn, Poley, Schulz
U.S.G.S
Menlo Park, California 94025

SEISMICITY PATTERNS

Efforts to bring the '66 hypocentral region into better focus continue. Our current best locations are shown in cross-section in Figure 2. In the blowup of the '66 hypocentral region (Figure 2b), MM3 is the box we assume will contain the foreshocks to the next Characteristic Parkfield Earthquake (CharPEQ). The hypocentral depths of the '66 foreshock and main event (small and large filled stars) have estimated standard errors of 1-2 km.

SEISMICITY RATES

The dominant features of the long-term seismicity are the increase in activity that accompanied the two M4.5-5 events in 1975 (open stars in Figure 2), and the apparent decrease in activity during 1984-5 in both the large Parkfield (Figure 3a) and the Middle Mountain (Figure 3b) boxes. (Box locations are shown in Figure 1).

In light of the long-term prediction for a CharPEQ in 1988, the quiescence since 1984 might be interpreted as evidence for something like Mogi's "Stage 3" of the seismic cycle, and as such might tend to reinforce the expectation that the next CharPEQ will occur by 1992. However in light of the variations in length of reported "periods of quiescence", and the lack of any clear correlation with the magnitude of the earthquakes that sometimes appear to follow them, it is not clear that a "quiescence", if real, would significantly perturb the conditional probabilities based on the historical data alone. In addition, two serious questions cloud any interpretation of the apparent decrease in seismicity rates in Figure 3 as a "premonitory quiescence".

The first complication is that the Coalinga earthquake (2 May 1983, M 6 3/4) had a profound effect on creep meters in the Parkfield area (Mavko et al, 1985), with two of the nearest sites ceasing right lateral motion altogether (Figure 4c). The Middle Mountain creepmeter (XMM1) resumed right lateral slip after about 14 months in July, 1984, but at a reduced rate. The seismicity in MM3 entirely ceased at the M1.5 level during this same time period (Figure 4c), strongly suggesting that the effects of the Coalinga earthquake at Parkfield were not confined to the near surface. Several of the creepmeters in the Parkfield area continue to record slip rates significantly below those observed prior to 1983; XPK1 still continues (as of July 85) to record no right-lateral slip (Figure 4d). The possibility that the apparent reduction in seismicity rate is due to continuing effects of the Coalinga earthquake cannot be discounted.

25-JUL-85

Report for NEPEC, (26 July 1985)

The second difficulty relates to one of the grim realities of running a large rapidly evolving seismic network, particularly in a time of changing technology for recording and processing the data; the difficulty of maintaining an absolute magnitude scale. Although formally the coda-magnitude relation has remained constant since 1969, subtle changes in the details of how things are done can potentially make a difference. Summarized in Table 1 are those changes in procedures, hardware, and network configuration, of which we are aware at this time, that might have affected magnitude values. While the effects of some these changes are probably negligible, and even when not should tend to be random, and thereby tend to cancel out to some degree, this unfortunately may not be the case for the last two changes. Between Jan and Apr 1984 the transition was made to processing almost all of the CALNET data on Carl Johnson's CUSP system, this meant an end to the use of coda lengths from develeocorder films for magnitude determinations. While efforts were made to ensure that this change did not result in any magnitude bias, the possibility that magnitude values crept downward over some magnitude ranges at this time cannot be eliminated. In addition in Nov '84 six new stations were added in the Parkfield area that operate at 6-12 db lower gain. No correction has yet been made for the shorter codas that result from this change, the effect may be particularly significant at lower magnitudes. Efforts to remedy this situation are underway; until the magnitude of the problem is ascertained, the apparent decrease in seismicity rate at Parkfield in 1984 is suspect.

TABLE 1

DATES	CHANGE
1972 - 1980	Gradual increase in number of stations
mid 1974	Digitizing table replaces Geotech viewers
1975 - 1985	Gradual decrease in % of stations on Develeocorder
Apr 1977	Decrease in average develeocorder gain
Feb 1981	Addition of significant quantity of RTP codas
	Algorithm Ia, b, c, ...
Jul-Sep 1983	RTP Coca algorithm II
mid 1983	Develeocorders slowed to 5mm/sec
Jan-Apr 1984	CUSP processing eliminates remaining develeocorders
Nov 1984	Addition of intermediate gain stations at Parkfield

FORESHOCKS

The last two CharPEDs (1934 and '66) were preceded by immediate foreshock sequences containing one or more M5 events of 72 and 4 hours duration, respectively. The two M5 foreshocks in '34 were located within 5 km to the NW of the main event (Wilson, '35; Bakun and McEvilly, '81), the M5 foreshock in 1966 was located about 1.5 km to the NW of the main event at the same approximate depth (Figure 2). Thus the prospects seem good that the next Parkfield

25-JUL-85

Report for NEPEC, (26 July 1985)

earthquake will be preceded by foreshock activity in the MM3 box, and if some means could be found to identify such foreshocks as they occur, they would provide a powerful short-term precursor.

Because of their potential for short-term prediction, some effort has been devoted to the question of foreshock identification, but to date no general applicable criteria have been established. Thus the only use of foreshocks which can be implemented at this time is statistical, in the sense that after the occurrence of a given earthquake which can be identified as a potential foreshock, the probability of occurrence of a larger earthquake might be enhanced for some time period. Lucy Jones has calculated such probabilities for earthquakes in southern California (Jones, '85) and for Parkfield (Jones, this meeting) and finds that for any M5 event at Parkfield there is a 33% chance of it being followed by a larger event within five days. On the basis of the seismicity data presented here, we can attempt an independent estimate.

Since we have already assumed that the hypocenter of the next Parkfield earthquake will be near the hypocenter of the last event, we can confine our calculations to seismicity near that point; given the practical limitations on resolving earthquake locations, this is essentially equivalent to confining our attention to events within the MM3 box (Figures 2b and 4c).

Primarily on the basis of detection and location capabilities, we have chosen two threshold levels that define the onset of a potential foreshock sequence within MM3; they are one M1.5 event, or two M1 events within a 72 hour period. Since 1980 when detection capabilities achieved this level in the Parkfield region, these alarm levels have been reached an average of about 5 times per year (Figure 4c). However since the apparent overall decrease in activity in 1983, they have averaged only three alarms per year. These numbers allow us to make a very simple -- and very approximate -- estimate of the probability gain (Ak1, 1981) associated with a potential foreshock sequence within MM3.

If we wish to estimate the empirical probability of a given event within MM3 being a foreshock, we need an estimate of the frequency of such events, and the probability that the next characteristic Parkfield event will be preceded by foreshocks. Since we know that at least two of the last four Parkfield events had foreshock sequences at the M3-5 level, an estimate of 0.5 for the probability of the next event having some foreshock activity at the M1 level seems conservative. Thus it remains to estimate the frequency of potential foreshock sequences within MM3.

We have estimated that there is a 95% chance that the next CarPERQ will occur by 1993, this implies that approximately 25 potential foreshock alarms will occur during the time interval within which the earthquake is expected. Assuming a 50% chance the next event will have some sort of foreshock sequence within MM3, this implies a 2% chance that any given foreshock alarm will be followed by a M6 Parkfield earthquake.

25-JUL-85

Report for NEPEC, (26 July 1985)

Based on a 21.7 year average recurrence interval, the Poisson estimate is just over 1 in 10,000 per day for a CarPEQ (Dashed curve in Figure 5). We estimated above that the probability that a potential foreshock sequence will be followed by a CharPEQ is approximately 1 in 100 for 24 to 72 hours following a foreshock alarm. This implies an average probability gain of about 100 associated with each foreshock alarm. Alarms associated with larger events will presumably be less frequent and thus imply a larger probability gain. Conversations with Lucy Jones on precisely how to interpolate between her values for M3-5 foreshocks, and ours for M1 foreshocks are underway.

The probability gain of 100 estimated above will be applied to whatever the current probability estimate is at the time the potential foreshock sequence occurs. Analysis of historical data has led to an estimate of 1988.2 for the next CharPEQ, with an estimate of 2.6 years for the standard error of that estimate (Bakun and McEvilly, 1984; Bakun and Lindh, 1985). If we apply a simple statistical model for estimating conditional probabilities (Hagawara, 1974; Lindh, 1983; Sykes and Nishenko, 1984), these long-term data result in probability estimates that increase rapidly in time, reaching about 30%/yr, or $8.4E-4/\text{day}$ by 1988 (Figure 5). Thus a probability gain of 100 associated with a potential foreshock sequence in the MM3 box in 1988 would result in a conditional probability estimate of almost 1 in 10 per day for a period of 1-3 days following the onset of the alarm.

Of course while a conditional probability estimate as high as 1 in 10 per day represents an enormous gain over the unconditional Poisson estimate of 1 in 10,000, it still does not correspond to what most people think of as a short-term earthquake prediction. Until better techniques are developed for recognizing foreshocks in real-time, this may be all we can get from seismicity data by itself.

This emphasizes the importance of a multidisciplinary approach; if we are to achieve more certain short-term estimates with high confidence, we will have to rely on changes in the pattern of deformation as measured by creepmeters, two-color geodetic measurements, downhole strain-meters, or deep waterwell measurements, all of which are underway in the Parkfield area. If we are so fortunate as to recognize a potential foreshock sequence as it occurs, and thereby achieve a short-term probability as high as 1 in 10, it would only take 2 or 3 other instruments contributing additional independent probability gains of 2 to move us to estimates over 50%/day, which if correct, would probably constitute a successful short-term prediction in most peoples eyes. However without confirming anomalies from other instrumentation, we might have to endure as many as 5-10 false alarms based on foreshocks alone.

25-JUL-85

Report for NEPEC, (26 July 1985)

ALARM IMPLEMENTATION

All the signals from the 400+ seismic components of the CALNET are telemetered in real time directly to U.S.G.S. Western headquarters in Menlo Park, California, where they are recorded on a variety of media, and also processed directly in real-time by computers which provide estimates of earthquake locations and magnitudes within 3-5 min. of their occurrence. These locations are used to trigger automatic alarm systems, which on the basis of hypocenter and magnitude activate paging systems and place phone calls to alert the seismologists responsible for surveillance. Alarms based on the foreshock scenarios in MM3 described above have been in operation since Apr 1985. The scientists responsible for surveillance have computer terminals in their homes, and thus when an alarm goes off, can quickly review the seismic data and contact those responsible for checking other kinds of data and/or making decisions.

The remaining question is determining the duration of the alarm periods. Most foreshock sequences are of short duration, with a large fraction of 24 hrs or less (Jones and Molnar, 1977; Jones, 1984). The two CharPEQ foreshock sequences for which we have data were of approximately 72 and 4 hours respectively. Thus somewhat arbitrarily we consider the ALERT PERIOD following each alarm to be of 72 hours duration, with the probability gain at 100 for the first 24 hours, 67 for the 2nd 24 hours, and 33 for the 3rd 24 hours following the alarm.

To illustrate with a concrete example, on 25 May 1985 a M3 event occurred at 419 GMT beneath Middle Mountain at a depth of 10 km, just south of the '66 hypocenter, well within MM3. The long term probability is currently .00036/day (Figure 5), so application of the foreshock alarm probability gains results in the following conditional probability estimates.

TIME PERIODS	DAILY PROBABILITY
25 May 0419 - 26 May 0419	.036
26 May 0419 - 27 May 0419	.024
27 May 0419 - 28 May 0419	.012
28 May 0419 - Present	.00036

Figure Captions

Figure 1. Map of earthquake epicenters (1975-June 1985) relative to the trace of the San Andreas fault (bold line) and the epicenters of the $M=5.1$ foreshock and the main shock in 1966, shown as small and large stars respectively. Parkfield epicenters were calculated using a crustal velocity model designed specifically for the Parkfield section of the San Andreas fault. Epicenter clusters near the western edge (faint line) of the San Joaquin Valley are aftershocks of the 1975 Cantua Creek, 1976 Avenal, 1982 New Idria, and 1983 Coalinga earthquakes. Epicenters for all $M \geq 2.3$ earthquakes are shown, except the very many $M \geq 3$ aftershocks of the 1983 Coalinga earthquake, which cover the Coalinga area when plotted. The Middle Mountain window (quadrilateral) includes the preparation zone of the characteristic Parkfield earthquake; the larger box is the general Parkfield alarm window.

Figure 2. Cross sections of seismicity for 1975-June 1985. Symbol size is proportional to magnitude; the smallest symbol represents 2.3-2.99 in (a) and 1.5-2.29 in (b). a) Cross-section of the seismicity of $M \geq 2.3$ along the section A-A' (Figure 1). Relative focal depths are generally accurate to 1 km or less; depths of the shallow shocks to the northwest of the Middle Mt. box are less accurate, with an uncertainty of about 2 km. For reference, the hypocenters of the immediate $M=5.1$ foreshock and the main shock in 1966 are shown as small and large solid stars respectively; the other two stars are the 1975 $M=4+$ shocks. The lines at B and B' denote the boundaries of the Middle Mt. box. Creepmeter locations are given by 3 letter names along the top of the figure. b) Blow-up cross-section of the seismicity of $M \geq 1.5$ along the section B-B' (Figure 1). Hypocenter locations are based on a revised set of station corrections for master events within the Middle Mt. box (locations will differ slightly from those in 2a). The section is divided into 3 boxes - MM1, MM2, and MM3 - denoting 3 clusters of events

Figure 3. Time histograms of seismicity (1969-1988) at 90 day intervals, $M \geq 1.75$. Time of the Coalinga main shock is shown by the vertical line. a) Parkfield seismicity. b) Middle Mt. seismicity (within the MM box in Figure 1). Stick figures with solid circles represent $M \geq 3.75$, those with X's $M \geq 4.0$ shocks.

Figure 4. Time histograms of seismicity $M \geq 1.6$, and cumulative creep near Middle Mt (1979-June 1985). Times of New Idria and Coalinga main events are shown by vertical lines. a) MM1 seismicity (Figure 2b). Note spurt of activity in May 1983. b) MM2 seismicity (Figure 2b). Note spurt of activity in late 1983. c) MM3 (1966 hypocentral area) (Figure 2b). Also shown as short vertical bars are those times when the MM3 foreshock alarm now in use (since April 1985) would have been triggered (see text). d) Cumulative creep near MM for creepmeters XMM and XPK (Figure 2a). Note the correlation between the decrease in seismicity and the decrease in rate of creep following the Coalinga earthquake in May 1983.

Figure 5. Time plot of the probability of the next characteristic Parkfield earthquake for two different set of assumptions. The lower dashed curve is the unconditional Poisson estimate for a mean recurrence time of 21.7 years. The upper solid curve is the conditional probability, given that an event has not yet occurred, for the estimate of Bakun and Lindh that the next event will occur in 1988.2 (+2.6) yrs, using the statistical formulation of Lindh. The left hand axis labeling is for annual probability, the right hand for daily probability.

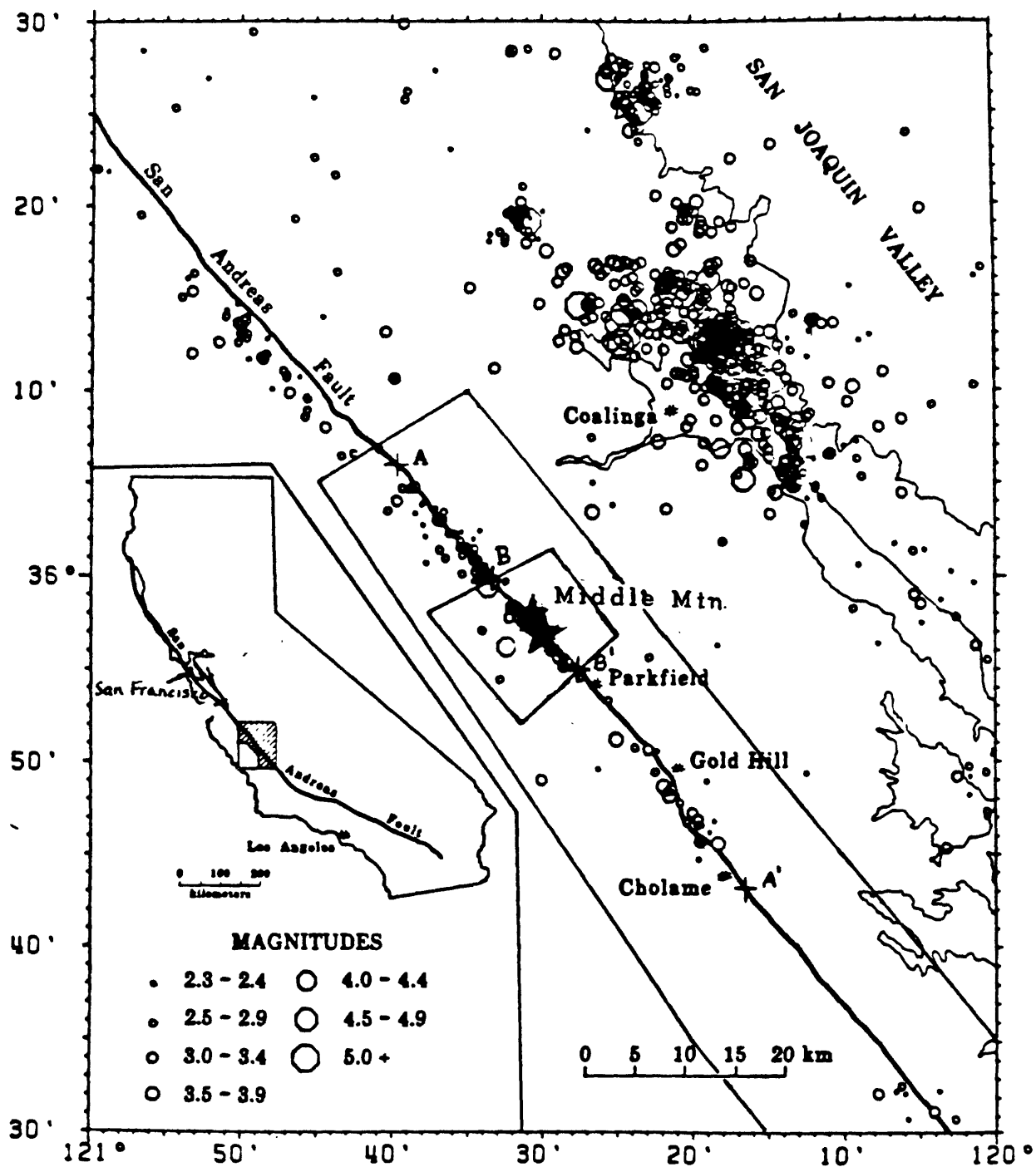


Figure 1

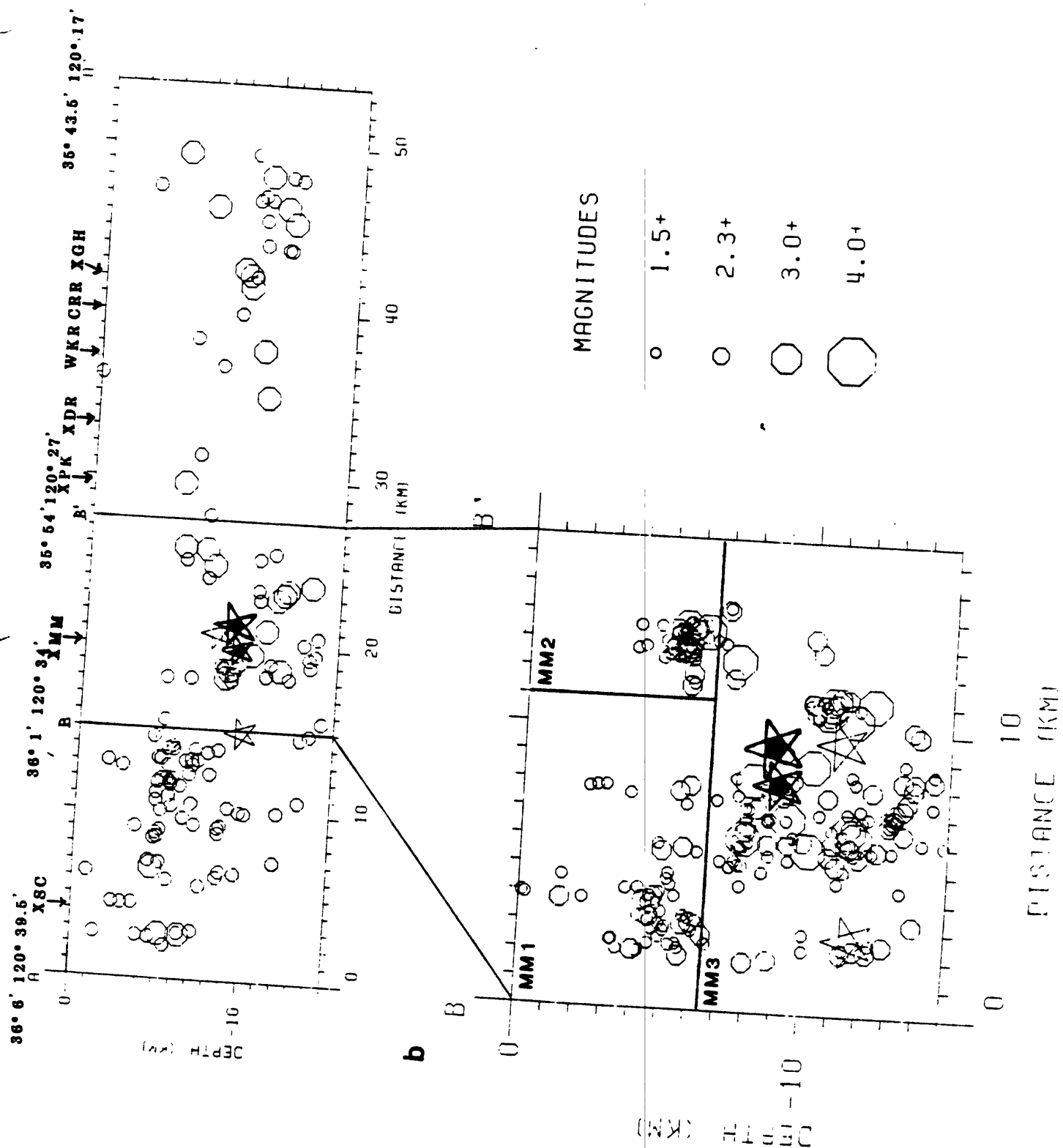


Figure 2

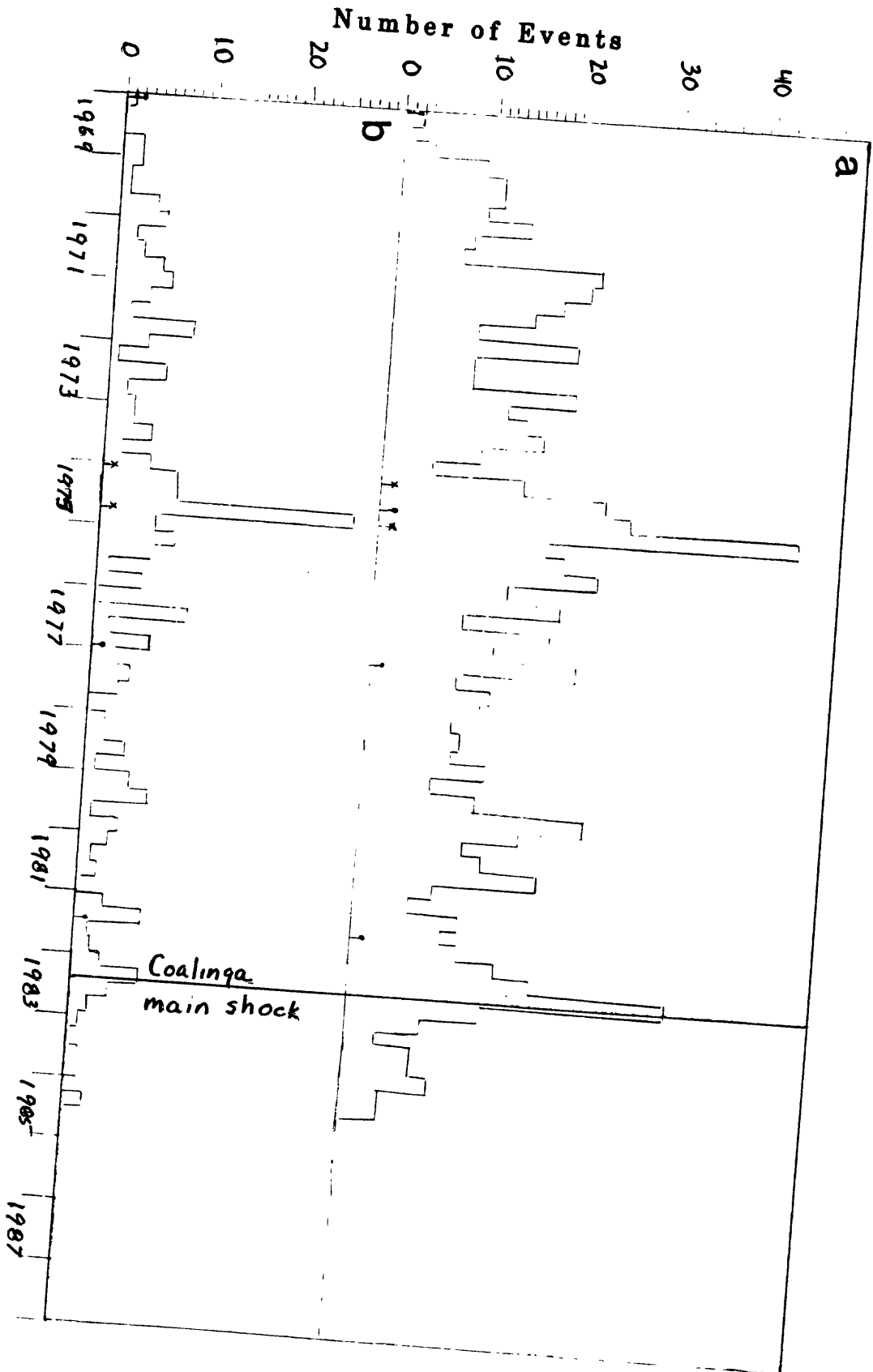


Figure 3

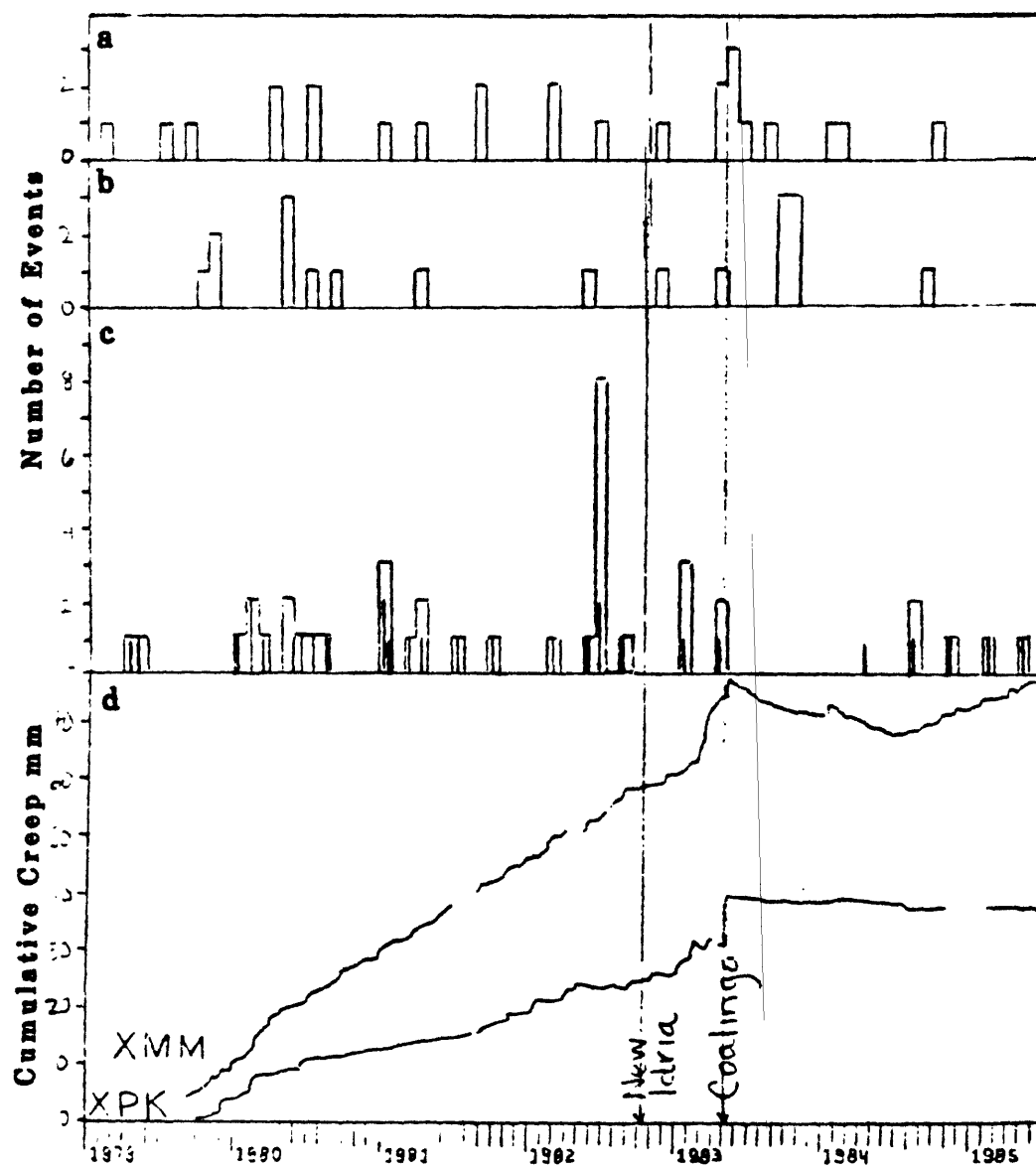


Figure 4

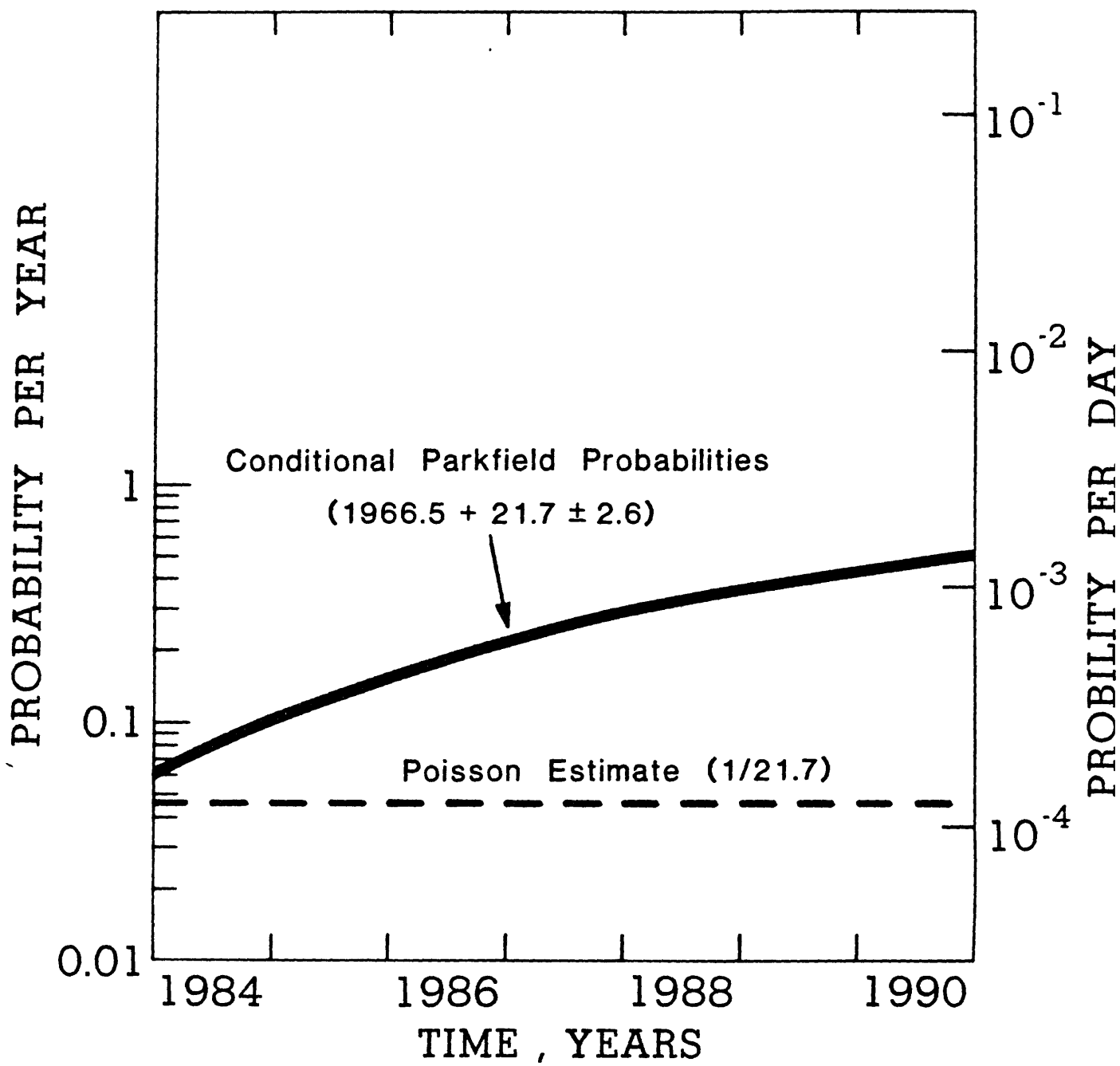


Figure 5

APPENDIX A. 2.

The Parkfield, California, Earthquake Prediction Experiment

W. H. Bakun and A. G. Lindh

Reprinted with permission of the author
and SCIENCE, volume 229, pp. 619-624,
August 16, 1985

The Parkfield, California, Earthquake Prediction Experiment

W. H. Bakun and A. G. Lindh

Certain sections of the San Andreas fault system in central California tend to fail in recurring, moderate-sized (magnitude 5 to 7), characteristic earthquakes (1, 2). Characteristic earthquakes are repeat earthquakes that have the same faulting mechanism, magnitude, rupture length, location, and, in some cases, the same epicenter and direction of rupture propagation as earlier shocks. The earthquakes in 1979 at Coyote Lake and in 1984 at Morgan Hill, both of magnitude 6 (Fig. 1, inset), on the southern Calaveras fault east of San Jose, California, are recent examples of characteristic earthquakes, apparently repeating shocks in 1897 and 1911, respectively (3, 4). The case for characteristic earthquakes on the Parkfield section of the San Andreas fault (Fig. 1) is more complete (5), at least in part because the interval between events at Parkfield is shorter (21 to 22 years) than the interval (70 to 85 years) that is apparently appropriate for the southern Calaveras fault (3, 4).

In recent years, earthquakes near Parkfield (Fig. 1) have occurred either on the San Andreas fault or in distinct clusters of activity near the western edge of the San Joaquin Valley (6). Northwest of the Parkfield section, slip on the San Andreas fault occurs predominantly as aseismic fault creep; although small shocks (magnitude <4) occur here frequently, shocks of magnitude 6 and larger are unknown and little, if any, strain is accumulating (7). In contrast, very few microearthquakes and no aseismic slip have been observed on the fault south-east of Cholame; this locked section ap-

parently ruptures exclusively in large earthquakes (magnitude >7), most recently during the great Fort Tejon earthquake of 1857 (8). Parkfield earthquakes occur within the transition zone between these contrasting modes of fault failure. The regular nature of Parkfield seismicity since 1857 may be due to the nearly

Summary. Five moderate (magnitude 6) earthquakes with similar features have occurred on the Parkfield section of the San Andreas fault in central California since 1857. The next moderate Parkfield earthquake is expected to occur before 1993. The Parkfield prediction experiment is designed to monitor the details of the final stages of the earthquake preparation process; observations and reports of seismicity and aseismic slip associated with the last moderate Parkfield earthquake in 1966 constitute much of the basis of the design of the experiment.

constant slip rate pattern on the adjoining sections of fault. Until recently, the Parkfield section had been relatively free of significant perturbations in stress caused by nearby shocks; the effect of the 2 May 1983 Coalinga earthquake [local magnitude (M_L) 6.7], 40 km northeast of Parkfield (Fig. 1), on the timing of the next Parkfield shock is not known.

Historic Parkfield Seismicity

The epicenters of two foreshocks of magnitude 6 in 1857, as well as the epicenter of the 1857 main shock, were probably located on the San Andreas fault near Parkfield (9). Since 1857, earthquake sequences with main shocks of magnitude 6 have occurred near Parkfield on 2 February 1881, 3 March 1901, 10 March 1922, 8 June 1934, and 28 June 1966. The times between sequences since 1857 are remarkably uniform, with

a mean interval of 21.9 ± 3.1 (standard deviation of the mean) years (Fig. 2b). Although the time of the 1934 sequence departs from the regular pattern by occurring a decade too early, the time of the 1966 sequence conforms to the regular pattern, in that the 44 years between 1922 and 1966 is twice the mean interval.

The last damaging Parkfield earthquake in 1966 was assigned a value for M_L of 5.6 (5, 10) and a seismic moment of 1.4×10^{25} dyne-cm (11). Although the shock might have caused significant damage if it had occurred in a metropolitan area, it caused only minor damage to the wooden frame homes in the sparsely populated Parkfield region (12, 13). The source of the 1966 earthquake can be described by a simple model: unilateral rupture propagation southeast over the rupture zone, a 20- to 25-km-long section of the San Andreas fault bounded by two

geometric discontinuities in the fault trace that apparently control the extent of rupture (14). The northwest discontinuity, adjacent to the epicenter of the 1966 main shock on Middle Mountain, is a 5° change in the strike of the fault trace; the southeast discontinuity is a 1-km echelon offset (right step) in the fault trace near Gold Hill. The Parkfield preparation zone is the 1- to 2-km-long section of fault at the northwest end of the rupture zone; the preparation zone is defined to include the 5° bend in the fault trace and the epicenters of the 1966 main shock and its foreshock (M_L 5.1) (Fig. 1).

The Characteristic Parkfield Earthquake

The 1934 and 1966 Parkfield sequences were remarkably similar (5, 10). The main shocks had identical epicenters, magnitudes, fault-plane solutions, and unilateral southeastward ruptures.

The authors are with the Department of the Interior, Geological Survey, Branch of Seismology, 345 Middlefield Road, Menlo Park, California 94025.

Moreover, identical foreshocks of M_L 5.1 preceded each main shock by 17 minutes (10), and the lateral extent of aftershock epicenters in 1966 (15) repeated that in 1934 (16). The location and extent of surface faulting in 1934 were similar to those in 1966, and anecdotal reports suggest that, after the 1922 and 1901 events, cracks were found in some of the same places as well (12). Intensity patterns for the Parkfield shocks in 1901, 1922, 1934, and 1966 are similar (9); the few reports available for the 1881 Parkfield shock (17) are consistent with the intensities reported for the more recent shocks. The epicentral location of the main shock in 1922 is constrained to the 18-km-long section of the fault northwest of the rupture zone (18). Comparisons of

seismograms for the 1922, 1934, and 1966 main shocks recorded in Europe, North America, and South America suggest that, within the experimental errors of 10 to 20 percent, the seismic moments for the three shocks were equal (5).

Although few data are available for Parkfield sequences before 1934, they are consistent with the proposal that the main shocks in 1881, 1901, and 1922 were similar to those in 1934 and 1966 (5). The similarities in the main shocks (19) suggest that the Parkfield section of the San Andreas fault is characterized by recurring earthquakes with predictable features. Thus, the design of a prediction experiment can be tailored to the specific features of the recurring characteristic earthquake.

A Recurrence Model for Parkfield Earthquakes

The limited data available on the recurrence of large and great earthquakes along plate boundaries around the world apparently are consistent with a time-predictable model, for which the time interval between successive shocks is proportional to the coseismic displacement of the preceding earthquake (20, 21). Unfortunately this simple model is not supported by the data available for the last three Parkfield earthquakes: although comparable coseismic displacements in 1922, 1934, and 1966 are inferred from the observations (5), the time intervals between the three events differ by more than a factor of 2 [1934 to 1922 (12 years) compared with 1966 to 1934 (32 years)].

However, simple adjustments result in another model, the Parkfield recurrence model, which partially accounts for the timing of the characteristic Parkfield shocks (see Fig. 2a). Both models assume a constant loading rate and an upper bound stress threshold, σ_1 , corresponding to the failure strength, or yield stress, of the fault. Whereas the time-predictable model permits a variable stress drop, the Parkfield recurrence model assumes the same stress drop for each characteristic earthquake but allows for the possibility of an occasional early failure, that is, before σ_1 is reached. The Parkfield recurrence model implies that the stress drop in a characteristic earthquake generally does not completely relieve stress in the rupture zone.

The features of the Parkfield recurrence model are easily described. Failure at or near σ_1 corresponds to those times when the failure stress is approached over the entire rupture zone, at which time failure must occur; according to this model there can be no late characteristic Parkfield earthquakes. However, triggering scenarios (22) can be devised that permit the occasional early characteristic earthquake.

There may be evidence for an early triggering mechanism in the seismicity preceding the 1934 event. The foreshocks during the 3 days before the main shock in 1934 were initiated by a cluster of magnitude 3 events and a subsequent shock of M_L 5.0 (23). This early M_L 5 foreshock, which occurred 55 hours before the 1934 main event and about 3 km northwest (16), was characterized by unilateral rupture expansion southeast toward the preparation zone (24), a particularly efficient mechanism for increasing right-lateral shear stress in the prepa-

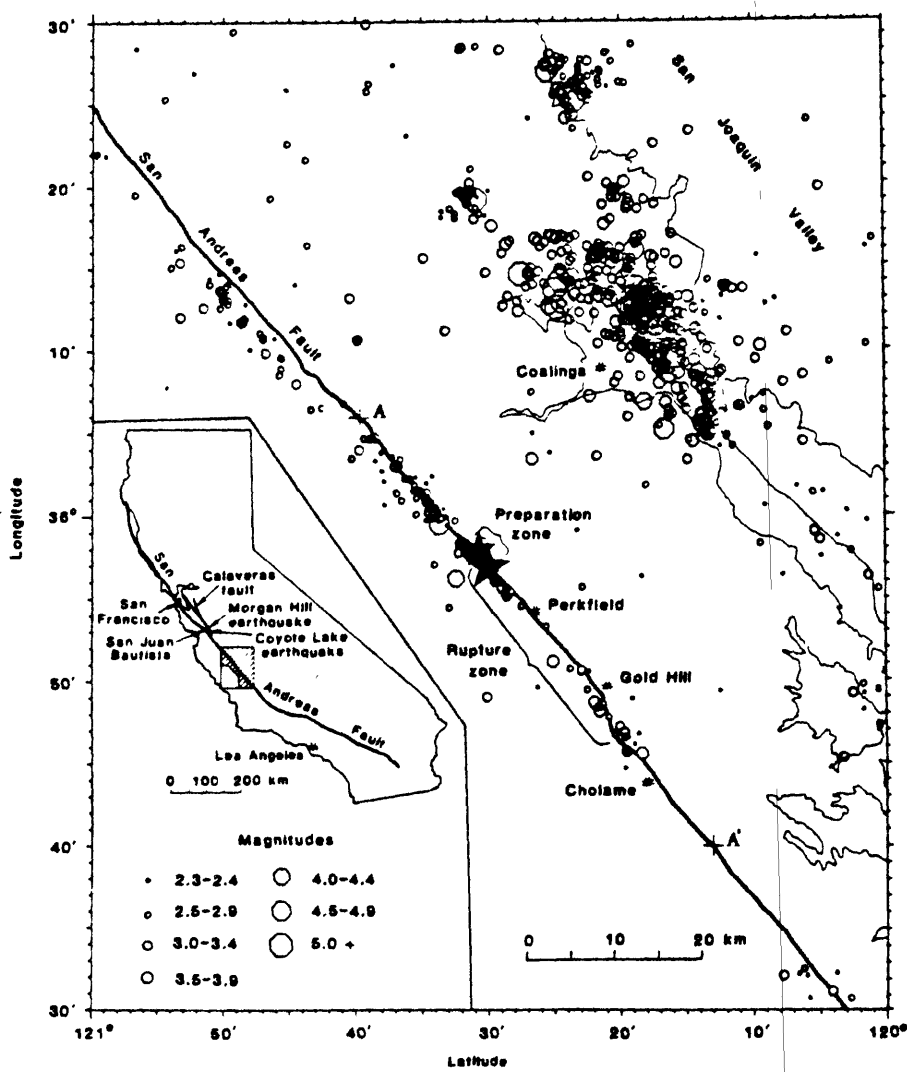


Fig. 1. Map of earthquake epicenters (1975-1984) relative to the trace of the San Andreas fault (bold line) and the epicenters of the foreshock (M_L 5.1) and the main shock in 1966 (small and large stars, respectively, near the center of the map). All epicenters were calculated from a crustal velocity model designed specifically for the Parkfield section of the San Andreas fault (55). Brackets along the fault show the preparation zone and rupture zone of characteristic Parkfield earthquakes. Epicenter clusters near the western edge (faint line) of the San Joaquin Valley are aftershocks of the earthquakes at Cantua Creek in 1975, at Avenal in 1976, at New Idria in 1982, and at Coalinga in 1983. Epicenters for all earthquakes of M_L 2.3 or greater are shown, except the very many aftershocks ($M_L < 3$) of the 1983 Coalinga earthquake, which cover the Coalinga area when plotted.

ration zone. This early foreshock may have triggered the failure within the preparation zone, including the immediate foreshock of M_L 5.1 and the main shock (25).

The Parkfield area was relatively quiet for shocks of M_L 4 or greater in the years following the 1934 and 1966 sequences (Fig. 2c); more active periods began in 1953 and 1975. This pattern is reminiscent of the seismic cycle modulations in regional seismicity that accompany great plate-boundary earthquakes (26). Perhaps there is an intermediate stress level, σ_2 , reached midway in the recurrence cycle (27), at which moderate seismicity ($M \geq 4$) resumes in the Parkfield area. The 1934 Parkfield sequence occurred approximately when σ_2 would have been reached (Fig. 2). We can speculate that, while the early foreshock in 1934 should have just marked the onset of the active half of the seismic cycle, it triggered a sequence of shocks near the preparation zone that culminated in the immediate foreshock and the 1934 characteristic earthquake.

According to the model, the next characteristic Parkfield earthquake should occur before σ_1 is exceeded (early 1988 from Fig. 2). The uncertainty in this predicted time can be estimated from the regression of times of characteristic earthquakes that we presume occurred at σ_1 (28). From the relation $T_O = 21.71 + 1836.2$ (line in Fig. 2b), where T_O is the time of origin (in years) and I is a characteristic earthquake counter (5), the 95 percent confidence interval for the predicted date is 1988.0 ± 5.2 (29). That is, the next characteristic Parkfield earthquake should occur before 1993.

Recent Seismicity

The significant recent seismic activity on the San Andreas fault near Parkfield is concentrated near the ends of the 1966 rupture zone (Figs. 1 and 3), the same spatial pattern that preceded the 1979 Coyote Lake and 1984 Morgan Hill earthquakes (3, 30). Seismic activity on the creeping section northwest of the preparation zone is characterized by shallow focal depths and a small average magnitude, which are typical features of seismicity along the creeping section of the fault northwest to San Juan Bautista (31). The recent seismicity within the rupture zone mimics the spatial and magnitude distributions of the 1966 aftershocks (32), even though the events shown in Figs. 1 and 3 occurred well after the end of the 1966 aftershock ac-

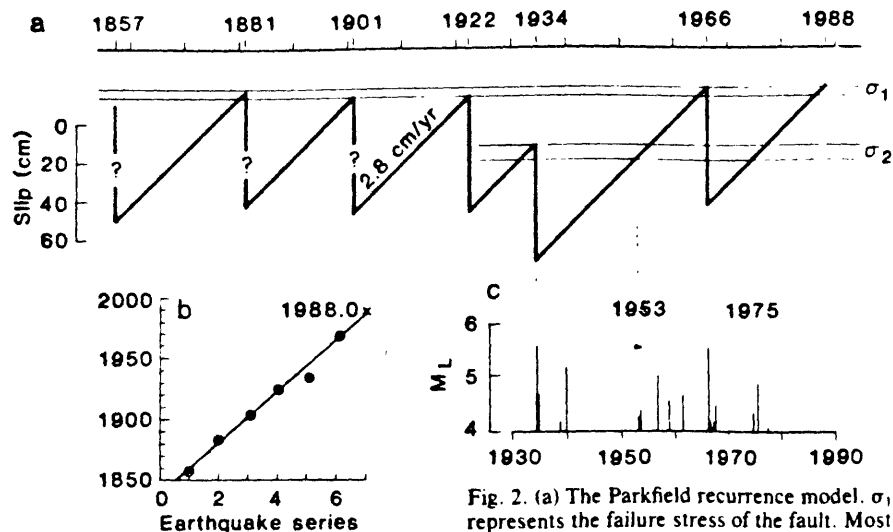


Fig. 2. (a) The Parkfield recurrence model. σ_1 represents the failure stress of the fault. Most characteristic earthquakes occur at σ_1 ; the 1934 shock occurred at σ_2 . A constant loading rate of 2.8 cm per year and a coseismic slip of 60 cm for the Parkfield earthquake sequences in 1881, 1901, 1922, 1934, and 1966 are assumed (56). (b) Series of earthquake sequences at Parkfield since 1850 (after [5]). The line represents the linear regression of the time of the sequence obtained without the 1934 sequence. The anticipated time of the seventh (that is, the next) Parkfield sequence for the regression is January 1988. (c) Shocks of M_L greater than 4 since 1930 have tended to occur when the stress exceeds σ_2 .

tivity (33). Apparently, the distribution of seismicity within the rupture zone is controlled by relatively stationary fault zone properties, such as geometry (30, 34) or rock type (35).

The seismic activity near the preparation zone (36) is most critical for short-term earthquake prediction. All but one of the $M \geq 4$ shocks in the Parkfield area since 1969 have occurred within 1 to 2 km of the preparation zone. On 13 September 1975, a shock of M_L 4.9 with low static stress drop (24) occurred 5 km northwest of the preparation zone; rupture propagated southeast, apparently stopping near the preparation zone. This shock appears to be similar in many respects to the early foreshock in 1934 (and to the shock of M_L 5 on 16 November 1956) (24), but it did not trigger an early characteristic earthquake, although it did initiate the current active phase of the seismic cycle (Fig. 2c). Since 1975, a number of clusters of magnitude 3 shocks, the most recent in June 1982, have occurred near the preparation zone.

The static stress drops of the immediate foreshocks of M_L 5.1 in 1934 and 1966 were marginally higher than those of other shocks of M_L 5 located near, but not within, the preparation zone (24). Higher static stress drops were also obtained for a set of recent smaller shocks located close to the preparation zone; sources of lower stress drop tend to occur around the sources of higher stress drop (37). Perhaps the preparation zone is characterized by sources of relatively

high stress drop, whether or not the earthquakes are foreshocks.

Signals from seismographs (38) near Parkfield (Fig. 4) are telemetered continuously to a central data-processing facility in Menlo Park, California. The signals are automatically and continuously monitored by a real-time processor (39) that, within a few minutes, routinely locates earthquakes in central California. Beeper and paging systems have been established so that the responsible scientists are notified within minutes of all significant seismicity near the preparation zone.

Crustal Deformation

An irrigation pipeline that crosses the rupture zone 2 km northwest of Gold Hill broke and separated about 9 hours before the 1966 Parkfield main shock (40). Also, fresh en echelon cracks of uncertain origin were observed in the fault zone near the center of the rupture zone 12 days before the 1966 earthquake; if the cracks were tectonic, they resulted from aseismic slip in the rupture zone (41). An optimistic interpretation of the broken pipeline and the fresh cracks is that a few centimeters or more of precursory fault creep occurred in the rupture zone just before the 1966 earthquake. Although these observations are fragmentary, and although subsequent earthquakes elsewhere in California have not produced any further evidence for premonitory slip, laboratory observations

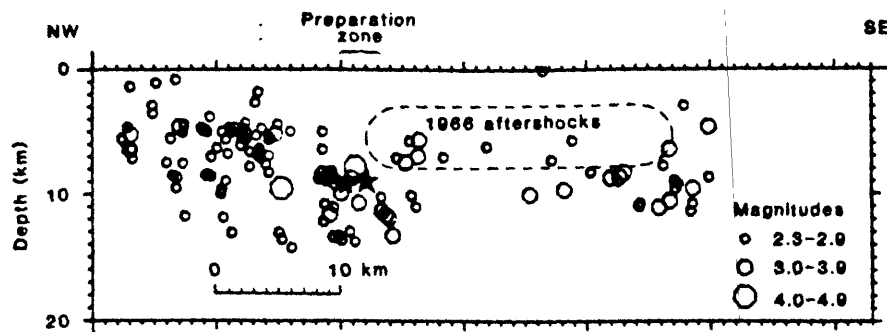


Fig. 3. Cross section of the seismicity for 1975-1984 along the section A-A' (Fig. 1) of the San Andreas fault. Relative focal depths are generally accurate to 1 km or less; depths of the shallow shocks northwest of the preparation zone are less accurate, with an uncertainty of about 2 km. For reference, the hypocenters of the immediate foreshock of M_L 5.1 and the main shock in 1966 are shown as small and large stars, respectively, and the approximate outline of the 1966 aftershock zone (rupture zone) is dashed.

and theoretical calculations (42) indicate that premonitory deformation should occur near the hypocenter, although the amount and timing are uncertain. In light of the crucial importance of this question for future directions in earthquake prediction research, a major effort has been undertaken at Parkfield to define whatever premonitory deformation precedes the next earthquake there.

On a more fundamental basis, the deformation measurements define the tectonic framework within which all the Parkfield observations must be interpreted. The Parkfield section of the San Andreas fault is a relatively simple part of the North American-Pacific plate boundary, with no major active intersecting faults nearby. Below 10 to 20 km, the relative motion of the Pacific and North American plates apparently occurs as steady right-lateral slip at about 3.5 cm per year (43). Relative plate motion on the San Andreas fault at shallower depths is accommodated by infrequent great earthquakes southeast of Cholame and by aseismic slip or small

shocks (or both) northwest of the preparation zone; the transition occurs near Parkfield (44).

Within this context, the Parkfield rupture zone is an asperity, or "stuck patch," on the fault plane approximately 5 km wide; that is, it extends 3 to 8 km in depth and about 25 km in length. This patch is being loaded by slipping portions of the fault northwest of and beneath it, and is either completely "stuck" between earthquakes, or is slipping, but at a rate much slower than the loading rate of 3.5 cm per year. As such, it is an analog for large plate-boundary earthquakes on transform faults, which typically involve widths of 10 to 20 km and lengths of 100 km and greater. Thus, the Parkfield experiment is most significant in that earthquakes here are apparently large enough to embody the essential features of a great plate-boundary earthquake. There is a period of strain accumulation (in this case, about 20 years) when slip within the rupture zone is less than the rate of relative plate motion. This period is followed by the

sudden slip in the earthquake when the rupture zone "catches up." The details of the crustal deformation preceding the next Parkfield earthquake should lead to a clearer understanding of the strain accumulation and release process at a plate boundary and thus should guide our efforts to predict great plate-boundary earthquakes elsewhere.

Efforts to monitor deformation at Parkfield address two specific questions:

1) Will the strain release during the next earthquake be approximately the inverse, both in amount and distribution, of the strain accumulation since the 1966 shock? The answer is crucial to the basic assumptions underlying earthquake recurrence models, such as the time-predictable and Parkfield recurrence models, which are the foundation of long-term prediction efforts.

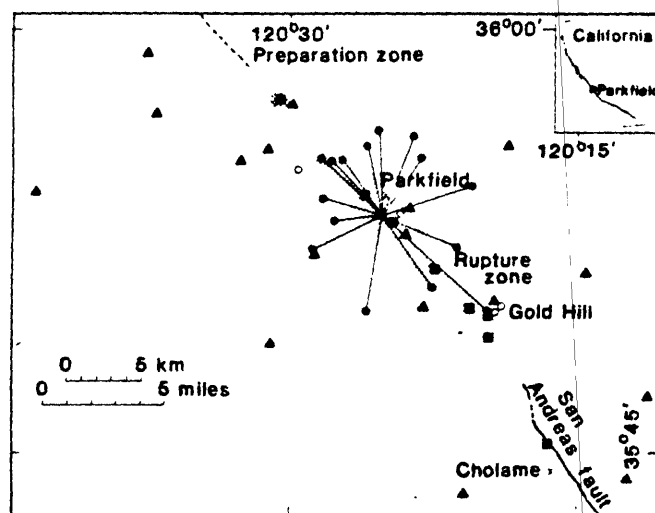
2) Are there changes in the details of the deformation field that might permit a refined estimate of the time of the next earthquake? The answer to this question will have a major impact on efforts toward medium- and short-term prediction.

Because of their importance, these questions are addressed by several projects to monitor deformation near Parkfield. A dense geodetic network with line lengths of 5 to 30 km spanning the fault has been measured every 1 to 2 years since 1969; the lengths are measured to a precision of 0.3 to 0.5 part per million, so that these data should establish the average slip during the next earthquake to an accuracy of better than 10 percent (45). Because of the inherent difficulties of resolving slip at depth and the uncertain time scale of the strain accumulation process, details of the deformation changes are perhaps better resolved by other techniques.

Lengths of lines spanning the rupture zone (Fig. 4) are measured several times each week with a two-color laser distance-measuring device that is capable of resolving length changes of about 1 mm over the 5- to 8-km-long lines (46). These observations should provide some additional resolution of the long-term deformation, but more important, they should resolve details of the deformation within the rupture zone during the days to months before the next earthquake.

While the geodetic observations are relatively insensitive to long-term systematic errors, they are difficult to measure frequently. In efforts to overcome this limitation and to improve the sensitivity to short-term changes, borehole volumetric strainmeters (47) are being installed in the Parkfield area (Fig. 4). These dilatometers provide continuous

Fig. 4. Seismometers (Δ), borehole dilatometers (\circ), creepmeters (\blacksquare), and lines of the geodetic figure monitored with two-color laser (\bullet) near the preparation and rupture zones of Parkfield characteristic earthquakes.



data with a sensitivity of about 1 part per billion over periods of a few hours. The resolution of these data overlaps the resolution of the two-color laser measurements for periods of a few weeks and is one to two orders of magnitude more sensitive at shorter periods.

In addition, a number of low-sensitivity 10- to 20-m-long wire strainmeters (creepmeters) span the surface trace of the San Andreas fault near Parkfield (Fig. 4). These creepmeters can detect a few millimeters of anomalous fault slip and are well suited to detect premonitory slip of the magnitude that may have occurred in 1966. However, interpretation of fault creep measurements along the San Andreas fault is complicated by the effects of the Coalinga earthquake (M_L 6.7) of 2 May 1983. Not only was the character of creepmeter recordings along a 40-km-long section of the San Andreas fault strongly affected by the Coalinga earthquake (48), but an unusual swarm of small shocks 18 km southeast of Cholame on the locked section of the San Andreas fault occurred a few days after the Coalinga main shock (49).

A Larger Shock

It is possible that the next characteristic Parkfield earthquake might break through the en echelon offset at the southeast end of the rupture zone and continue southeast along the San Andreas fault, growing into a major earthquake. Alternatively, the characteristic earthquake might stop at the en echelon offset and, by analogy to the triggering mechanism of the early foreshock of M_L 5.0 in 1934, increase the right-lateral shear stress on the fault southeast of the rupture zone. The latter case has been suggested (9) as the triggering mechanism for the great Fort Tejon earthquake of 1857.

Slip in 1857 along the 50-km-long section of the San Andreas fault southeast of Cholame was about 3.5 m, appreciably less than the 9-m offset farther southeast (50). Continuation of a Parkfield earthquake southeast might result in a rupture length of about 90 km, which is consistent with a magnitude 6.5 to 7 earthquake (2). Since the average Holocene offset rate across the San Andreas fault at Wallace Creek is 3.5 cm per year (51), it seems likely that the 3.5 m of slip in 1857 has largely been recovered, so that the possibility of an earthquake breaking this segment must be taken seriously. There are few data available to suggest what precursors there might be for this hypothetical larger shock. Minor

differences in the stress field near the offset, the strength of the offset, and the dynamic stress ahead of the rupture could all be important (52). Although foreshocks or deformation (or both) at the southeast end of the Parkfield rupture zone might portend a shock significantly larger than a characteristic Parkfield earthquake, there is certainly no evidence that such precursors need occur.

Discussion

Experiments in predicting the detailed characteristics of the source of a significant earthquake, such as the next Parkfield earthquake, provide opportunities for many kinds of investigations. In addition to the elements of the prediction experiment, geophysical instrumentation is being deployed near Parkfield that will take advantage of the predicted features of the coming earthquake to address specific outstanding issues of earthquake mechanics. For example, a network of nearly 50 strong-motion accelerographs operated by the California Division of Mines and Geology near the Parkfield rupture zone is designed to provide a direct measure of the velocity of rupture, estimates of the history and amplitude of the seismic slip along the rupture length, detailed information about high-frequency radiation and directivity effects, and a test of the idea that the low-rigidity fault zone might act as a wave guide that significantly distorts seismic radiation (53).

Two fundamentally different models of the earthquake generation process have been used in our description of the phenomena at Parkfield. The propagating crack models (type 1) derived from analyses of seismograms feature discontinuous slip beginning at a point (the hypocenter) and expanding over the rupture surface (54). For these type 1 models, precursory aseismic slip is generally not considered, precursors are expected near the epicenter (the preparation zone), and the preparation zone is viewed as a relatively strong point on the fault surface. The evidence for larger stress drops for earthquakes within the Parkfield preparation zone would support the type 1 models. However, laboratory experiments in rock mechanics (42) suggest that stick-slip events—the earthquake analog in rock mechanics—are always preceded by stable sliding—the fault creep analog in rock mechanics. These observations have been used in support of strain-softening models (type 2) of the earthquake generation process

(42). For these type 2 models, at least some precursory aseismic slip is required near the hypocenter; zones of precursory aseismic slip might have significant lateral extent, perhaps extending beyond the preparation zone. For the type 2 models, earthquake precursors should be concentrated near the relatively weak places on the fault surface where the aseismic slip occurs. The anecdotal reports of the broken irrigation pipeline and the en echelon cracks observed before the 1966 Parkfield earthquake are qualitative evidence supporting the type 2 strain-softening models of the earthquake generation process. The evaluation of these two different types of models, implicit in the design of the Parkfield prediction experiment, is essential before focused efforts to record short-term precursors can be undertaken in other earthquake-prone areas.

References and Notes

1. A. G. Lindh, *U.S. Geol. Surv. Open-File Rep.* 83-63 (1983).
2. L. R. Sykes and S. P. Nishenko, *J. Geophys. Res.* 89, 5905 (1984).
3. W. H. Bakun *et al.*, *Science* 225, 288 (1984).
4. P. Reasenber and W. L. Ellsworth, *J. Geophys. Res.* 87, 10637 (1982).
5. W. H. Bakun and T. V. McEvilly, *ibid.* 89, 3051 (1984).
6. The 1982 New Idria sequence (main shock M_L 5.4) and the 1983 Coalinga sequence (main shock M_L 6.7) shown in Fig. 1 are examples of the seismic activity associated with the development of the prominent fold structures between the San Andreas fault and the San Joaquin Valley [see J. Eaton, R. Cockerham, F. Lester, *Calif. Div. Mines Geol. Spec. Publ.* 66, 261 (1983)].
7. J. C. Savage and R. O. Burford, *J. Geophys. Res.* 76, 6469 (1971).
8. C. R. Allen, *Stanford Univ. Publ. Geol. Sci.* 11, 70 (1968).
9. K. E. Sieh, *Bull. Seismol. Soc. Am.* 68, 1731 (1978).
10. W. H. Bakun and T. V. McEvilly, *Science* 205, 1375 (1979).
11. Y. B. Tsai and K. Aki, *Bull. Seismol. Soc. Am.* 69, 275 (1969).
12. R. D. Brown, Jr., J. G. Vedder, R. E. Wallace, E. F. Roth, R. F. Yerkes, R. O. Castle, A. O. Waananen, R. W. Page, J. P. Eaton, *U.S. Geol. Surv. Prof. Pap.* 579 (1967).
13. C. A. von Hake and W. K. Cloud, *United States Earthquakes, 1966* (U.S. Coast and Geodetic Survey, Washington, D.C., 1968).
14. A. G. Lindh and D. M. Boore, *Bull. Seismol. Soc. Am.* 71, 95 (1981).
15. T. V. McEvilly, W. H. Bakun, K. B. Casaday, *ibid.* 57, 1221 (1967).
16. J. T. Wilson, *ibid.* 26, 189 (1936).
17. T. R. Toppozada, C. R. Real, D. L. Parke, *Calif. Div. Mines Geol. Open-File Rep.* 81-11 SAC (1981).
18. The data permit a common epicenter for the 1922, 1934, and 1966 main shocks near the southeast end of the preparation zone (5). There are no seismograms that might constrain the epicenter locations of the 1881 and 1901 shocks.
19. Although the features of the main shocks are similar, there are notable differences in the foreshock activity. The 1934 main shock was preceded by a nearly 3-day-long foreshock sequence, including a foreshock (M_L 5.0) 55 hours before the main shock (16). Although the immediate (17 minutes before) foreshocks of M_L 5.1 in 1934 and 1966 were identical (10), early foreshock activity comparable to that in 1934 did not occur in 1966. There are no reports of felt foreshocks preceding the main shocks in 1881, 1901, or 1922, so that foreshocks of M_L 5 probably did not precede these characteristic shocks. Furthermore, no foreshocks in 1922 are evident on the Bosch-Omori seismograms written at Berkeley; shocks of M_L 4.5 near Parkfield probably would be noticeable on these records.
20. K. Shimazaki and T. Nakata, *Geophys. Res.*

- Lett.* 7, 279 (1980); L. R. Sykes and R. C. Quittmeyer, *Am. Geophys. Union Monogr. Earthquake Prediction*, 217 (1981).
21. The fundamental principles of the time-predictable model are well established [H. F. Reid, *The California Earthquake of April 18, 1906* (Carnegie Institution of Washington, Washington, D.C., 1910), part 2]. That is, an earthquake occurs when the strain accumulated since the preceding earthquake results in sufficient stress to rupture the fault surface. Adding the concepts of a constant failure stress threshold, a constant rate of strain accumulation, and variable stress drop results in the time-predictable model.
 22. J. N. Brune, *J. Geophys. Res.* 84, 2195 (1979).
 23. G. S. Buhr and A. G. Lindh, *U.S. Geol. Surv. Open-File Rep.* 82-205 (1982); W. H. Bakun and A. G. Lindh, *Earthquake Pred. Res.*, in press.
 24. W. H. Bakun and T. V. McEvilly, *Bull. Seismol. Soc. Am.* 71, 423 (1981).
 25. While the foreshock cluster may have provided the immediate triggering mechanism, the conditions that permitted this to occur only in 1934 are not resolved. Accelerated loading rate associated with nonuniform regional strain accumulation [W. Thatcher, *Nature (London)* 299, 12 (1982)], accelerated fault creep near the preparation zone, temporal changes in the fault strength associated with fluctuations in pore pressure, and so forth could have contributed. Such "out of sequence" events may simply be statistical fluctuations resulting from the nonlinear interaction of a large number of factors, such as an ensemble of asperities in the preparation zone, each obeying a somewhat different strain-softening constitutive law.
 26. D. Tocher, *Calif. Div. Mines Geol. Spec. Rep.* 57, 39 (1959); S. A. Fedotov, in *Seismic Zoning of the U.S.S.R.*, S. Medvedev, Ed. (U.S.S.R. Academy of Science, Moscow, 1968).
 27. K. Mogi, *Am. Geophys. Union Monogr. Earthquake Prediction*, 43 (1981).
 28. The 1934 time, corresponding to σ_1 , rather than σ_2 , was not used in these calculations. Although the details of seismicity at Parkfield in 1857 are uncertain, the 1857 date is used since we presume that it represents failure at σ_1 (Fig. 2).
 29. The standard error in the estimated origin time (given the sequence counter) is 1.2 years [W. J. Dixon and F. J. Massey, Jr., *Introduction to Statistical Analysis* (McGraw-Hill, New York, 1957)]. The significance of the 95 percent confidence interval calculation is extremely limited given the small sample size (3 degrees of freedom) and the apparent inconsistency of the Gaussian assumption. An analysis of long-term probabilities (1) yields an estimate of 67 percent probability of a characteristic Parkfield earthquake by the spring of 1993 (1988.0 + 5.2 years). The corresponding Poisson expectation, $1 - \exp(-8.2/21.9)$, is 31 percent.
 30. W. H. Bakun, *Bull. Seismol. Soc. Am.* 70, 1181 (1980).
 31. The abrupt termination of this shallow seismicity, about 6 km northwest of the preparation zone, coincides with the southeast limit of the contact of Franciscan melange with the San Andreas fault trace. For 150 km northwest, the creeping section is associated with Franciscan melange east of the fault; no melange material outcrops farther southeast, and the surface creep decreases to zero near Cholame.
 32. J. P. Eaton, M. E. O'Neill, J. N. Murdock, *Bull. Seismol. Soc. Am.* 60, 1161 (1970).
 33. All shocks of M_L 4 or greater and most of M_L between 3 and 4 occur within the two distinct clusters at 8 to 10 km depth at the two ends of the 1966 aftershock zone, similar to the results obtained for late aftershocks in 1966 (32).
 34. W. H. Bakun et al., *Bull. Seismol. Soc. Am.* 70, 185 (1980).
 35. Although there is little basement outcrop adjoining the rupture zone northeast of the San Andreas fault, there are slivers of granite and crystalline metamorphic rocks on Middle Mountain and a large outcrop of gabbro near Gold Hill, suggesting that the basement adjacent to the rupture zone is of higher density, and possibly higher strength, than the Franciscan melange rocks that adjoin the creeping section to the northwest (31).
 36. The locations for the two 1966 shocks are relative to precise hypocentral locations for several of the largest shocks near the preparation zone since 1975: epicenter and focal depth precisions are 1 km and 2 km, respectively.
 37. M. E. O'Neill, *Bull. Seismol. Soc. Am.* 74, 27 (1984).
 38. Telemetered, high-gain, short-period seismic stations in the U.S. Geological Survey's central California seismic network have operated continuously in the Parkfield region since April 1969. The network has expanded from a small regional network of 4 single-component vertical stations to a comprehensive network of 14 high-gain, short-period vertical stations and 8 3-component stations with improved dynamic range. The 14 high-gain vertical stations are being upgraded with improved dynamic range instruments, and data transmission is being transferred from long-distance, dedicated phone lines to a microwave telemetry system.
 39. R. A. Allen, *Bull. Seismol. Soc. Am.* 68, 1521 (1978).
 40. The broken irrigation pipeline has been attributed to 1 to 2 feet of southeast movement of the northeast end relative to the southwest end (12), consistent with right-lateral strike-slip displacement across the fault. However, the history of the movement is unknown, so that perhaps only a small part occurred in the days and weeks just before the 1966 earthquake.
 41. The discovery of these cracks in June 1966 (12) led to a 24-hour microearthquake survey of the area on 18 and 19 June 1966, 8 days before the main shock; no identifiable shocks of M_L 1 or greater occurred within a distance of 24 km [C. R. Allen and S. W. Smith, *Bull. Seismol. Soc. Am.* 56, 966 (1966)]. Seismograms at Gold Hill showed that no shocks of M_L 1 or greater occurred within the rupture zone in the 6 days before the 1966 main shock and that only six occurred in the preceding 5.5 months [G. Buhr, G. Matooka, A. Lindh, M. Frosenbaugh, *Earthquake Notes* 49 (No. 4), 41 (1978)]. This level of seismicity is about 15 percent of the average seismicity level within the rupture zone; the significance of this relative quiescence is difficult to assess in light of the clustered nature of the recent seismicity.
 42. J. H. Dieterich, *J. Geophys. Res.* 83, 3940 (1978); J. R. Rice, *Gerlands Beitr. Geophys.* 88, 91 (1979); W. D. Stuart, R. J. Archuleta, A. G. Lindh, *J. Geophys. Res.* 90, 592 (1985); S. T. Tse, R. Dmowska, J. R. Rice, *Bull. Seismol. Soc. Am.* 75, 709 (1985).
 43. W. Thatcher, *J. Geophys. Res.* 84, 2283 (1979).
 44. Surface slip rates since 1966 are 3.0 to 3.5 cm per year to the northwest, 2 cm per year above the preparation zone, less than 1 cm per year near Gold Hill, and 0 southeast of Cholame [M. Lisowski and W. H. Prescott, *Bull. Seismol. Soc. Am.* 71, 1607 (1981)]. Whereas nearly continuous aseismic surface slip (fault creep) is common to the northwest, creep within the rupture zone tends to be episodic, with events of up to a few millimeters of slip occurring in a few hours [S. S. Schulz et al., *J. Geophys. Res.* 87, 6977 (1982)]. Creep events apparently extend down less than 1 km, propagating to the surface over a few days [N. R. Goult and R. Gilman, *J. Geophys. Res.* 83, 5415 (1978)].
 45. W. F. Slawson and J. C. Savage, *Bull. Seismol. Soc. Am.* 73, 1407 (1983).
 46. The two-color laser is a prototype instrument operated in cooperation with L. Slater of the University of Colorado. Noise levels on a similar array near Hollister, California, were 10^{-7} to 2×10^{-7} strain [J. O. Langbein et al., *Science* 218, 1217 (1982)].
 47. The Sacks-Everson volumetric strainmeter (or borehole dilatometer) measures changes in pressure within a fluid-filled cylinder cemented in place at depths of 100 to 500 m [I. S. Sacks, S. Suyehiro, D. W. Everson, *Proc. Jpn. Acad.* 47, 707 (1971)]. These instruments are an important component of earthquake prediction efforts in Japan [K. Mogi, *Am. Geophys. Union Monogr. Earthquake Prediction*, 635 (1981)].
 48. The maximum calculated stress change along the San Andreas fault was not more than about 1 bar [G. M. Mavko, S. Schulz, B. D. Brown, *Bull. Seismol. Soc. Am.* 75, 475 (1985)]. Nevertheless, the pattern of fault creep recorded by the Middle Mountain creepmeter located atop the Parkfield preparation zone was drastically altered. Left lateral slip occurred from 2 May 1983 to mid-August 1984, when the normal right-lateral movement resumed [S. S. Schulz, G. M. Mavko, B. D. Brown, *U.S. Geol. Surv. Prof. Pap.*, in press].
 49. W. L. Ellsworth et al., *Eos* 64, 749 (1983). Earlier moderate shocks east of the San Andreas fault were also followed by small shocks on the San Andreas fault north of Simmler: a magnitude 2.9 shock occurred 32 days after the Avenal earthquake (M_L 4.7) of 14 January 1976 and a magnitude 2.1 shock occurred 2 days after the New Idria earthquake (M_L 5.4) of 25 October 1982.
 50. K. E. Sieh, *Bull. Seismol. Soc. Am.* 68, 1421 (1978).
 51. K. E. Sieh and R. H. Jahns, *Geol. Soc. Am. Bull.* 95, 883 (1984).
 52. S. Das and K. Aki, *J. Geophys. Res.* 82, 5658 (1977).
 53. R. D. McJunkin and A. F. Shakal, *Calif. Geol.* 36, 27 (1983).
 54. See, for example, N. A. Haskell, *Bull. Seismol. Soc. Am.* 54, 1811 (1964); J. N. Brune, *J. Geophys. Res.* 75, 4997 (1970); R. Madariaga, *Bull. Seismol. Soc. Am.* 66, 639 (1976).
 55. R. Nowack, unpublished data. Epicenters not near Parkfield are less accurate.
 56. Right-lateral plate motion of 29 mm per year was obtained (43) in an inversion of geodetic measurements near the creeping section of the San Andreas fault northwest of Parkfield. For slip between 3 and 8 km depth and a rupture length of 25 km, coseismic slip in 1966 was 60 cm (14).
 57. We thank J. Dieterich, W. Ellsworth, A. McGarr, R. Page, and J. Savage for comments on the manuscript. K. Poley for her help with the data analysis and preparation of the figures, and the people of the Parkfield area for their generous cooperation, interest, and friendship. Without their help this experiment would not have been possible.

APPENDIX A. 3.

Foreshocks and Short-Term Earthquake Hazard Assessment at Parkfield

L. M. Jones

Foreshocks and Short-term Earthquake Hazard Assessment at Parkfield

Lucile M. Jones
U.S. Geological Survey
525 So. Wilson Avenue
Pasadena, CA 91106

Abstract

The probability that a $M > 5.0$ earthquake near Middle Mountain on the San Andreas fault will be followed within 5 days by a characteristic Parkfield earthquake is estimated to be $80\% \pm 40\%$. The probability that the Parkfield earthquake will occur within 1 hour of the possible foreshock is approximately 20% and decays as $\text{time}^{-0.9}$ with elapsed time after the possible foreshock. The probabilities that the Parkfield earthquake will occur within 5 days after a $M=2.0$, $M=3.0$, or $M=4.0$ earthquake at Middle Mountain are estimated to be 5%, 18%, and 40%, respectively. These numbers are based on a statistical study of the earthquakes recorded in the Parkfield area since 1932.

Introduction

The U.S. Geological Survey has issued an intermediate term earthquake prediction for the Parkfield section of the San Andreas fault. This prediction states that there is a 90% probability that the Parkfield section (between $35^{\circ} 42' \text{ N}$ and $35^{\circ} 56' \text{ N}$) will produce a $M \sim 6$ earthquake by 1993. Six similar earthquakes that have occurred in the same place over the last 130 years and thus an earthquake in this site has been called a characteristic Parkfield earthquake (Bakun and Lindh, 1985). Because of the high probability of a moderate earthquake within the next 8 years, Parkfield is the site of intensive monitoring effort. This work is aimed at documenting short term changes in the earth prior to a moderate earthquake as well as possibly issuing a short-term prediction to the Parkfield event.

One of the earthquake precursors likely to occur before a characteristic Parkfield earthquake is a foreshock sequence. Two of the three

previous earthquakes at Parkfield have been preceded within hours or days by foreshock sequences (Bakun and Lindh, 1985) and it is thus considered likely that foreshocks will precede the next Parkfield earthquake. If the occurrence of foreshocks is to be useful in preparing a short-term prediction of the Parkfield earthquake, however, the probability that an earthquake occurring near the initiation site of the Parkfield event will be a foreshock must be determined. The purpose of this paper is to determine this probability as well as its dependence on time and magnitude.

Previous work analyzed the average time-dependent probability that an earthquake will be a foreshock to a larger event as a function of magnitude of the first event in southern California (Jones, 1985). This paper will present an application of this method to the Parkfield section of the San Andreas fault. In addition, the seismicity catalog for the Parkfield region is analyzed to determine site-specific probabilities. These results are compared with the average southern California values. The goal is to make the best possible estimate of the probability that an earthquake on the San Andreas at Parkfield will be a foreshock to the characteristic Parkfield earthquake.

Previous Work

A study of the 50 year southern California earthquake catalog has shown that after the occurrence of a $M \geq 3.0$ earthquake, the probability of a larger event occurring within 5 days and within 10 km of the epicenter of the first event is 6%, independent of the magnitude of the first event (Jones, 1985) (Figure 1). This value was determined by

assuming that the two sets of mainshocks with foreshocks and mainshocks without foreshocks form a binomial distribution. In this case, the percentage of earthquakes that were foreshocks in the past is the probability that an event will be a foreshock in the future. In addition, the rate of mainshock occurrence after foreshocks was found to decay by approximately the inverse of elapsed time from the event (Figure 2). The number of foreshock-mainshock pairs with a difference in magnitude greater than or equal to ΔM plotted against ΔM formed a log-linear distribution with a coefficient (b-value) of 0.75, close to the average b-value for independent events (0.83) (Figure 3). These three factors have been combined to determine the probability that an mainshock of magnitude M_m will occur at time $t(\text{hr})$ after an earthquake of magnitude M_f of:

$$P(\text{hr}) = 0.016 * t^{-.9} * 10^{-0.75*(M_m-M_f)}. \quad (1)$$

Aki (1981) presented a method by which the probabilities, derived from independent precursors, of an earthquake occurring could be combined to determine the total earthquake hazard. In this formulation, the total probability that an earthquake will occur within a given time window, $P(t)$, is:

$$P(t) = P_0 * P_a/P_0 * P_b/P_0 * \dots \quad (2)$$

where P_0 is the background rate of occurrence, P_a is the probability from precursor a, P_b is the probability from precursor b, etc. The probability gain, P_a/P_0 from foreshocks may be quite high depending on

the size of the possible foreshock and the background rate. One precursor, independent of foreshocks, that can be used in many instances in California is the temporal position of a given fault segment within its earthquake cycle when the cycle is known.

Application to Parkfield

Parkfield is included in the southern California region used to determine the foreshock probabilities described above. Thus, the first approximation of the probability of the characteristic Parkfield earthquake occurring after the occurrence of a possible foreshock is the probability derived from Equation (1). To examine the question in more detail, the analysis conducted for all of southern California has been repeated using only data from Parkfield. This analysis tests whether the magnitude and time dependences found in general for southern California foreshock-mainshock sequences apply in the specific case of Parkfield. It also produces values of the probability more representative of the Parkfield region, but the small number of earthquakes available for study leads to larger error estimates. The probability of the Parkfield earthquake following a possible foreshock is calculated using both the average southern Californian probabilities as well as probabilities derived solely for the Parkfield region.

Parkfield Data. The catalog used for Parkfield is the data collected by CIT for 1932-1969 and that collected by USGS's CALNET for 1970-1984 within a box surrounding the Parkfield section of the San Andreas fault (Figure 4). This is the same box used by Lindh et al. (1985). Only $M \geq 3.0$ earthquakes were used for 1932-1969 and only $M \geq$

2.0 earthquakes were used for 1970-1984. These magnitude thresholds are approximately the estimated levels of completeness for these time periods. Aftershocks were removed using the same algorithm as was used for the southern California catalog (Jones, 1985). As was done for all of southern California, foreshocks were defined as events that were followed within 5 days and 10 km by another earthquake with a larger magnitude. There were 534 earthquakes in this data set with aftershocks removed of which 53 were foreshocks to larger events.

Temporal Dependence. The probability that an earthquake will be a foreshock decreases quickly with elapsed time after the possible foreshock. The average decay rate is $\text{time}^{-0.9}$ for all of southern California (Figure 2). Figure 5 shows the temporal distributions of mainshocks after foreshocks for Parkfield alone. The decay in the rate of occurrence of mainshocks after foreshocks is the same at Parkfield as for southern California but the fit to the data is not well constrained at Parkfield. Thus, the average southern Californian value is the best approximation for the Parkfield case.

Foreshock Percentages. The percentage of earthquakes that have been followed by larger events within 5 days and 10km at Parkfield is higher than the average for southern California. On the average, 6% of the earthquakes in southern California are followed by larger earthquakes, independent of the magnitude of the first event between $M=3.0$ and $M=5.0$. At Parkfield, however, the percentage of earthquakes to be followed by larger events is dependent on the magnitude of the first event (Figure 6). Only 9% of the $M \geq 3.0$ earthquakes have been followed by larger events but 33% of the $M \geq 5.0$ earthquakes have been foreshocks to larger earthquakes. The percentage of all $M \geq 3.0$ earthquakes that

have been foreshocks at Parkfield (9%) is also larger than for southern California in general. Because of the smaller data set available for analysis at Parkfield, the error bars for Parkfield alone are larger than for southern California. It should be noted that even considering these larger error bars, the probability that a $M \geq 5.0$ earthquake at Parkfield will be a foreshock ($33\% \pm 16\%$) is larger than elsewhere in southern California ($6\% \pm 4\%$).

Magnitude Dependence. The cumulative number of foreshock-mainshock pairs at Parkfield with a magnitude difference equal to or greater than ΔM are plotted against ΔM in Figure 7. The slope of this curve is 0.56 ± 0.15 which is lower than the slope found for all events in southern California (Figure 3). This dependence on magnitude is also seen in the percentage of earthquakes that were foreshocks. In Figure 6, the percentages of earthquakes that have been foreshocks to $M \geq 4.0$ mainshocks and foreshocks to $M \geq 5.0$ mainshocks are shown along with the percentage of events that were foreshocks to a mainshock of any size. All $M \geq 3.0$ earthquakes at Parkfield that have been foreshocks to anything have been foreshocks to a characteristic Parkfield earthquake ($M \geq 5.0$ - either the 1934 or the 1966 earthquake).

The percentage of earthquakes that have been foreshocks to $M \geq 5.0$ mainshocks at Parkfield (Figure 6) is the percentage of earthquakes that have been foreshocks to characteristic Parkfield earthquakes. The magnitude dependence plotted in Figure 7 is incorporated in the $M \geq 5.0$ mainshock curve in Figure 6. The reason that the magnitude dependence can be seen so clearly in the percentage versus magnitude curve at Parkfield (Figure 6) but not in the same curve for all of southern California (Figure 2) is that there is essentially only one possible

mainshock at Parkfield. The same difference in magnitude between foreshock and mainshock, M , at Parkfield can give only one possible magnitude of foreshock. In southern California, many possible mainshock magnitudes give many possible foreshock magnitudes for the same M .

Recurrence Intervals. To determine the total probability of the Parkfield earthquake using Equation (2), it is necessary to know both the background rate of occurrence (P_0) and the rate due to the present position in the seismic cycle (P_F). The Parkfield earthquakes have occurred on the average once every 22 years (Bakun and Lindh, 1985) so the background daily probability of the Parkfield earthquake is $1/22\text{yr} \times 365\text{day/yr} = 1.245 \times 10^{-4}/\text{day}$. Because the last Parkfield earthquake occurred in 1966, the present probability is 90% in 8 years (Bakun and Lindh, 1985) or $0.9/(8\text{yr} \times 365\text{day/yr}) = 3.1 \times 10^{-4}/\text{day}$. This gives a probability gain for being near the end of the seismic cycle of approximately 2.5.

Results

The preceding analysis has shown that the temporal distribution of foreshocks determined using southern California data are applicable to foreshocks occurring on the Parkfield section of the San Andreas fault. However, this analysis also suggests that the probability that an earthquake at Parkfield will be a foreshock to a larger event is larger than elsewhere in southern California. Moreover, the dependence on the magnitude of the possible foreshock of the probability of being a foreshock is incorporated in the probability of being a foreshock at Parkfield. The probabilities determined for Parkfield are less reliable

than those determined using data from all of southern California because of the smaller data set.

Immediate foreshocks (those occurring within hours or days of their mainshocks such as those used in this analysis) occur very close in space to the hypocenter of their mainshock (Jones, 1984, 1985; Utsu, 1970). The previous characteristic Parkfield earthquakes appear to have all originated in the same area of the San Andreas fault near Middle Mountain and their foreshocks have also been located very nearby (Bakun and Lindh, 1985). Thus for a possible foreshock to be a foreshock to the Parkfield earthquake it must occur near Middle Mountain and it is only in this case that the probability gain resulting from the position in the seismic cycle can be incorporated into the probability analysis using Equation (2). The percentages of earthquakes that are followed by larger events as shown in Figure 6 are determined using a larger area than just the Middle Mountain area. It is thus possible that even the probabilities determined using the Parkfield data may be too low for the earthquakes occurring actually at Middle Mountain.

Because of all of these uncertainties, it is not possible to state unequivocally the probability of the Parkfield earthquake occurring after an earthquake of magnitude M at Middle Mountain. It is possible to give bounds to the possible values. The values determined using the average southern California data (Equation 1) is probably the lower bound of the possible probabilities. An upper bound could be determined using a deterministic approach to the earthquakes actually within the proposed hypocentral area as is done by (Lindh et al., 1985). The probabilities determined in this study using the Parkfield data are intermediate values.

The lower bound of the Parkfield probabilities are given in Table I. This table shows the probability of the Parkfield earthquake occurring within 1 hour, 6 hours, 12 hours, 1 day or 5 days after an earthquake of magnitude M_f ($M_f=2.0$ to $M_f=5.0$). The numbers were calculated using equation 2 with a foreshock probability from equation 1 and a probability gain for the position in the earthquake cycle of 2.5. The values are shown graphically in Figure 8 where the probability per hour of the characteristic Parkfield earthquake occurring is plotted as a function of time after an earthquake of magnitude M at Middle Mountain.

The intermediate values for the Parkfield probabilities are shown in Table II. The numbers were also calculated using Equation 2 and a probability gain for the seismic cycle of 2.5. The foreshock probabilities were calculated by:

$$P_f(t) = P' * t^{-0.9} \quad (3)$$

where t is in hours. A graphical representation of these values are shown in Figure 9. The probability P' is taken from the Parkfield results shown in Figure 6.

The probabilities calculated using Parkfield data suggest that there would be a high probability of the Parkfield earthquake occurring if an earthquake were to occur at Middle Mountain. If a $M \geq 5.0$ earthquake were to occur, the probability that the Parkfield earthquake would occur in the next 5 days is $80\% \pm 40\%$. The probability that it would occur within the first hour after a $M \geq 5.0$ event is $20\% \pm 10\%$ (Table II). This is 15,000 times more likely than the background rate

of occurrence. Even a $M=2.0$ event would increase the probability of the Parkfield earthquake occurring by a factor of 1,000. There would be a 1.2% chance of the Parkfield earthquake occurring in one hour after a $M = 2.0$ event.

The values given in Table II give a first order approximation of the probability of the Parkfield earthquake occurring within a short period of time after a smaller event at Middle Mountain. However, it must be noted that the number of earthquakes in the data set used to compute these values is small and the uncertainties are large.

Conclusions

The probability that a $M \geq 5.0$ earthquake near Middle Mountain on the San Andreas fault will be followed within 5 days by a characteristic Parkfield earthquake is estimated to be $80\% \pm 40\%$. The probability that the Parkfield earthquake will occur within 1 hour of the possible foreshock is approximately 20% and decays as $\text{time}^{-0.9}$ with elapsed time after the possible foreshock. The probabilities that the Parkfield earthquake will occur within 5 days after a $M=2.0$, $M=3.0$, or $M=4.0$ earthquake at Middle Mountain are estimated to be 5%, 18%, and 40%, respectively.

REFERENCES

- Aki, K., 1981. A probabilistic synthesis of precursory phenomena, in Earthquake Prediction: An International Review, Maurice Ewing Volume 4, Simpson, D.W., and P.G. Richards (eds), Amer. Geophys. Union, Washington, DC., 566-574.
- Bakun, W. H., and A. G. Lindh, 1985. The Parkfield, California, prediction experiment, in press, Earthquake Prediction Research.
- Jones, L. M., 1984. Foreshocks (1966-1980) in the San Andreas System, California, Bulletin Seismological Society America, 74, 1361-1380.
- Jones, L. M., 1985. Foreshocks and time-dependent earthquake hazard assessment in southern California, in press, Bulletin Seismological Society America.
- Lindh, A. G., W. K. Bakun, and K. Poley, 1985. Report on possible seismic precursors to the Parkfield earthquake, Report to NEPEC, 1985.
- Utsu, T., 1970. Aftershocks and earthquake statistics (II) - Further investigation of aftershocks and other earthquake sequences based on a new classification of earthquake sequences, J. of Faculty of Science, Hokkaido Univ., Series VII (Geophysics), 3(4), 197-266.

Table I
The Probability of the Parkfield Earthquake Occurring
within Time T after an Earthquake of Magnitude M_f
at Middle Mountain
(Determined from southern California data, Minimum Estimate)

Event	Time Interval				
	1 hr	6 hrs	12 hrs	1 day	5 days
Background Rate	0.000014	0.00009	0.00017	0.00034	0.0017
$M_f = 2$	0.0001	0.0002	0.00024	0.00028	0.0004
$M_f = 3$	0.0005	0.001	0.0012	0.0014	0.002
$M_f = 4$	0.003	0.0059	0.007	0.008	0.012
$M_f = 5$	0.017	0.033	0.04	0.048	0.07

Table II
The Probability of the Parkfield Earthquake Occurring
within Time T after an Earthquake of Magnitude M_f
at Middle Mountain
(Determined from Parkfield data, Intermediate Estimate)

Event	Time Interval				
	1 hr	6 hrs	12 hrs	1 day	5 days
Background Rate	0.000014	0.00009	0.00017	0.00034	0.0017
$M_f = 2$	0.012	0.024	0.029	0.034	0.048
$M_f = 3$	0.044	0.086	0.12	0.12	0.18
$M_f = 4$	0.10	0.20	0.24	0.28	0.40
$M_f = 5$	0.20	0.39	0.48	0.57	0.80

FIGURES

Figure 1. The probability that an earthquake in southern California will be followed by a larger earthquake within 5 days and 10 km as a function of the magnitude of that earthquake (solid line). The vertical bars show the standard deviation in the estimates of probability for each magnitude level. The dashed line shows the probability of being followed by a $M \geq 4.0$ mainshock and the dotted line shows the probability that an earthquake will be followed by a $M \geq 5.0$ mainshock.

Figure 2. The number of mainshocks still to occur as a function of elapsed time for the foreshock for the 287 foreshock-mainshock pairs in the southern California data set.

Figure 3. The cumulative number of foreshock-mainshock pairs in southern California with a difference in magnitude at or above each level of magnitude difference as a function of difference in magnitude. Only pairs recorded after 1943 (when magnitudes were first given to the nearest .1 unit instead of .5 unit) are used.

Figure 4. A map showing the Parkfield area used to determine the probabilities of the Parkfield earthquake.

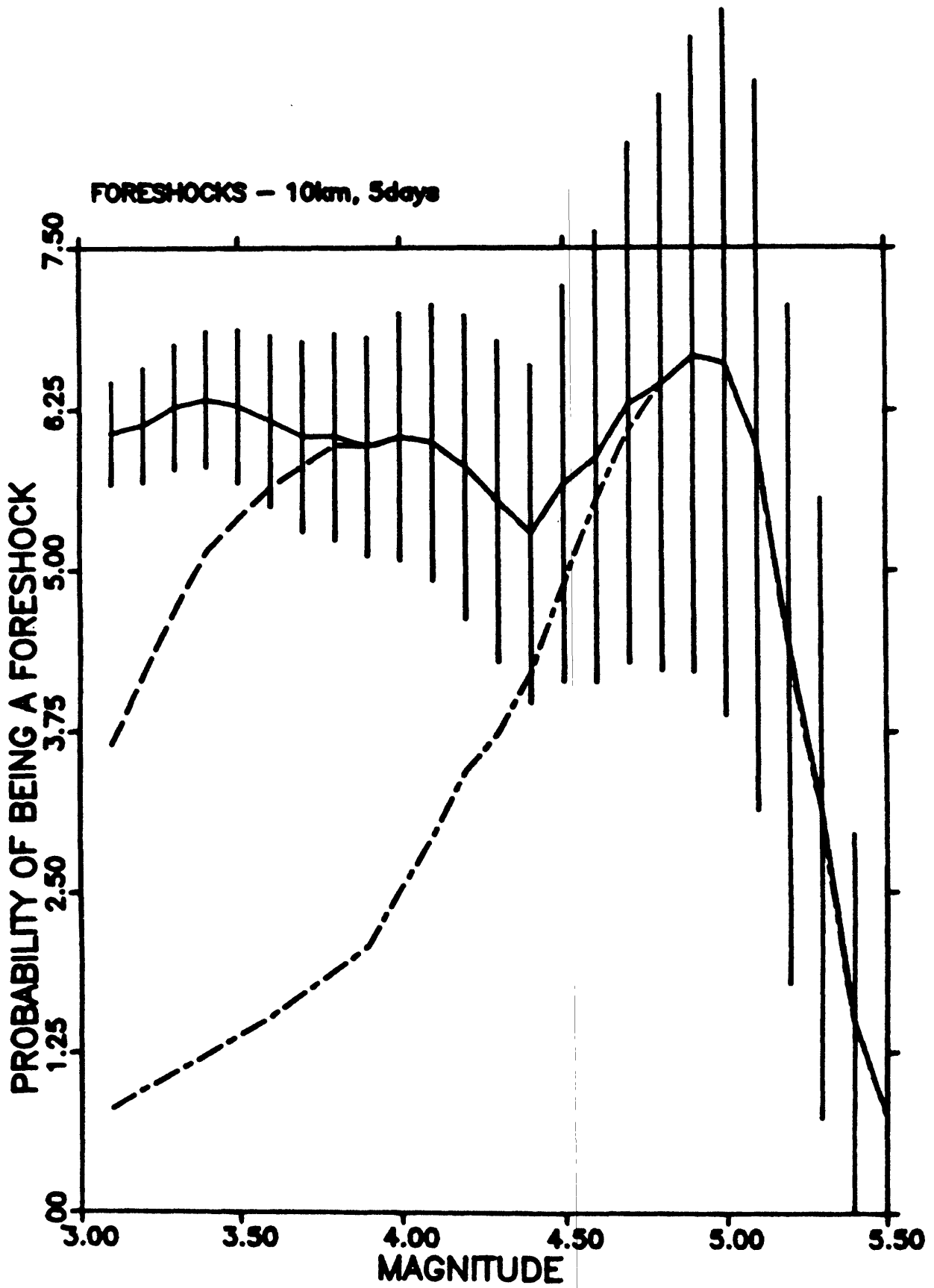
Figure 5. The number of mainshocks still to occur as a function of elapsed time from the foreshocks in Parkfield.

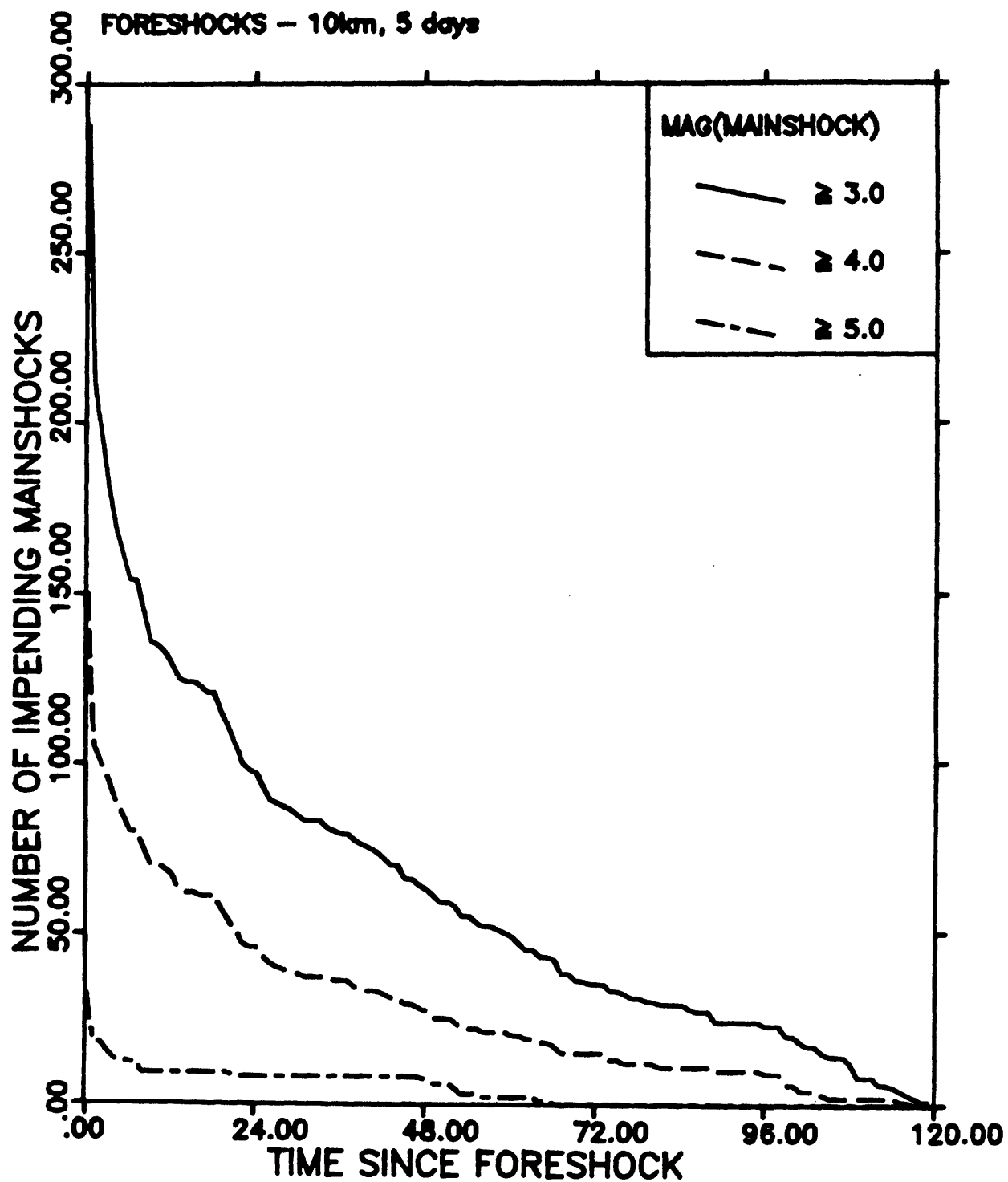
Figure 6. The probability that an earthquake at Parkfield will be followed by a larger earthquake within 5 days and 10 km as a function of the magnitude of that earthquake (solid line). The vertical bars show the standard deviation in the estimates of probability for each magnitude level. The dashed line shows the probability of being followed by a $M \geq 4.0$ mainshock and the dotted line shows the probability that an earthquake will be followed by a $M \geq 5.0$ mainshock.

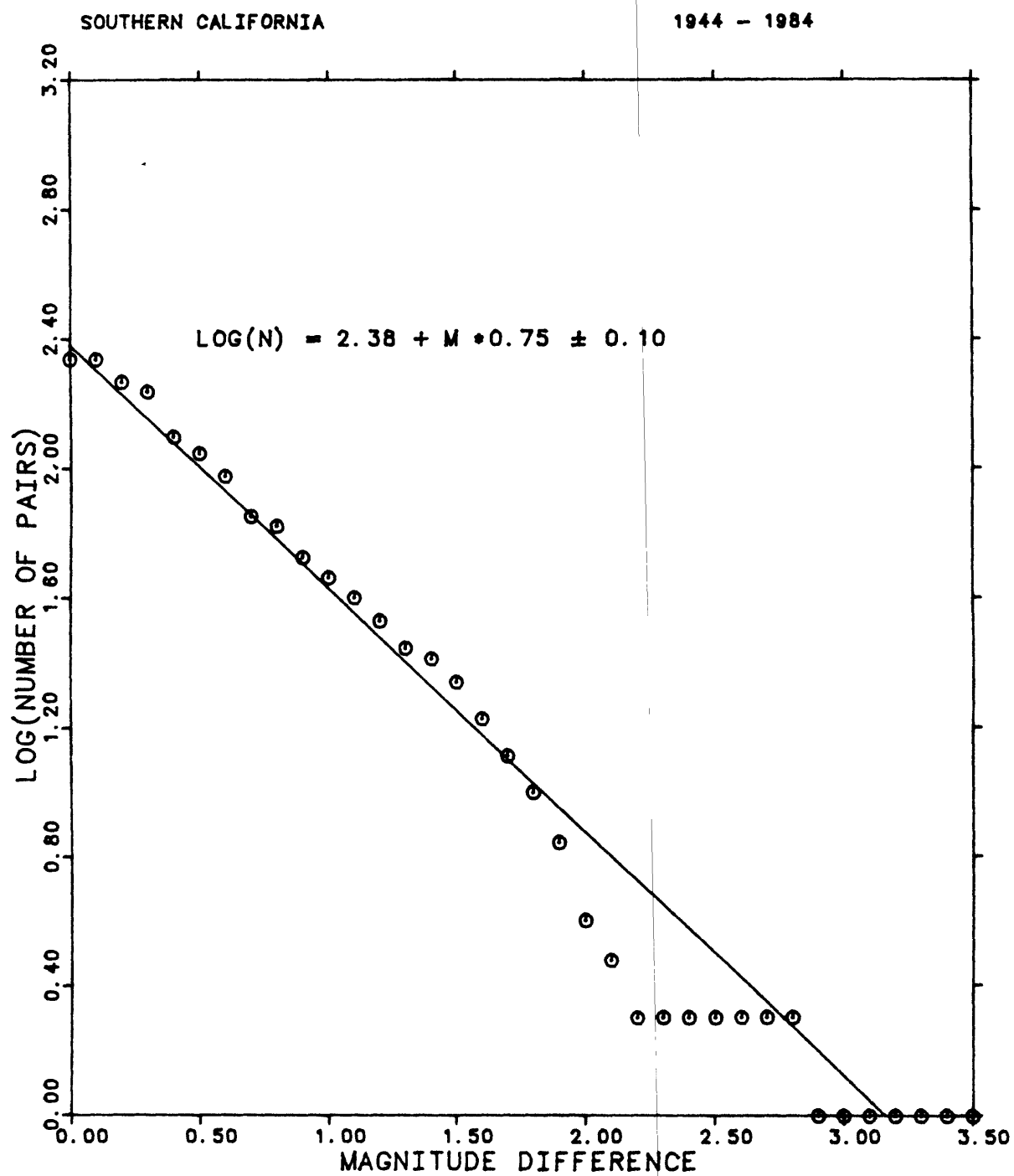
Figure 7. The cumulative number of foreshock-mainshock pairs with a difference in magnitude greater than or equal to ΔM as a function of ΔM for Parkfield.

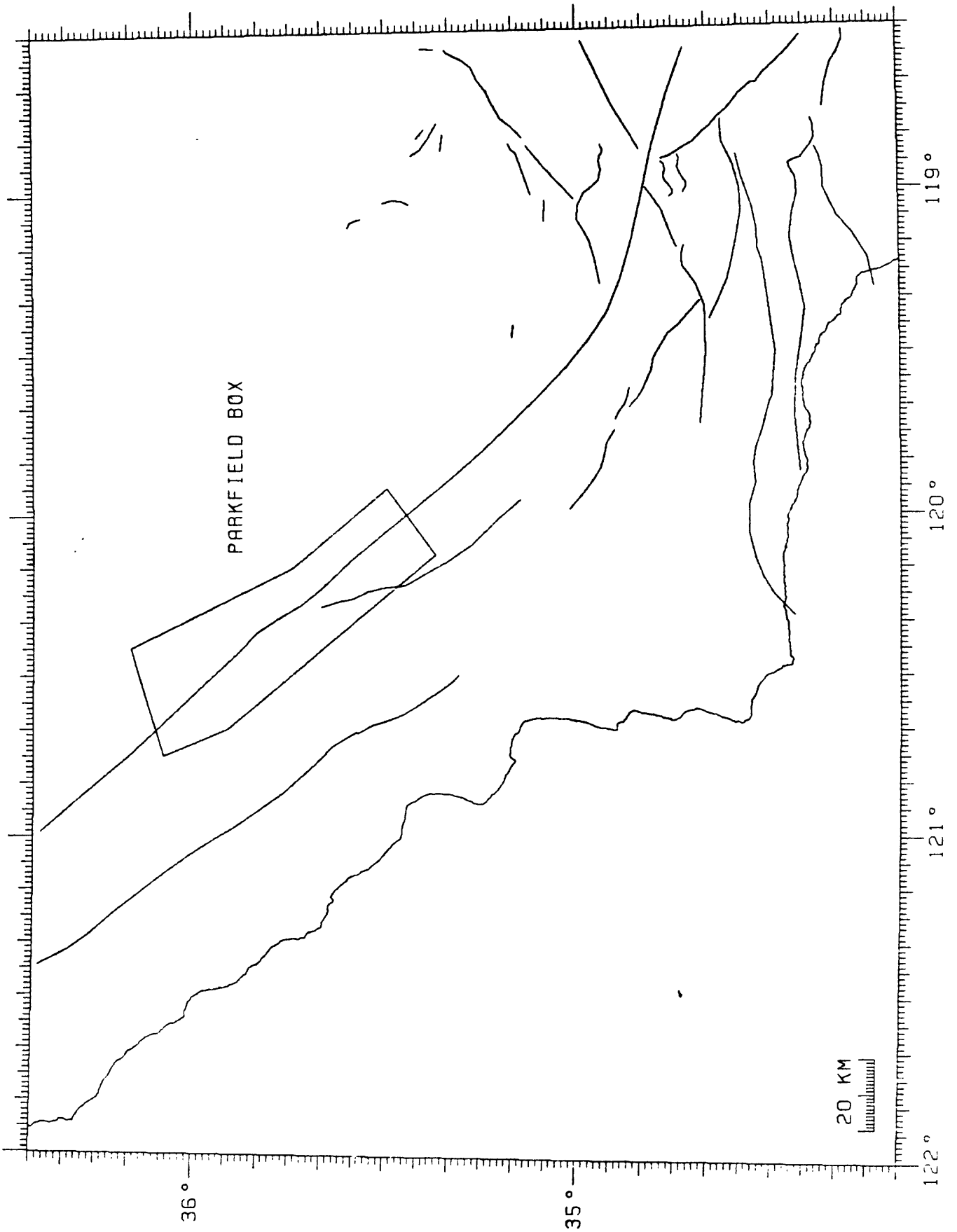
Figure 8. The minimum value for the probability per hour of the Parkfield earthquake occurring as a function of time after a possible foreshock at Middle Mountain determined using southern California data. The minimum values of the probability are shown for possible foreshocks of $M = 2.0, 3.0, 4.0$, and 5.0 .

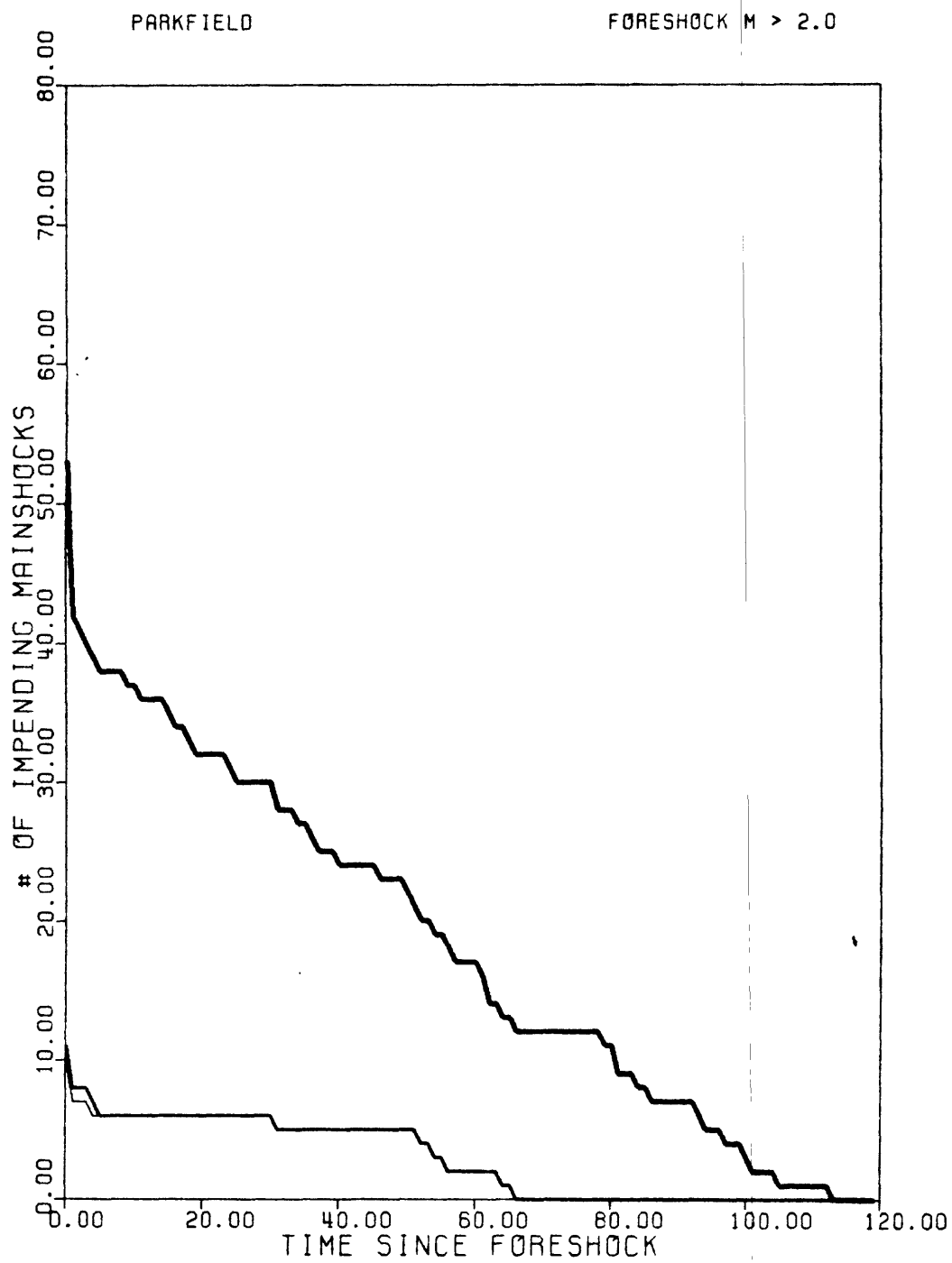
Figure 9. The intermediate value of the probability per hour of the Parkfield earthquake occurring as a function of time after the possible foreshock at Middle Mountain determined using Parkfield data. The intermediate value of the probabilities are shown for possible foreshocks of $M = 2.0, 3.0, 4.0$ and 5.0 .

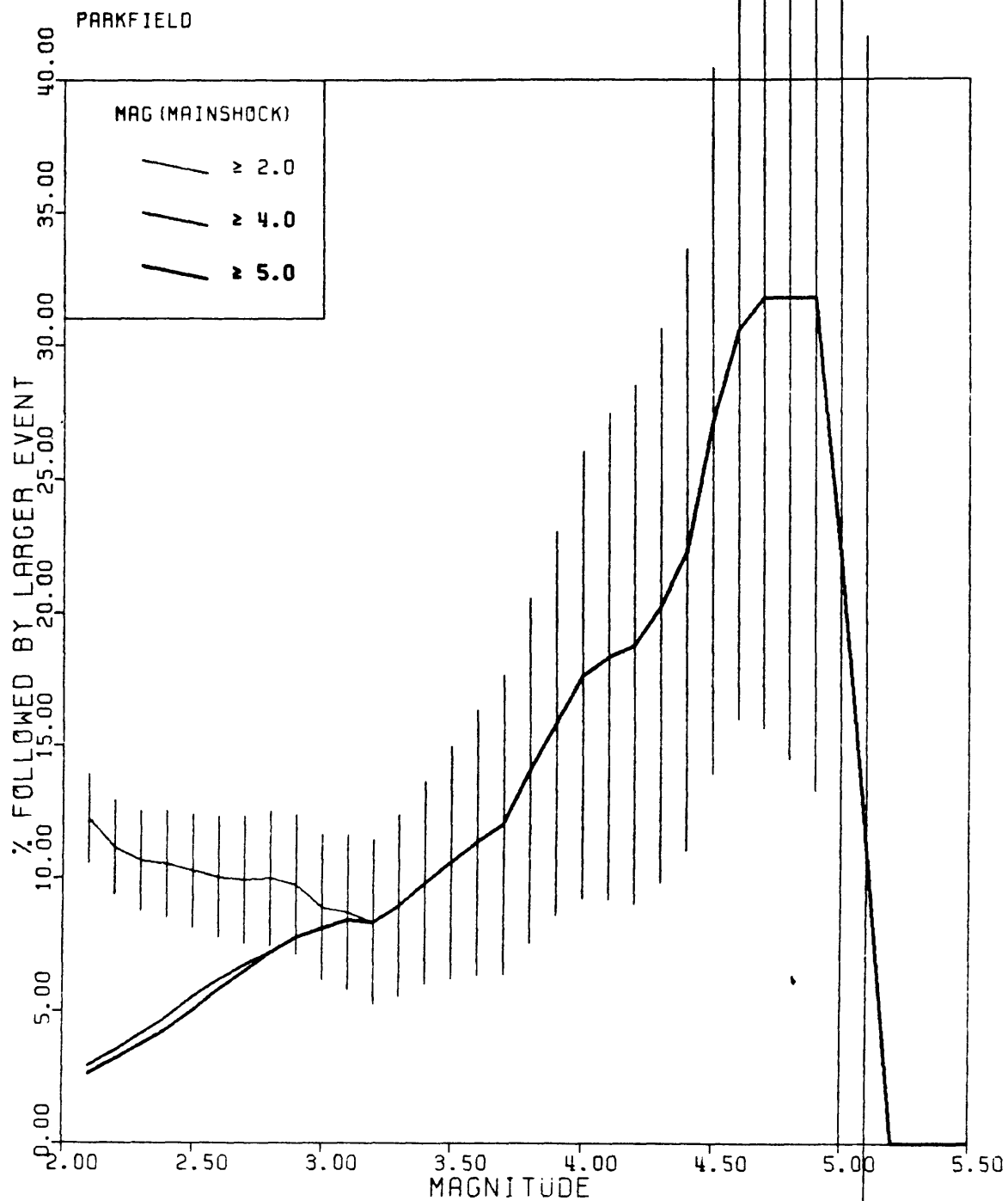


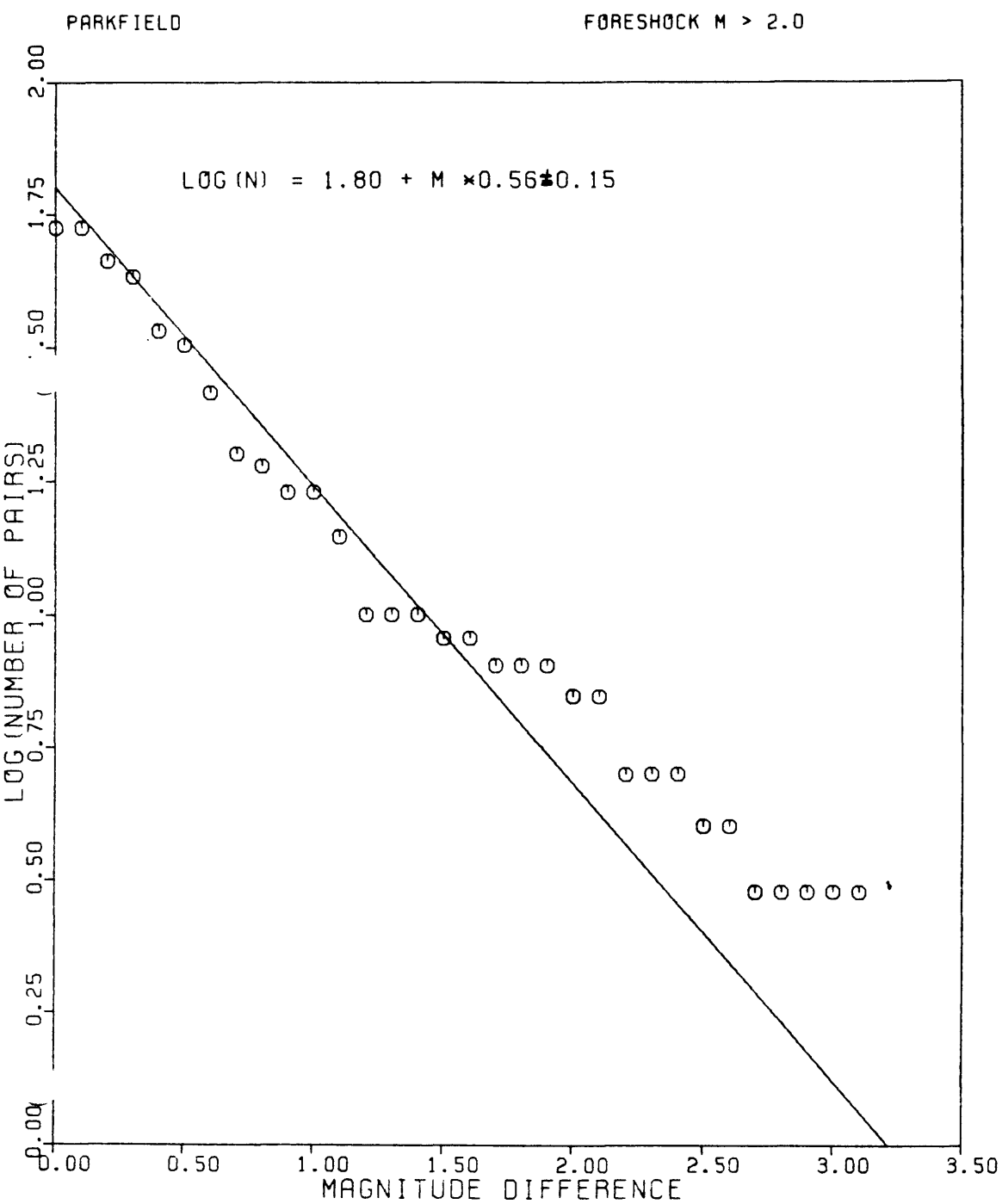


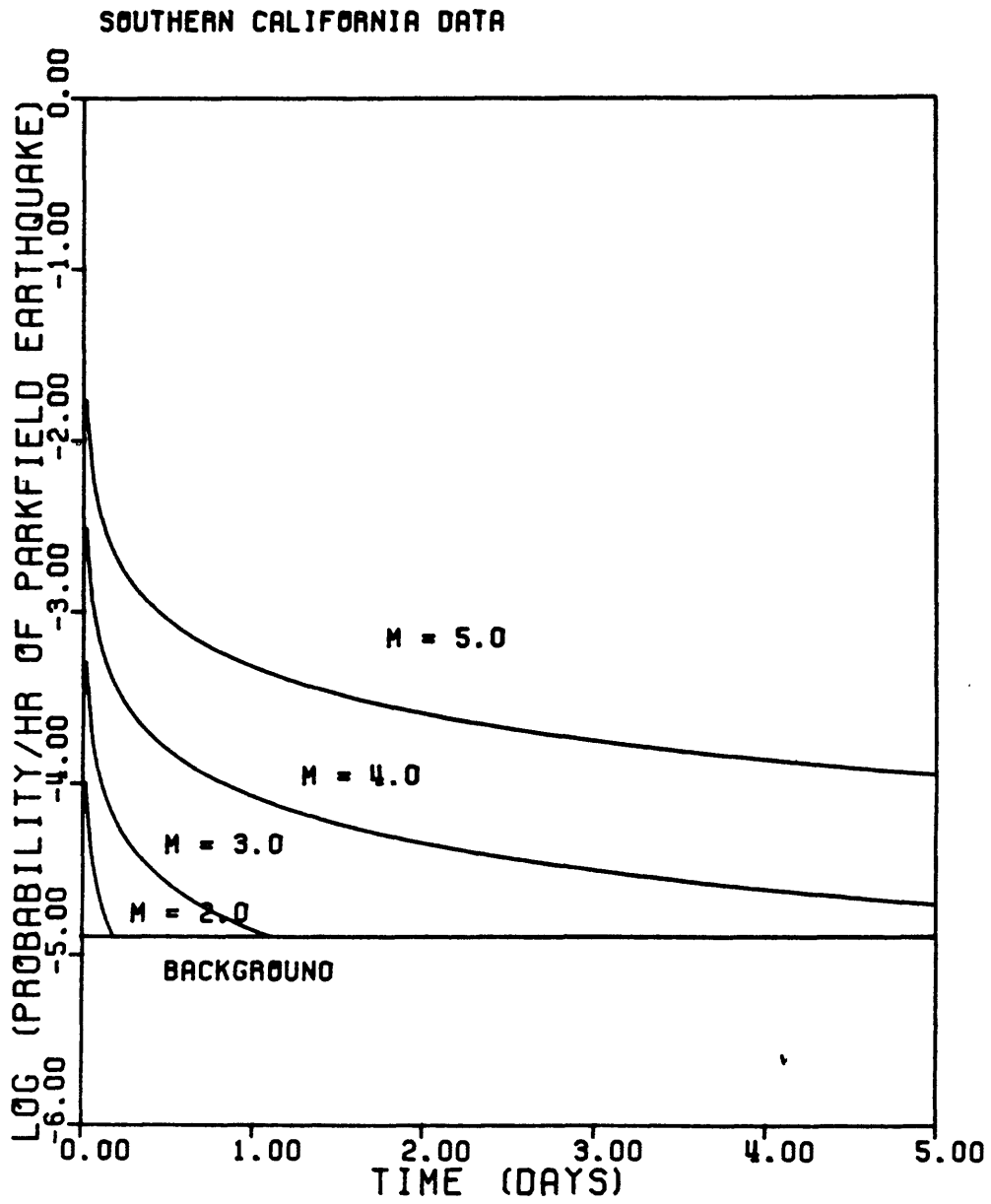


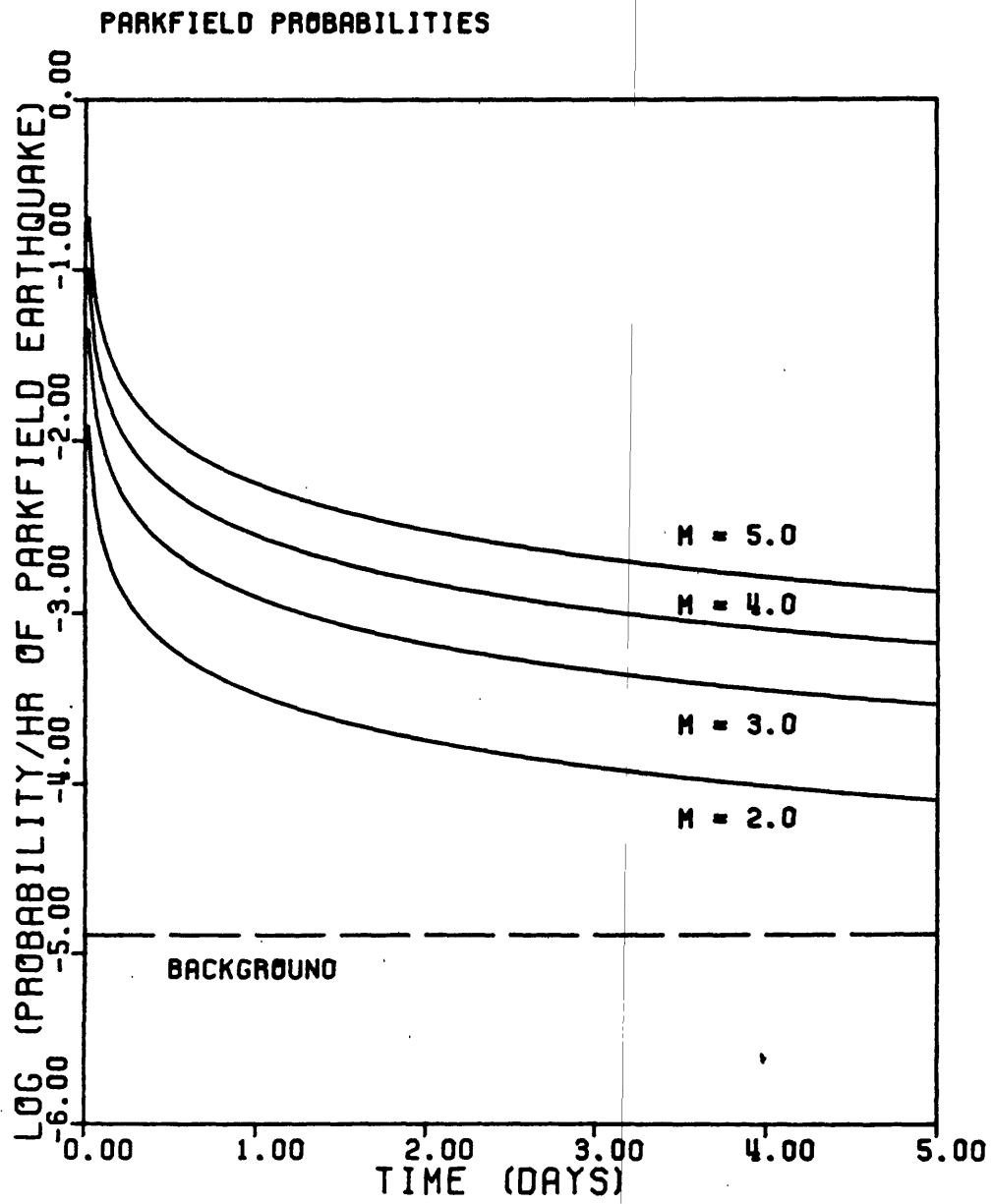












APPENDIX A. 4.

The Detection History of the Parkfield Segment of
the San Andreas Fault: A Preliminary Assessment

R. E. Habermann

The Detection History of the Parkfield Segment
of the San Andreas Fault: A Preliminary Assessment

R.E. Habermann
School of Geophysical Sciences
Georgia Institute of Technology
Atlanta, Georgia 30332

Many people have proposed that changes in seismicity rates can occur as part of the process of preparation for large earthquakes. Numerous rate changes can be observed in any seismicity data set. Most of these changes are not followed by large earthquakes and, therefore, are not precursors. If these changes are to be used as part of an earthquake prediction program, one must be able to distinguish between those that are possible precursors and those that are not. We have found that a great deal of information about seismicity changes can be obtained by examining the distribution of such changes in the magnitude domain. This technique is particularly useful for recognizing man-made changes in seismicity data.

Quantitative techniques for making comparisons of seismicity rates are essential for insuring objectivity and balance in any study of changes in these rates. We use the z-test for a difference between two means for our comparisons. This test is the most general of the statistical tests for evaluating the difference between two means.

In order to examine the distribution of an observed seismicity change in the magnitude domain we display the z-values which result from comparisons of rates during two time periods in a number of magnitude bands. These plots are described in Figure 1. In our work on the California catalog we examine cutoffs between $M_d = 0.5$ and $M_d = 3.0$.

MAN-MADE SEISMICITY CHANGES

Two types of man-made changes are observed in the seismicity data from the Parkfield region, detection increases and magnitude decreases. These types of changes have different characteristics which affect the appearance of magnitude signatures. These characteristics are summarized graphically in Figure 2 and described here.

Detection Increase.

A schematic magnitude signature for this type of change is shown in Figure 2A. Detection increases are characterized by the following features:

- * Strong increases (negative z-values) in the data sets which contain smaller events (trough on the left side of the plots).
- * Lack of change (z-values near 0) in the data sets which contain larger events (on the right side of the plot).
- * Negative z-values throughout the magnitude signature.
- * A plateau of negative z-values in the data sets which contain the larger small events (as you approach the center of the plot from

the left).

Magnitude Decrease.

A schematic magnitude signature for this type of change is shown in Figure 2B. A magnitude increase has the same characteristic appearance, but the signs of all the z-values are the opposite. The principal characteristics which identify magnitude shifts are:

- * The occurrence of z-values of different signs in the magnitude signature.
- * The occurrence of waves or other aberrations of the shape of normal detection related magnitude signatures.

The effects of detection changes can be taken care of by using a magnitude cutoff which eliminates the smaller events affected by the change. The magnitude cutoffs which would be appropriate are illustrated in Figure 2A. Magnitude shifts can be corrected for by using magnitude corrections, simply reversing the magnitude change.

EXAMPLES FROM THE PARKFIELD REGION

Detection Increase.

The magnitude signature which compares the rates between January 4, 1978 and December 18, 1979 to those between December 19, 1979 and September 2, 1980 shows all of the expected characteristics of a detection increase (Figure 3). The trough and platform on the left side of the plot indicates strong increases in the smaller events. These increase drop off as one considers larger events (on the right side of the plot). The magnitude cutoff in this case is $m_d \geq 1.3$.

Magnitude Decrease.

The magnitude signature which compares the rates between December 19, 1979 and September 2, 1980 to those between September 3, 1980 and March 23, 1982 shows all of the expected characteristics of a magnitude decrease (Figure 4). The magnitude bands which include larger events show decreases (on the right side of the plot). Those that include smaller events show rate increases.

We use synthetic magnitude signatures as an aid in interpreting magnitude signatures which indicate magnitude shifts. The process of constructing the synthetics is described in Figure 5. The best fit to the magnitude signature in Figure 4 resulted from decreasing the magnitudes of the events with $0.8 \leq m_d \leq 3.0$ by 0.15 units. This synthetic is shown in Figure 6.

Real Changes.

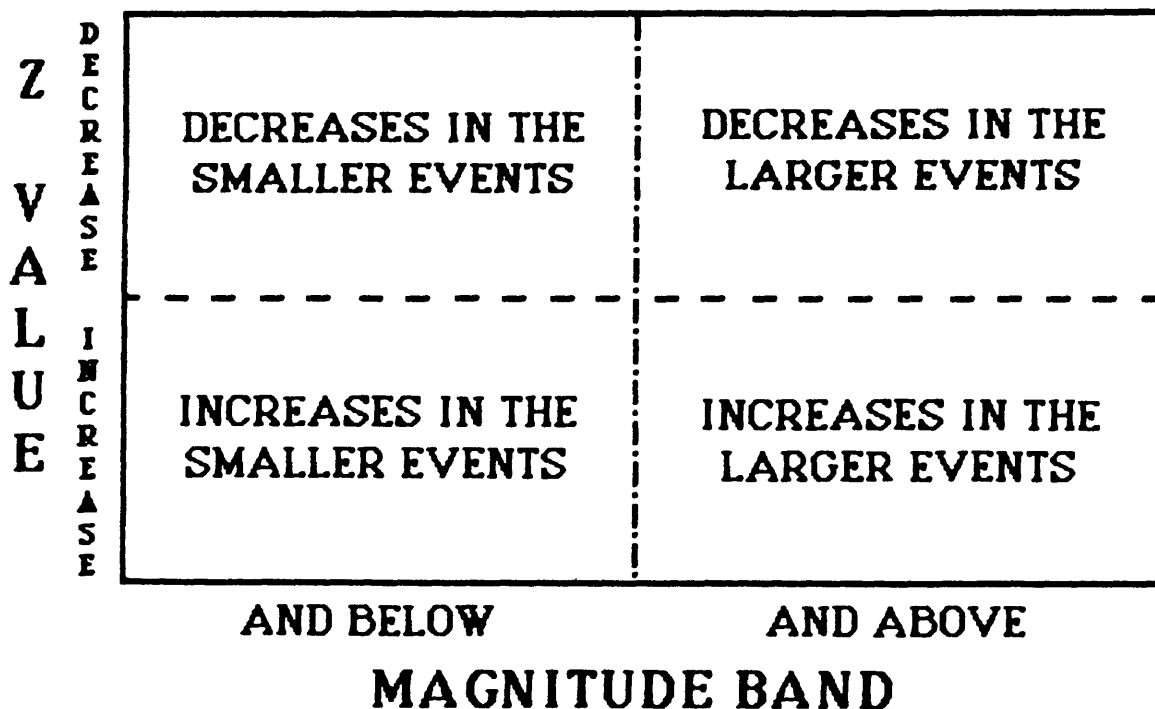
We found that the number of aftershocks in the Parkfield seismicity data was small enough so that these events could be retained without seriously affecting the results. This provided an opportunity to examine the magnitude signature generated by a real seismicity rate change. The period between April 23 and December 30, 1975 was a period

of increased activity in the Parkfield area. This activity included a swarm during April and May and aftershocks of a large event ($m_d = 4.9$) on September 13, 1975.

The magnitude signature comparing the rates between June 5, 1974 and April 22, 1975 to those between April 23 to September 15, 1975 is shown in Figure 7. Note that this magnitude signature shows strong increases in the data sets which include the larger events. This is the characteristic expected for real seismicity changes. The significance of the increase falls off for the smaller events because these events were not well detected in this region during this time.

A second change in the Parkfield region which appears to be real occurred during January, 1978. The magnitude signature for this change is shown in Figure 8. Note that it includes strong decreases in the larger events. The period of low numbers of larger events lasts until December 1979, the time of the detection increase shown in Figure 3. This period of low activity is suspect for several reasons. First, the beginning and end of the period correspond to beginnings of years. Second, the period of low numbers of large events (January 1978) marks the beginning of the preliminary catalog for this region. We have examined the final catalog for the first six months of 1978 which suggests that this change is real, but the length of time is too short to make unambiguous decisions for the larger magnitudes. We are presently trying to determine the spatial extent of this quiet period which should shed light on its origin. In any event, completion of the of the seismicity catalog for Parkfield for the last seven years should have high priority.

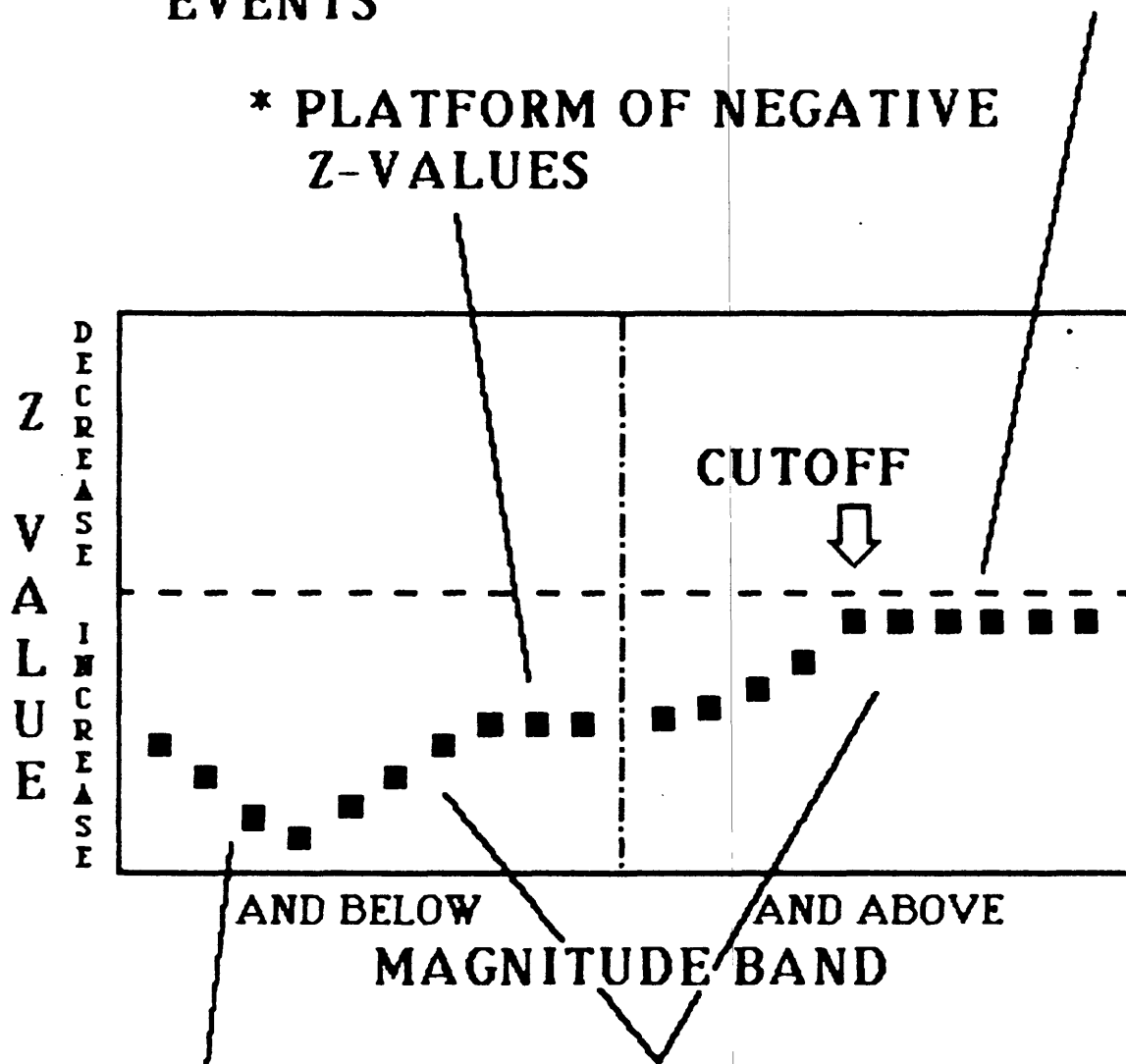
Detection and reporting changes naturally divide seismicity data into a subset of smaller events which are affected by the change and a subset of larger events which are unaffected. **The goal of our work is to find the boundary between these sets, a magnitude cutoff which eliminates the affected events from consideration.** Each cutoff divides the data set into two subsets, those above the cutoff, and those below. In order to find the correct cutoff, we examine a wide range of possible cutoffs using a plot called a **magnitude signature**. These plots show the significance of an observed seismicity change as a function of magnitude cutoff. The vertical axis of a magnitude signature shows the z-value which results from comparing the rates during two time periods. The **upper half** of the plot has positive z-values which indicate **rate decreases**, the **lower half** of the plot has negative z-values which indicate **rate increases**. The horizontal axis of the magnitude signature shows the magnitude bands which are being examined. The subsets which are **below the cutoffs** are on the **left** side of the plot and those **above the cutoffs** are on the **right**. When these two divisions are combined, four quadrants are generated. The Figure below shows what the occurrence of points in each of the four quadrants indicates about the change which is being examined.



DETECTION INCREASE

* LACK OF CHANGE IN THE LARGER EVENTS

* PLATFORM OF NEGATIVE Z-VALUES

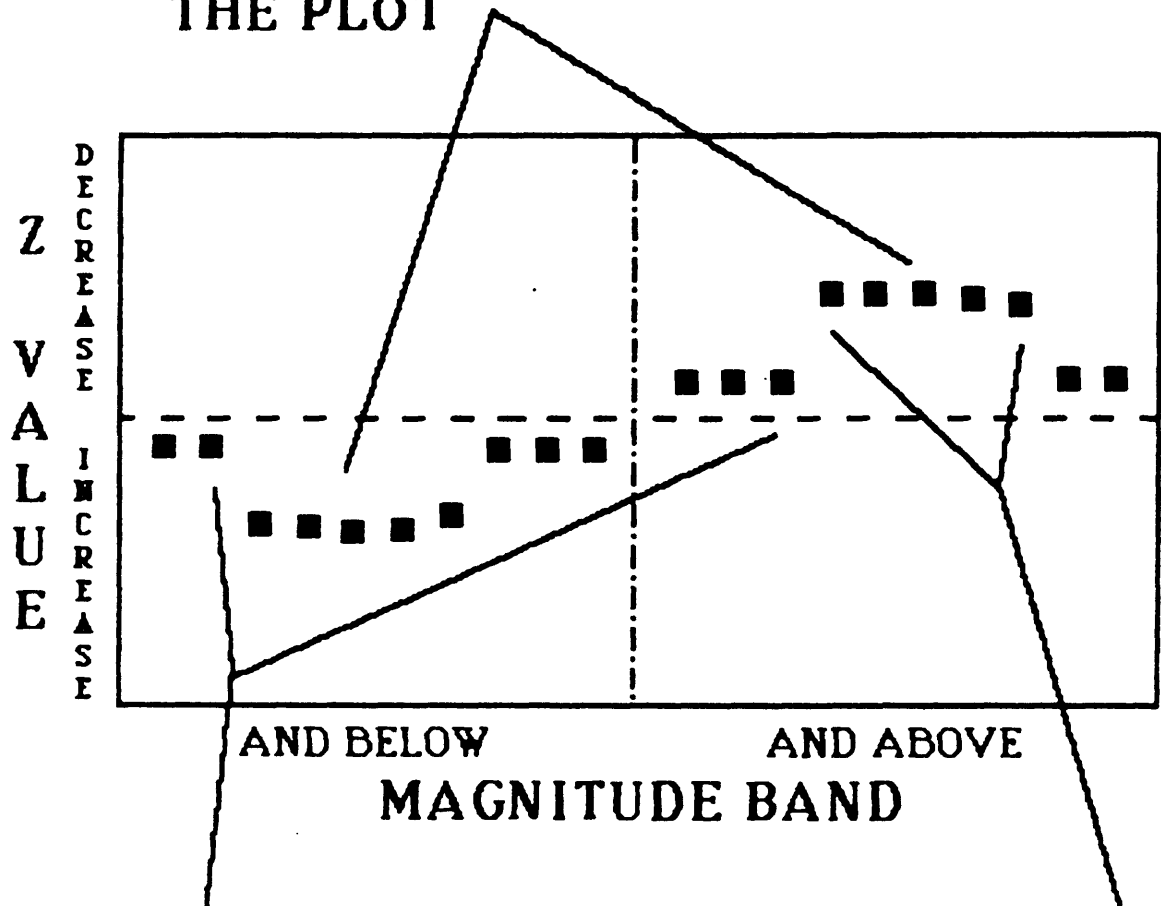


* NEGATIVE Z-VALUES
IN ALL MAGNITUDE BANDS

* STRONG INCREASES IN THE SMALL EVENTS

MAGNITUDE DECREASE

* Z-VALUE SIGN CHANGE ACROSS THE PLOT

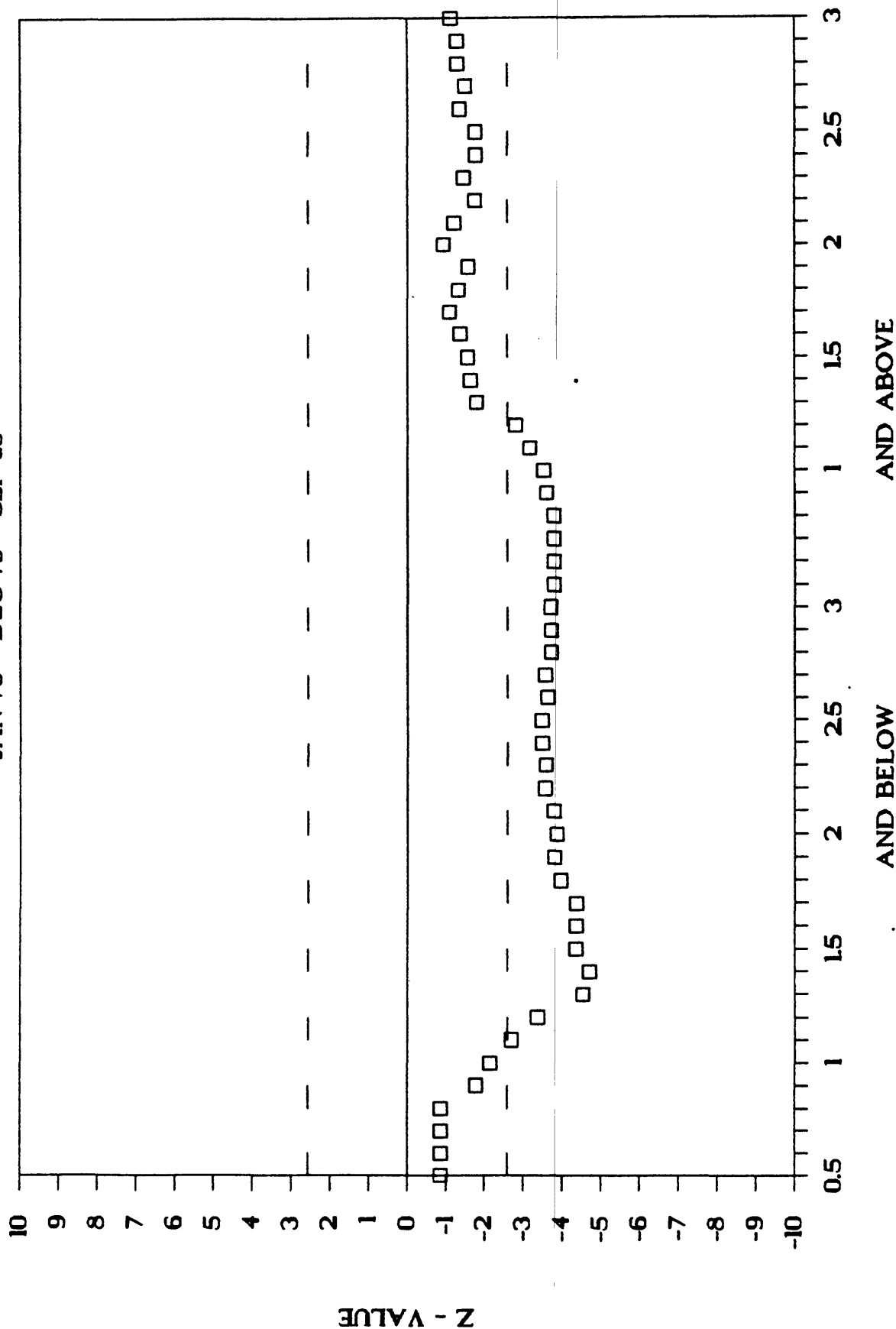


* WIDTH OF PEAK INDICATES SIZE OF EVENTS AFFECTED

* RELATIVE POSITION INDICATES AMOUNT OF SHIFT

OBSERVED MAGNITUDE SIGNATURE

JAN 78 - DEC 79 - SEP 80



OBSERVED MAGNITUDE SIGNATURE

DEC 79 - SEP 80 - MAR 82

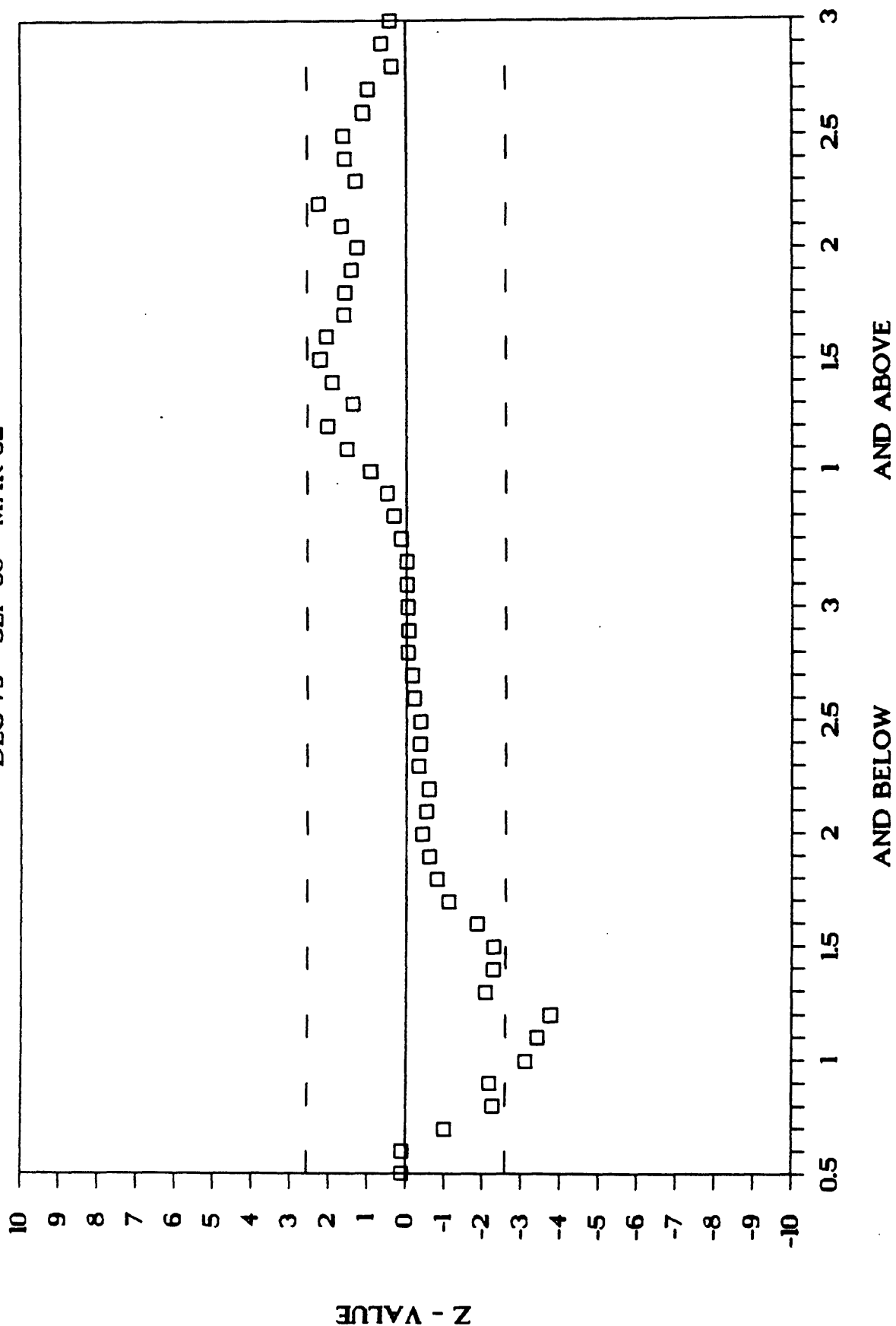
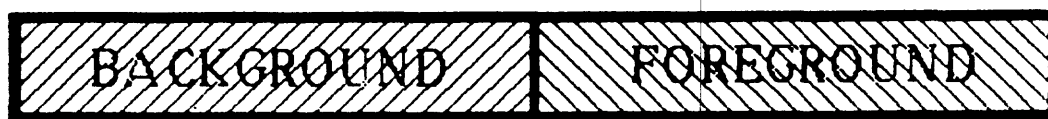


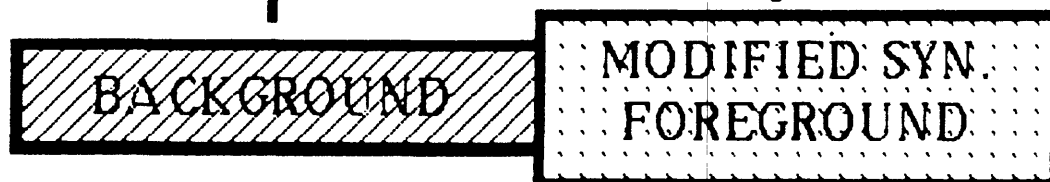
Figure 3. Synthetic Magnitude Signatures

Magnitude signatures compare rates during two time periods. Call these the background and foreground periods.



The first step of the synthesis is shifting the background period in time, forming a synthetic foreground ground period.

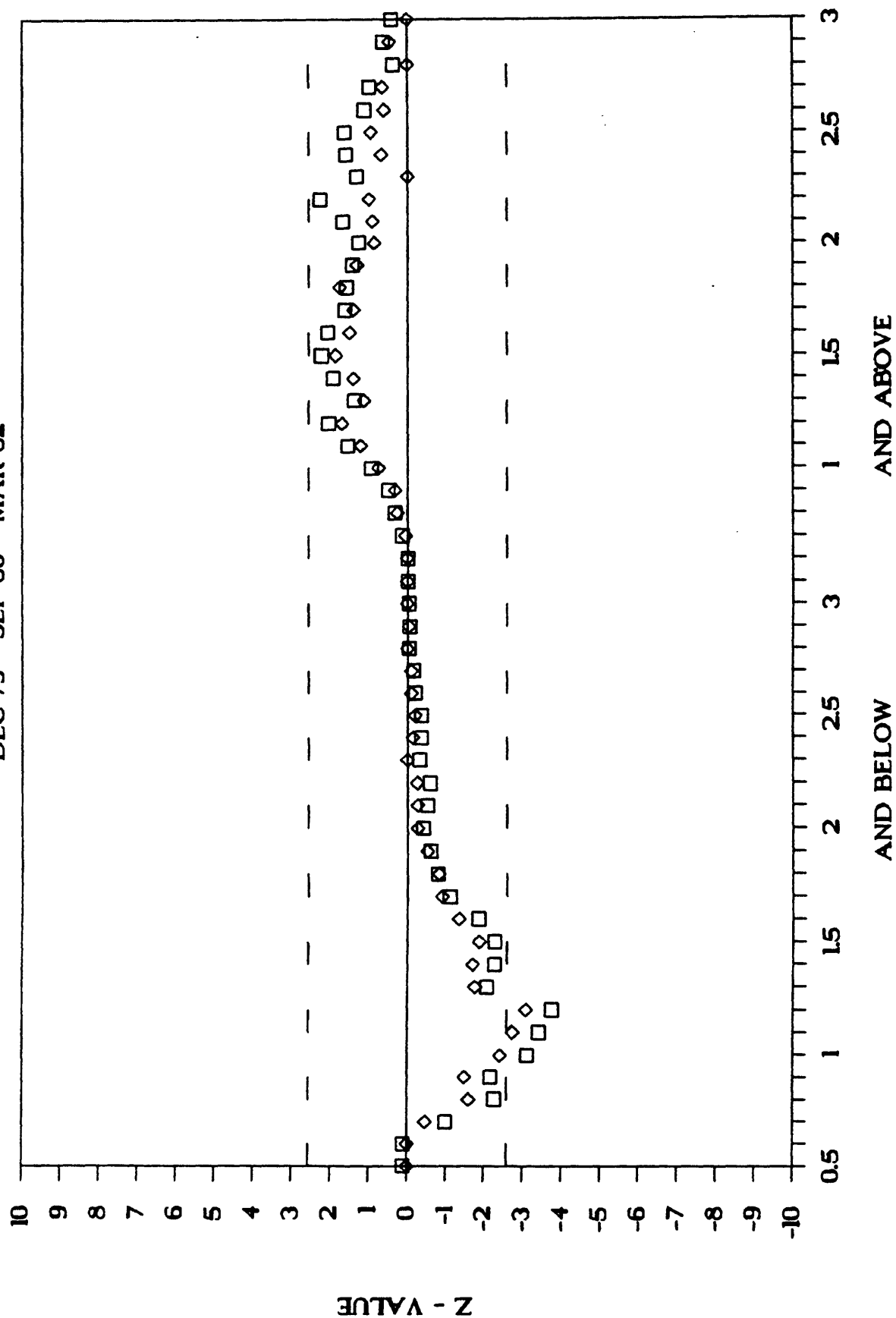
Next, the events during the synthetic foreground are modified by shifting their magnitudes or repeating events.



Finally, the modified synthetic foreground is compared to the original background period to form the synthetic magnitude signature. This process is then repeated until a satisfactory fit is achieved.

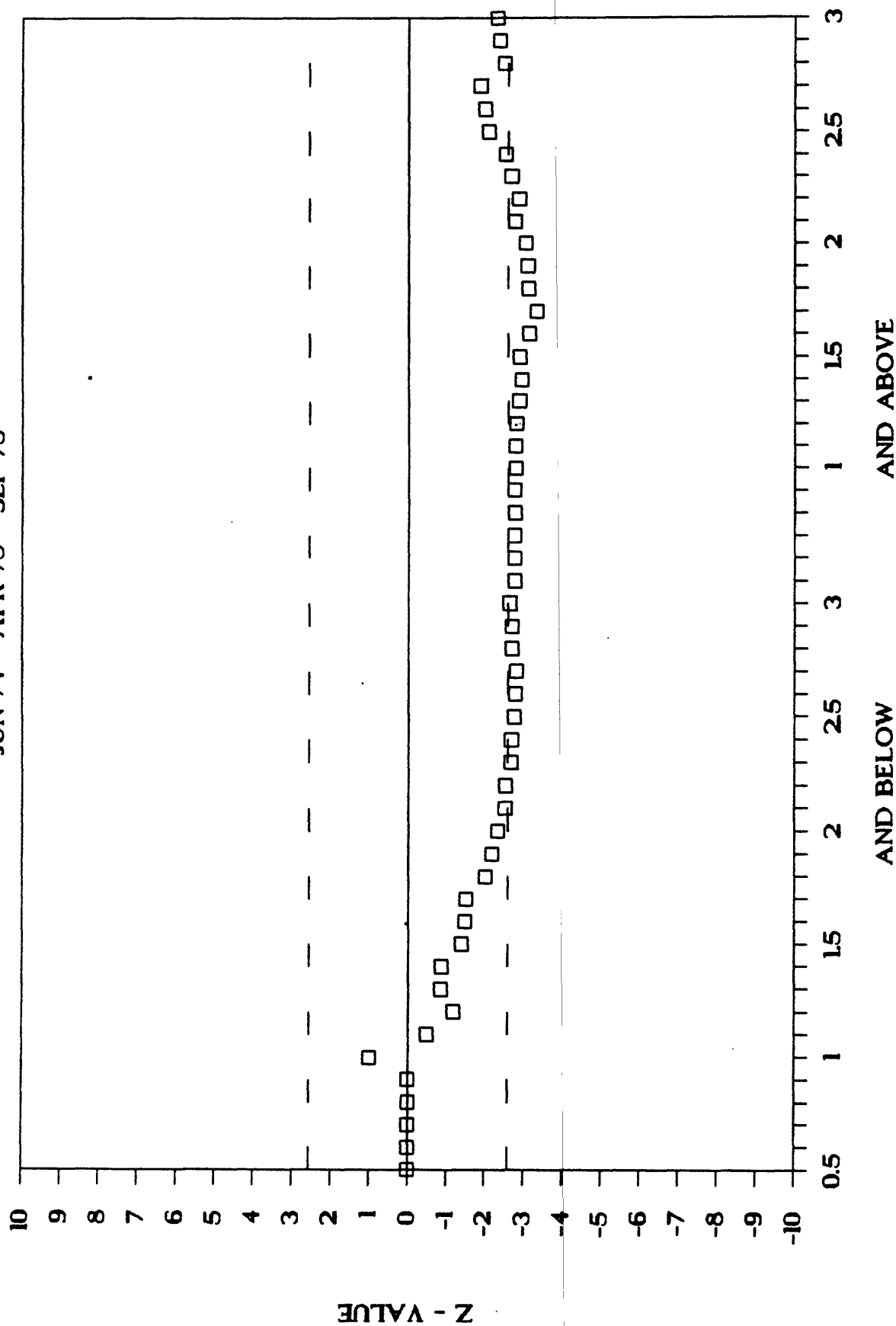
EQUAL SYNTHETIC

DEC 79 - SEP 80 - MAR 82



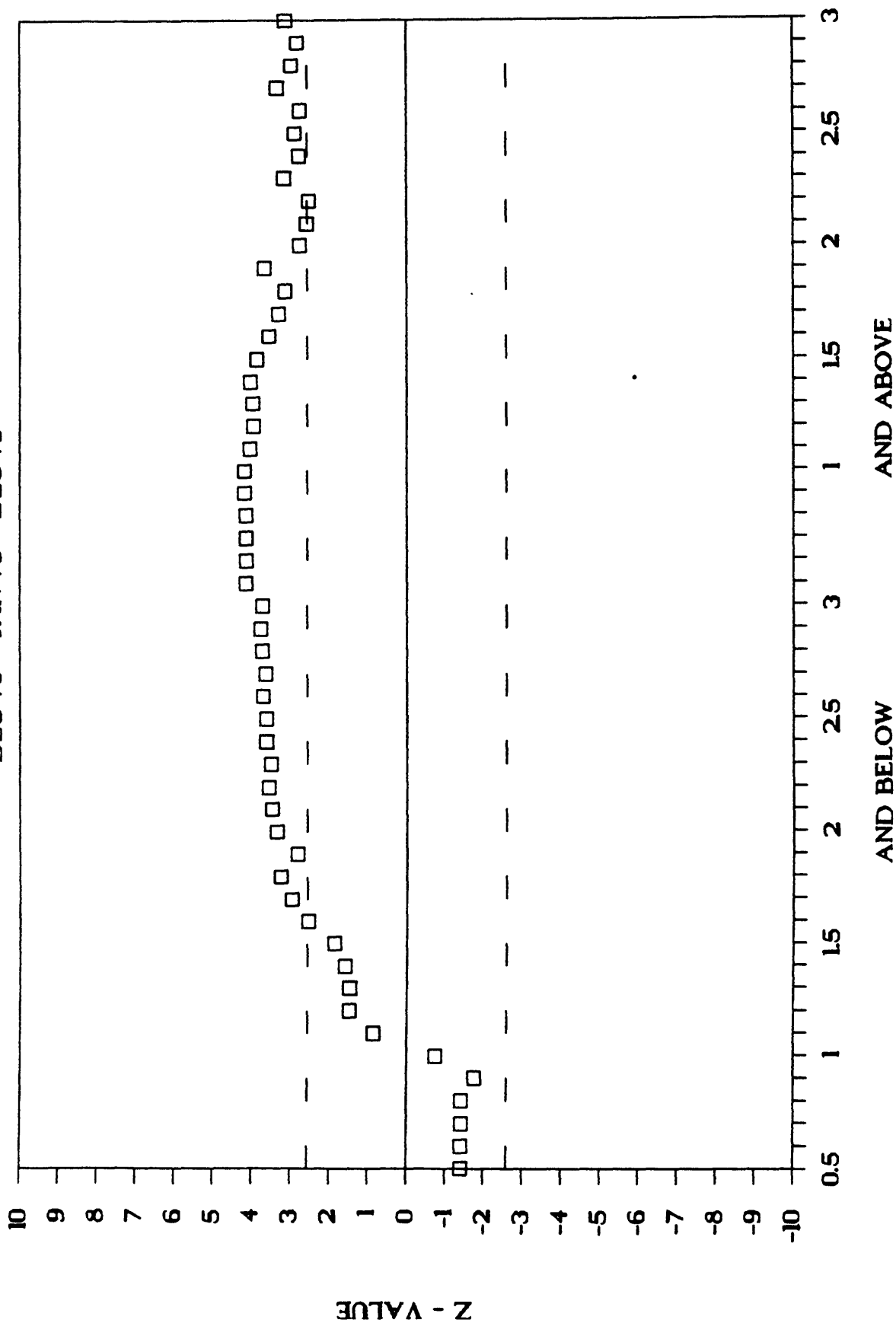
PARKFIELD

JUN 74 - APR 75 - SEP 75



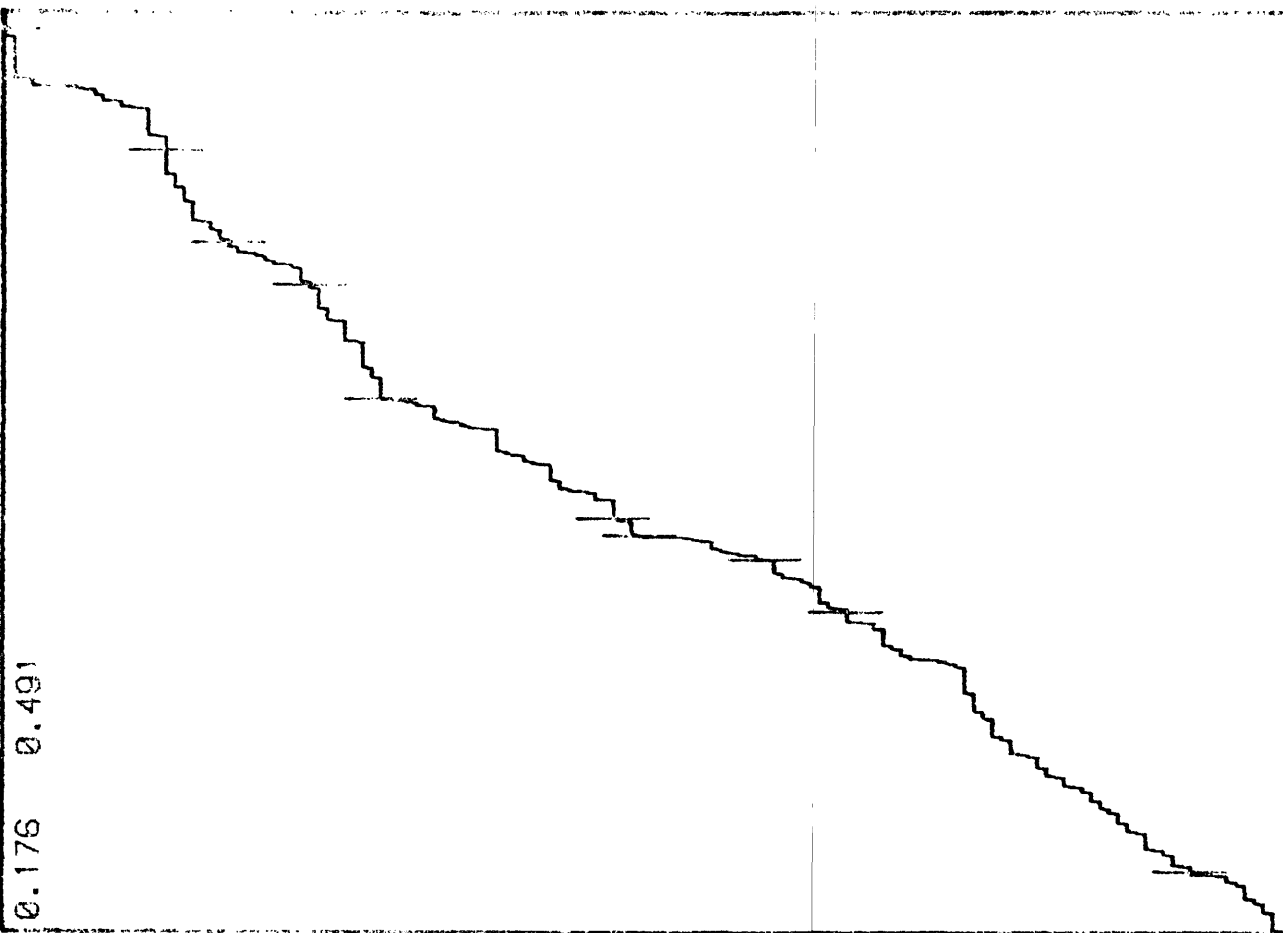
OBSERVED MAGNITUDE SIGNATURE

DEC 75 - JAN 78 - DEC 79



DATA SET 47 HAS 143 EVENTS LONG TERM MEAN =
DATA SET 47 HAS 0 TARGETS

53
284
330
351
366
471
573
610
691
799



OBSERVED MAGNITUDE SIGNATURE

DEC 79 - SEP 80 - MAR 82

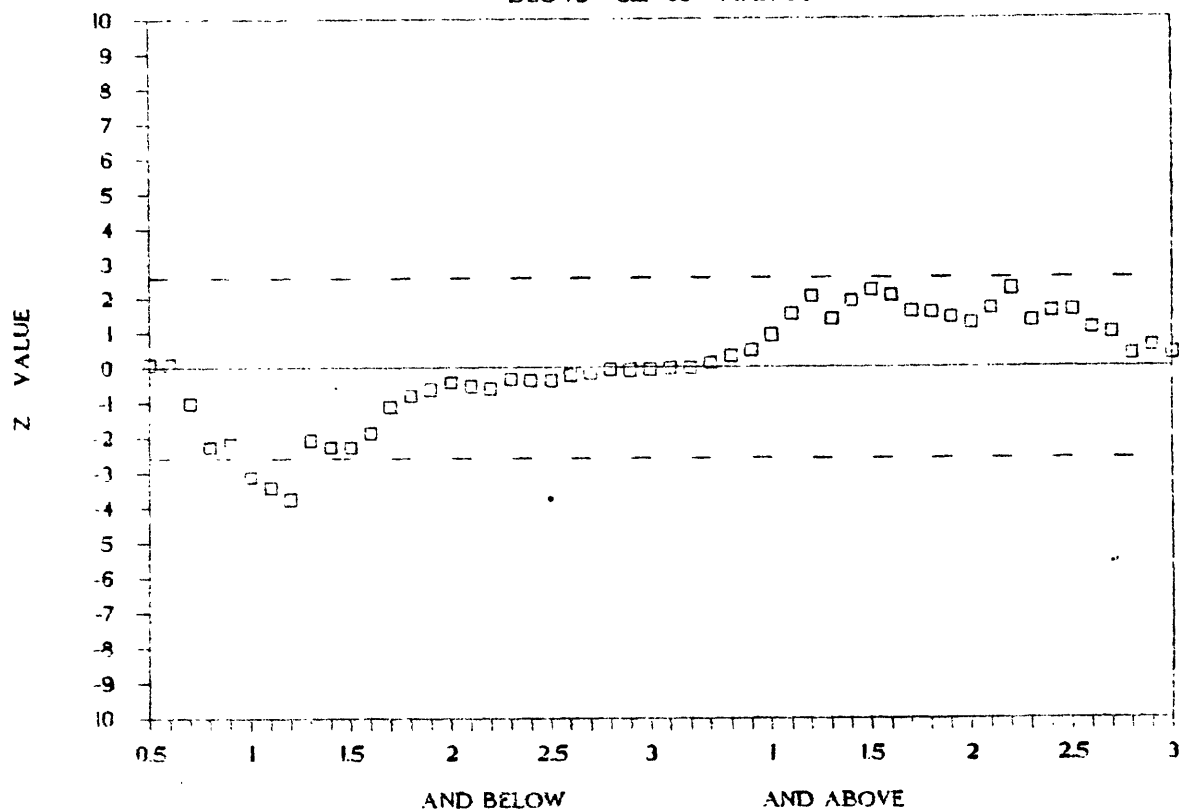


Fig. 5A

CORRECTED MAGNITUDE SIGNATURE

DEC 79 - SEP 80 - MAR 82

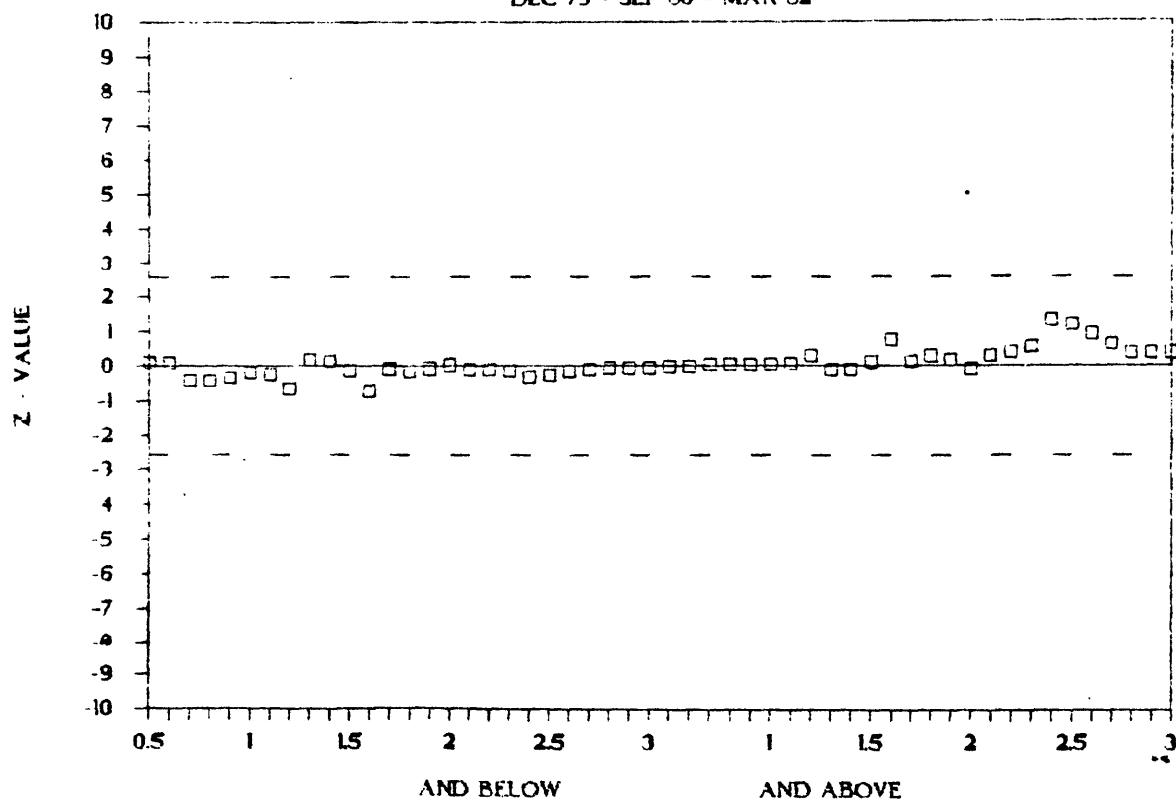


Fig. 5B

APPENDIX A. 5.

Review of Seismic Wave Monitoring in Central California

R. Clymer and T. V. McEvilly

REVIEW OF SEISMIC WAVE MONITORING
IN CENTRAL CALIFORNIA

by R. Clymer and T.V. McEvelly

USGS Contract 14-08-0001-21985

July 26, 1985

Hollister Area P-Wave Travel-Time Monitoring

P-wave travel-time monitoring has continued in the Hollister area (Figure 1) with our aging (10-year-old), single-channel recording system (Figure 2).

The precision of the measurements is indicated by the results of stability tests consisting of repeated measurements of an 8-sec deep-crustal reflection (Figures 3 and 4) on path T-Z in Bickmore Canyon (Figure 1). With the system in its present configuration, travel times on such tests scatter over about 1 msec and amplitude varies about 20%. Applying these results to our actual monitoring data indicates: 1) In Bear Valley, on path W-B, repeated measurements indicate a scatter of 5-10 msec, and 2) at the Winery and Stone Canyon areas, first-arrival travel times scatter over about 1 msec or somewhat less, depending on signal-to-noise ratio.

While precision appears to be quite good, accuracy is degraded considerably by seasonal variations of up to about 6 msec for first arrivals at the Winery and Stone Canyon areas (Figure 5). The cause is very-near-surface seasonal moisture variations. Our solution has been to monitor near-surface times with geophones below the water table at most source and receiver sites, and then to simply subtract the near-surface variations from the path data. The results are shown in Figures 6 and 7. The efficacy of the procedure is difficult to quantize. We suspect that the 1-3 msec long-term variations shown cannot be considered meaningful. A travel-time change of 4-5 msec would probably indicate a real change occurring at depth.

We have chosen a different method of dealing with this problem at Parkfield. All receivers are to be in boreholes at depths of several hundred feet. With the vibrator fixed, data from several sites will be recorded simultaneously. Data for a path on which changes are not expected will be used as a reference to remove spurious changes from the other paths. This should produce a correction at least as accurate as the present procedure, with a considerable increase in field efficiency.

Shear-Wave Vibrator (Figure 8)

In the summer of 1984, Amoco Production Company donated a shear-wave vibrator in excellent condition to the UCB Seismographic Station, giving us the capability of monitoring S-wave travel time and amplitude. In addition, we believe we can monitor S-wave velocity anisotropy by a simple procedure. Roberts and Corrigan (1983) have shown that an S-wave vibrator will radiate S_V or S_H waves towards the receiver depending on the orientation of the vibrator baseplate, and that this could be used to measure anisotropy in a near-surface shale. Results of a vertical seismic profile accomplished with our S-wave vibrator at the Geysers geothermal area in the fall of 1984 confirmed these results. Here, S_V and S_H waves parallel and

perpendicular to a known fracture pattern showed distinct velocity changes. (Figures 9 and 10. Further processing of the data with software that can rotate the axes and accentuate a particular mode of vibration show the change in S-wave velocity more clearly.)

We think this new capability has exciting implications for earthquake prediction research at Parkfield, since S-wave amplitude and anisotropy may be more sensitive indicators of fault-zone properties than P-wave parameters.

New Recording System

To monitor S-wave and P-wave parameters at Parkfield will require 3-component receivers and recording of a considerably larger data set than that at Hollister. This will only be practical if we record data from several 3-component receivers simultaneously. Figure 11 shows the system chosen and presently on order. It will be used for this and other UCB/LBL projects.

Parkfield Accomplishments

Figure 12 shows sites for 3-component borehole seismometer installations. Four of these were accomplished in the spring of this year, and two more will be finished this summer. The Gold Hill package is clamped in an open hole. The installations are a cooperative effort involving the USGS, UC Santa Barbara, and UC Berkeley.

One week of preliminary data gathering with the S-wave vibrator and the single channel recording system laboriously produced the following results (Fig 13-16):

- 1) A surprisingly high signal-to-noise ratio, even at a source-receiver offset of 10-11 km. This is 2-3 times the offset used at Hollister with the P-wave vibrator. Coherent, reproducible, source-generated signals were present to 12-15 sec travel time, with an indication of a coherent event at 20 sec.
- 2) Complex S-wave arrivals that change in character when the vibrator baseplate is rotated.

We plan to determine if further processing of these records will provide evidence of anisotropy. Regardless, we conclude that we can detect changes in the dissimilarity of these waveforms. Such changes, should they occur, would indicate variations in fault zone properties.

References

- Clymer, R.W. and T.V. McEvilly (1981). Travel-time monitoring with VIBROSEIS, Bull Seism Soc Am, 71, 1903.
- Peacock, Sheila and Stuart Crampin (1985). Shear-wave vibrator signals in transversely isotropic shale, Geophysics, 50, No 8 (in press).
- Robertson, James D. and Dennis Corrigan (1983). Radiation patterns of a shear-wave vibrator in near-surface shale, Geophysics, 48, 19.

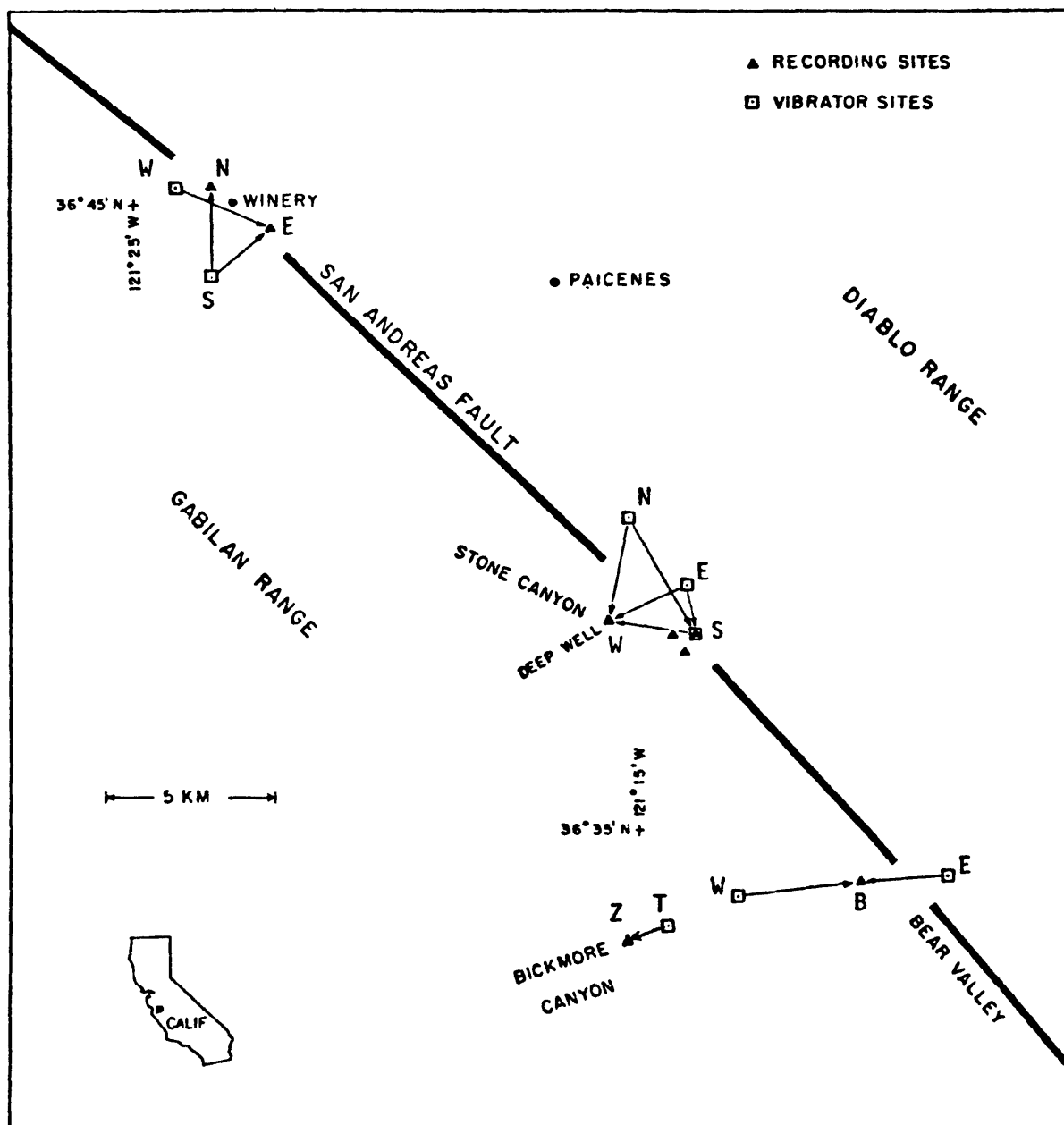
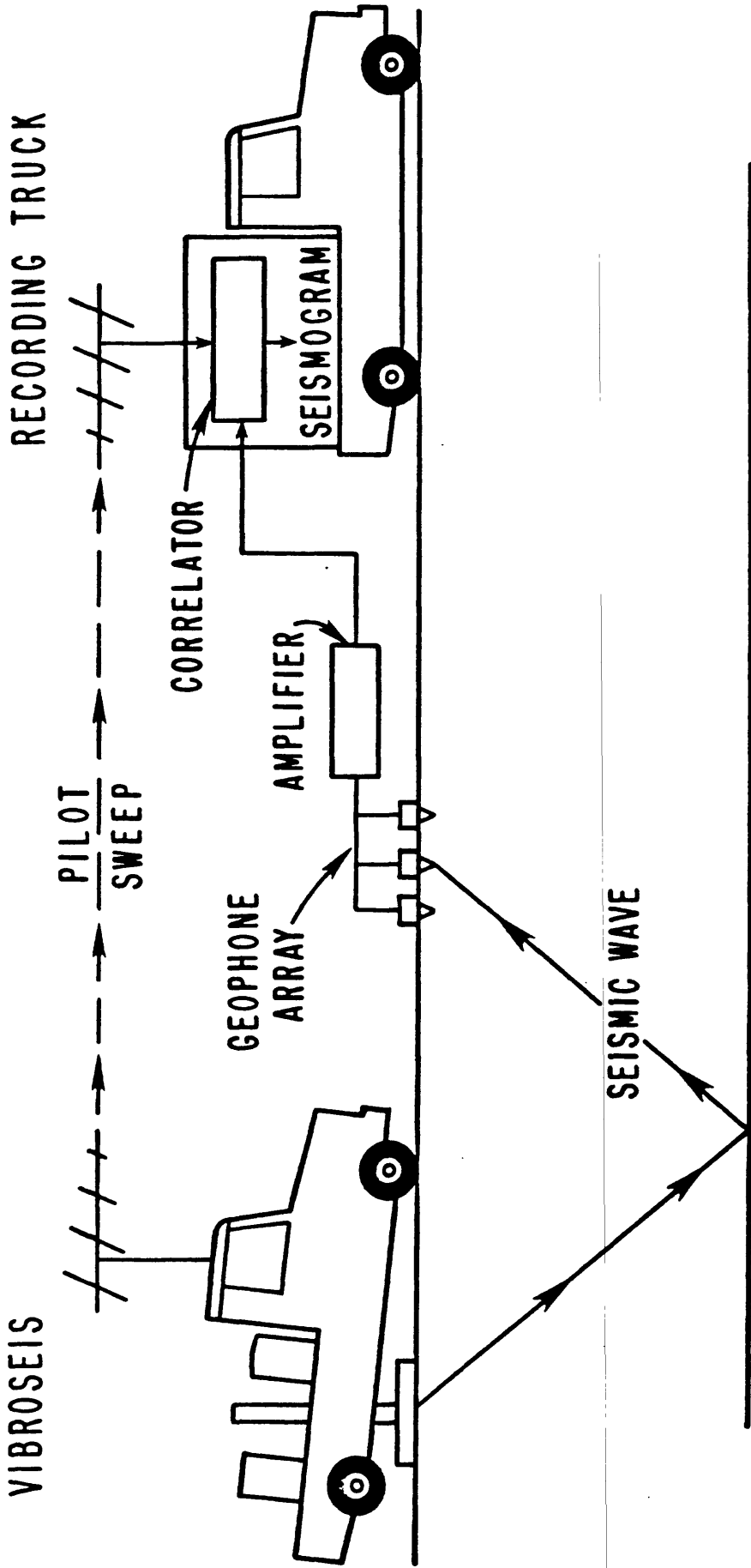


FIGURE 1. Source and receiver sites, Winery, Stone Canyon and Bickmore Canyon areas.



XBL 758 - 3660

Figure 2 . Schematic of VIBROSEIS field system in operation.

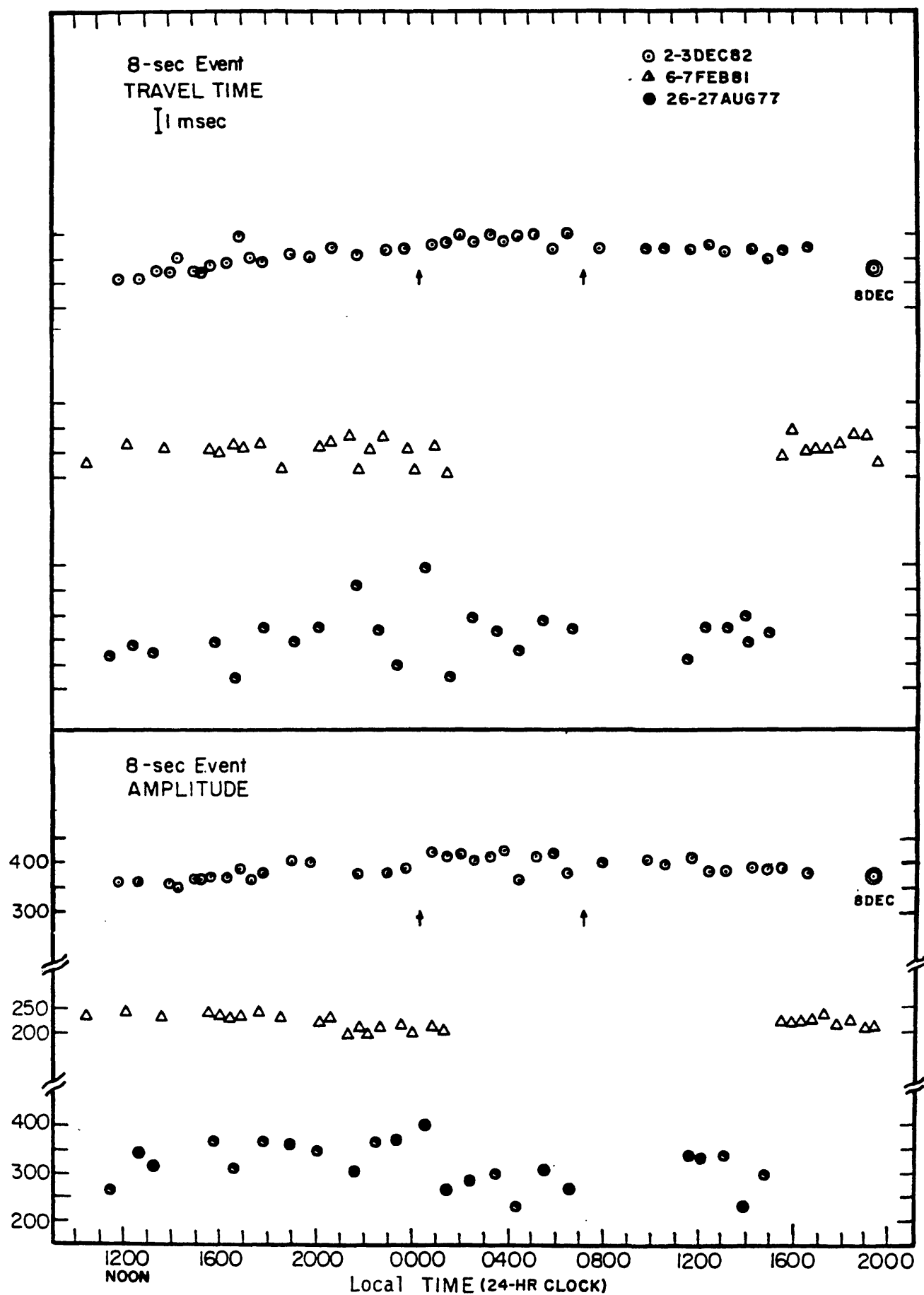


Figure 3. Variations in travel time and amplitude of a deep crustal reflection at 8-sec travel time during three stability tests. Path: T-Z (Figure 1).

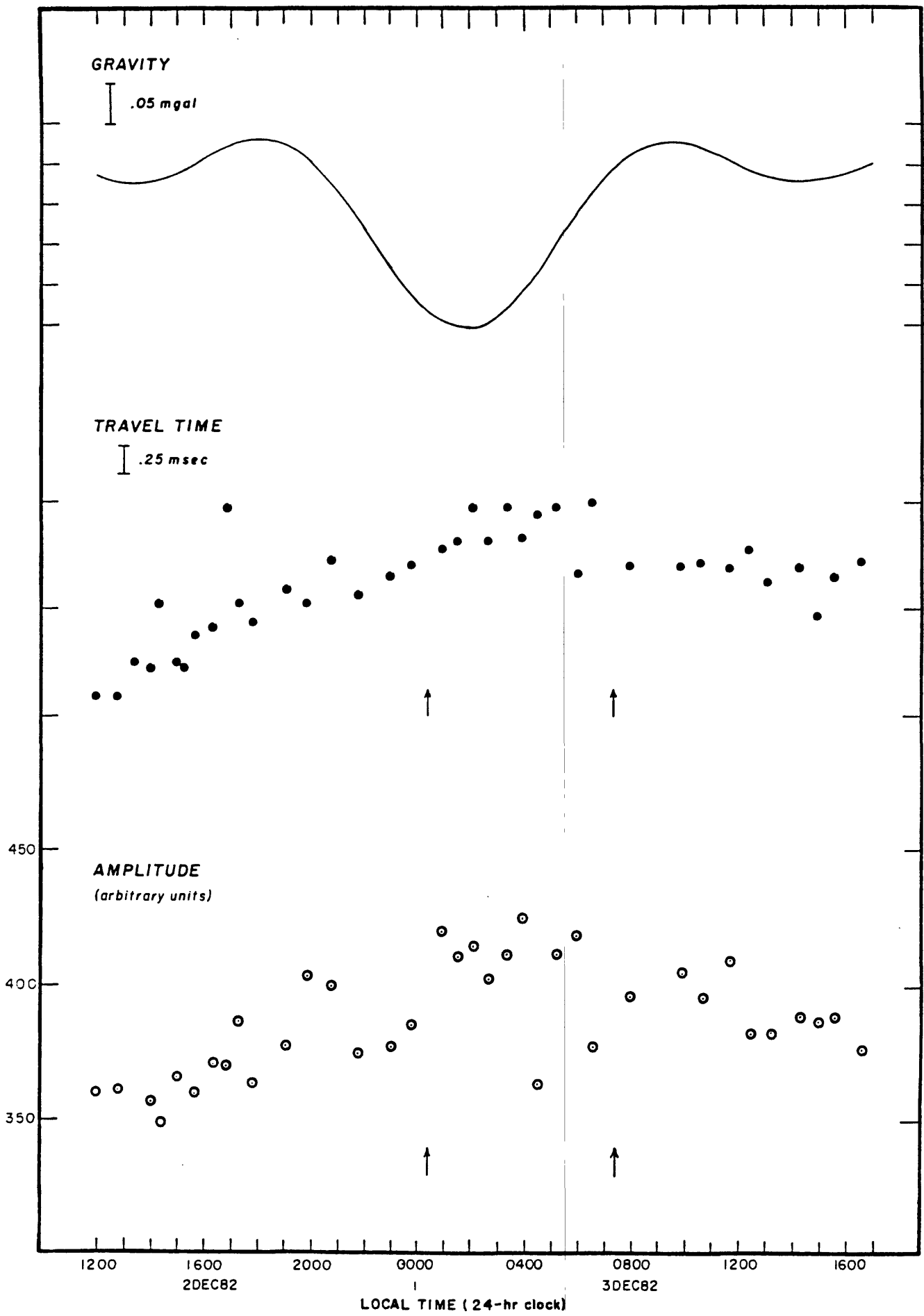


Figure 4. Calculated gravity tide and variations in travel time and amplitude of the 8-sec deep crustal reflection, path T-Z (see Figure 1). The arrows indicate instrument or vibrator changes.

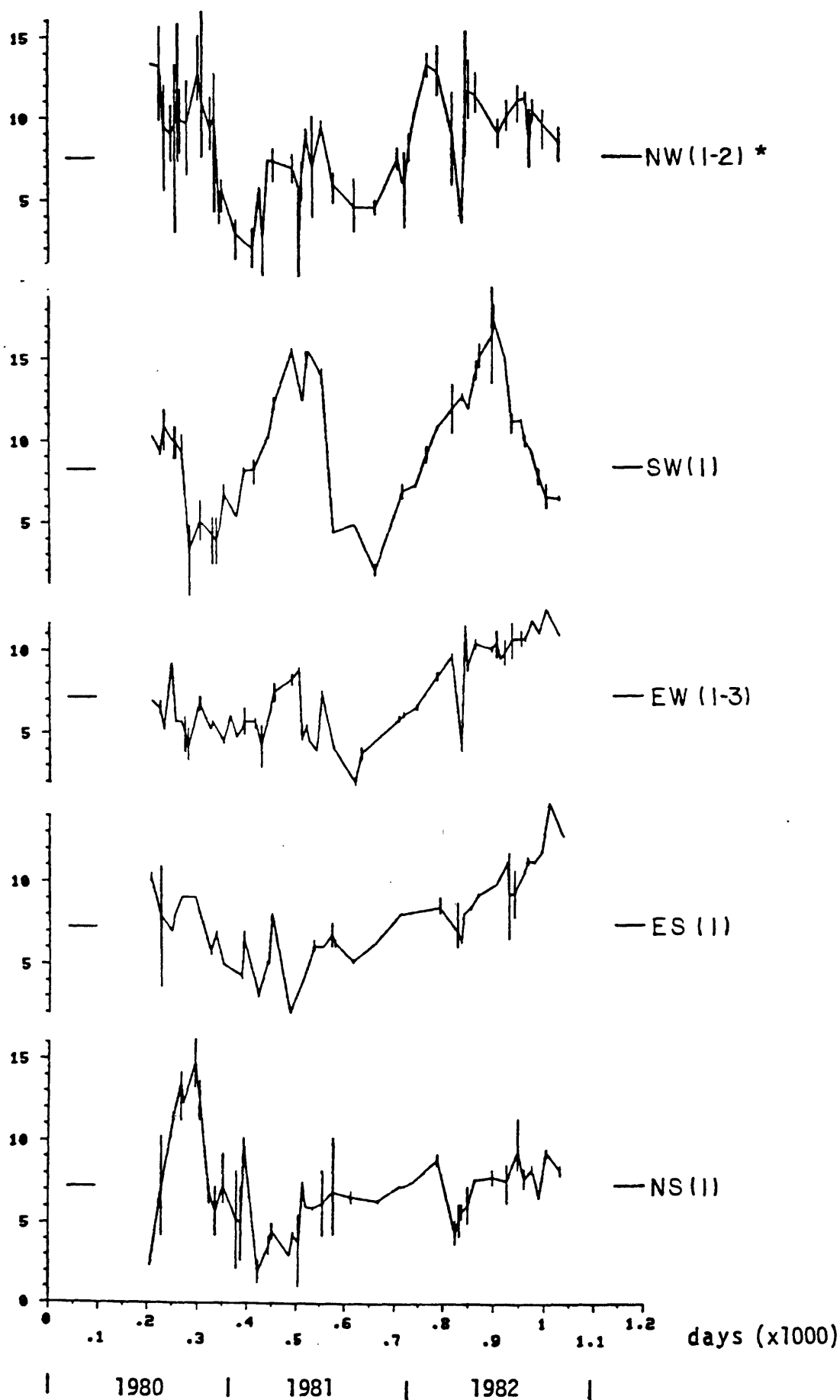


Figure 5. First arrival travel times, without near-surface corrections.

* Nomenclature: Path name (picks in average)

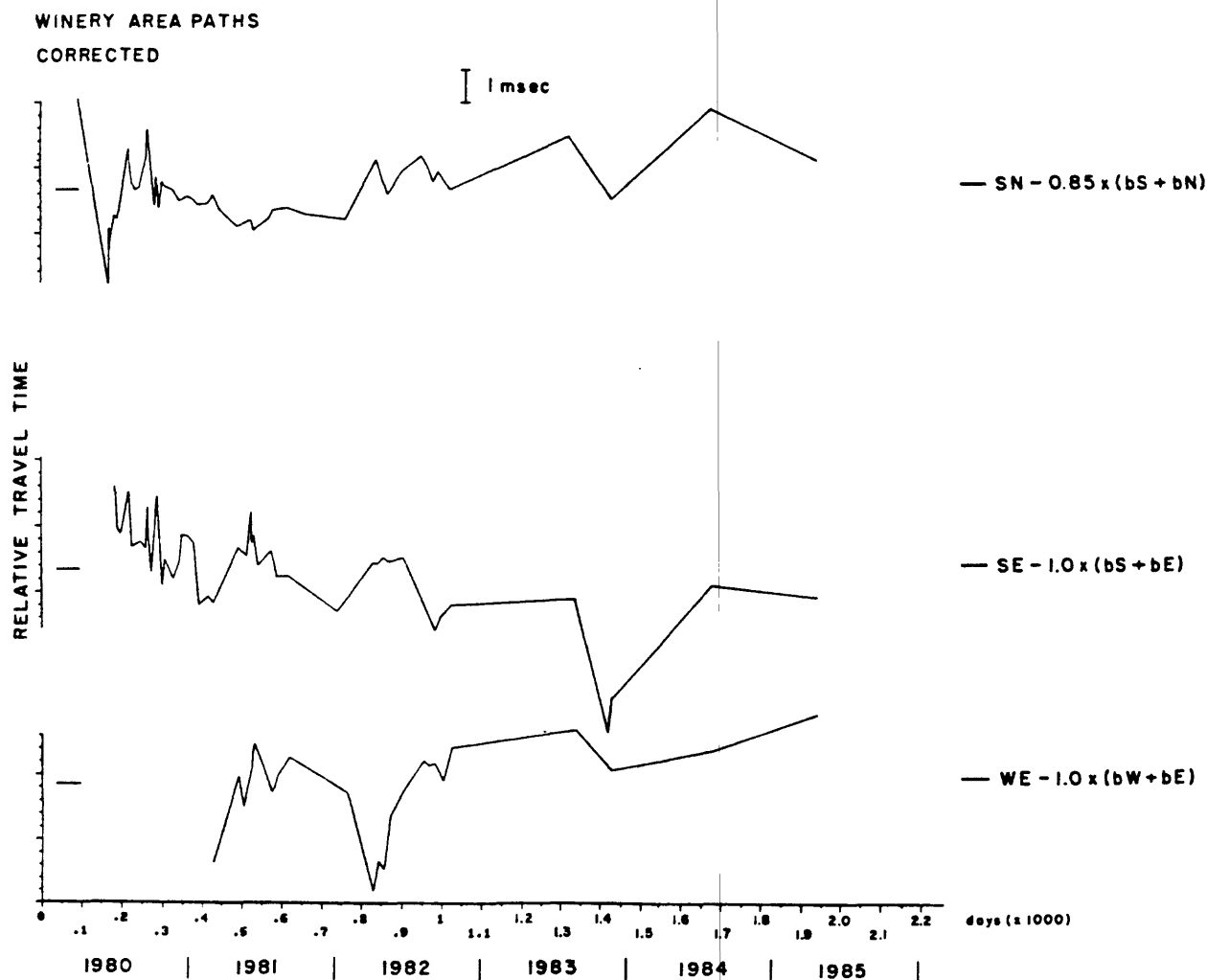


Figure 6. Winery area first-arrival travel times with near-surface (seasonal) corrections. Upper-case letters refer to site designations shown in Figure 1. Two upper case letters together indicate the source and receiver ends of a path, respectively. A lower-case 'b' followed by an upper-case letter implies that a borehole data set at that site was used for near-surface corrections to the path data. The associated numbers are scale factors.

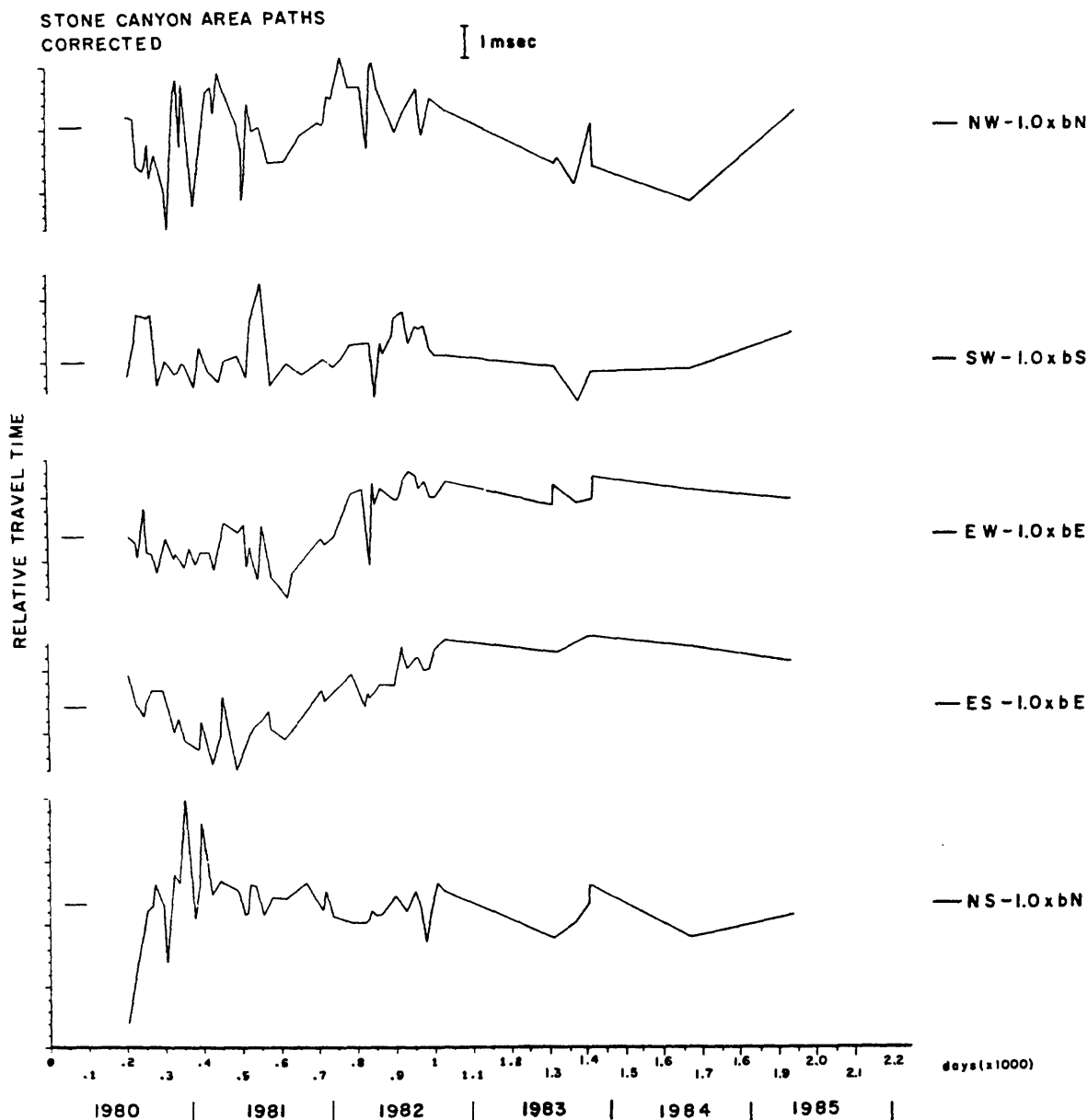


Figure 7: Stone Canyon area first-arrival travel times, with near-surface (seasonal) corrections. Site W has a surface geophone array and no borehole geophone for near-surface control. Thus paths NW, EW, and SW only have vibrator-end near-surface corrections applied. The receiver at site S is a borehole package, thus no receiver-end near-surface correction is necessary for paths NS and ES. Site designations as in Figure 6.

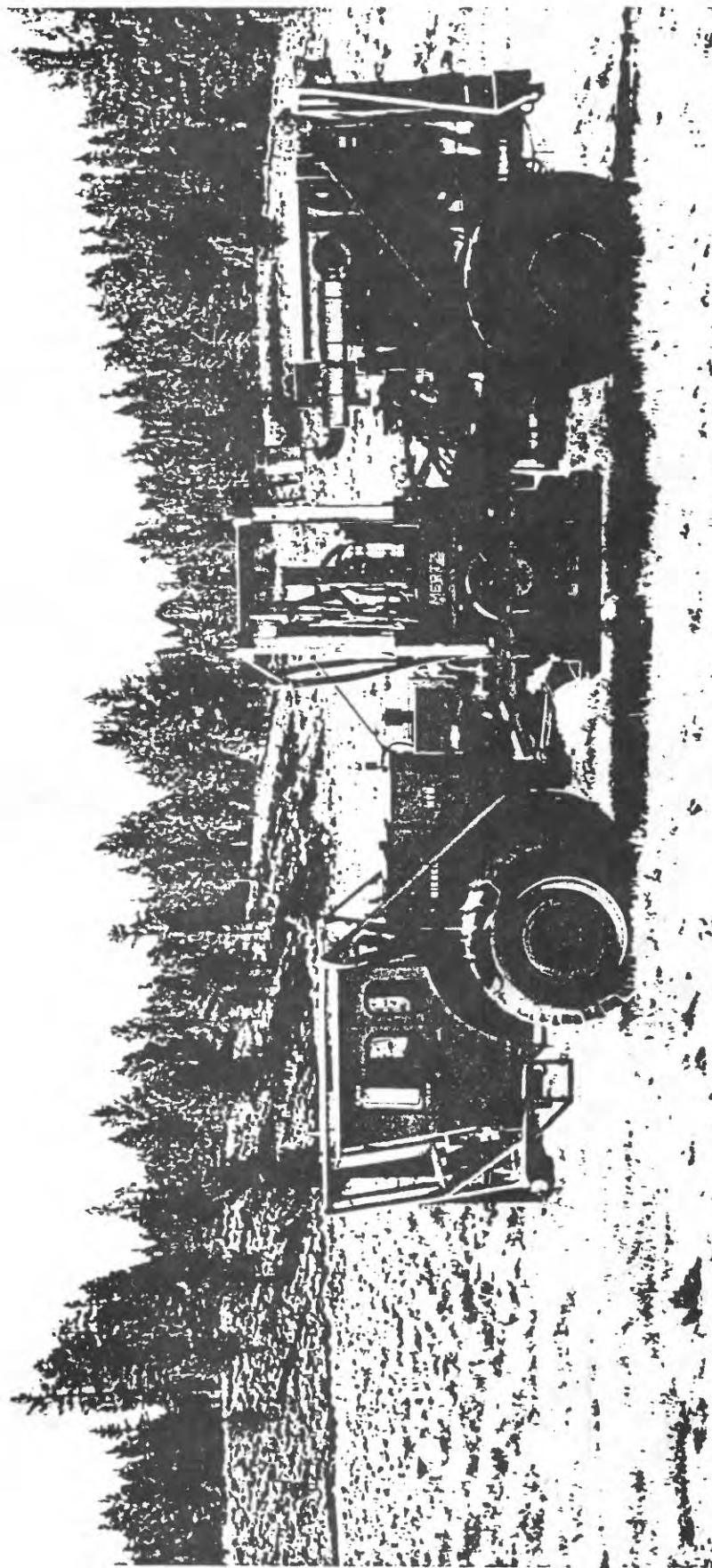


Figure 8. UCB shear-wave vibrator on-site in Long Valley, California.

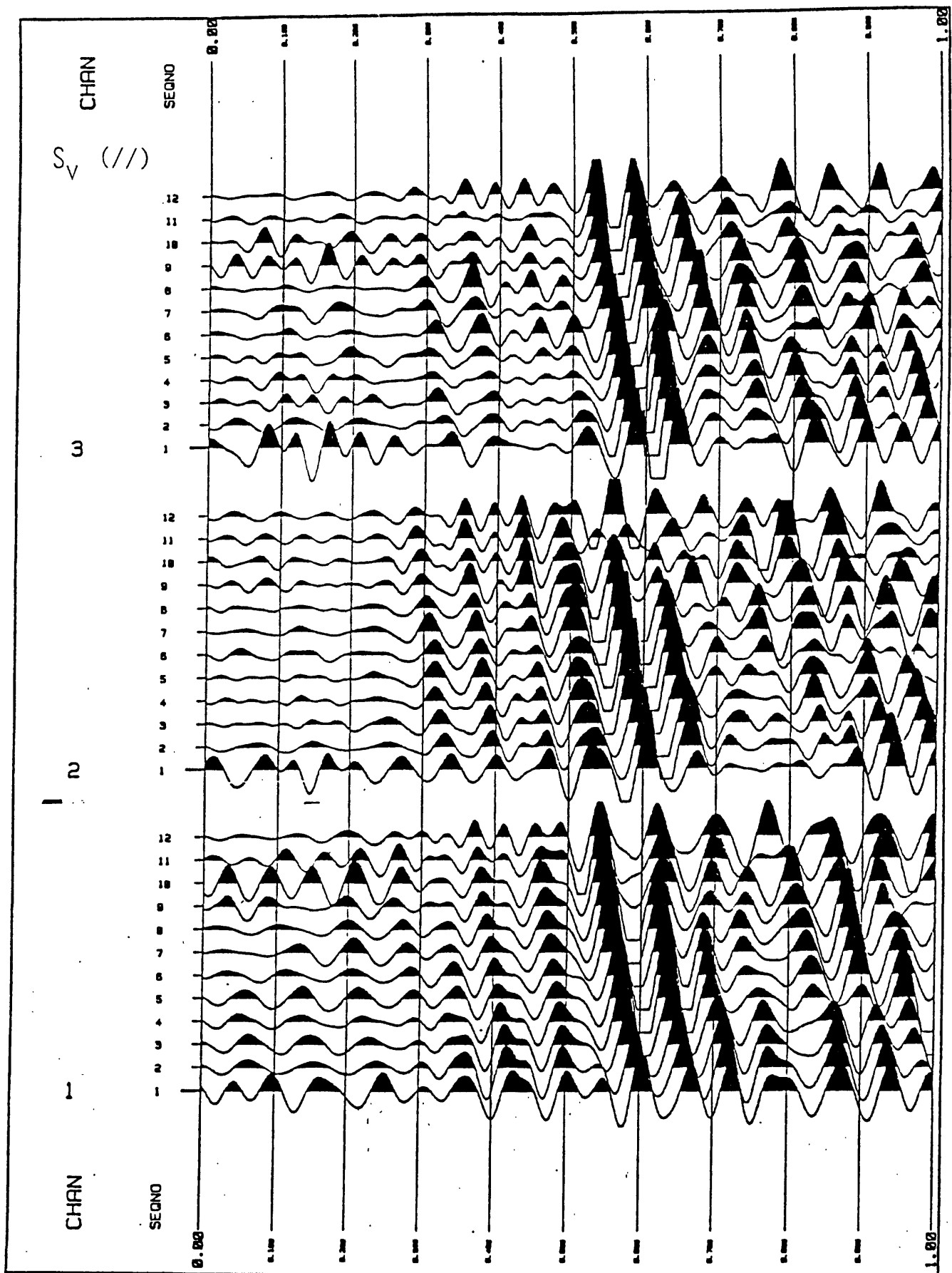


Figure 9. Shear-wave vertical seismic profile (VSP) data. Three-component (channel 1 is vertical) traces for 1000'-2100' depth range, 1700' source offset, 10-55 Hz sweep, shear-wave vibrator, at The Geysers geothermal field. Polarization is S_y (parallel to expected subsurface fracture grain).

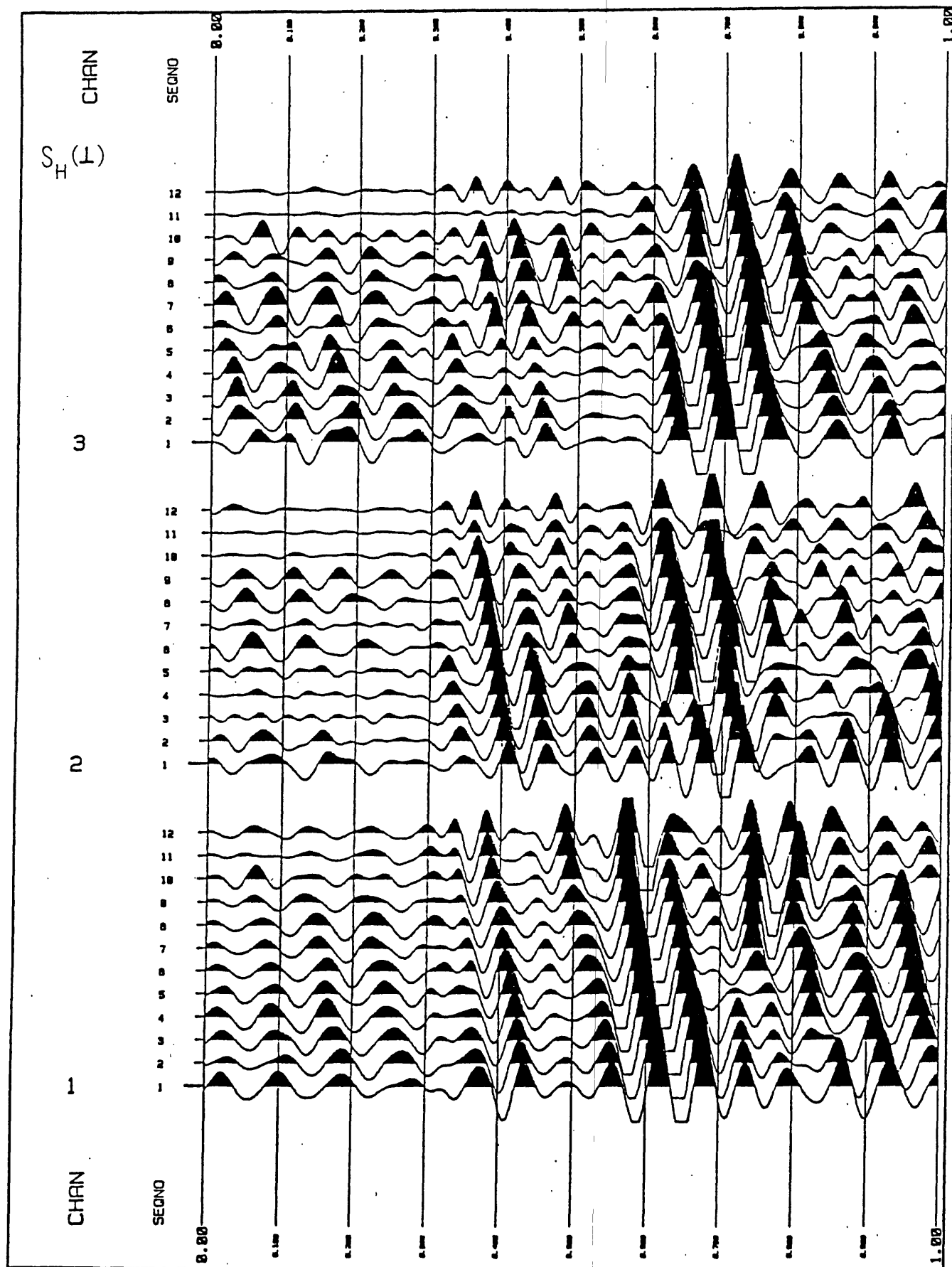


Figure 10. S_H -polarized (perpendicular to expected fractures) VSP, source location and parameters (except polarization) identical to previous figure. Note approximately 120 msec delay for S_H polarization. This anisotropy is presumed to be due to the dominant fracture fabric of the reservoir.

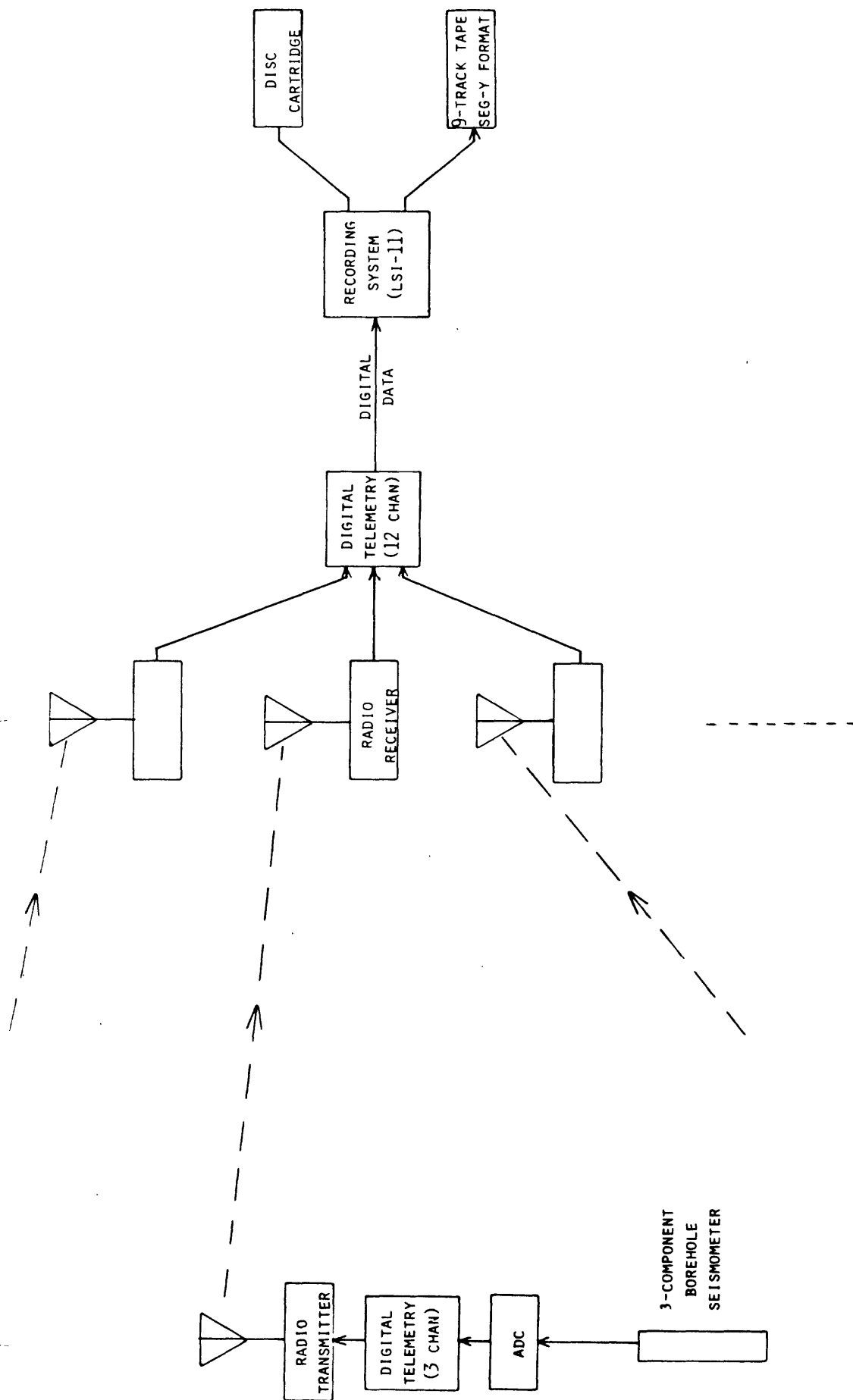


Figure 11. Schematic diagram of planned UCB/LBL seismic data acquisition system, featuring digital telemetry and computer-based recording and in-field processing. The system will be expandable to many more channels than shown, and is expected to be capable of recording both VIBROSEIS and earthquake data, the latter with triggered event recording. SEG-Y 9-track tapes will allow processing with DISCO software at the Center for Computational Seismology at Lawrence Berkeley Laboratory.

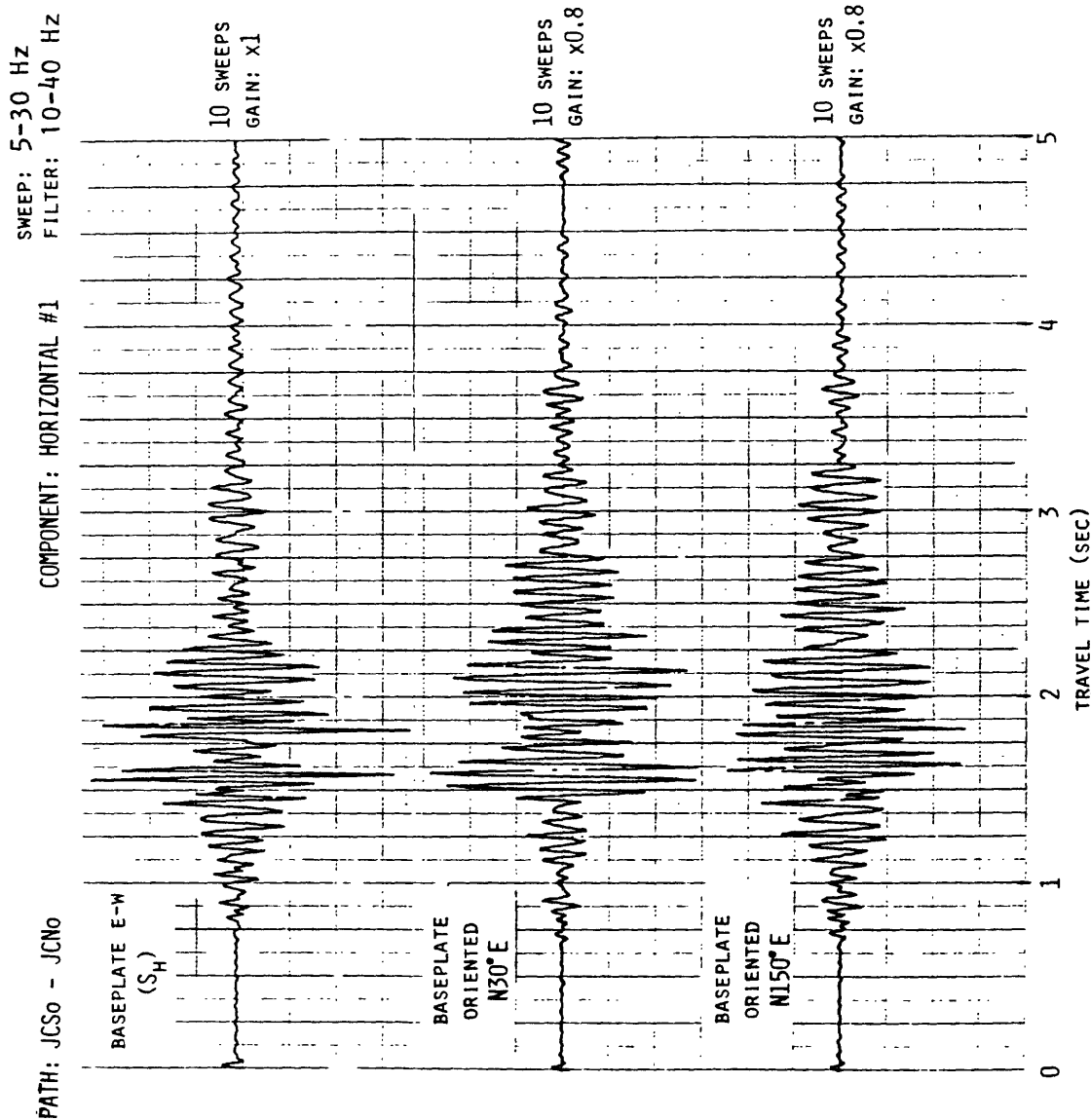


Figure 13. Shear-wave vibrator data recorded in June, 1985 at Parkfield. For the top trace, the vibrator baseplate motion was perpendicular to the source-receiver azimuth (S_H mode). The lower two traces show the same (horizontal) seismometer component with the vibrator baseplate rotated first 120 east, then 120 west of the S_H orientation. The source-receiver offset was 2.1 km. The path was located in Joquin Canyon (see Figure 12).

PATH: JCS0 - JCNO
 COMPONENT: HORIZONTAL #2
 SWEEP: 5-30 Hz
 FILTER: 10-40 Hz

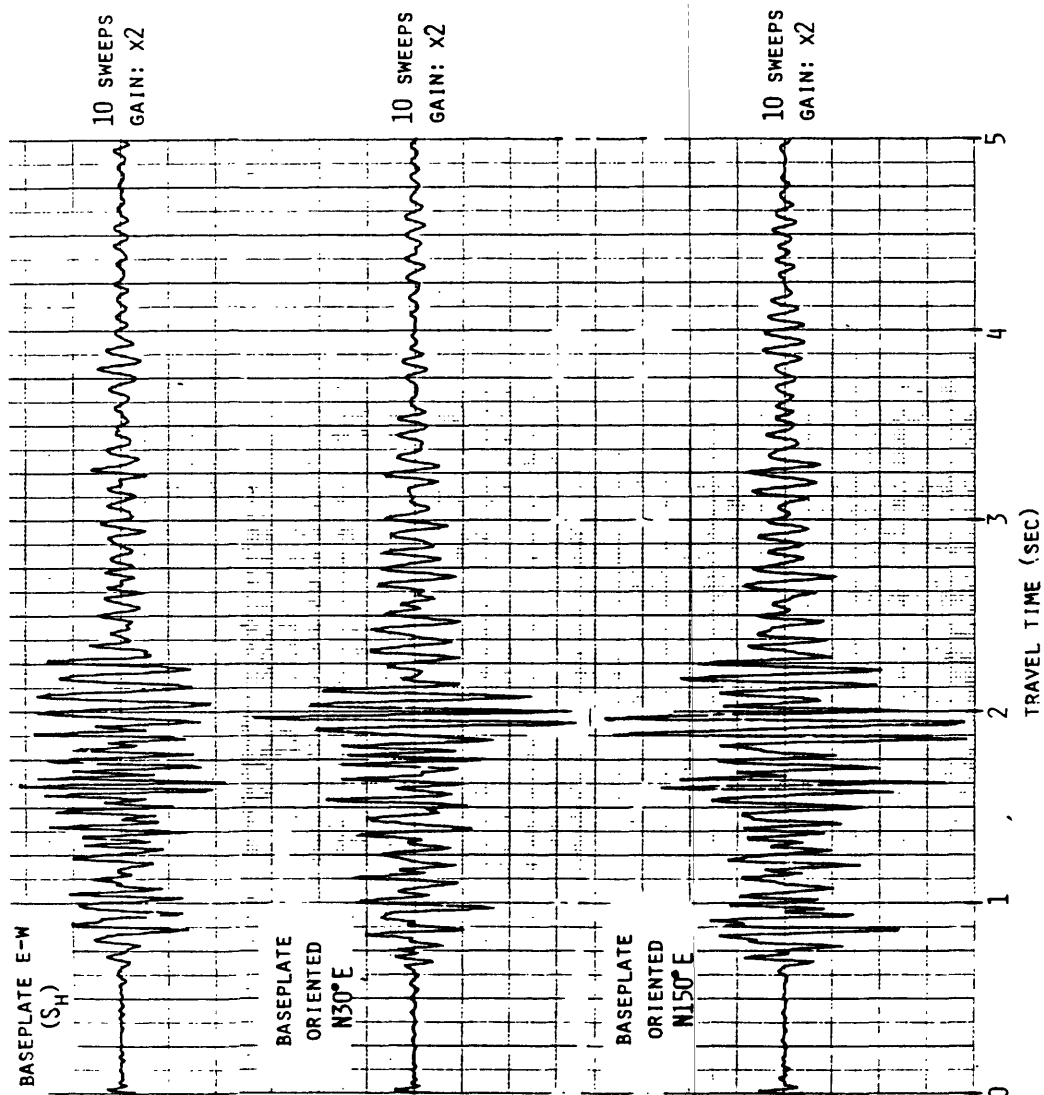


Figure 14. Shear-wave vibrator data as in Figure 13, except for receiver component.

PATH: VCRD-JCNO SWEEP: 5-30 HZ FILTERS: OUT-40 HZ

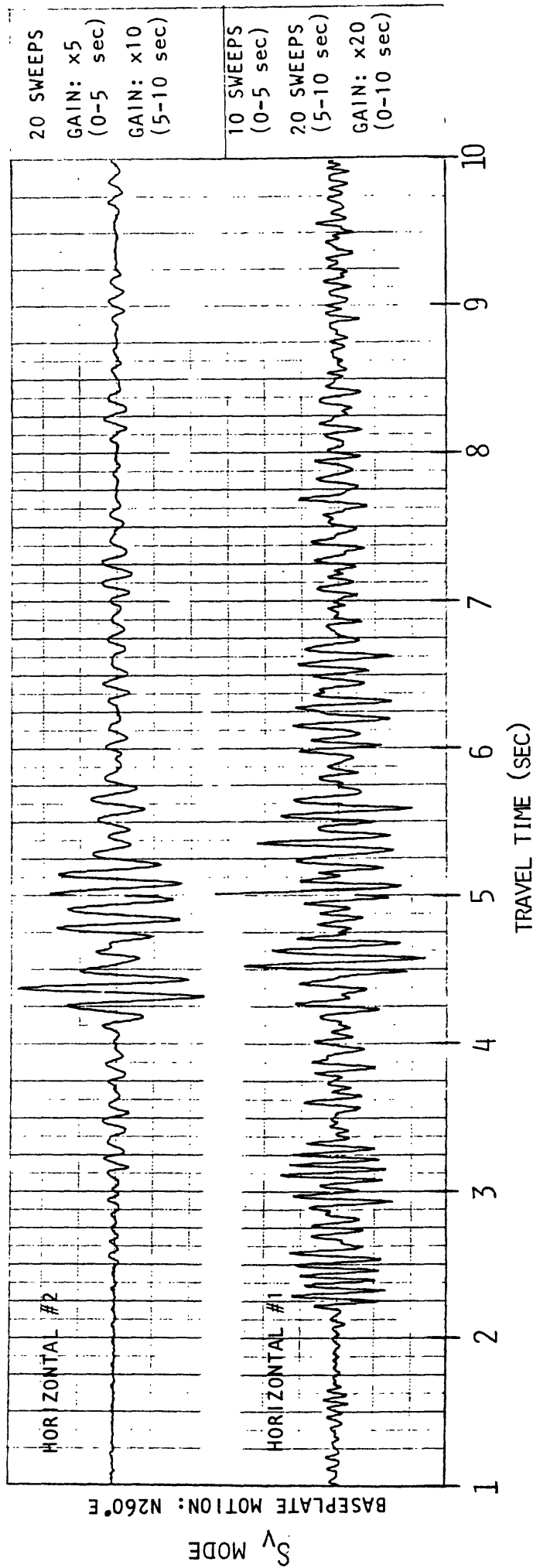
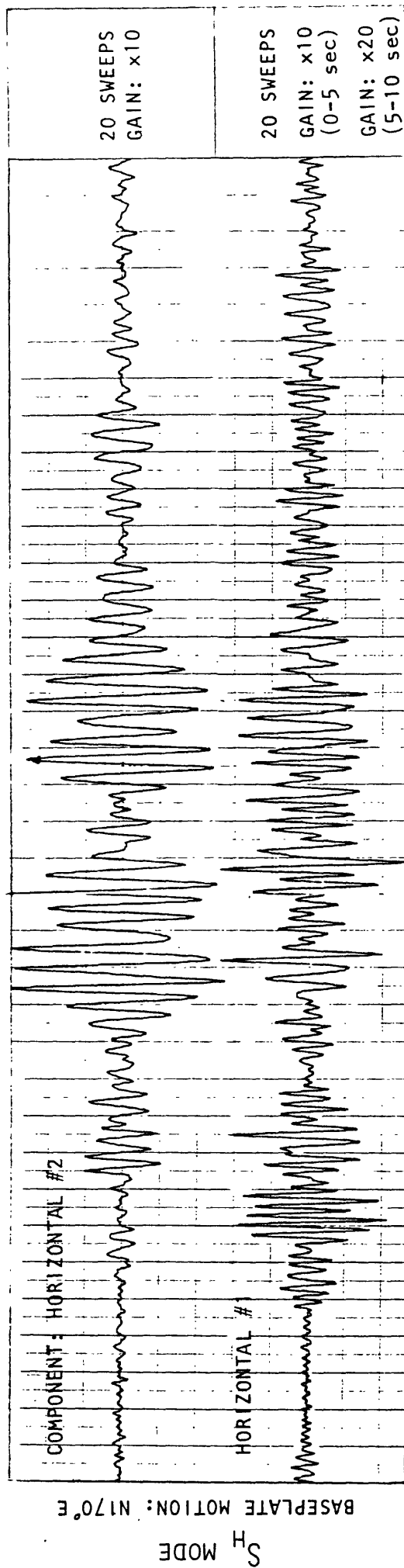


Figure 15. Shear-wave vibrator data recorded in June, 1985 at Parkfield, with a 6.7 km source-receiver offset. Separate 5-sec records were recorded at two time windows to produce the 10 sec of data shown. Note the gain discrepancies indicated at the right.

PATH: SLRD - JCNO SWEEP: 5-30 Hz FILTERS: OUT-40 Hz BASEPLATE MOTION: $190^\circ (S_H)$

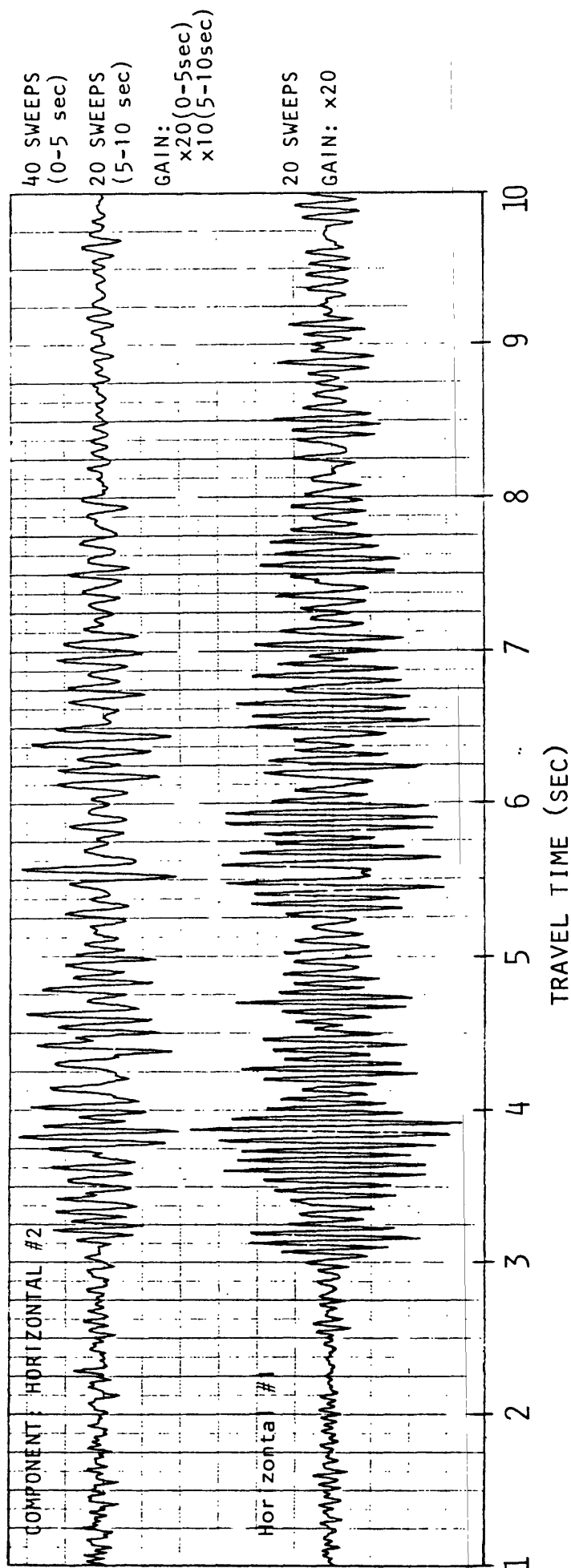


Figure 16. Shear-wave vibrator data recorded in June, 1985 at Parkfield, with a 10.8 km source-receiver offset. Time windows as for Figure 15. For the top trace, note that the 1-5 sec segment has an effective gain (considering both the instrumental gain and the number of vibrator sweeps) that is four times that of the 5-10 sec segment.

APPENDIX A. 6.

Preliminary Results from Vertical Seismic Profiling
of Oroville Microearthquake S-Waves

P. E. Malin and J. A. Waller

Reprinted with permission of the
American Geophysical Union

PRELIMINARY RESULTS FROM VERTICAL SEISMIC PROFILING OF OROVILLE MICROEARTHQUAKE S-WAVES

P. E. Malin and J. A. Waller¹Marine Sciences Institute and Department of Geological Sciences
University of California Santa Barbara

Abstract. Seismograms recorded along a 0.5 km-deep borehole in Oroville, CA., show that ground-level s-wave velocity spectra at this location are a product of site effects. In the 6.25 to 50 Hz range studied, both the Cleveland Hill fault, through which the borehole was drilled, and the rock above it contribute to a substantial loss of s-wave energy. In first-order approximation, the average apparent s-wave quality factor, Q_s^a , along the well is 9. Across the fault zone the Q_s^a drops to a low of 3. Downhole, the seismograms can readily be separated into longitudinal and transverse components. Particle motion diagrams show that the s-arrival is made up of two differently polarized waves. This splitting is possibly an effect of wave propagation in the highly cracked and probably anisotropic rock of the region.

Introduction

A common feature of ground-level earthquake observations is that their velocity spectra start decreasing before the corner frequencies predicted by some models of the earthquake source [Brune, 1970]. For a given site, the frequency at which this "crash" occurs is not dependent on the size or distance of the earthquake [Frankel, 1982]. At recording sites near Oroville, for example, the spectra of different earthquakes may drop off at 20 Hz for one site and at 40 Hz for another [Hanks, 1982; Fletcher, 1980]. As a result, conclusions on the mechanics of Oroville earthquakes suffer from a degree of doubt.

At least two suggestions have been made to account for this variability in microearthquake velocity spectra. First, the velocity spectra may be a product of the material immediately (0.5 km) below the observation site [Frankel, 1982; Hanks, 1982]. Second, the earthquake source itself may be responsible for the missing frequencies [Archuleta et al., 1982; Aki, 1984]. These two mechanisms are not mutually exclusive and a combination of them may be needed for a full explanation of the observations. As evidence that at least the first mechanism is taking place at the Oroville site, we present some microearthquake s-wave velocity spectra recorded along a 0.5 km well at Oroville.

Oroville lies in the tectonically active foothills of the Sierra Nevada Mountains. The observation borehole was drilled through the cracked and faulted Smartsville ophiolite typical of this region [McJunkin, 1983; Moos et al., 1983]. In addition to affecting the spectra of local earth-

quakes, these rocks also complicate the particle motions of these events.

It is possible to separate seismograms recorded at the bottom of the well into relatively unmixed longitudinal (p-wave) and transverse (s-wave) components. At this depth, the s-arrival is composed of two differently polarized waves. These waves may represent the "splitting" known to exist in anisotropic rock [Crampin et al., 1984].

In a broader context, the results of the Oroville microearthquake-VSP experiment show the value of borehole seismometer arrays in studying tectonically active areas. Such arrays allow the recording of very small earthquakes, near-surface wave propagation effects, and depth-dependent apparent attenuation. These features are likely to be of value in the study of the seismic phenomena that precede and accompany larger earthquakes.

The Microearthquake-VSP Experiment

The Oroville borehole was drilled by the United States Geological Survey to study the Cleveland Hill fault, site of the 1975 Oroville earthquakes [Lahr et al., 1976; Anderson et al., 1983]. In 1983 the site was made available for cooperative experiments. In April of that year, we used hydraulic hole locks to deploy a recoverable array of vertical and 3-component seismometers into the borehole. The array was retrieved in September, after 4 months of full operation.

The seismometer array is shown schematically in Figure 1. The seismometers had natural frequencies of 4.5 Hz and each was shunted so as to produce the same degree of damping (0.7 of critical). Recording of seismic events was accomplished with 2 GEOS digital event recorders [Maxwell et al., 1983]. The recorders were set to trigger on Station 5 and to sample at 200 Hz/channel. To suppress 60 Hz pickup, a 42 dB/octave high-cut filter was applied at 50 Hz. To eliminate instrument-related DC offsets, an equivalent low-cut filter

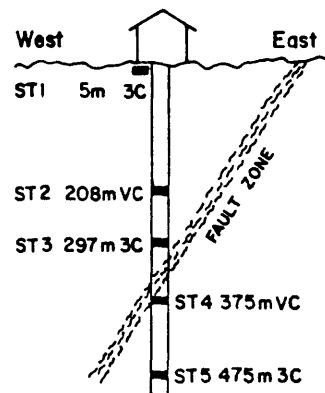


Figure 1. The Oroville VSP array as seen along the strike of the Cleveland Hill fault zone. Depth in meters, 3C=3-component, VC=vertical.

¹Now at Evergreen Geophysical Associates, Inc., Lakewood, CO.

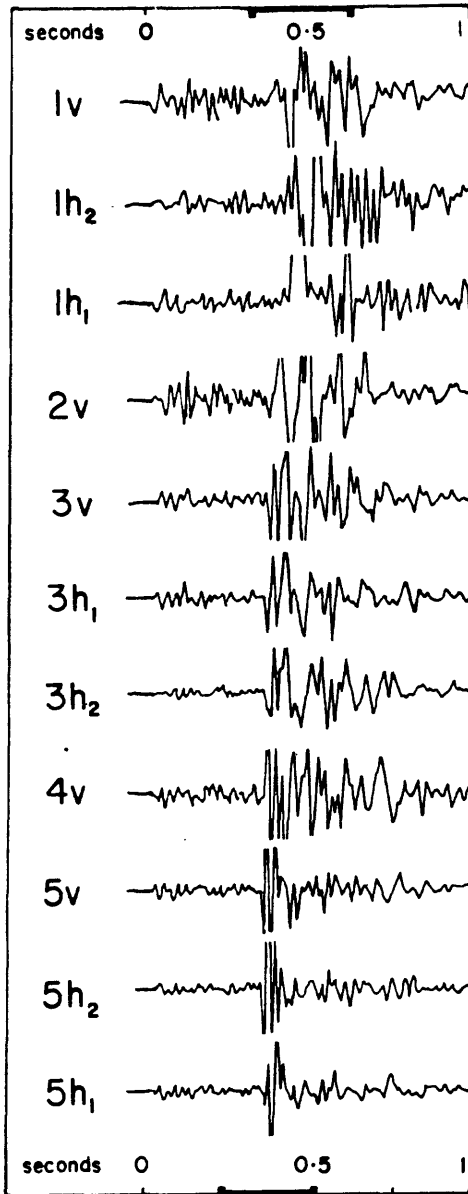


Figure 2. Seismograms for the J.D. 259 microearthquake shifted so that the p-waves are aligned. Brackets on the time axes show the earliest and latest windows used for the spectral analysis. Overlapping seismogram peaks have been omitted.

was applied at 3.125 hz during processing.

Over the 4-month period the array was operated, 11 microearthquakes and 19 other seismic events were recorded. Here, we discuss the $M_{\text{coda}}=0.4$ event of J.D. 259, a typical microearthquake. As seen in Figure 2, it was received with high signal-to-noise ratio at each station.

Depth-Dependent S-Wave Velocity Spectra

The s-wave velocity spectrum at Station 5 for the J.D. 259 event is shown in Figure 3a. In comparison to the seismic background and GEOS system noise, the signal-to-noise ratio of this spectrum at 50 hz is on the order of 150. Over the 6.25 to 50 hz band in which the raw data are reliable, the spectrum increases roughly with the first power in frequency. Such behavior is pre-

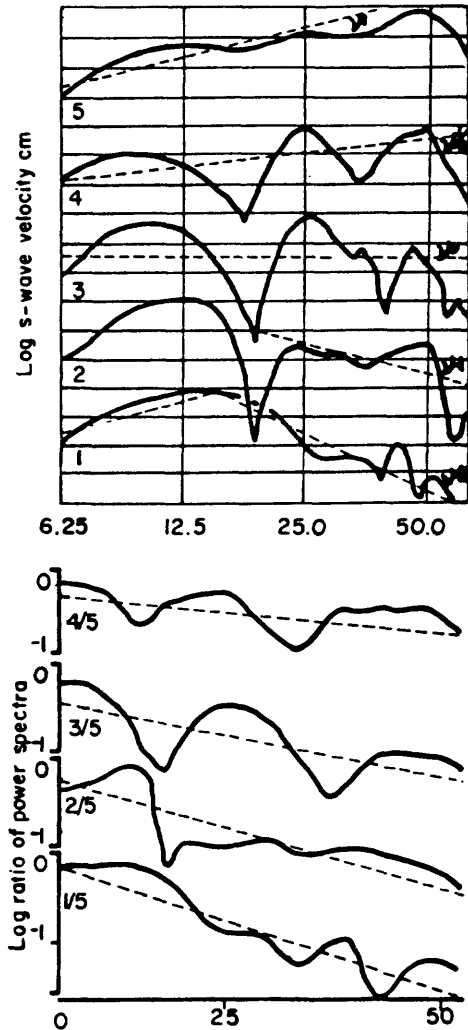


Figure 3. a. Log of the s-wave velocity spectra for the J.D. 259 as a function of depth. The grid lines are separated by factors of 2. Note the 48 db/octave high-cut filter at 50 hz. The spectra have been successively lowered for plotting. Thin dashed lines show slopes of ν^n , $-2 \leq n \leq 1$. b. Log of the ratios of the s-wave power spectra. The dashed lines show least-squares lines.

dicted by, for example, the Brune model of the earthquake source [Brune, 1970]. The latter model also suggests that the s-wave corner frequency of the J.D. 259 event should be roughly 70 hz, which is beyond the raw band-pass of our data (a 5 bar stress drop was assumed based on Fletcher, 1980).

The seismograms in Figure 2 seem to show a general loss of high-frequency s-wave energy with decreasing depth. The progressive character of this damping can be seen in the velocity spectra shown in Figure 3a and in the spectral ratios in

TABLE 1. Apparent attenuation between stations. *

Station	4/5	3/5	2/5	1/5	3/4	2/4	1/4	1/3	1/2
Q_s^a	11	7	7	9	3	9	8	8	9

* $Q_s^a = 2\pi \cdot \delta t \cdot s$, δt = s travel-time, s = slope

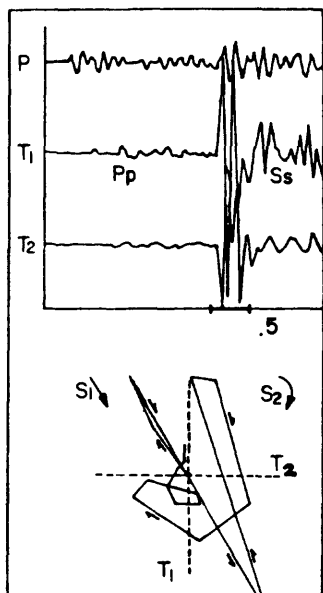


Figure 4. a. The longitudinal and transverse components at St. 5. T_1 and T_2 are the transverse components in the vertical and horizontal planes. The heavy line on the time axis marks the window of the s-wave hodogram. b. The s-wave hodogram.

Figure 3b. For comparison, the slopes of various powers of frequency, ν^n , are shown on the spectral plots. Likewise, least-squares fit lines are shown along with the spectral ratios. The loss of energy from the s-wave is clearly a function of frequency and position along the borehole. The velocity spectra also show signs of interfering waves. The effects of interference are evident in the notched character of the velocity spectra.

We have done preliminary modeling of the velocity spectra and their ratios, assuming 1D acoustic wave propagation and first-order attenuation theory. The results show that these simple theories do not accurately describe the observed data. For example, it seems that the Cleveland Hill fault and the weathering layer are zones of strong scattering, and thus zones of wave conversion and frequency-dependent damping.

Nevertheless, the models do establish that the spectral notches at 20 and 40 Hz are related to the 40 to 80 m low-velocity zone of the Cleveland Hill fault [Moos et al., 1983]. Also, to first order, the slopes of the least-squares lines fit to the spectral ratios give an estimate of the apparent quality factor Q_s^a along the borehole. The ratios in Figure 3b can be used to approximate the average Q_s^a between the bottom of the borehole and each station above it. The resulting Q_s^a values are listed in Table 1, and are comparable to ones found in shallow explosion studies of the upper crust [McDonal et al., 1958].

While the lowest Q_s^a occurs across the fault zone, it is the cumulative Q_s^a along the well that accounts for the ground-level spectrum. Viewing only the spectrum of Station 1, the apparent s-wave corner frequency of this microearthquake is 17 Hz. In effect, the high-frequency s-wave energy has crashed by the time it reaches ground level, so the spectrum at this level is not useful for estimating source parameters.

S-Wave Particle Motion

To help identify different arrivals in the seismograms, an attempt was made to rotate them into principal longitudinal and transverse components (aligned along the direct p- and s-waves polarization directions). This step was also aimed at detecting s-wave splitting due to anisotropy [Crampin, 1984]. Since neither the location of event J.D. 259 nor the orientation of the seismometers was known, the rotation was done in a step-wise fashion, station by station.

First, the horizontal b_1 and b_2 components were rotated about the vertical v component so that the first oscillations of the b_1 component fit, in a least squares sense, those of the v component. (The resulting seismograms are the best fit vertical, radial, and horizontal motions.) Next, the vertical and b_1 component were rotated around b_2 until the first oscillations of b_1 vanished. The resulting components were relabeled P , T_1 , and T_2 . In a uniform isotropic halfspace, these components should have only p and Rayleigh waves, s and Rayleigh waves, and s waves, respectively.

This procedure was most successful at Station 5. As seen in Figure 4a, the transverse components have relatively little energy in the time window between the p- and s-wave arrivals. The notable exception is the arrival marked Pp, corresponding to the theoretical arrival time of the p-wave reflection from ground level. This phase is seen on the T_1 component because, when reflected, the p-wave motion is no longer entirely in the P direction. A similar geometry applies to the reflected s-wave, labeled Ss in the figure.

The transverse particle motion of the direct s-arrival is plotted in the polarization diagram (hodogram) of Figure 4b. The time window of the diagram is shown in Figure 4a and small arrows point out the relative sense of motion. The nearly linearly-polarized first motion, labeled s_1 , is interrupted after about one cycle (25 msec) by a second, relatively large s-wave, s_2 , producing elliptic motion.

The origin of s_2 is not clear. Based on travel times and amplitudes, it does not appear to be a reflection from the fault nor a converted wave from ground level. (Phases of the latter sort, which have been described by Evans, 1984, can be found in the s-wave hodograms of Station 1.) If the s wave followed a path similar to that of s, their average speed would differ by about 4%. Further, similar waves from other Oroville microearthquakes show that this splitting of the s-arrival is not unique to the J.D. 259 event.

Discussion

In this first, short research note on the Oroville microearthquake-VSP experiment, the VSP seismometer array and the s-wave motion of the J.D. 259, 1983, $M_{\text{coda}} = 0.4$ microearthquake are described. The array had 5 stations located at various depths in a 0.5 km-deep borehole. The J.D. 259 event was reliably recorded on the array out to a frequency of 50 Hz, where the s-wave signal-to-noise ratio was 150.

As a function of depth, the s-wave velocity spectra of this microearthquake show a significant loss of high-frequency s-waves with decreasing depth. To first order, the apparent Q_s^a associated

with this loss has an average value of 9, with a low of 3 across the Cleveland Hill fault. Downhole, the s-wave corner frequency is above 50 Hz; at ground level it occurs at about 17 Hz.

The particle motion of the J.D. 259 event shows that the s-arrival is made up of two differently polarized waves. The two waves are of comparable amplitude and the second wave has an apparent speed 4% slower than the first.

Perhaps the safe conclusion to draw from these data is that the cracked and faulted rocks of Oroville strongly affect s-waves. The apparent Q_s^a found for the borehole includes the intrinsic losses, scattering losses, and wave interference produced by these structures. The complex polarization of the s-arrival may represent evidence for the splitting of this phase by anisotropy.

It is less safe but more tempting to suggest that, in tectonically active regions, the upper half km or so of crust controls the high-frequency s-wave energy observed at ground level. This conclusion does not rule out special source effects in the high-frequency spectrum; it simply makes them more difficult to observe. The mechanism of the apparent attenuation remains unknown. However, the lower velocities and lateral heterogeneities present near ground level are sure to make s-wave scattering an important factor in addition to intrinsic attenuation.

It is equally tempting to identify the second s-wave as a product of crack-induced anisotropy [Crampin, 1981]. Evans [1984] has argued that this type of anisotropy should be a ubiquitous feature in faulted regions of the crust. Both the time separation and the change in polarization of the two s-waves are within the theoretical and observational bounds reported for s-wave splitting [Crampin et al., 1984]. Demonstration of this possibility for Oroville, however, is incomplete and must await further work.

A final point is simply to underscore the potential of microearthquake-VSP measurements. As shown here, microearthquake-VSP can provide direct evidence on subsurface ground motion, for either scientific or engineering purposes. Moreover, given the low noise conditions downhole, the quality of such data is high, even for microearthquakes as small as the one discussed here.

Acknowledgements. The work of many helping hands can be found in the Oroville experiment. T.L. Heney, University of Southern California, loaned the VSP equipment. Numerous people at the USGS, Menlo Park, deserve recognition: R. Borchardt, G. Jensen, and J. Van Schaack for the GEOSs; E. Cranswick and D. Moos for the analysis software; M. Zoback for access to the borehole; S. Wegener and T. Denham for help in the field; and W. Ellsworth and F. Fisher for the 3-component seismometers. The polarization analysis was suggested by S. Crampin. The authors also thank A. Lindh, USGS, Menlo Park, and the reviewers.

References

Aki, K., Asperities, barriers, characteristic earthquakes and strong motion prediction, *J. Geophys. Res.*, 89, 5867-5872, 1984

- Anderson, R. N., M. D. Zoback, S. H. Hickman, J. H. Healy, In-situ stress and physical property measurements in the Cleveland Hills fault zone, Oroville, California, *EOS Trans. AGU*, 64, 834, 1983.
- Archuleta, R. J., E. Cranswick, C. Mueller, and P. Spudich, Source parameters of the 1980 Mammoth Lakes, California, earthquake sequence, *J. Geophys. Res.*, 87, 4595-4607, 1982.
- Brune, J. N., Tectonic stress and the spectra of seismic shear waves from earthquakes, *J. Geophys. Res.*, 75, 4997-5009, 1970.
- Crampin, S., A review of wave motion in anisotropic and cracked elastic-media, *Wave Motion*, 3, 343-391, 1981.
- Crampin, S., Evaluation of anisotropy by shear-wave splitting, *Geophysics*, in press, 1984.
- Crampin, S., E. M. Chesnokov, and R. G. Hipkin, Seismic anisotropy - the state of the art: II, *Geophys. J. R. Astron. Soc.*, 76, 1-16, 1984.
- Evans, R., Anisotropy: a pervasive feature of fault zones, *Geophys. J. R. Astron. Soc.*, 76, 157-164, 1984.
- Evans, R., Effects of the free surface on shear wavetrains, *Geophys. J. R. Astron. Soc.*, 76, 165-172, 1984.
- Fletcher, J. B., Spectra from high-dynamic range digital recordings of Oroville, California, aftershocks and their source parameters, *Bull. Seismol. Soc. Am.*, 70, 735-755, 1980.
- Frankel, A., The effects of attenuation and site response on the spectra of microearthquakes, *Bull. Seismol. Soc. Am.*, 72, 1379-1402, 1982.
- Hanks, T. C., F_{max} , *Bull. Seismol. Soc. Am.*, 72, 1867-1880, 1982.
- Lahr, K. M., J. C. Lahr, A. G. Lindh, C. G. Bufo, and F. W. Lester, The August 1975 Oroville earthquakes, *Bull. Seismol. Soc. Am.*, 66, 1085-1099, 1976.
- Maxwell, G. L., E. G. Jensen, R.D. Borchardt, J. P. Fletcher, R. McClearn, J. R. Van Schaack, and R. E. Warrick, GEOS, *EOS Trans. AGU*, 64, 775, 1983.
- McDonal, F. J., F. A. Angona, R. L. Mills, R. L. Sengbush, R. G. Van Nostrand, and J. E. White, Attenuation of shear and compressional waves in Pierre shale, *Geophysics*, 23, 421-439, 1958.
- McJunkin, R.D., Geology of the Bangor quadrangle and data from a deep well into Smartsville ophiolite, Butte County, California, *California Division of Mines and Geology, open file report*, pp. 1-29, 1983.
- Moos, D., S. H. Hickman, and M. D. Zoback, Sonic velocity and fracture patterns or distribution in a well drilled through the Cleveland Hills fault, Oroville, California, *EOS Trans. AGU*, 64, 834, 1983.

P. E. Malin, Department of Geological Sciences, University of California Santa Barbara, Santa Barbara, CA, 93106

J. A. Waller, Evergreen Geophysical Associates, 927 West Alameda St., Lakewood, CO, 80226

(Received January 2, 1985;
accepted January 16, 1985.)

APPENDIX A. 7.

Summary of Geodetic Survey Measurements near Parkfield

P. Segall, W. Prescott, R. Stein, N. King, R. Harris and A. Lindh

SUMMARY OF GEODETIC SURVEY MEASUREMENTS NEAR PARKFIELD

P. Segall, W. Prescott, R. Stein, N. King, R. Harris, A. Lindh
 U.S. Geological Survey
 Menlo Park, CA 94025

I. TRILATERATION DATA

A. 1966 Coseismic Period

From 1959 to 1969, the California Department of Water Resources (CDWR) observed 13 lines that span the rupture zone of the 1966 Parkfield earthquake (heavy lines in Figure 1). CDWR used a Model 2A Geodimeter, and estimated refractivity using end-point (and often mid-point) measurements of pressure, temperature, and humidity. Coseismic line length changes are calculated assuming that the preseismic and interseismic changes are linear functions of time with constant rate.

The coseismic line length changes can be used to determine the fault slip during the 1966 earthquake. The length, width, and depth of the fault surface are estimated from the distribution of aftershocks and surface offset following the earthquake. The aftershocks defined a nearly vertical plane extending 30 km SE of the mainshock epicenter, and from the surface to a depth of 10-12 km (Eaton et al., 1970). The concentration of aftershocks at depths of 2-4 km and 8-10 km (Eaton et al., 1970), together with the inferred absence of surface slip immediately following the shock (Smith and Wyss, 1968), have led most investigators to model the mainshock as extending from a depth of 2-4 km to 8-10 km, with lengths ranging from 20 to 40 km.

Once the dislocation geometry is specified, the coseismic line length changes are used to solve for least-squares estimates of fault slip. Although the geodetic data are insensitive to the details of the slip distribution, they do yield a reasonably well-constrained estimate of the seismic moment.

Table 1 lists results for a number of possible uniform slip models. In each case the northwest end of the dislocation is fixed at the mainshock epicenter.

Table 1: Coseismic Models

Length (km)	Depth (km)	Slip (cm)	$M_0 \times 10^{25}$ (dyne-cm)	Reduced χ^2
25	3-8	106 ± 9	4.0	2.3
30	3-8	91 ± 8	4.1	1.8
35	3-8	86 ± 7	4.5	1.3
30	2-10	59 ± 5	4.2	1.7
30	4-10	99 ± 8	5.3	1.5

In general models with slip between 2-4 km and 8-10 km provide acceptable fits to the data. Dislocations significantly shorter than 30 km tend to have larger misfits than those with lengths of 30-35 km. (In theory, models with reduced chi-squared values greater than 2.0 are rejectable at the 98% confidence level. Longer slip zones are permitted by the geodetic data, but are inconsistent with the aftershock distribution.

In the final analysis it is the seismic moment that is best determined by the geodetic observations. The minimum moment consistent with the data is 4×10^{25} dyne-cm. This is in reasonably good agreement with estimates of $0.9-2.1 \times 10^{25}$ dyne-cm obtained from surface waves by Tsai and Aki (1968). The larger moment estimate obtained from the geodetic data may be partially due to post-seismic slip. Note that the procedure used to estimate the coseismic line length changes tends to incorporate post-seismic effects into the "coseismic" change.

B. Interseismic Period (1966-1985)

During the 1970's, the California Division of Mines and Geology (CDMG) took over and expanded the CDWR network. CDMG used a Model 8 Geodimeter, and estimated refractivity from end-point pressure measurements and aircraft-flown profiles of temperatures and humidity. Since the mid 1970's the network has been measured by the U.S. Geological Survey. USGS uses a Geodolite, and refractivity is estimated using end-point pressure measurements and aircraft-flown profiles of temperature and humidity. The measurement procedure is described in detail by Savage and Prescott (1973). Four small-aperture networks, spanning the San Andreas fault within the larger network, have been measured by USGS since the middle 1970's: Red Rock, Parkfield, Jacks Ranch, and Cholame (Figure 2). These measurements are made with a Hewlett-Packard 3800/3808A, or occasionally with a Geodolite. Refractivity is estimated using end-point measurements of pressure, temperature, and humidity. The procedure is described in detail by Lisowski and Prescott (1981).

1. Reobservation Schedule

- a. The 80 aircraft-flown (Geodolite) lines illustrated in Figure 1 will be surveyed once a year.
- b. 31 of the near-fault short aperture lines will be surveyed semi-annually.
- c. The four "monitor" lines from station Red Hill will be surveyed quarterly.

C. Errors

The standard deviation of a single line-length measurement σ is given by

$$\sigma = [a^2 + b^2 L^2]^{1/2}$$

where a is fixed error, b is proportional error, and L is line length.

Savage and Prescott (1973) found that this equation with $a = 3 \text{ mm}$ and $b = 2 \times 10^{-7}$ adequately described repeated U.S.G.S. Geodolite measurements.

A histogram of normalized residuals, calculated from linear fits to the monitor net data are shown in Figure 4. The observed residuals are nearly normally distributed, however, large residuals are found to occur more frequently than would be predicted by a normal distribution (see table with Figure 4).

D. Detection Threshold for Red Hill Monitor Net

The observed distribution of residuals can be used to calculate the amount of fault slip that is required to produce a change in line length that would be larger than expected random errors at a given confidence level. Results are shown in Table 2 assuming that the slip is localized to the 1966 rupture surface. We conclude that buried slip with a moment equal to 25% of the 1966 earthquake would produce a line length change on Park-Red Hill that occurs randomly only 3.2% of the time.

Table 2: Detection Threshold for Red Hill Monitor Net

	Park - Red Hill		Cotton - Red Hill	
	2σ (89%)	3σ (96.8%)	2σ (89%)	3σ (96.8%)
Minimum Detectable Slip on 1966 Rupture Surface (cm)	14	21	38	57
Equivalent Moment ($\times 10^{25}$ dyne-cm)	0.75	1.1	2.0	3.0

E. Determination of Interseismic Slip Distribution on the San Andreas Fault

Two models of the distribution of interseismic slip on the Parkfield section of the San Andreas fault have been proposed in the literature. In the first model, (Lindh and Boore, 1981) the 1966 rupture surface, extending from 3 to 8-10 km depth, is locked between earthquakes. In this model the observed surface creep extends only to the top of the locked zone ($\sim 3 \text{ km}$). In the second model (Slawson and Savage, 1983) the surface creep rates were extrapolated through the seismogenic zone. Both models assume approximately 30 mm/yr below the 1966 rupture zone (10-12 km depth) and rigid block motion at a comparable rate northwest of Middle Mountain.

We have inverted the interseismic trilateration data for the distribution of average fault slip-rate. The data consists of average rate of line length change for all lines with four or more measurements (the 31 heavy lines in Figure 5). The slip rate at the surface is chosen to be consistent with creepmeter alignment array, and small-aperture trilateration data (Figure 6). Slip northwest of Middle Mountain is assumed to

accumulate at 25 mm/yr from the surface to a depth of 14 km. Below 14 km the slip rate is taken to be 30 mm/yr everywhere.

Figure 7 illustrates our "starting model". The slip distribution is one that both satisfies the constraints and in some sense minimizes the slip-rate gradient. Figure 8 shows an "improved model", which satisfies the previous constraints and fits the trilateration data in a least squares sense. Comparing Figures 7 and 8 it is clear that the line-length data require low interseismic slip rates in the 1966 rupture zone. To this extent the data favor the locked rupture zone model as opposed to models involving significant amounts of buried interseismic slip.

II. LEVELING DATA

A 51-km-long network of leveling lines has been resurveyed periodically since 1979. The network is well located to measure the vertical deformation that accompanies strike slip displacement during Parkfield earthquakes. Since 1984 we have concentrated on measurement of potential pre-seismic deformation in the vicinity of the 1934 and 1966 epicenters. A 10-km-long line oriented perpendicular to the San Andreas fault at the town of Parkfield has been surveyed four times since 1980 (Park 1 on Figure 9). Two new lines in the vicinity of Middle Mountain, totalling 32 km in length, were monumented and surveyed in April 1984 and were resurveyed in March 1985 (Park 2A and 2B in Figure 9). A 24-km-long line running parallel to the San Andreas between Parkfield and Cholame, and a 17-km-long line oriented perpendicular to the fault at Cholame have not been resurveyed since 1983.

Profiles of the Park 1 leveling route topography and elevation change for the period 1980 to 1985 are shown in Figure 10. The data show a marginal down to the west tilt, however, this is only marginally significant given the expected random errors for the line (dashed envelope on Figure 10).

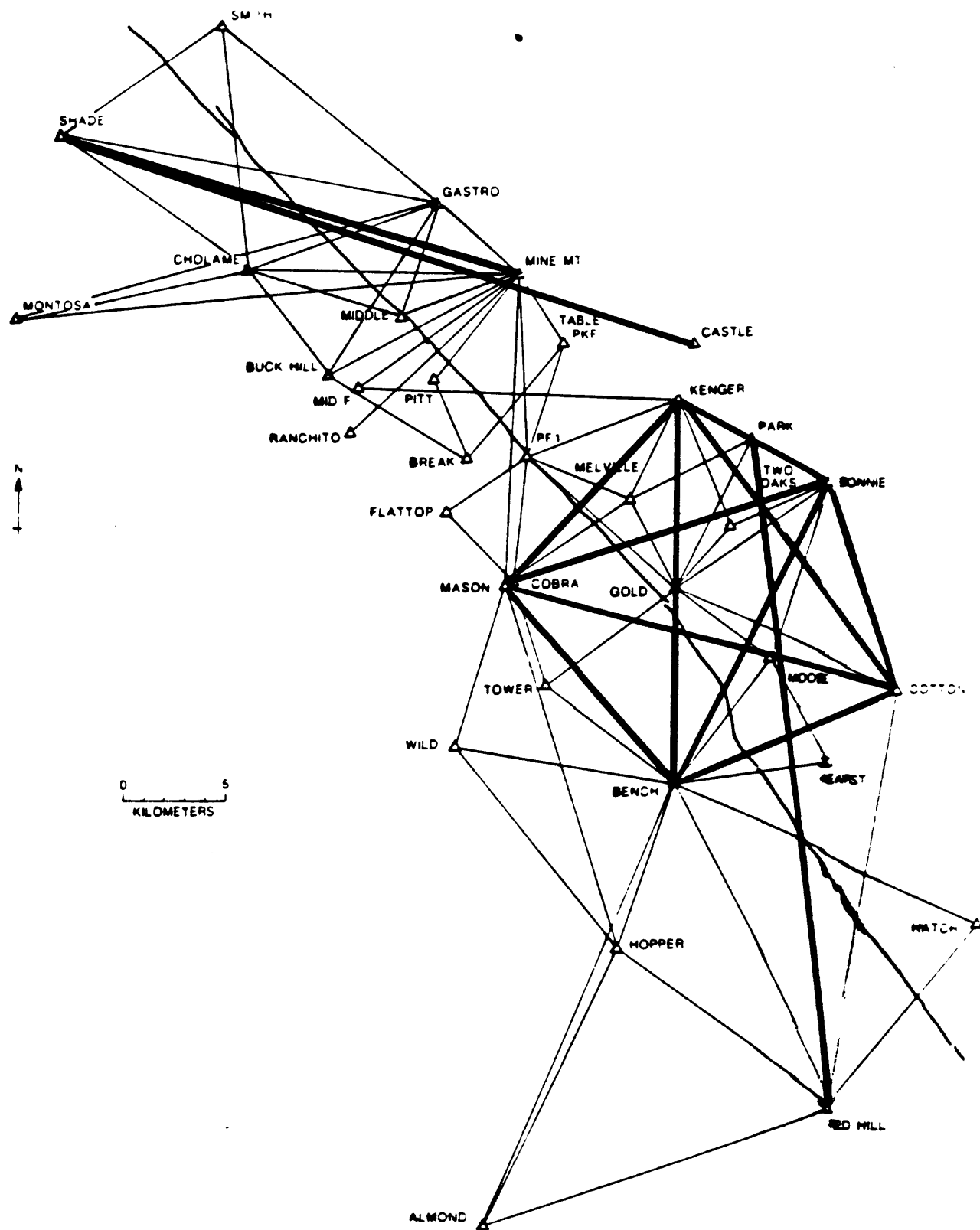
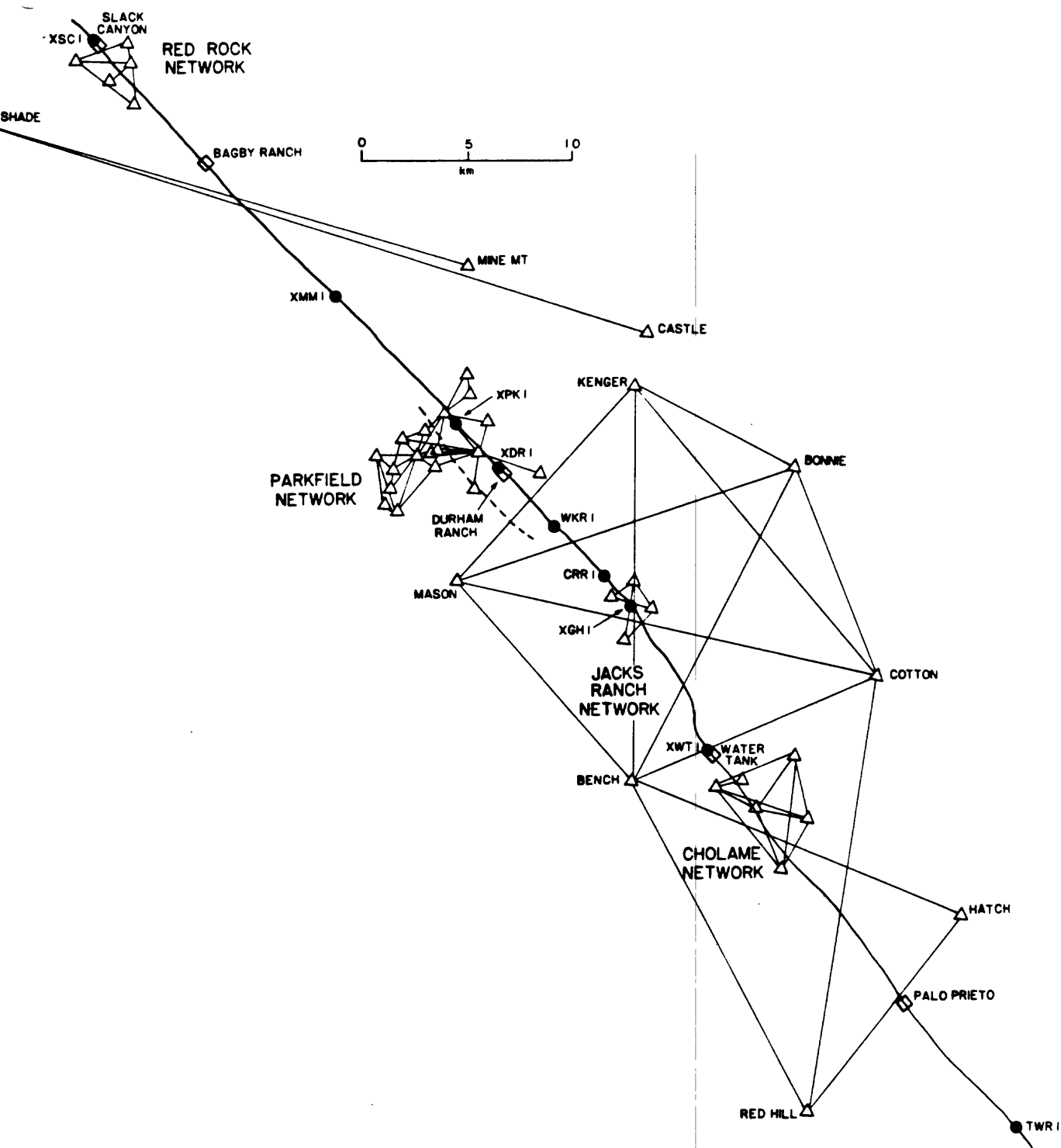
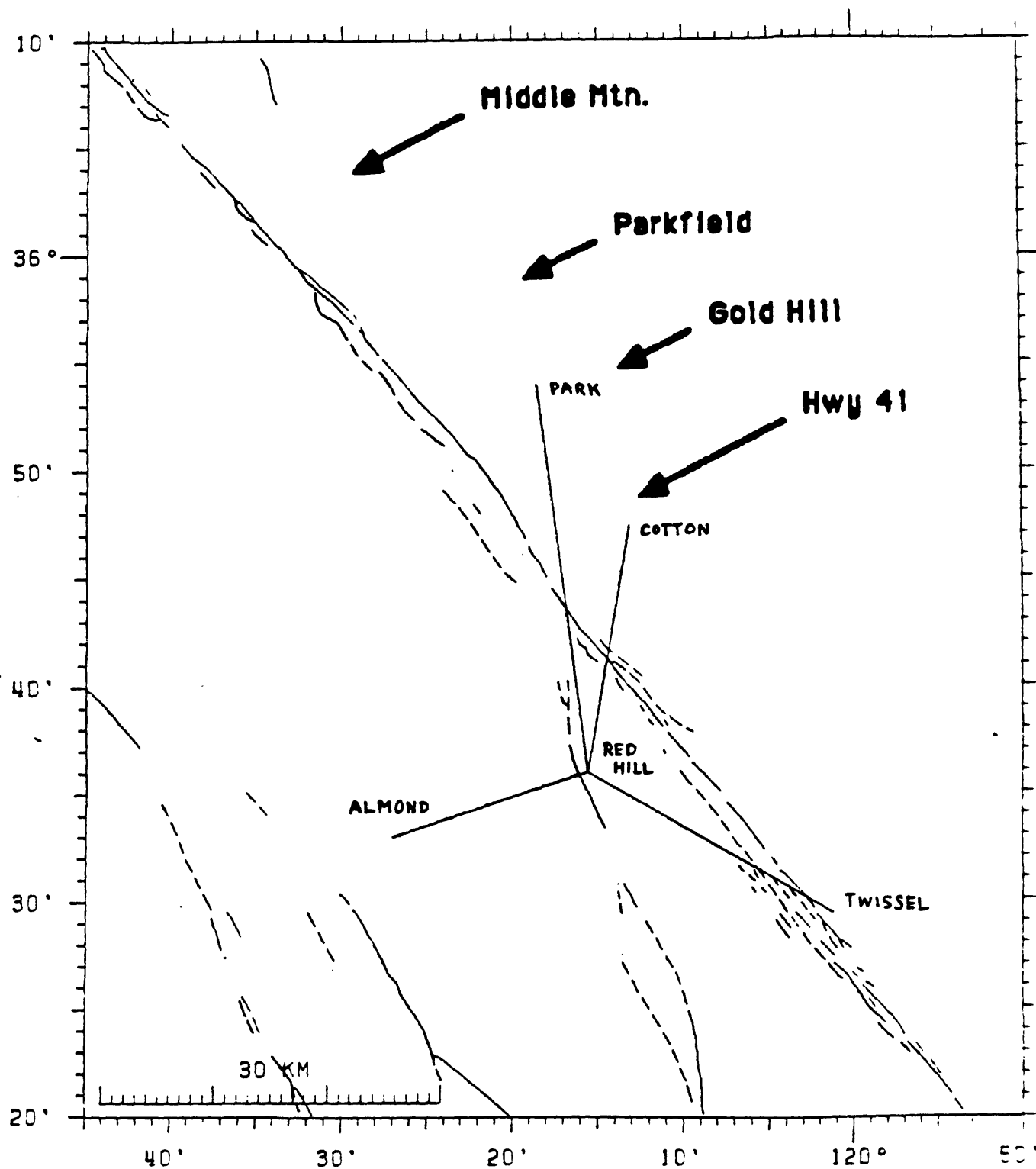
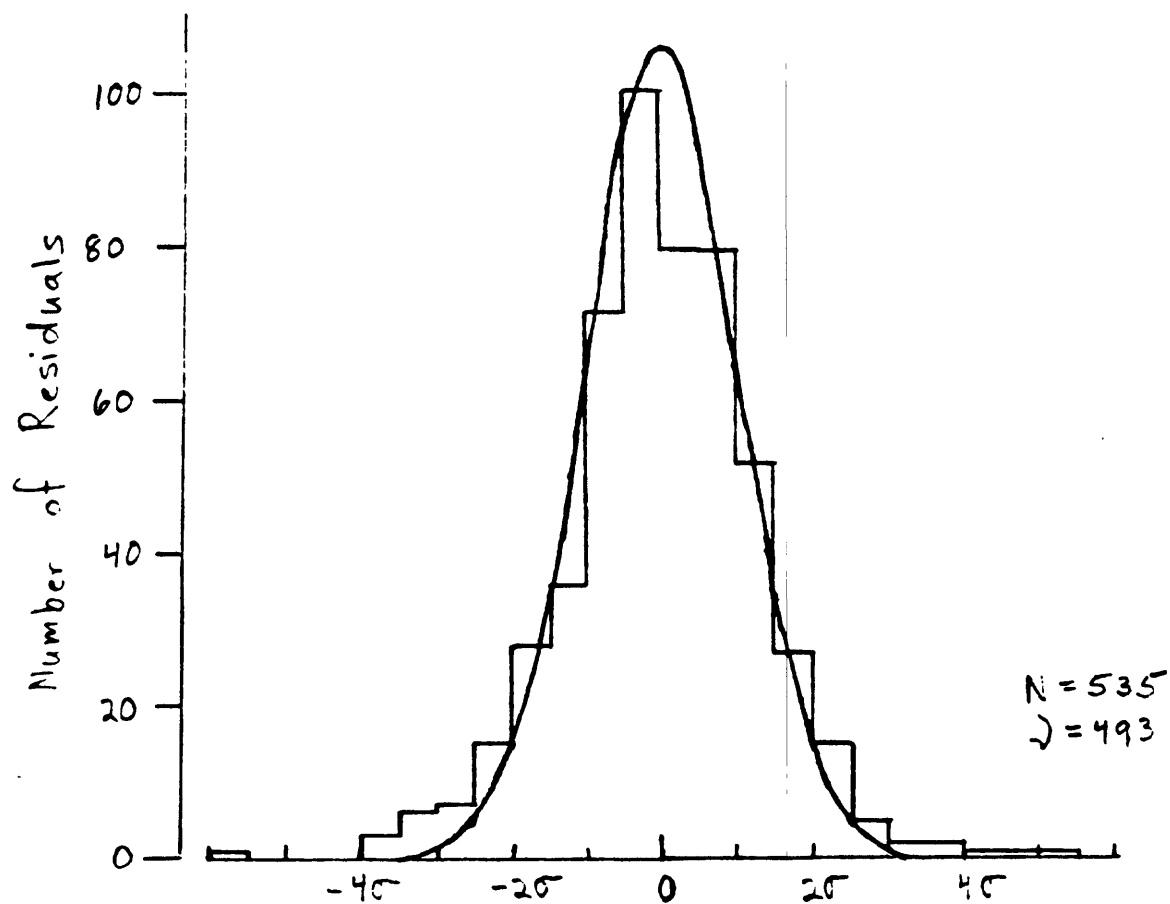


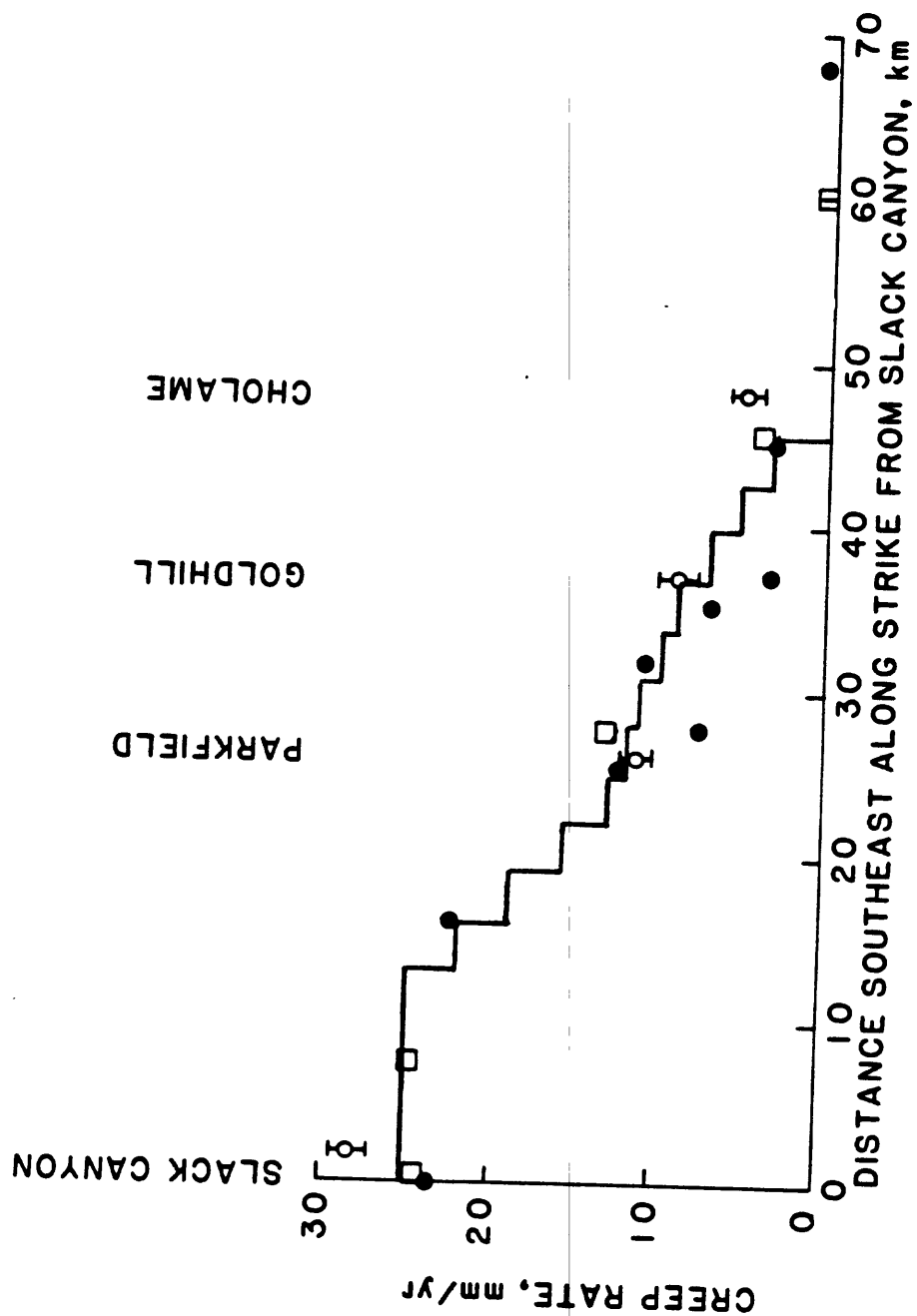
Fig 2

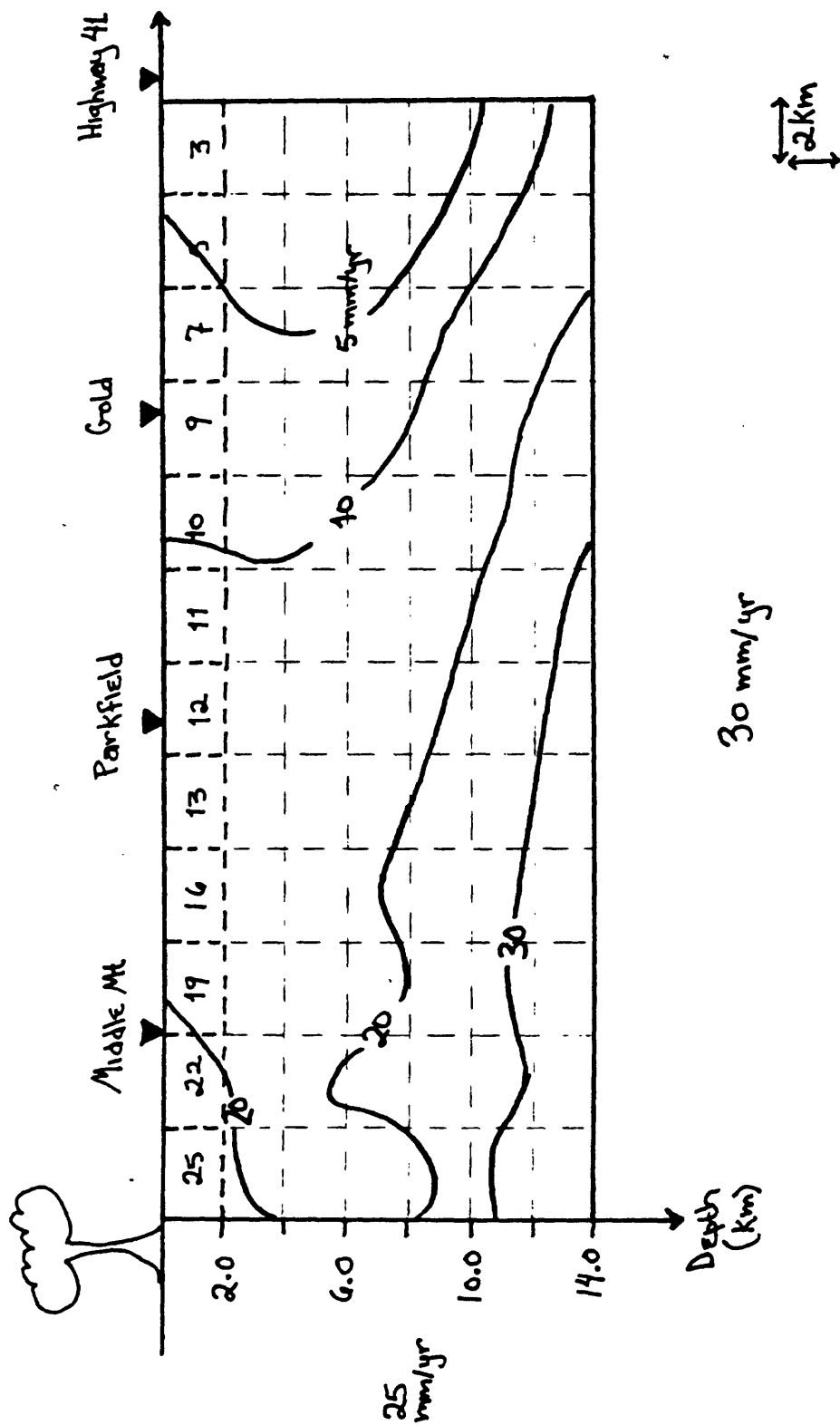






<u>OBSERVED DISTRIBUTION</u>	
<u>Half width</u>	<u>Area %</u>
2σ	89.0
3σ	96.8
4σ	99.2
5σ	99.6





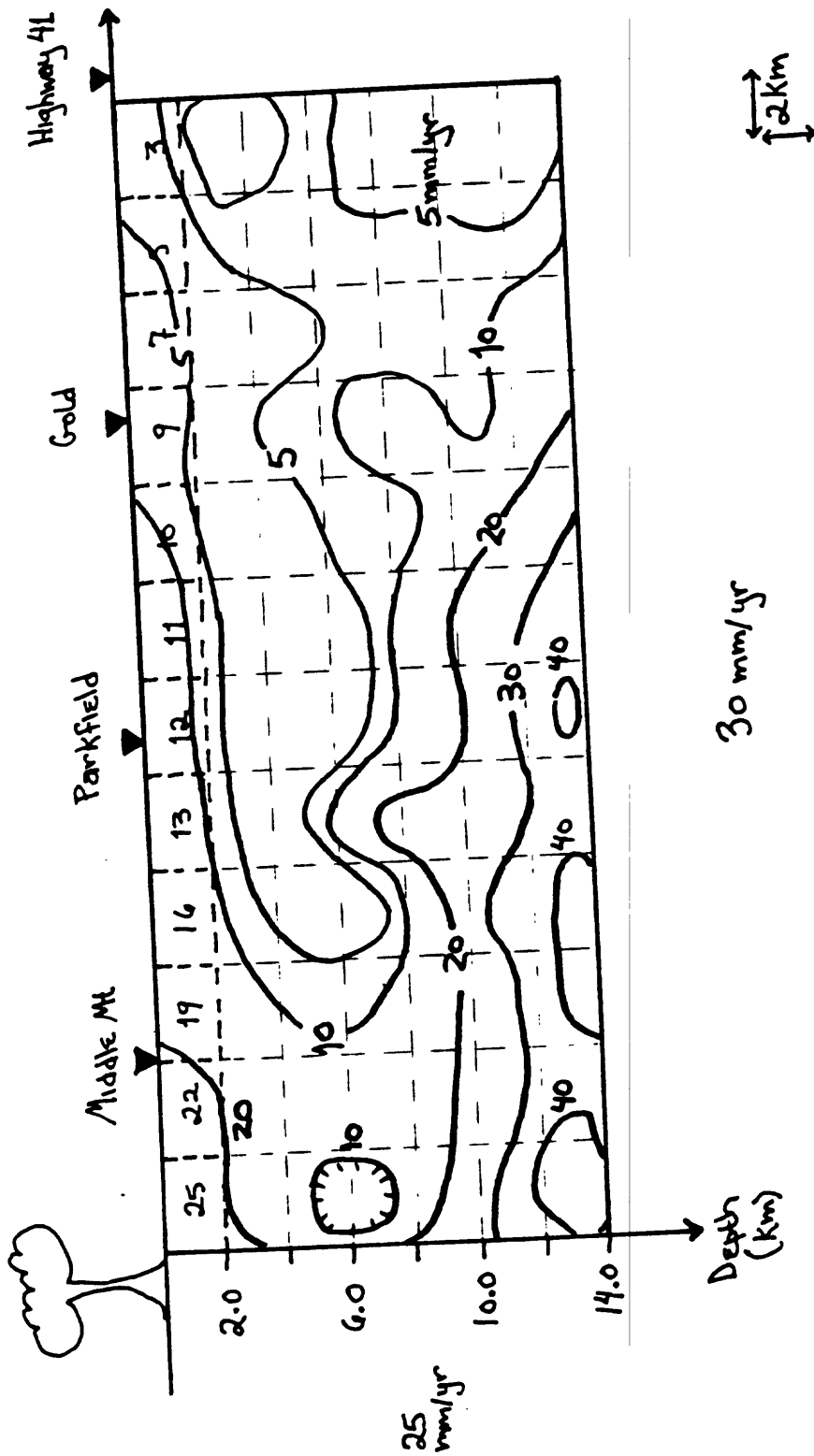
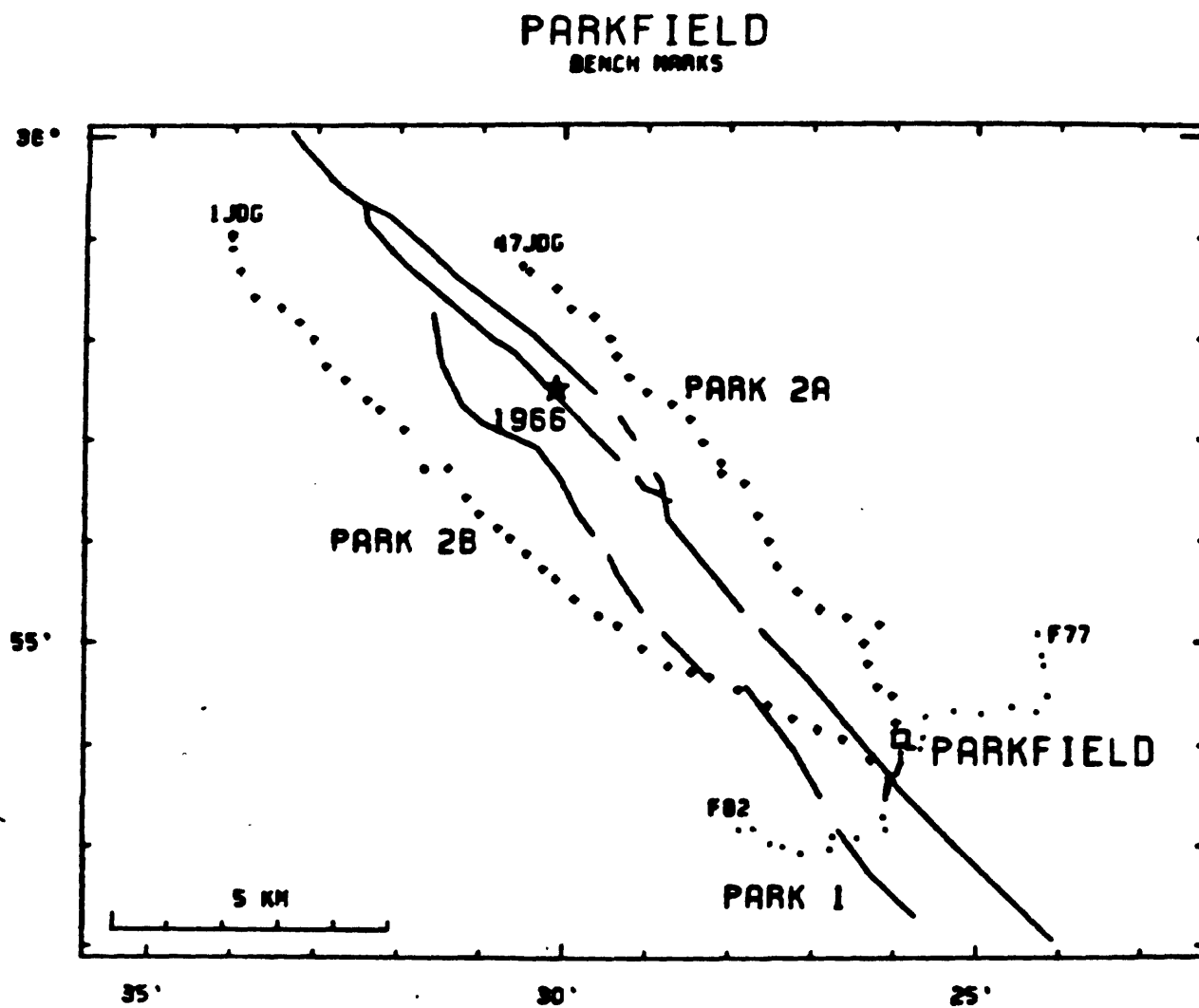
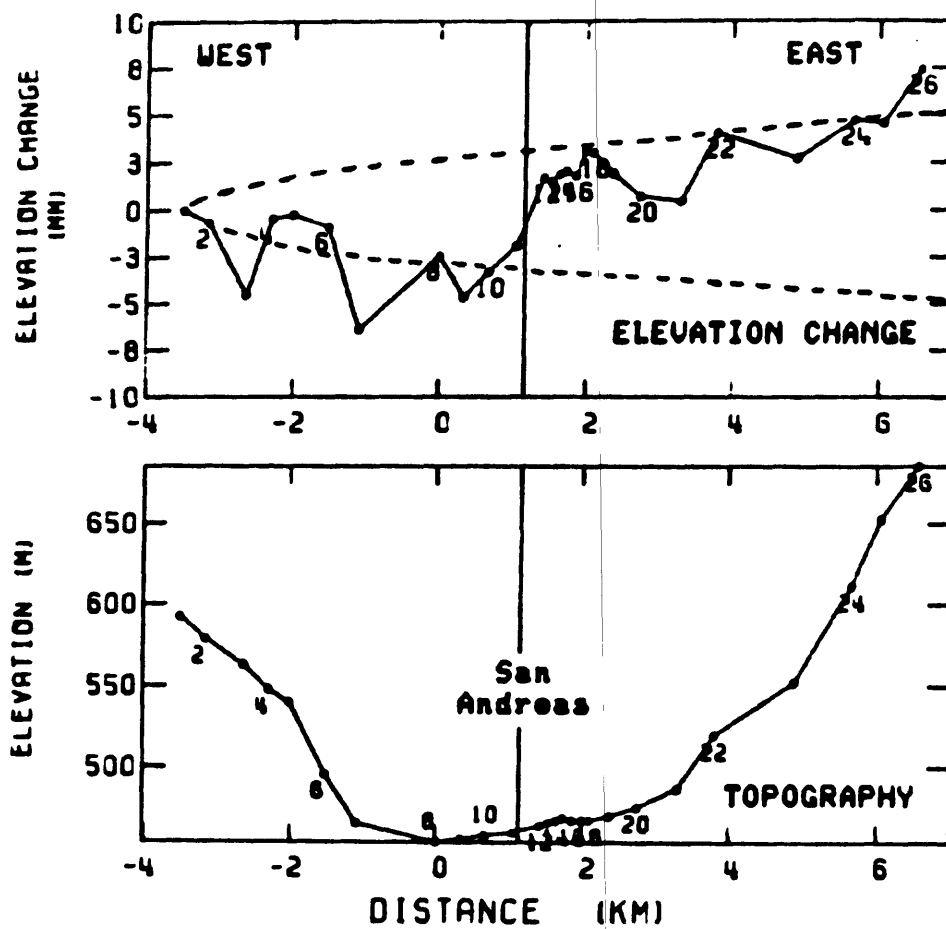


Figure 9



PARKFIELD 1

1985/MAR - 1980/FEB



APPENDIX A. 8.

Two-Color Laser Strain Monitoring in the Parkfield Region

R. O. Burford and L. E. Slater

TWO-COLOR LASER STRAIN MONITORING in the PARKFIELD REGION

R.O. Burford

Office of Earthquakes, Volcanoes, and Engineering
U.S. Geological Survey
Menlo Park, California 94025.

and

L.E. Slater

CIRES, University of Colorado
Boulder, Colorado 80309

The Parkfield 2-color laser strain-monitoring system consists of a central observatory facility at Car Hill, 1.4 km SSE of Parkfield, surrounded at present by 20 reflector sites at ranges between 1.5 and 9.2 km (Figure 1). The Car Hill observatory houses the 2-color laser transmitter/receiver plus its supporting electronics and a small computer, whereas the reflector sites consist only of passive telescope devices. The 2-color laser instrument uses mixed red (helium-neon, 6329A) and blue (helium-cadmium, 4416A) laser sources, each modulated at a frequency of about 3 gigahertz, to measure distance variations to each reflector within a particular modulation wavelength (~ 5 cm peak-to-peak, round-trip basis). The path-integrated differential effect of atmospheric refraction (density) on red and blue wavelengths is detected and is used to correct the transit-time of the red light. Metrological data obtained at Car Hill and a nominal constant range to the target reflector are entered into the onsite computer at the beginning of each measurement. The system is programmed to average range determinations over 10-second intervals and to accumulate the resulting 10-second values for at least 4 minutes, if possible, thereby accumulating 20 or more range readings for each recorded measurement. A mean value and a standard deviation are then calculated for all the 10-second averages accumulated during the 4- to 5-minute monitoring period. After rejection of readings failing to meet a limit of $\sigma < 1.5$ mm, typical errors for 20- to 30-sample data points vary between about ± 0.55 mm (~ 4 -km range) and ± 0.76 mm (~ 6 -km range). Considering the amplitudes of typical short-term length fluctuations of unknown origin in each data set, the practical level of strain resolution (simple extension) over intervals of 1 month or so is about ± 0.2 ppm.

Twelve lines were monitored during the past year (site names underlined in Fig. 1). Length measurements to permanent reflector sites CREEK, HOG-S, LANG and MASON-W were started by late July, 1984, to MID and MID-E by late August and to BARE, CAN, MEL-S, PITT and TABLE by early October. Measurements to the portable reflector at BREAK were conducted on November 8, 1984, and on March 20, 1985. Permanent reflector facilities were recently completed at NORM, EAST, FLAT, GOLD-NW and TODD (July, 1985), and another permanent site will be established at BENCH. Initial measurements to the 5 new permanent sites await the delivery of additional reflective telescopes. As for station BREAK, lines to JUMP and SLOPE will be measured only occasionally when occupied with a portable reflector. A number of additional sites of this type may be added as needed.

Measurements to permanent reflectors are attempted about 3 times each week. However, successful measurements are recorded much less frequently on several of the more difficult lines. Moreover, there have been periods of as long as a few weeks when system malfunctions or adverse atmospheric conditions have prevented the acquisition of reliable data, but to date, none of the instrument down-times have resulted in demonstrable offsets of apparent ranges.

Average length values composed of less than 20 ten-second samples or with standard deviations of greater than ± 1.5 mm are not included in final plots or as input for strain analysis. Time-series displacement and strain results are obtained by running various programs using the

files containing filtered data. Plots of all filtered data obtained to date for lines to permanent reflector sites are shown in Figure 2 (MID2=MID after unknown offset for new reflector). Details of these data since April 1, 1985 are shown in Figure 3.

High readings during April thought to be due to system instability were removed from these displays. From July 1984 through January 1985, E-W trending lines were extending (HOG, LANG, MELVILLE, and TABLE), while N-S and NW-SE trending lines were either stable or were extending at very low rates (BARE, CAN, CREEK, MASON, and MID). The line to MID-E showed strong extension between November and February. This pattern reversed during early February, indicating onset of areal contraction (negative dilatation). Following the passage of slip activity by about May 20, trends on most of the lines have been relatively flat.

Rapid contraction on the line to MID-E occurred between April 21 and May 9, possibly owing to 5 mm right-lateral slip on the main fault along the Middle-Mountain section. Lines to BARE and CAN show similar signals. Lines to MASON, CREEK, MELVILLE, and TABLE show a contractional pulse with maximum values developing on about May 4, followed by equal or greater extension lasting until about May 20. These signals may have resulted from right-lateral slip of the order of 5 mm propagating southeastward through the network area.

Results of a simple fault-slip, strain model used to calculate average slip and strain histories for the past 11 months are shown in Figure 4. Dextral simple shear (tensor value) accumulated at a nearly constant rate of ~ 1 ppm/yr until March, 1985, when the rate dropped to nearly zero. Resolved shallow slip (modeled as occurring between 0 and 1.5-km depth, but not significantly different at 0 to 6.5-km depth) indicates episodic shallow yielding on the main fault with high slip rates from the onset of monitoring through September, 1984, and again since about the beginning of April, 1985. The latest onset of increased slip rate corresponds to the onset of near-zero dextral-shear rate, indicating that slip, even though modeled as shallow, may nevertheless be deep enough to effectively reduce strain accumulation (a case for near rigid-block translation). The slip rate is ~ 1 cm/yr. Average slip rates during the two seasonal (?) episodes are approximately 2.7 mm/month. The recent increase in slip rate and corresponding decrease in rate of dextral shear are accompanied by a reversal of trend in apparent areal dilatation (+2.3 ppm/yr to -2.9 ppm/yr). This occurred mainly as a reversal of trend in the component of extensional strain normal to the main fault. The fault-parallel extensional component shows a similar pattern, but at much reduced amplitude such that both the maximum change and the cumulative value do not differ significantly from zero.

FIGURE CAPTIONS

Figure 1. Map of the Parkfield 2-color laser network showing traces of the 1966 surface breaks within the San Andreas fault zone. Solid rays designate lines to permanent reflectors that are monitored frequently. Dotted rays designate lines to portable reflector sites that will be measured about once a month. Underlined site names indicate the 12 lines measured during 1984 (11 permanent sites plus BREAK). Distances from CAR to BREAK and all longer lines except TODD were measured on 10/24/84 with the Geodolite system.

Figure 2. Line lengths from CAR to the 11 permanent reflector sites as repeatedly resolved by the 2-color laser system (filtered data). Variations in resolved distances and error bars are plotted in millimeters.

Figure 3. Line lengths from CAR to the 11 permanent reflector sites from March 15 through May 31, 1985 (filtered data).

Figure 4. Results of model of uniform strain combined with laterally uniform slip on the San Andreas fault through the entire 2-color network. a) Slip constrained between surface and 1.5-km depth. b) Slip constrained between surface and 6.5-km depth.

PARKFIELD 2-COLOR NETWORK

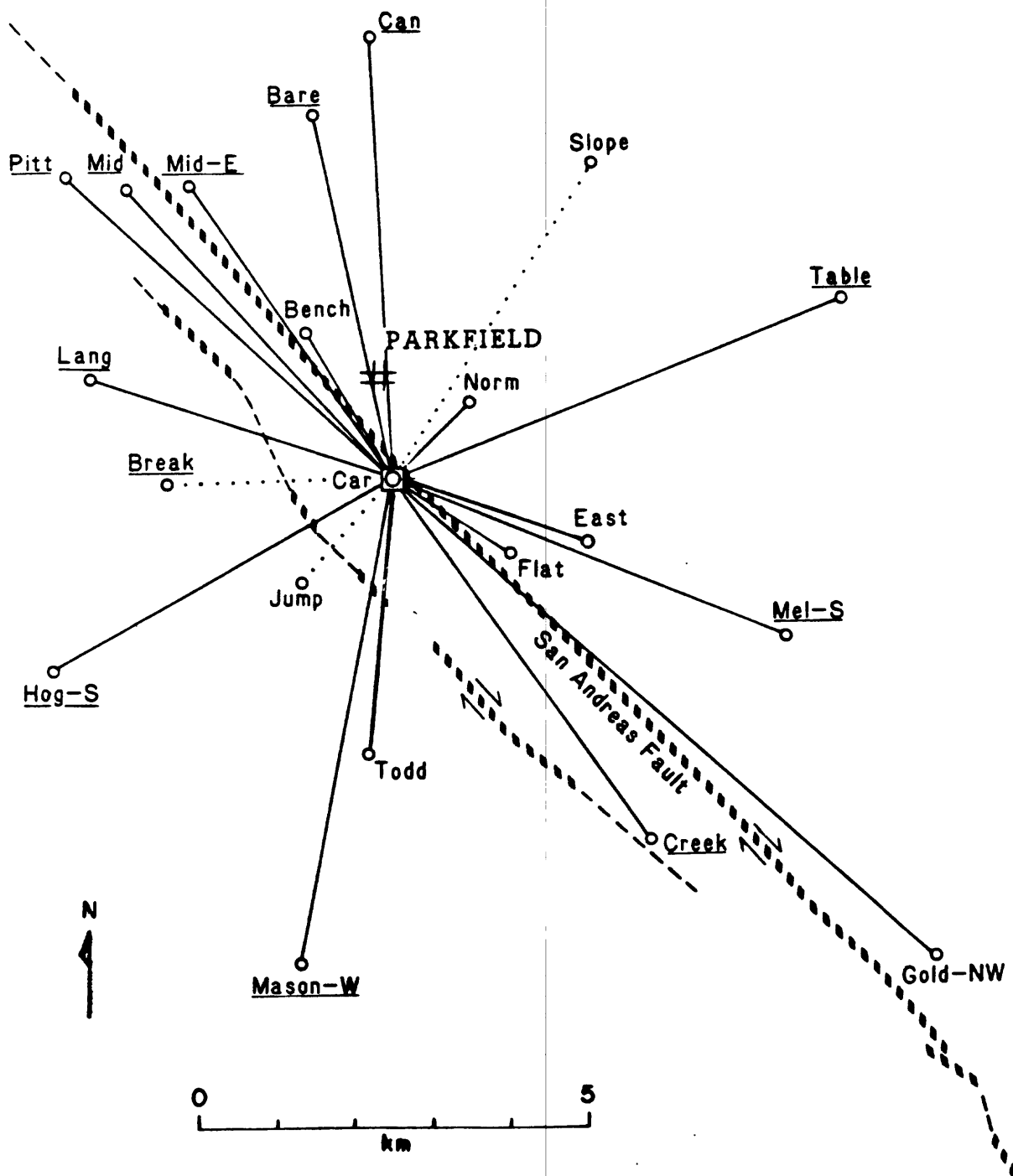


Figure 1.

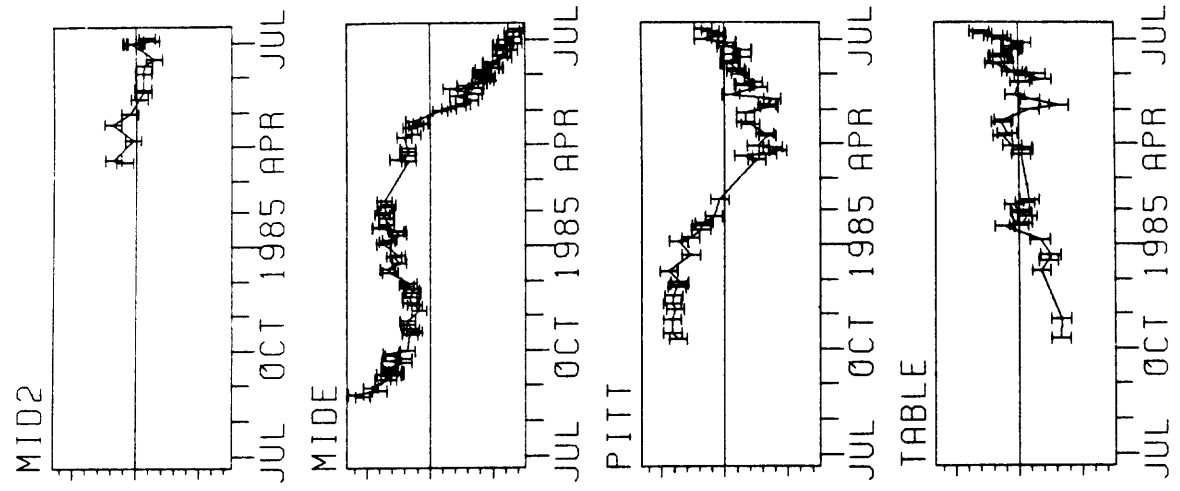
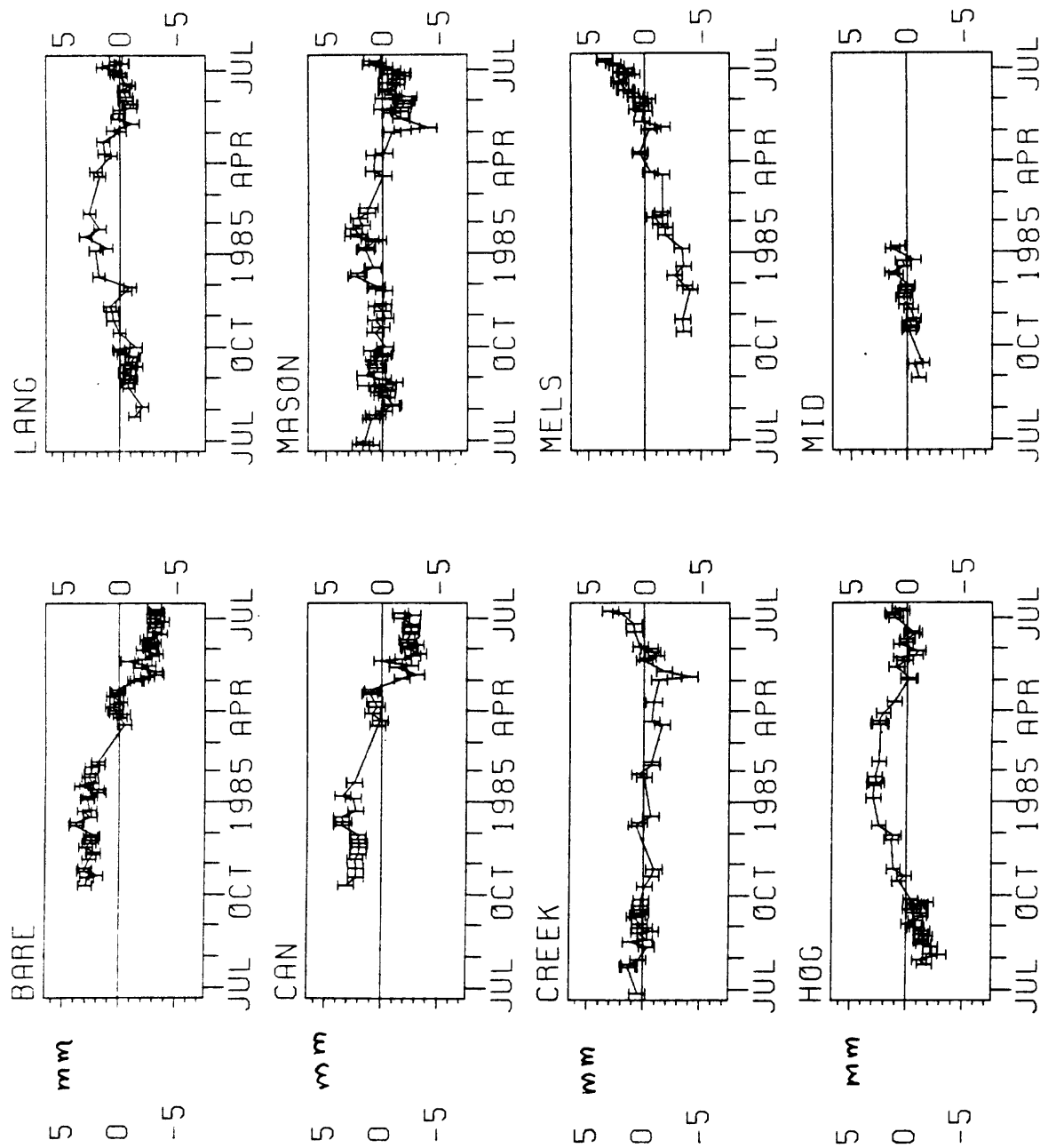


Figure 2.

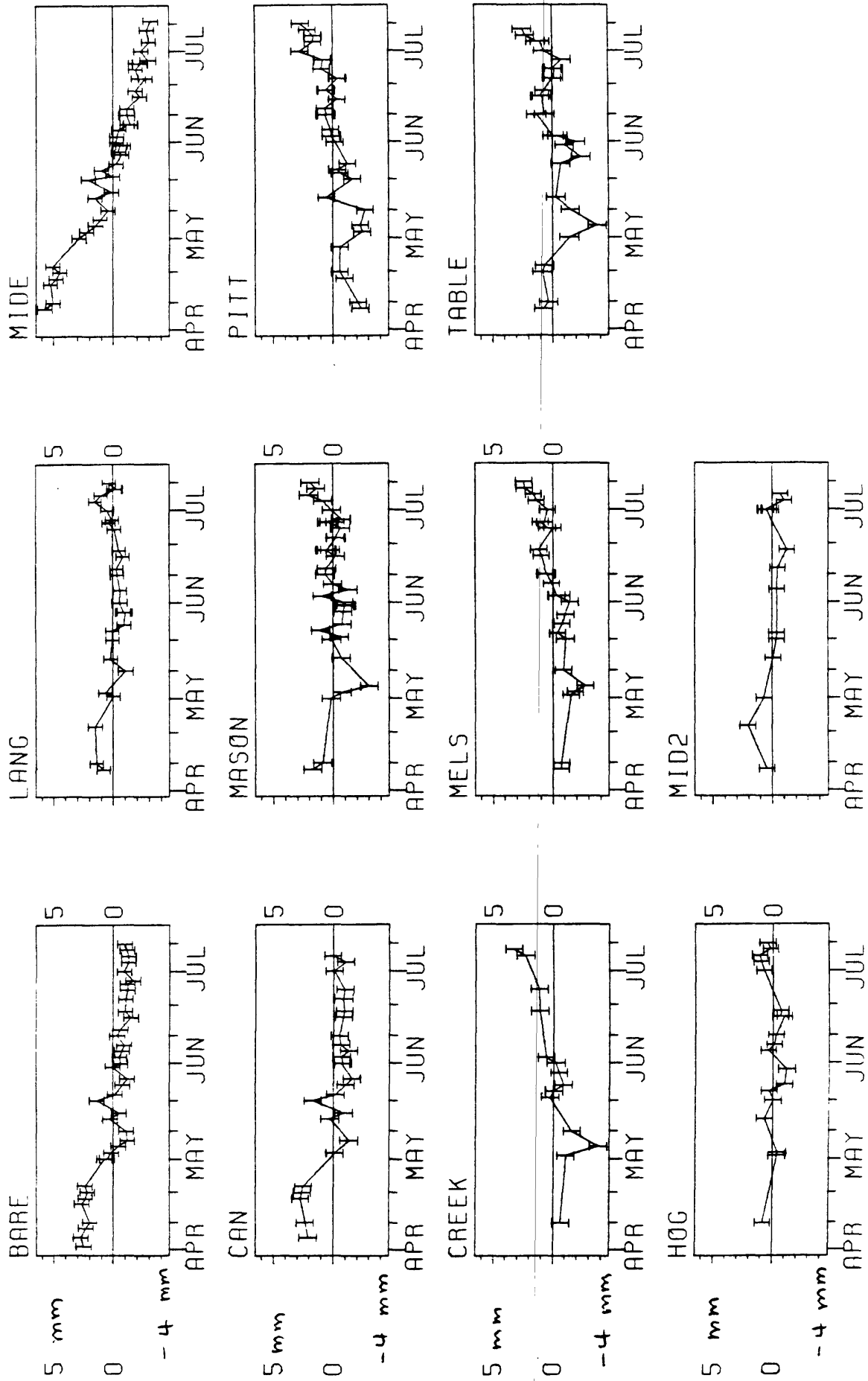
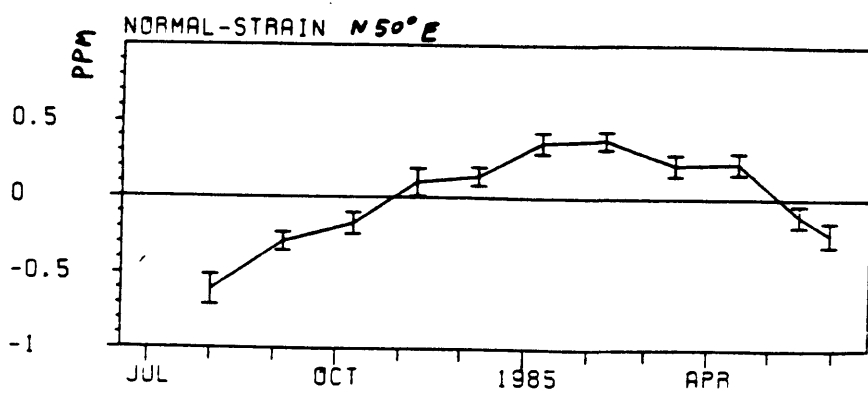
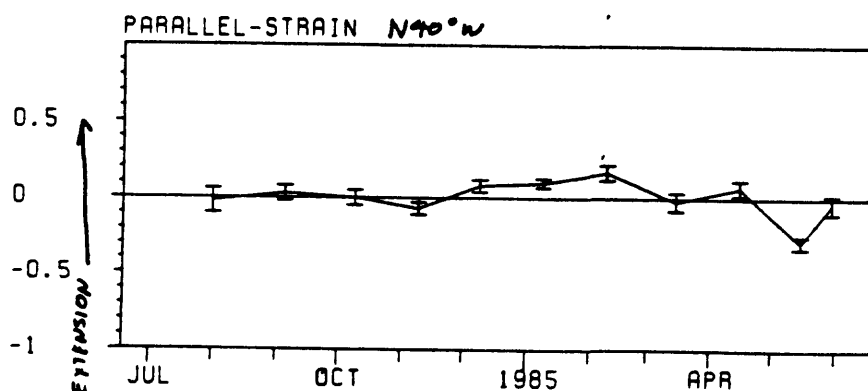
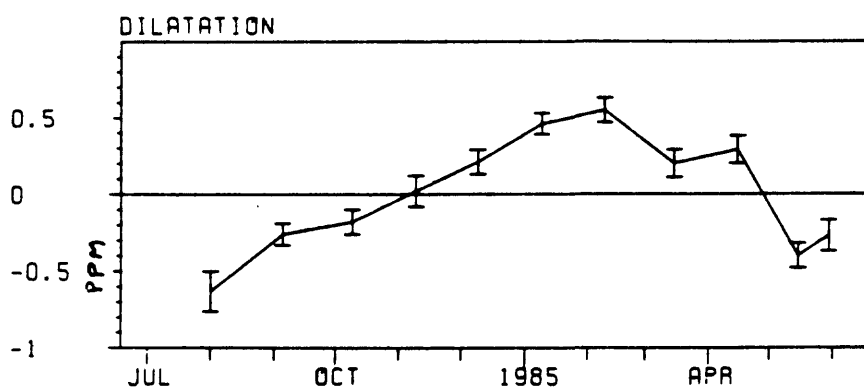
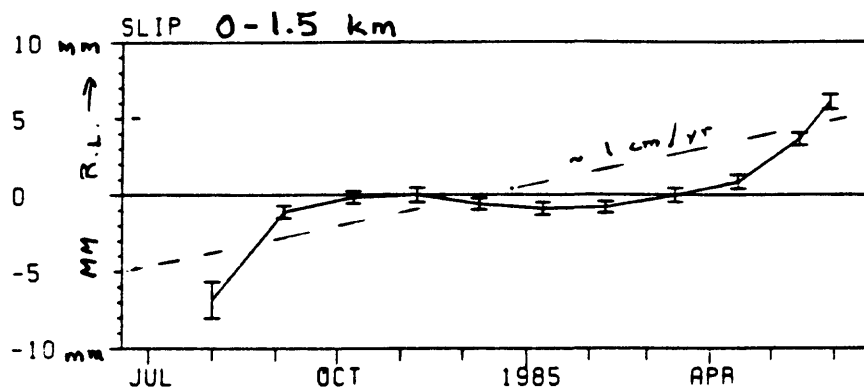
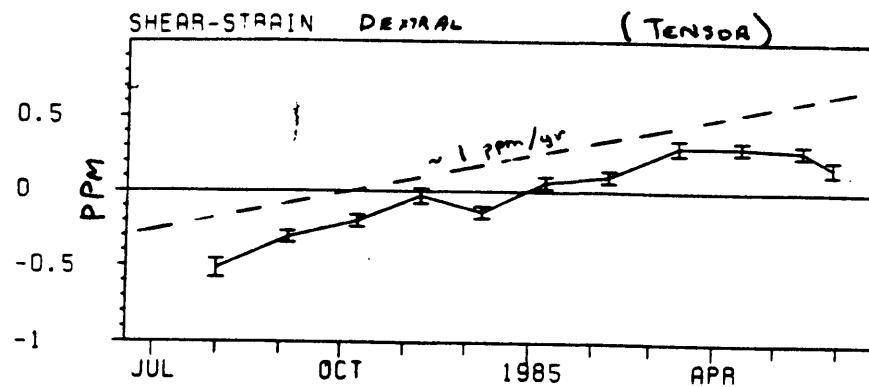


Figure 3.



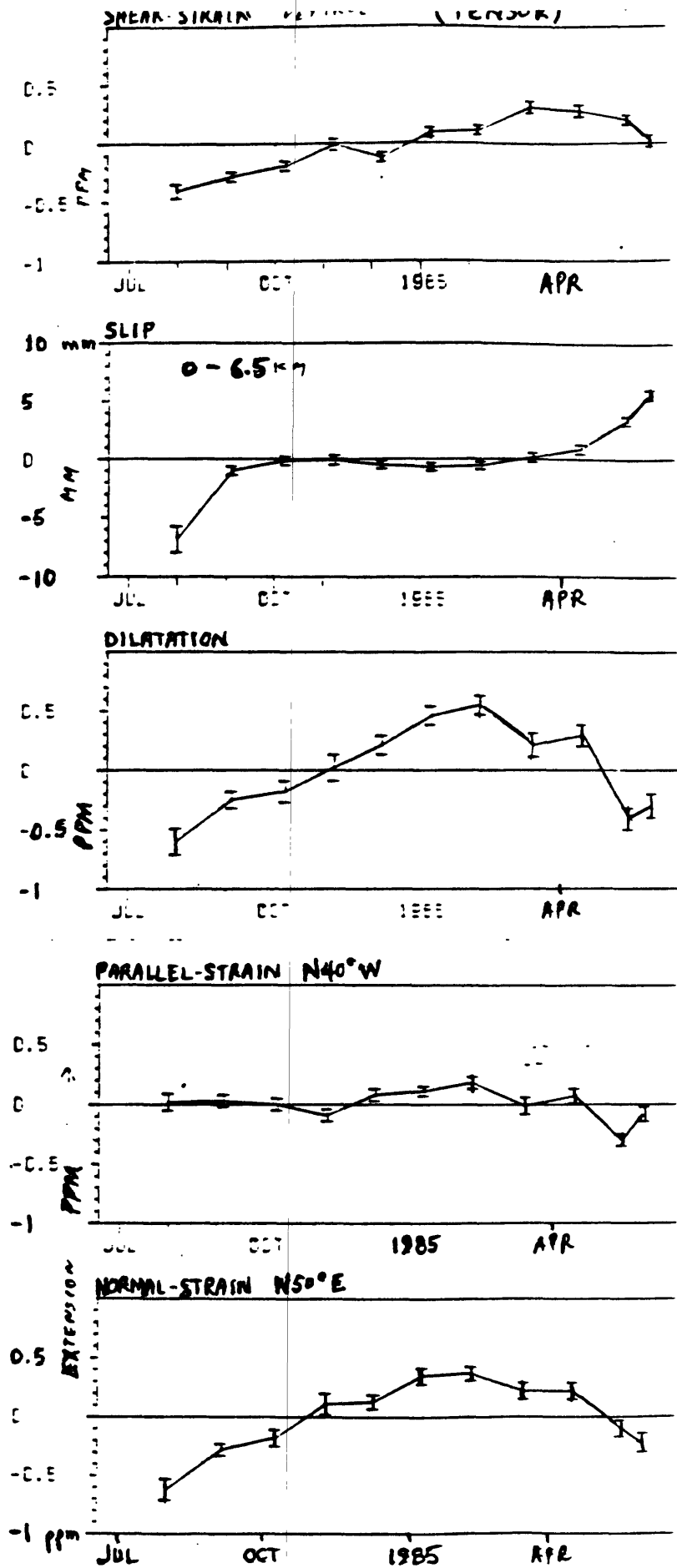


Figure 4 b.

TWO-COLOR LASER STRAIN MONITORING in the PARKFIELD REGION

R.O. Burford

Office of Earthquakes, Volcanoes, and Engineering
U.S. Geological Survey
Menlo Park, California 94025.

and

L.E. Slater

CIRES, University of Colorado
Boulder, Colorado 80309

FIGURES NOT CITED IN TEXT:

Figure 5. Comparison of dilatometer record from Gold Hill, site 1a, with length changes on line Car Hill to Mid-E, 12/1/84 through 7/9/85, the 2-color line most sensitive to fault slip and/or close-in, shallow strain.

Figure 6a. Comparison of creep record from XMM1 creepmeter, 5.6 km NW of 2-color reflector site Mid-E and ~ 10 km NW of Car Hill, with inverted length change record for 2-color line to Mid-E.

Figure 6b. Same comparison as for 6a, with XMM1 record detrended.

Figure 6c. Same comparison as for 6a, with XMM1 record detrended on short-term base and smoothed.

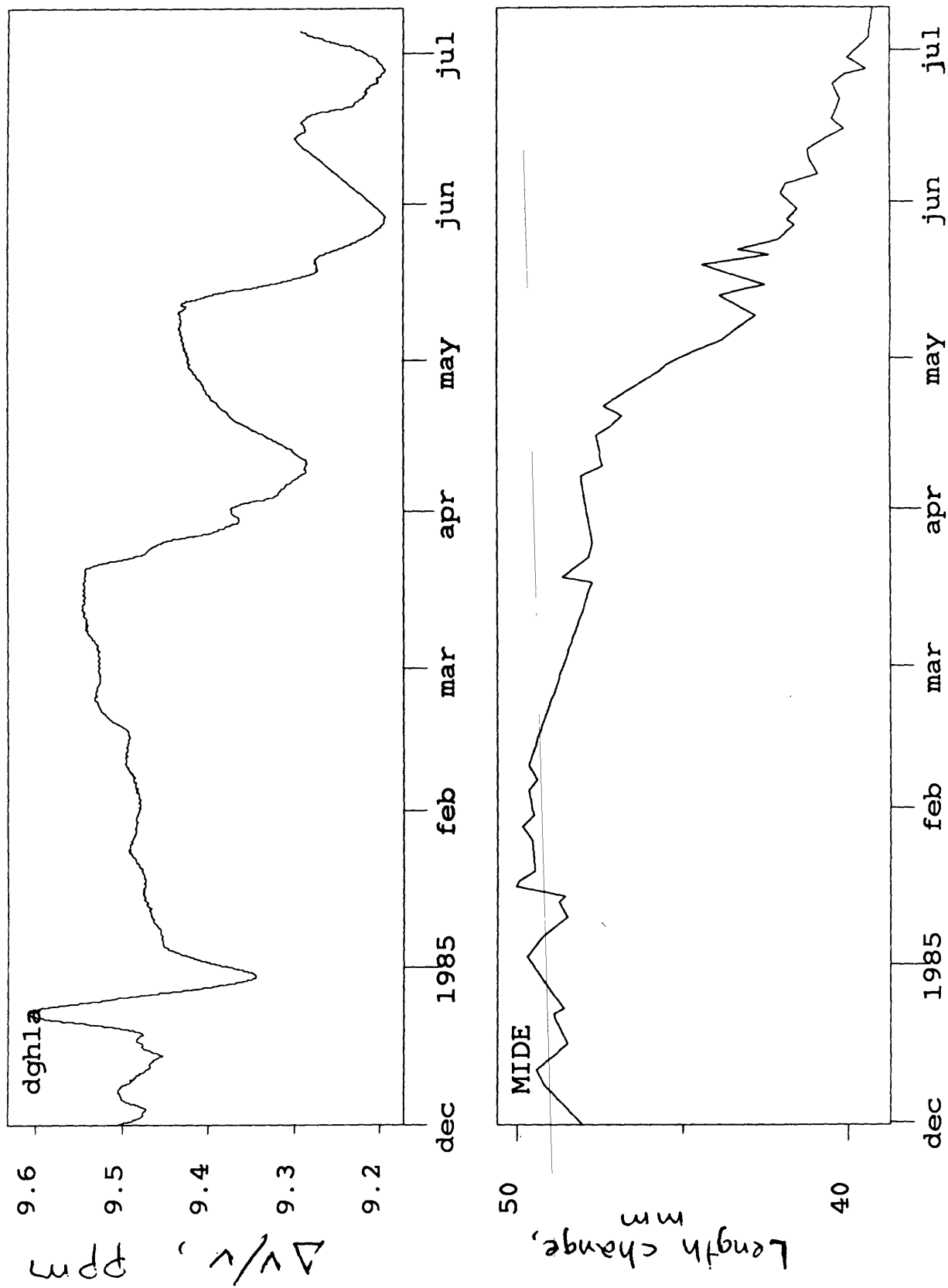


Figure 5.

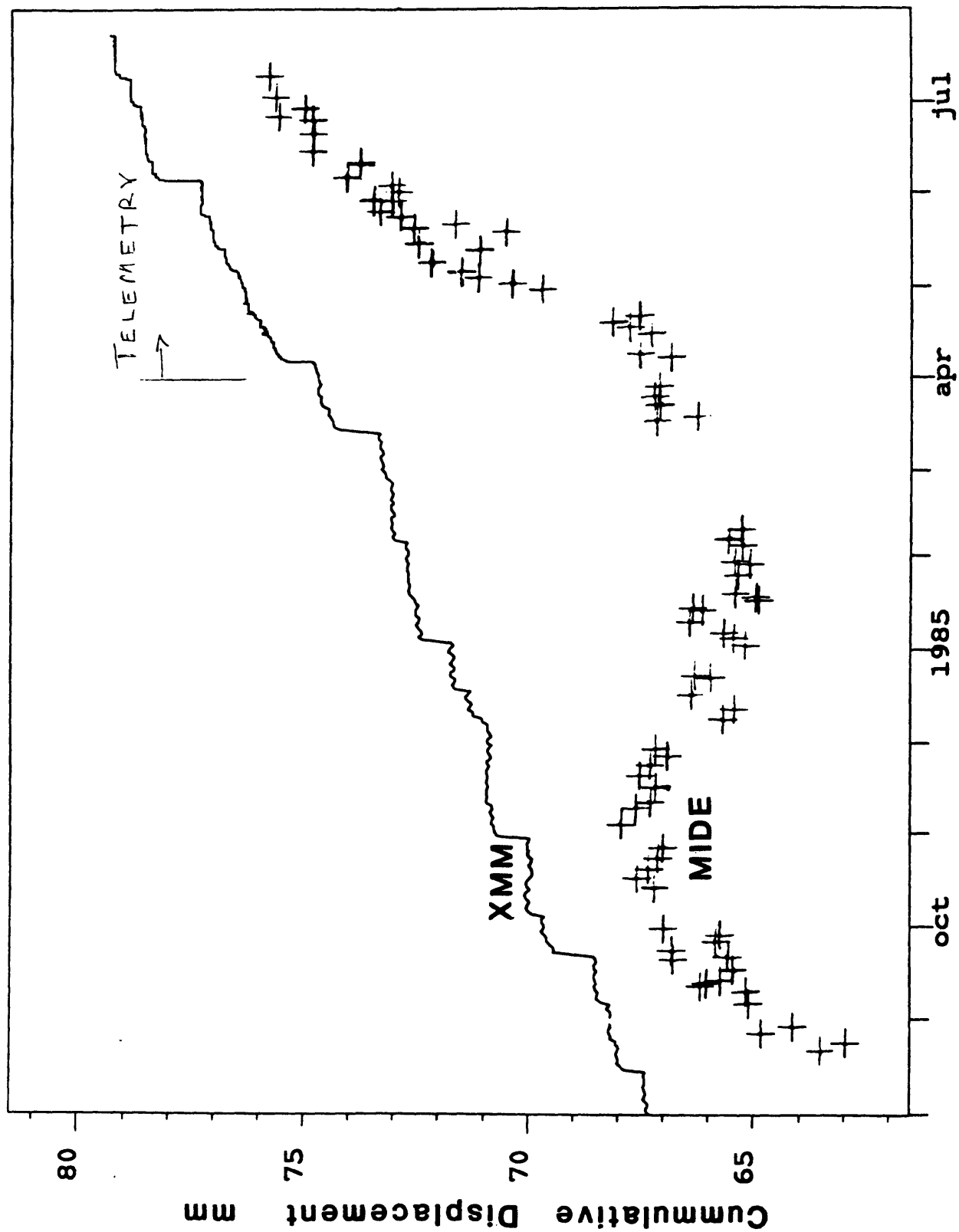


Figure 6 a.

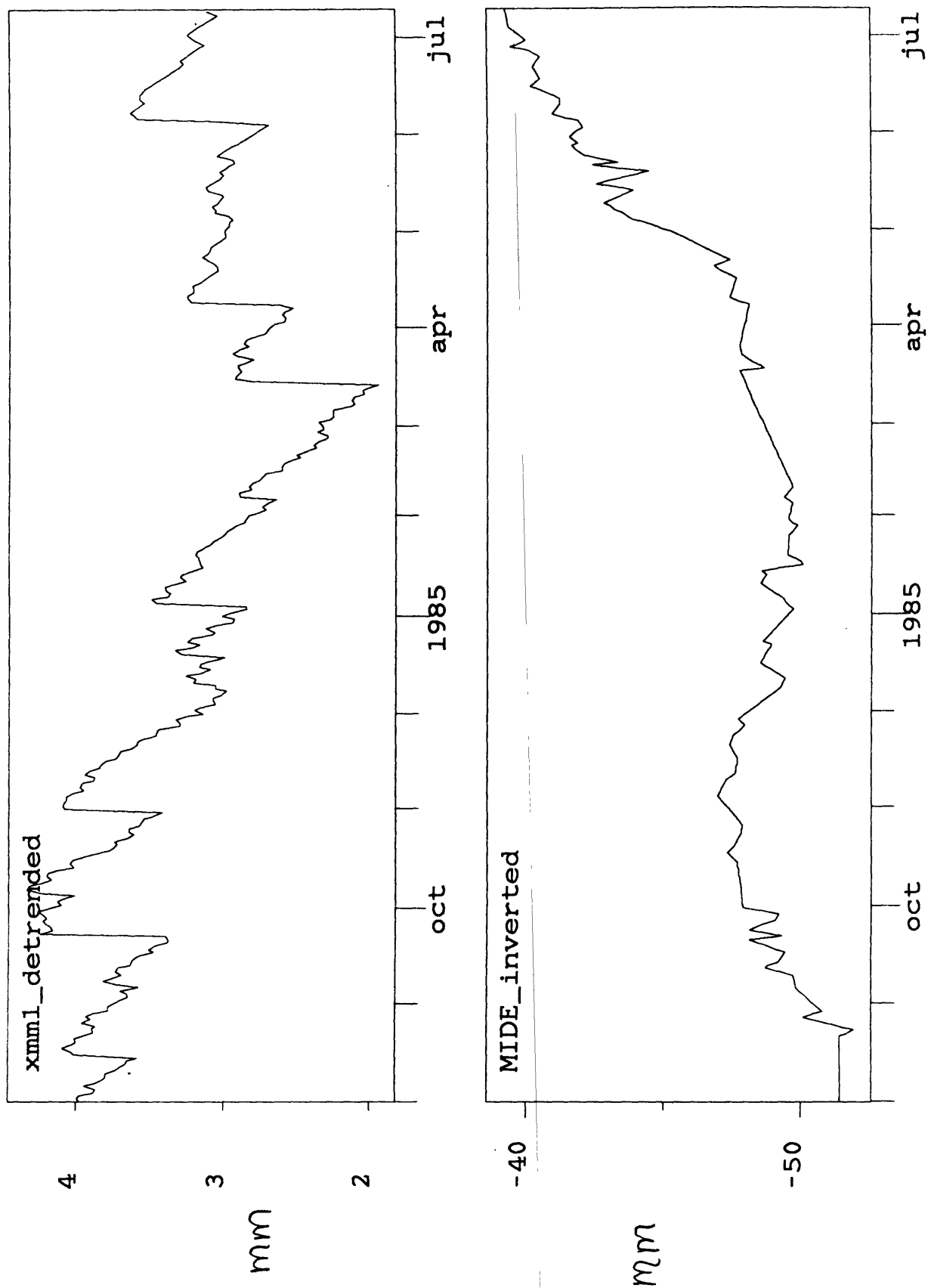


Figure 6b.

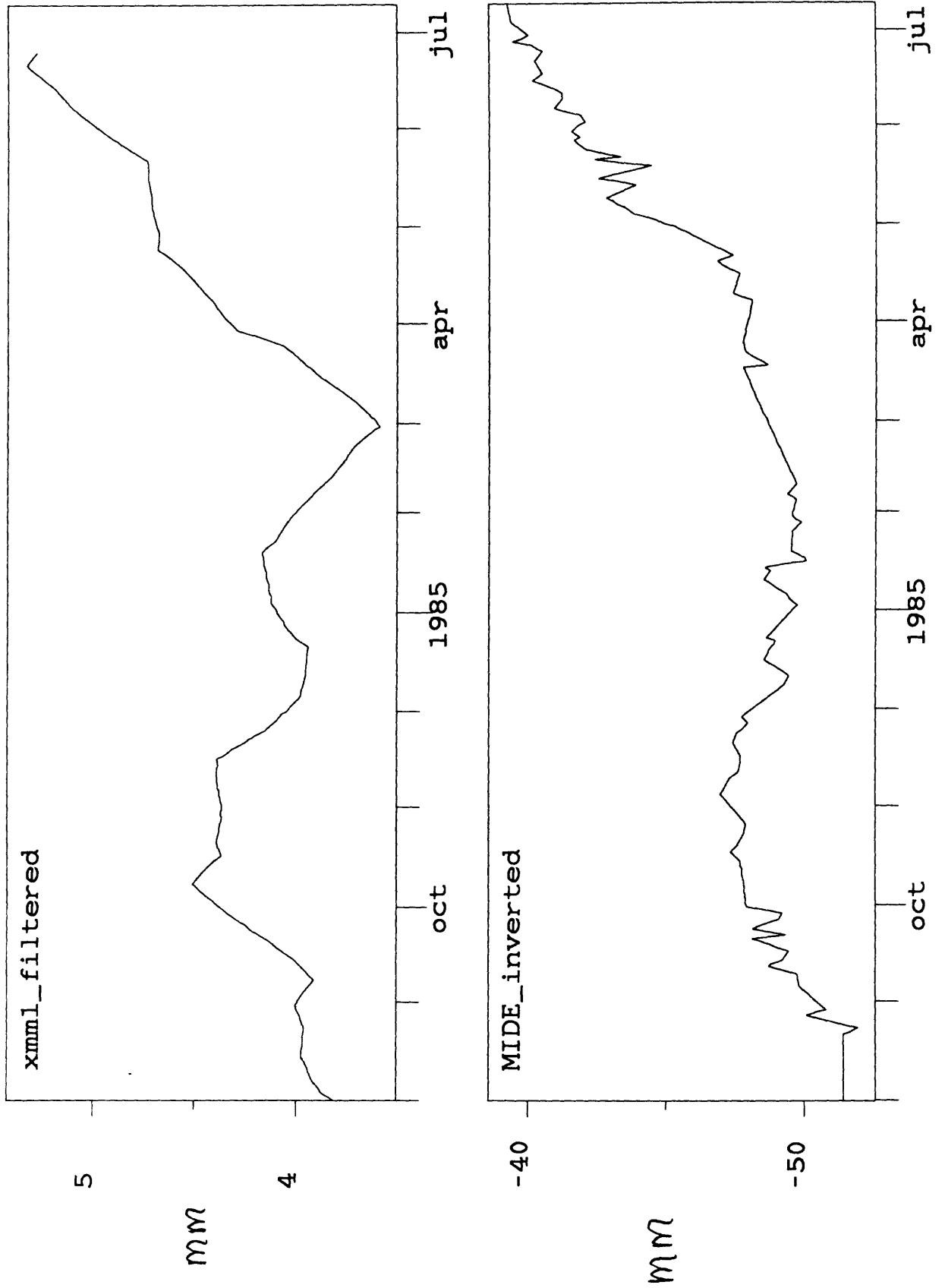


Figure 6 c.

APPENDIX A. 9.

Strain, Creep, Magnetic, and Tilt Data

M. Johnston, S. Schulz, R. Mueller, and C. Mortensen

STRAIN, CREEP, MAGNETIC AND TILT DATA

M. Johnston, S. Schulz, R. Mueller, and C. Mortensen

INTRODUCTION

Real-time monitoring is of crucial importance in attempts to detect and define the state of crustal strain, particularly before, and during fault failure. Many issues must be faced in order to obtain these continuous deformation data in the heterogeneous materials encountered near active fault zones. For this meeting we will be considering in each of these data sets

- * The array designs
- * The main characteristics of the data
- * The approximate measurement resolution for each type of data
- * Recent exciting results
- * Currently operating algorithms for detection of anomalous behavior

I. STRAIN INSTRUMENTATION

Continuous strain measurements at tidal sensitivity are presently being obtained in the Parkfield region from borehole strainmeters in a cooperative experiment between the USGS and Carnegie Inst of Washington and from a single 10 m extensometer. The locations of the sites are shown in Figure 1.

Data from all strainmeters are recorded on site on analog recorders and are transmitted using digital telemetry every 10 minutes to a host computer in Menlo Park. Data are also recorded at some sites on standard seismic telemetry and on wide band digital recorders running in trigger mode to record in the band 0.02 to 1000 seconds during local and teleseismic events.

Strain Resolution

The power spectral plot in Figure 2 shows that the strain noise from the Parkfield dilatometer sites (eg GH2A) referenced to 1 (strain)²/Hz falls off at 20 dB per decade of frequency from about -80 dB at 10⁷ seconds to -220 dB at 0.1 seconds. Least count noise of 10⁻¹¹ corresponds to about -220 dB. If these spectra are transformed into displacement spectra in order to compare with spectra from low noise seismic systems, the strain noise agree quite well in the band 1 to 10 seconds but extend the recording band to D.C. Over periods of weeks to months strains of better than 0.1 microstrain can be resolved, particularly if earth tides and atmospheric loading effects are predicted and removed from the data. Because of cement curing effects strain rates comparable to geodetic rates are not observed or expected to be observed yet. By comparison, equivalent spectra from the surface strainmeters are typically 10 to 20 dB noisier than the deep borehole instruments but have the same general frequency dependence.

Data Summary

Figures 3 and 4 show the complete history of data from the two dilatometers at Gold Hill. The main features of these data are long term drift due to cement curing (other reasons also exist), earth tides (which can't be seen on this scale),

atmospheric pressure loading effects($\sim 10\%$ of the tide), and strain events. The sequence of cleaning operations to remove tides and atmospheric pressure loading is shown in Figure 5. This sequence of events are seen on both instruments and, as we will see later on nearby water well records, are quite unique and unusual. Much of our effort this year has been focussed on attempts to independently constrain the source location, length scale, and source geometry of these events. There are also curious relations to local seismicity in the area. The first strain event occurred in late December and continued through the beginning of the year. A magnitude 3.2 earthquake occurred on January 4 in the middle of the event, but about 20 km to the north along the fault. The second event started in the last week of March and continued through the first week of April. An unusual sequence of earthquakes occurred to the south of Gold Hill near Highway 46 of April 9. At this time the strain reversed sense back to its previous trend. The latest sequence started on May 12. A magnitude 3 earthquake occurred on May 20 near Gold Hill. The strain reversed sense after this event and on the 23 rd went onto extension again. Another magnitude 3 event occurred on the 25 th. These events are most clearly seen on GH1A and GH2A after tides and pressure effects are predicted and removed from the data (Figure 5). Independent records of water level at the well next to GH1A, when scaled using the earth tides overlay, almost perfectly, the records obtained here.

Various attempts have been made to fit these data to simple models of slip on the San Andreas fault and on other faults in the region. The moments of point source dislocation models at the hypocenters of the two magnitude 3 earthquakes required to generate 0.1 microstrain perturbations at Gold Hill are much larger than those of the earthquakes alone.

II. PARKFIELD CREEPMETERS

Instrumental Sensitivity

The Parkfield creepmeters consist of two distinctly different models. Five creepmeters (XSC, XMM, XPK, XDR, XGH) are the U.S.G.S. invar-wire design with 0.05 mm resolution, and three (WKR, CRR, TWR) are the CalTech invar-rod design with 0.5 mm resolution (Figure 7a and 7b).

Data Summary

Mechanical design and physical condition of an instrument, together with local site conditions and variation in surface creep rate from site to site, produce signals so characteristic as to provide almost a 'signature' for that instrument. For example, XMM is a new creepmeter in good mechanical condition located on a fast-moving section of the fault. XMM records a smooth daily background change of about 0.02 mm, with occasional 0.02 to 1 mm events superimposed on it. In contrast, XDR is a 16-year-old instrument in relatively poor mechanical condition that records not only a diurnal change of greater than 0.06 mm, but a large 10 mm or so response both to rainfall and subsequent dewatering of the site. This seasonal response is noticeably absent during the drought years of 1976-77 (Figure 8). The CalTech creepmeters display the usual tendency of rod instruments to move in friction steps. Thus, their records normally are unchanging with an occasional abrupt change to a higher or lower number.

In spite of this several important results are apparent in the data. The most important is the definition of slip rate from north to south along the fault. As pointed out by Lisowski and others these rates agree quite well with those determined geodetically. Independent verification of the rates is obtained from alignment array data.

We must emphasize, however, that these are current patterns, subject to change. For example, as seen on Figure 2, the Coalinga earthquake had a profound retarding effect at several of the creepmeters. This retarding effect followed an overall gradual retardation at several sites that had been in progress since about 1980. The two periods of retardation were separated by an unexplained surge at several stations in late-1982 early-1983 and by the coseismic step on May 3. It is likely that the retardation effects represent a precursor to the earthquake predicted for Parkfield by 1988. Table 1 summarizes present slip rate patterns.

III. MAGNETOMETER INSTRUMENTATION

Local magnetic fields have been monitored in the Parkfield area at three sites (LG, GD, and AG, see Figure 9a) since 1976 and since 1979 at GR. In 1985 three new telemetered sites were installed (by transferring stations from other locations in California to sites near Parkfield used for portable magnetometers) so better coverage and array design could be achieved. The locations of all sites in relation to the signals predicted from a simple tectonomagnetic model of the Parkfield earthquake is shown in the Parkfield Binder. In essence the predicted signals have a form similar to that expected in dilational strain with a quadrupole distribution with the peak signal occurring at about 0.3 fault depths from the fault. The purpose of the experiment is to detect magnetic perturbations that result from changes in the mean state of crustal stress since both magnetic remanence and magnetic susceptibility have a stress sensitivity of about 0.0001 per bar. For a 10 bar stress change, this translates into a local field of about 1 nT if the magnetization is 0.1 A/m.

The data recorded are absolute total field data. These data are transmitted every 10 minutes in digital form to Menlo Park where they are differenced to isolate changes of local origin.

Detection threshold

Changes in magnetic field of about 1 nT can fairly readily be detected in the raw data over the period range days to months or at periods of a few hours or less. Processing using Weiner Predictive filters reduces this threshold to 0.1 to 0.2 nT. Figure 10 shows a plot of standard deviation in difference field data as a function of station separation. Coherent changes of about 1 nT across the array, but not necessarily with the same sense, would constitute anomalous behavior in these data.

Data Summary

Summary plots of the complete difference field records for the past years are shown in the Parkfield Binder. These records are spectacularly uneventful at the sub nanotesla level except for two features. at the

a step of about 3 nT at GRAM several months before the Coalinga earthquake (Figure 11). This step was seen only on the one instrument and this instrument was not the closest to the subsequent earthquake.

increased secular rates on the Parkfield instruments that are clearly evident when the data are corrected for secular variation and other internal and external effects in the data using Weiner Filtering. This is evident in Figure 12 which shows the rates in nT/a across the whole array.

IV. TILTMETER INSTRUMENTATION IN THE PARKFIELD REGION

A small network of shallow-borehole tiltmeters has been operated in the Parkfield region since May 1976. In September 1980 the array assumed

approximately its present configuration and an experiment was commenced which entailed operating a cluster of five shallow tiltmeters within an area of about 100 square meters. The results of this experiment are that long-term tilt trends from the shallow-borehole installations are not generally coherent between instruments and therefore reflect only the movement of the material immediately surrounding the instruments, while agreement between instruments improves as frequency increases.

Signal detection

Throughout most of the records the noise level of the data is on the order of $10E-6$, or a little better, for periods ranging from hours to a few days. Phenomenon of particular interest that occur in this frequency range include creep events, and the capability to observe propagating deformation fields associated with creep events using these instruments has been established (Johnston & McHugh, 1976; and Mortensen, et. al., 1977).

Currently the array of tiltmeters near Parkfield consists of three instruments in the closely-spaced cluster situated at Gold Hill, about 2.4 km east of the San Andreas fault (Figure 13). These instruments have station identifiers GOA, GOB and GOC. A fourth tiltmeter, GOH, is located about 1.75 km east of the fault, between the cluster and the fault. The GOH instrument was the one originally installed at Gold Hill in 1976.

Resolution and Data Summary

Examples of the data from the various north and east tiltmeters for the last 6 months during the time of the strain events on the deep borehole strainmeters is shown in Figures 14 and 15. It is clear that over periods of several weeks to a month we cannot resolve the 0.1 microradian signals expected on the tiltmeters due to the strain events. At short periods the instruments can resolve strains of better than 0.01 microradians. This issue can be more completely demonstrated with a noise power spectra of the data.

ANOMALY DETECTION ALGORITHMS

Alarm detection algorithms operating on low frequency data are of several different types. (Figure 16) The systems currently used operationally are of two types:

- * Amplitude detectors. This system is used on the creepmeters feeding the 'Creep Beeper'
- * Rate detectors. This system is used on the continuous strain and tilt data.

Both of these systems can be scaled according to the level of background noise. In the more general problem we would also want to define group behavior (Figure 17). The systems used are based on;

- * Simultaneity
- * Coherence and anticoherence functions

Alarm thresholds for Parkfield creepmeters

Some evidence exists that surface creep may have occurred in the weeks or hours before the 1966 earthquake. If so, similar creep may occur before the next earthquake. Once each hour, the Unix 44 computer samples real-time telemetry data from the seven creepmeters starred in Figure 7b. A change of 0.25 mm or greater causes the computer to dial the paging service, actuating a beeper. The alarm is set purposely low so we can start watching early in the event. After noting which instrument has tripped the alarm, all Parkfield creepmeters are checked for unusual changes. If the event is confined to one instrument, its signal is monitored until movement returns to a more normal rate.

Since the beeper was purchased in September, 1984, less than half the alarms have been true creep events. (The creep events usually are ≤ 2 mm in amplitude, last approximately 45 minutes to 1 hour, and are confined to one station, often the Middle Mountain creepmeter.) The remainder of alarms have been failures of phone lines, electronics, telemetry units, or batteries, producing signals that are identified with varying degrees of difficulty.

Five General Alarm Thresholds for Parkfield Creepmeters

If precursory creep does occur, its signal may have an unusual appearance. Here are five extraordinary creep signals, listed in order from most obvious to more subtle, that would prompt the spread of an alarm.

- 1) Abrupt aseismic movement* on one or more creepmeters that exceeds instrumental range within a few telemetry transmissions (10 min apart), or is sustained longer than 1 hour at a rate high enough to exceed instrumental range within 24 hours. Note: if movement occurs only at one creepmeter and quickly exceeds instrumental range, perhaps breaking the wire before telemetry counts can increase, and especially if adjacent creepmeters show nothing unusual and there is no sudden increase in seismicity, this alarm could be confused with possible electronic failure. Confirmation (surface cracks noted at site, eventual change at an adjacent creepmeter) might delay alarm hours to days. To deal with this problem, one station (Middle Mountain) is also equipped with a special creepmeter (XMBC) designed to withstand 24 cm of movement, compared to the usual 25 mm range of the other creepmeters.
- 2) Within an hour, onset of aseismic movement* at two or more creepmeters, adjacent or not, if movement exceeds 0.5 mm at each site the first hour and shows no tendency to slow during the second hour. This latter condition would be extraordinary, even if rain is falling. Continuation of the events at unabated levels into the third hour would constitute an unmistakable anomaly, particularly at stations that have shown retardation since 1983.
- 3) Onset as described in (2) above, but limited to one creepmeter. Note: This would not necessarily be an anomaly for XDR1 (Durham Ranch) during rainfall or in springtime. This behavior would also be suspect if 2 years had passed since the last battery change at a station.
- 4) Onset of aseismic movement* simultaneously or within moments at three or more creepmeters, even if amplitudes are sub-millimeter and movement is sustained through only a few telemetry transmissions (10 min apart). The key in this case is near-simultaneous onset, which in the past has been associated only with earthquakes, and thus would be significant whether or not stations were adjacent. Coincident heavy rainfall could cast some doubt on this alarm, depending on which stations were involved.
- 5) Near-simultaneous cessation of movement at all 7 stations, sustained for at least 12 hours. Certainty that an anomalous situation was developing would increase with each hour after the initial 12-hour period.

Alarm thresholds for Parkfield strainmeters

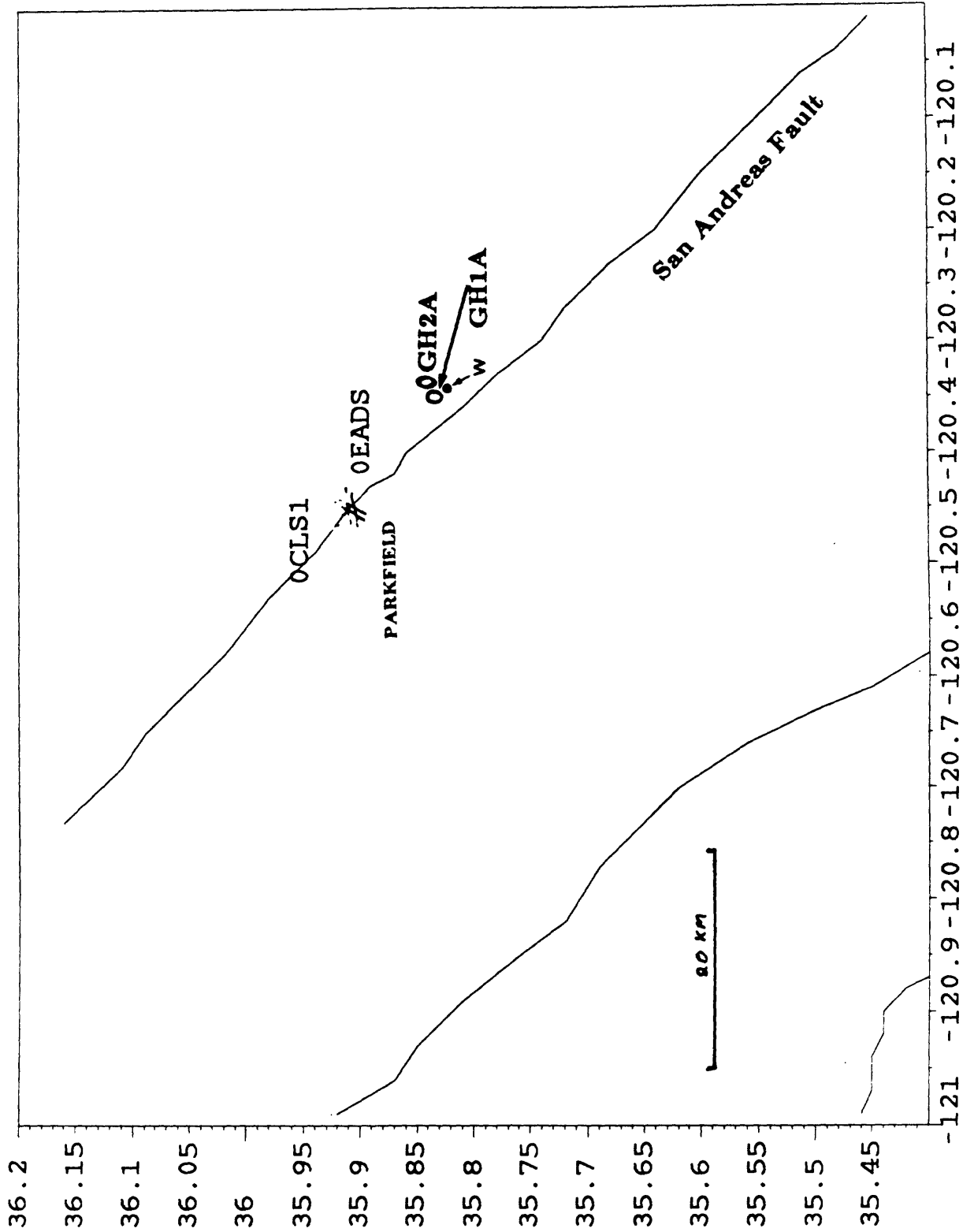
Figure 18 shows the output from the rate alarm detector running on the strain data discussed earlier.

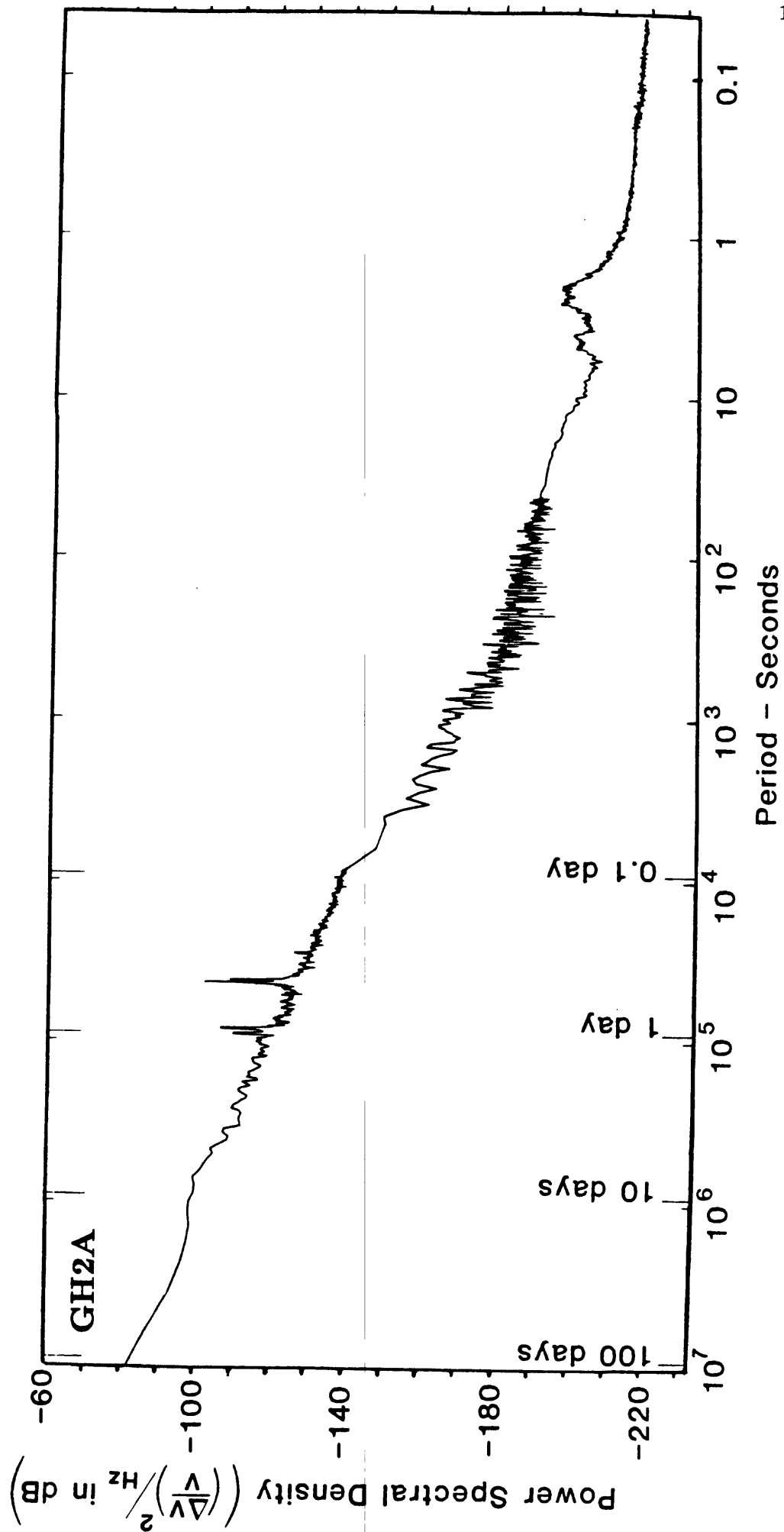
* Either right- or left-lateral, but particularly right-lateral.

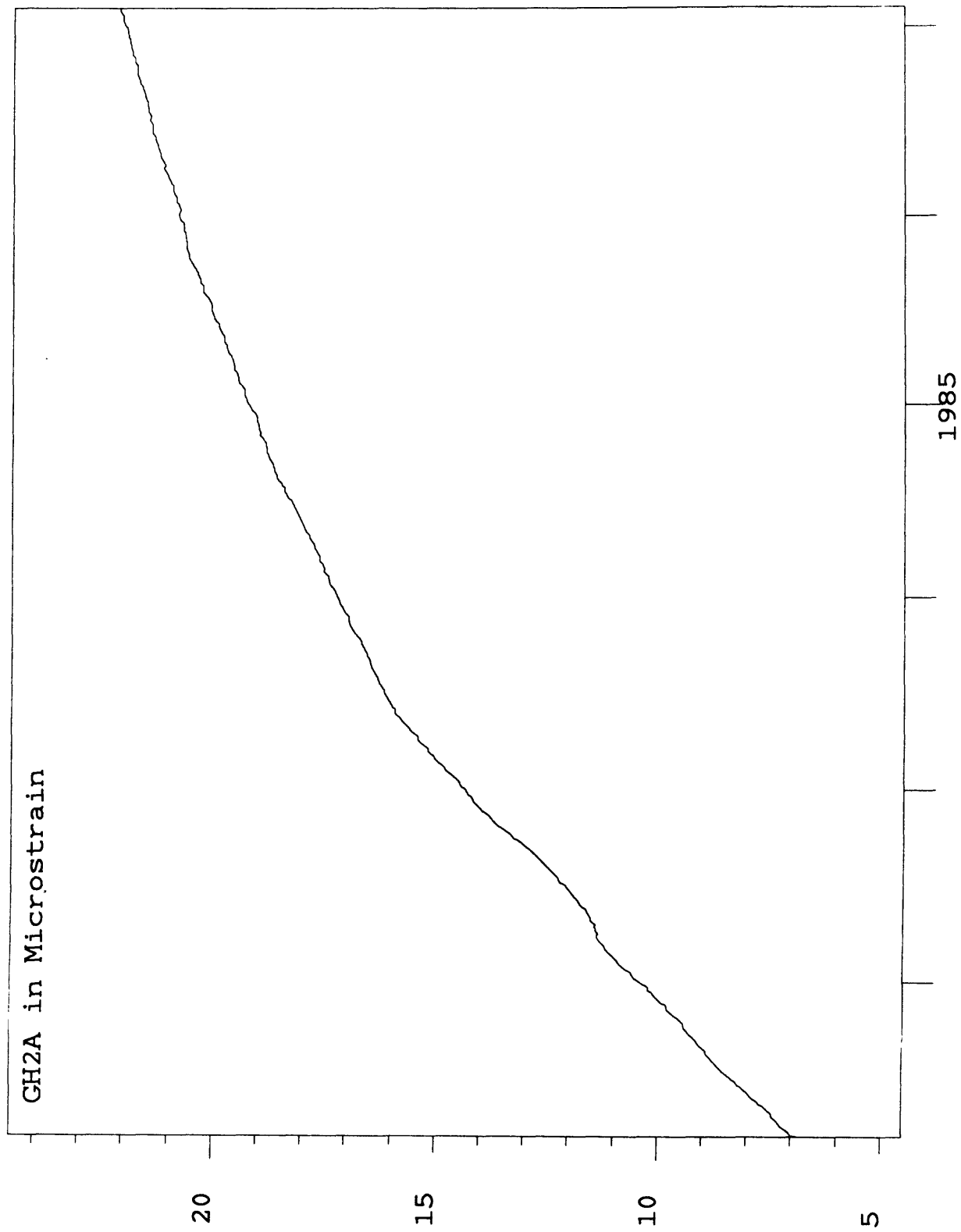
LOW-FREQUENCY INSTRUMENTATION AT PARKFIELD

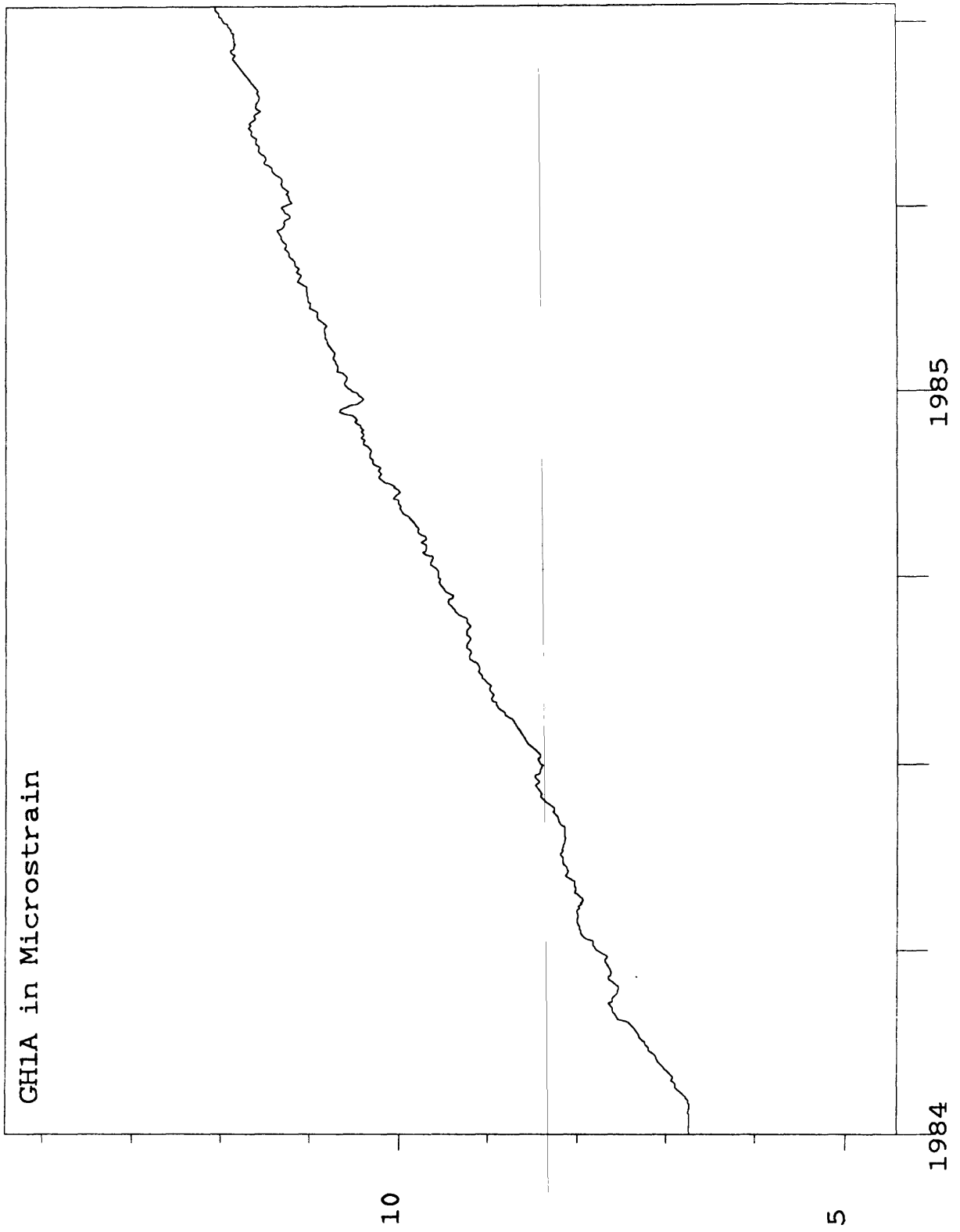
- **MEASUREMENT METHOD -FAULT CREEP**
 - BOREHOLE AND NEAR-SURFACE STRAIN
 - DIFFERENTIAL MAGNETOMETRY
 - NEAR-SURFACE TILT
- **SITE LOCATIONS**
- **DESCRIPTION OF INSTALLATIONS**
- **ON-SITE RECORDING AND TELEMETRY**
- **CALIBRATION -Instrumental**
 - Tidal
 - Surface waves
- **DATA SUMMARY AND RECENT RESULTS**
- **RESOLUTION AND DETECTION OF ANOMALOUS BEHAVIOR**
- **CROSS-COMPARISON OF DATA**
- **CONCLUSIONS**

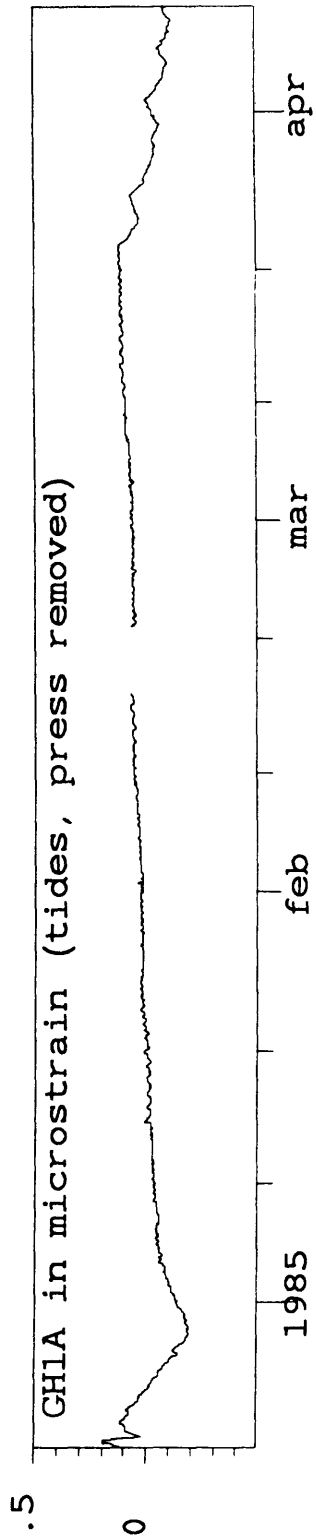
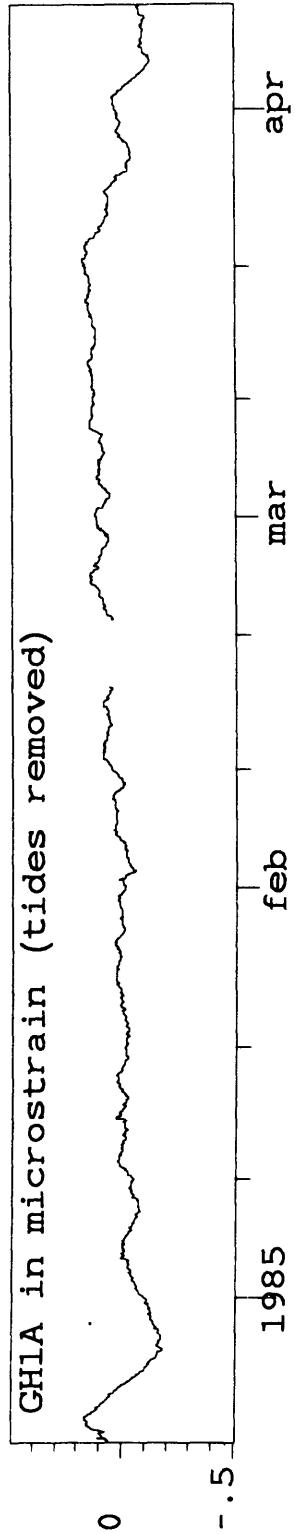
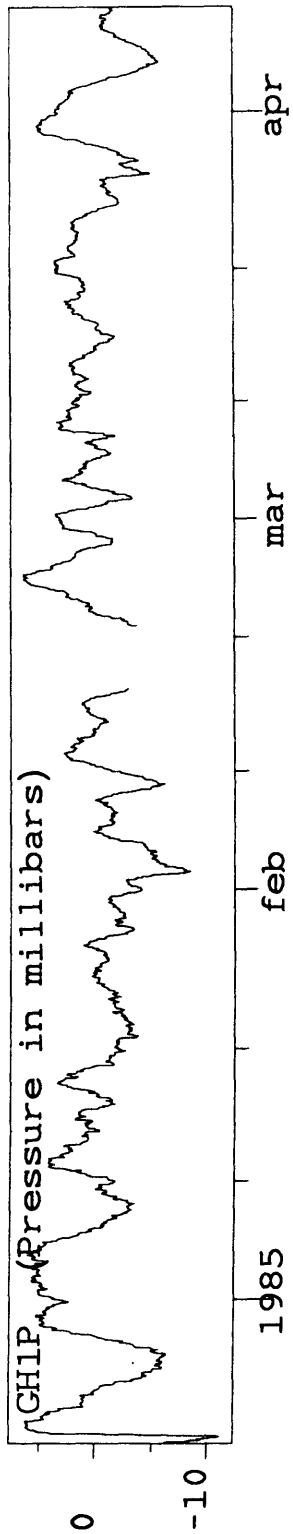
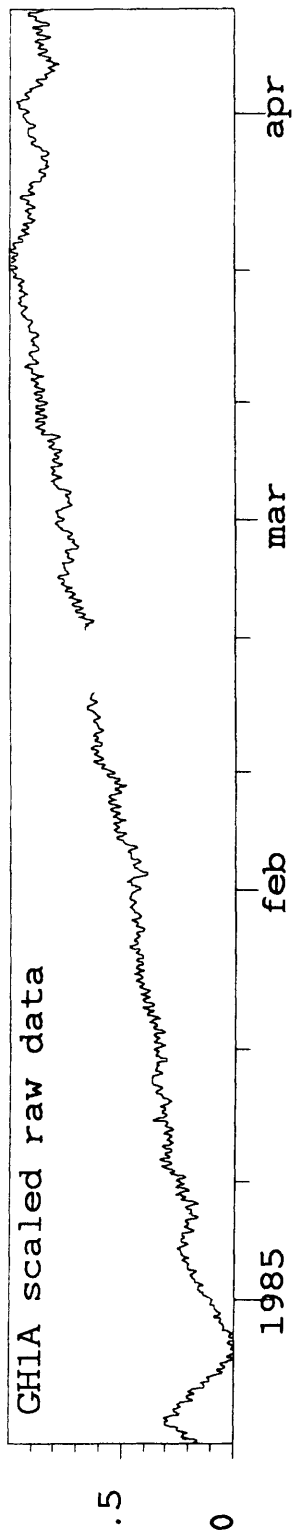
PARKFIELD STRAINMETER ARRAY

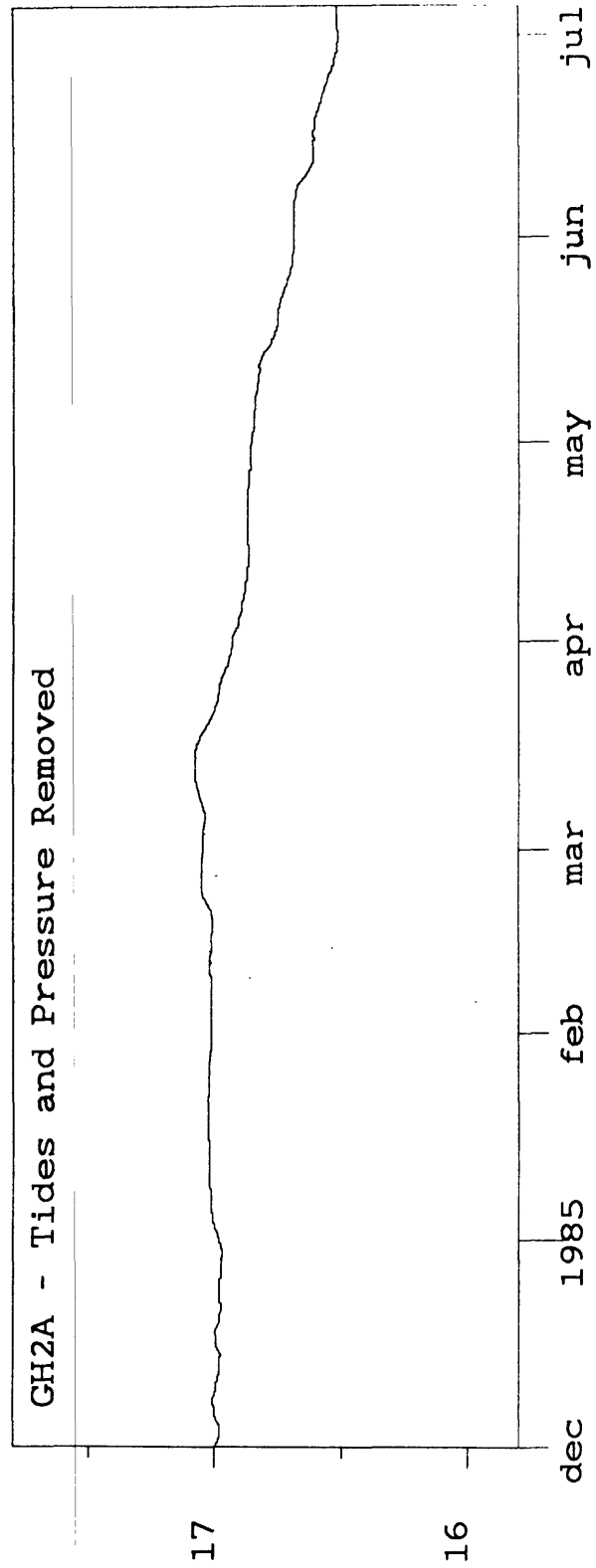
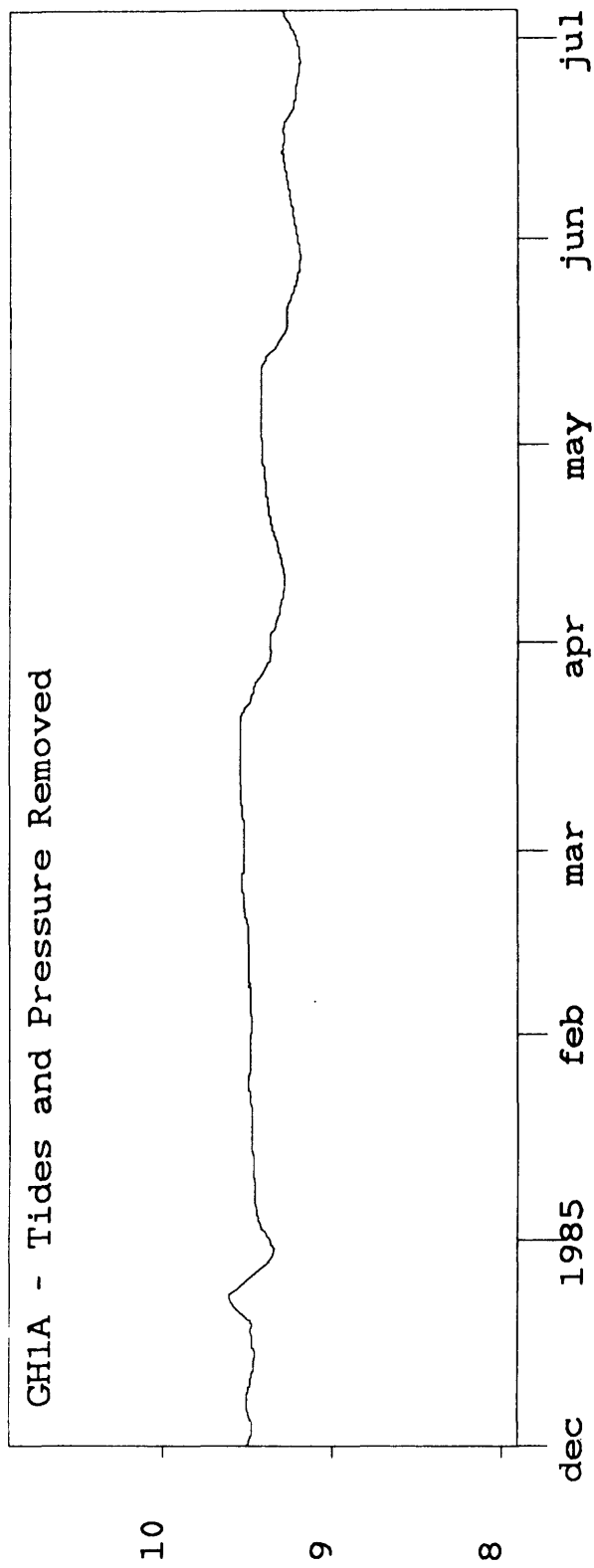












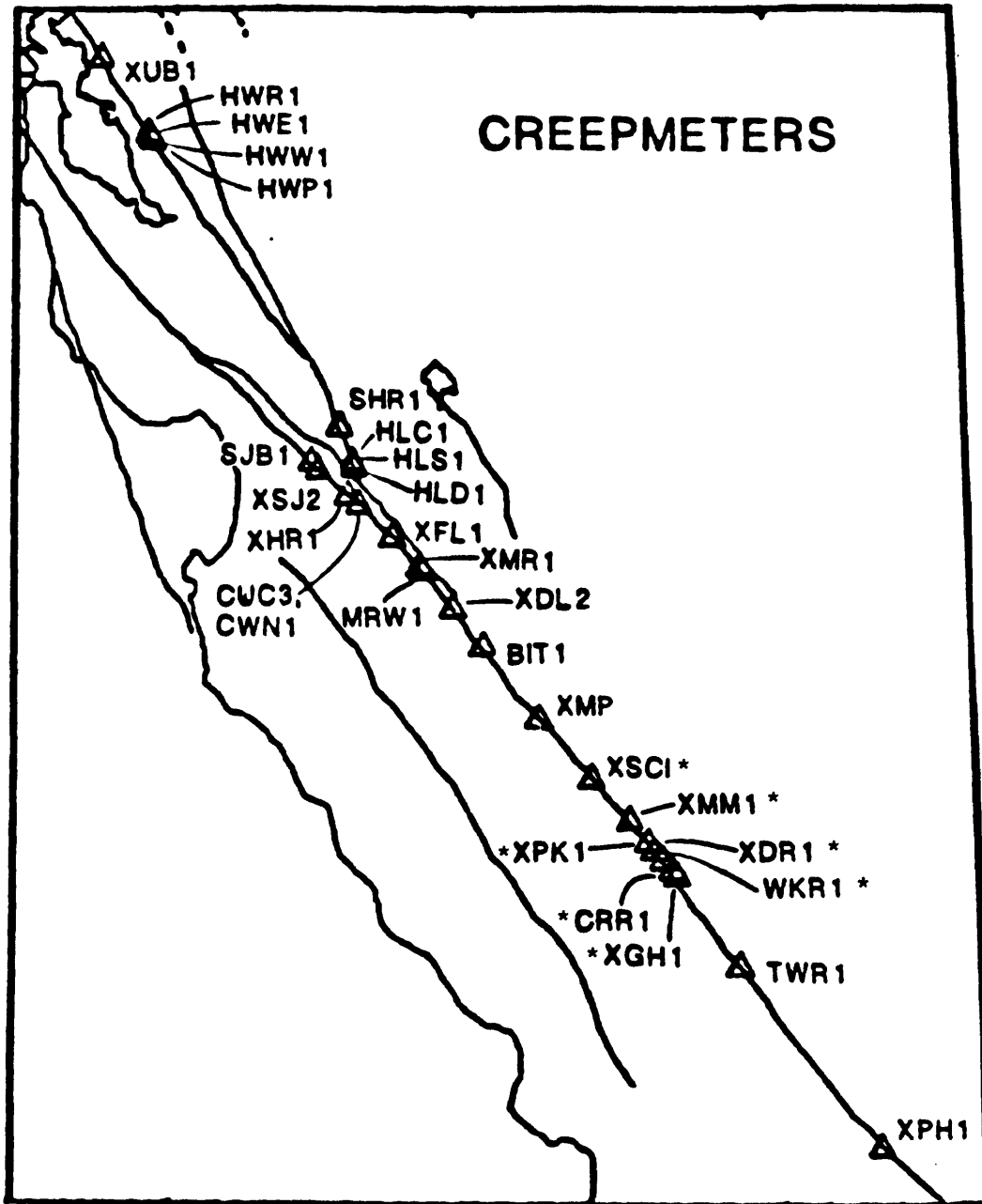


Figure 7a

*Starred stations are on alarm beeper system

Creep and Alinement : Parkfield , CA

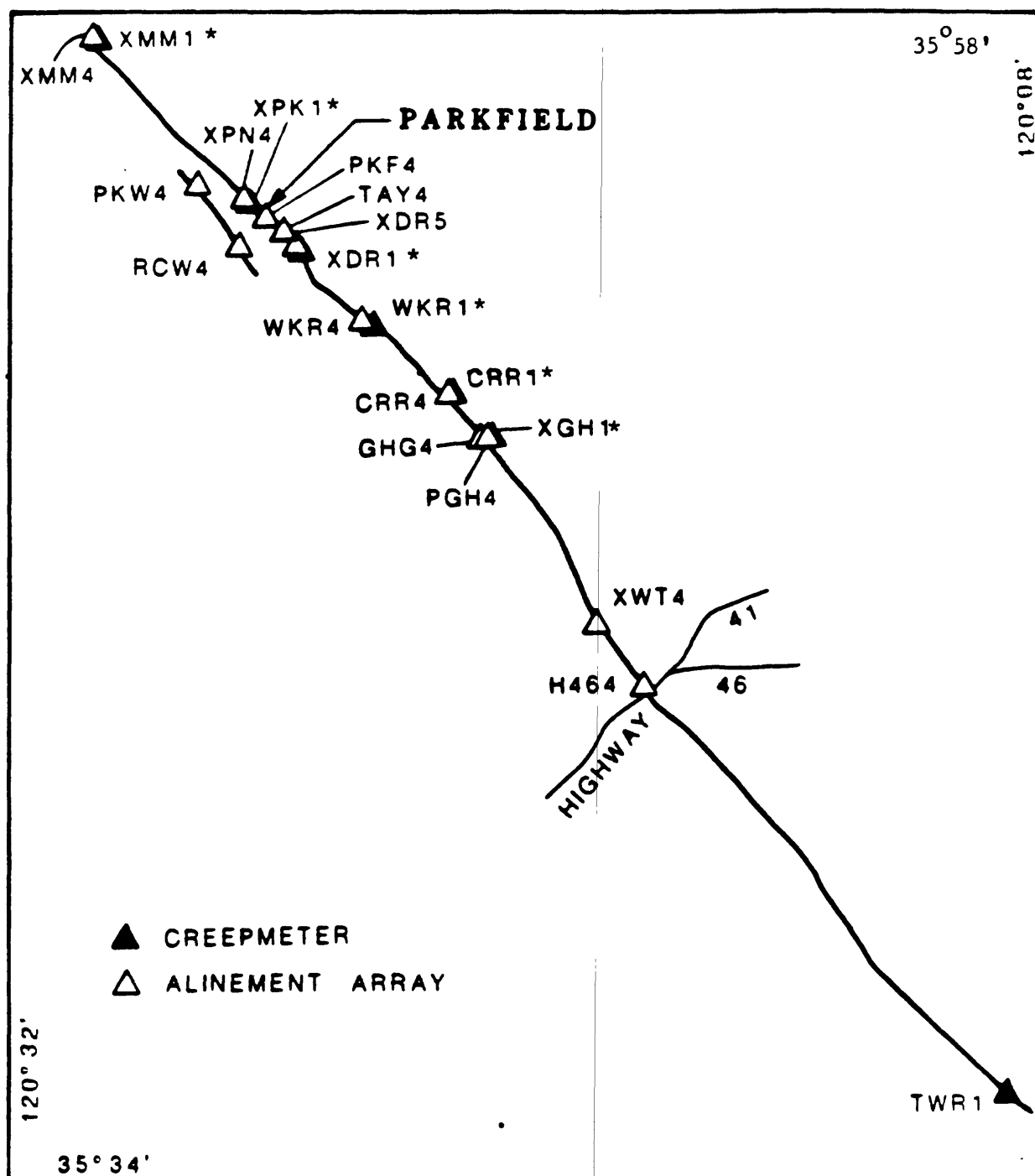
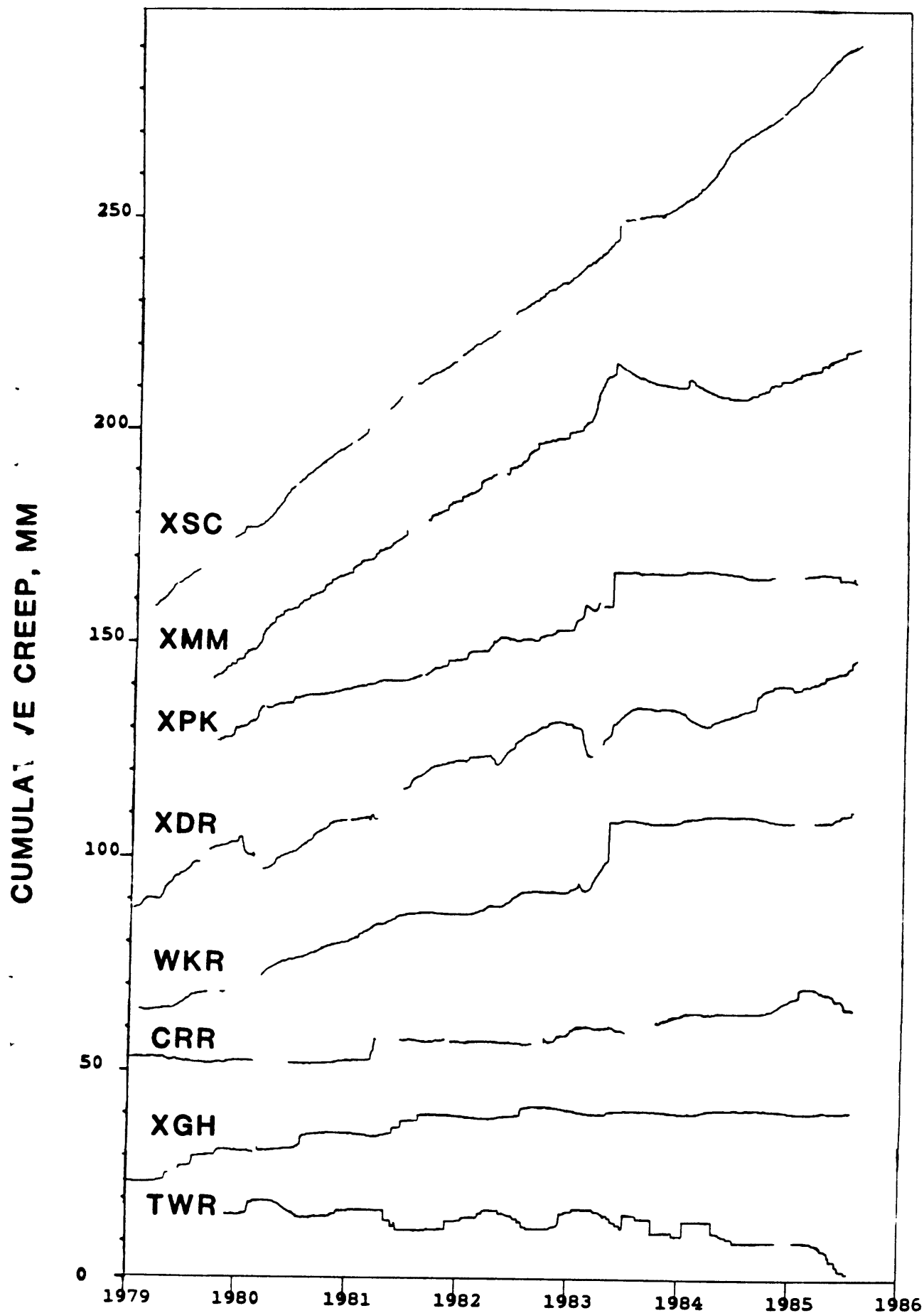


Figure *Fb*

*Starred stations are on alarm beeper system



PARKFIELD CREEPMETERS

JAN 1979 to JULY 22, 1985

Table 1

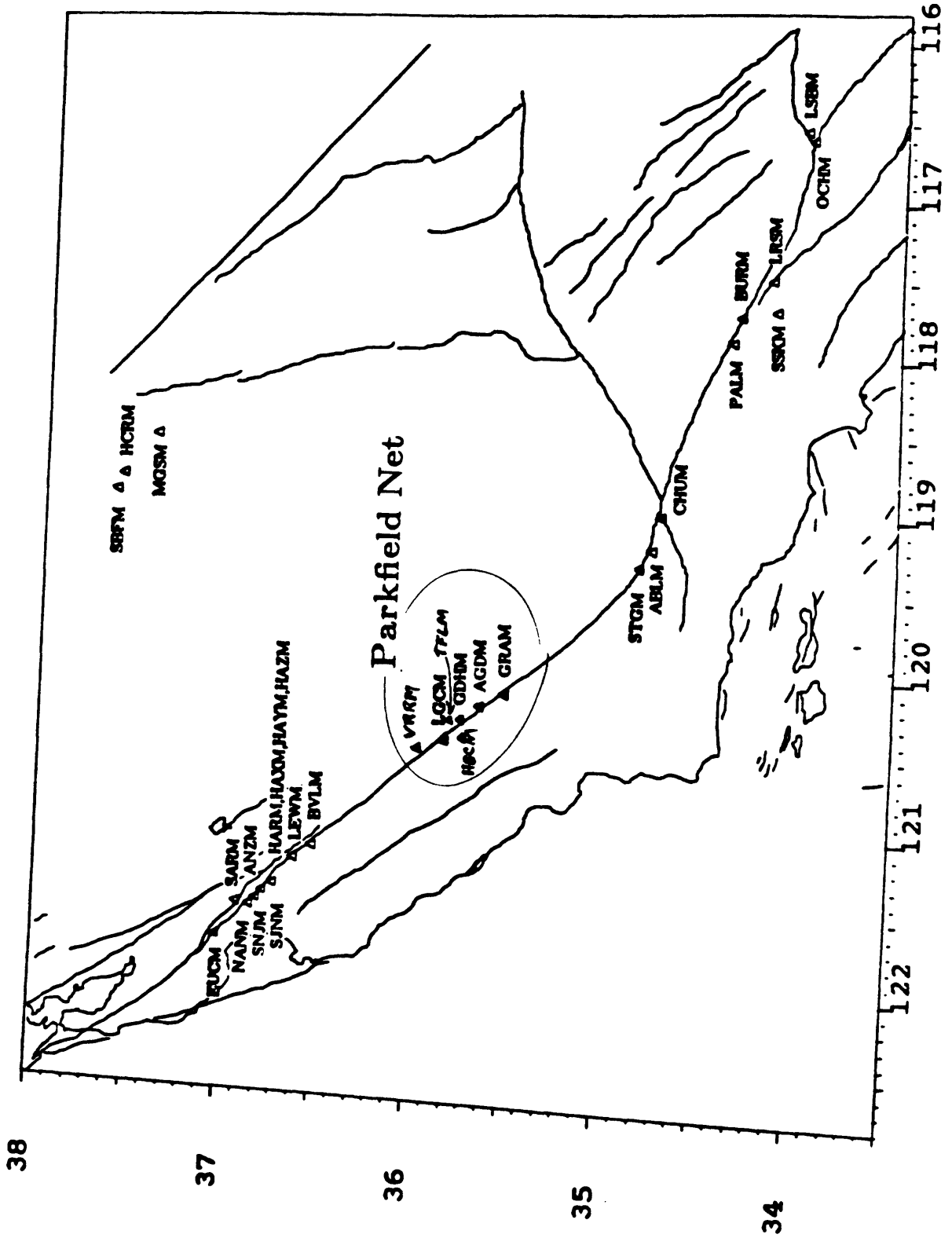
Creep-meter	Year of Install.	Avg annual rate prior to May 1983 (mm/year)	Avg annual rate since May 1983 (mm/year)	Avg Daily change in tele. counts*	Conversion factor** (cnts/mm)
XSC	1969	23	23 (since 11/83)	13	150
XMM	1979	20.1	11 (since 7/84)	3	150
XPB	1979	8.6	-0.8	1	150
XDR	1969	10	10	10	150
WKR	1976	8	0.2	3	105
CRR	1966	5	5	3	105
XGH	1969	3.7	-0.9	1	150
WTR	1976	0.4	-6.6	1	335

* Excepting events

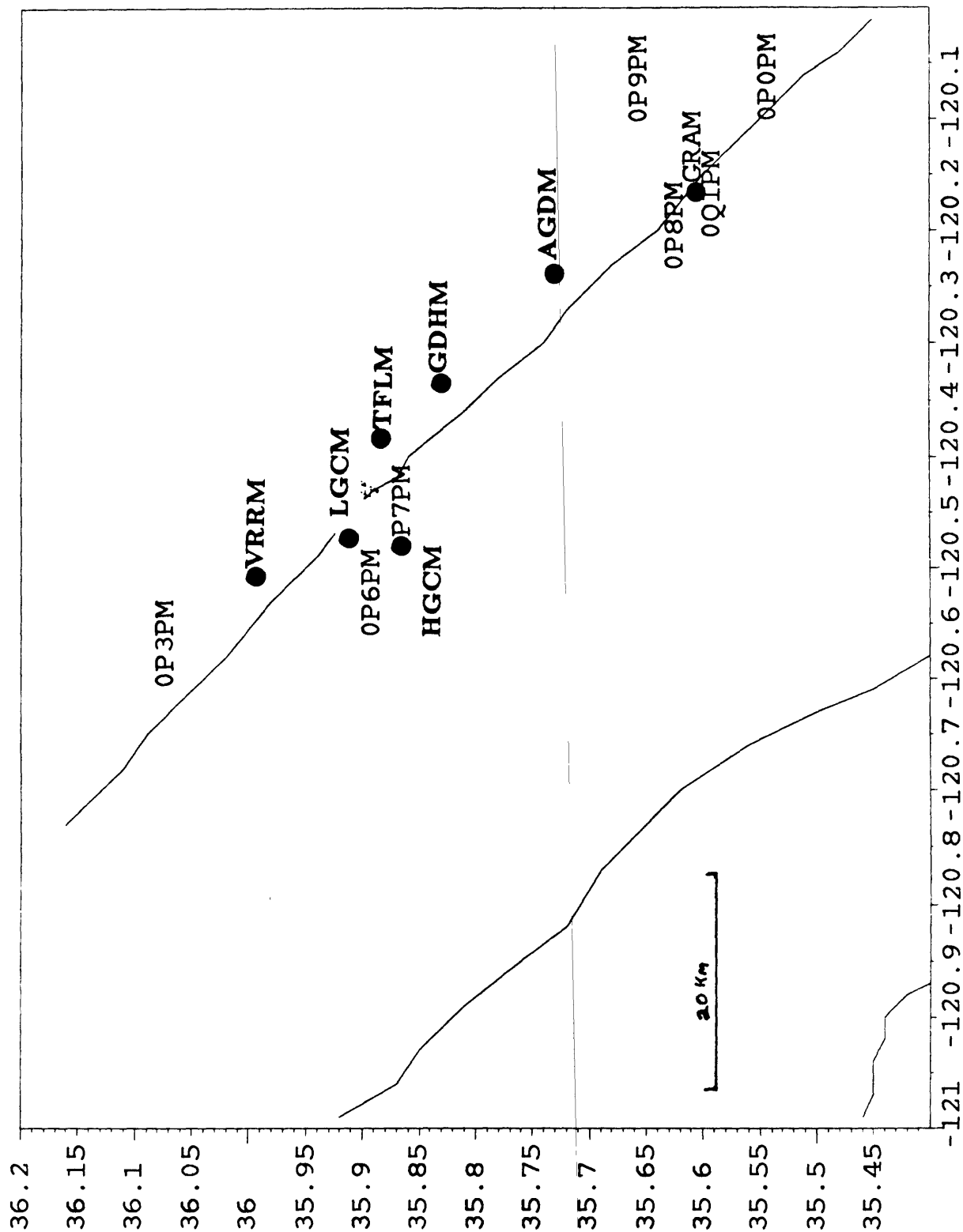
** Uncorrected for angle of station to fault.

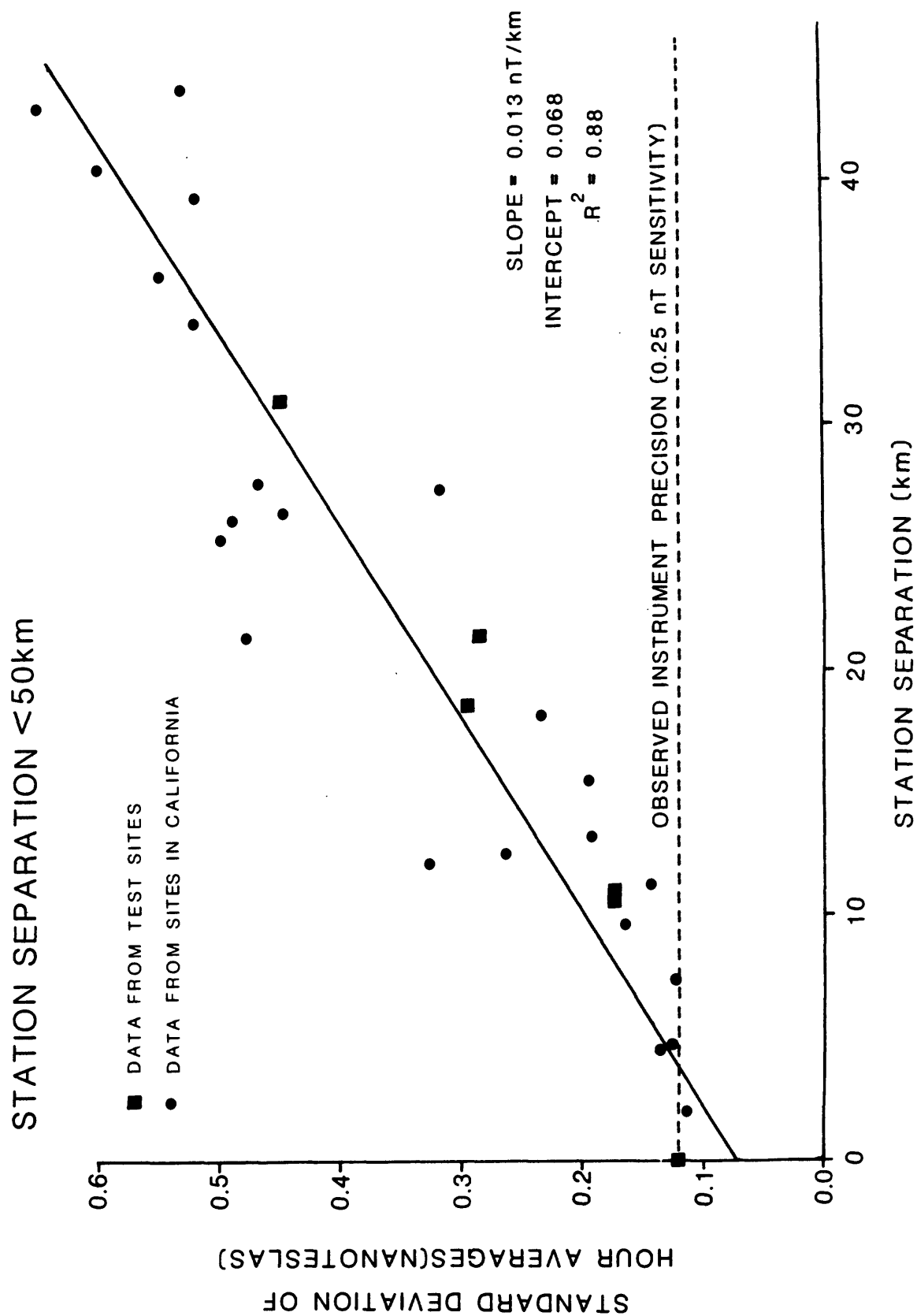
PERMANENT MAGNETOMETERS

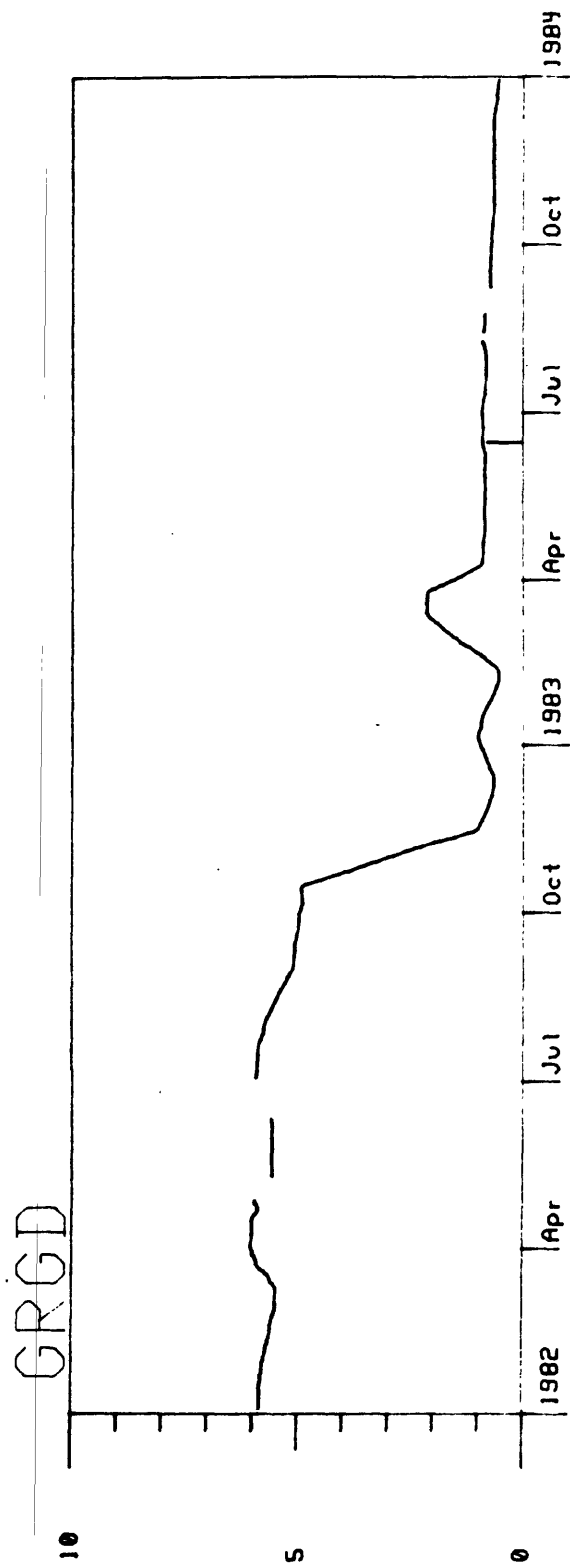
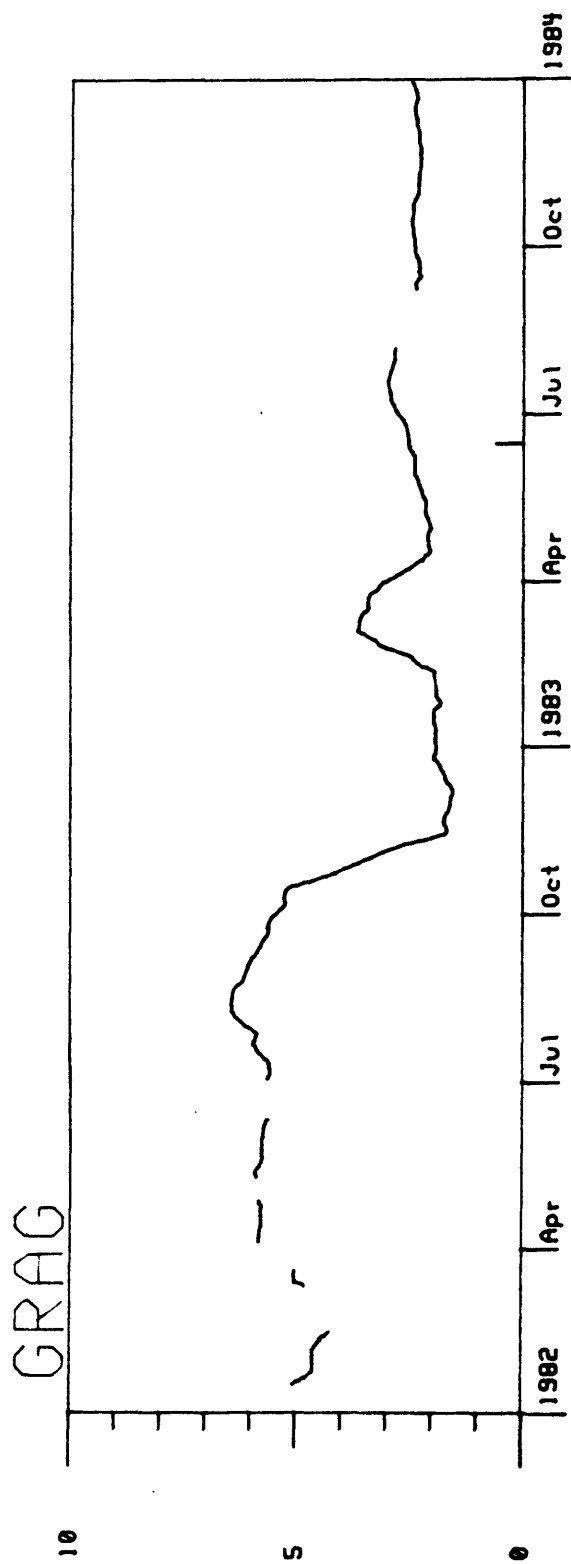
92

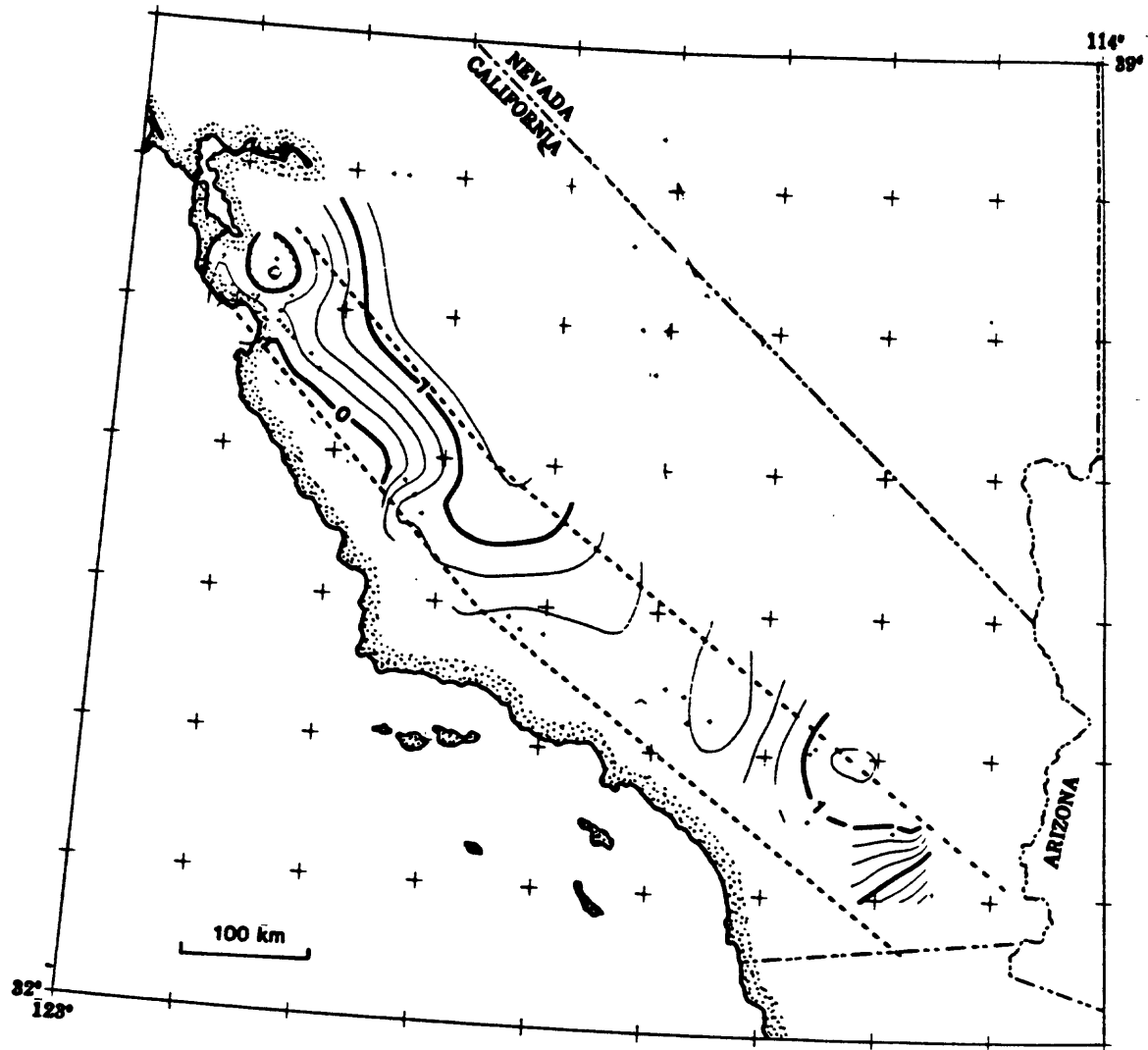


PARKFIELD MAGNETOMETER ARRAY









(12)

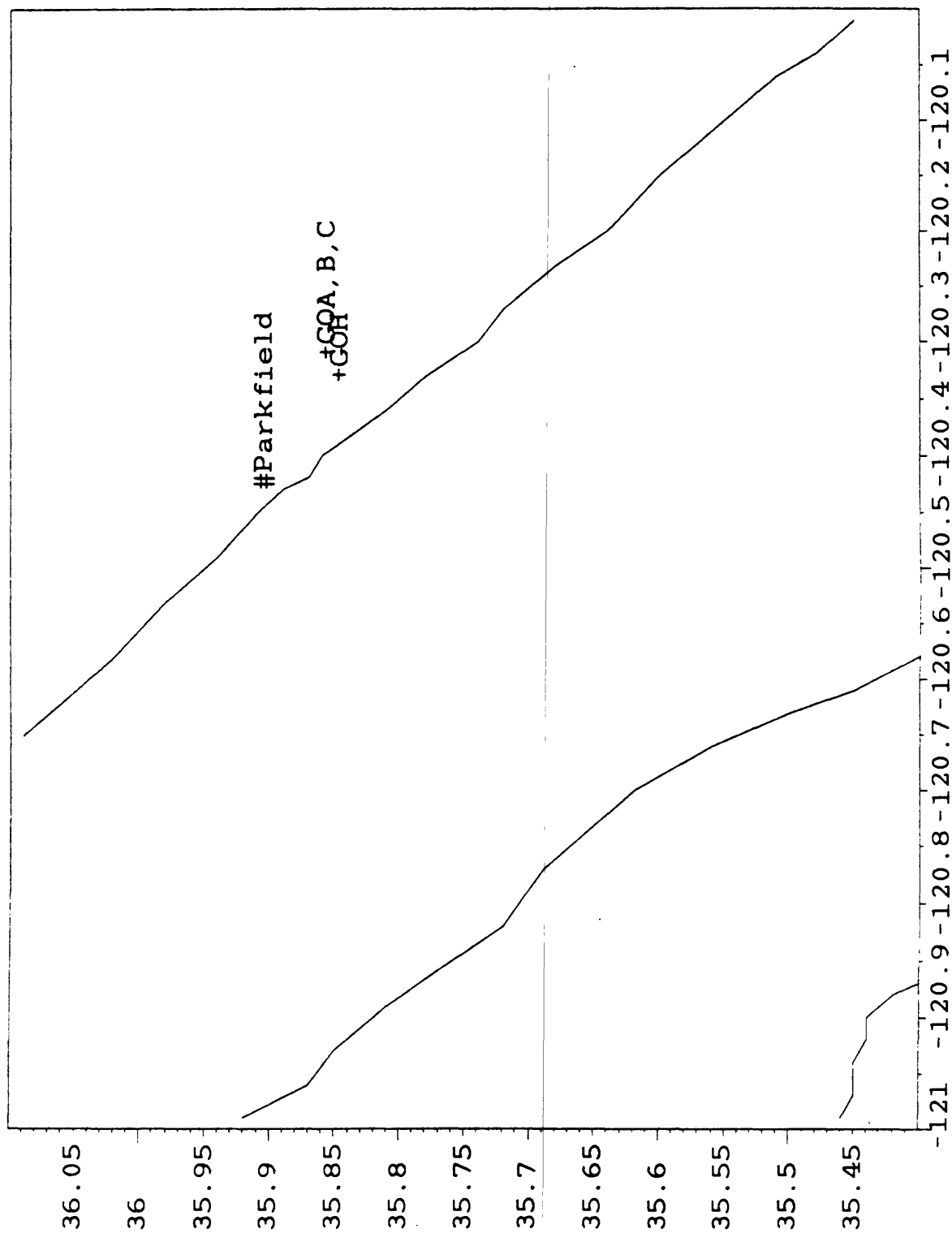
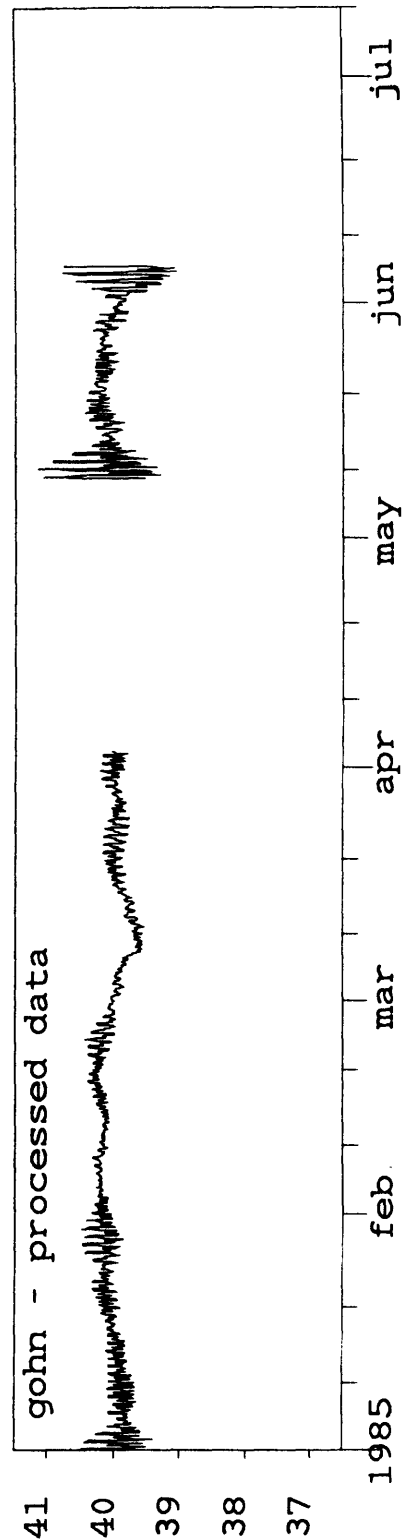
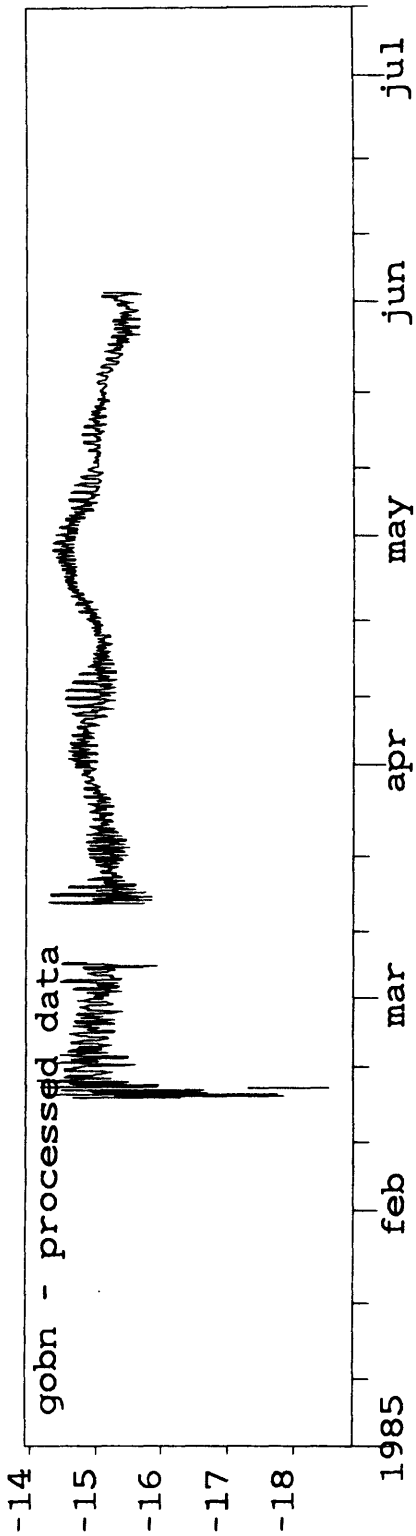
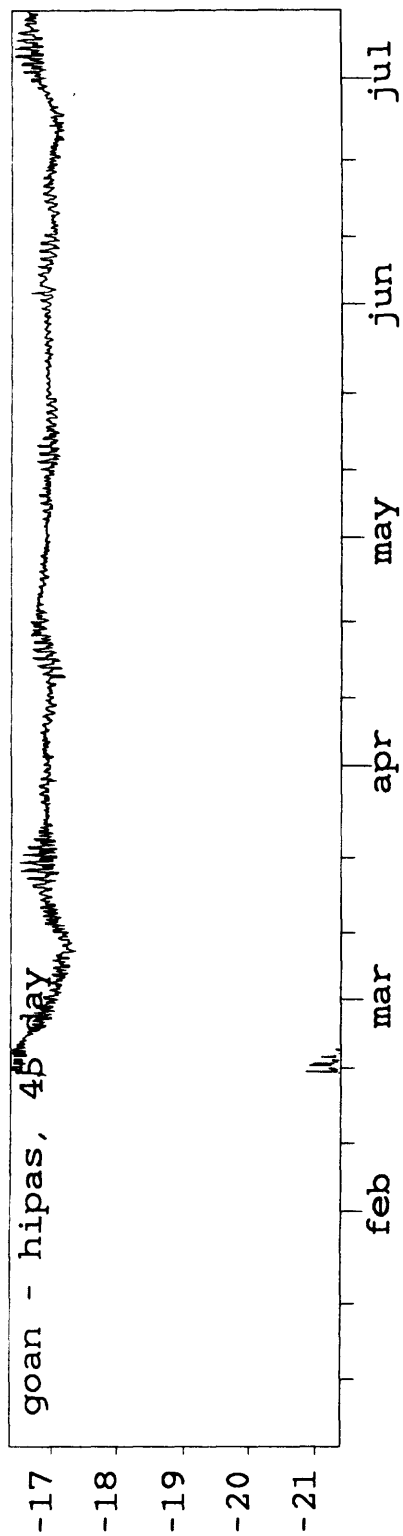
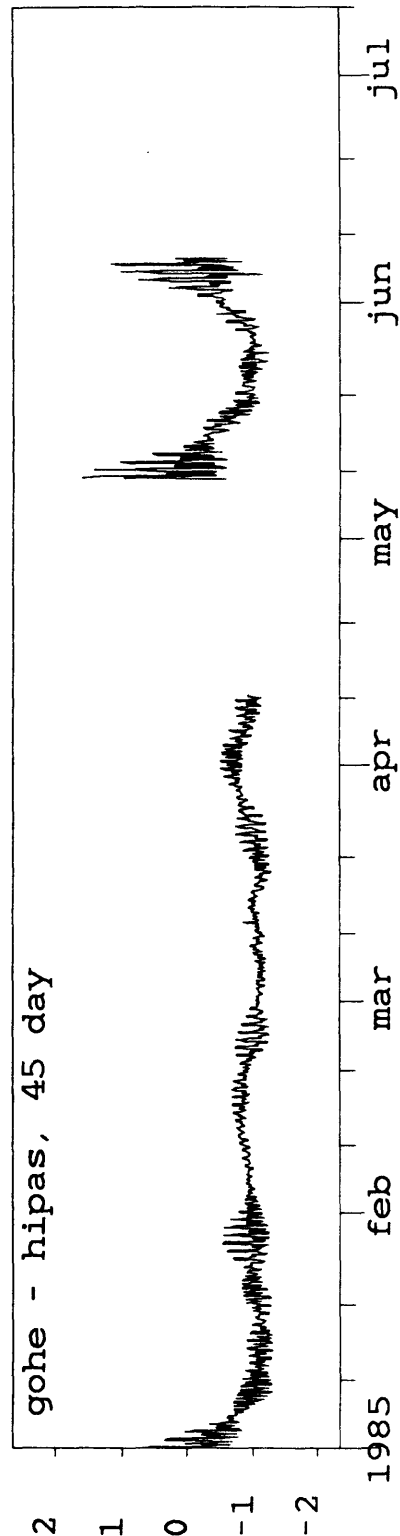
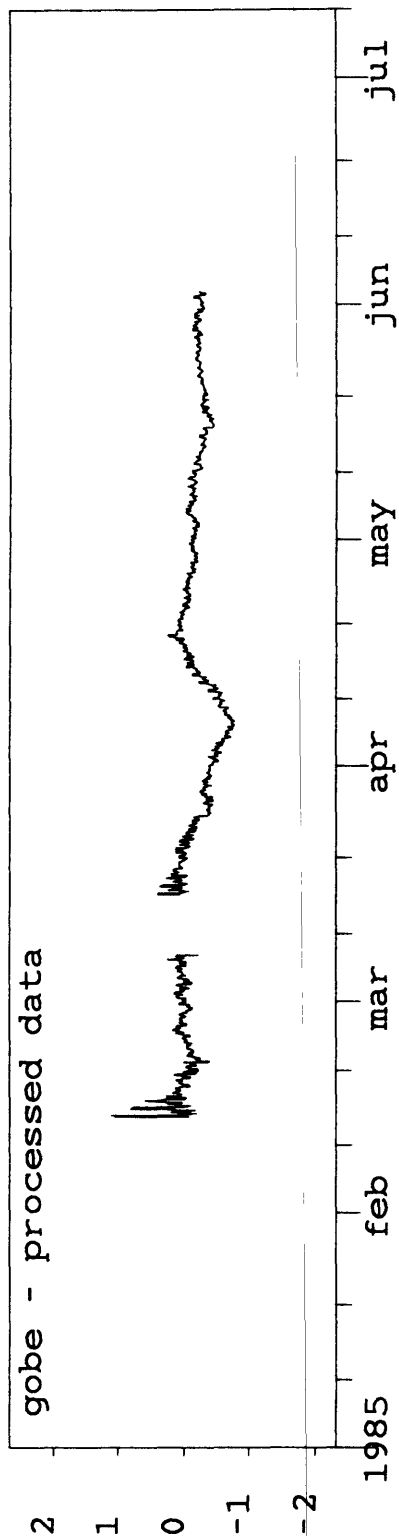
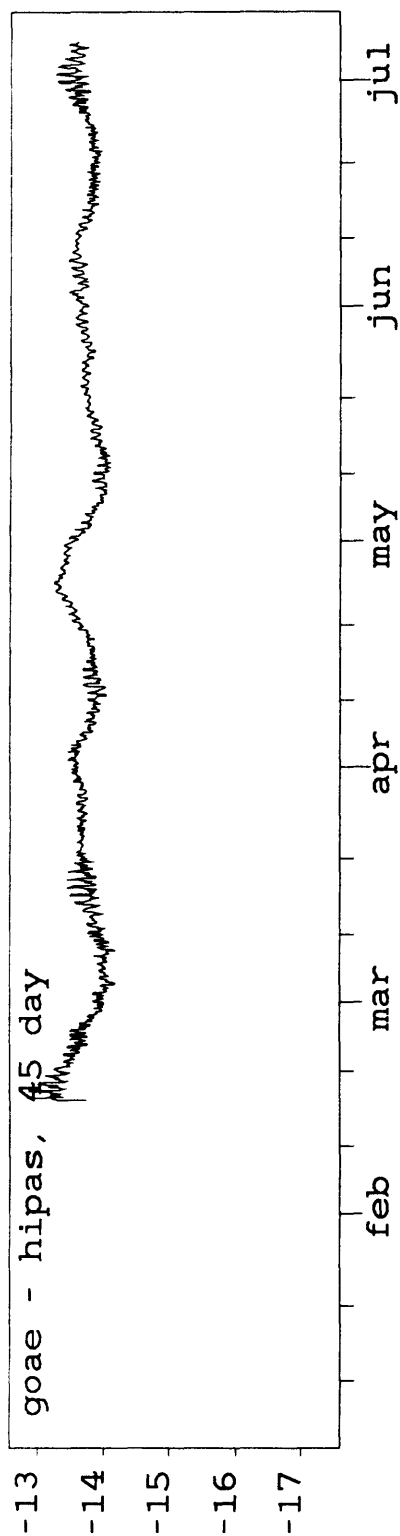


FIGURE 13.

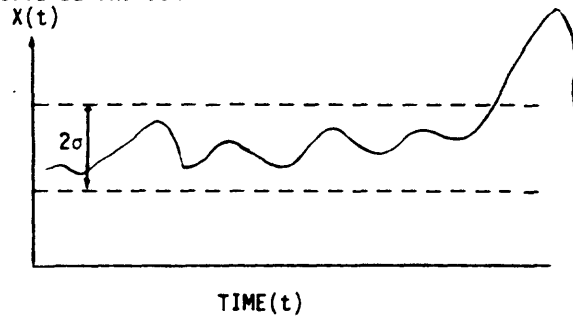




ANOMALY DETECTION ALGORITHMS

SINGLE STATION PRECURSOR DEFINITION

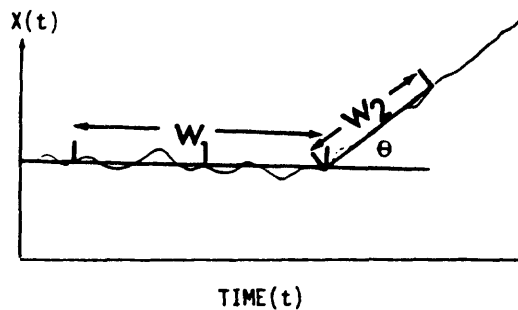
A) SIGNAL/NOISE DEFINITION



$$\begin{aligned} A(t) &= X(t) && \text{for } X(t) > 2\sigma \\ A(t) &= 0.0 && \text{for } X(t) \leq 2\sigma \end{aligned}$$

B) DATA FORM DEFINITIONS

1) RATE CHANGE



$$A(t) \propto \frac{\text{PROBABILITY FOR } W_1 \text{ and } W_2 \text{ THAT } \theta = 0.0}{\text{NOISE ESTIMATE}}$$

2) SIGNAL TYPE

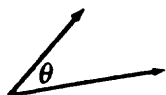
16

PRECURSOR DEFINITIONS FOR GROUPS OF STATIONS WITH THE SAME OR
DIFFERENT DATA TYPES.

A) SIMPLE SIMULTANEITY

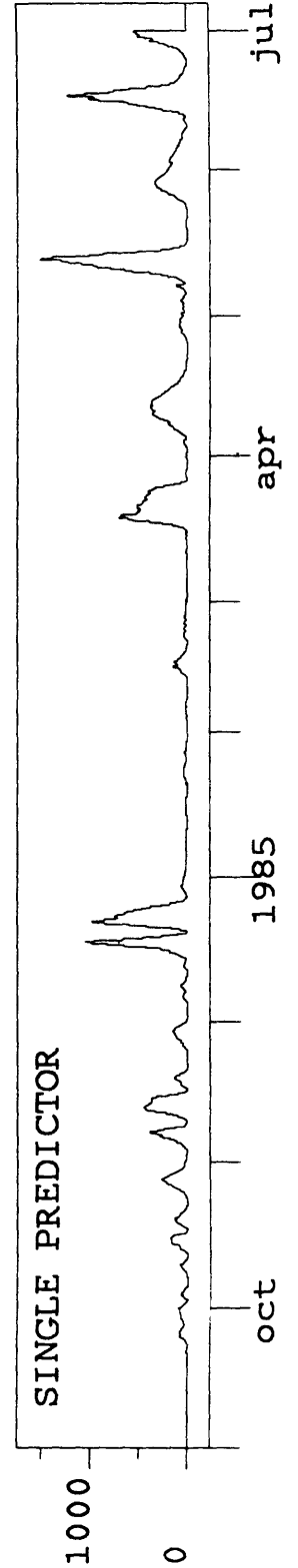
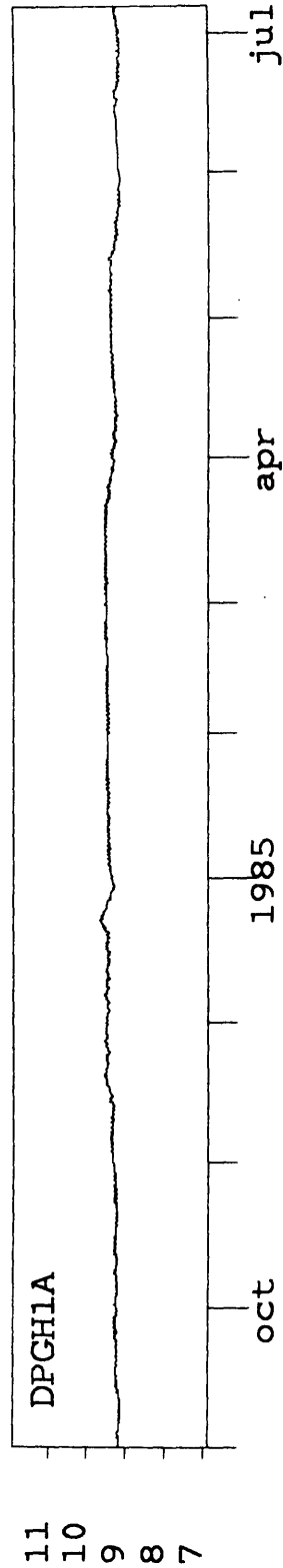
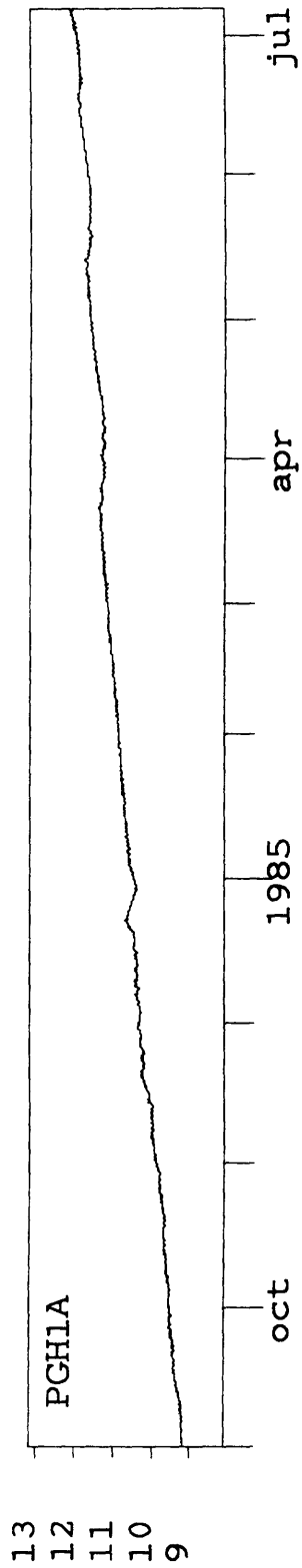
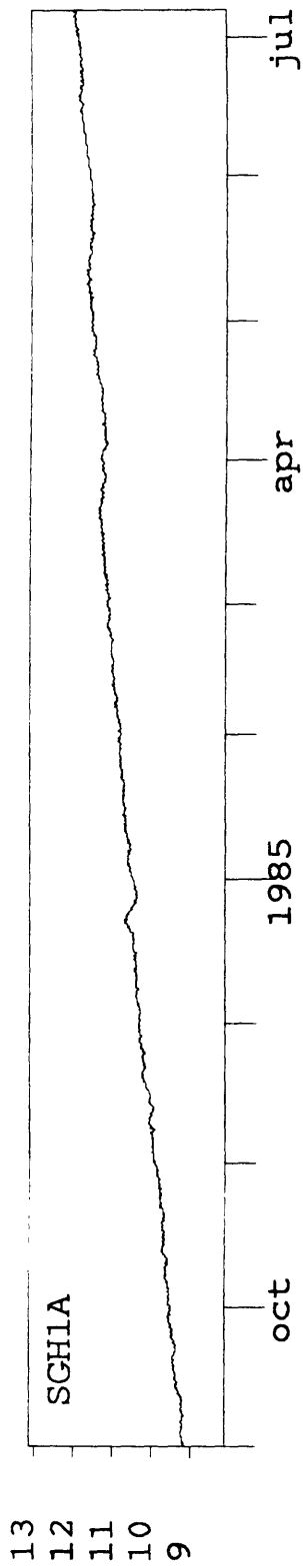
$$A_G(t) = K \sum A^J(t)$$

B) COHERENCE AND ANTICOHERENCE FUNCTIONS



$$A_G(t) = K (1 - \cos \theta)^2 L$$

C) OTHERS



APPENDIX A. 10.
Water Level Monitoring
J. D. Bredehoeft



United States Department of the Interior

GEOLOGICAL SURVEY

Water Resources Division
345 Middlefield Road, Mail Stop 66
Menlo Park, California 94025

WATER LEVEL MONITORING

J. Bredehoeft

For the past decade or so, water levels in a network of water wells have been measured in the Palmdale area as part of the earthquake prediction program. Three groups were engaged in the monitoring: Lamar and Merrifield, an independent geological consultant; Dick Mogle of the USGS, Water Resources Division; and Tom Hengey, University of Southern California.

Starting in 1982, a group under my direction began instrumenting some of the wells previously monitored by Dick Mogle with satellite telemetry. At each location the instrumentation includes: 1) pressure transducer for measuring water-level fluctuations in the well, 2) a barometer, and 3) a rain gage. Each location is self-powered by batteries which are charged from solar panels. A microprocessor collects and stores data at 15 minute intervals. Every three hours the data is transmitted in a one minute window via GOES satellite. In our case it is received at the Water Resources Division (WRD) offices in Phoenix, and transmitted via WRD data network to our WRD PRIME minicomputer in Menlo Park. The Phoenix receive site is backed-up by another WRD receive site in Denver. Initially we used LaBarge data collection platforms; in 1984 we replaced these with more up-to-date, Synergetic platforms. This technology was initially developed for "real-time" stream monitoring.

In considering which wells to instrument, only those which appeared to show earth-tide responses were selected. It is not uncommon for wells which tap confined aquifers to have good earth-tide responses--a double amplitude of several hundredths of a foot fluctuation in water level, or more. The extent of our current network is indicated in Table 1. Figure 1 shows the location of the wells at Parkfield.

Our recent focus has been on establishing a network of six or seven wells in the Parkfield area. We have been drilling these wells ourselves, locating them in what we hope is a reasonably optimal network designed to observe the co-seismic dilatational strain associated with a Parkfield earthquake. Hopefully, by using the co-seismic dilatation as a guide, we will also observe a possible precursor to the earthquake.

Comparison: Dilatometer versus Water Well

At Gold Hill we have a water well and a dilatometer within 30 meters of one another. Figure 2 is a fast fourier transform of a period of the Gold Hill water-level data. As indicated on the figure, a number of the prominent tidal constituents are apparent: M_2 , N_2 , S_2 , O_1 and K_1 .

Figure 3 shows a comparison of the fast fourier transforms for the dilatometer, water level and barometric records for the same period, November through December, 1984, at Gold Hill. As is apparent, the same tidal constituents are identified in both the dilatometer and the water-level data. However, the water level data is more strongly influenced by the diurnal and semi-diurnal barometric fluctuations than is the dilatometer.

Figures 4 and 5 are fast fourier transforms of data from the Turkey Flat and Flinge Flat wells. The Turkey Flat well has the major tidal constituents, indicating a good well for strain measurements. The Flinge Flat well has an M_2 peak; however, it is diminished in comparison to the semi-diurnal, S_2 peak. The Flinge Flat well is probably not as good a strain indicator as the other wells. However, Flinge Flat is strategically located with respect to a preparation zone at Middle Mountain.

As Table 1 indicates, we have only just completed drilling at Joaquin Canyon and Vineyard Canyon. Currently, we are drilling at Hog Canyon. The seventh well site at Parkfield is still problematical.

The largest tidal fluctuations we have observed in our California network are in a 1900 foot granite hole that Jack Healy drilled at Hi Vista in the Palmdale area. The tidal fluctuations in this well exceed a 0.1 foot. Figure 6 is a fast fourier transform of data from the Hi Vista well. The transform shows an M_2 peak much larger than the semi-diurnal S_2 peak. Figure 7 is a fast fourier transform of barometer data from Hi Vista. The barometric transform shows prominent diurnal, semi-diurnal and higher harmonic peaks. These peaks are also present in the water-level data, as is shown in Figure 6.

Two typical records for wells at Littlerock and Crystallaire are shown in Figure 8. The upper two traces are the raw data. The third trace is the barometer. The lower two traces are superimposed plots of the filtered records, both the barometer and the tides have been removed.

During the several years we have been collecting data, we have only observed a few events which seemed to be tectonic in nature. Figure 9 is a plot of the filtered Gold Hill water-level

record which shows the March-April, 1985 event. This event has an offset in water-level of approximately 0.2 feet--approximately 3 to 4 times the tidal amplitude.

Table 1. Water wells instrumental for strain measurements.

<u>Location</u>	<u>Date Instrumented</u>	<u>Comments</u>
Crystallaire (Palmdale area)	Feb. 1982	
Littlerock (Palmdale area)	Feb. 1982	
Hi Vista (Palmdale area)	Aug. 1982	
Fremont Valley (Garlock Fault)	Feb. 1982	Discontinued July 1985
Gold Hill (Parkfield area)	Jan. 1983	
Flinge Flat (Parkfield area)	Apr. 1984	
Turkey Flat (Parkfield area)	Aug. 1984	
Joaquin Canyon (Parkfield area)	(July 1985)	Drilled June 1985
Vineyard Canyon (Parkfield area)	(July 1985)	Drilled July 1985
Hog Canyon (Parkfield area)	-----	Drilling July 1985
(Middle Mountain) (Parkfield area)	-----	To be drilled Aug. 1985

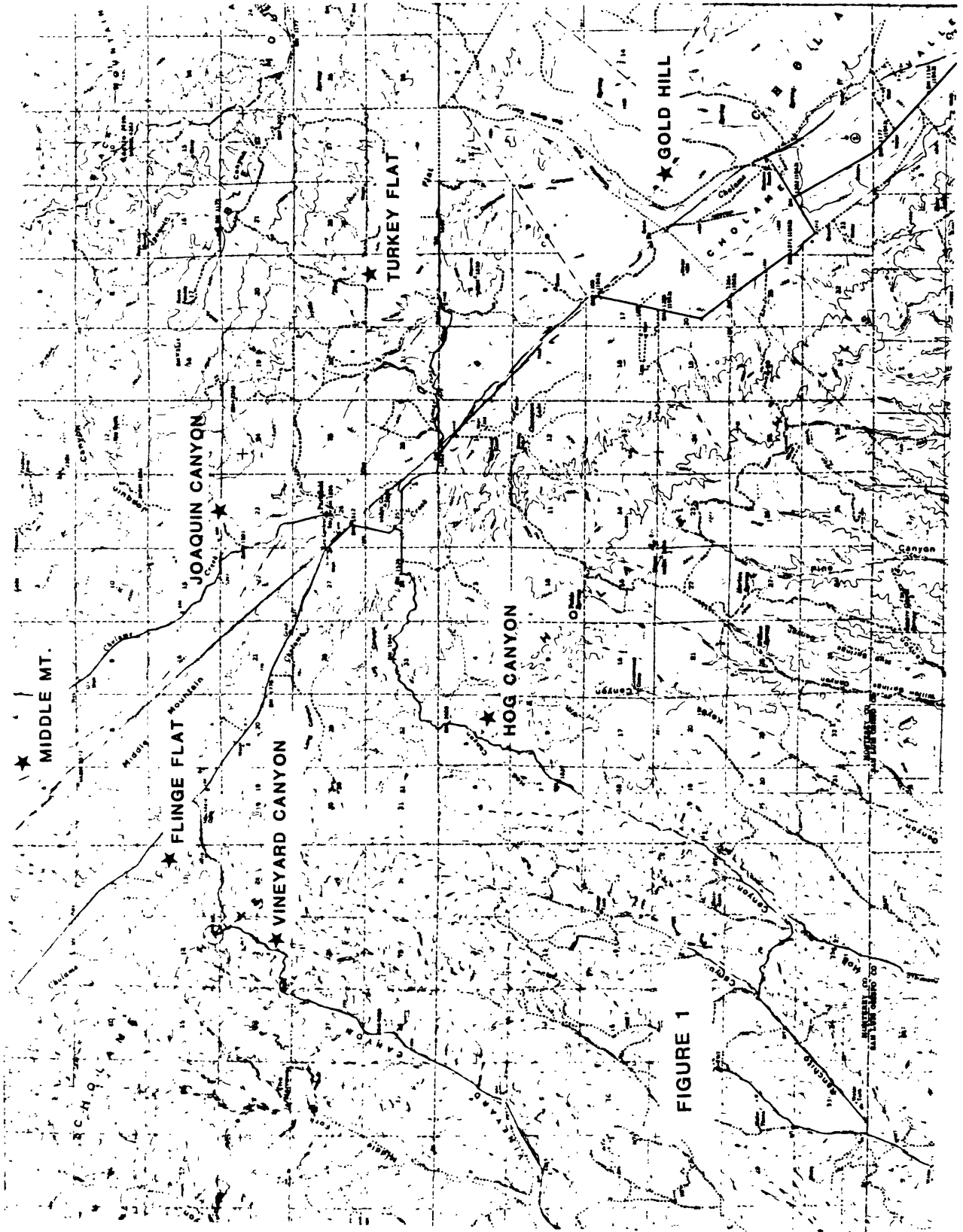


FIGURE 1

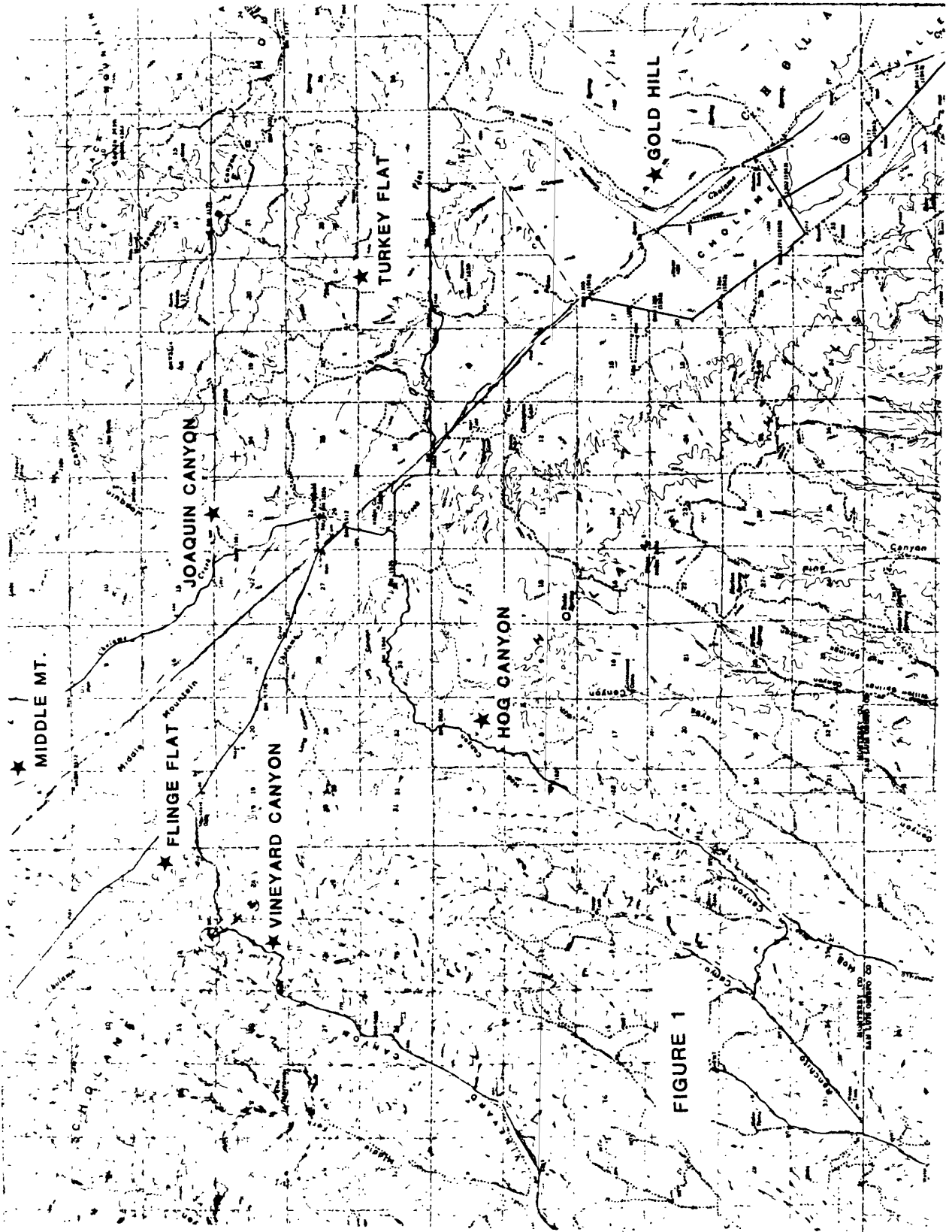


FIGURE 1

FIGURE 2

GOLD HILL

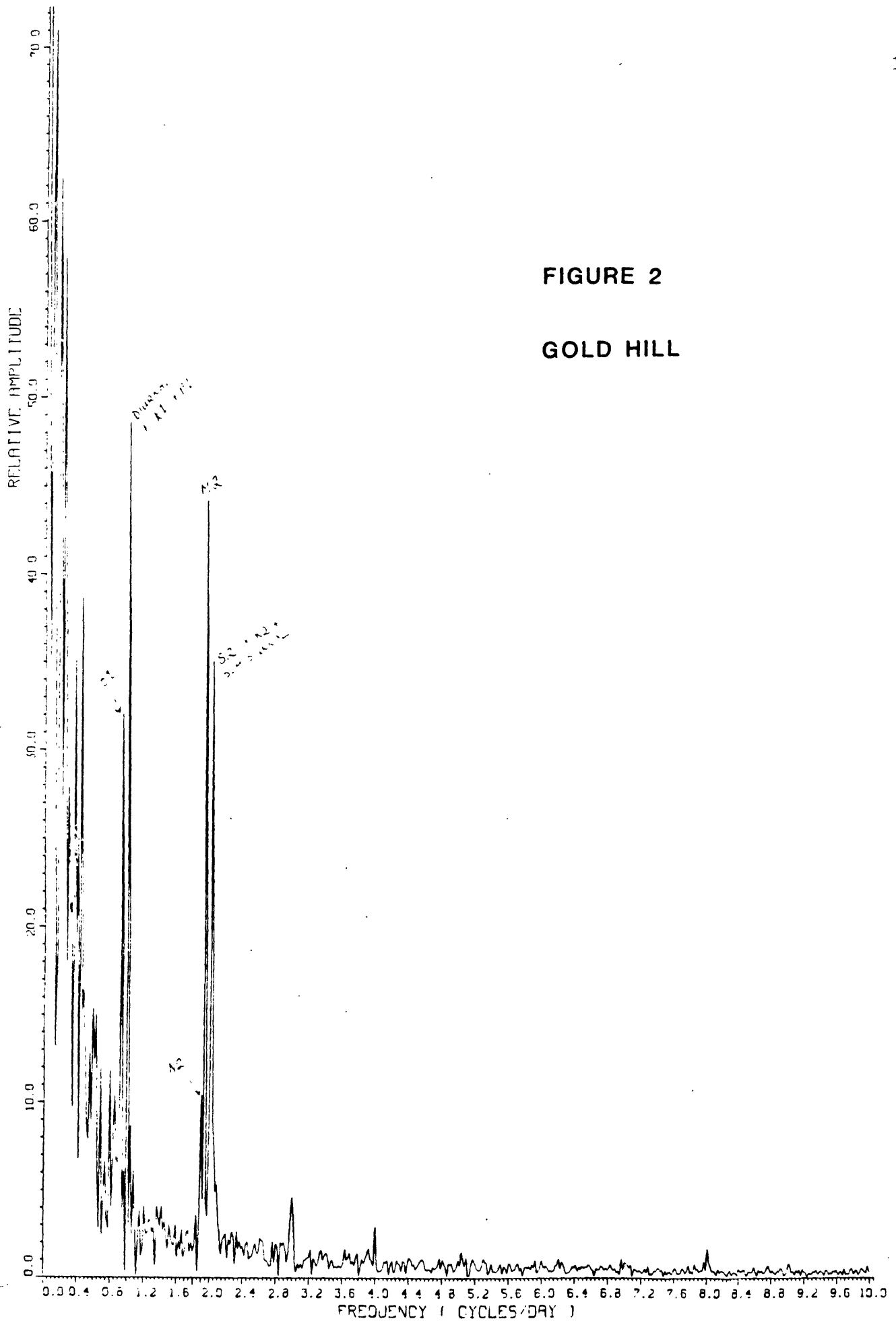


FIGURE 3

OLD HILL

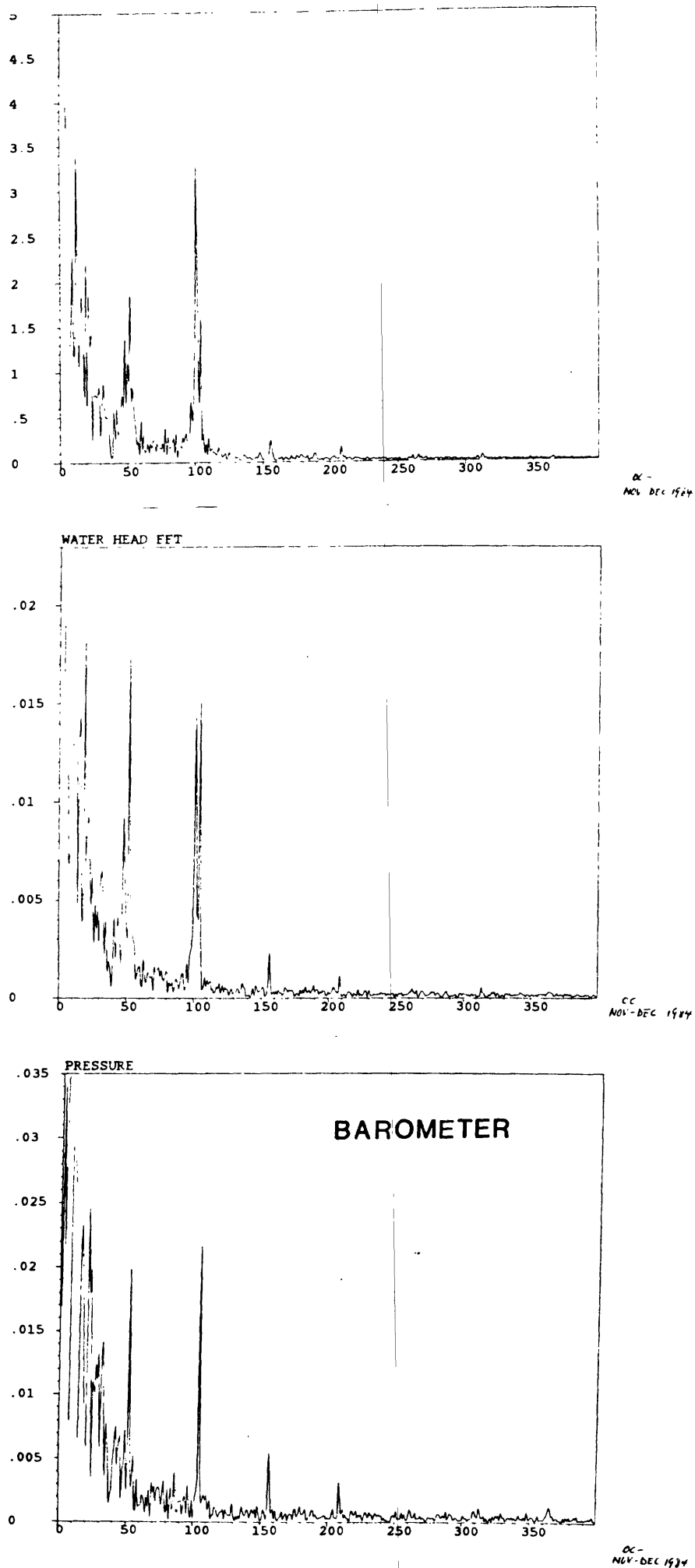


FIGURE 4

TURKEY FLAT

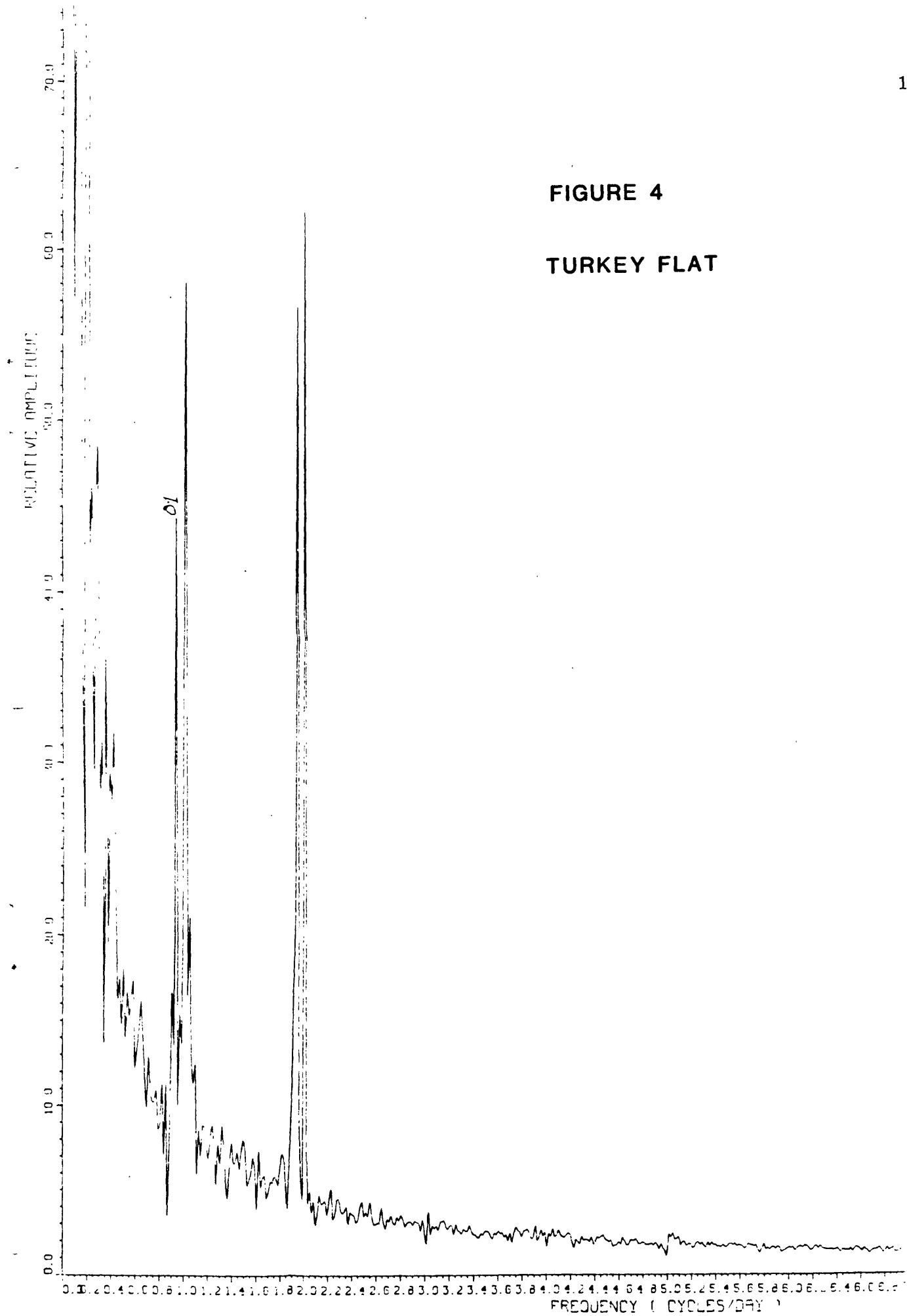


FIGURE 5

FLINGE FLAT

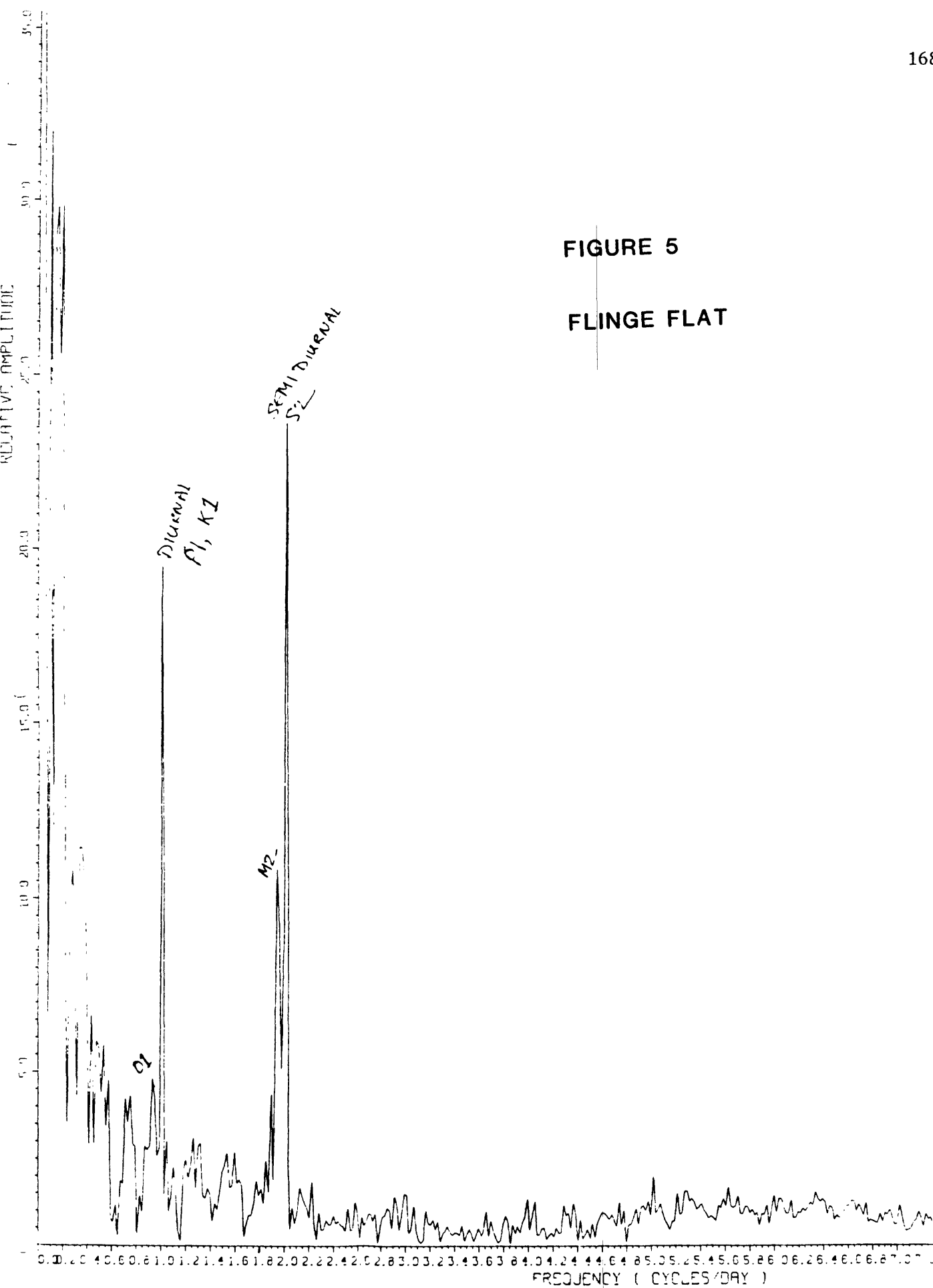


FIGURE 6

HI VISTA

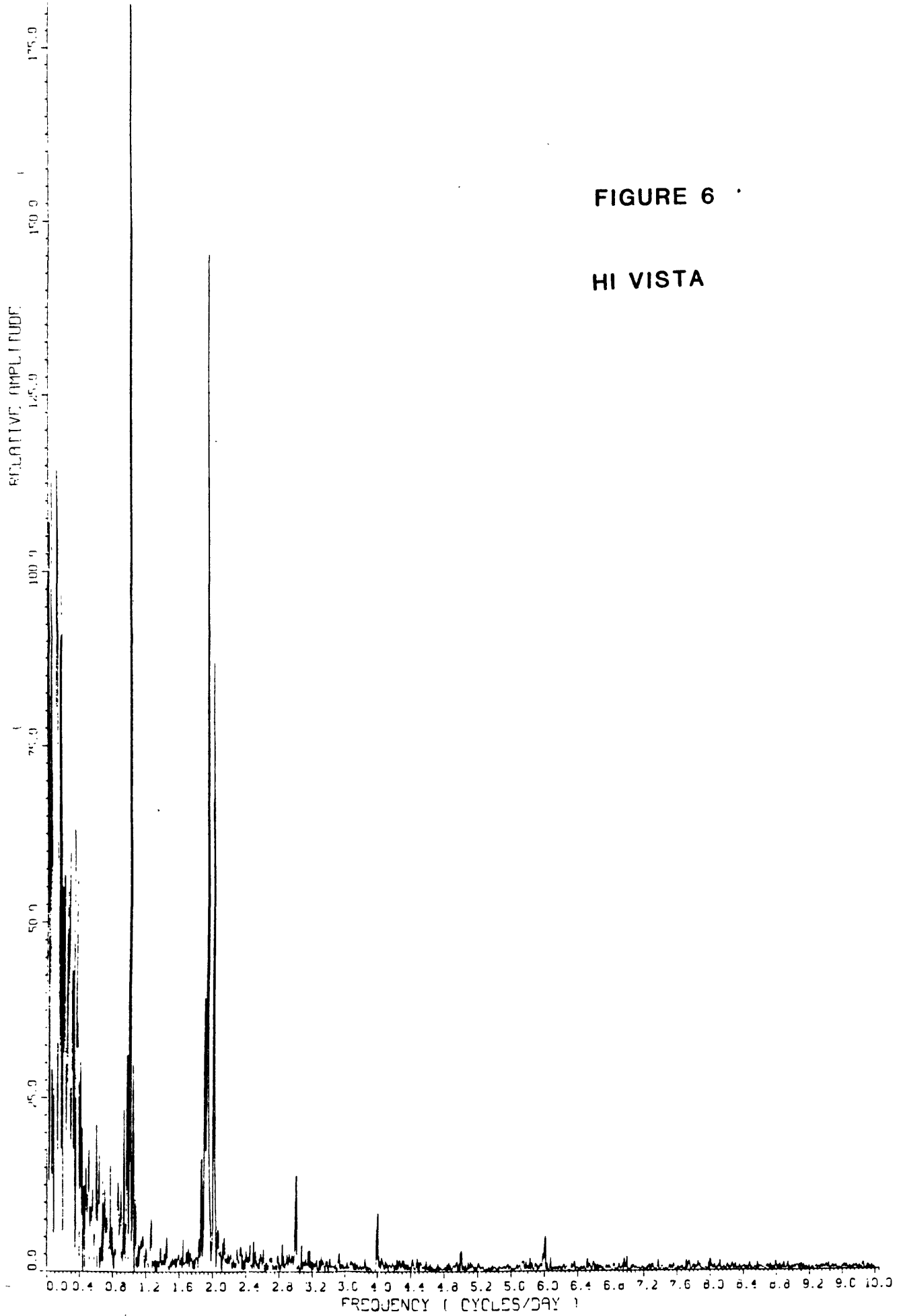
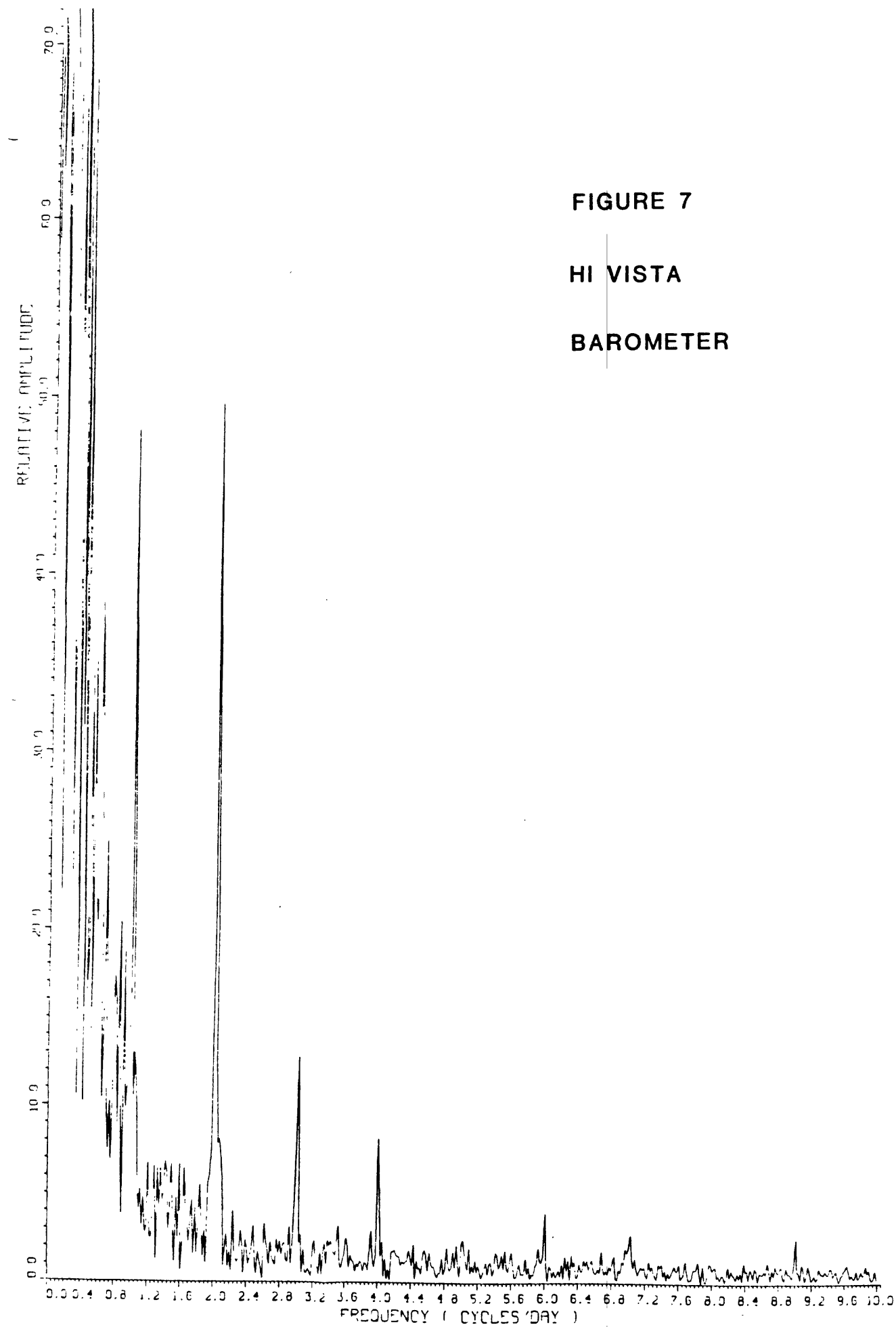


FIGURE 7

HI VISTA

BAROMETER



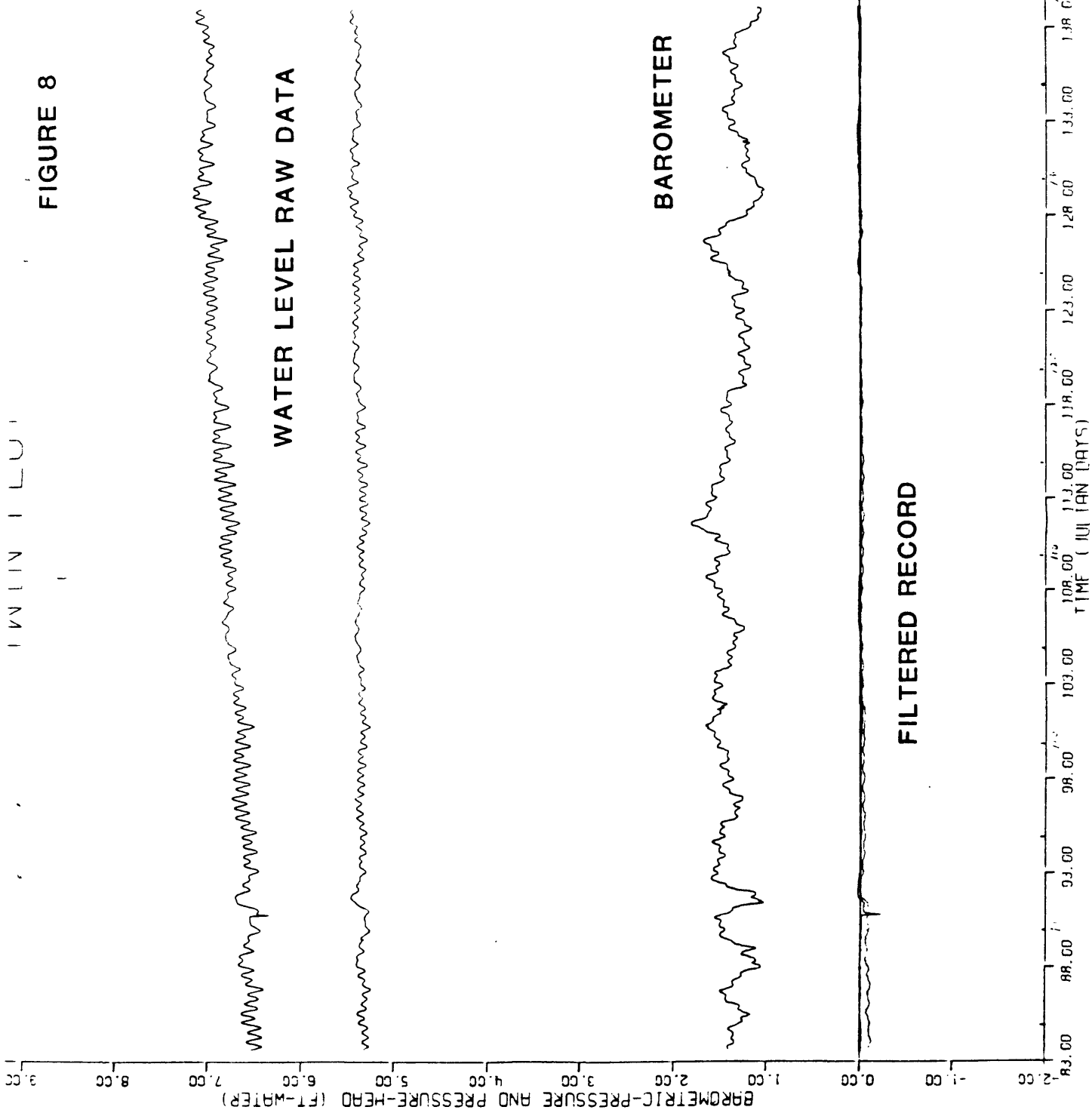
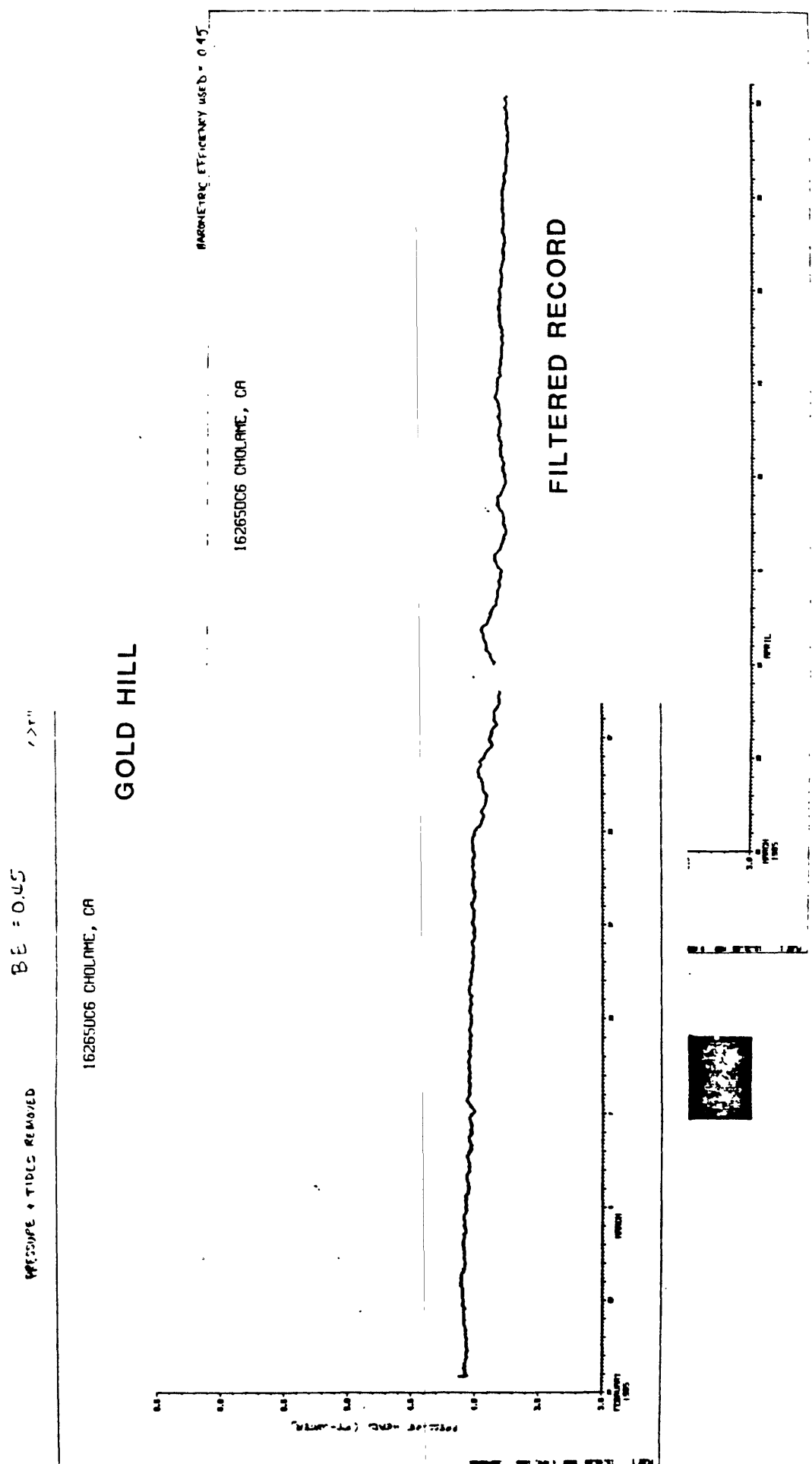


FIGURE 8

FIGURE 9



APPENDIX A. 11.

The Significance Expected of Near-Surface Tiltmeter
Data from Parkfield, California

S. Morrissey

The Significance Expected of Near-Surface
Tiltmeter Data From Parkfield, California

Sean-Thomas Morrissey
Saint Louis University

I. Introduction

The National Earthquake Prediction Evaluation Council has approved a formal prediction for an earthquake to occur within the next few years in the Parkfield area of central California. The Council will continue to evaluate this prediction and consider refinements of the time and place of occurrence in the light of new data as it becomes available. Parkfield has become heavily instrumented for this purpose, including not only intense seismological monitoring, but a broad array of geodetic and surface deformation investigations. Among these is a program to install near-surface tiltmeters in the area to provide data on any significant strain changes that would precede the anticipated earthquake, particularly during the final rapid stress loading stage anticipated by the model described by Stuart et al. (Parkfield Forecast Model, JGR, 90, 592-604). This paper will outline the task of determining the significance expected of near-surface tilt measurements.

II. Defining the "Noise" Level Above Which an "Event" Occurs

A) With geodetic data, including tilt, a baseline or reference-continuum of data points must be determined before any significant changes in the slope or rate of the data can be designated as significant "events." The variance about the baseline is generally considered to be a measure of the quietness of the background data, while "noise" consists of random data points or serial excursions of the data from a baseline for extended periods of time. The "noise level" is directly dependent upon the sensitivity of the data scale plotted, where a plot of the baseline data near the threshold of the instrument system resolution and/or stability will show the noisiest data.

B) This brings up the question of what can be done to improve the data after it has been acquired. Known noise spikes, etc., are always removed, but often little else is done, and meaningful interpretation is attempted of data series that have obvious contaminants in them, such as direct environmental effects. Efforts are always made to minimize these in the course of instrument design and installation, but acknowledging that well known residual series are contaminating the raw data is very important when an instrument system is being pushed to its maximum performance. Often linear correction of the data can improve the "flatness" of the baseline, hence the noise threshold, by an order of magnitude or more, if the sources of the noise are properly understood and monitored.

C) Noise sources for the tiltmeter system include the following:

1) Temperature variations in the electronics: The electronics have been completely redesigned, and the current system has a noise figure of less than 2 nano-radians per degree C. If it is housed with care, direct effect of temperature on the electronics should not be a problem.

2) Linear temperature variation in the sensor: The sensor is a biaxial liquid electrolyte bubble, made of glass and housed in a stainless steel chamber that is fastened to the bottom of a 60 cm tapered cast stainless steel pipe. The glass bubble is free to move ± 1 mm laterally within the mount, and its pressure spring (that presses the glass surface against the chamber top - the reference surface) is similarly free to move. This causes a direct (mostly) linear temperature effect that is independent in each channel; it seems to be wholly dependent on where the bubble and spring happen to be within the mounting, and can be changed by striking the housing. No remedy has been tried, but this is probably the main cause of the annual thermal cycles in the tiltmeter data that vary in amplitude and polarity from component to component, but repeat annually as long as the sensor is not disturbed.

3) Stress and thermal variation of the borehole pipe: The mounting of the borehole pipe to the rock, with the bubble housing screwed onto the bottom, is an important interface. Much experimentation has resulted in a procedure that results in very rapid stabilization of the tiltmeter, usually to the annual cycle baseline within a few hours. Figure 1 shows two examples of this. Figure 1a is a plot of the installation of the Adak south site, North unit, at a 2 meter depth, in August 1984. Figure 1b shows the reinstallation of the three tiltmeters at Pinon Flat, California, in May 1985. Alpha and Beta stabilized very rapidly; with Delta, there was a temporary wiring problem, but also the bubble mount threads seized when it was fitted to the borehole pipe creating a highly stressed condition. This resulted in the large excursions of the data. However, later figures will show that this stress seems to have relaxed. The bonding procedure, and the construction of the tapered pipe, provide a close impedance match to the host rock. Some linear thermal dependence may remain.

4) Local thermal sensitivity: That the sensor can confidently be mounted to a rock volume does not guarantee that the local rock represents the regional terrain or even adjacent rock volumes. Experience has indicated that the deeper a sensor is installed, the more likely the rock it is interfaced to will represent the regional stress, strain, or tilt pattern. Overcoring strain work has shown that up to a depth of about 6 meters, random results are found in the same location, but deeper than 6 meters, consistent results are often found. The Parkfield tiltmeters will be installed in holes of at least 10 meters depth. (We have repeatedly practiced 10 m deep installations at the test site, and are completing new equipment to work at any reasonable depth.) Most of the improvements with depth of installation reduce thermal noise and other direct environmental effects. A very general guideline is that thermal noise decreases with the cube of the depth

Figure 1a.

ADAK TILTMETER ARRAY, RAW DATA South Site, North Tiltmeter

176

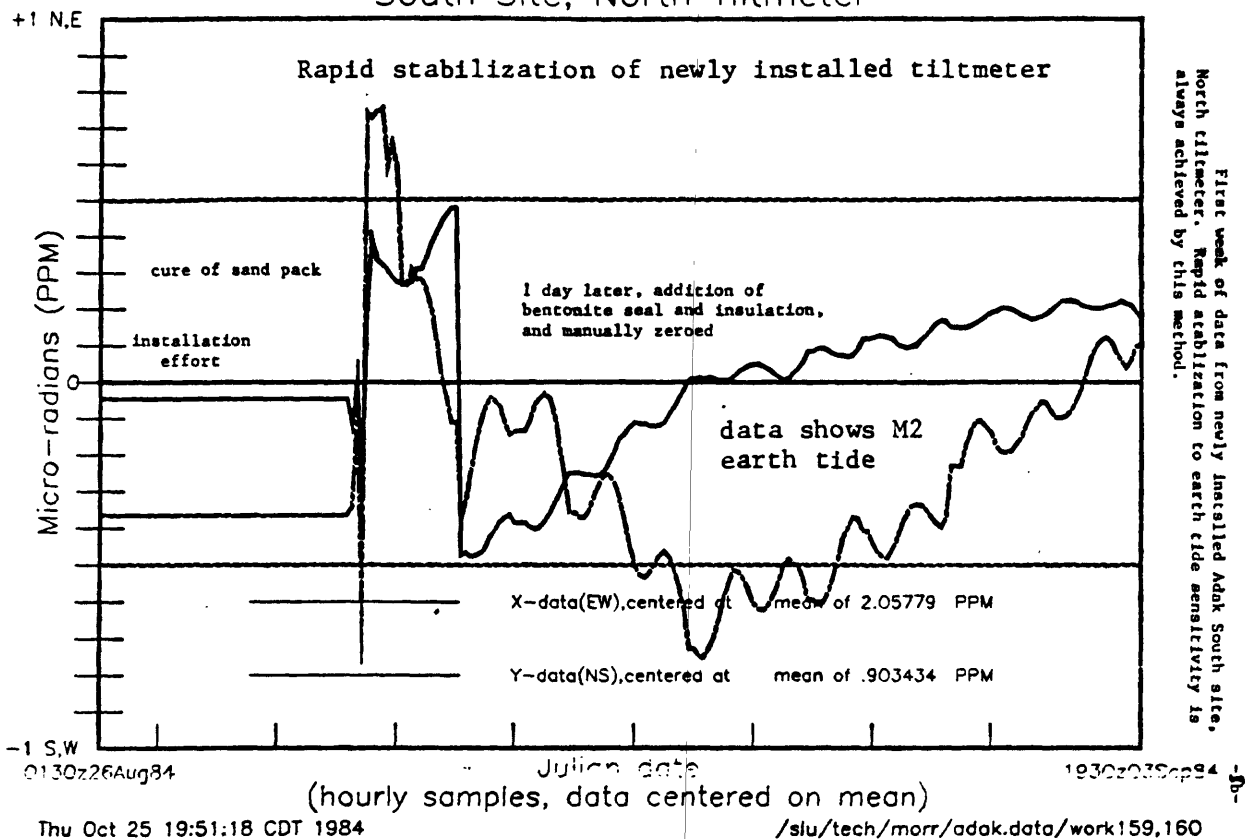
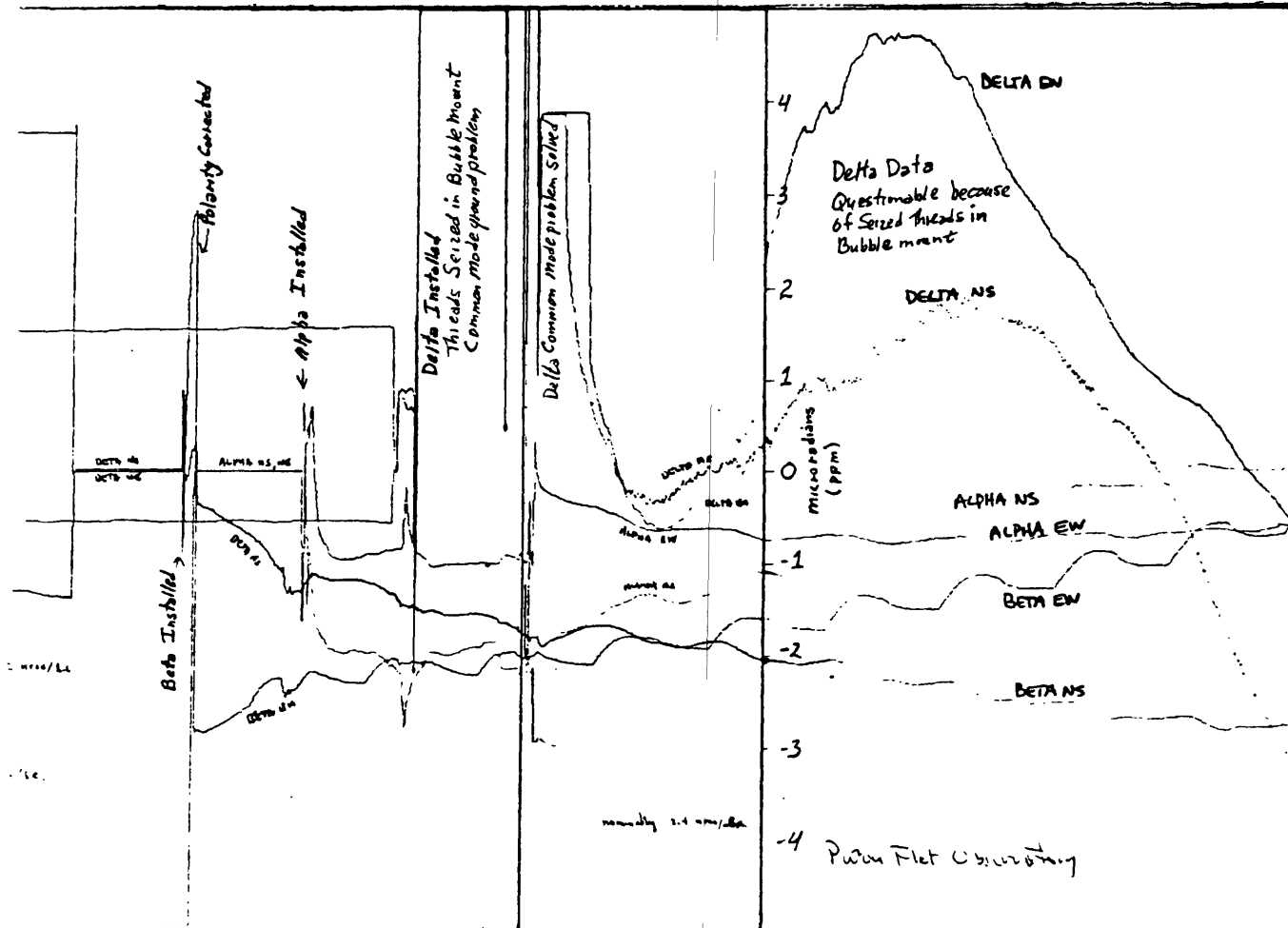


Figure 1b. First data after reinstallation of bubble tiltmeters at Pinon Flat.



increment.

5) Natural or cultural causes of tilt "noise": Even when a sensor is installed at a "quiet" depth, it does not mean that seasonal and other noise effects will not be a problem. With attenuation of shorter wavelength surface noises, long term regional effects will become evident, both natural and man-made. Pumping for irrigation is an obvious example. This should not be a problem at Parkfield. And, of course, the "natural" event we are looking for is the pre-event acceleration of tilt. By installing three instruments at each site, we expect that regional tilt events will be coherently recorded by all three, providing confidence in such data even if it is very near the noise level.

D) Estimates of Temperature Change in the Ground

1) Direct attenuation of surface temperature with depth can be estimated for temperature cycles of various periods. Figure 2, adapted from D.C. Agnew (unpublished paper on tiltmeters), shows the attenuation of the power spectral amplitude for a range of depth-squared X frequency values. The vertical bars show the attenuation of diurnal (D) and annual (A) thermal cycles for various depths in meters. For reference to plotted data, amplitude ratios are also indicated. As is quite clear, the diurnal signal is attenuated more at the 2 meter depth than the annual thermal cycle is at the 30 meter depth. These figures are based, of course, on totally closed ("ideal") holes in the halfspace; the open 2 m pits at Adak show only 10% of the attenuation expected here. The figure also indicates that even at 30 meters, a direct annual thermal effect on the sensor may be evident in the data.

2) Other causes of temperature change are more difficult to model, particularly rainfall, since it also causes hydrological stress changes, and can be warmer or colder than the ground. A heat flow sensor at Adak has provided an interesting analogue of the rainfall effect that often fits the observed rainfall noise at the south site, but also shows such events as the spring snow melt. Deeper installation, of course, should diminish these effects.

3) Unusual thermal noise sources have been encountered in deep holes, such as vertical water flow between two aquifers. At the present time, this tiltmeter installation method requires a dry, uncased hole, precluding depths where this would be a problem.

III. Examples of Noise Level from Available Data

A) The 2 meter deep units at Adak, Alaska

These units are installed in 1-2 meter deep pits 1 meter in diameter made by hand in hard rock with a gasoline powered jackhammer. A smaller 60 cm deep by 15 cm diameter hole is made for installing the borehole pipe. A bonded sand mixture is tamped into place around the borehole pipe, which is maintained to within 1 ppm of vertical during

Direct effect of temperature on sensor

SEMI LOGARITHMIC
MULTIPLYING
SCALE FACTORS

358.01

()

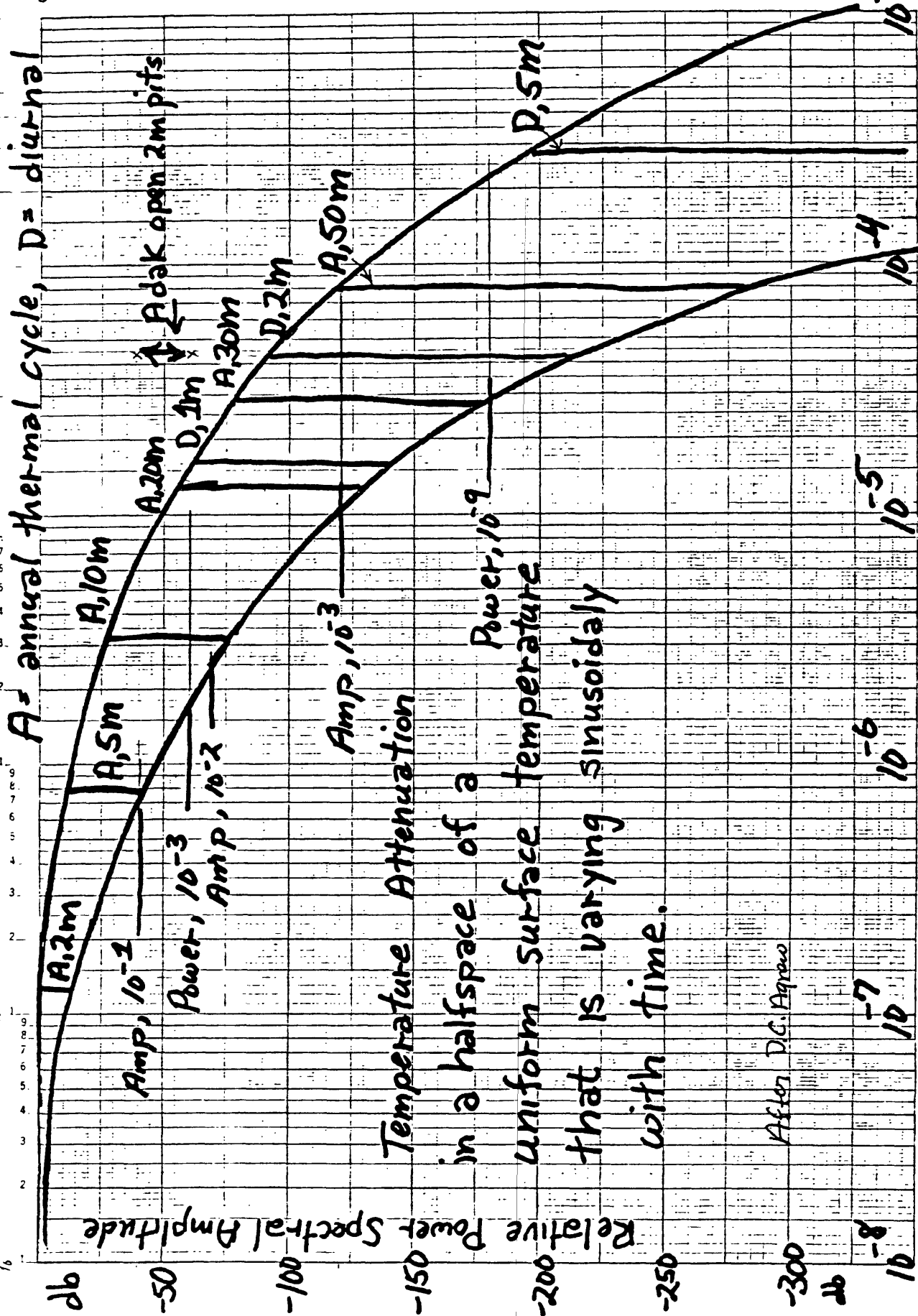
()

()

()

Figure 2

A = annual thermal cycle, D = diurnal



Zzf (m²h²)

the process. The pit is afterwards partially filled with bags of vermiculite insulation and protected with a highway "crash barrel" with several layers of insulation in the sides and top. There is now no specific research program to operate the Adak instruments, but they are continued in operation as long as the Adak seismic network, sponsored by CIRES of the University of Colorado and the USGS, is operated by this principal investigator. The tiltmeter system at Adak requires minimal annual maintenance, and the data are automatically recorded on floppy disks that are mailed to St. Louis every 8 days for analysis. Little routine analysis is done, other than a plot of the raw data to assure that the instruments are working.

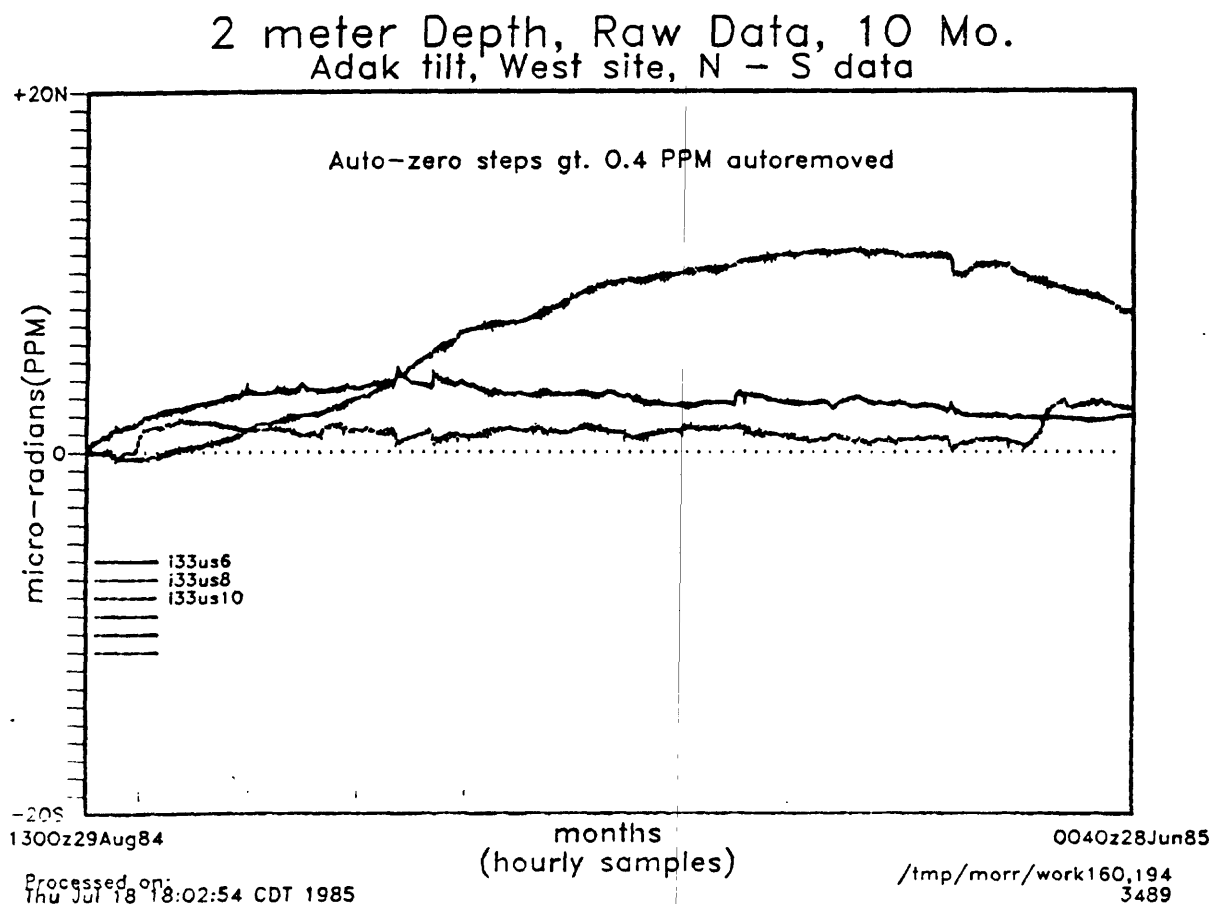
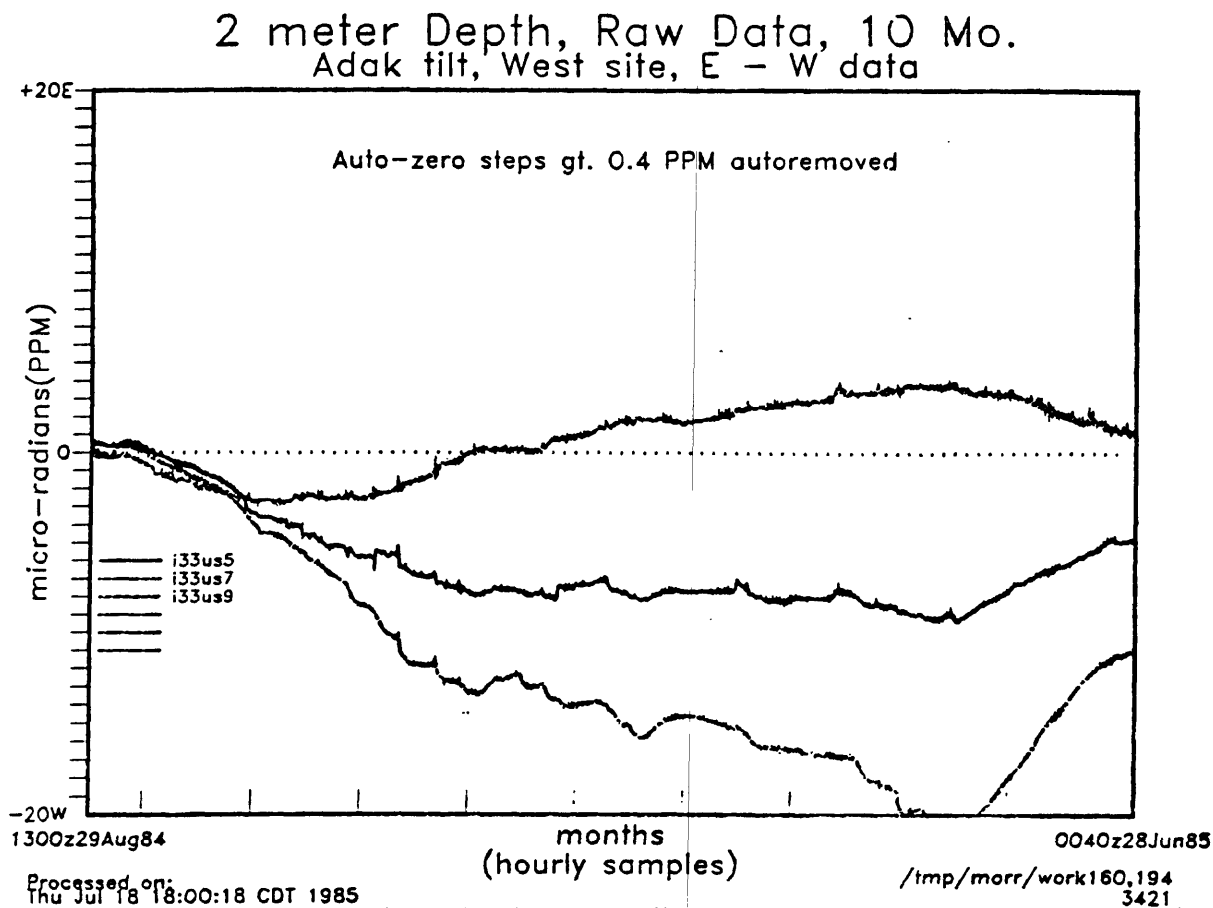
1) An arbitrary short 10 month sample of the data was chosen to see what the noise level would be for such a short data base. This happened to be the data from 29 August 1984 through 28 June 1985 that was stored on disk in the PDP 11/70 on July 7 when the author received the letter regarding the NEPEC meeting. Automatic routines that were developed for processing the data were applied to this set. The only improvement made was a refinement in generating the thermal profiles.

A valid criticism of the work done in February was that inflections of a month or more duration in the thermal profiles were reflected in the resulting residual tilt series, suggesting an apparent coherence at these periods. To avoid this problem, the thermal data was smoothed twice by using a cubic spline, first fitted at one point every 24 hours averaged (triangularly) over 48 hours, to produce a daily mean function, then again with a point every 840 hours (35 days), averaged over the same width of 840 hours. Also, since the cubic spline always fits the end points of the series, these were selected to represent the mean of the first or last 10 days of the data, thus avoiding artificial inflections at the beginning and ends of the series. The resulting curves are very smooth, and the week-to-month period events remaining in the residual tilt series after deconvolution of the temperature are not artifacts of the processing; site coherency shows that these are real tilt events.

The following figures will show this 10 month data set from Adak, using only the West site data, where three tiltmeters are operating. There are a total of 8 at Adak, currently at two other sites, but the data from these other sites is of less value for this analysis because of more recently understood shortcomings with the site selection and borehole construction. For example, the North site is in relatively flat terrain, the pits are over 3 m deep, and are always flooded, but the boreholes were made in badly weathered rubble rather than any sort of competent rock.

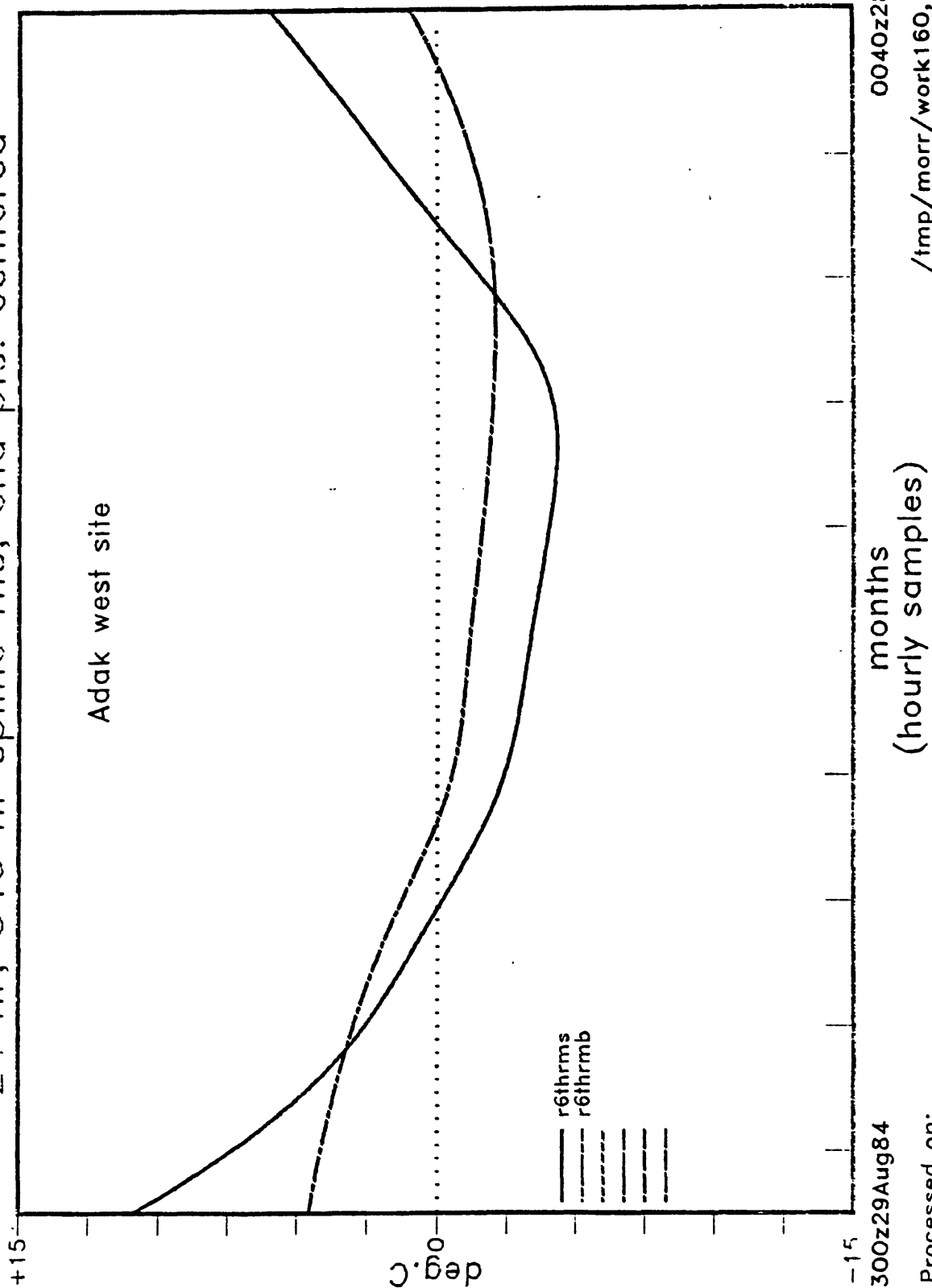
a) Figure 3 is a plot of the raw data for the three instruments. The only processing done has been a program that removes the steps caused by the auto-zeroing system (any step greater than 0.4 ppm/hour).

b) Figure 4 shows the thermal profiles for the West site. The borehole temperature is from the east borehole, and the surface temperature sensor is in the site microprocessor/digitizer enclosure. The smoothing process was described above.



10 Mo. Surface and Borehole Thermal Profiles 24 hr, 840 hr spline fits, end pts. centered

Figure 4



c) Figure 5 shows the residual tilt data after least-squares fitting of the two thermal profiles. It is plotted at the same scale as the raw data of Figure 3. The periodic fuzziness of the trace is the earth tide. The spike-like events are periods of rainfall or snow melt.

d) Figure 6 is an enlargement of the residual tilt of Figure 5. The scale here is ± 10 ppm, and linear regression lines have been fitted to the data. The earth tides, rainfall, snow melt events, etc., are rather obvious. There is also a long period term remaining in the data, with a period of about 1 year, that may be part of the annual thermal cycle that has not been properly fitted. The linear regression lines have a scatter in slope of ± 2 ppm/year with this short data base. Examination of the details of the data shows that large anomalous excursions have sometimes dominated the fitting process. For example, the N-S component of the W.S. tiltmeter shows a positively sloped regression line, while most of the data follows the negatively sloped line of the W.E. data. The step-like excursions in the first and last months of that series have had a strong influence on the linear regression. Clearly, a longer time series is required for a representative linear regression.

e) Table 1 is a summary of the statistical data produced during the least-squares fitting process for the whole suite of tiltmeters. (The E (east site) tiltmeter was discontinued in 1984, so the series contains only a fragment of data; the remainder is a zero line.) The % fit data is unity minus the ratio of the standard deviation of the input to the standard deviation of the output of the fitting process, expressed as a percentage. Conversely, if the variance of the input equalled the variance of the output, no fit was accomplished, and the % fit is small. The mcrR is the multiple correlation coefficient, relating the significance (expressed here as a percentage) of the fit of the linear regression line to the residual tilt data. It is an estimate as to whether the line itself is meaningful. For example, the N-S data of the W.S. tiltmeter is dominated by the above mentioned step in the first and last months, but contains little of the annual thermal cycle. Thus the fit percentages are all small, and even the fit of the straight line is less than 5%. Similarly, the mcrR is also very small (less than 0.5 or, here, only 30%).

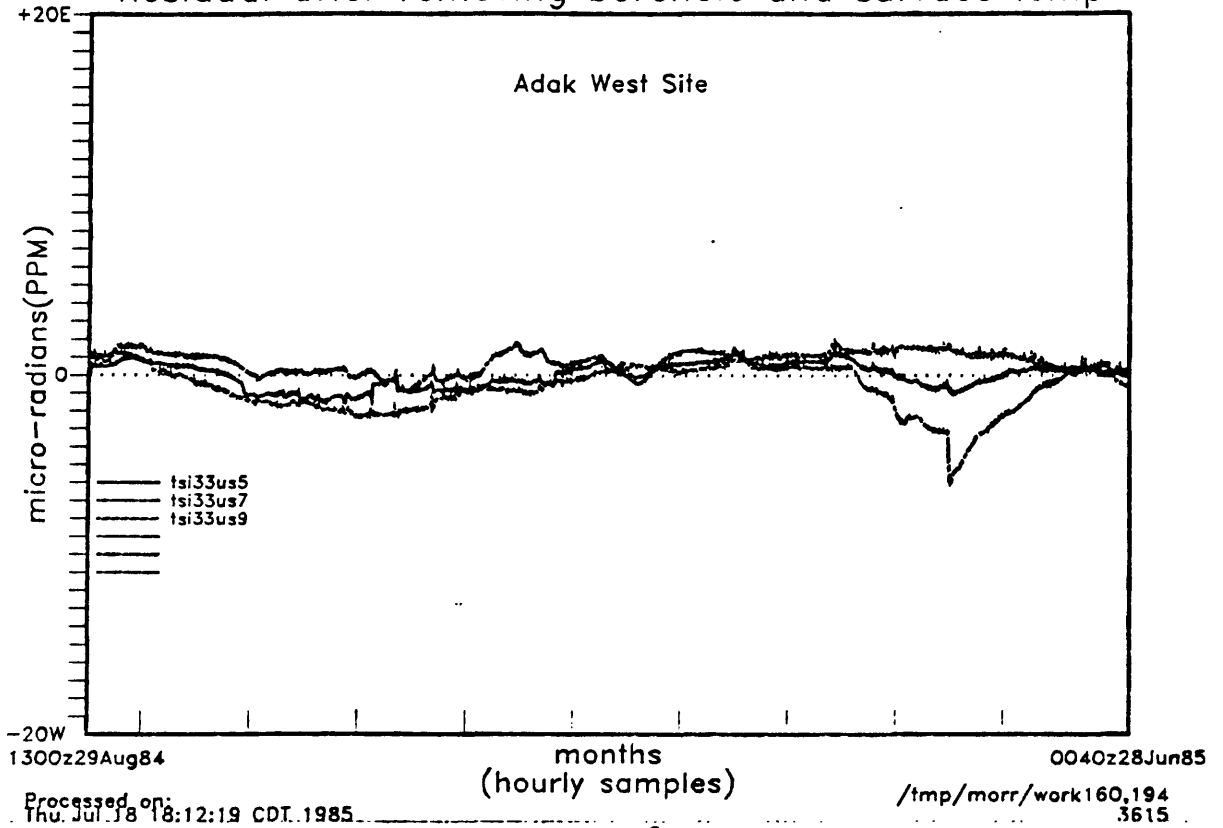
2) A 20 month data set had been prepared in January for a preliminary paper on estimates of secular tilt at Adak (which is when all the processing was developed). This 20 month set was remounted and the thermal profile series were reprocessed as described above. Slightly better fits resulted, but the linear regression values were similar to the previous values. This data set overlaps the 10 month data set by 11 floppy disks, or about 3 months.

a) Figure 7 is a plot of the raw data from the West site, as described above for Figure 3. A major portion of the W.E. unit, NS data is missing due to a shorted cable.

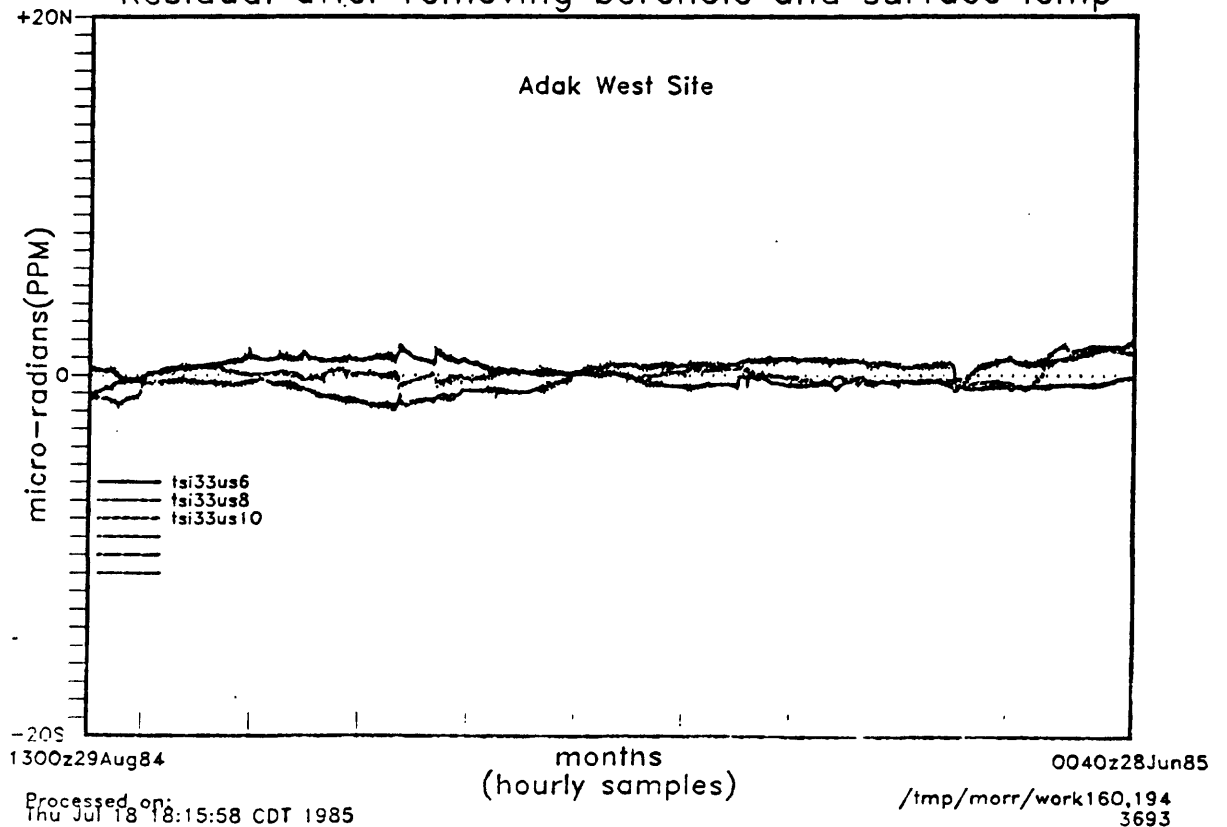
b) Figure 8 is a plot of the thermal profiles derived from successive cubic spline fitting as described above.

c) Figure 9 is the residual tilt data plotted at the same scale as

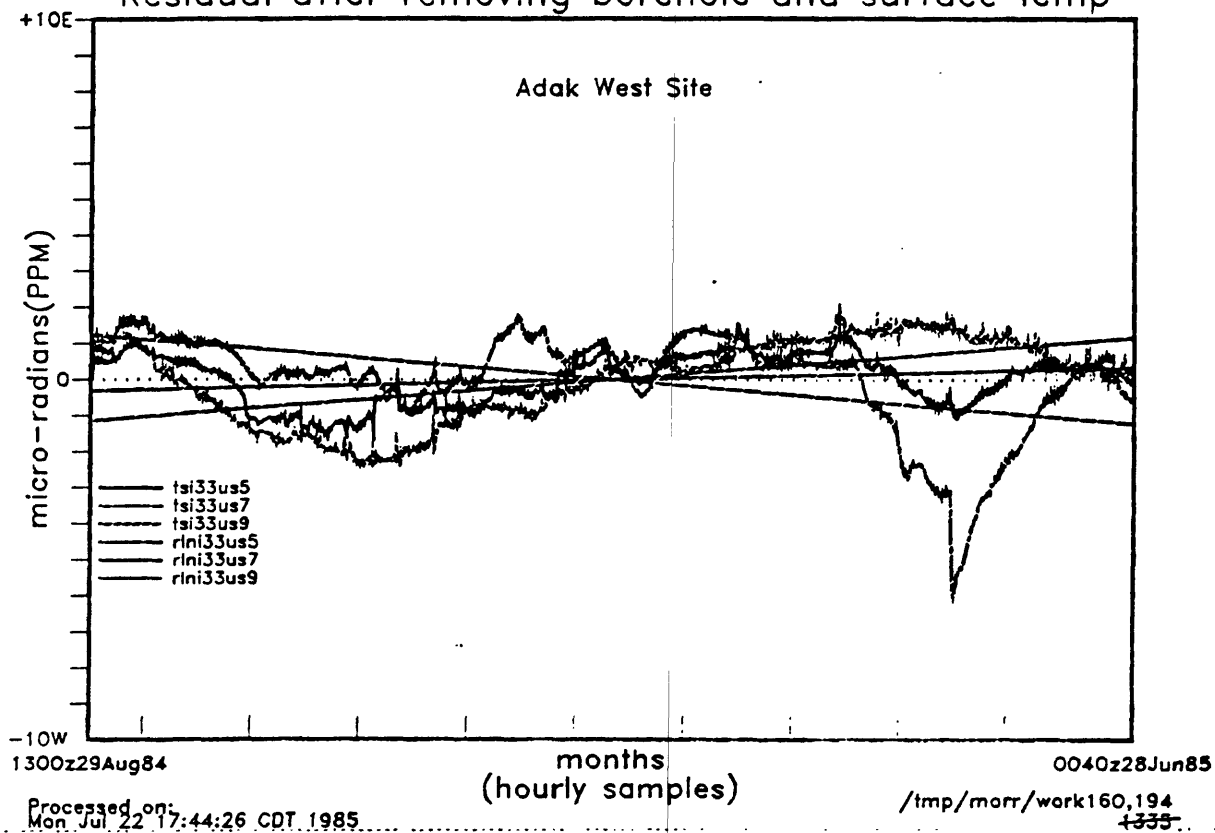
E - W Tilt, 10 mo., Corrected for Temperature
Residual after removing borehole and surface temp



N - S Tilt, 10 mo., Corrected for Temperature
Residual after removing borehole and surface temp



E - W Tilt, 10 mo., Corrected for Temperature
Residual after removing borehole and surface temp



N - S Tilt, 10 mo., Corrected for Temperature
Residual after removing borehole and surface temp

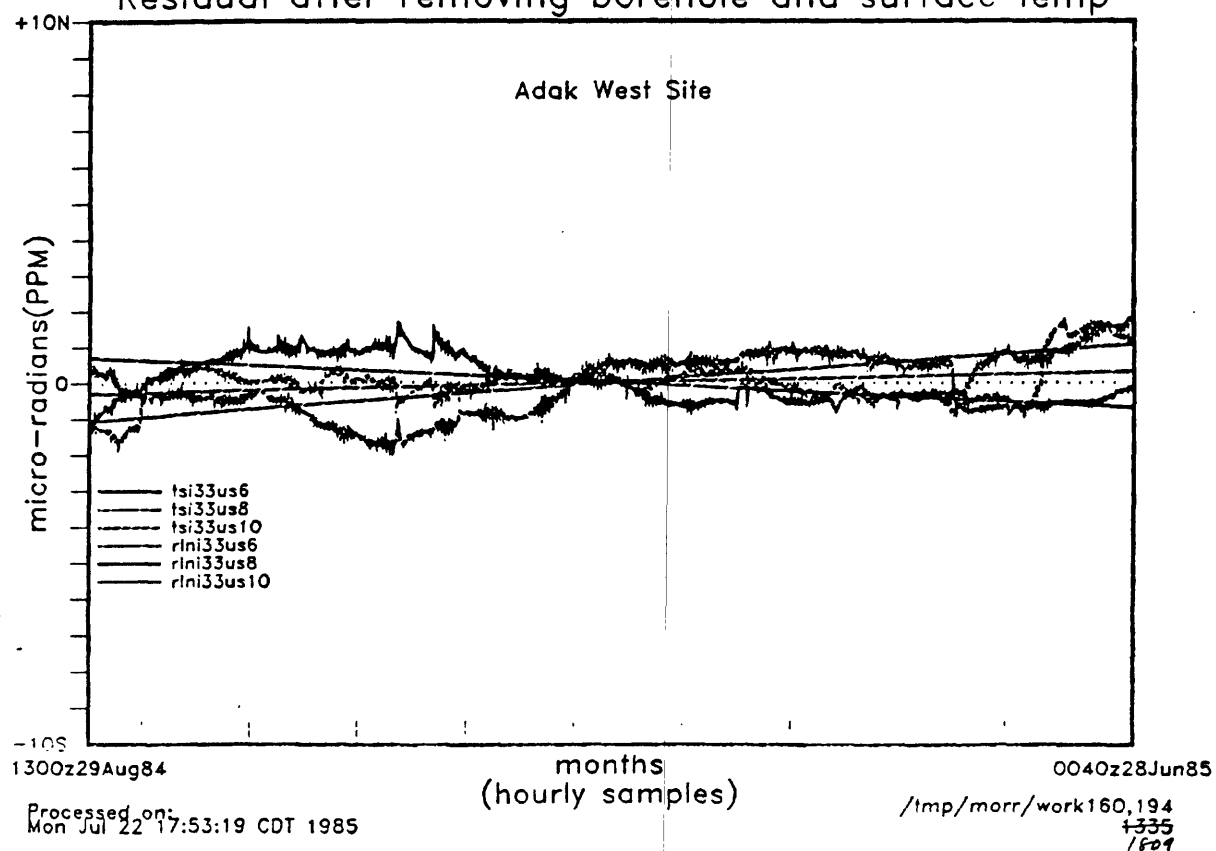


Table 1. Summary Statistics from analysis of 10 month data set.

Process date: Mon Jul 15 19:08:21 CDT 1985

decimation is 7

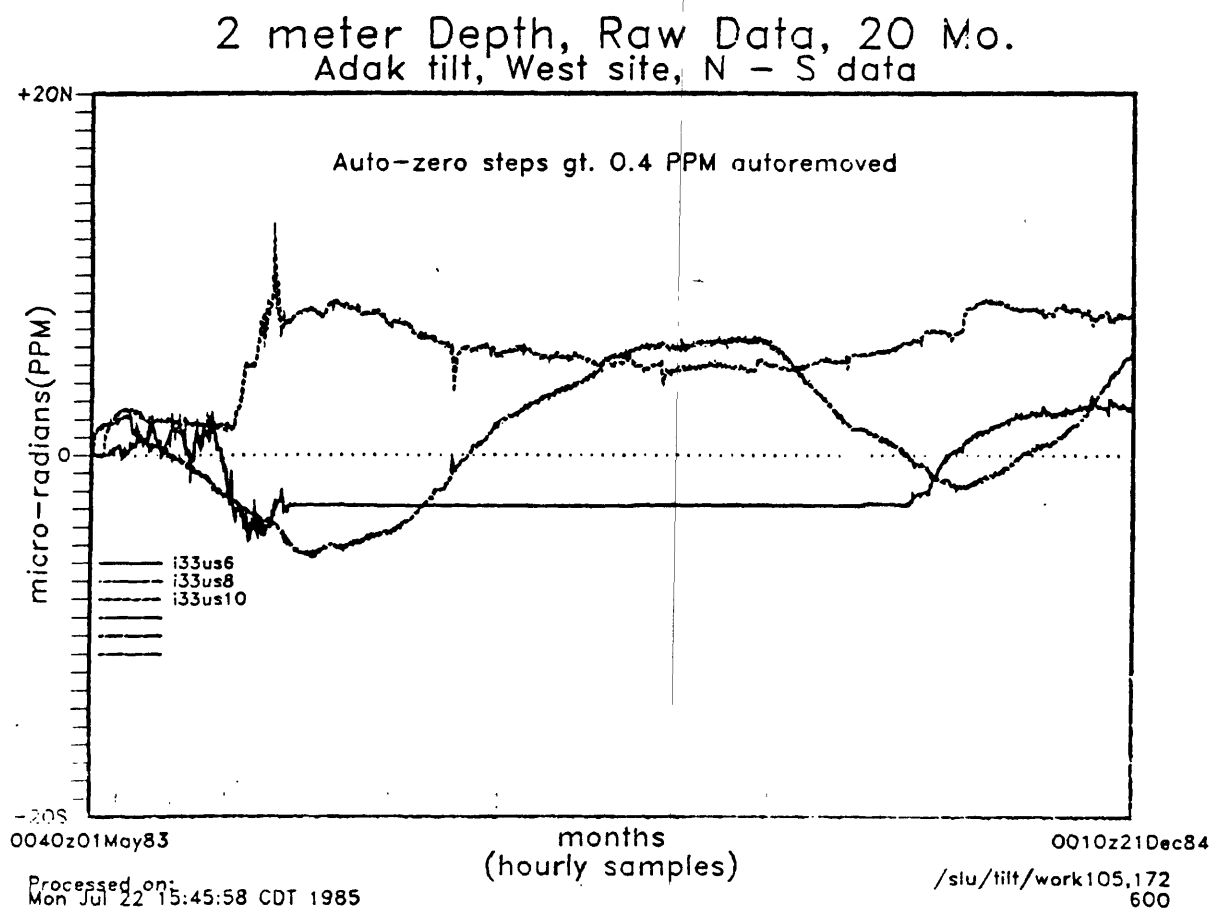
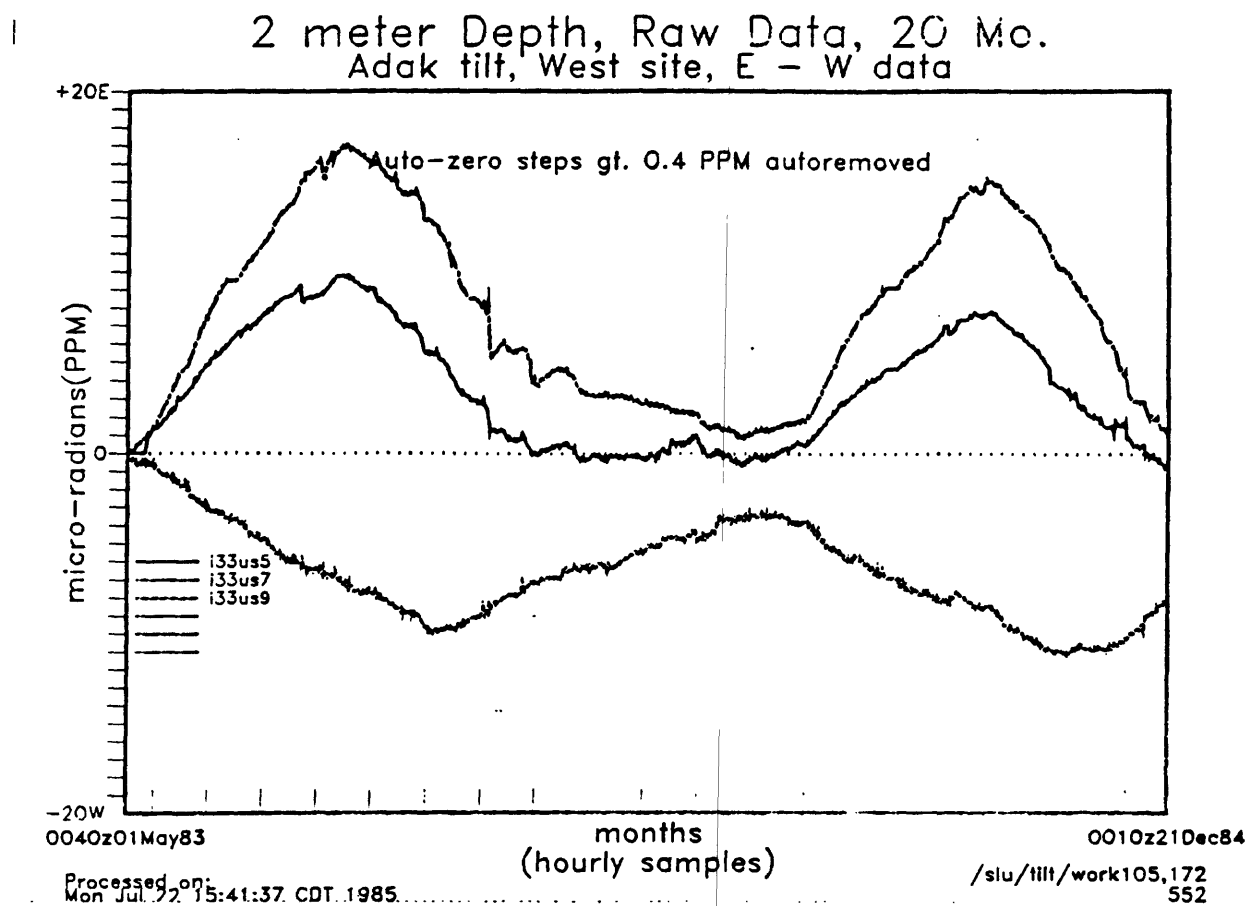
Summary of x (EW) data:

channel	unit	borehole thermal		surface thermal		straight line		meanF	mccR
		%Fit	fit(b)	%Fit	fit(b)	%Fit	fit(b)		
131us5	SE	78.7	-9.440	11.6	-0.525	27.3	-0.249	39	69 %
131us7		64.2	4.981	10.8	-0.470	13.6	-0.171	30	50 %
132us5	NE	0.1	-0.054	14.3	-0.464	46.9	-0.238	20	85 %
132us7	NW	0.2	0.093	2.7	0.196	7.3	0.113	3	37 %
133us5	WE	73.5	3.133	2.5	0.104	3.5	0.044	26	26 %
133us7	WW	75.3	7.005	8.5	-0.393	14.8	-0.170	33	52 %
133us9	WS	39.1	-2.033	11.4	0.396	18.2	0.158	23	58 %
134us5	E	31.1	0.646	1.8	0.064	0.1	0.005	11	4 %
Averages		45.3		8.0		16.4		23	48 %

Summary of y (NS) data:

channel	unit	borehole thermal		surface thermal		straight line		meanF	mccR
		%Fit	fit(b)	%Fit	fit(b)	%Fit	fit(b)		
131us6	SE	25.8	-2.478	0.3	-0.113	3.1	-0.134	10	25 %
131us8		59.2	-14.690	15.6	1.923	39.9	0.882	38	80 %
132us6	NE	41.2	-1.178	3.7	-0.126	9.8	-0.071	18	43 %
132us8	NW	16.2	0.821	3.4	0.178	9.3	0.102	10	42 %
133us6	WE	1.6	-0.154	13.4	-0.233	24.5	-0.097	13	66 %
133us8	WW	75.7	-4.638	11.6	0.296	31.1	0.148	39	73 %
133us10	WS	0.2	0.049	0.3	0.031	4.8	0.043	2	30 %
134us6	E	25.5	-0.404	2.7	-0.056	0.2	-0.006	9	7 %
Averages		30.7		6.4		15.3		17	46 %

(Note: mccR is multiple correlation coefficient, expressed as percent.)



20 Mo. Adak Thermal Profiles 24, 840 hr splines, and pts. centered

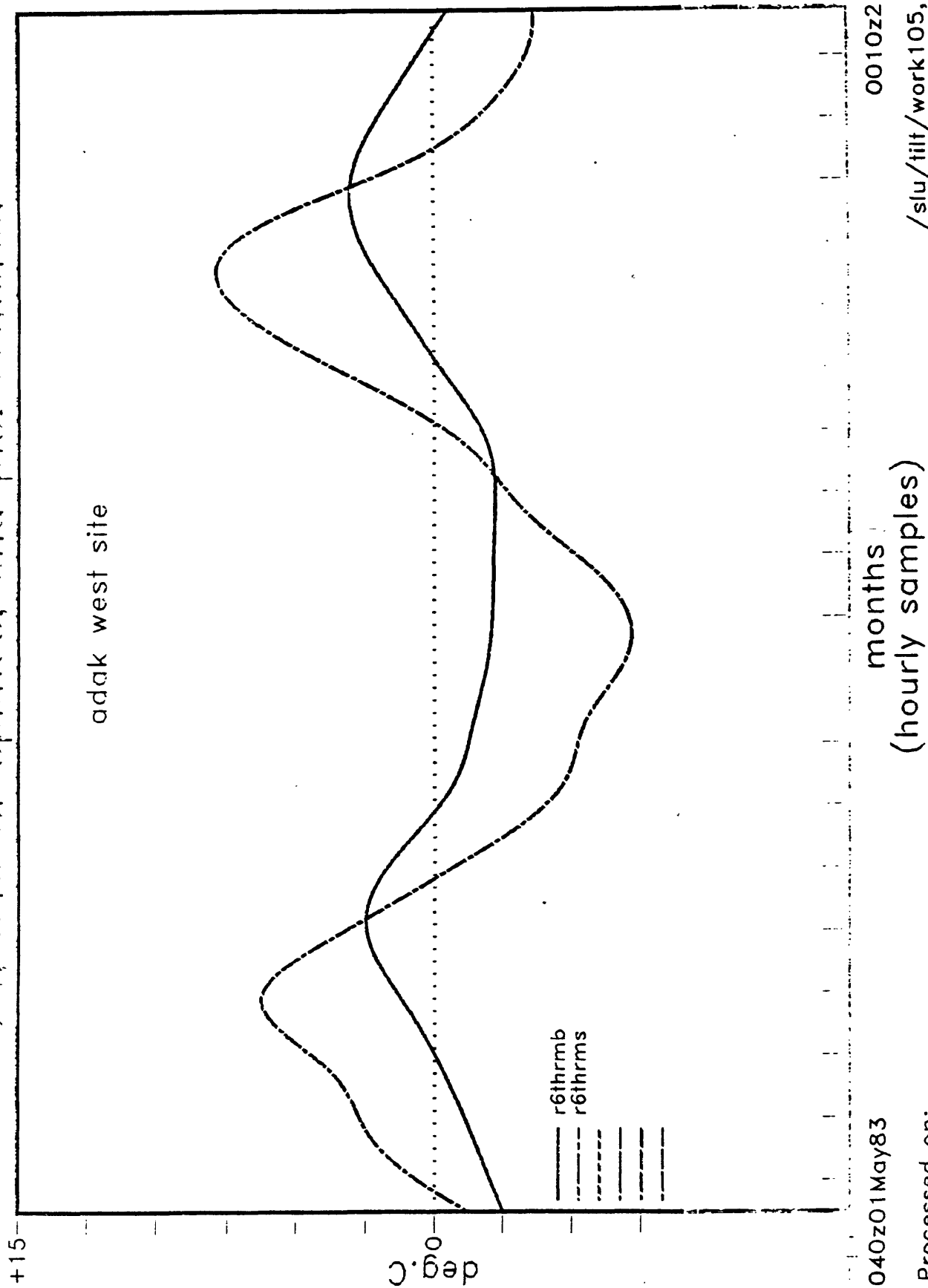
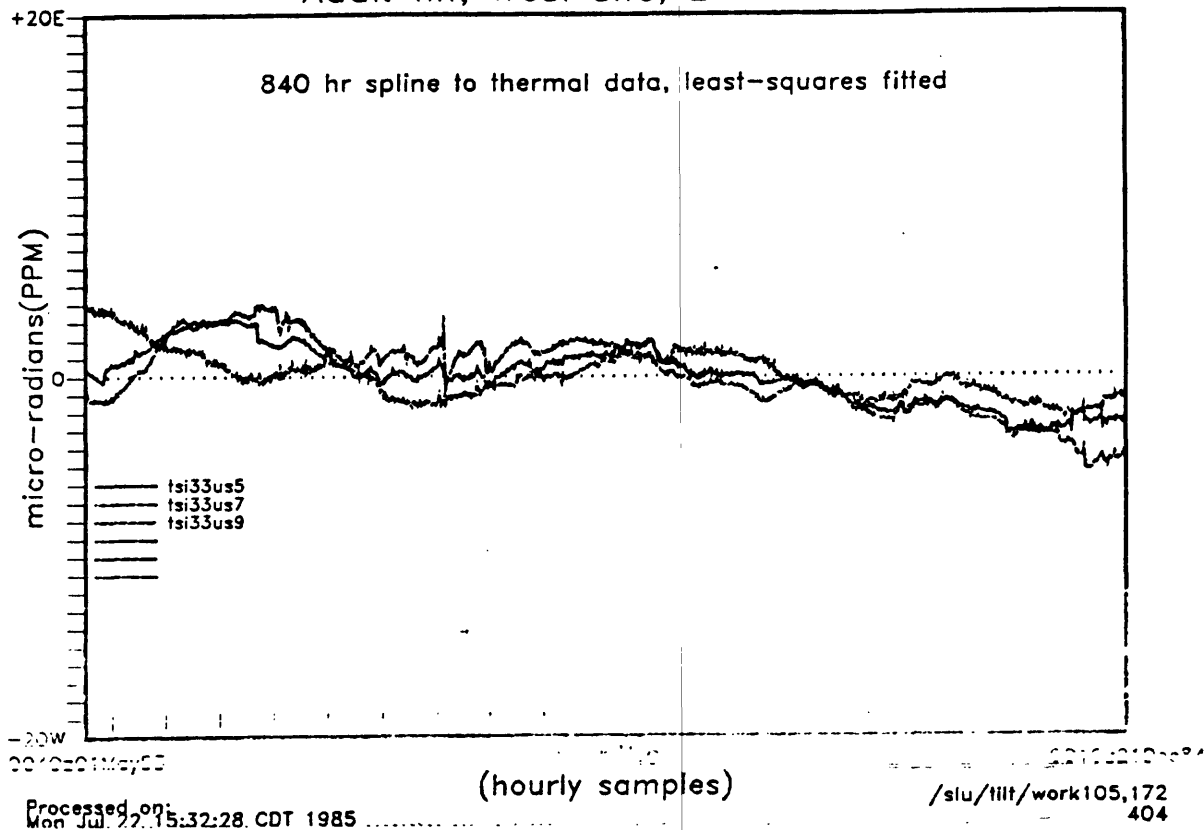
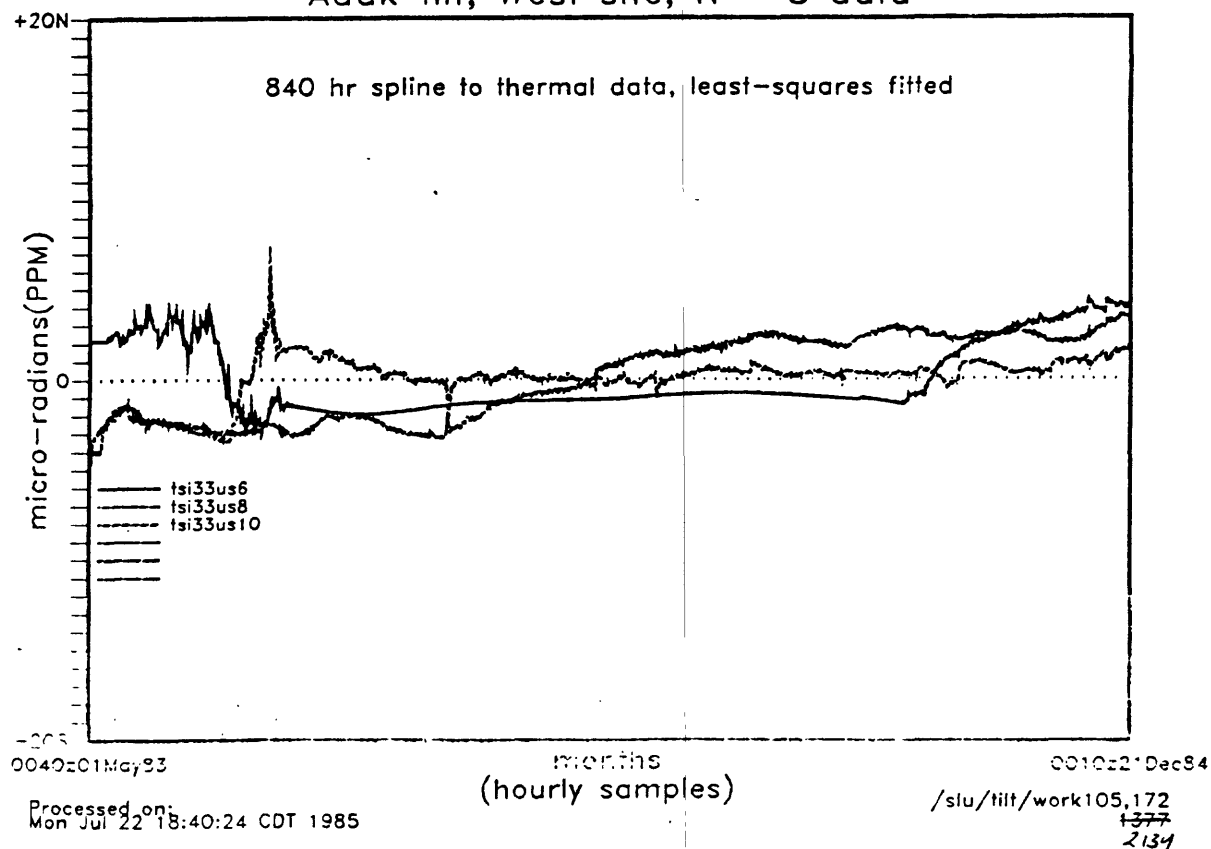


Figure 8

2 meter Depth, Corrected Data, 20 Mo.
Adak tilt, West site, E - W data



2 meter Depth, Corrected Data, 20 Mo.
Adak tilt, West site, N - S data



the raw data. The W.E. unit, N.S. data is an artifact.

d) Figure 10 is of the same residual tilt plotted at twice the sensitivity, with the linear regression lines shown. The linear regression fits have a mean of 1.1 ppm/year for the EW data, and 1.4 ppm/year for the NS data at the West site. The remnant annual cycle seen in the 10 month data is not as evident here.

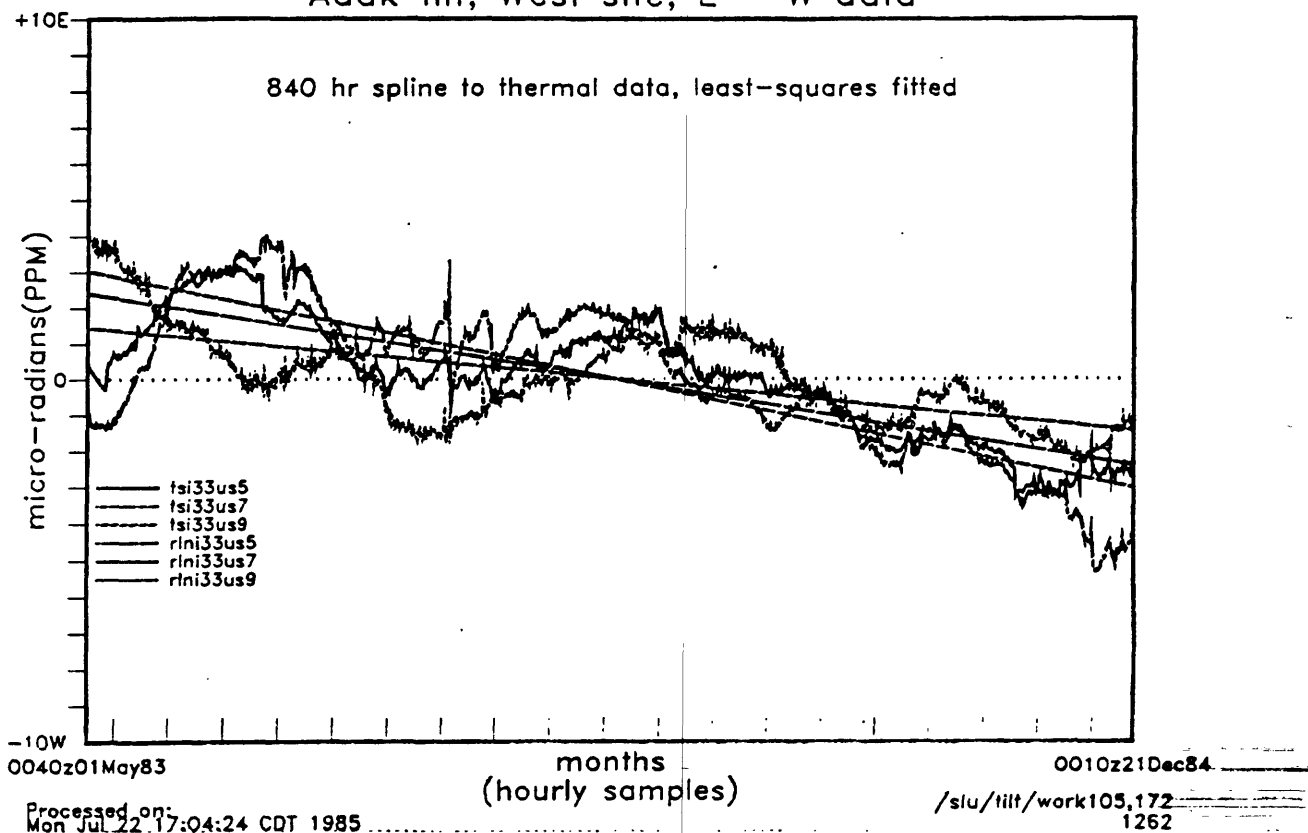
e) Table 2 is a summary of the statistics of the least-squares deconvolution of temperature and of the fitting of the regression line. In general, the numbers indicate significantly better fits of the line than those of the 10 month data set of Table 1, while the thermal fits are about the same or worse. This latter fact indicates that either the thermal profiles are in error, or that in the longterm series there is more secular tilt with regard to the annual thermal cycles, or that there are other annual or longer noise series that need to be modeled and removed from the data, or all of the above. The possibilities are interesting.

B) Data from 5 Meter Depth at the Crustal Deformation Observatory (CDO) at the Pinon Flat Observatory (PFO)

1) The Pinon Flat Observatory is where UCSD is operating the 3/4 km laser strainmeters and fluid tiltmeters, most of which have "optical anchors" that correct for movement of the surface piers with regard to the rock 30 meters below. The data are exquisite, and define maximum resolution/stability goals for surface measurements of crustal deformation. There they have been operating commercial bubble sensor tiltmeters similar to those used by the USGS for several years, and this Principal Investigator has a research program to attempt an improvement of the signal/noise values of these relatively inexpensive instruments and their longterm stability by: stage 1) removing the existing sensors and reinstalling them with the tapered pipe and new electronics in the existing 5 meter deep by 1 meter diameter pits; stage 2) drilling 10 meter holes with a 30 cm diameter and installing new instruments in them; and stage 3) drilling 26 m deep, 30 cm diameter holes and reinstalling the shallow open-pit instruments in them.

2) The three open-pit instruments were reinstalled in late May of 1985. (See II.C.3 above.) The data available to-date has consisted of weekly plots of the raw data. These were hand-digitized at 2 day intervals and are plotted in Figure 11. The large gyration of the Delta unit (with the seized mounting) is quite evident. Otherwise, the data have stabilized into a linear trend that seems to be a portion of an annual thermal cycle, most likely a function of the bubble sensor temperature. In the reinstallation, special efforts were made to force thermal stratification in the 5 m access pits, but it was only partially successful because the anticipated materials (4" ethofoam sheets) were not locally available. Improvements are planned in the near future. It will remain uncertain that these data actually represent a "typical" 5 m depth in California until the temperature data become available (it is in the pipeline).

2 meter Depth, Corrected Data, 20 Mo.
Adak tilt, West site, E - W data



2 meter Depth, Corrected Data, 20 Mo.
Adak tilt, West site, N - S data

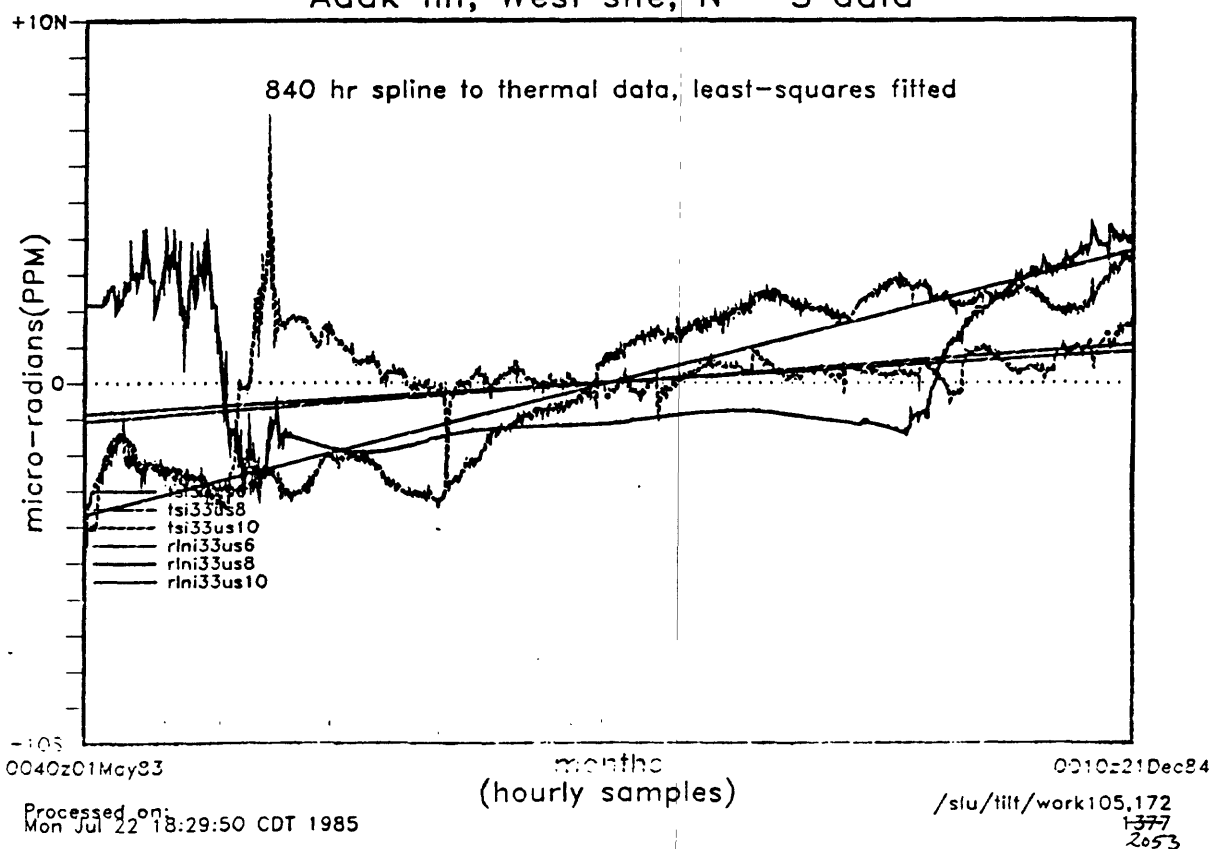


Table 2. Summary statistics from analysis of 20 month data set.

Process date: Fri Jul 19 17:26:20 CDT 1985

decimation is 14

Summary of x (EW) data:

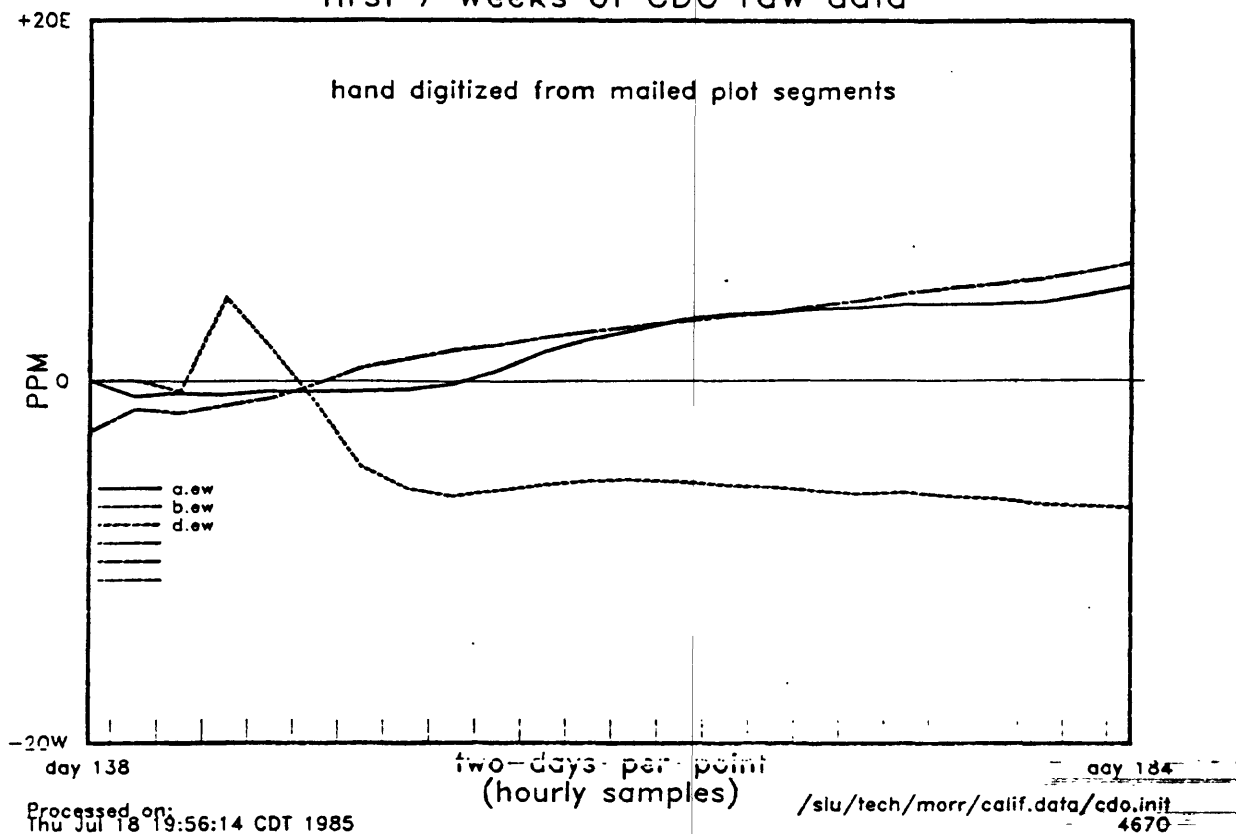
channel	unit	borehole thermal		surface thermal		straight line		meanF	mccR
		%Fit	fit(b)	%Fit	fit(b)	%Fit	fit(b)		
i31us5	SE	27.0	-9.800	26.7	-2.809	13.8	0.165	22	51 %
i31us7		40.0	8.209	10.4	-1.081	72.3	0.226	41	96 %
i32us5	NE	5.0	-1.022	9.0	-0.510	16.2	-0.066	10	55 %
i32us7	NW	1.2	0.396	0.5	-0.099	24.4	-0.072	9	65 %
i33us5	WE	38.3	3.592	18.0	0.636	46.7	-0.083	34	85 %
i33us7	WW	53.8	6.326	7.5	0.493	40.9	-0.105	34	81 %
i33us9	WS	33.7	-2.790	25.1	0.646	22.7	-0.050	27	63 %
i34us5	E	3.1	-1.746	7.9	1.055	73.2	-0.259	28	96 %
Averages		25.2		13.1		38.8		26	74 %

Summary of y (NS) data:

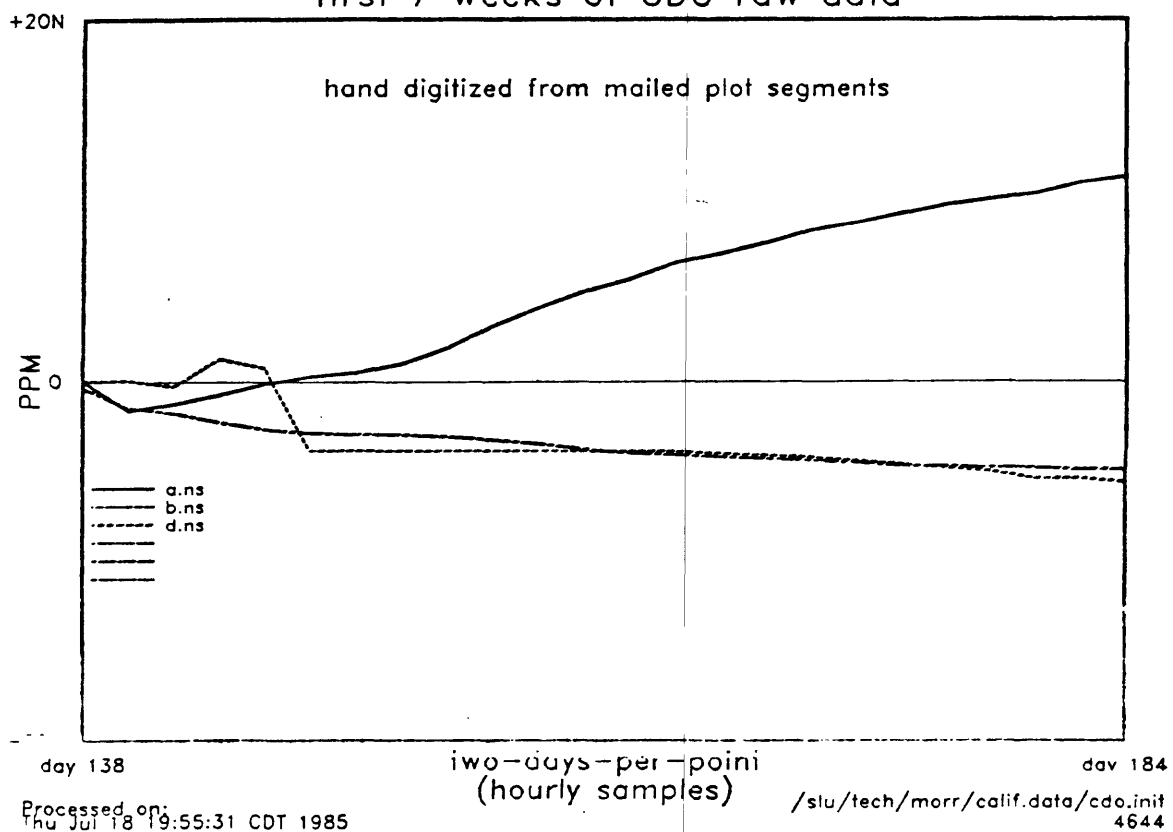
channel	unit	borehole thermal		surface thermal		straight line		meanF	mccR
		%Fit	fit(b)	%Fit	fit(b)	%Fit	fit(b)		
i31us6	SE	19.5	-6.307	2.9	0.803	63.0	-0.328	28	93 %
i31us8		45.2	-12.685	1.2	0.506	26.4	0.236	24	68 %
i32us6	NE	0.3	-0.117	3.2	-0.140	1.8	0.011	2	19 %
i32us8	NW	0.0	-0.135	7.1	0.984	63.7	-0.249	24	93 %
i33us6	WE	3.2	0.727	0.9	-0.147	3.4	0.030	2	26 %
i33us8	WW	34.2	-3.730	1.3	-0.207	62.5	0.127	33	93 %
i33us10	WS	26.6	1.939	15.7	-0.445	13.0	0.037	18	49 %
i34us6	E	1.3	1.078	12.0	-1.239	57.0	0.223	23	90 %
Averages		16.3		5.5		36.3		19	66 %

(Note: mccR is multiple correlation coefficient, expressed as percent.)

5 meter depth, E - W data first 7 weeks of CDO raw data



5 meter depth, N - S data first 7 weeks of CDO raw data



3) This short segment of 5 meter open pit data is hardly enough basis to estimate longterm trends; nonetheless, the thermal noise data is of about the same range of amplitudes as the Adak data at 2 meters depth. More data are needed from CDO before more is said. D.C. Agnew made a special effort to assemble some "before and after" data with respect to this upgrading of the shallow tiltmeters at CDO. It is generally inconclusive as to whether previous trends are continued or not; it does suggest that the range of thermal noise, although often of opposite sense after the changes, may be of about the same order, if one is bold enough to make longterm projections from 46 days of data. If the thermal noise is a linear effect on the bubble, as at Adak, it can readily be removed, as shown above.

C) Installations at 10 Meter Depth

1) These have only been accomplished at the CCMO test site, where a 8 m tower with a platform over a 2 m hole was built to simulate installations in the Palmdale area of the western Mojave. Successful practice installations have been made at the test facility, but the bubble/borehole pipe is always removed immediately afterwards, so as to facilitate cleaning out the hole for the next practice. All the practices have been with a hand-held pre-leveling extension of the tiltmeter installation tool and hand-operated 11 m long sand tamping tools. This process works, but is clumsy. For the Palmdale instruments, five 10-meter deep holes were drilled in April 1983 at two sites. The instruments were not installed because of uncertainties of the future of the Palmdale project.

IV. Projections of the Noise Level for Installations at Depths of 10 Meters or More

A) The attenuation of environmental noise with depth, particularly thermal noise, is generally estimated to be an (depth)³ factor. The data of Figure 2 have shown this, but still show that even at 30 meters depth significant annual temperature variations remain. The Adak data has shown that these variations can readily be removed if they are a linear function of temperature at the sensor. The initial installations at Parkfield are planned to be at the 10 m depth. There is insufficient drilling funding in the present budget to go deeper.

B) Deeper depths, possibly in excess of 100 meters, will be possible in the near future. A new electric-pneumatic installation system has been designed at Saint Louis University and is undergoing preliminary testing. A biaxial motor driven beam-bending technique is used to pre-level the borehole pipe to within 1 ppm of vertical and hold it there. A variable height pneumatic tamping mechanism, the heart of which is eight miniature double-acting compressed air cylinders, has been designed to tamp the sand and "steer" the tiltmeter under electrical control from the surface. Down-hole reservoirs for the dry bonded sand and water to add to it have been tested. The sand dispensers have pneumatic gate valves to control sand addition increments. This system will be available for later phases of tiltmeter installation at

Parkfield if funding is provided for additional sites.

C) Even with the 10 meter depth installations, we can make some rough estimates of the baseline stability to be achieved after removing the annual thermal effects from the data. The Adak data, at 2 m, shows linear regression fits of 20 months of data that have a mean of about 1.25 ppm/year. But in examining the tilt data in detail after thermal correction, one can see tracking of all three instruments for several months at a time to much less than 1 ppm. One would expect that with more elegant deconvolution of the environmental noise, this coherence would be improved throughout the data base. Coherence between co-sited instruments essentially establishes the baseline or noise threshold of the data.

Based on the 2 meter deep data from Adak, and allowing that a coherence of 1 ppm/year is plausible with at least 1 year of data, installations at 10 meters should be 125 times more stable $(10/2)^3$. In reality, something like 25 times more stable and coherent would be a worthwhile achievement. A corrected baseline coherence of 0.1 ppm/year for three instruments at a given site is then not too unreasonable to expect for installations at only 10 meters depth in central California.

V. Implications for the Parkfield Prediction

A) The model of Stuart *et al.* (JGR, 90, 592-604) seems to be accurate enough to predict creep that has actually been measured on creepmeters located along the fault from the freely slipping region northwest of Middle Mountain, southeast through Parkfield, and into the locked lobe of the 1857 earthquake south of Highway 46. So it makes sense to use the model to select sites of the greatest potential deformation for the installation of tiltmeters. Figure 12 is based on their figure that shows theoretical uplift rates at three phases of the pre-earthquake process. The x-axis is measured in km from the 1966 epicenter on Middle Mountain, trending southeast along the fault. The tiltmeters are represented as arrows originating ± 1 km from the fault. The vertical deformation is in units of 1 mm/bar, which is the equivalent of 0.11 mm/year according to the paper. But 0.1 mm/year/km is 0.1 ppm/year of tilt, near the anticipated threshold of the instrumental data, after thermal correction, at the 10 meter depth.

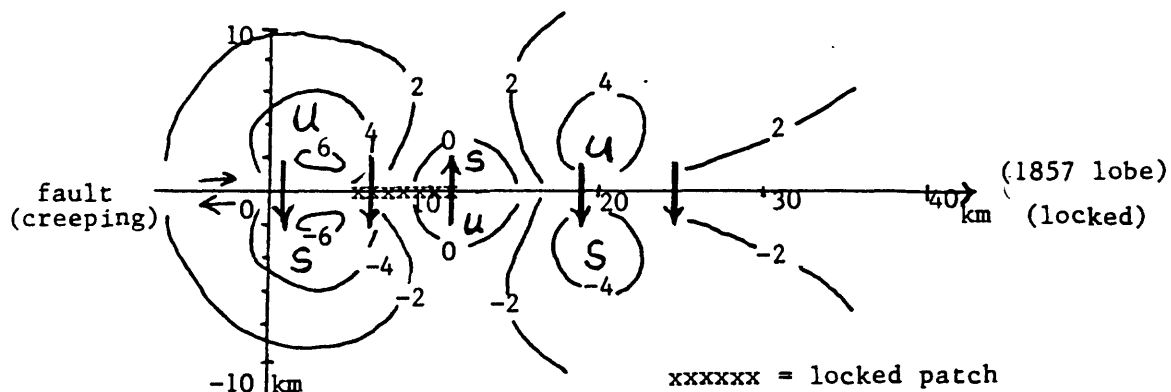
As the figure shows, the initial state of the locked patch at the state of greatest patch resistance, produces areas of uplift and subsidence as indicated in Figure 12a. Tiltmeters located as shown would show alternating azimuths of down tilt. (U and S indicate uplift and subsidence.) As the patch shrinks and the stress increases, the tilt pattern of the unit at Km 11 rotates, as in Figure 12b. At the end of the precursor stage, when the maximum stress is on the patch, the deformation to the northwest of it will reverse the tilt direction, while the tilt measured to the southeast will rapidly accelerate. This will be a tilt of over 0.5 microradians in a period of a few months, and should readily be detected by the present instrumentation.

The paper notes that the deformation model is based on pure

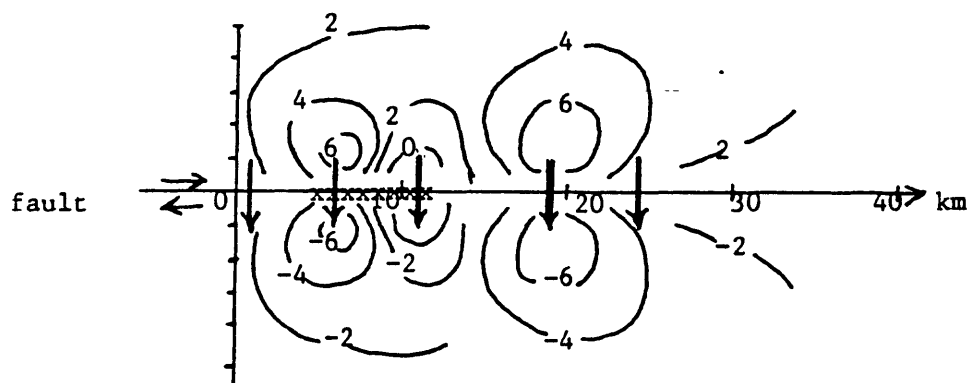
Figure 12. Theoretical uplift rates at the ground surface at three phases of the pre-earthquake process at Parkfield, CA.
(after Stuart et al: Parkfield Forecast Model, JGR, 90, 592-604)

(Uplift/subsidence rates in mm/bar, where 10 mm/bar = 1.1 mm/yr)
(Tiltmeter long term stability at 10m depth is 0.1ppm/yr, or 0.1mm/km/yr)

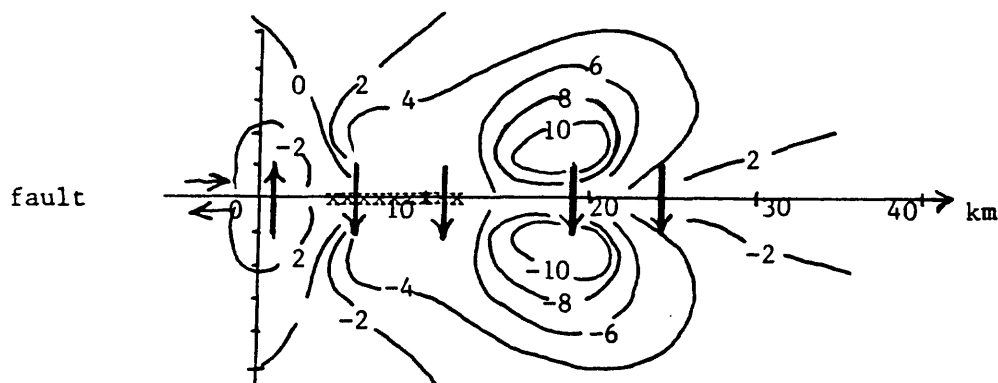
A) Maximum resistance of locked patch: shear stress = 0.10



B) End of slow load stage: shear stress = 1.00



C) End of precursor stage: time of incipient failure: shear stress = 1.20



Tiltmeters are indicated as large arrows in the direction of subsidence.
All the tiltmeters will be within 1 km of the fault; the unit at km 1 may not be installed because of the topography.

strike-slip motion, whereas some dip-slip motion is quite likely, which would greatly enlarge the tilt signals expected from the model. Indeed, some recent precision leveling data has detected tilting in the Parkfield area well above the baseline statistics (Al Lindh, private communication).

B) The tiltmeter installation plan at Parkfield is shown in Figure 13. This figure also shows the locations of the creepmeters and other geodetic experiments along the fault segment, where distances are, as above, measured in km from the 1966 epicenter. The model of the paper would ideally have tilt measurements at km 1, 7, 11, 19, and 24 kms. The site at km 1 on Middle Mountain is unsuitable topographically for shallow tilt measurements. The sites at 7, 11, and 19 are accessible and have been permitted, and the near surface structure determined at km 11 and 19 by shallow refraction in May. A site at km 24 would be very desirable to examine the behavior of that locale with respect to the model. If the rapid attenuation of tilt with respect to the units at km 11 is not seen, significant involvement of the 1857 lobe in the failure process might be expected.

Current plans are to drill three holes each at sites KM 11, Turkey Flats Road, and KM 19, Gold Hill, on the Jack ranch; the drilling is planned for September. If the driller provides a lower quotation, we will also establish a site and drill just off the beginning of Joaquin Creek, near Km 7. The instruments are available, since the western Mojave program has been discontinued. Data acquisition will be by on-site 12- and 16-bit digitization and telemetry to the 2 color geodimeter hut on Carr Hill. Logging will be on floppy disks, as at Adak, for mailing to Saint Louis University, and also tape cassette, for telephone dump to Menlo Park. Backups consist of a 132 column printer at the telemetry receive site and on-site slow speed strip chart recorders. A full meteorological system will be implemented at each site.

C) Data analysis will be done by whoever has the time. At St. Louis, routine analysis and assembly will be done, as for the Adak data. Deconvolution of the thermal noise will begin after about 6 months of data are acquired, and the least squares coefficients can then be used on any selected portion of the data if desired. They can also readily be improved as the data base expands in time.

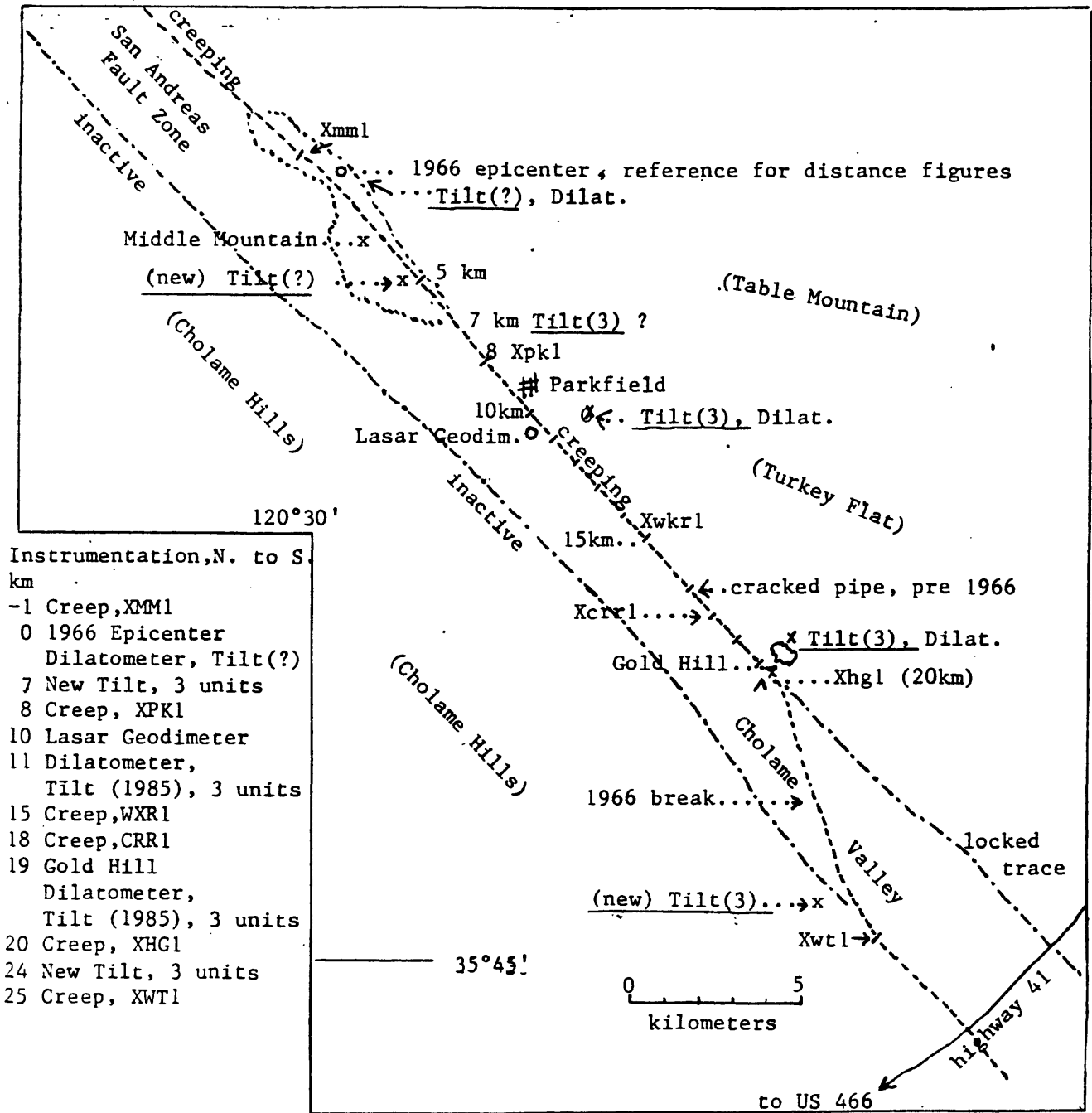
Sean-Thomas Morrissey
Senior Research Scientist
Saint Louis University

21 July 1985

Figure 13.

San Andreas Fault zone in the vicinity of Parkfield, CA., showing locations of active deformation monitoring experiments.

120°15'
36°00'



Note that most of the instrumentation is east of the fault zone, in the competent formations of the North American plate. The surface structure west of the fault is mostly north-west bound rubble.

APPENDIX A. 12.

Seismicity Record, $M_L \geq 2.5$, for the Central Coast
Region of California

R. A. Uhrhammer

SEISMICITY RECORD, $M_L \geq 2.5$, FOR THE CENTRAL

COAST REGION OF CALIFORNIA

by

Robert A. Uhrhammer

Seismographic Station

University of California, Berkeley

Berkeley, California 94720

The seismicity record in this study is coalesced from three primary sources: 1) Townley and Allen (1769-1927); 2) Topozada and others (1812-1949); and 3) the Bulletin of the Seismographic Stations, University of California, Berkeley (October 1910-June 1985). From January 1800 through June 1985, 4059 earthquakes ($M_L \geq 2.5$) have been observed in the central coast region shown in Figure 1. The two rectangles (150 km long by 20 km wide) shown in Figure 1 are the spatial windows used to select events associated with the San Andreas and Calaveras fault zones for analysis.

Clustering in the seismicity list was removed using the magnitude dependent time and space windows shown in Table 1. The window distances and times were empirically derived from an analysis of California earthquake sequences. All subsequent analysis uses only the mainshocks for each cluster. Approximately 42 per cent of all earthquakes ($M_L \geq 2.5$) are associated with clusters containing at least two events.

The time interval for which the seismicity catalog is considered complete at a given M_L threshold is shown in Table 2. The 1948 date for completeness at the M_L 2.5 threshold is attributed largely to the installation of a Benioff seismograph at Mt. Hamilton (magnification = 100k).

The cumulative rates of seismicity ($2.5 \leq M_L \leq 6$) for the San Andreas and Calaveras fault segments are shown in Figures 2 and 3 and Tables 3 and 4, respectively. The rate of seismicity along the Calaveras fault zone is 50 per cent higher than the rate along the San Andreas fault zone. The b-values are typical for California seismicity.

Identified foreshock sequences ($M_L \geq 2.5$, 1948-1985) are shown in Tables 5 and 6. The probability that a mainshock has a foreshock sequence and the probability that an event is a foreshock is given in Tables 7 and 8. Note that one-third of the $M_L \geq 5$ earthquakes on the San Andreas had foreshocks. This is in agreement with the observations of L. Jones.

The distribution of seismicity along the faults as a function of time (1940-1985) is given in Figures 4 and 5. Note the presence of regions of low seismicity (commonly called "seismic gaps"). It may be more appropriate to identify anomalous regions by variations in the b-value as done by W. Smith. Smith estimates the temporal and spatial variation of b-value and the gradient of the cumulative sum (cusum) of the differences between the individual values and the mean (of M_L). There were no significant variations in the b-value prior to the 1979 Coyote Lake earthquake (M_L 5.9) or the 1984 Morgan Hill earthquake (M_L 6.2).

Frequency spectra of mainshocks along the fault zones are given in Figures 6 and 7. No significant periodicities are present in the range from a few weeks to ten years.

Wavenumber spectra of mainshocks along the fault zones are given in Figures 8 and 9. The larger amplitudes at low wavenumbers is attributed to the relatively higher rate of seismicity at the southern ends of the regions.

Table 1 - Declustering Window

Magnitude	Time (hr)	Distance (km)
2.5	32	10
3.0	59	10
3.5	110	10
4.0	210	10
4.5	390	17
5.0	720	20
5.5	1300	30
6.0	2500	45
6.5	4700	67
7.0	8800	100
7.5	16000	150
8.0	31000	220
8.5	57000	330

Table 2 - Magnitude Threshold for
Completeness of Catalog
Threshold

Magnitude	Year	Interval (yr)
2.5	1948	37
3.0	1942	43
3.5	1935	50
4.0	1932	53
5.0	1852	133

Table 3 - Cumulative Rate of Seismicity
San Andreas Fault Zone

Magnitude	Time (yr)	Number of eqk	Rate (eq/yr)	Sigma (eq/yr)
2.5	37	540	14.6	.628
3.0	43	264	6.14	.378
3.5	50	96	1.92	.196
4.0	53	42	.792	.122
4.5	53	21	.396	.086
5.0	133	16	.120	.030
5.5	133	8	.060	.021
6.0	133	2	.015	.011

Table 4 - Cumulative Rate of Seismicity
Calaveras Fault Zone

Magnitude	Time (yr)	Number of eqk	Rate (eq/yr)	Sigma (eq/yr)
2.5	37	797	21.5	.763
3.0	43	354	8.23	.438
3.5	50	143	2.86	.239
4.0	53	59	1.11	.145
4.5	53	23	.434	.091
5.0	128	20	.156	.035
5.5	128	12	.094	.027
6.0	128	4	.031	.016

Table 5 - Identified Foreshocks - San Andreas Fault Zone

Number	Date	Magnitude							
1	48 mar 28	4.0	4.6						
2	49 may 10	2.5	2.7						
3	53 dec 16	3.5	3.8						
4	54 apr 22	3.8	4.3	3.0	5.3				
5	55 dec 23	2.6	2.8						
6	57 mar 22	2.7	3.5	3.8	2.6	5.3			
7	57 dec 10	3.0	2.8	3.0	3.2				
8	58 aug 30	2.6	2.9	3.2					
9	59 may 25	3.0	3.1						
10	59 oct 14	3.4	2.5	3.6					
11	61 jan 03	3.6	4.1						
12	63 may 22	2.7	2.8						
13	63 jul 16	2.8	3.6						
14	65 jan 01	2.5	2.6	3.1					
15	66 mar 16	3.4	3.6						
16	66 jun 22	2.6	3.0						
17	72 sep 23	2.9	3.5	3.5	4.0	4.1	2.9	4.8	
18	73 aug 02	2.9	3.0						
19	74 apr 22	2.5	3.0						
20	75 apr 22	2.9	3.0						
21	77 jul 08	2.7	2.8						
22	79 aug 02	2.9	3.1	3.0	3.9				
23	80 jun 18	3.7	4.2						
24	81 feb 24	2.7	2.8	3.1					
25	81 jun 14	2.6	2.8						

Table 7 - Foreshock Probabilities - San Andreas Fault Zone

Magnitude	Total Number of Sequence	Number of Foreshock Sequences	P1 (%)	P2 (%)
2.5	540	25	4.6	4.6
3.0	214	20	9.3	5.1
3.5	80	11	14	5.0
4.0	35	6	17	2.9
4.5	17	4	24	
5.0	6	2	33	

P1 - probability of mainshock having a foreshock sequence

P2 - probability that event is a foreshock

Table 6 - Identified Foreshocks - Calaveras Fault Zone

Number	Date	Magnitude				
1	48 apr 27	4.0	4.4			
2	51 oct 30	4.0	4.2	3.9	3.4	4.8
3	56 apr 10	2.9	3.2			
4	57 dec 11	3.0	2.8	3.0	3.2	
5	57 dec 17	2.8	3.0			
6	59 mar 03	2.6	4.4			
7	59 oct 14	3.4	2.5	3.6		
8	59 dec 29	4.7	5.0			
9	63 jul 31	2.7	3.9			
10	66 jan 09	2.5	3.3			
11	66 jan 17	3.3	4.1			
12	68 nov 05	3.1	3.2			
13	70 may 25	2.8	2.7	2.7	2.9	3.0
		3.5	2.5	2.8	3.8	
14	70 jun 11	3.4	3.0	2.6	3.3	4.3
15	70 jul 05	2.6	2.9			
16	71 dec 19	2.6	3.2	3.6		
17	71 dec 28	3.7	3.4	3.1	2.8	3.9
18	72 sep 04	2.8	2.9			
19	72 dec 12	2.7	2.6	2.8	3.0	
20	73 jul 05	2.9	3.1			
21	74 mar 08	2.5	2.9			
22	74 jun 12	2.5	3.7			
23	76 aug 15	3.0	3.3			
24	76 sep 03	2.7	3.5			
25	77 jan 18	3.5	3.9			
26	77 jul 08	2.7	2.8			
27	77 aug 09	2.8	2.9			
28	77 dec 10	2.6	3.6			
29	78 may 08	3.4	2.9	3.3	3.8	
30	78 sep 17	3.3	3.0	3.9		
31	80 mar 05	2.8	3.8	4.0		
32	80 jun 26	2.7	3.2			
33	81 feb 22	2.8	3.1			
34	82 aug 19	2.9	3.3			
35	82 oct 17	2.8	2.8	3.0		
36	84 oct 31	3.2	3.6			

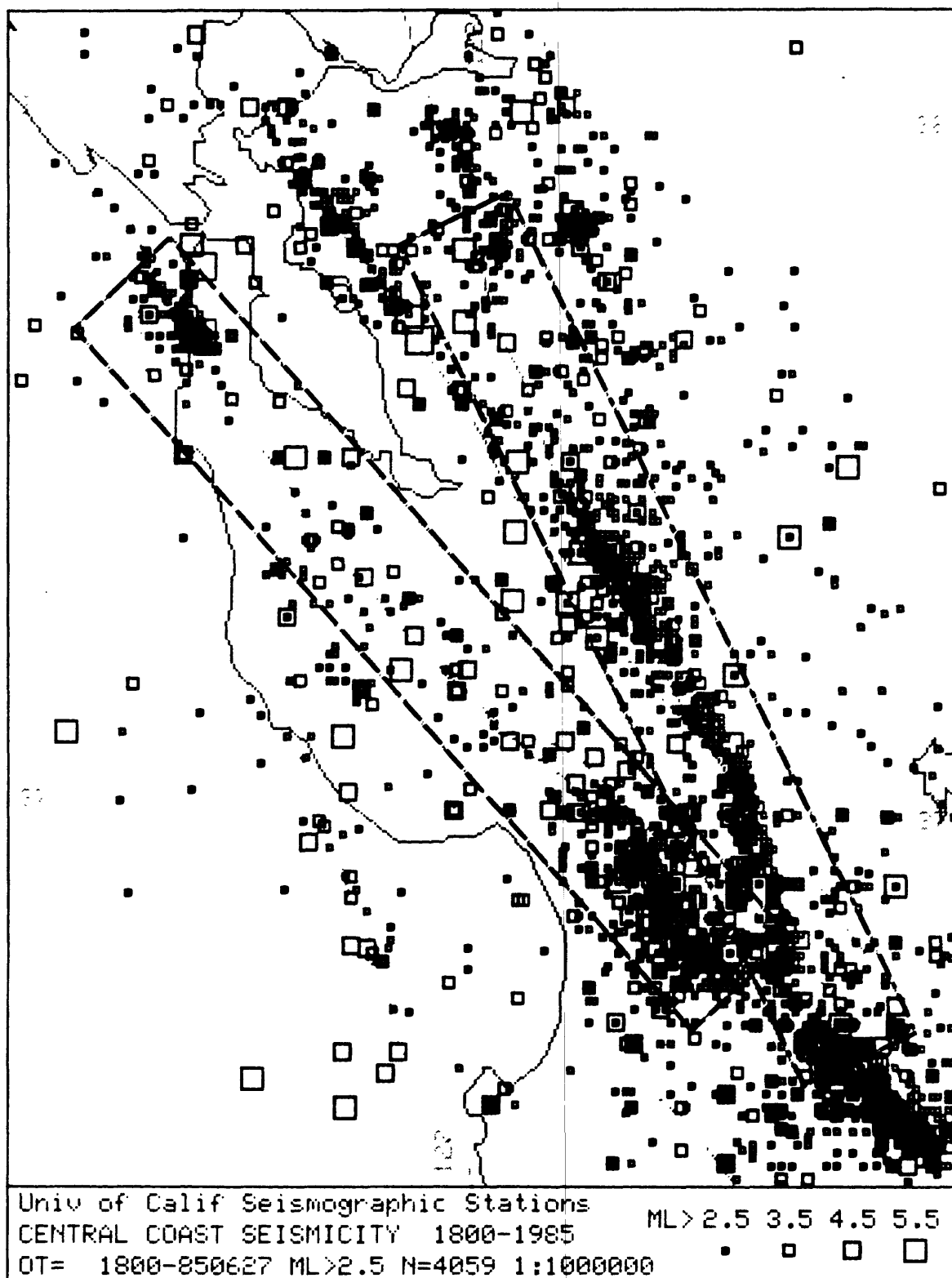
Table 8 - Foreshock Probabilities - Calaveras Fault Zone

Magnitude	Total Number of Sequences	Number of Foreshock Sequences	P1 (%)	P2 (%)
2.5	797	36	4.5	4.5
3.0	315	30	10	5.1
3.5	132	17	13	3.8
4.0	42	7	17	7.1
4.5	19	2	11	5.3
5.0	7	1	14	

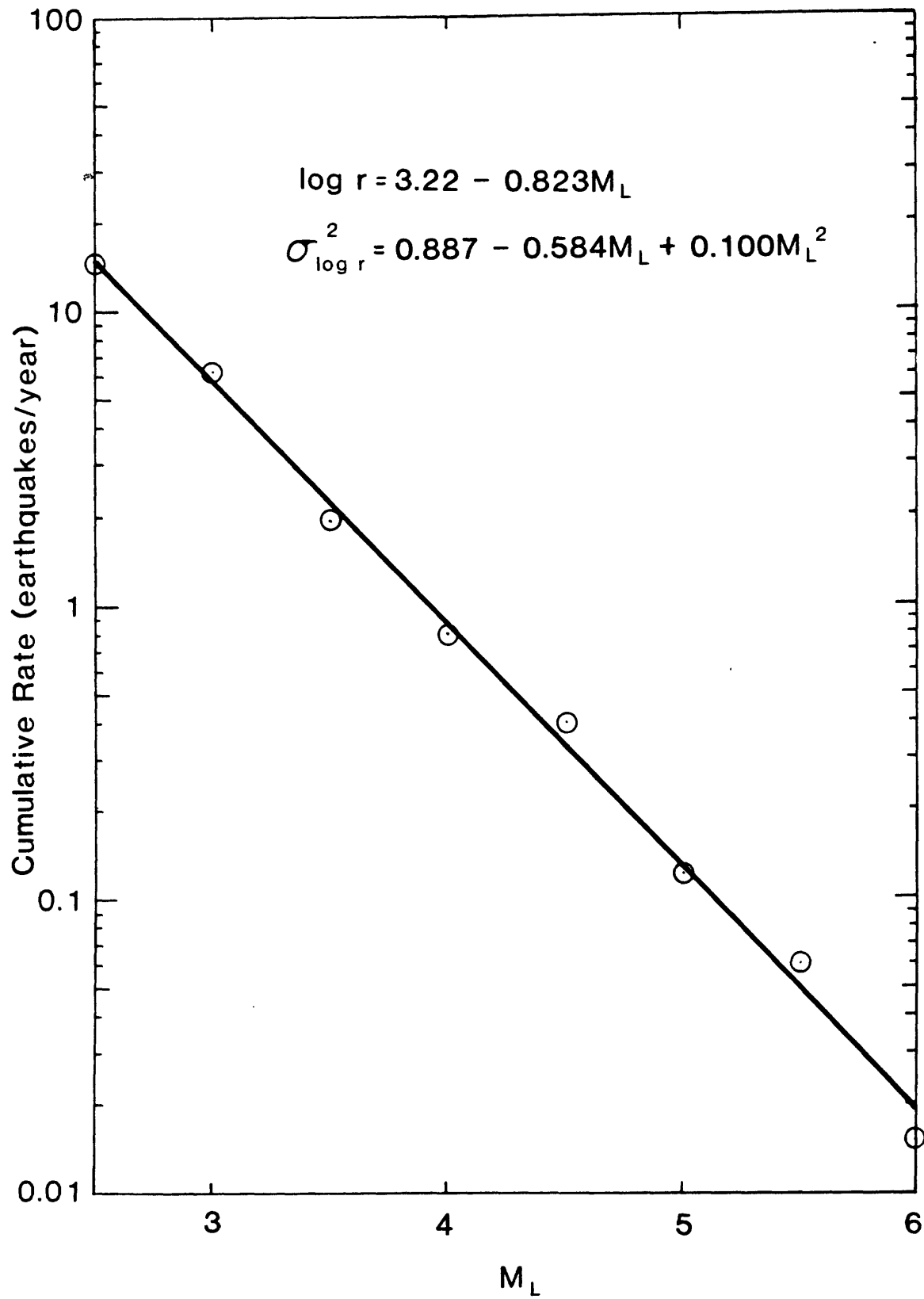
P1 - probability of mainshock having a foreshock sequence

P2 - probability that event is a foreshock

Figure 1



SAN ANDREAS FAULT ZONE



CALAVERAS FAULT ZONE

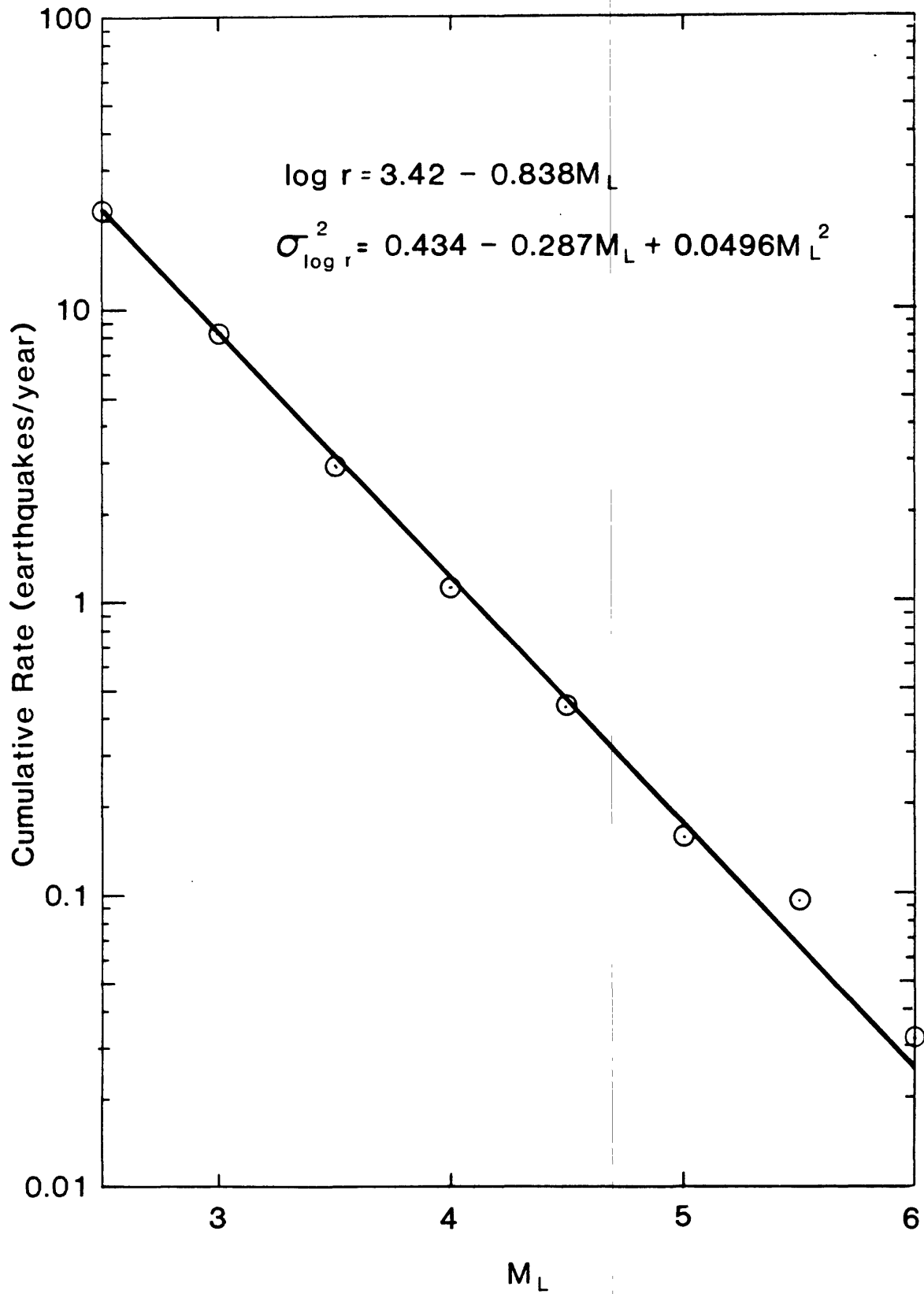


Figure 4

SAN ANDREAS FAULT ZONE

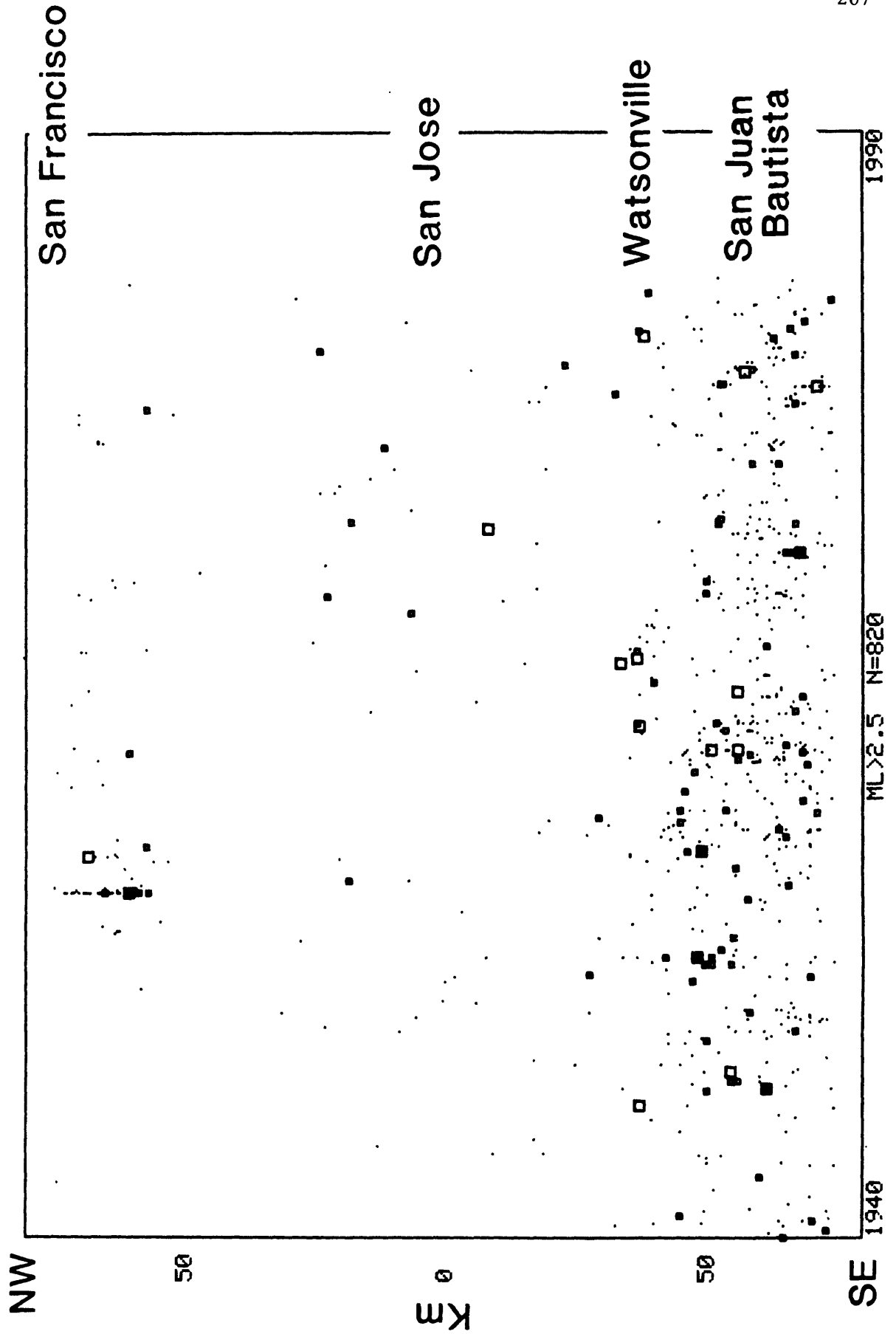
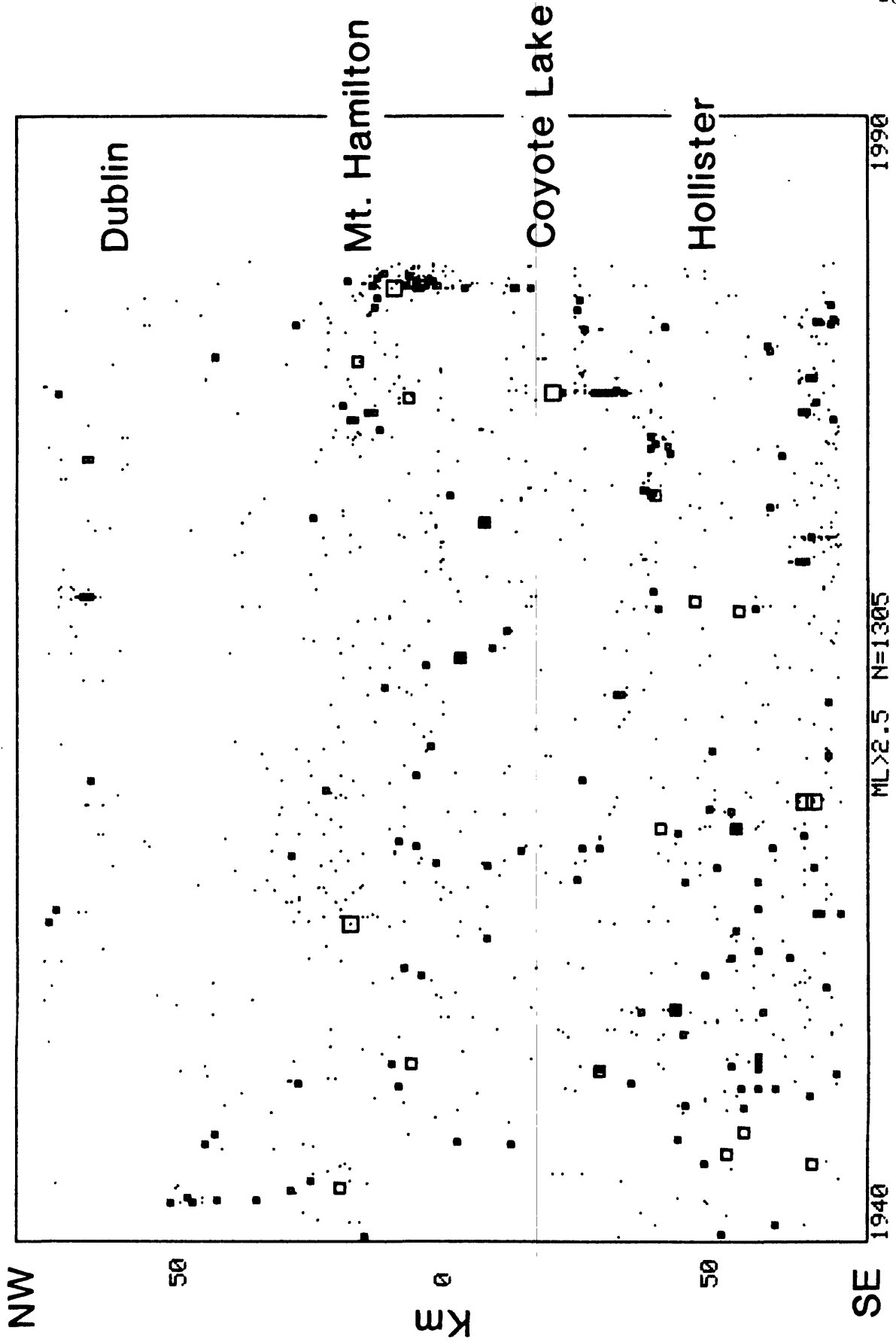


Figure 5

CALAVERAS FAULT ZONE



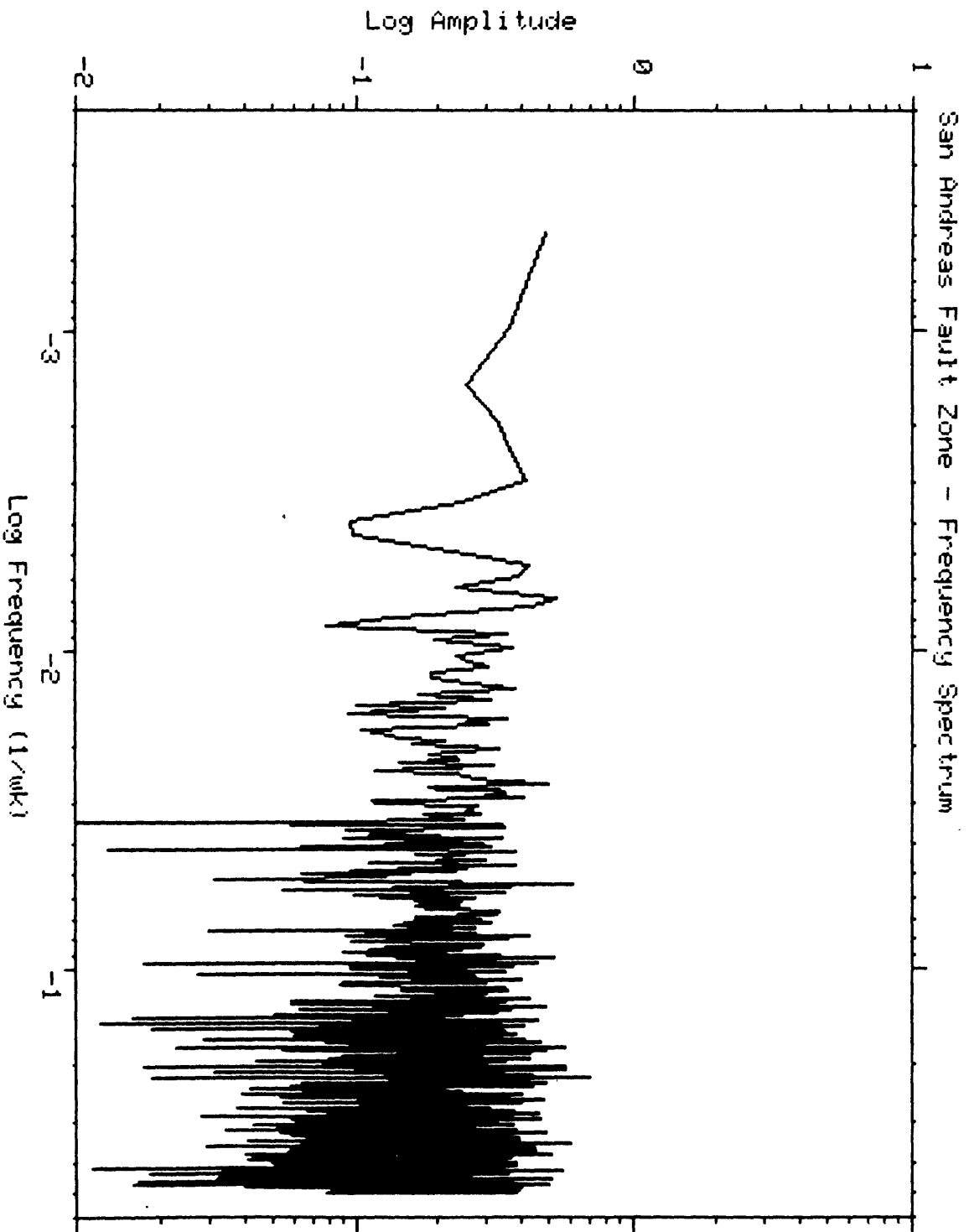


Figure 6

Figure 7

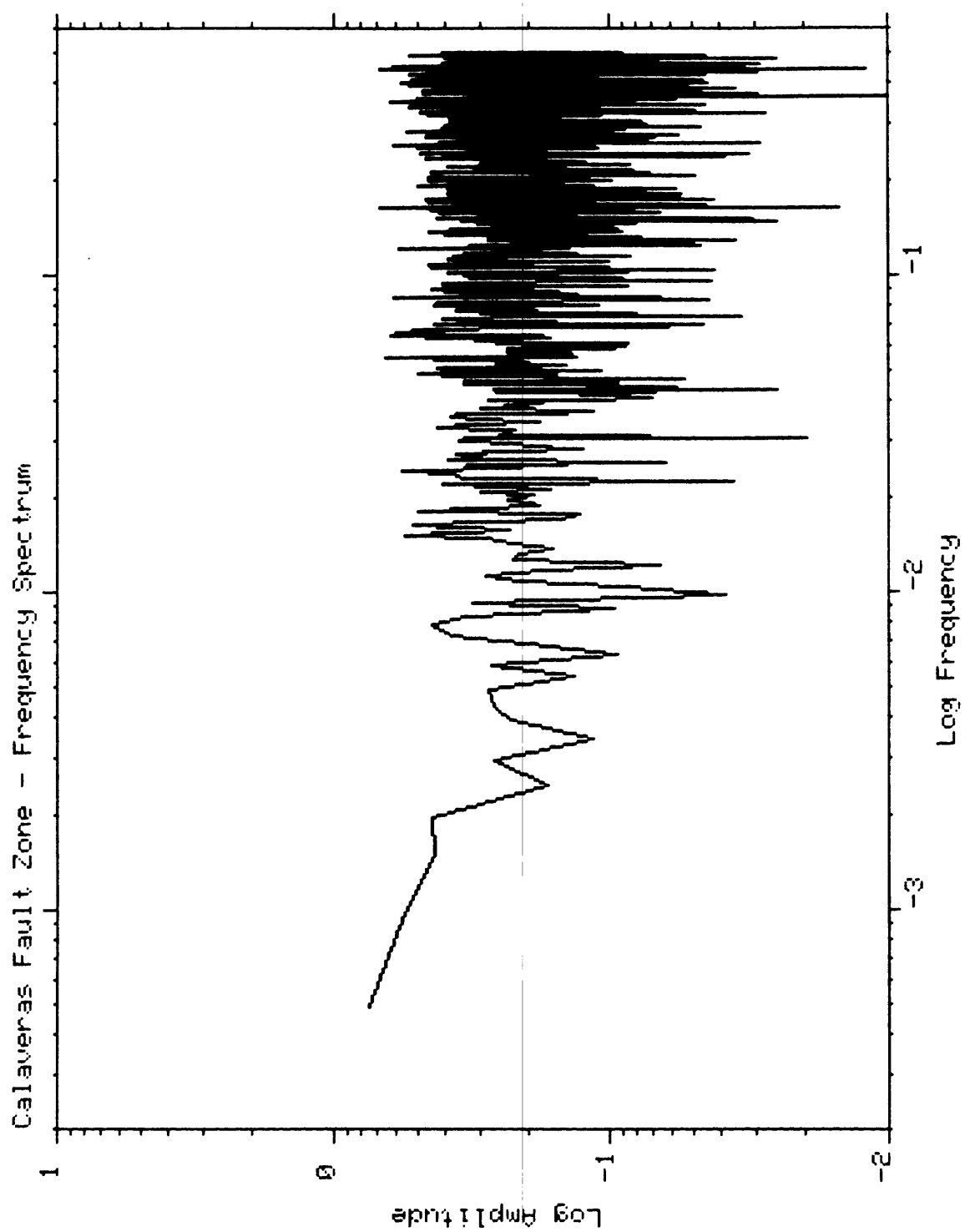


Figure 8

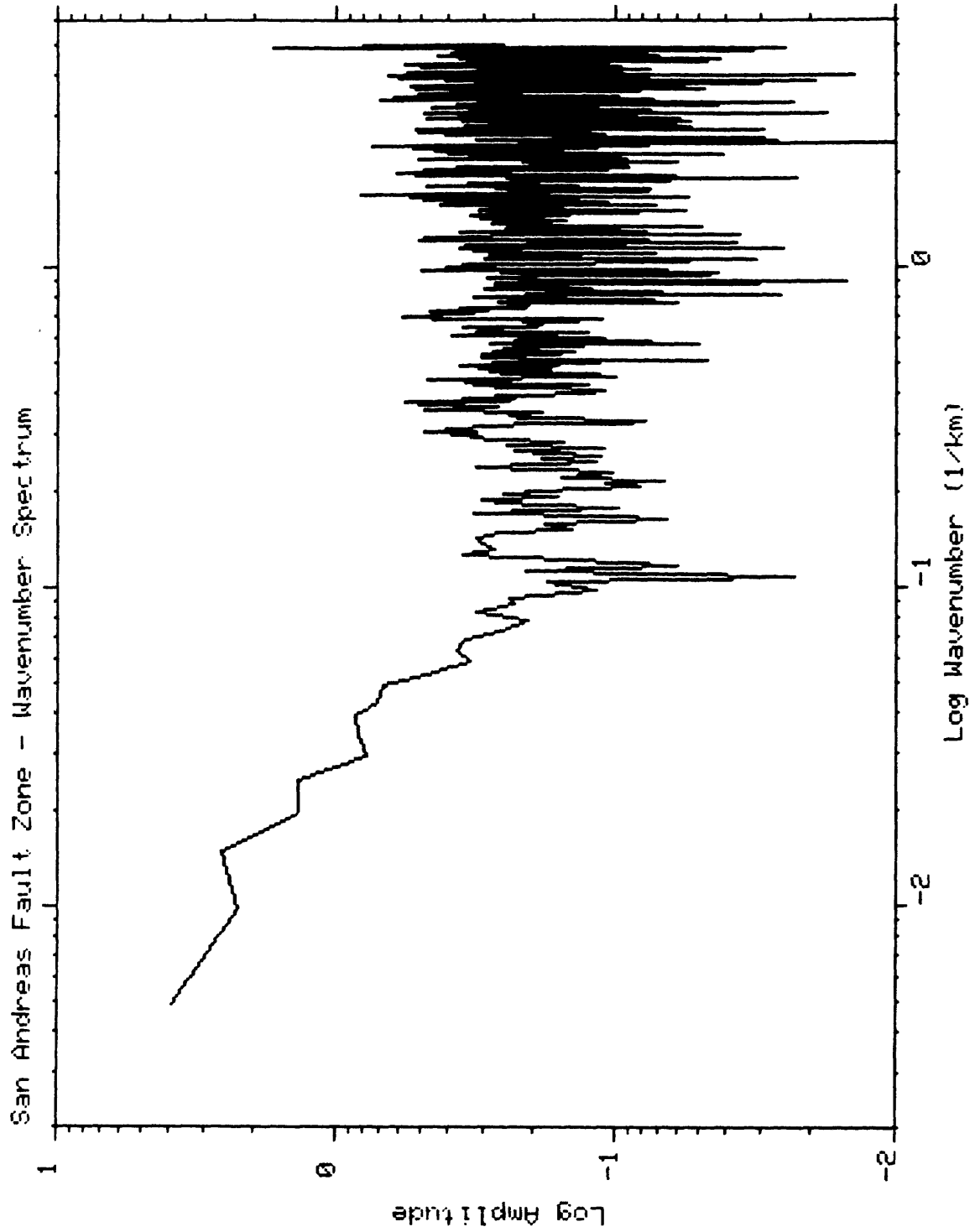
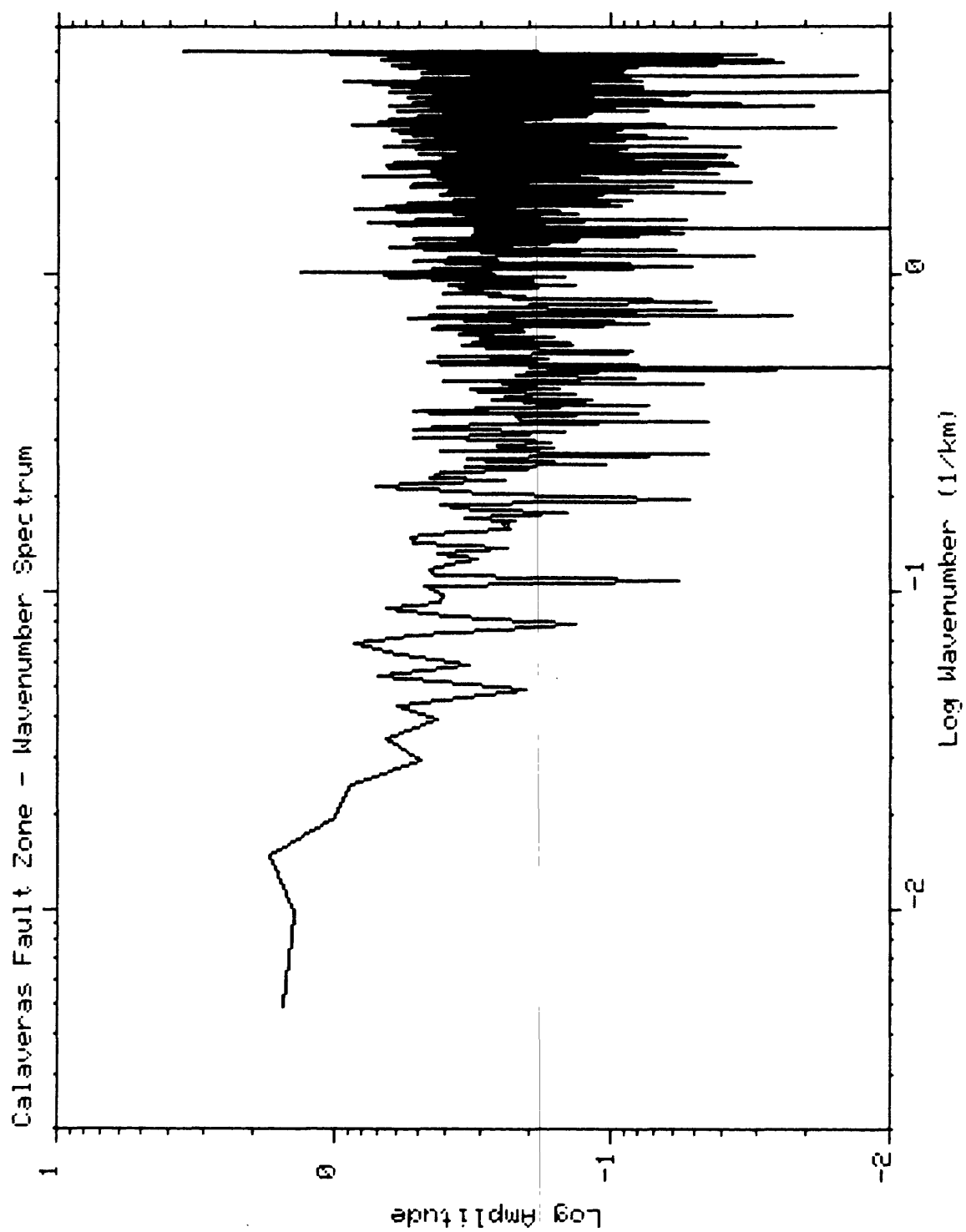


Figure 9



APPENDIX A. 13.

Earthquakes of $M \geq 6$ in the South San Francisco Bay Area

T. Toppozada

Earthquakes of $M \geq 6$ in the South San Francisco Bay Area

T. Topozada, Division of Mines and Geology

Introduction

This paper summarizes the history of damaging earthquakes in the South San Francisco Bay area. The occurrences are listed and discussed, and for the earthquakes after 1850 when newspaper reporting was common, isoseismal maps are presented. Pre-instrumental epicenters are assumed to fall in the area of highest intensity, and magnitudes are estimated from the extent of the areas shaken at different intensities.

Since 1850, two $M > 7$ earthquakes have occurred; $M \sim 7$ on the Hayward fault in 1868, and $M \sim 8$ on the San Andreas in 1906. It is interesting that in the years before and after the Hayward earthquake (1864-1890) most of the $M > 6$ events were on the San Andreas. Also, in the years before and after the San Andreas event (1897-1984) most of the $M \geq 6$ events were on the Hayward-Calaveras zone.

History

Occurrences of $M > 6$ earthquakes in the South San Francisco Bay area are listed in Table 1, and discussed below. The epicenters are shown in Figure 1. The sources of information are: Topozada et al. (1981) for 1800-1897, Topozada and Parke (1982) for 1903 and 1906, Topozada (1984) for 1911 and 1984, and U.S. Earthquakes for 1979.

The first earthquake damage in California was reported in 1800 from San Juan Bautista: "...there is not a single habitation, although built with double walls that has not been injured from roof to foundation, and that all are threatened with ruin; and that the fathers are compelled to sleep in the wagons to avoid danger, since the houses are not habitable. At the place where the rancharia is situated, some small openings have been observed in the earth, and also in the neighborhood of the river Pajaro there is another deep opening all resulting from the earthquakes." The San Andreas fault passes through San Juan Bautista near the Mission and crosses the Pajaro River about 11 km northwest of San Juan Bautista. This segment of the San Andreas fault also ruptured during the magnitude 6.0 earthquake on 24 April 1890 causing similar damage in San Juan Bautista. Aftershocks of the 1800 event were felt for seven weeks, suggesting a $M > 6$ mainshock.

In 1808, from 21 June to 17 July, 18 earthquakes were felt in the Presidio of San Francisco, cracking houses and destroying an antechamber. This suggests a $M > 6$ earthquake, possibly on the San Andreas fault.

In 1836, an earthquake occurred, "...the effects of which were felt along the foothills from San Pablo to Mission San Jose. There were large fissures in the earth...there were innumerable lesser (aftershocks)...for a month..." This is comparable to the 1868 Hayward earthquake on the Hayward fault, and the same magnitude was assumed ($M_{6.8}$).

In 1838, the San Andreas fault reportedly ruptured from near Santa Clara to San Francisco, suggesting a $M \sim 7$ event. The damage at Mission Dolores in San Francisco, was comparable to that in 1906. Also, the damage in Monterey was at least as high as in 1906, suggesting that faulting may have extended southward of Santa Clara.

Before the 1849 gold rush, the record is probably not complete for $M \sim 6$ earthquakes. For example, there are unconfirmed reports of damage at Santa Clara in 1822. After 1849, earthquake effects reported in the newspapers made the construction of isoseismal maps possible. Maps for events of $M \geq 6$ in the subject area are attached.

Table 1. SOUTH SAN FRANCISCO BAY AREA EARTHQUAKES $M \geq 6$

No. x	Date	Lat ^{OW}	Long ^{ON}	I	M	Fault*
1.	11-31 Oct. 1800	36.9	121.6	VII		SA
2.	21 June 1808	37.8	122.5	VIII		SA
3.	10 June 1836	37.8	122.2	VIII	6.8	H
4.	June 1838	37.6	122.4	VIII	7	SA
5.	26 Nov. 1858	37.5	121.9	VII	6.1	C
6.	26 Feb. 1864	37.1	121.7	VI	5.9	
7.	8 Oct. 1865	37.3	121.9	IX	6.3	SA
8.	21 Oct. 1868	37.7	122.1	IX	6.8	H
9.	17 Feb. 1870	37.2	122.1	VII	5.8	SA
10.	24 Apr. 1890	36.9	121.6	IX	6.0	SA
11.	20 June 1897	37.0	121.5	VIII	6.2	C
12.	11 June 1903	37.4	121.9	VII	5.8	H
13.	3 Aug. 1903	37.3	121.8	VII	5.8	H
14.	18 Apr. 1906	37.7	122.5	XI	8.3	SA
15.	1 July 1911	37.25	121.75	VIII	6.2	H
16.	6 Aug. 1979	37.1	121.5	VII	5.8	C
17.	24 Apr. 1984	37.33	121.67	VII	6.2	C

x Sequential numbers used in Figure 1.

* SA - San Andreas, H - Hayward, C - Calaveras

The 1858 earthquake in the East Bay threw down an adobe building and the corner of a new building in San Jose. It also threw down a cornice in San Francisco and part of a chimney in Mountain View.

The 1864 earthquake cracked adobe walls in Monterey and tipped over light furniture in Watsonville.

The 1865 earthquake threw houses down at New Almaden, toppled chimneys in Santa Cruz, and threw down walls in San Jose. Ground cracking occurred near the San Andreas fault. More aftershocks were reported at Santa Cruz than at San Jose, suggesting a source on the San Andreas.

The 1868 earthquake resulted from rupture of 50 km of the Hayward fault. The courthouse at San Leandro was ruined, and similar damage occurred from San Jose to the lowlands of both San Francisco and Oakland.

In 1870, chimneys were dislocated at Los Gatos and Santa Cruz.

The 1890 earthquake toppled most chimneys between San Juan Bautista and Corralitos and damaged some brick and frame buildings. Probable faulting occurred along the San Andreas fault where it crosses the Pajaro river.

The 1897 earthquake greatly damaged brick buildings from Gilroy to San Felipe. Fissures reported on the Pacheco Pass road and near San Felipe suggest possible rupture of the Calaveras fault.

Earthquakes occurred near San Jose and the Hayward fault in June and August 1903. These earthquakes have intensity distributions that are comparable to the 1911 event, but they are somewhat smaller in size.

The great 1906 San Francisco earthquake was followed by the 1911 earthquake, that was damaging from Morgan Hill to Santa Clara.

After 1911, no earthquakes of $M \geq 6$ occurred in the area for 68 years, until 1979 when a damaging earthquake occurred near Gilroy (Coyote Lake).

Finally, in 1984 an earthquake occurred that was damaging between Gilroy and Mount Hamilton (Morgan Hill).

Observations

The largest earthquakes ($M > 7$) have occurred on the San Andreas fault in 1838 and 1906, and on the Hayward fault in 1836 and 1868.

The next largest earthquake ($M \sim 6 \frac{1}{2}$) occurred on the Santa Cruz Mountains portion of the San Andreas fault in 1865.

$M \geq 6$ earthquakes generally occur at intervals of 7 years or less in the South San Francisco Bay area. The longer intervals before 1850 probably reflect the incompleteness of the record. The 20-year quiescence (1870-1890) apparently resulted from the large release of stress in the $M \sim 7$ earthquake of 1868, and the 1911 to 1979 quiescence apparently resulted from the large release of stress in the $M \sim 8$ earthquake of 1906.

The earthquakes of $M \geq 6$ have occurred on the Hayward-Calaveras zone east of San Jose in 1858, 1897, 1903, 1911, 1979, and 1984, and on the San Andreas between San Juan Bautista and Los Gatos in 1864 (apparently), 1865, 1870, and 1890.

It is interesting to relate these occurrences to the two largest post-1850 earthquakes. The Hayward-Calaveras earthquakes occurred mostly from the decade before the 1906 San Andreas earthquake and have continued to date. The San Andreas earthquakes occurred from the decade before the 1868 Hayward earthquake and continued to 1890. This suggests that $M \geq 6$ activity on the Hayward-Calaveras zone precedes and follows $M \geq 7$ activity on the San Andreas, and that $M \geq 6$ activity on the San Andreas precedes and follows $M \geq 7$ activity on the Hayward-Calaveras zone.

References

- Toppozada, T.R., Real, C.R., and Parke, D.L. (1981). Preparation of isoseismal maps and summaries of reported effects for pre-1900 California earthquakes, California Division of Mines and Geology, open file report 81-11 SAC.
- Toppozada, T.R., and Parke, D.L. (1982). Areas damaged by California earthquakes, 1900-1949, California Division of Mines and Geology, open file report 82-17 SAC.
- Toppozada, T.R. (1984). History of earthquake damage in Santa Clara county and comparison of 1911 and 1984 earthquakes, in The 1984 Morgan Hill, California Earthquake, J.H. Bennett and K.W. Sherburne editors, California Division of Mines and Geology, Special Publication 68.
- U.S. Earthquakes, 1979. U.S. Dep. of Interior, Geological Survey, and U.S. Dep. of Commerce, National Oceanic and Atmospheric Administration.

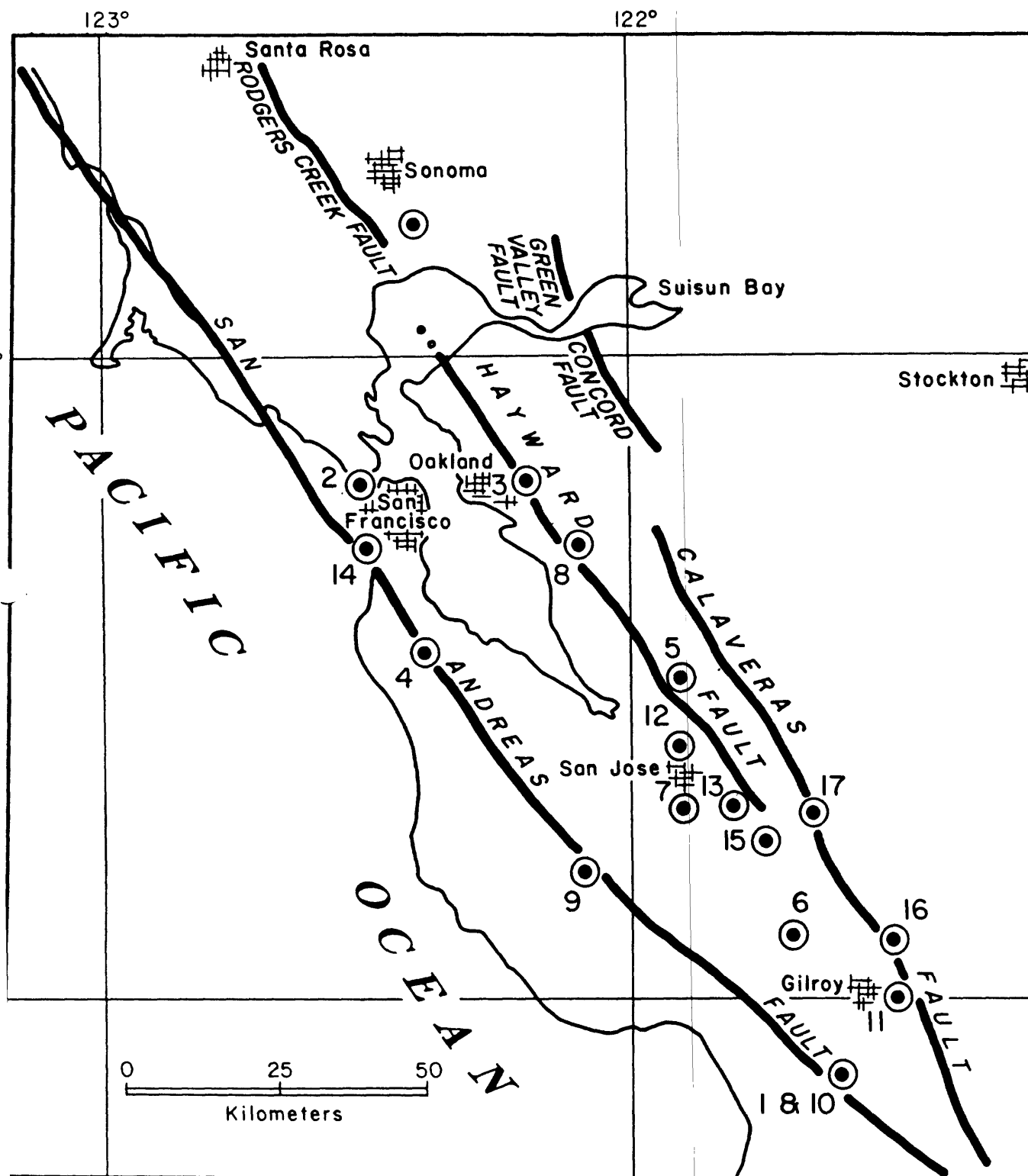


Figure 1 Approximate epicenters of earthquakes of magnitude about 6 and greater in south San Francisco Bay area. The sequential numbers are keyed to Table 1.

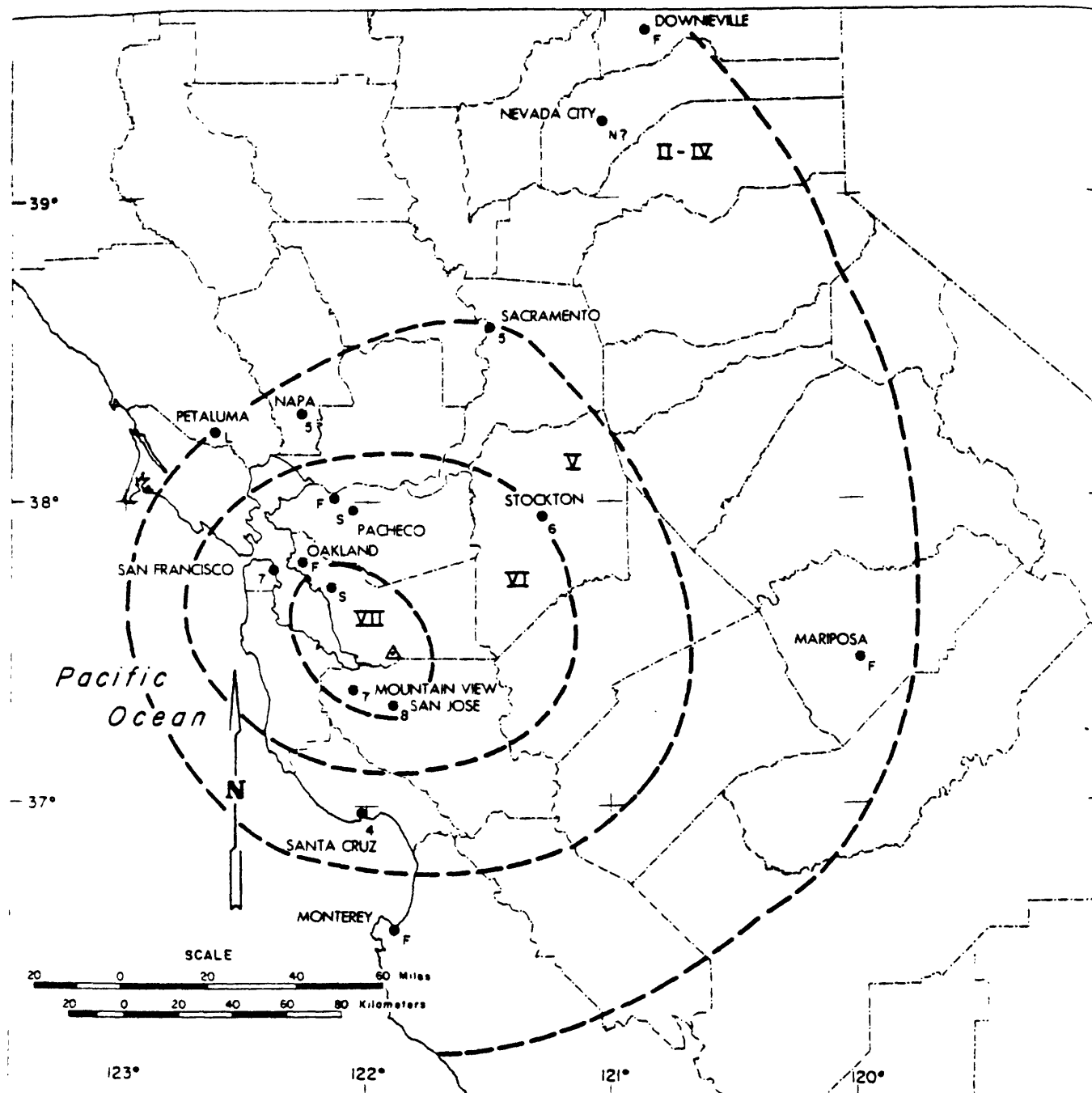


FIGURE 2. MODIFIED MERCALLI ISOSEISMAL MAP
DATE: 26 NOV., 1858 TIME: 08:35 GMT



- | | | |
|---|-----------------------|---------------------------|
| ● ₅ Site reporting intensity 5 effects | ● _F Felt | } Indeterminate intensity |
| ● _N Reported not felt | ● _L Light | |
| Ⅴ Zone of intensity 5 effects | ● _H Heavy | |
| △ Estimated epicenter | ● _S Severe | |

— — — — — Smoothed isoseismal line, dashed where data is lacking

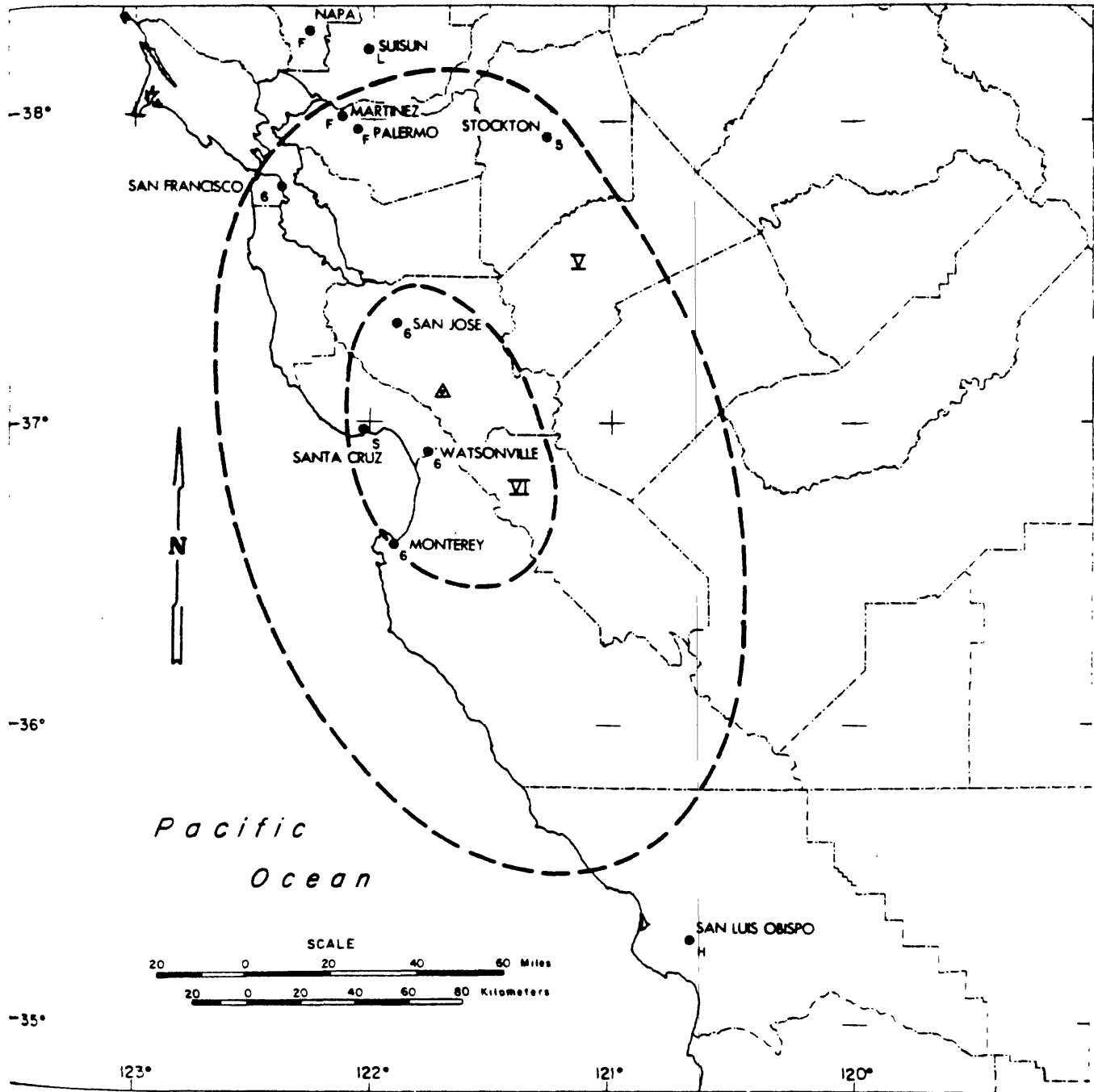


FIGURE 3. MODIFIED MERCALLI ISOSEISMAL MAP
DATE: 26 FEB., 1864 TIME: 13:47 GMT



1981

- ₅ Site reporting intensity 5 effects
- _N Reported not felt
- ∇ Zone of intensity 5 effects
- △ Estimated epicenter

- _F Felt
- _L Light
- _H Heavy
- _S Severe

} Indeterminate intensity

— — — Smoothed isoseismal line, dashed where data is lacking

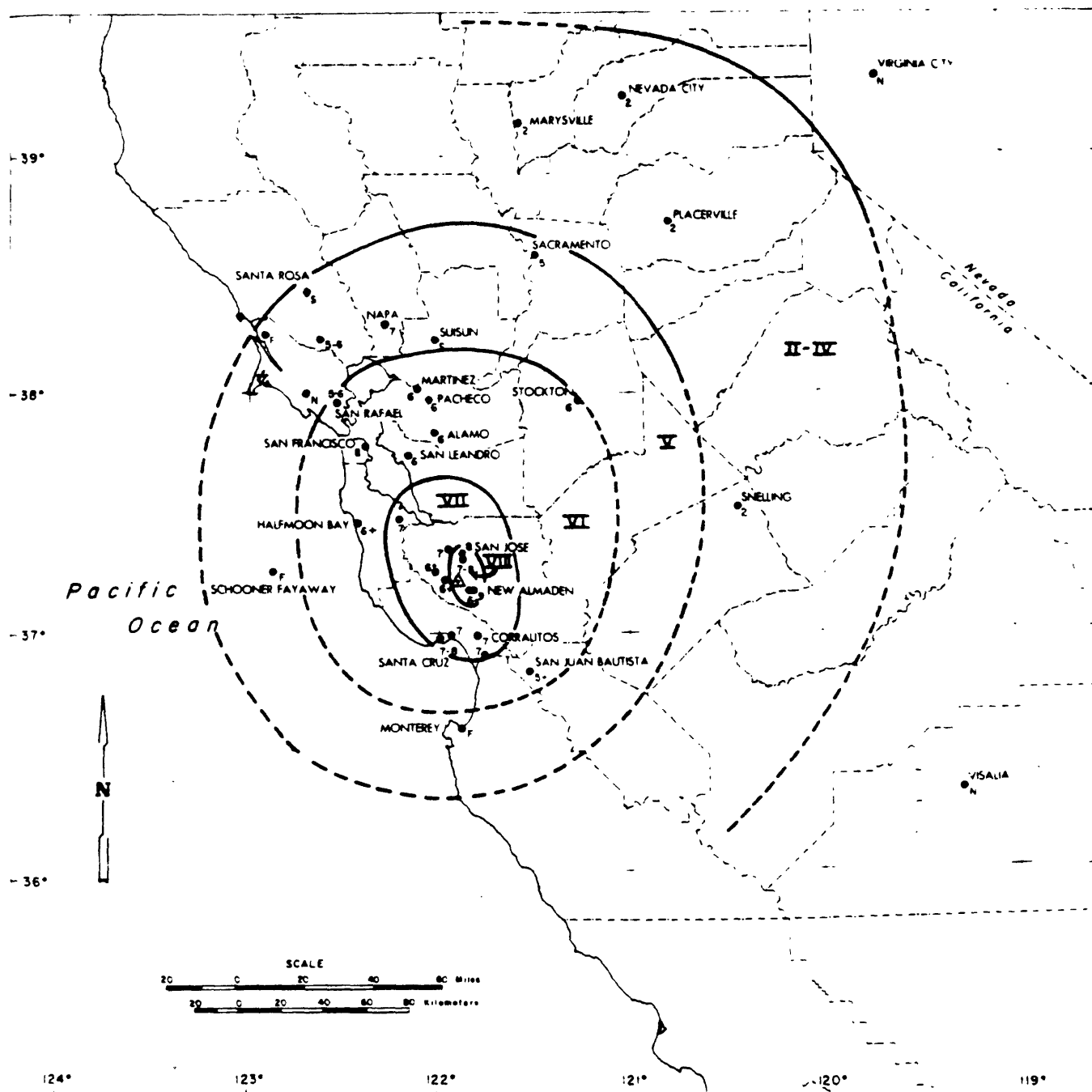


FIGURE 4 . MODIFIED MERCALLI ISOSEISMAL MAP
DATE: 8 OCT., 1865 TIME: 20:46 GMT



1981

- | | | |
|---|-----------------------|---------------------------|
| ● _S Site reporting intensity 5 effects | ● _F Felt | } Indeterminate intensity |
| ● _N Reported not felt | ● _L Light | |
| Ⅴ Zone of intensity 5 effects | ● _H Heavy | |
| △ Estimated epicenter | ● _S Severe | |

— — — — — Smoothed isoseismal line, dashed where data is lacking

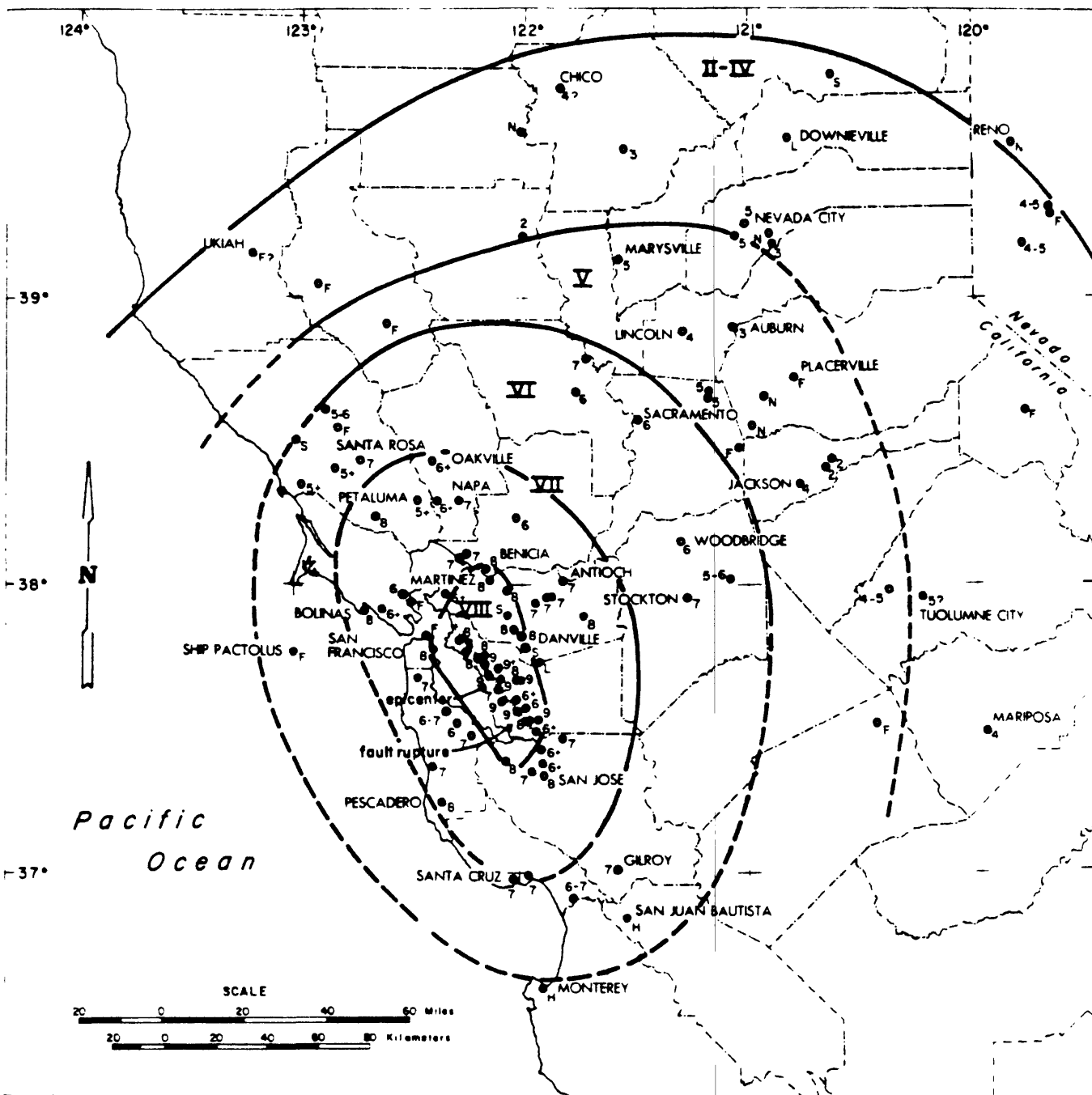


FIGURE 5 . MODIFIED MERCALLI ISOSEISMAL MAP
DATE: 21 OCT., 1868 TIME: 15:53 GMT

- ₅ Site reporting intensity 5 effects
- _N Reported not felt
- Ⅴ Zone of intensity 5 effects
- △ Estimated epicenter

- _F Felt
- _L Light
- _H Heavy
- _S Severe

} Indeterminate intensity

— — — — — Smoothed isoseismal line, dashed where data is lacking



CALIFORNIA DIVISION OF MINES AND GEOLOGY

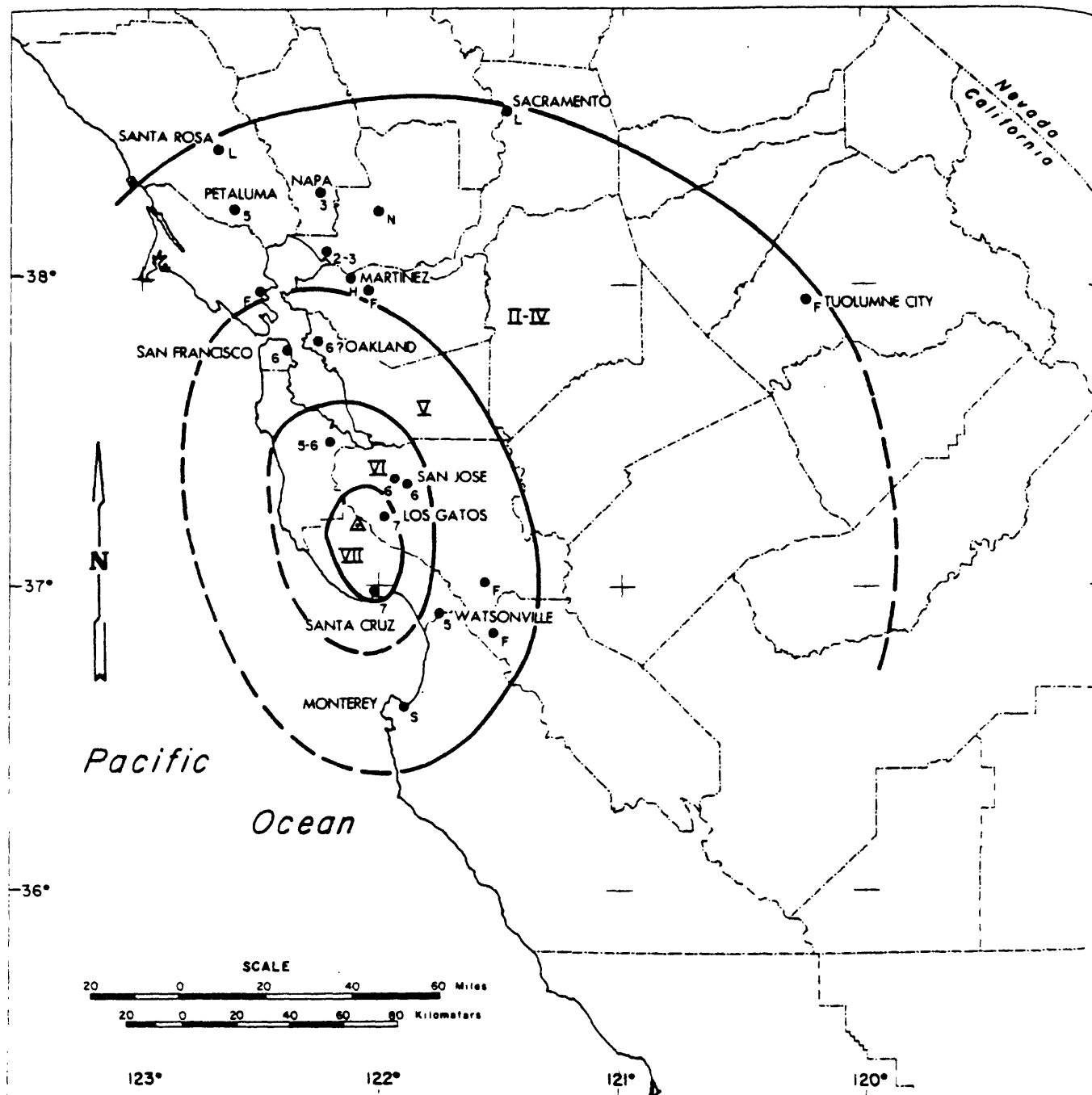


FIGURE 6. MODIFIED MERCALLI ISOSEISMAL MAP
 DATE: 17 FEB., 1870 TIME: 20:12 GMT



1981

- ₅ Site reporting intensity 5 effects
- _N Reported not felt
- Ⅴ Zone of intensity 5 effects
- △ Estimated epicenter

- _F Felt
- _L Light
- _H Heavy
- _S Severe

} Indeterminate
intensity

— — — — — Smoothed isoseismal line, dashed where data is lacking

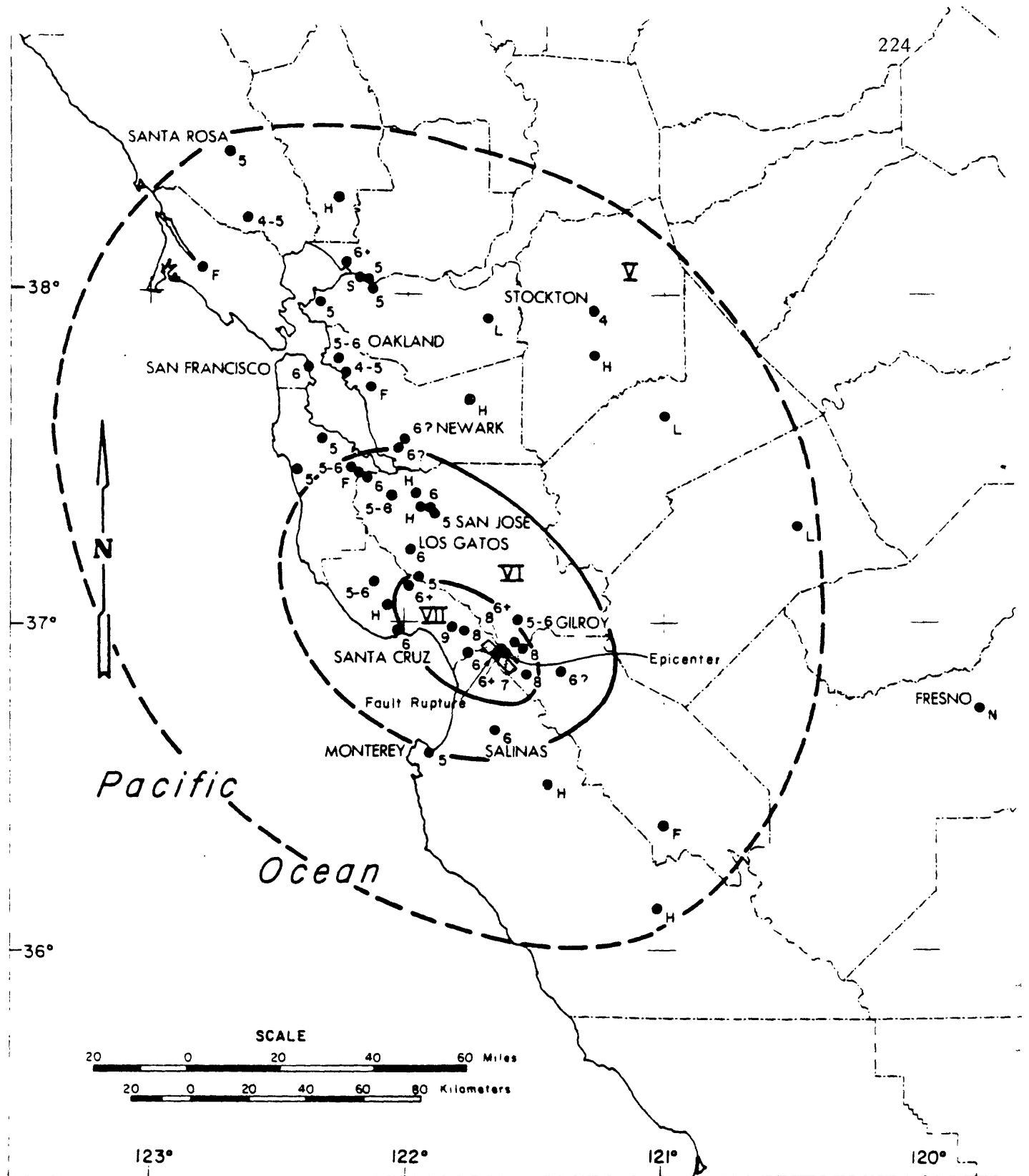


FIGURE 7 . MODIFIED MERCALLI ISOSEISMAL MAP
DATE: 24 APR., 1890 TIME: 11:36 GMT



- | | |
|---|-----------------------|
| ● ₅ Site reporting intensity 5 effects | ● _F Felt |
| ● _N Reported not felt | ● _L Light |
| Ⅴ Zone of intensity 5 effects | ● _H Heavy |
| △ Estimated epicenter | ● _S Severe |

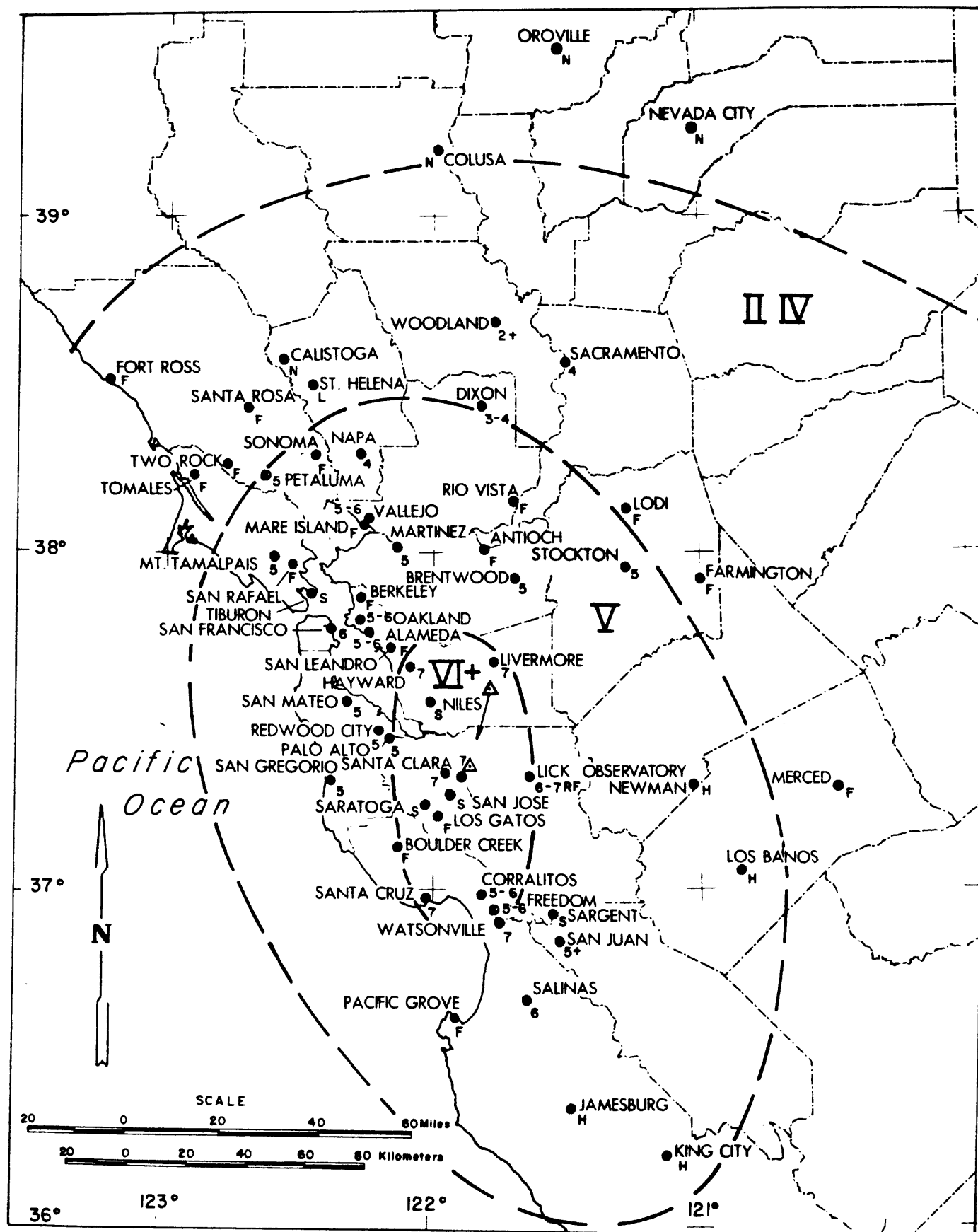


Figure 9

11 JUNE 1903

CALIFORNIA DIVISION OF MINES AND GEOLOGY

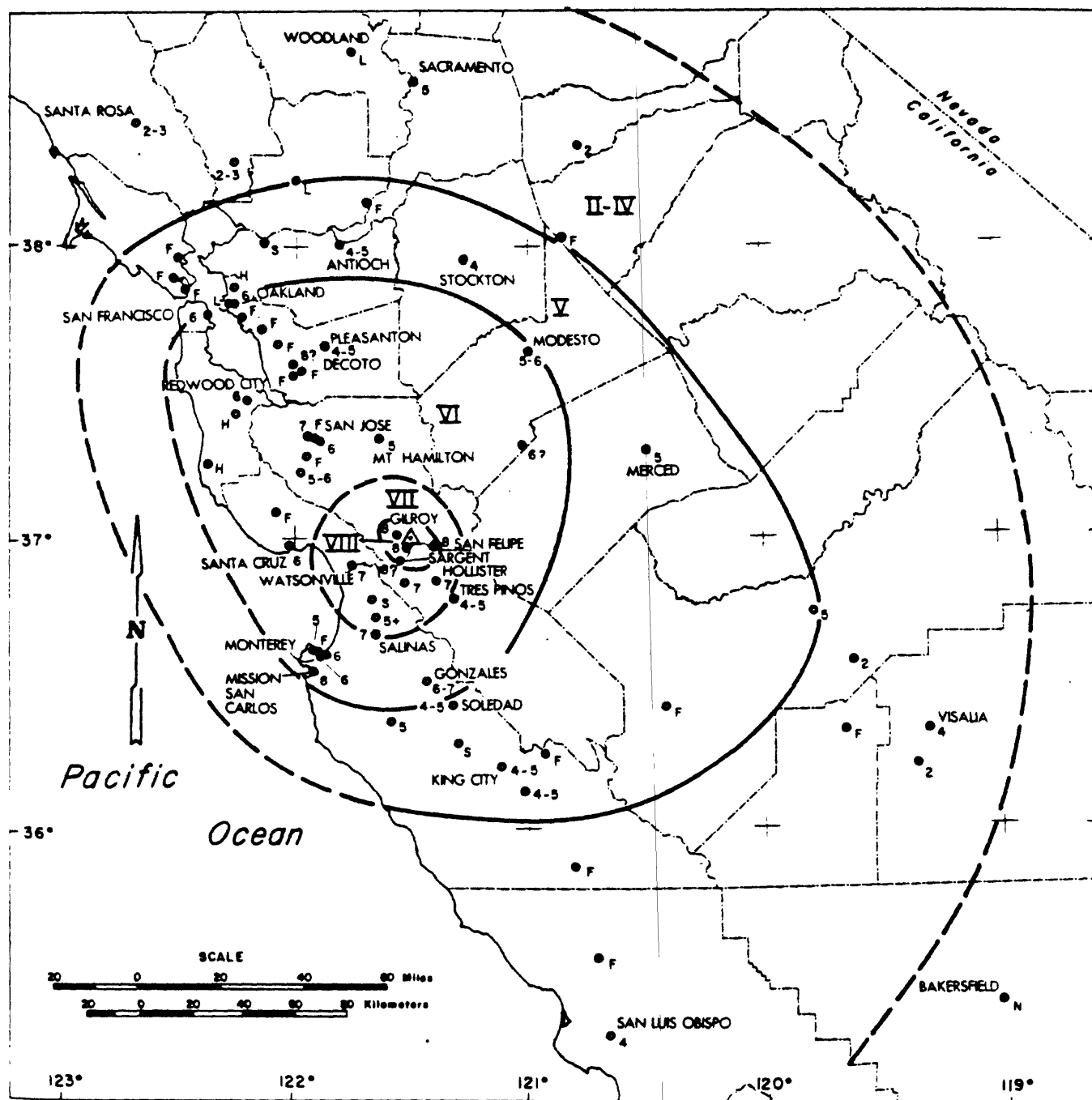


FIGURE 8 MODIFIED MERCALLI ISOSEISMAL MAP
DATE: 20 JUNE, 1897 TIME: 20:14 GMT



- ₅ Site reporting intensity 5 effects
- _N Reported not felt
- Ⅴ Zone of intensity 5 effects
- △ Estimated epicenter

- _F Felt
 - _L Light
 - _H Heavy
 - _S Severe
- } Indeterminate intensity

— — — — — Smoothed isoseismal line, dashed where data is lacking

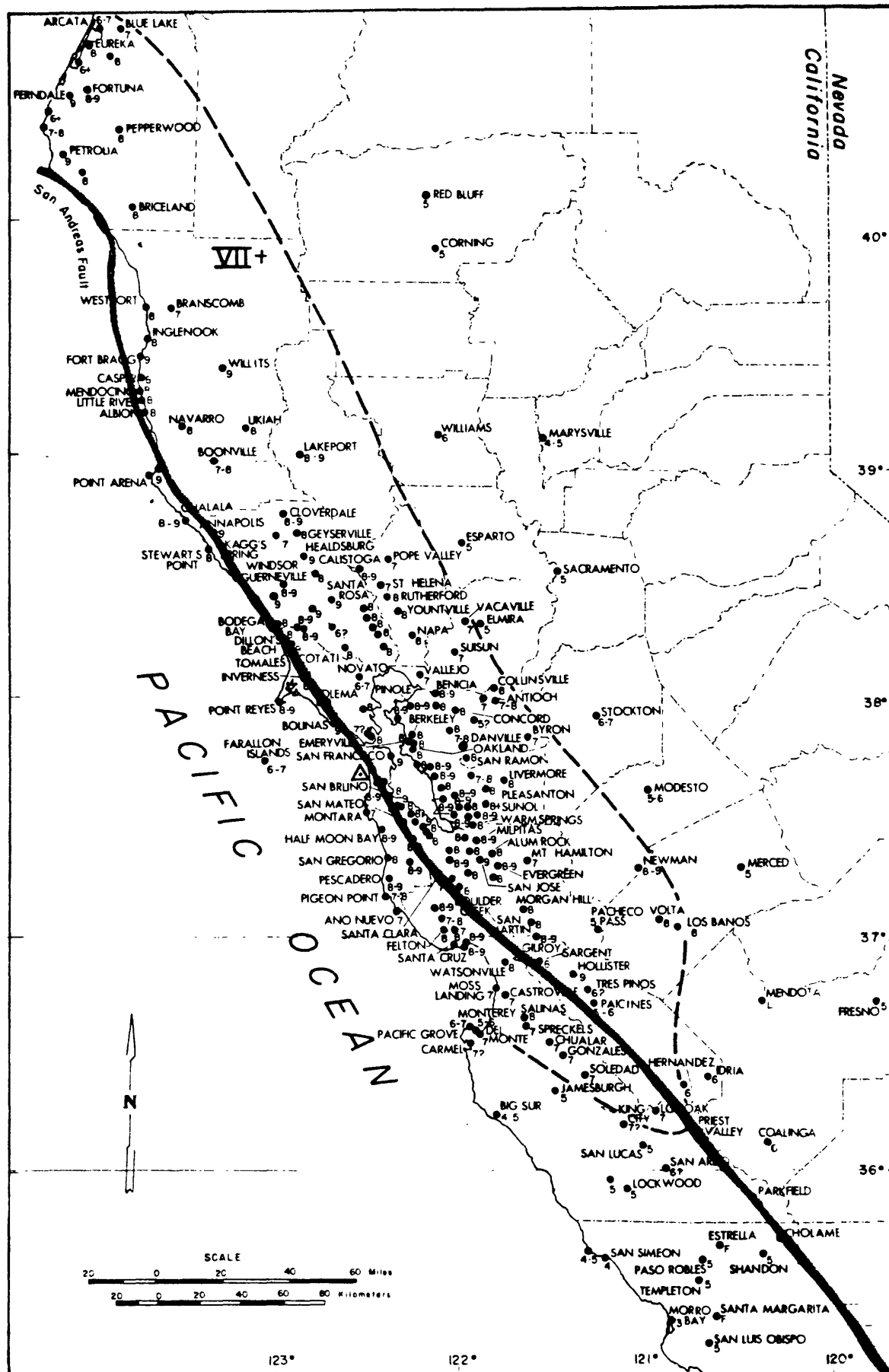


Figure 11

18 APRIL 1906

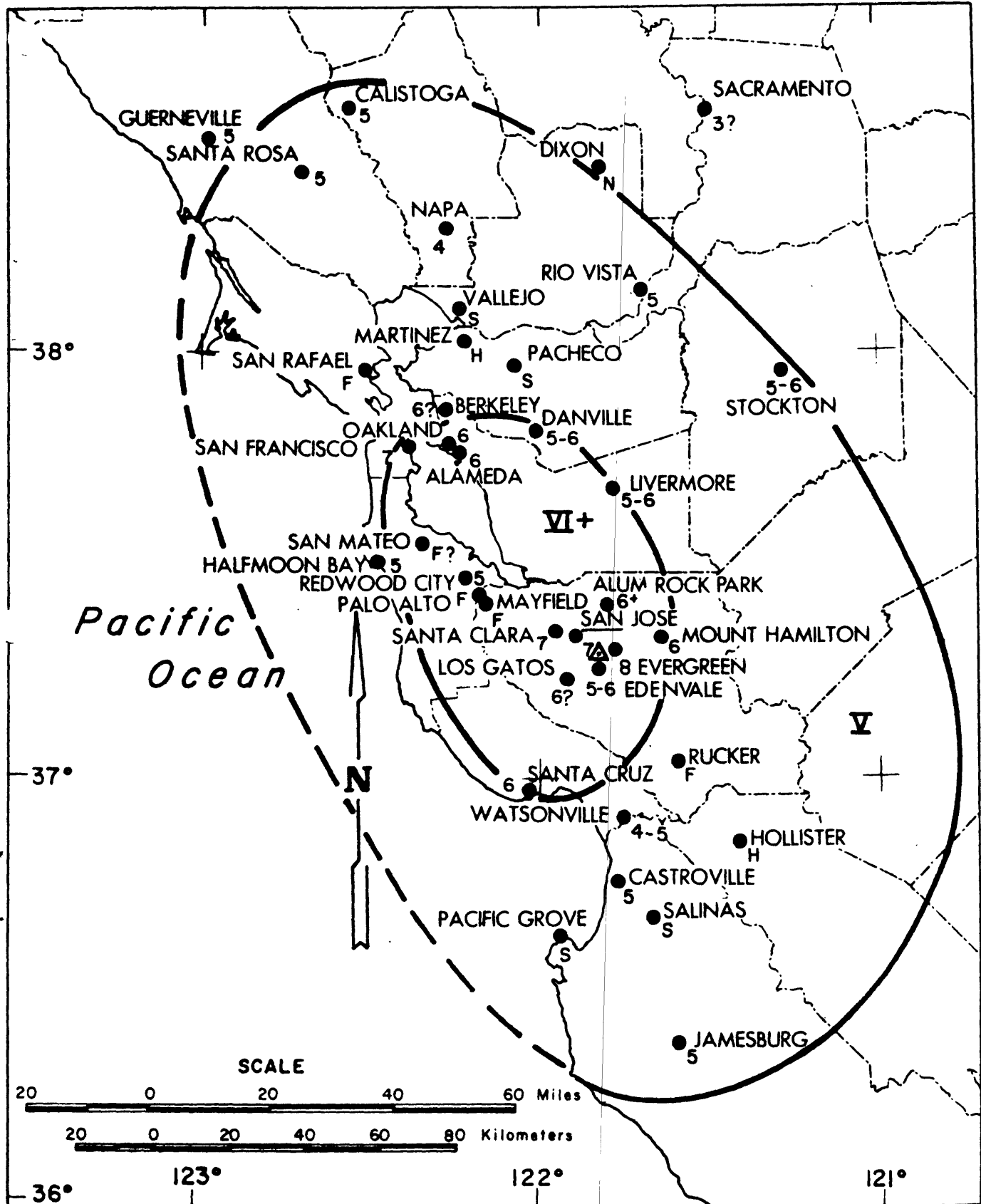


Figure 10

3 AUGUST 1903

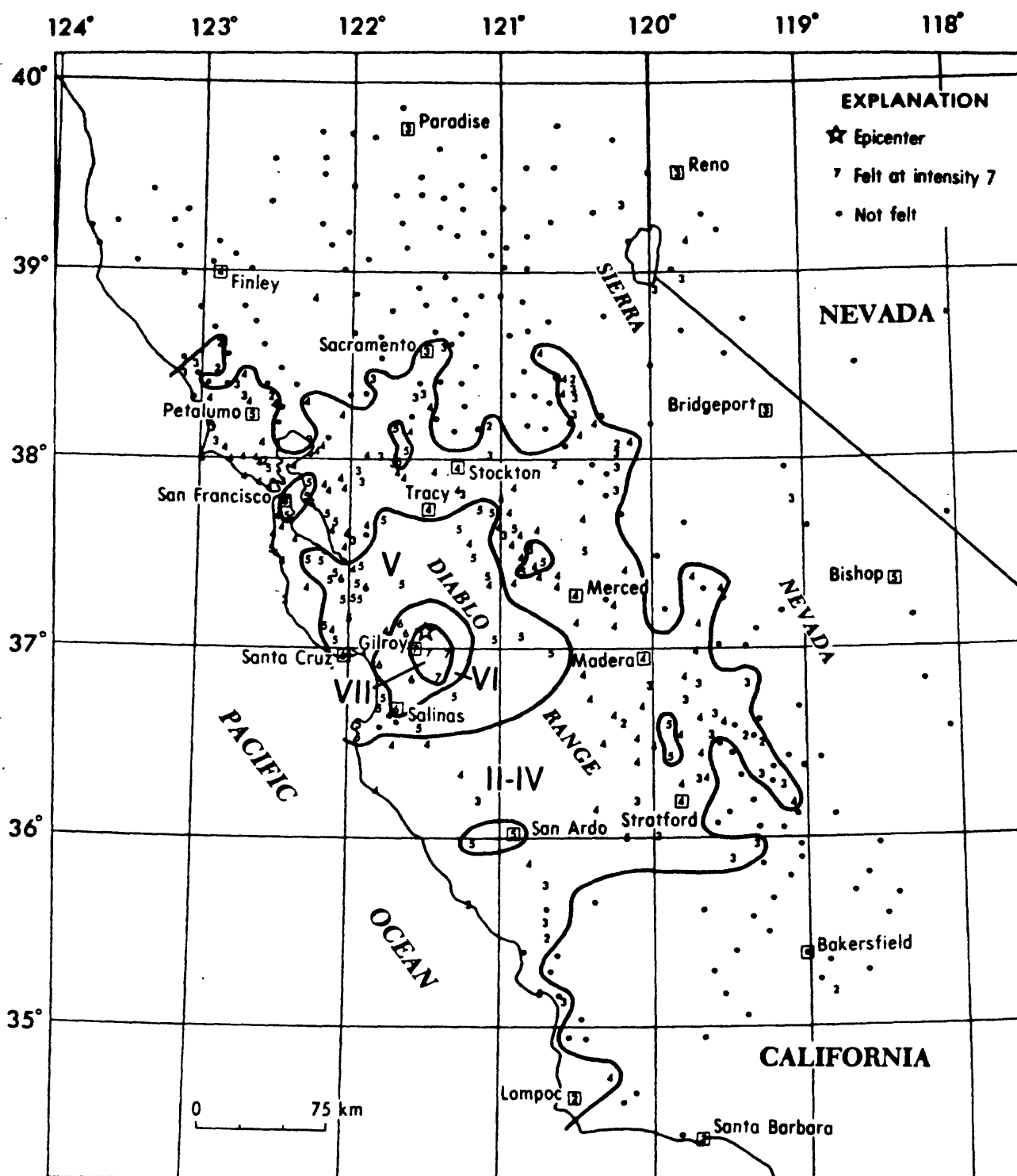


FIGURE 13--Iseseismal map for the central California earthquake of 6 August 1979, 17 05 22.7 UTC. Roman numerals represent Modified Mercalli intensities between isoseismals; Arabic numerals are used to represent these intensities at specific sites.

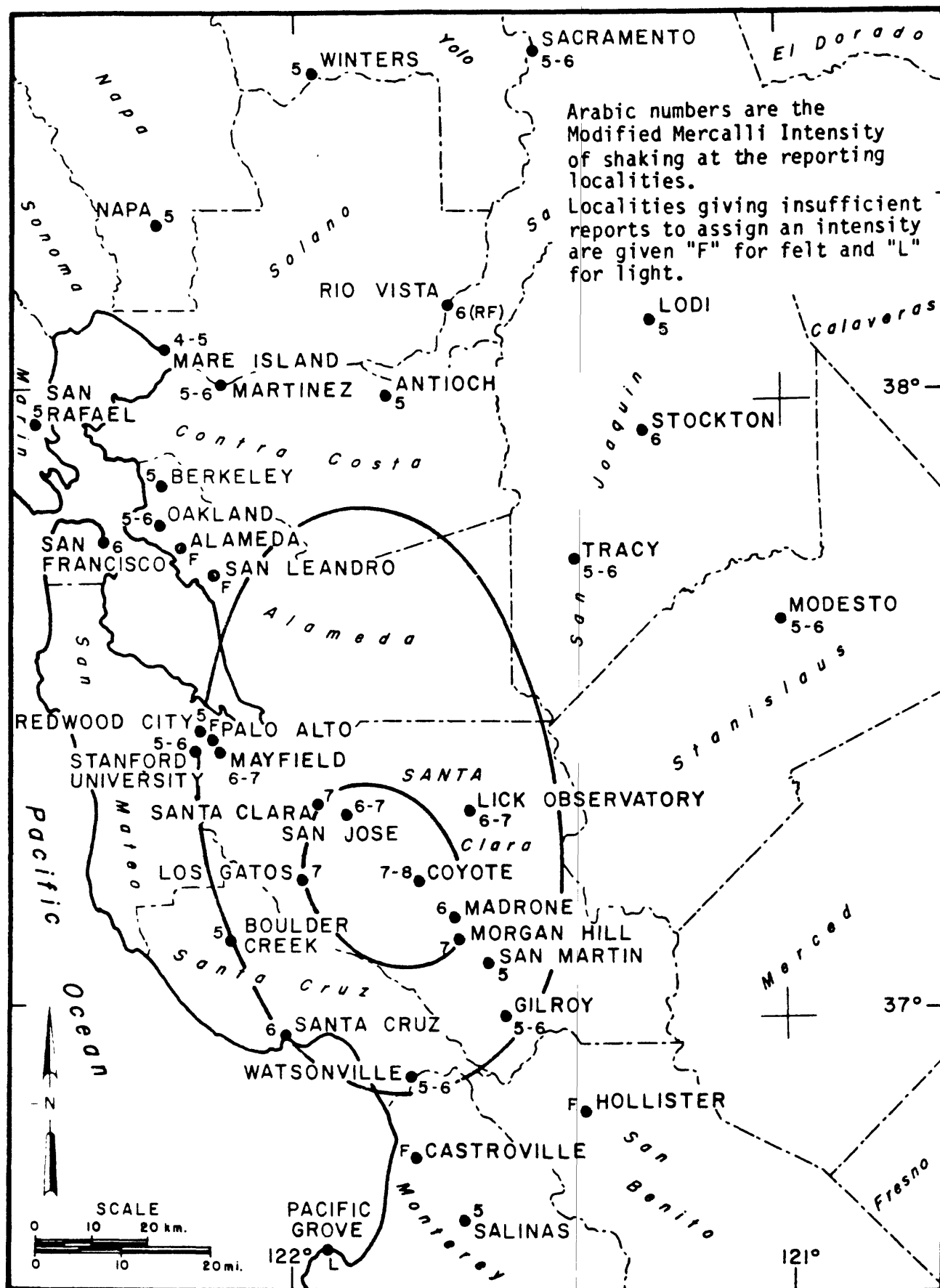


Figure 12 Isoseismal map of 1 July 1911 earthquake. The smoothed isoseismal lines outline the area of minor damage (outer contour) and significant damage (inner contour).

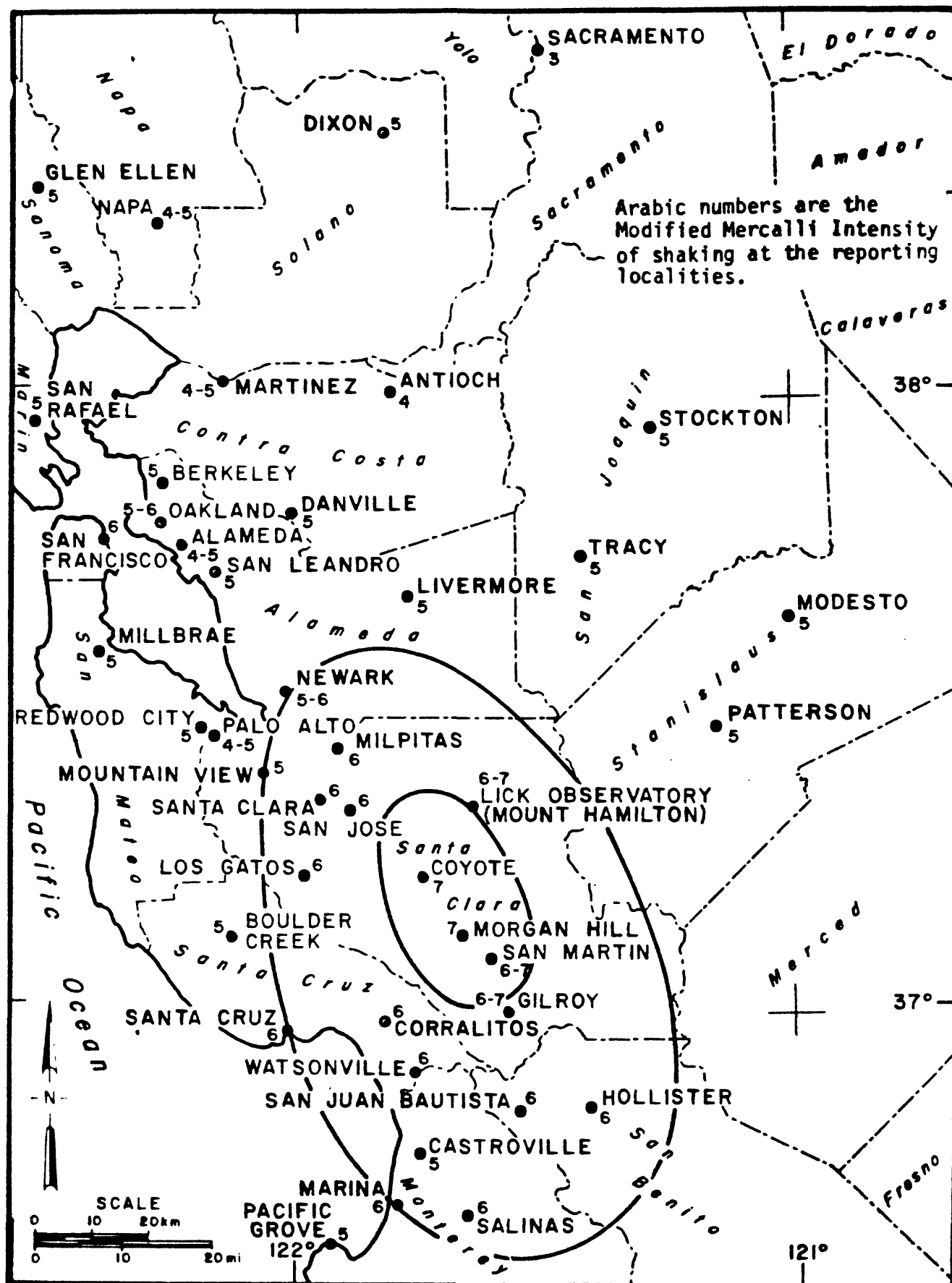


Figure 14 Isoseismal map of 24 April 1984 earthquake. The smoothed isoseismal lines outline the area of minor damage (outer contour) and significant damage (inner contour).

APPENDIX A. 14.

An Overview of the Distribution of Relative Plate Motion
along the San Andreas Fault System from Hollister, California,
to the Mendocino Triple Junction

W. H. Prescott

An Overview of the Distribution of Relative Plate Motion along the San Andreas Fault System from Hollister, California to the Mendocino Triple Junction

William H. Prescott
U.S. Geological Survey
25 July 1985

Abstract. Recent work on the distribution of the relative motion between the Pacific and North American plates suggests that a fundamental change in the nature of the fault system occurs at Hollister, California. North of Hollister the plate motion is not concentrated on the San Andreas fault, either seismically or aseismically. Rather the San Andreas is accomodating only about one-third of the plate motion, while the rest is distributed over a broad zone to the east of the fault. The transition occurs over a relatively short distance, and then the fault system behavior appears to remain constant all the way north to perhaps beyond the Mendocino triple junction.

Introduction. South of Hollister, it is well known that the plate motion is all accomodated by aseismic slip on the San Andreas fault. [The relative plate motion rate in this part of California appears to be 30–35 mm/yr, at least over the last 70 years or so (Thatcher, 1979; Prescott et al., 1981; Prescott et al., 1985). Consequently, in this paper, reference to the total plate motion rate will refer to this rate of 30+ mm/yr.] In this discussion I will try to convince you of some general conclusions about what happens to this 30+ mm/yr farther to the north along the San Andreas fault system. These conclusions are of relevance to a discussion of earthquake hazard in the San Francisco Bay area for several reasons. Knowledge of the overall pattern of deformation provides a framework for understanding the details in any one area. If we can place limits on the rate of strain accumulation, or equivalently slip deficit, it may assist us in estimating recurrence intervals. Finally, knowledge of the overall pattern of relative motion distribution can aid us in knowing which faults are likely to be seismically active in the future.

Evidence. There is a large network of geodetic lines (Fig. 1) covering the plate boundary between Hollister and the Mendocino triple junction. The length of all of these lines has been measured with a geodolite using

aircraft-obtained meteorology to control the influence of refraction. Most of the lines have been measured many times. In the following discussion we will work north from the Hollister area examining briefly the distribution of motion in each area.

In the Hollister area there are approximately 100 lines (Fig. 2) covering the region where slip on the San Andreas fault system ceases to occur on a single well defined fault trace and becomes more complex. Analysis of this network (Savage et al., 1979; Gu and Prescott, in press) indicates that the 30 mm/yr slip coming up from the south, divides neatly between the Calaveras and San Andreas faults. There is no evidence of internal deformation of the blocks between the faults; just rigid block motion on the two fault systems. Although the division is neat, it is not equal: the Calaveras fault gets about two-thirds of the slip. Gu's least squares adjustment of the observations for station velocities is the subject of Fig. 3. Relative to the central block, the western block is moving at 8.9 ± 0.8 mm/yr; also relative to the central block, the eastern block is moving at 14.5 ± 0.5 mm/yr. Notice that there is little difference between the length of the vectors within an individual block. At this latitude the slip has distributed but it is all accommodated as rigid block motion. Savage et al. (1979) obtained a relative block motion rate of 13.4 ± 2.2 mm/yr across the San Andreas fault south of San Juan Bautista. The major difference between the study of Savage et al. and that of Gu and Prescott is the latter study's inclusion of stations Vargo, Chamber, Gal, Mulligan and Brush (Fig. 2). It is not clear why this would decrease the apparent slip rate. However, the fact that including these more distant stations does not increase the slip rate argues against an appreciable amount of relative motion to the west of the San Andreas fault, a point that will be confirmed by data from further north.

The next profile to the north is across the southern end of San Francisco Bay. Fig. 4 shows the lines that were used to infer a displacement profile across the entire area. Station velocities were obtained from an adjustment of data for all of the lines shown in Fig. 4. These velocities have been resolved into components parallel and perpendicular to the plate boundary (Fig. 5). The upper profile in Fig. 5 shows some distributed shear in the vicinity of the San Andreas fault (near -20 km), at the SW end of the profile. There is an abrupt displacement where the profile crosses the Hayward fault (3 km) and the Calaveras fault (7 km) with

the single station Allison in between. Although it appears that there is some distributed shear east of the Calaveras fault, it can be shown that this motion is produced by rotation of the block east of the Calaveras fault (Prescott et al., 1981). Overall there is a displacement of 32.1 ± 7.4 mm/yr across the entire area. There is no clear evidence of motion on the southwest side of the San Andreas fault although the data are not very definitive.

North of San Francisco Bay the network (Fig. 6) allows a better resolution of relative motion. Once again we constructed a profile of the component of displacement parallel to the fault system (Fig. 7). The important features of this profile are the absence of deformation on the SW side of the San Andreas fault, and the broad distribution of displacement to the NE of the San Andreas fault. The absence of any offsets at the fault crossings. This profile includes a station on the Farallon Islands as well as a number of stations in the vicinity of Point Reyes. All of these stations are either SW of the San Gregorio fault or north of the junction of the San Andreas and San Gregorio faults. The absence of deformation at the SW end of the profile places limits on the slip that can be occurring on the San Gregorio fault (Prescott et al., 1985). The total slip across the entire zone is 25 ± 6 mm/yr.

Further north (Fig. 8), no profiles of displacement have been constructed; but there is ample evidence of extensive shear deformation well to the east of the San Andreas fault. Both historical triangulation data and recent trilateration data along the Maacama and Lake Mountain faults indicate strain rates of 0.4 to .07 μ rad/yr. There is no recent data available near the San Andreas fault. Seismicity in this area, 1982 is shown as a sample in Fig. 9, clearly indicates that deformation is occurring in the area to the east of the San Andreas fault. While the absence of seismicity near the San Andreas fault is ambiguous (it is consistent with both an inactive area, and a completely locked fault) the absence of seismicity to the west of the fault confirms our conclusion that all of the deformation is occurring to the east of the San Andreas fault. It may not be a coincidence that the seismicity and high strain follows the extension of the small circle about the Minster and Jordan (1979) pole from central California to northern California (Fig. 9). Smith, Knapp and McPherson (1985) have argued that a few million years ago the plate boundary was located 50 km to the west of the present San Andreas fault. The extensive deformation occurring east of the San

Andreas fault may be the result of a continuing migration of the plate boundary to the east. Perhaps the present San Andreas fault is being abandoned in favor of boundary in the vicinity of the Lake Mountain-Maacama system. Fox (1983) argues that, at the latitude of Point Reyes, the crust near the San Andreas fault is undeformed while the crust further to the east is highly deformed.

A final bit of evidence to suggest that the change in the style of deformation that occurs at Hollister is permanent is provided by the comparison of near field strain rates along the San Andreas fault. Small networks within 5 km of the fault, three along the San Francisco peninsula (Prescott et al., 1981) and one at Point Reyes Station (Prescott and Yu, 1985) indicate that there is very intense deformation occurring very near the San Andreas fault. For all of these nets the rate has been about $0.6\text{--}0.7\text{ }\mu\text{rad/yr}$, double the rate observed from trilateration elsewhere. There is no difference between the nets on the peninsula and the net at Point Reyes Station even though the San Gregorio fault intersects the San Andreas fault between the two locations.

Conclusions and Implications. This interpretation of recent geodetic work has several implications for the earthquake prediction in the San Francisco Bay area:

- 1) The total relative motion between the two plates in this area (Hollister to Mendocino) is $30\text{--}35\text{ mm/yr}$ rather than 55 mm/yr .
- 2) There is no detectable difference between the behavior of the San Andreas fault at Point Reyes, where the slip in 1906 was 4 m, and the peninsula, where the slip in 1906 was 2 m.
- 3) The present rate of slip at depth on the San Andreas fault is 12 to 15 mm/yr from Hollister to Pt. Reyes.
- 4) The balance about 20 mm/yr of relative motion that must be absorbed by East Bay faults.
- 5) There is no evidence in recent geodetic observations that there is relative motion occurring in the material southwest of the San Andreas fault.
- 6) In particular there is no evidence in recent geodetic observations that there is any strain accumulating due to slip at depth on the San Gregorio fault. Nor is there any evidence of an increase in movement on the San Andreas fault north of its junction with the San Gregorio fault.

7) There is some weak evidence that the 2/3 of the relative motion which occurs east of the San Andreas fault, is occurring as distributed shear, and that it may not be associated with slip on discrete faults.

8) Hence even though the evidence suggests that most of the relative motion is located east of the San Andreas fault, the likelihood of great earthquakes here may not be very large.

References.

Fox, K.F., Jr., 1983, Tectonic Setting of Late Miocene, Pliocene, and pleistocene Rocks in Part of the Coast Ranges North of San Francisco, California, U.S.G.S. Prof. Pap. 1239.

Gu, G.-H., and W.H. Prescott, 1985, Discussion on displacement analysis: Detection of Crustal Deformation, submitted to JGR.

Minster, T.H. and J.B. Minster, 1978, Present day plate motions, JGR, 83 (B11), 5331-5354.

Prescott, W.H., M. Lisowski, and J.C. Savage, 1981, Geodetic measurement of crustal deformation across the San Andreas, Hayward and Calaveras faults near San Francisco, California, JGR, 86 (B11), 10853-10869.

Prescott, W.H. and S.-B. Yu, 1985, Geodetic measurement of horizontal deformation in the northern San Francisco Bay Region, California, submitted to JGR.

Prescott, W.H., N.E. King, M. Lisowski, and J.C. Savage, Deformation of the Pacific Plate near San Francisco, California, 1985, submitted to Science.

Savage, J.C., W.H. Prescott, M. Lisowski, and N.E. King, 1979, Geodolite measurements of deformation near Hollister, California, JGR, 84 (B13), 7599-7615.

Smith, S.W., J. Knapp and R. McPherson, 1985, A double planed seismic zone at Cape Mendocino, EOS, 66 (18), 299.

Thatcher, W., 1979, Systematic inversion of geodetic data in central California, JGR, 84 (B5), 2283-2295.

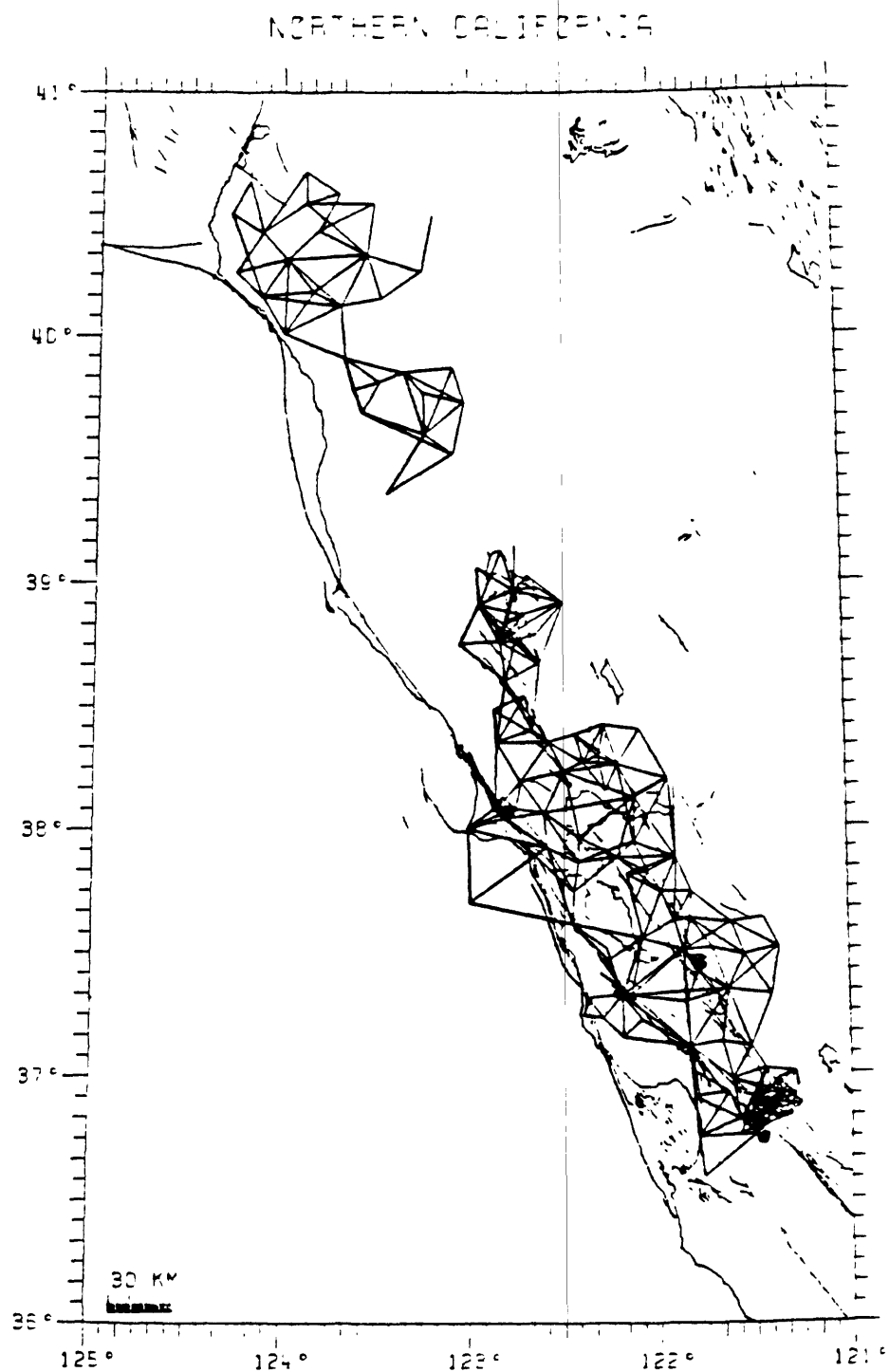


Figure 1. Map of Northern California. All straight line segments shown have been observed by geodolite during last 15 years.

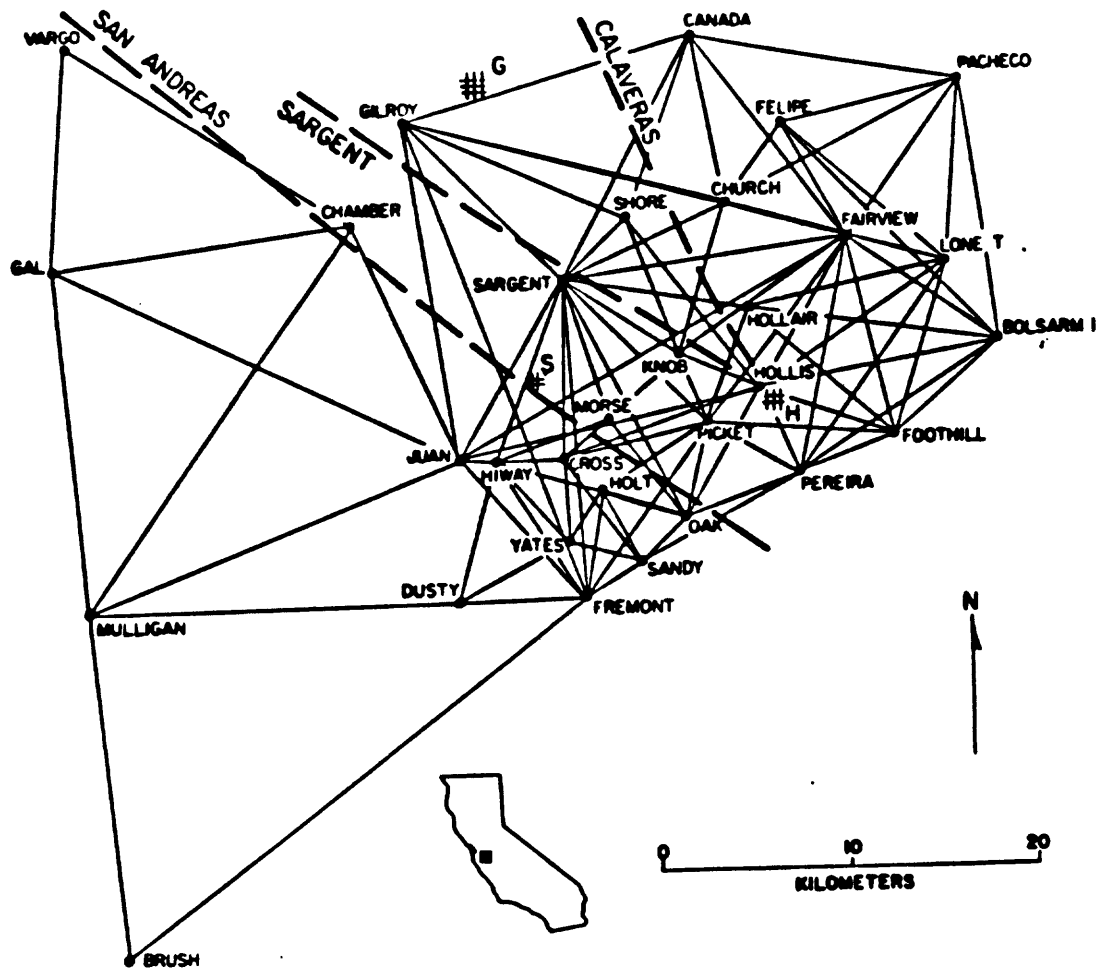


Figure 2. Diagram of the Hollister Network. This network is the southernmost one shown in Fig. 1.

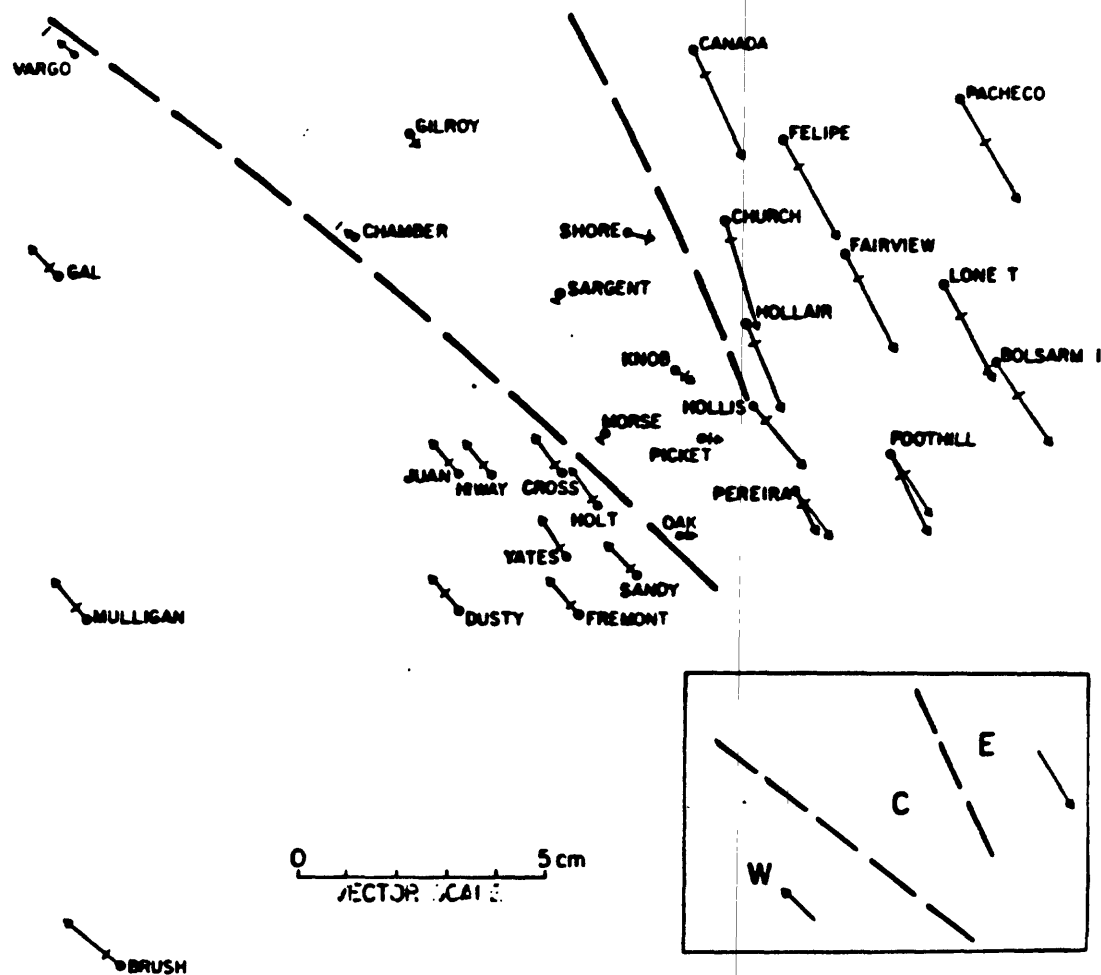


Fig 3

Figure 3. Station velocities for the Hollister network. Vectors indicate the direction and magnitude of the annual rate of movement of the station as deduced from geodolite measurements over the period 1970 to 1982.

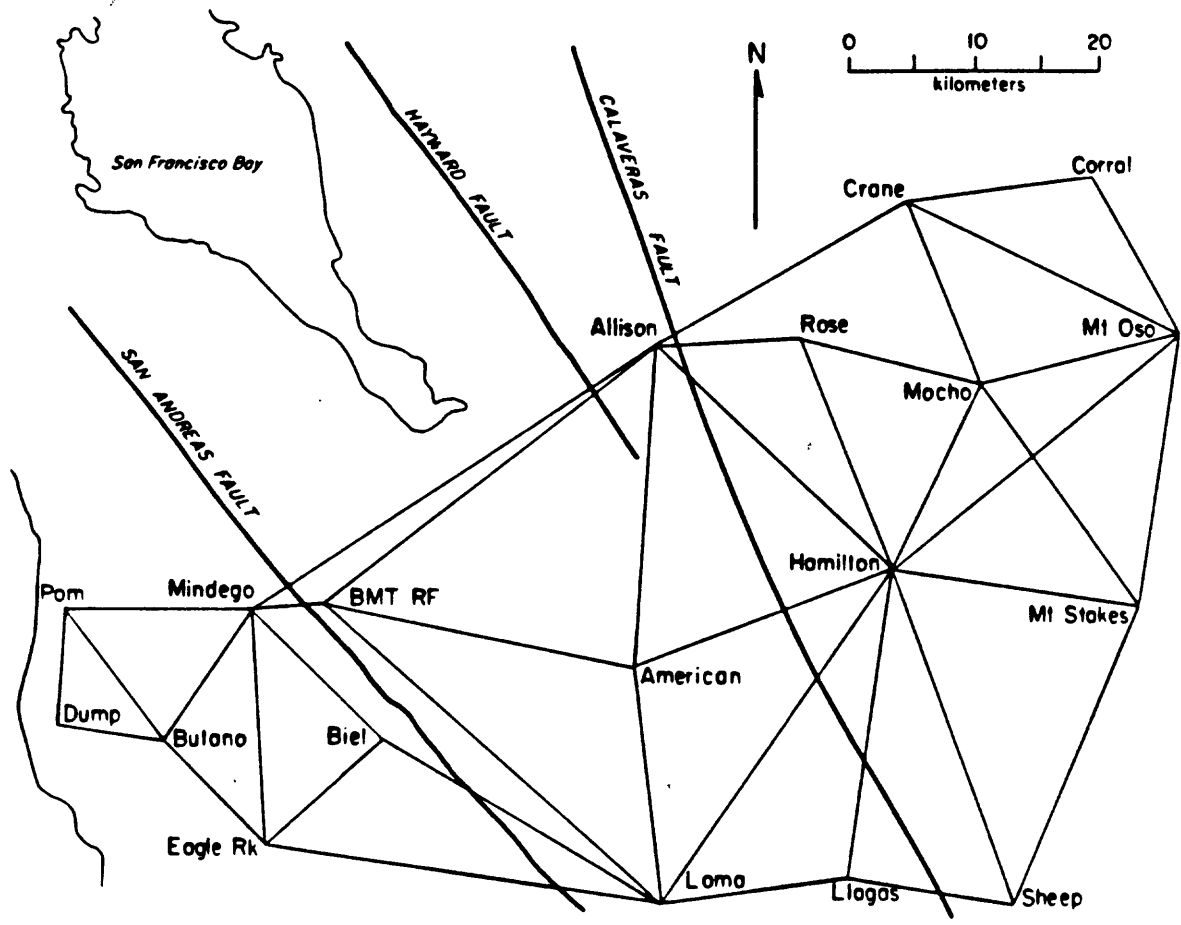


Figure 4. Diagram of the network at the southern end of San Francisco Bay.

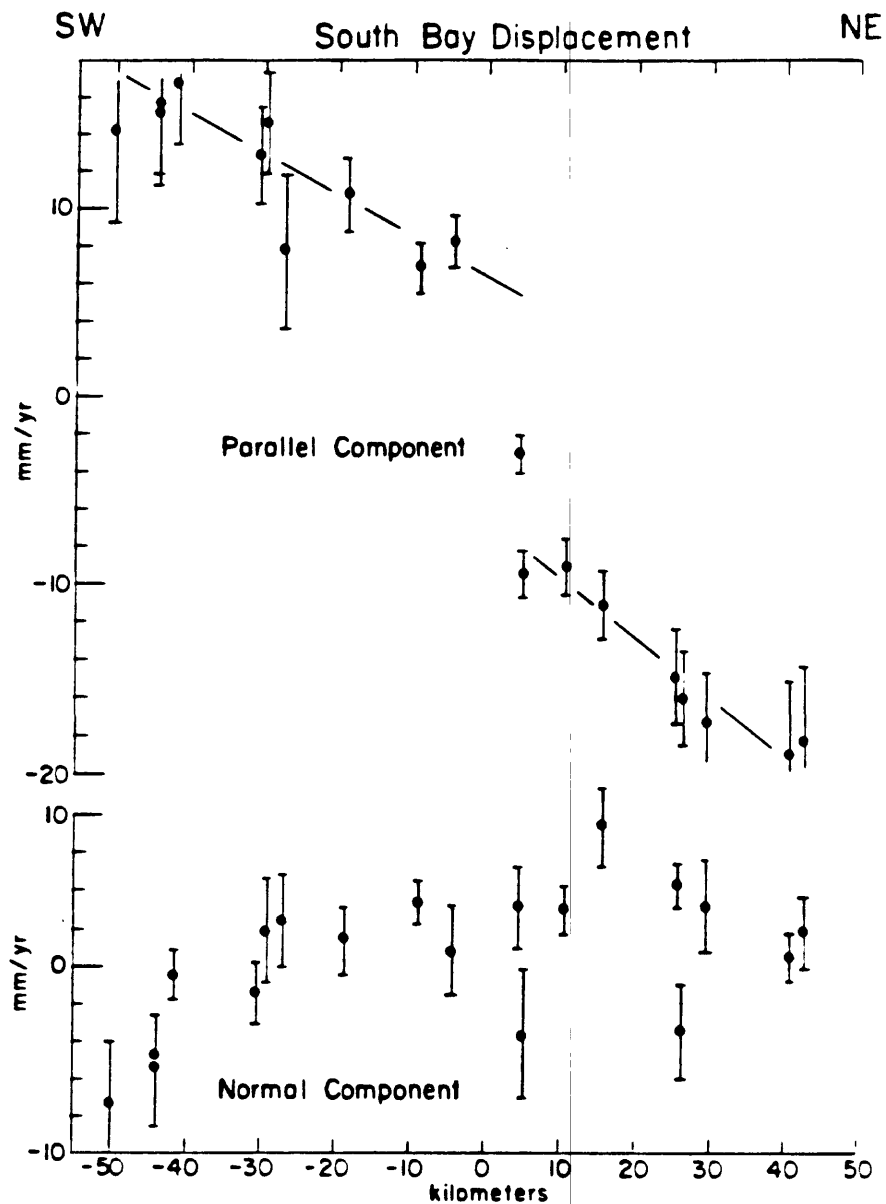


Figure 5. Profile of components of the velocity vector for stations of the network in Fig. 4. At top is the component of motion parallel to the faults; at bottom is the component of motion perpendicular to the faults. Both components are plotted as a function of distance along a normal to the fault plane (with arbitrary origin on both axes).

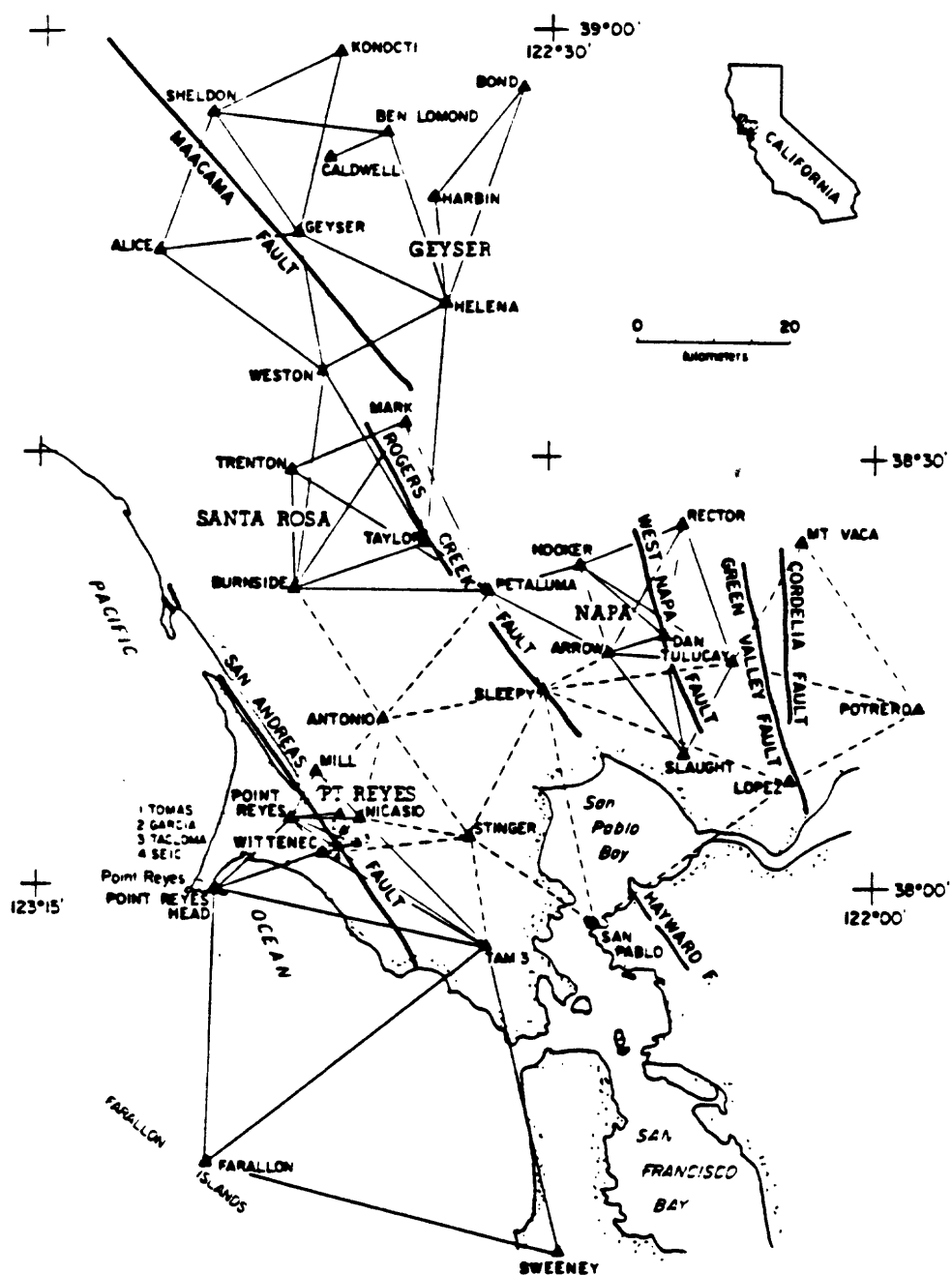


Figure 6. Network diagram for the lines north of San Francisco Bay.

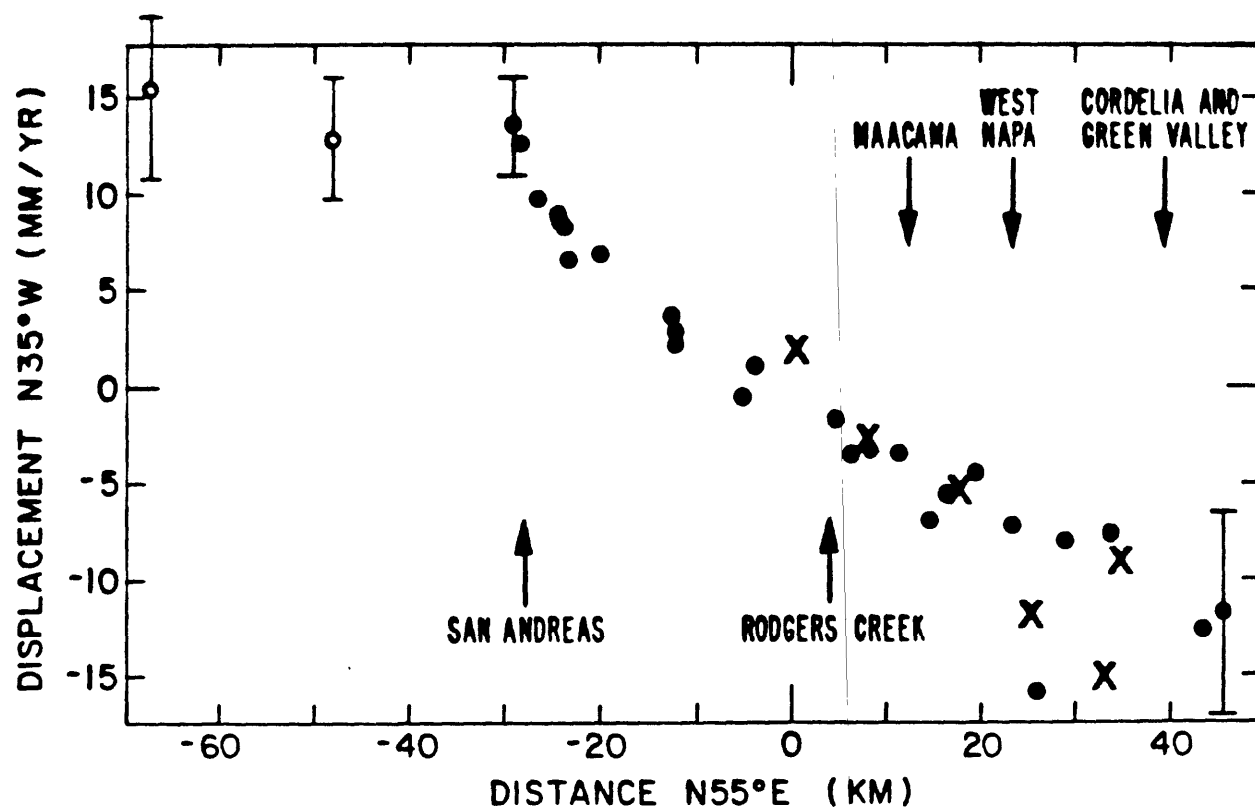


Figure 7. Profile of parallel component of the velocity vector for stations of the network in Fig. 6. Component is plotted as a function of distance along a normal to the fault plane (with arbitrary origin on both axes).

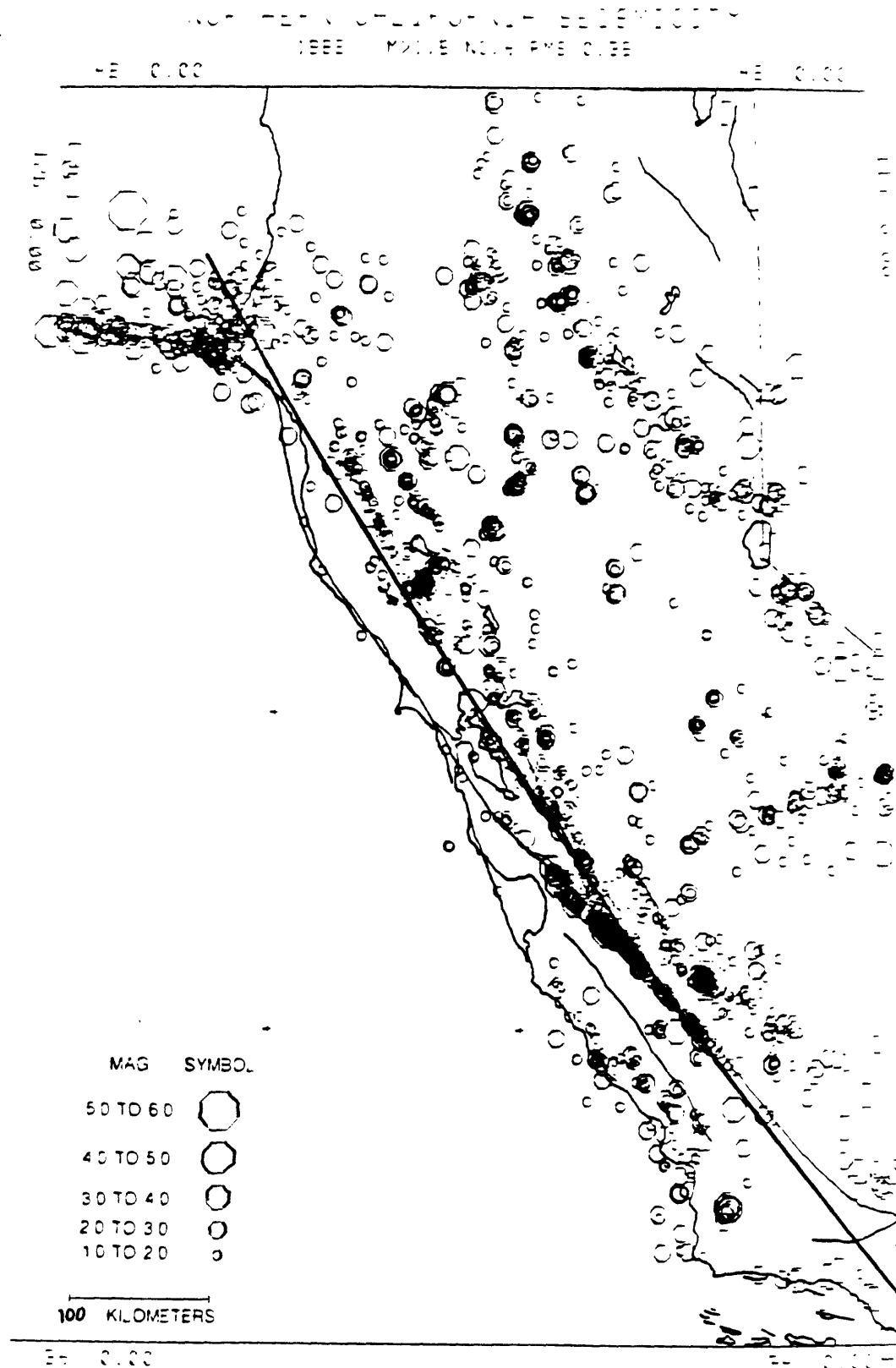


Figure 9. Plot of seismicity for central California for the year 1982 and for $M_L > 1.5$ (Courtesy of R. Lester, U.S.G.S.). Long solid line is a small circle about the Minster-Jordan pole for relative motion between the Pacific and North American plates.

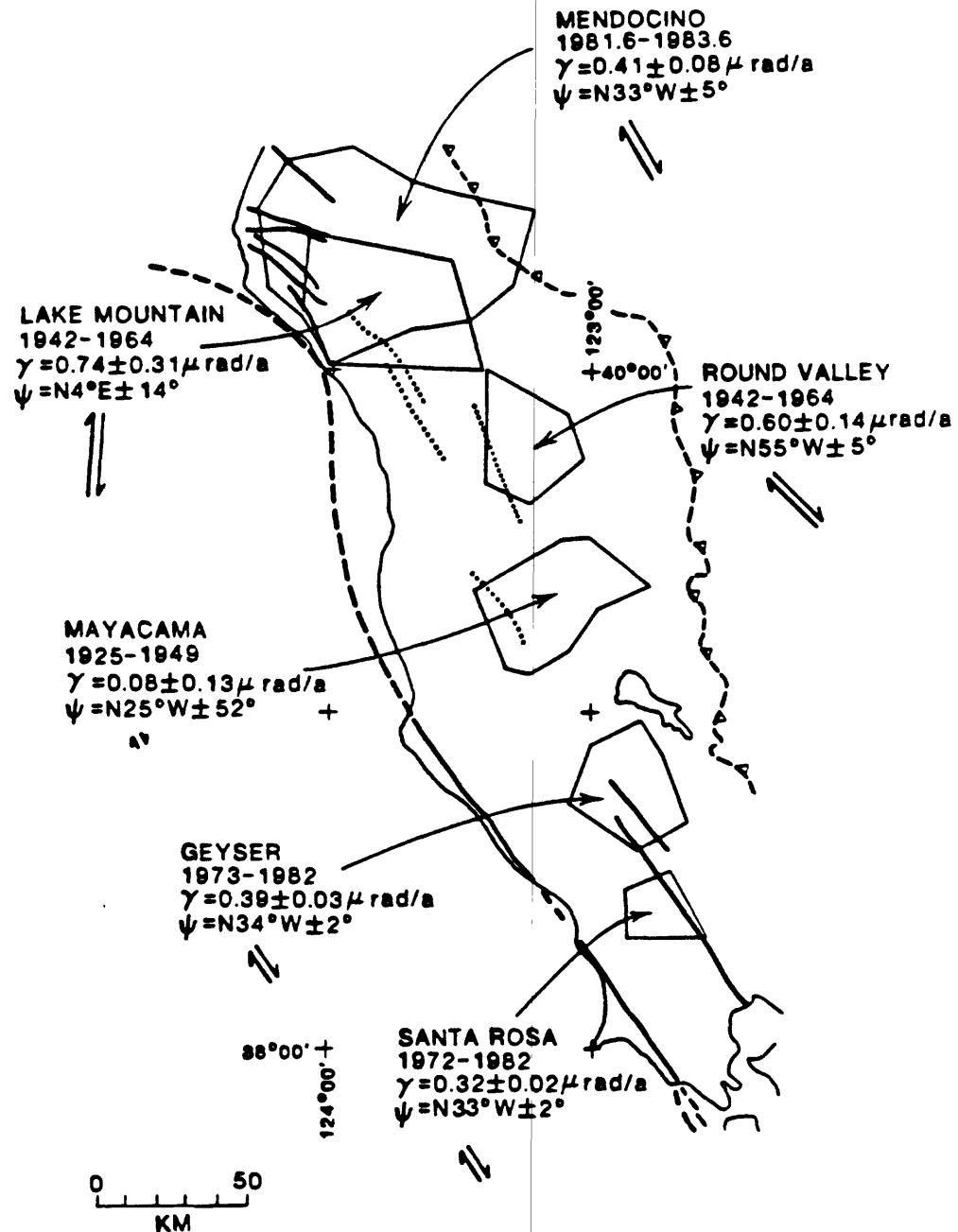


Figure 8. Map of northern California indicating strain rates determined from trilateration or triangulation surveys. γ is the rate of engineering shear. ψ is the direction across which right lateral shear is maximum.

APPENDIX A. 15.

Seismic Slip on the Calaveras Fault, California

W. H. Bakun, G. C. P. King, and R. S. Cockerham

SEISMIC SLIP ON THE CALAVERAS FAULT, CALIFORNIA

William H. Bakun, Geoffrey C. P. King, Robert S. Cockerham

ABSTRACT

The 1969-1984 history of seismic slip on the Calaveras fault in central California illustrates different modes of fault failure. The recent rate of seismic slip along the creeping section near Hollister has lagged the geodetic slip rate in recent years and the seismic slip rate to the northwest where moderate earthquakes apparently occur every 75-80 years. The rupture zones of the $M_L = 5.8$ Coyote Lake earthquake of 6 August 1979 and the $M_L = 6.2$ Morgan Hill earthquake of 23 April 1984, located northwest of the Hollister section, were relatively deficient in seismic slip in the decade before the earthquakes, suggesting that slip histories can be used to help identify fault sections where significant future seismic slip is most likely. The recent rate of seismic slip over the 20-km-long section of fault northwest of the Morgan Hill rupture zone is much less than that to the southeast and lags the geodetic slip rate; although undetected aseismic slip or off-fault deformation may be responsible, an interpretation of the discrepancy as potential for a future damaging shock cannot be rejected.

CONCLUSIONS

The distribution of seismic slip on the Calaveras fault for 1969-1984 suggest that:

1. Larger shocks tend to occur within regions of slip deficit left by earlier earthquakes. This is most clearly seen for the 1984 Morgan Hill earthquake, even though only 15 years of detailed seismic history exist and the apparent recurrence interval of larger shocks on the south half of the Calaveras fault is 75-80 years. Consideration of earlier significant shocks on the Calaveras fault enhances the pre-Morgan Hill slip deficit, indicating that it would be more apparent if a larger period of detailed seismicity were available. It is also apparent that in the Morgan Hill case shallow seismicity above the 5-9 km deep brittle zone partly obscures the slip deficit, emphasizing the importance of looking at slip as a function of depth.
2. Comparison of the seismic slip distribution with the potential slip inferred from geodetic observations illustrates details of the earthquake generation process. There are limited areas of the 5-9 kilometer deep brittle zone, such as near the energetic late Morgan Hill earthquake source, where the seismic slip is comparable to the potential slip. Seismic slip on adjoining areas of the brittle zone over the past 80 year

recurrence time has not matched the potential slip. The seismic-versus-geodetic slip discrepancies may be explained by a combination of processes-fault creep, incomplete seismicity catalogs, and off-fault deformation - as well as a not yet realized potential for seismic slip in future shocks.

3. Seismic slip on the Hollister section since 1969 is significantly less than the seismic slip elsewhere on the Calaveras fault and is much less than the slip rate inferred from geodolite measurements. There are no known earlier shocks on the Hollister section large enough to alter the geodetic-versus-seismic slip rate discrepancy. Given the geodetic evidence for rigid block motion near Hollister, irreversible fault creep or near-fault deformation must account for much of the discrepancy.

4. There exists a considerable geodetic-versus-seismic slip rate discrepancy on the section of the Calaveras fault northwest of the rupture zone of the 1984 Morgan Hill earthquake. A considerable part of this discrepancy might be explained by permanent deformation, either as fault creep or off-fault deformation. An interpretation of the discrepancy in terms of continuing elastic deformation with increasing potential for a damaging shock should not be rejected.

FIGURE CAPTIONS

- Figure 1. Seismicity (magnitude > 1.3) in the San Francisco Bay area for 1976-1984. The polygon encloses epicenters of shocks associated with the Calaveras fault, Calaveras-Sunol fault, and Concord Fault (see Figure 2). Hypocenters of shocks with epicenters located by the USGS CALNET inside the polygon are projected onto the vertical plane beneath profile A-A'.
- Figure 2. Seismicity within the polygon (Figure 1) for 1969-1984. a) map and b) vertical cross sections of hypocenters of all earthquakes in the USGS CALNET earthquake catalogs. The catalogs include some relatively inaccurate locations. c) and d) are map and cross sections of hypocenters subject to stringent accuracy criteria (we use all hypocenters with DMIN, the epicentral distance to the closest seismograph that recorded the shock, less than 5 km, the std. error of the epicenter less than 2.5 km, and the std. error of the hypocenter < 2.5 km. Also included are shocks with DMIN < 2 focal depths.) Slip distributions obtained using these two data sets are essentially identical; the sole exception is the details of the Morgan Hill aftershock slip since some of the larger aftershocks have poor locations.
- Figure 3. Normalized cumulative seismic slip for 1969-1984 for the USGS CALNET catalogs for the Calaveras fault study area (polygon in figure 1) is shown in the inset. Shocks with magnitude < 3.5

contribute less than 1% of the total seismic slip.

Figure 4. Distribution of slip(cm) on the fault plane for
a) $M_L=4$ and b) $M_L=5$ earthquakes. Rectangular source areas are bounded by dashed lines. Slip is distributed among the $1 \times 1 \text{ km}^2$ cells whose centers(x) lie within the $L \times W$ source areas.

Figure 5. a) Cross section showing aftershocks of the 1984 Morgan Hill earthquake with epicenters located within a 2.1-km-wide band along the Calaveras fault (taken from Cockerham and Eaton, 1984). Dashed line outlines a central quiet area interpreted by Cockerham and Eaton to be the section that slipped during the main shock. The hypocenter of the Morgan Hill main shock is shown as a star.

b) Contours of constant seismic slip(cm) obtained using two sources: an $M_L 5.8$ source to the northwest and an $M_L 6.1$ source to the southeast (Bakun et al., 1984). The location, length, and width of the sources were adjusted so that the boundary of significant slip mimics the dashed line in a).

c) The 10-, 50-, and 100-cm-slip contours from b) superimposed on a).

Figure 6. a) Longitudinal cross section along the Calaveras fault showing the 1979 Coyote Lake main shock and magnitude 0.5 and larger aftershocks located on Zone 1, the easternmost section

(taken from Reasenber and Ellsworth, 1982). Symbol size is proportional to magnitude. The hypocenter of the Coyote Lake main shock is shown as a star. Dashed line outlines a central area around which larger aftershocks are located. Although aftershocks on Zones II and III are located farther southeast, there is no evidence that rupture during the main shock extended to these segments.

b) Contours of constant seismic slip(cm) obtained using two sources: an $M_L=5.75$ event near the main shock hypocenter and an $M_L=5.2$ source located 9 kilometers to the southeast. The two sources were arbitrarily adjusted so that the slip contours mimic the spatial pattern of larger aftershocks on Zone 1.

The 12-cm-slip contour from b) superimposed on a).

Figure 7. Contours of constant seismic slip before the Morgan Hill earthquake on the section of AA' (Figure 1) from 70 to 125 kilometers for (a) 1 Jan 1969 to 5 Aug 1979, (b) 6 Aug 1979 to 6 Nov 1979, (c) 7 Nov 1979 to 23 Apr 1984, and (d) 1 Jan 1969 to 23 Apr 1984. Contour interval = 0.25 cm. Hypocenter (star) and 1-cm seismic slip contour (dashed line) of the Coyote Lake mainshock (Figure 6) are superposed on a), b), and c).

Figure 8. Seismic slip on the section of AA' (Figure 1) from 70 to 135 kilometers. (a) Boundary contour (0.25 cm) of seismic slip from figure 7d. (b) Slip contours for 24 Apr 1984 to 23 July

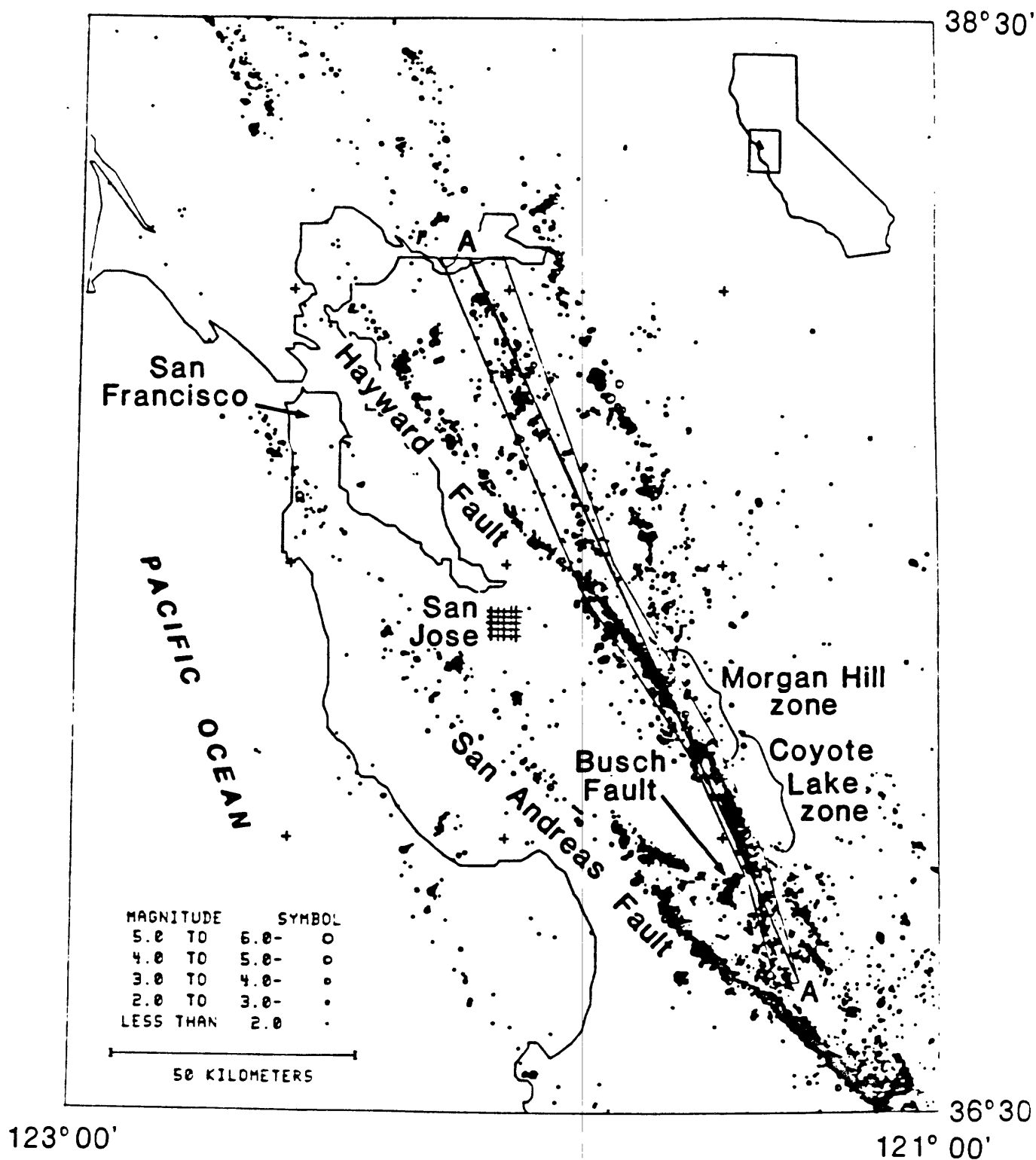
1984. Contour interval = 0.25 cm. Hypocenter (star) and 1-cm contour of seismic slip (dashed line) of the Morgan Hill main shock (Figure 5b) are superposed on (a) and (b). (c) Seismic slip (per km² of fault area) for the Morgan Hill main shock (Figure 5b) averaged over the depth interval of 0 to 15 km is shown as a bold dashed line. The time from 1 Jan 1969 to 23 April 1984 (Figure 7d) averaged over depths of 0 to 15 km and 6 to 15 km are shown as dotted and thin solid lines respectively. The time from 1 Jan 1969 to 23 April 1984 plus the 9 March 1949 ($M_L=5.2$) and the 5 Sept 1955 ($M_L=5.5$) shocks averaged over depths of 0 to 15 km is shown as a thin dashed line.

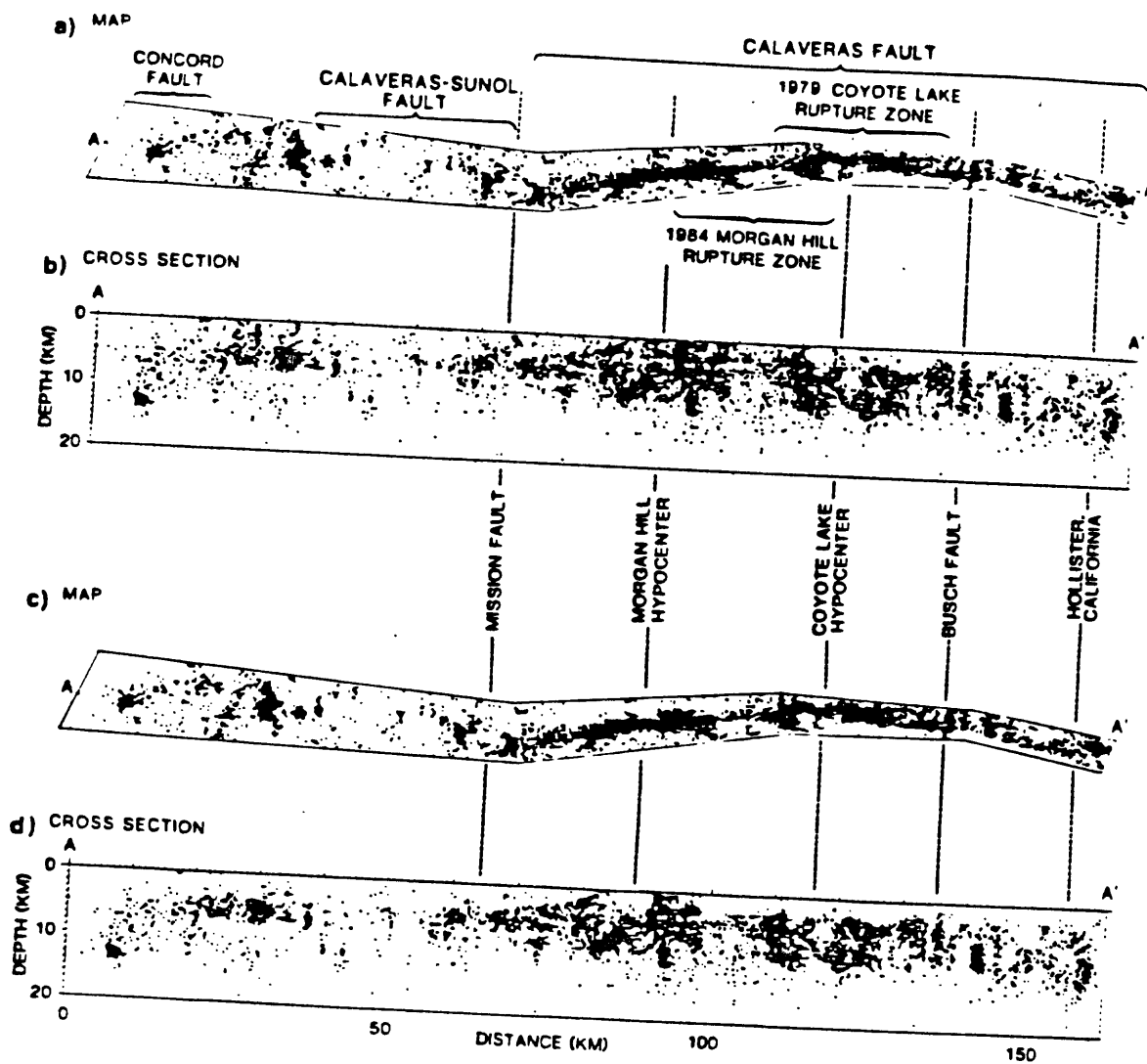
Figure 9.

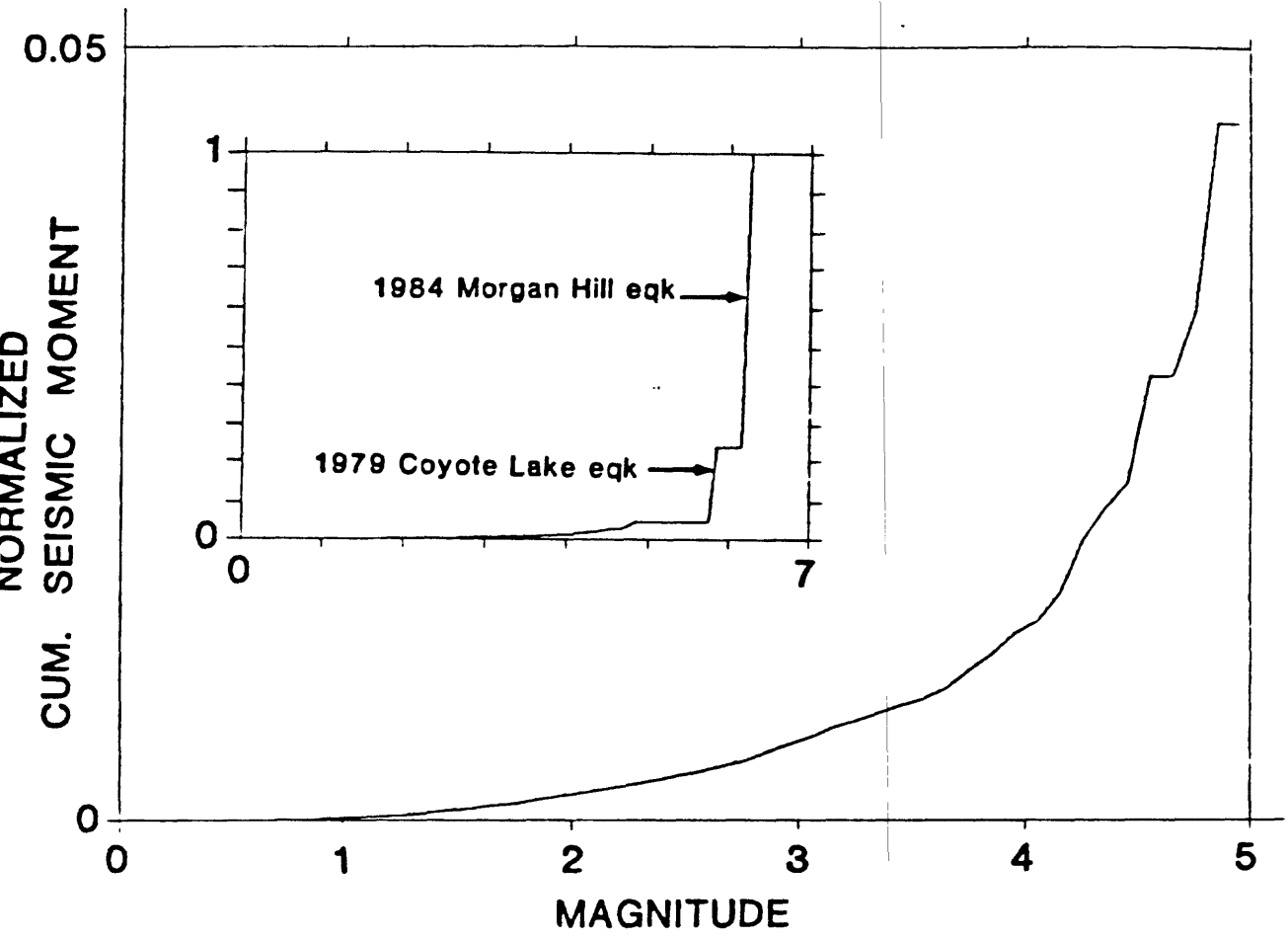
Seismic slip on the section AA'. (a) Cross section for 1 Jan 1969 to 1 Jan 1985 with contour interval = 0.50 cm. (b). Slip on (a) averaged over depth intervals of 0-4, 5-9, 10-14, and 6-8 km compared with slip (wavy lines) for 15 and 80 years inferred from geodetic observations. The geodetic slip uses 1.5 cm/yr (Savage et al., 1979) for 80-162 km and 0.7 cm/yr (Prescott et al., 1981) for 30-75 km. The transition at 75-80 km is arbitrarily drawn midway between the intersections of the Mission and Hayward faults with the Calaveras fault. (c) and (d). (a) and (b) with seismic slip for the 9 March 1949 ($M_L=5.2$), the 5 Sept 1955 ($M_L=5.5$), and the 24 October 1955 ($M_L=5.4$) shocks added. The length, and especially the width, of spatial slip shown for these pre-1969

shocks is arbitrary.

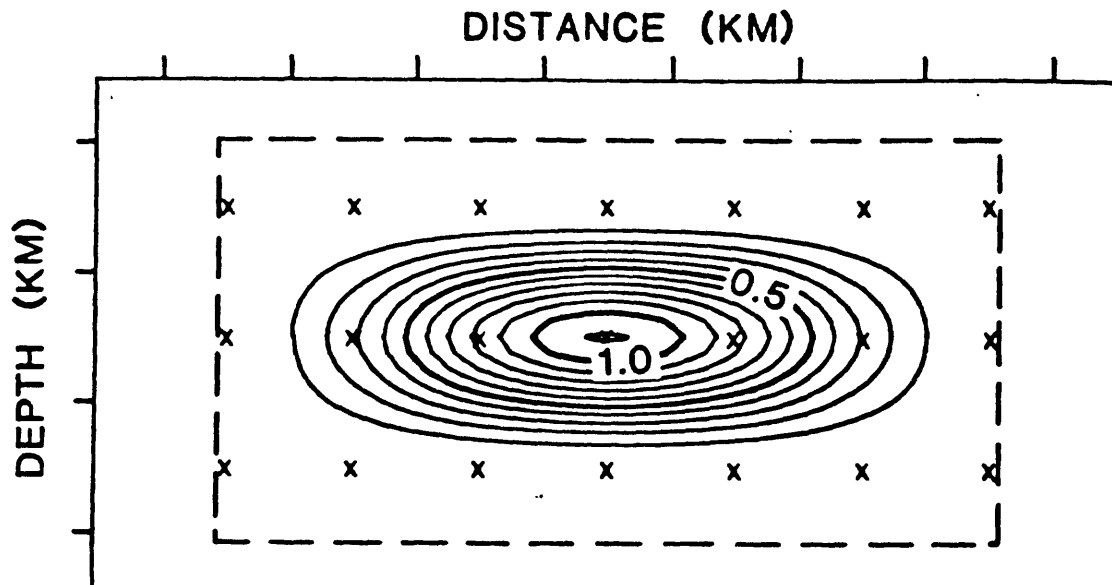
(e) Figure 2b repeated for comparison.



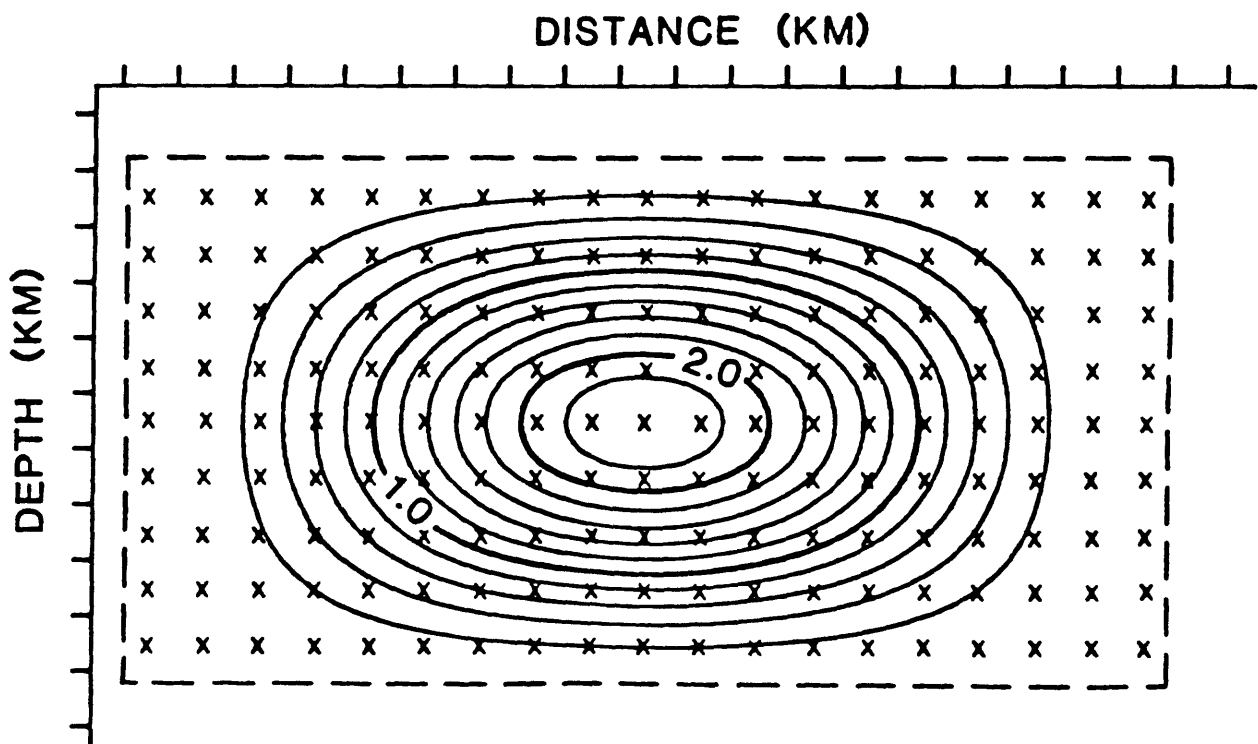


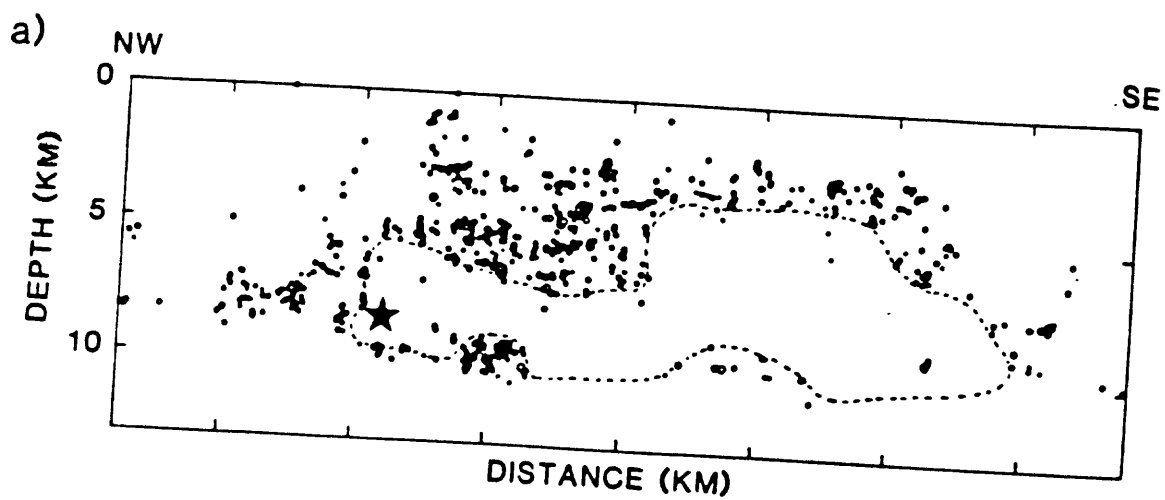


a) $M_L = 4$ ($L = 2W = 6$ KM)

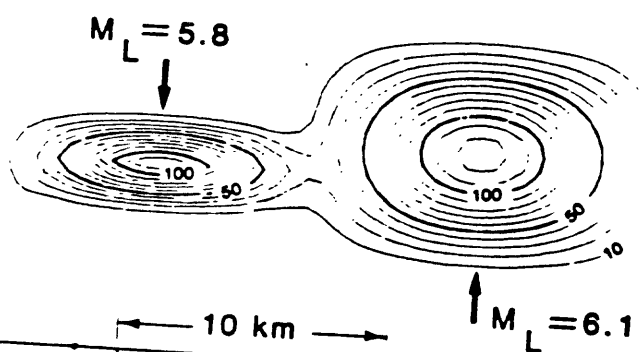


b) $M_L = 5$ ($L = 2W = 19$ KM)

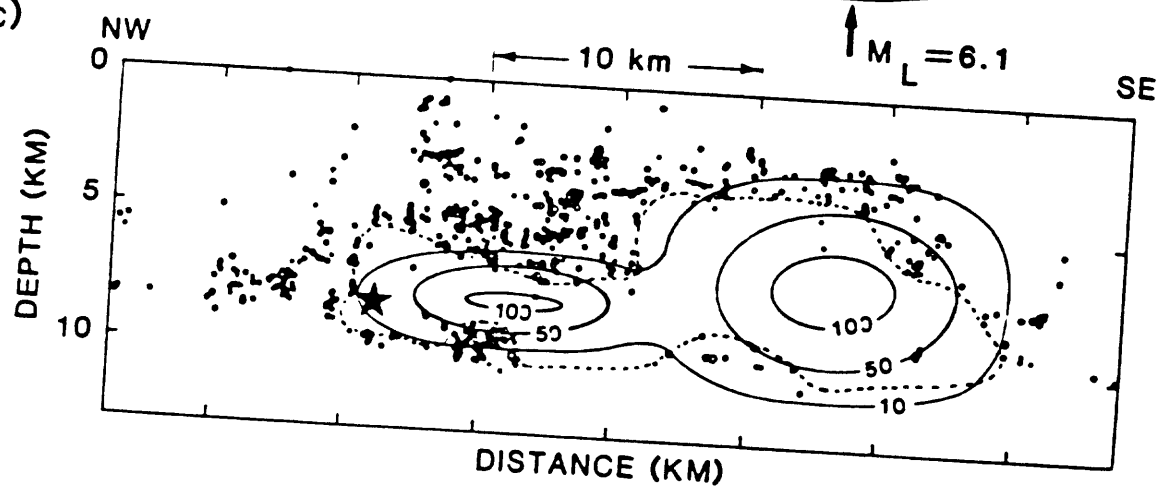




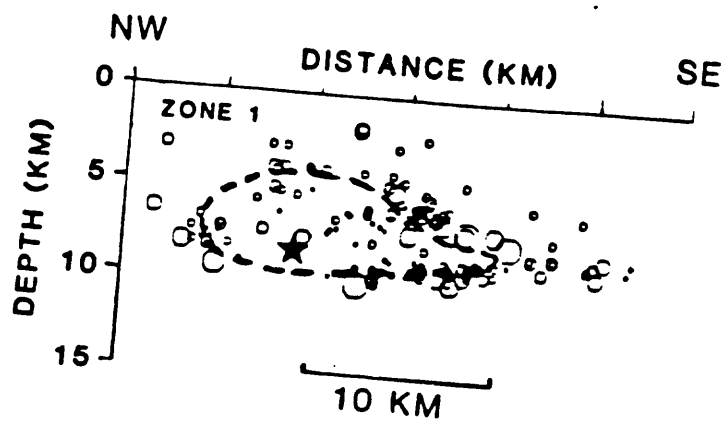
b)



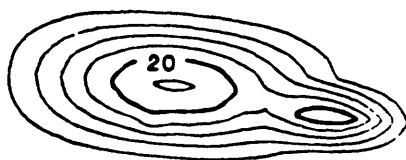
c)



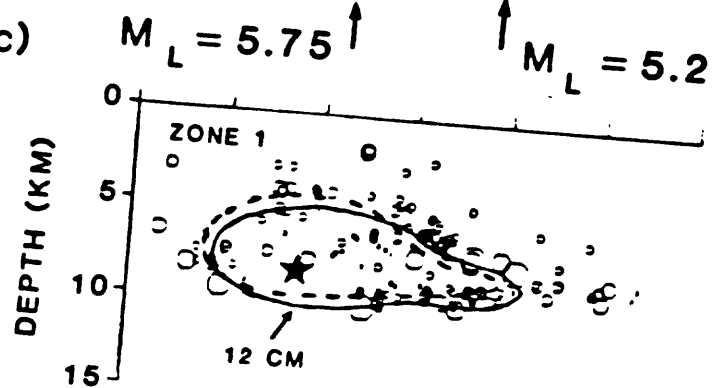
a)

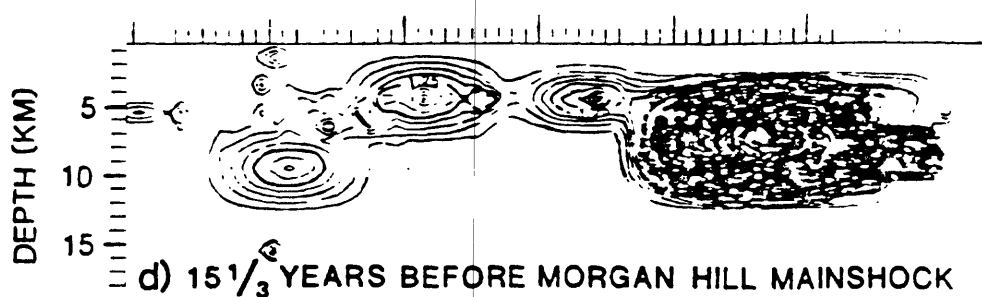
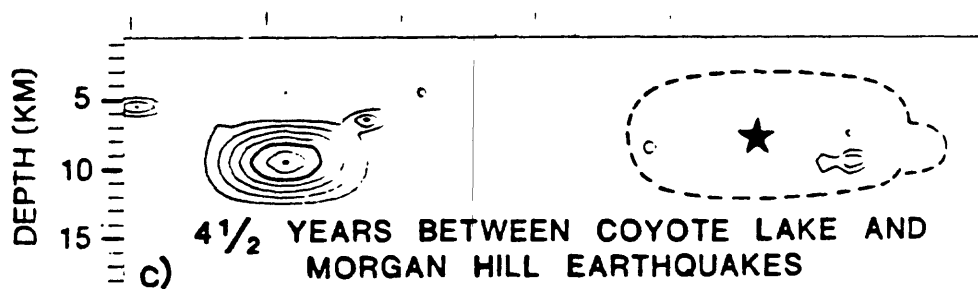
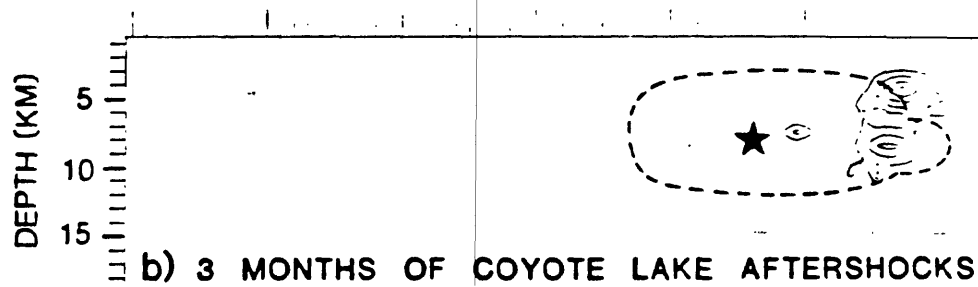
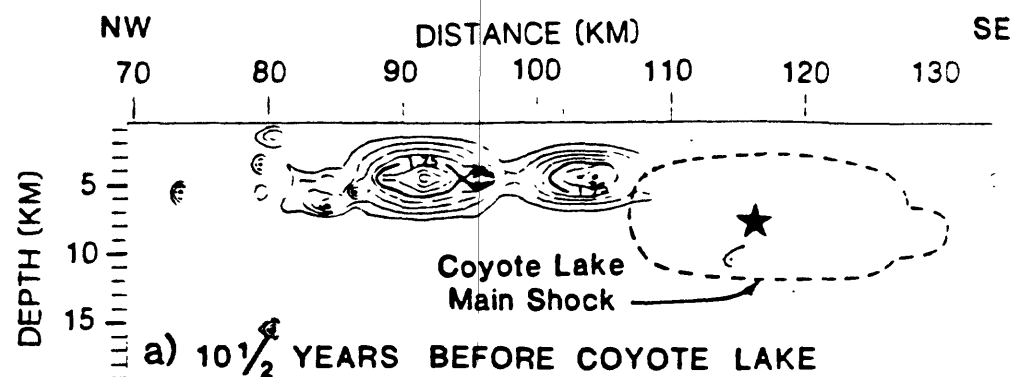


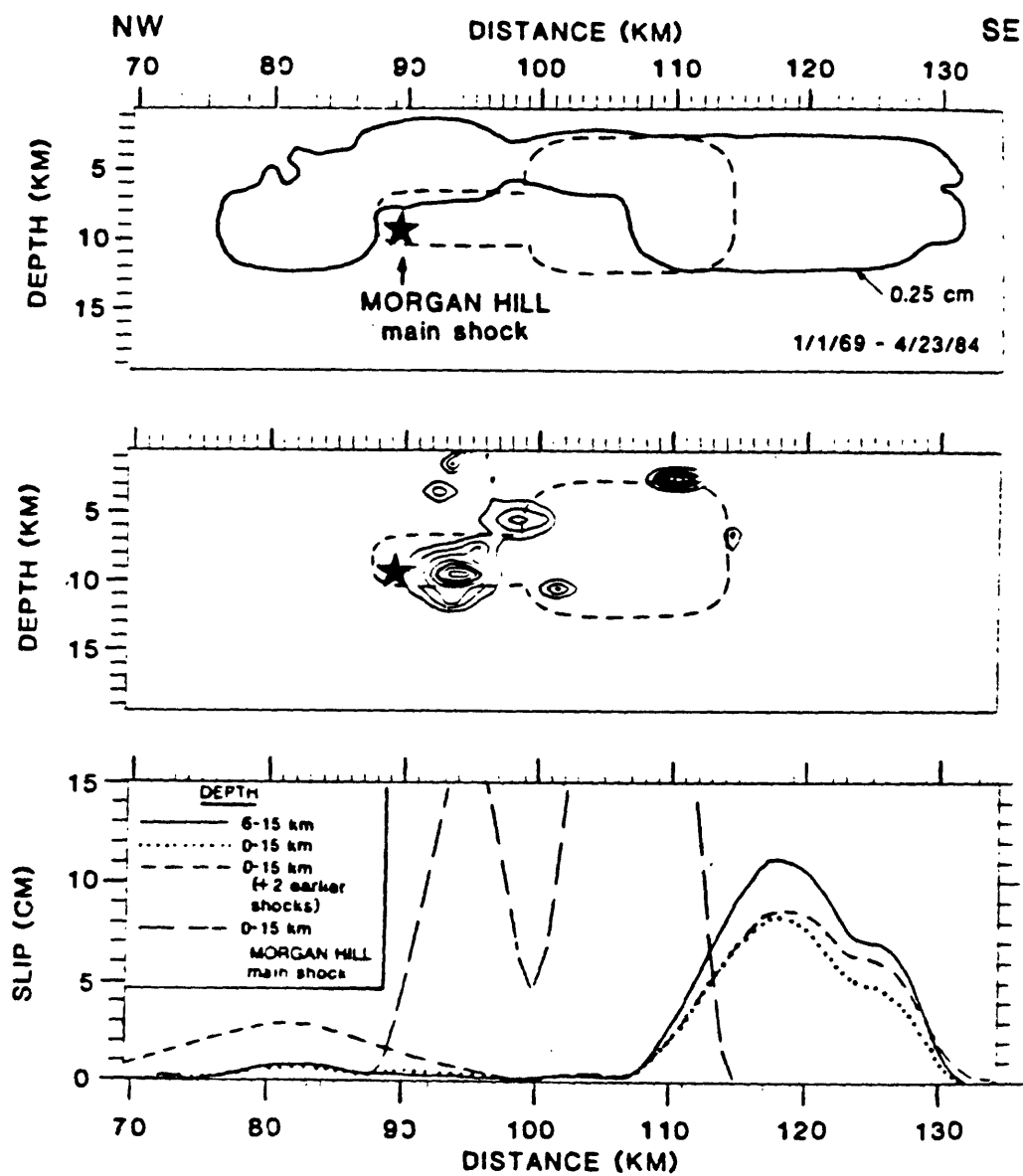
b)

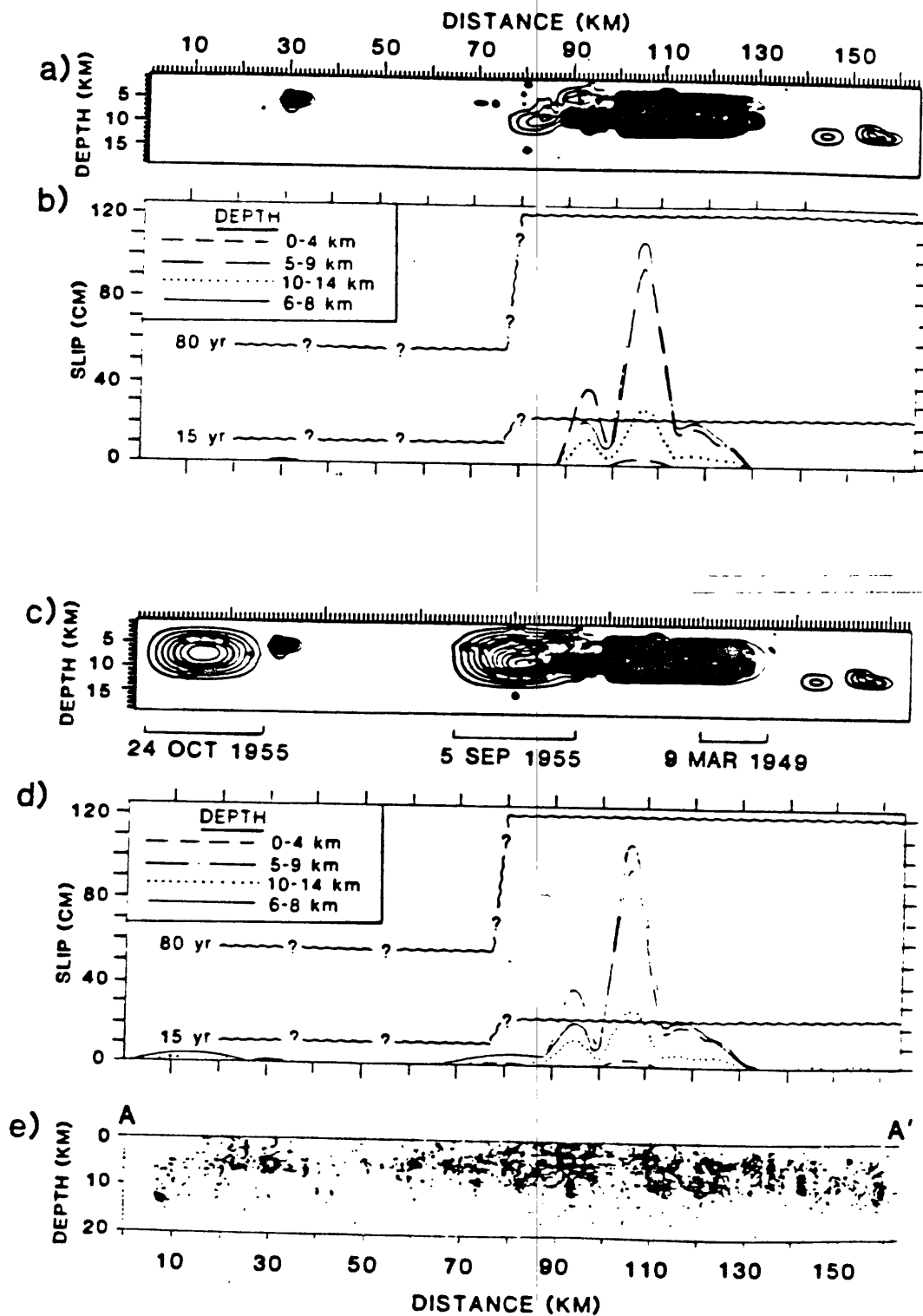


c)









APPENDIX A. 16.

Potential for Future Damaging Shocks on the
Calaveras Fault, California

W. H. Bakun and A. G. Lindh

POTENTIAL FOR FUTURE DAMAGING SHOCKS ON
THE CALAVERAS FAULT, CALIFORNIA

W. H. Bakun and A. G. Lindh

The $M_L = 5.8$ Coyote Lake earthquake on August 6, 1979 and the $M_L = 6.2$ Morgan Hill earthquake on April 24, 1984 have focused a great deal of attention on the potential for future damaging shocks on the Calaveras fault (Figure 1). The Coyote Lake and Morgan Hill earthquakes apparently were repeats of shocks in 1897 and 1911, suggesting recurrence intervals of 82 and 73 years respectively for the central Coyote Lake and Morgan Hill sections of the Calaveras fault (Reasenbergs and Ellsworth 1982; Bakun et al., 1984). The slip potential for an 80-year-long recurrence interval inferred from geodetic observations and the seismic slip since 1969 over these sections are comparable, suggesting that the potential for damaging shocks on these sections in the near future is low (Bakun et al., 1985). Given the geodetic evidence for rigid block motion along the Hollister section of the Calaveras fault (Savage et al., 1979), the observations of aseismic slip or fault creep (Schulz, 1984), and the lack of the $M_L \geq 5$ shocks in historic time (Bakun et al., 1985), it appears that the Hollister section is characterized by fault creep that must accommodate a significant part of the discrepancy between the geodetic and seismic slip rates.

In this note, we discuss the potential for future damaging shocks on the Calaveras Reservoir section, defined in this paper to be the 20-to-25-km-long section of Calaveras fault between Halls Valley and the intersection of the Calaveras fault and the Mission fault of Hall (1958). Our discussion is based on two reasonable assumptions: (1) the recurrence times of 82 and 73 years obtained for the central sections can be extrapolated to the north, and (2) two magnitude 5.8 shocks occurred on the Calaveras Reservoir section in 1903. Seismic slip on the Calaveras Reservoir section over the past 80 years significantly lags the potential slip inferred from geodetic observations (Prescott et al., 1981), which can be interpreted in terms of continuing elastic deformation with increasing potential for a future damaging shock (Bakun et al., 1985). We conclude that it would be prudent to anticipate the occurrence of a magnitude 6 shock on the Calaveras Reservoir section in the next several years.

80-YEAR RECURRENCE INTERVAL

The idea that certain sections of the San Andreas Fault system tend to fail in characteristic earthquakes occurring with predictable interevent times (e.g., Bakun and McEvilly, 1984; Sieh and Jahns, 1984) is the basis for recent evaluations of seismic potential (e.g., Lindh, 1983; Sykes and Nishenko, 1984) on the San Andreas fault system. The 1979 Coyote Lake and 1984 Morgan Hill shocks are examples of characteristic magnitude 6 earthquakes on the Calaveras fault; the interevent times of 82 and 73 years suggest a recurrence interval of about 80 years.

It is possible that subsections of these 20- to 25-km long central segments also tend to fail every 80 years or so in smaller shocks

characteristic of the shorter fault segments, adding support to the 80-year recurrence interval. An $M_L = 5.2$ earthquake apparently ruptured the south half of the Coyote Lake section on March 9, 1949 (Bakun, 1980). Intensities (see Table 1) for the shock (Murphy and Ulrich, 1951), are comparable to those reported by (Toppozada et al., 1981) for the earthquake of March 26, 1866. Although Toppozada et al (1981) note that the intensity pattern is similar to that of the 1979 Coyote Lake earthquake, it is clear from Table 1 that the size of the 1866 shock was more like that of the $M_L = 5.2$ shock in 1949. The 82 years between the 1866 and 1949 shocks is consistent with the 80 year recurrence interval inferred for the larger magnitude 6 shocks.

THE 1903 EARTHQUAKES

One major uncertainty concerning the current seismic potential of the Calaveras Reservoir section is the size and location of the event on September 5, 1955. This $M_L = 5.5$ is the only magnitude 5 or larger shock in the past 80 years that might have occurred on the Calaveras Reservoir section of the Calaveras fault. Newspaper accounts of the effects of shocks on June 11, 1903 and on August 3, 1903 were used by Toppozada and Parke (1982) to infer a magnitude of 5.8 for both events and epicenter locations of $37.4^\circ\text{N}; 121.9^\circ\text{W}$ and $37.3^\circ\text{N}; 121.8^\circ\text{W}$ respectively. The epicenter location of the September 5, 1955 shock at $37^\circ 22'\text{N}; 121^\circ 47'\text{W}$ (Bolt and Miller, 1975), is indistinguishable from those assigned to the 1903 shocks by Toppozada and Parke (1982). There are no reports of surface fractures in 1903 or in 1955 that might be used to infer the causative faults.

The modified Mercalli (MM) intensities (Murphy and Cloud, 1957; Topozada and Parke, 1982) for the 3 shocks at common reporting locations are shown in Figure 2. Peak intensities (MM VII and VIII) for the 3 shocks were reported at sites near the instrumentally-located 1955 epicenter, consistent with the indistinguishable epicenters assigned to the shocks. Intensities at common reporting sites for each of the 1903 shocks are generally larger (average difference = 1 MM unit) than for the $M_L = 5.5$ 1955 shock, consistent with the $M_L = 5.8$ determined for each 1903 event from the size of the isoseismal areas (Topozada and Parke, 1982). Thus we conclude that slip in the 1955 event was significantly less than in 1903 so that the 1955 shock was not sufficient to account for the slip potential incurred since 1903.

The difference in intensities (1903 minus 1955) is larger northwest of the 1955 epicenter, perhaps reflecting directivity toward the northwest in the seismic radiation from the two 1903 shocks. In summary, our comparison of the intensity data confirms Topozada and Parke's 1982 magnitude and epicenter estimates for the 1903 shocks; the relative northwest skew in intensity differences might reflect rupture propagation toward the northwest in the 1903 shocks. While there is no compelling evidence to associate the 1903 shocks with the Calaveras fault, the only plausible alternative, the south end of the Hayward fault, appears less likely since it has been seismically inactive at the microseism level in recent years when accurate epicenters are available.

DISCUSSION

Extrapolation of the 80-year recurrence interval to the Calaveras Reservoir section implicitly requires a detailed comparison of the "slip budget" on the different fault sections. By slip budget, we mean the necessary equivalence, given a sufficiently long time period, of the geodetically-determined deformation potential and the sum of seismic slip,

fault creep, and off-fault crustal folding (Bakun et al., 1985). Although little is known about the rate of fault creep or off-fault crustal folding either along the central Morgan Hill and Coyote Lake sections or along the Calaveras Reservoir section, there is no reason to expect significant differences in fault creep or off-fault folding between these adjoining fault sections. Most of the seismic slip occurs in the infrequent larger shocks (Bakun et al., 1985) so that in comparing seismic slip it is sufficient to consider only the larger earthquakes characteristic of each section. The comparable size ($M_L \sim 6$) of the larger shocks on each of the sections and the comparable 20- to 25-km-long section lengths suggest that seismic slip on the sections should be similar, if the 1903 shocks are assumed to be characteristic of the Calaveras Reservoir section.

Geodetic observations suggest that crustal deformation east of San Francisco Bay is distributed over a broad region that includes the Calaveras and Hayward faults (Prescott et al., 1981). The geodetically-determined right-lateral slip rate is 7 ± 1 mm/yr for the Calaveras-Sunol fault and $7 \pm$ mm/yr for the Hayward fault (Prescott et al., 1981). Savage et al. (1979) inferred from geodetic observations a rate of 15 mm/yr of right-lateral rigid block motion along the Hollister section of the Calaveras fault. Unfortunately there is little data to infer the details of the change from rigid block motion across a single fault zone near Hollister to the distributed deformation east of San Francisco Bay. Of particular interest is the deformation within and around the crustal block bounded by the Calaveras, Hayward and Mission faults (hatched area in Figure 1), as the details of that deformation are necessary to justify the extrapolation of the 80-year recurrence interval to the Calaveras Reservoir section. The transfer of

microearthquake activity from the Calaveras to the Hayward fault along the Mission fault (Ellsworth et al., 1982) suggests that the section of the Hayward fault south of the Mission fault intersection might now be bypassed in the accomodation of relative plate motion. If such is the case, then the combined east Bay deformation rate of 14 mm/year might be interpreted as a loading rate for future seismic slip on the Calaveras Reservoir section so that the recurrence interval of 80 years obtained for the adjoining central sections of the Calaveras fault would be appropriate. That recurrence interval, combined with the low seismic slip in the past 80 years (Bakun et al., 1985) and the 1903 dates for the last characteristic shocks, would imply that the Calaveras Reservoir section is a likely spot for a damaging magnitude 6 earthquake, or earthquakes, in the next several years.

There is little seismic activity on the Calaveras-Sunol fault (Ellsworth et al., 1982), the north extension of the Calaveras fault, and cumulative seismic slip there has lagged that on the Calaveras fault (Bakun et al., 1985). While the combined east Bay deformation rate of 14 mm/year (Prescott et al., 1981) might be appropriate for the Calaveras Reservoir section of the Calaveras fault, it is unlikely that it is appropriate for the Calaveras-Sunol fault since slip on the seismically active and creeping north sections of the Hayward fault must account for a significant part of the potential for right-lateral slip in the east Bay. For a lower rate of deformation (i.e., a lower rate of potential seismic slip accumulation), a slip budget comparison with the Calaveras fault would imply a recurrence interval significantly larger than 80 years for the Calaveras-Sunol fault. If 7 mm/year = 1/2 the combined east Bay deformation rate is appropriate (Prescott et al., 1981),

then a recurrence interval of 150-170 years is appropriate for the Calaveras-Sunol fault. Although the seismic history of the Calaveras-Sunol fault is uncertain, it is plausible that the last moderate-size shock on the Calaveras-Sunol fault occurred about 1865, as there were several poorly-located shocks in the east Bay at about that time (Toppozada et al., 1981). These arguments, although highly speculative, suggest that the Calaveras-Sunol fault poses less of an immediate threat than does the Calaveras Reservoir section of the Calaveras fault; however the uncertain division of the east Bay deformation rate between the Hayward and Calaveras-Sunol faults suggests that the absence of significant shocks on these faults in the past 120 years might reasonably be interpreted as evidence that magnitude 6 or larger shocks on these faults are due as well.

TABLE 1. MODIFIED MERCALLI INTENSITIES FOR THE MARCH 26, 1866 AND
THE MARCH 9, 1949 EARTHQUAKES

<u>Location</u>	<u>March 26, 1866+</u>	<u>March 9, 1949++</u>
Gilroy	7*	6
Hollister	**	7
Napa	2	4
San Francisco	6	6
San Jose	5	6
Stockton	3	5

-
- * Old Gilroy, located on the Pacheco Pass Highway, a few miles southeast of current Gilroy (personal communication, Janet Brians, San Benito CA. Historical Society, 1985)
- ** Ranches were first established near Hollister in 1866. The town of Hollister was began in 1872 (personal communication, Janet Brians, San Benito Ca. Historical Society, 1985)
- + Intensities from the Topozada et al., (1981)
- ++ Intensities from Murphy and Ulrich (1951)

REFERENCES

- Bakun, W. H., G. C. P. King, and R. S. Cockerham, (1985) Seismic slip on the Calaveras fault, California, submitted to Proc. Ewing Symposium α5.
- Bakun, W. H. (1980). Seismic activity on the southern Calaveras fault in central California, Bull. Seism. Soc. Am. 70, 1181-1197.
- Bakun, W. h., M. M. Clark, R. S. Cockerham, W. L. Ellsworth, A. G. Lindh, W. H. Prescott, A. F. Shakal, and P. Spudich (1984). The 1984 Morgan Hill, California earthquake, Science 225, 288-291.
- Bakun, W. H., and T. V. McEvilly (1984). Recurrence models and Parkfield, California, earthquakes, J. Geophys. Res. 89, 3051-3058.
- Bolt, B. A., and R. D. Miller (1975). Catalogue of earthquakes in northern California and adjoining areas 1 January 1910-31 December 1972, Seismographic Stations, Univ. of California, Berkeley, 567 pp.
- Ellsworth, W. L., J. A. Olson, L. M. Shijo, and S. M. Marks (1982) Seismicity and active faults in the eastern San Francisco Bay area, in Hart, E. M., S. E. Hirschfeld, and S. S. Schulz, eds., Proceedings, Conference on Earthquake Hazards in the Eastern San Francisco Bay Area, Calif. Div. Mines and Geol. Spec. Publ. 62, p. 83-92.

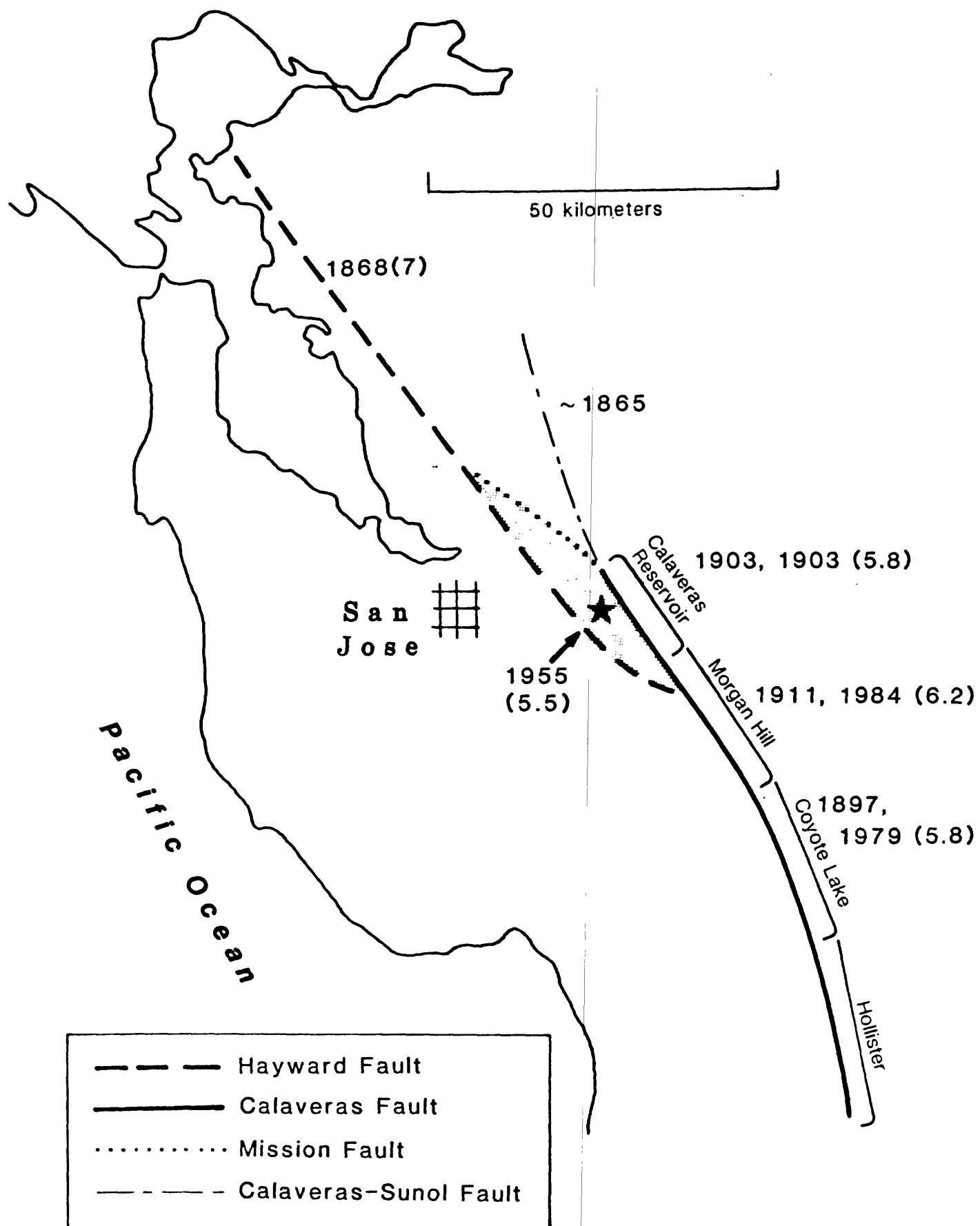
- Hall, C. A., Jr. (1958). Geology and paleontology of the Pleasanton area, Alameda and Contra Costa counties, California, Univ. of Calif. Publ. in Geol. Sci. 34, 89 pp.
- Lindh, A. G. (1983). Preliminary assessment of long-term probabilities for earthquakes along selected fault segments of the San Andreas fault system in California, U.S. Geol. Surv. Open File Rept. 83-63, 15 pp.
- Murphy, L. M., and F. P. Ulrich (1951). United States Earthquakes 1949, U. S. Dept. of Comm. Coast and Geol. Surv. Serial 748, Washington, D. C., 64 pp.
- Murphy, L. M., and W. K. Cloud (1957). United States Earthquakes 1955, U. S. Dept. of Comm. Coast and Geol. Surv., Washington, D. C., 83 pp.
- Prescott, W. H., M. Lisowski, and J. C. Savage (1981). Geodetic measurements of crustal deformation on the San Andreas, hayward, and Calaveras faults near San Francisco, California, J. Geophys. Res. 86, 10853-10869
- Reasenber, P. and W. L. Ellsworth (1982). Aftershocks of the Coyote Lake, California, earthquake of August 6, 1979; A detailed study, J. Geophys. Res. 87, 10637-10655.
- Savage, J. C., W. H. Prescott, M. Lisowski, and N. King (1979). Geodolite measurements of deformation near Hollister, California, 1971-1978, J. Geophys. Res. 84, 7599-7615.

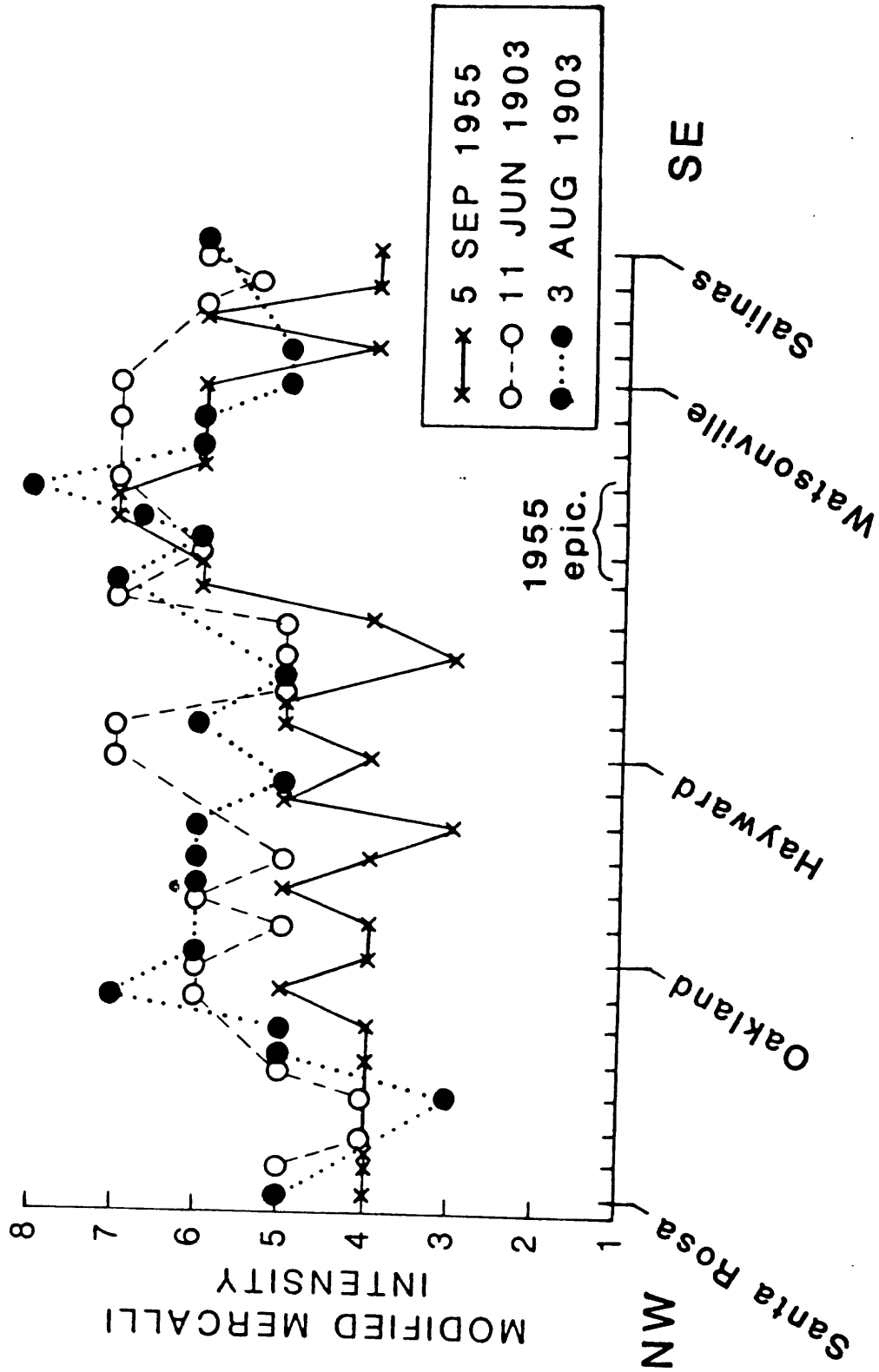
- Schulz, S. S. (1984). Triggered creep near Hollister after the April 24, 1984, Morgan Hill, California, earthquake, in the 1984 Morgan Hill, California earthquake, Calif. Div. Mines and Geol. Spec. Pub. 68, J. H. Bennett and R. W. Sherburne, eds., p. 175-182.
- Sieh, K. E., and R. H. Jahns (1984). Holocene activity of the San Andreas fault at Wallace Creek, Geol. Soc. Am. Bull. 95, 883-896.
- Sykes, L. R., and S. P. Nishenko (1984). Probabilities of occurrence of large plate rupturing earthquakes for the San Andreas, San Jacinto, and Imperial faults, California, 1983-2003, J. Geophys. Res. 89, 5905-5927.
- Toppozada, T. R., C. R. Real, and D. L. Parke (1981). Preparation of isoseismal maps and summaries of reported effects for pre-1900 California earthquakes, Open File Report 81-11 SAC, Calif. Div. Mines Geol., 182 pp.
- Toppozada, T. R., and D. L. Parke (1982). Areas damaged by California earthquakes, 1900-1949, Open File Rep. 82-17 SAC, Calif. Div. Mines Geol., 65 pp.

FIGURE CAPTIONS

Figure 1. Schematic map of the Calaveras and Hayward fault systems. The Calaveras fault is divided north-to-south into the Calaveras Reservoir, Morgan Hill, Coyote Lake, and Hollister sections. The epicenter (star) of the 1955 shock (Bolt and Miller, 1975) is shown. Hatchured area is bounded by the Mission fault (Hall, 1958), the Calaveras fault, and the currently aseismic south section of the Hayward fault.

Figure 2. Modified Mercalli intensities for the September 5, 1955 (Murphy and Cloud, 1957) and the June 11 and August 3 shocks in 1903 (Topozada and Parke, 1982). Common reporting locations are ordered along the abscissa according to the approximate northwest -to-southeast distance from the epicenter (Bolt and Miller, 1975) of the 1955 shock. The abscissa scale does not reflect true or relative epicentral distances.





APPENDIX A. 17.

The Detection History of the Calaveras Fault:
A Preliminary Assessment

R. E. Habermann

The Detection History of the Calaveras Fault: A Preliminary Assessment

R.E. Habermann
School of Geophysical Sciences
Georgia Institute of Technology
Atlanta, Georgia 30332

A major goal of network operators, and seismologists in general, is the improvement of methods for monitoring the seismicity in some region. Progress towards this goal is marked by increases in the detection and reporting of small earthquakes. Many seismologists make the assumption that all seismicity catalogs are improving monotonically as a function of time because of presumed progress towards this goal. This assumption can be tested by examining the rate of reporting of small events as a function of time. These rates for the Calaveras Fault are shown in Figure 1 for several magnitude bands. The time periods in these plots are times of consistent reporting which we have recognized (Table 1).

	START	END		START	END
1	01-Jan-69	28-Oct-69	12	30-Apr-75	10-Feb-76
2	29-Oct-69	19-May-70	13	11-Feb-76	13-Apr-76
3	20-May-70	08-Sep-70	14	14-Apr-76	14-Aug-79
4	09-Sep-70	11-Jan-72	15	15-Aug-79	29-Jul-80
5	12-Jan-72	28-Nov-72	16	30-Jul-80	25-Nov-80
6	29-Nov-72	20-Mar-73	17	26-Nov-80	08-Sep-81
7	21-Mar-73	11-Dec-73	18	09-Sep-81	03-May-83
8	12-Dec-73	14-May-74	19	04-May-83	24-Jan-84
9	15-May-74	20-Aug-74	20	25-Jan-84	17-Apr-84
10	21-Aug-74	10-Dec-74	21	18-Apr-84	31-Jul-84
11	11-Dec-74	29-Apr-75			

The periods between September 1970 and January 1972 (period 4) and between May 1974 and August 1974 (period 9) are consistently low. The period between March and December 1973 (period 10) is consistently high.

A surprising observation is that the number of small events reported progressively decreases between December 1974 and July 1980 (the final period of this group is the aftershock period of the Coyote Lake event, during which events were removed prior to analysis) reaching its lowest value (not including the aftershock period) between April 1976 and August 1979. The period between November 1980 and September 1981 (period 17) is the time of the highest rate of reporting of small events.

It is clear that the rate of reporting of smaller events is not increasing monotonically. This simple demonstration clearly indicates the need for careful determination of detection and reporting histories.

CHANGES IN REPORTING

We examined the detection and reporting histories using techniques described elsewhere in this report. These techniques involve examination of observed seismicity changes as a function of magnitude band. This is helpful for identifying man-made changes in seismicity

catalogs because such changes generally affect events with different sizes in different ways. We used synthetic magnitude signatures as an aid in interpreting complex changes.

The changes we identified are summarized in Table 2 which lists two characteristics of each magnitude signature we synthesized: 1) the amount of magnitude shift used to fit the observations and the range over which the shift is applied. 2) The range in which the number of events reported changed and the factor by which it changed. Repeat factors of less than one indicate detection decreases, factors greater than one indicate increases. Table 2 also gives a number of indications of how well the observations are fit by the synthetics. These include the sum of the residuals of the equal and truncated/expanded synthetics, and the sum of the absolute values of the observed and corrected magnitude signatures. In a perfectly modeled magnitude signature the sums of the residuals and the corrected magnitude signature would be zero. In most cases this ideal is not realized, but the residuals are small and the sums of the magnitude signatures are significantly reduced.

Table 2. Summary of Changes Observed in the Calaveras Fault Region

Date	Shift		Repeat		Residuals		Sums	
	Range	Amount	Range	Factor	Equal	Trun/Exp	Observed	Corrected
29-Oct-69	0-1.4	-0.15	0-2.0	1.25	23.02	44.34	57.50	49.68
20-May-70	0-2.19	0.20	0-.69	0.50	18.54	38.71	76.28	23.35
09-Sep-70	1.3-2.19	-0.20	0-1.19	0.50	21.34	28.93	85.61	32.57
12-Jan-72	.8-2.19	-0.10	0-.79	3.00	42.90	56.19	130.37	82.11
29-Nov-72	.7-1.9	-0.15			19.84	33.61	46.51	25.05
21-Mar-73	0-1.4	-0.20	0-2.0	2.00	21.49	27.57	144.32	45.29
12-Dec-73		No synthetic generated						
15-May-74	.9-1.59	-0.10	0-1.1	0.50	18.31	27.70	146.58	19.22
21-Aug-74	0-1.29	0.10	0-10	2.50	16.91	22.07	177.30	35.26
11-Dec-74	1.6+	-0.30	0-1.39	0.50	15.18	21.65	145.43	26.69
30-Apr-75	1.1-1.79	-0.20			23.35	27.16	41.40	30.33
11-Feb-76	1.0-2.5	0.20			18.80	17.60	79.64	17.58
14-Apr-76	0-2.39	-0.20	0-1.29	0.50	41.34	33.44	68.40	27.98
15-Aug-79		No synthetic generated						
30-Jul-80		No synthetic generated						
26-Nov-80	2.0-2.49	-0.10	0-1.29	2.00	88.21	76.84	243.29	29.25
09-Sep-81	0-.99	-0.30	0-1.59	0.50	57.46	62.35	187.47	34.41
04-May-83	.9-1.79	-0.10	0-.69	0.20	24.37	37.12	163.25	32.23
25-Jan-84	1.4-1.89	-0.10	0-1.1	2.00	25.55	78.62	151.17	40.74
11-Apr-84		No synthetic generated						

Detection Decrease.

The magnitude signature which compares the rates between March 21 and December 11, 1973 to those between December 12, 1973 and May 14, 1974 (Figure 2) shows all of the characteristics expected for a detection decrease. The peak on the left side of the plot indicates strong decreases in the smaller events. The z-values near zero on the right side of the plot indicate lack of change in the larger events. A magnitude cutoff which is appropriate for eliminating the effect of this change can be determined from the magnitude band at the left end of the platform on the right side of the plot. This is the smallest cutoff above which the observed behavior is independent of magnitude cutoff.

In this case it is $m_d \geq 0.9$.

Detection Increase.

The magnitude signature which compares the rates between July 30 and November 25, 1980 to those between November 26, 1980 and September 8, 1981 (Figure 3) shows all of the expected characteristics of a detection increase. Note that this is the increase which begins the period of highest reporting shown in Figure 1. The peak on the left side of the plot indicates strong increases in the number of small events reported. The z-values near zero on the right side of the plot indicate lack of change in the larger events. The appropriate magnitude cutoff in this case is $m_d \geq 1.3$ (although there is some magnitude decrease above this level indicated by the small peak on the right side of the plot).

Magnitude Shift.

The magnitude signature comparing the rates between October 29, 1970 and May 19, 1970 to those between May 20 and September 8, 1970 (Figure 4) shows the characteristics expected for a magnitude increase. These include increases in the data sets which include larger events (on the right) and decreases in the data sets which include smaller events (on the left). This effect cannot be corrected for using a magnitude cutoff, it requires changing the magnitudes of some events.

REGIONAL VARIATIONS IN DETECTION AND REPORTING CHANGES

One possible way to assess whether an observed seismicity change is real or due to changes in reporting and detection is to examine its scale. The basis for this approach is the assumption that detection and reporting changes will occur in regions which are larger than precursory zones for moderate earthquakes. In order to get a handle on this problem we compared the detection histories determined from the entire Calaveras fault to those observed in the northern and southern segments of the fault.

Figure 5A shows a magnitude signature observed in the entire Calaveras fault zone. This magnitude signature shows decreases in the data sets which include larger events (on the right) and increases in the data sets which include smaller events (on the left). This is the pattern expected for a magnitude decrease. In fact, this magnitude signature can be very well modeled as a magnitude decrease. Figure 5B compares the observed magnitude signature with a synthetic generated by decreasing the magnitudes of events between x and x by x . One would conclude from this fit that these magnitudes should be adjusted for events all along the Calaveras fault.

If one examines magnitude signatures comparing the rates during the same time periods on the northern and southern segments of the Calaveras fault, however, a different picture emerges. These are shown in Figure 5C and D. The northern segment of the fault shows a simple detection increase with a magnitude cutoff of $m_d \geq 1.3$. The southern segment shows a slight detection decrease (indicated by the platform on the left side of the plot) combined with a magnitude decrease. The southern segment contains many more events for these time periods, so it

dominates the magnitude signature for the entire fault zone.

These results indicate that detection and reporting histories vary substantially on the Calaveras fault. These variations make the task of correctly interpreting these variations more difficult, but they can also be used to shed light on the causes for these changes.

CALA VERAS FAULT

MAGNITUDE 1.5-

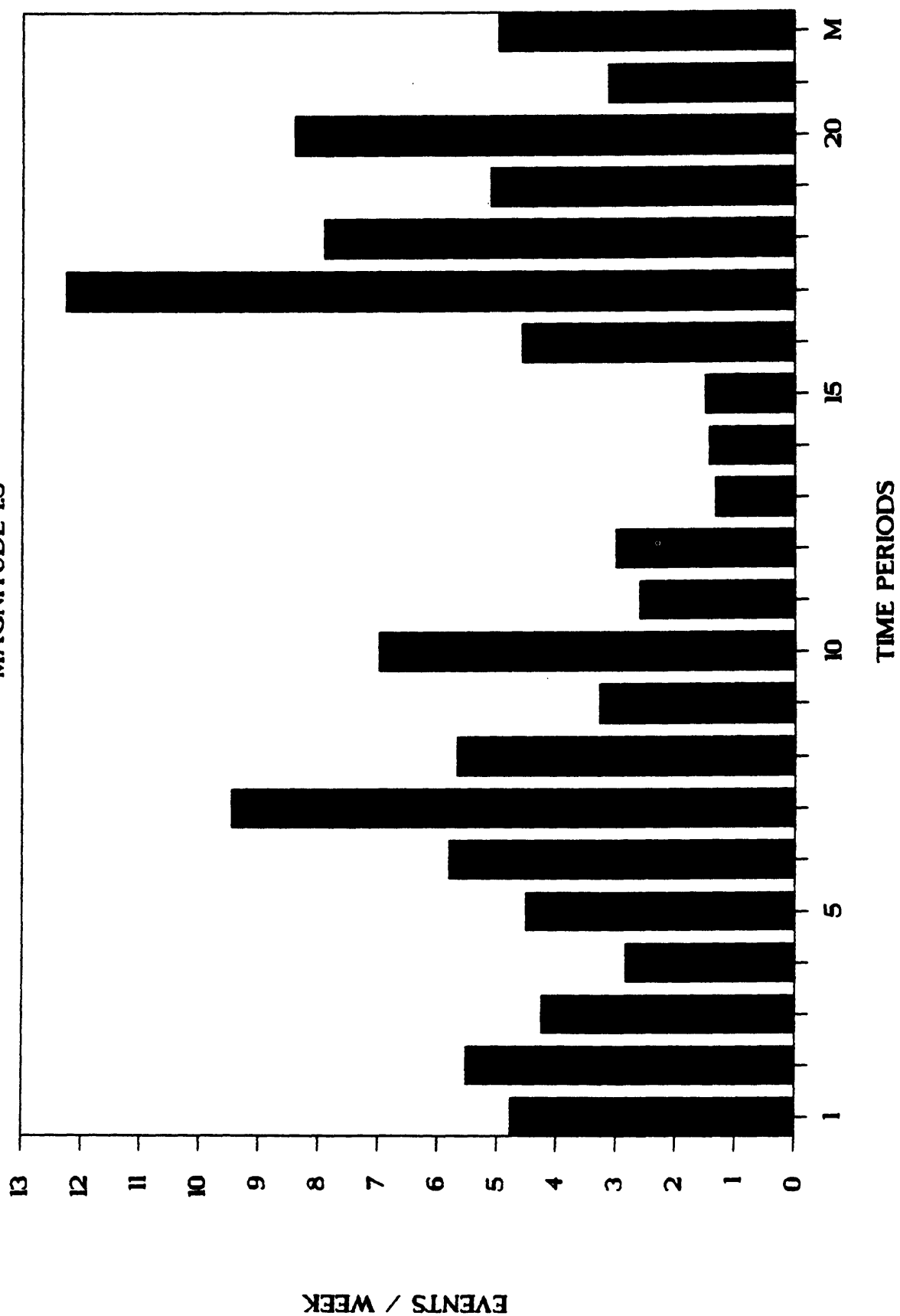


FIG. 1A

CALAVERAS FAULT

MAGNITUDE 2.5-

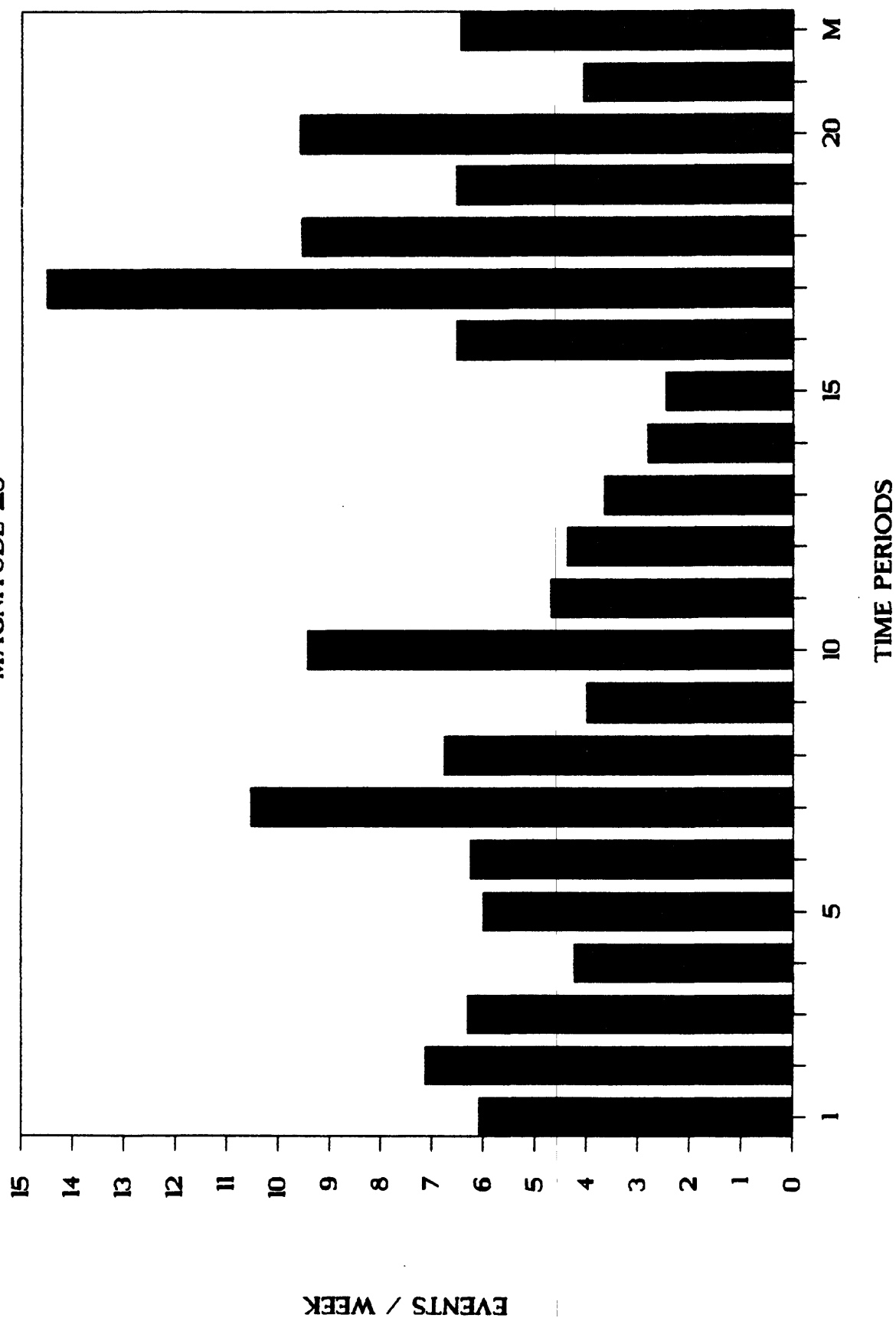
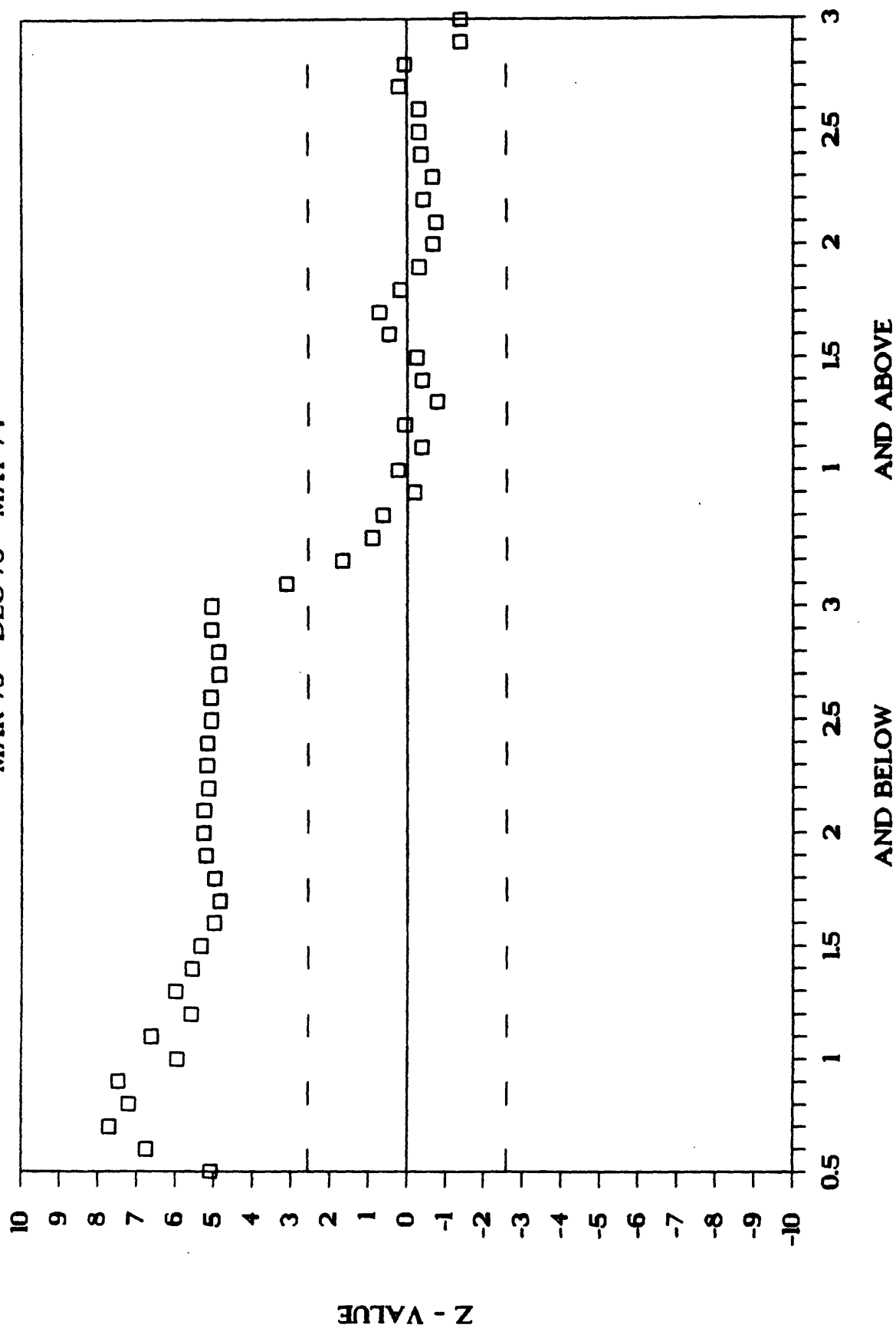


Fig. 1B

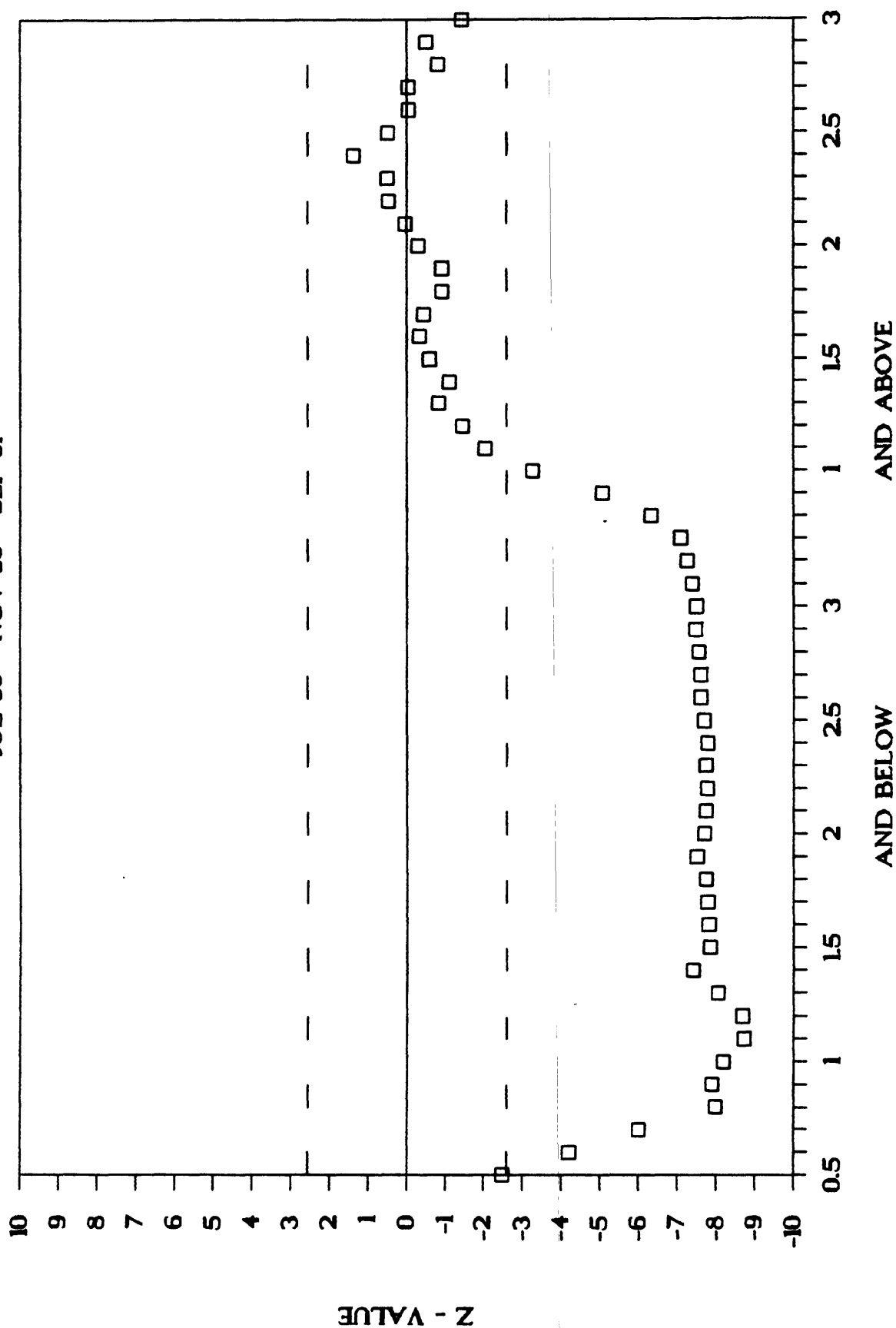
OBSERVED MAGNITUDE SIGNATURE

MAR 73 - DEC 73 - MAY 74



OBSERVED MAGNITUDE SIGNATURE

JUL 80 - NOV 80 - SEP 81



OBSERVED MAGNITUDE SIGNATURE

OCT 69 - MAY 70 - SEP 70

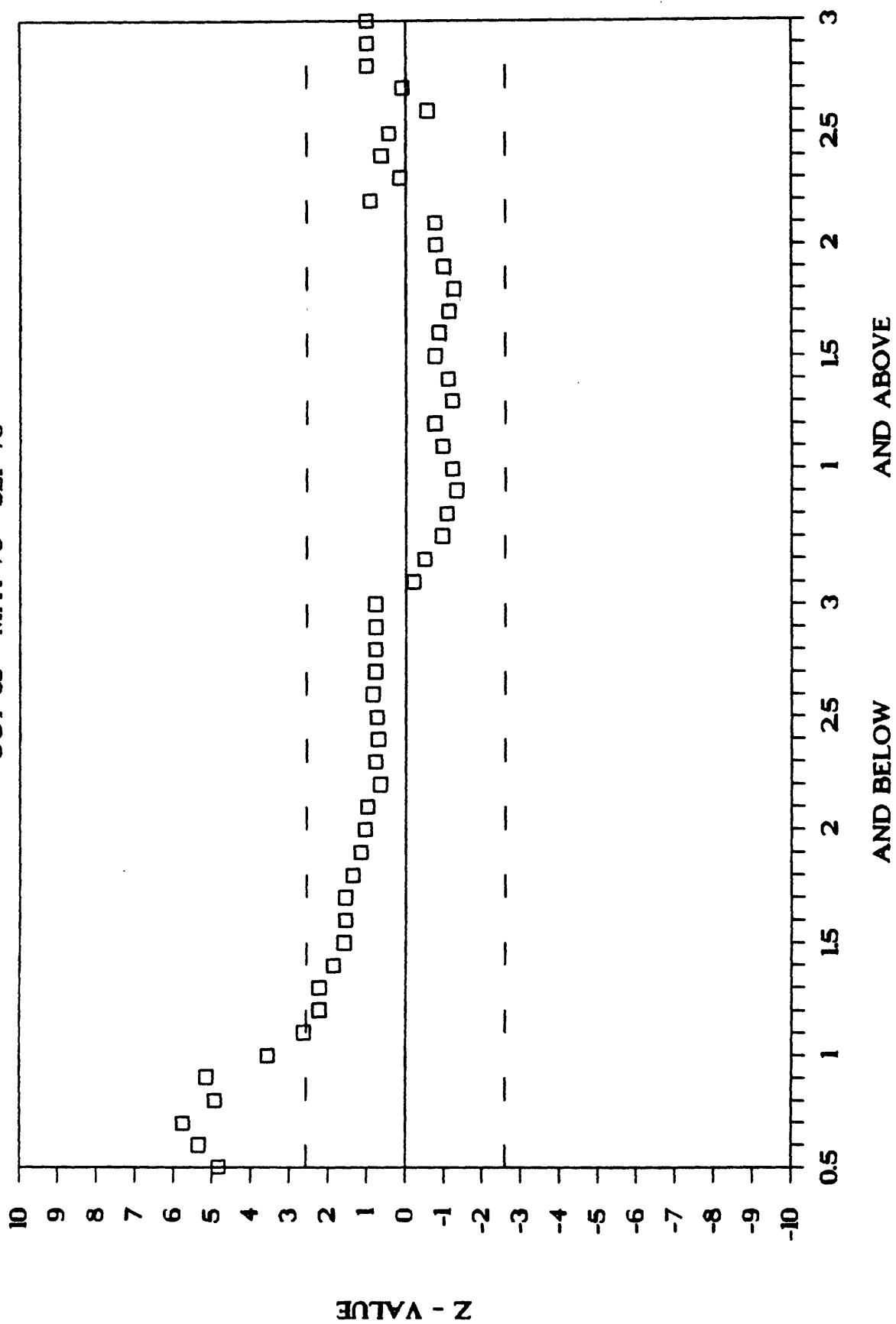


Fig 4

OBSERVED MAGNITUDE SIGNATURE

JAN 69 - JUN 69 - MAY 70

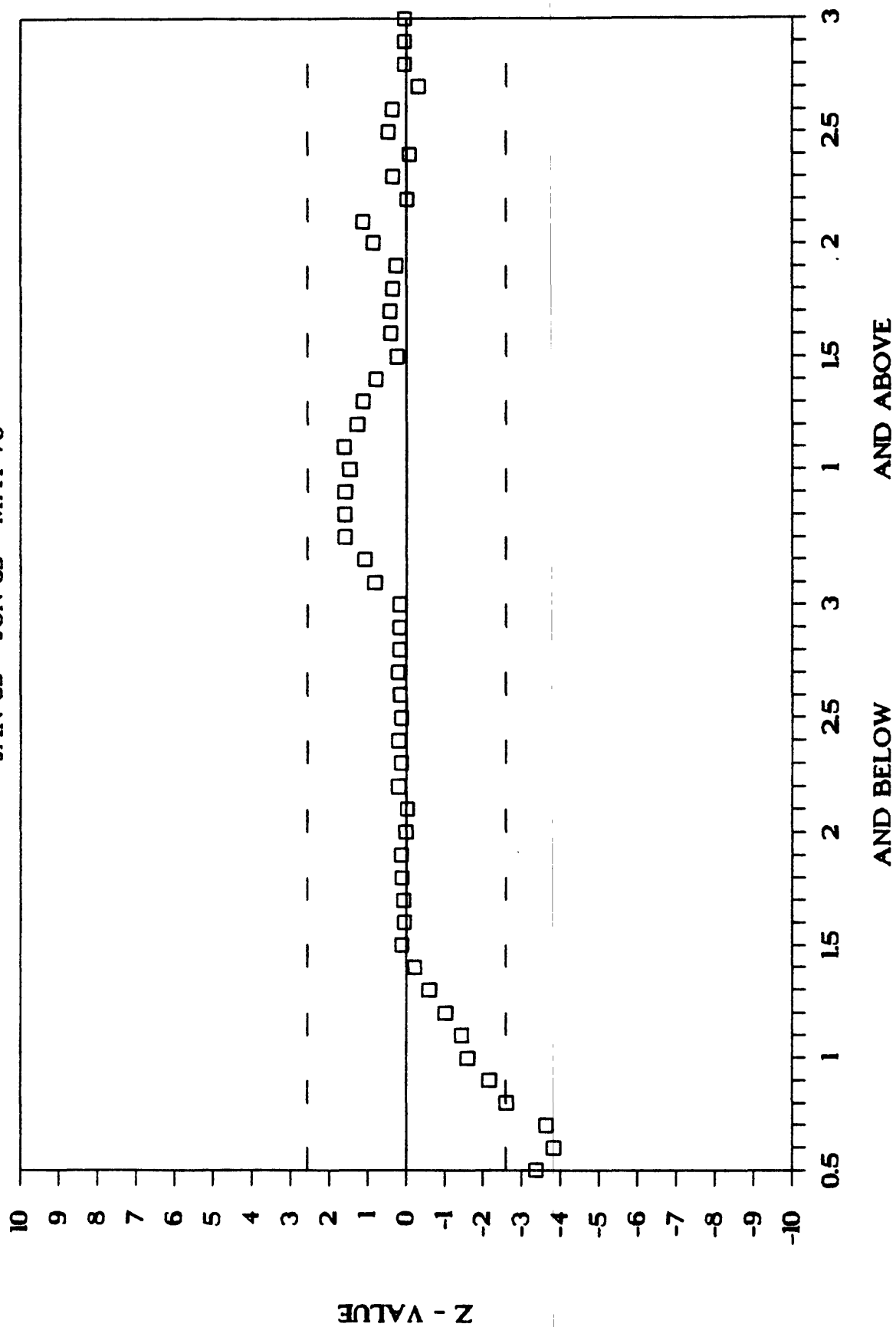
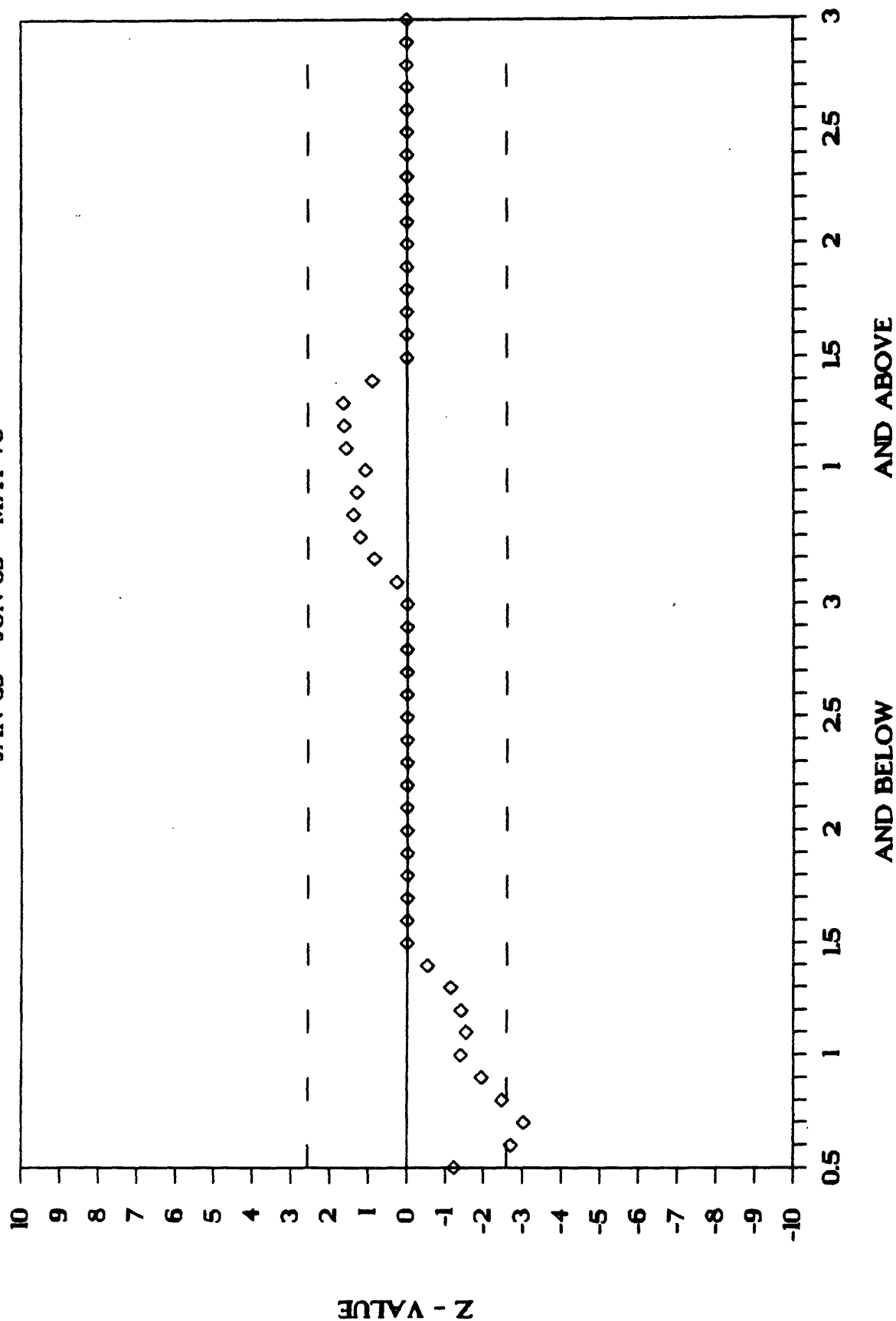


Fig. 5 A

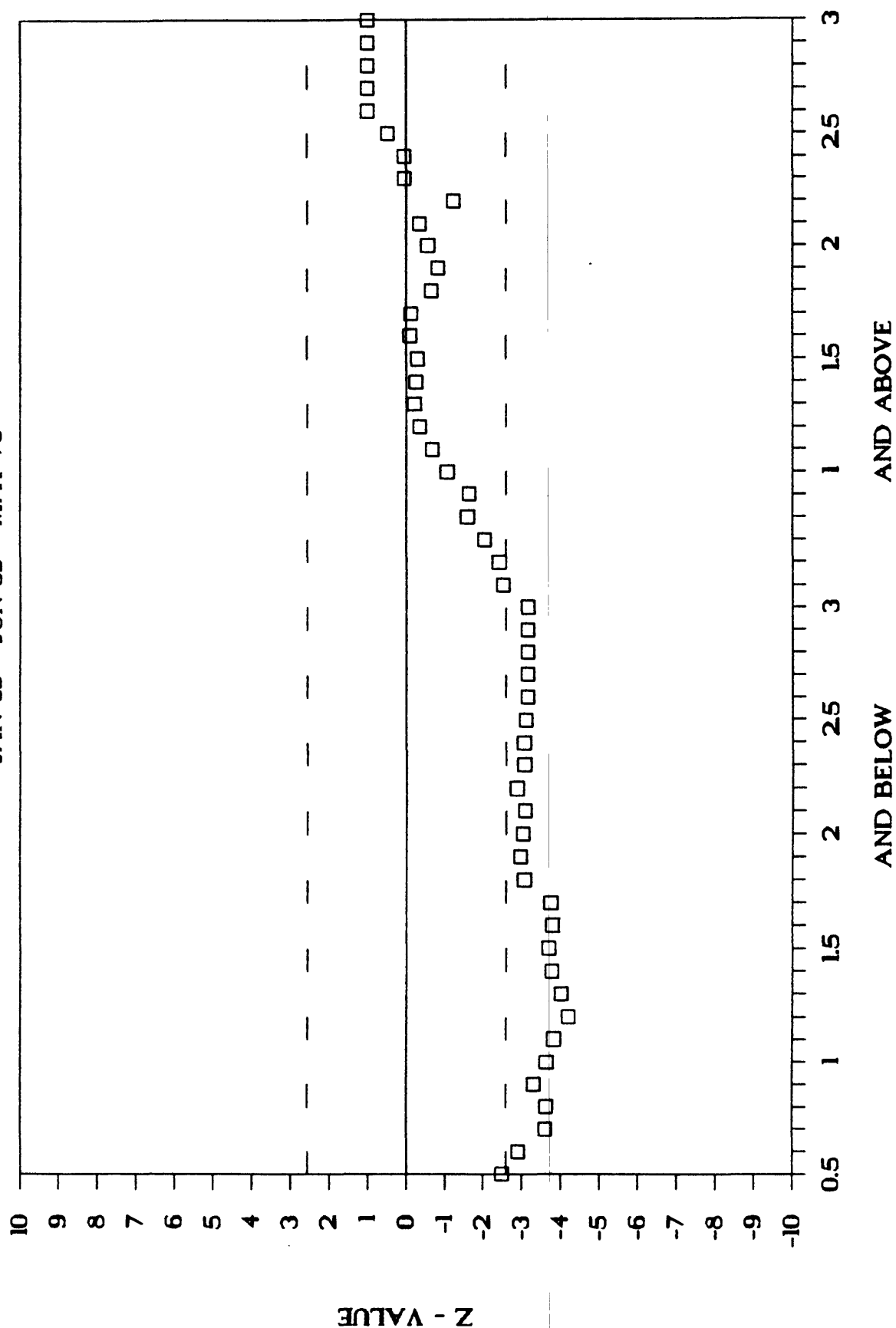
EQUAL SYNTHETIC

JAN 69 - JUN 69 - MAY 70



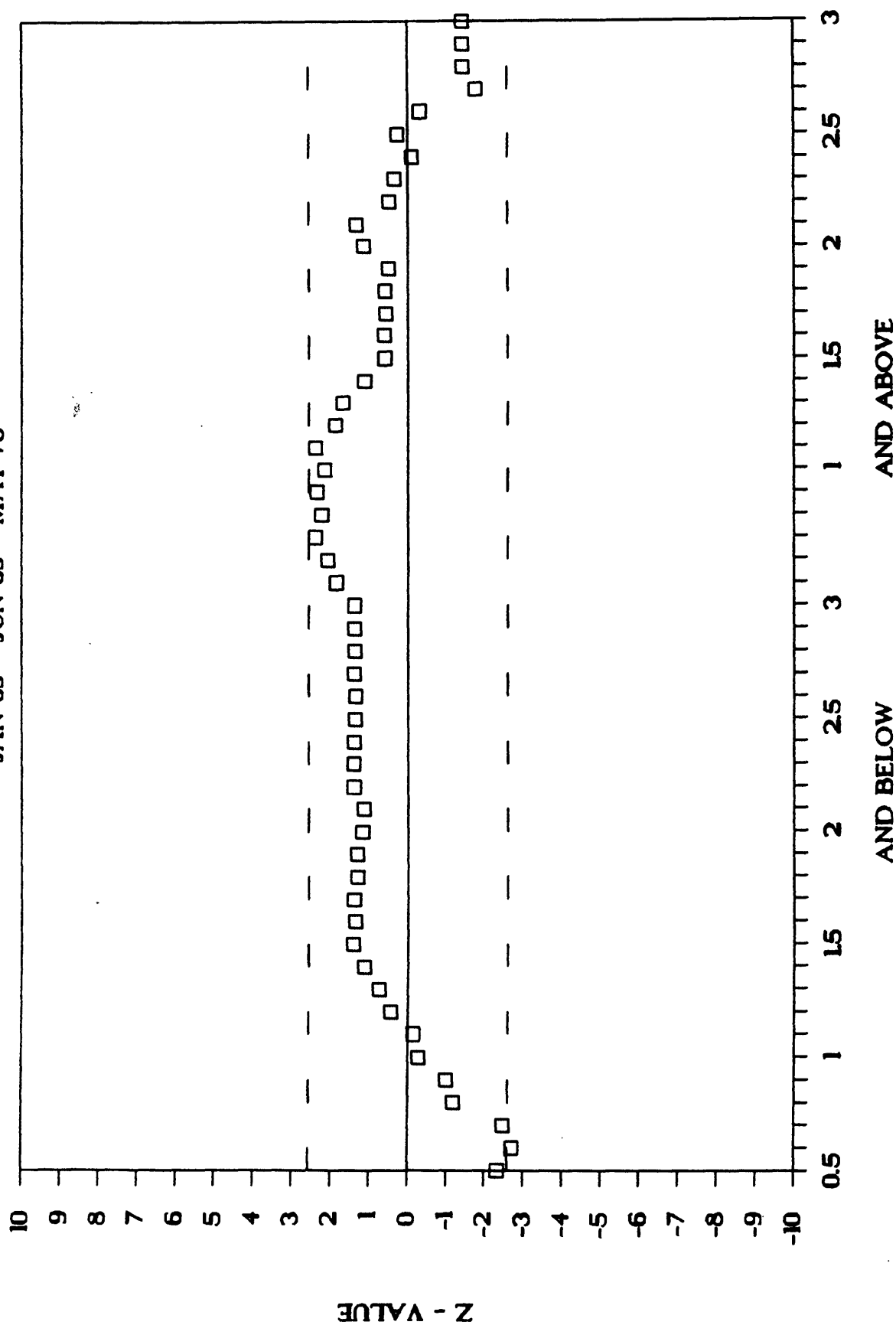
NORTHERN SEGMENT

JAN 69 - JUN 69 - MAY 70



SOUTHERN SEGMENT

JAN 69 - JUN 69 - MAY 70



APPENDIX A. 18.

Retardations in Aseismic Slip Rates Along the Calaveras
and San Andreas Faults in the Monterey Bay Region, California

R. O. Burford and S. S. Schulz

RETARDATIONS IN ASEISMIC SLIP RATES
ALONG THE CALAVERAS AND SAN ANDREAS FAULTS
IN THE MONTEREY BAY REGION, CALIFORNIA

R. O. Burford and S. S. Schulz

Office of Earthquakes, Volcanoes, and Engineering
U.S. Geological Survey
Menlo Park, California 94025.

July 27, 1985

ABSTRACT

Active fault traces in the Monterey Bay region have been monitored for surface slip activity by repeated surveys on alignment arrays and by installation and operation of various creepmeter devices since about 1968/69. However, monitoring at the Cienega Winery site on the San Andreas fault 14 km south of Hollister was started in 1956, following construction of the main building in 1948, and nearly continuous recording has been maintained at the site since about mid-1958. A map of active fault traces in the Monterey Bay region showing creepmeter locations and epicenters of earthquakes in the class $M_l \geq 4.0$, 1969 to present, is presented in Figure 1. Possible retardations in aseismic slip rates prior to moderate shocks during the 1971-73 Bear Valley, San Juan Bautista earthquake sequence were noted, in retrospect, as the afterslip effects of the sequence were being recorded. Unfortunately, monitoring was begun too late at most sites to establish an adequate pre-perturbation baseline (Fig. 2). Thus, the possibility of precursory creep-rate retardations could not be distinguished from at least one important alternative possibility that coseismic surface slip and subsequent accelerated afterslip effects were simply superimposed on nearly steady, lower-rate backgrounds. This ambiguity remains at certain sites despite the addition of useful data over the subsequent decade.

To date, the clearest case for precursory retardation in surface creep rate is provided by the 14-yr record from the Shore Road creepmeter (SHR1) on the Calaveras fault ~ 11 km NW of Hollister (Fig. 3). Conspicuous decreases in creep rate to near-zero values occurred at SHR1 during 1976-79 and again during 1982-84. Both of these periods of low creep rate were terminated by abrupt increases in slip rate associated with moderate earthquakes on the Calaveras fault northwest of the creepmeter (08/06/79, $M_l=5.9$, 15 km NW; 04/24/84, $M_l=6.2$, ~ 50 km NW). An earlier possible example of creep retardation at SHR1 occurred during 1973-74 prior to a moderate earthquake on the adjacent Busch fault (Fig. 1; 11/28/74, $M_l=5.1$, ~ 5 km SW). In this case, however, the period of retardation was terminated by a large creep event (~ 9 mm) that started on 09/14/74, 75 days before the earthquake. Note that the duration of retardation in these cases may be roughly proportional to the moment of the subsequent earthquake, perhaps modified by inverse proportionality to distance between creep site and epicenter (or to center of rupture zone?). The possibility of a quantitative relation of this sort has not been tested as yet.

Interaction between various active faults in the Hollister area may play an important role in initiating creep-rate retardations, as indicated by modeling work of Mavko (1982). Despite these results, it remains difficult, in our opinion, to explain the relationship between the record at SHR1 and the two larger moderate shocks to the northwest, on the same fault, in terms of fault interaction. However, the correspondence between the record at SHR1 and the records from adjacent sites along the San Andreas fault such as XSJ2 (Fig. 1) provides an intriguing indication of possible fault interaction effects (Fig. 4). Fluctuations in the creep rate at XSJ2 after 1974 seem to follow, more-or-less, those of SHR1 with a lag of about 9 to 10 months. This possible correspondence has some interesting, if weak implications concerning near-future activity along the San Juan Bautista section of the San Andreas fault, but we shall refrain, for the moment, from pursuing this line of discussion any deeper into the realm of "arm waving."

The focus of our concerns at present will instead be turned to the apparent development of fresh, on-going retardations in creep rates along the San Andreas fault at XFL1, XHR1, and XSJ2 (Figs. 1 and 5). These sites cover the same section of the fault where apparent, concurrent seismic quiescences have been detected, as documented in a companion presentation. A notable lack of definite retardation at Cienega Winery, at the heart of the Winery seismic gap and current quiescence, is admittedly perplexing. However, the hint of an incipient retardation onset at the Winery near the beginning of 1983 will be watched with great interest (Fig. 6).

The hypothesis presented here is that local creep-rate retardations associated with local seismic quiescences may relate to changes in combined seismic/aseismic slip processes within and near the fault-surface source areas for impending moderate mainshocks. Simplified elements of this hypothesis are presented in Figure 7. Here we propose that a persistently "slow" patch on a creeping fault consistently lags behind both the steady, regional-block motion and the slip on adjacent patches for an interval representing a late, yet significant fraction of the recurrence interval for the characteristic moderate earthquake (upper left, Fig. 7). This feature of the local slip budget will produce local strain accumulation across the patch coupled with quasi-steady stress increase. A creepmeter at any nearby surface location influenced by these conditions would record a steady slip rate well below the long-term average block-displacement rate (left-hand side, surface-slip versus time). The corresponding stress increase across the area of impending seismic rupture is depicted in the lower curve (left-hand side). At some stage in the accumulation of stress, we propose that stress will reach a threshold value that will induce, for instance, a change in the modulus of the slip-zone material such that a rather sudden onset of increased resistance to slip will result. Whatever the mechanism (stress or slip-geometry related?), it is clear that if such slip retardations occur *within* the seismogenic zone, the effects may eventually reach the shallow, creeping zone. Sites immediately above the source will be affected sooner and more profoundly than more distant sites that may ultimately be reached. Thus, according to our hypothesis, surface creep retardations associated with evidence of seismic quiescence may reflect a period of rapid increase in shearing stress across a subjacent, fault-surface area of impending seismic rupture.

FIGURE CAPTIONS

Figure 1. Map of active fault traces in the Monterey Bay area of California showing creepmeter sites and the epicenters of earthquakes of $M_l > 3.99$ that have occurred since the beginning of 1969.

Figure 2a. Creep records from 5 sites along the San Andreas fault from San Juan Bautista to Lewis Ranch. Site locations are indicated in Figure 1.

Figure 2b. Creep records from the same section of the fault represented in Fig. 2a showing details of possible creep-rate retardations and periods of afterslip associated with moderate shocks during 1971-73 (Bear Valley, San Juan Bautista sequence).

Figure 2c. Detrended creep records from San Juan Bautista to Bitterwater Valley (73 km) showing degree of coherence bracketting the 1971-73 moderate earthquake sequence. Discontinuous vertical lines labeled with magnitudes mark the times and approximate positions of epicenters along the fault. Variable scales at left (mm) apply to residual values for creep curve immediately to right.

Figure 3. Raw and detrended creep records from Shore Road site, 11 km NW of Hollister on the Calaveras fault. Times and approximate positions of moderate mainshocks are indicated by dots (distance scale on left).

Figure 4. Comparison of detrended creep records from SHR1 (Calaveras fault) and XSJ1,2 (San Andreas fault). Note ~ 9-10 month lag at XSJ for inflection points similar to those recorded at SHR (after 1974). Times and magnitudes of local moderate shocks near each creep site are indicated at top and bottom of plot.

Figure 5a. Combined creep records from the San Andreas fault between San Juan Bautista and Melendy Ranch (Bear Valley). Times and locations of nearby moderate earthquakes are indicated by dots.

Figure 5b. Detail of NW portion of Fig. 5a.

Figure 5c. Detail of central portion of Fig. 5a.

Figure 5d. Detail of SE portion of Fig. 5a.

Figure 6. Summary of detrended creep records from the San Andreas fault between San Juan Bautista and Melendy Ranch (Bear Valley). Note the coincidence of single and multiple moderate earthquake occurrences with several of the prominent inflection points on some of the creep records, especially XSJ 1980/81 and XFL mid-1982. Clearly there is the possibility of a weak retardation onset at Cienega Winery (CWC, CWN), approximately coincident with that of XFL, 14 km SE of Winery.

Figure 7. Hypothetical case for possible relation between 1) proposed seismic/aseismic slip-rate retardation within and near the fault-surface source area for a moderate earthquake, 2) surface creep behavior, and 3) stress changes across the impending seismic rupture. Contours represent average slip-velocity distribution on the fault plane in mm/yr. The left-hand side represents a 10-yr pre-shock average condition from ~ 13 years to ~ 3 years before rupture. The right-hand side represents a 2-yr pre-shock average condition from ~ 2.1 years to ~ 1 month before rupture. Corresponding surface slip-rate behavior and changes in stress across the "slow" patch on the fault are indicated in the lower half of the figure.

CAPTIONS FOR EXTRA FIGURES NOT CITED IN TEXT:

Figure 8. Slip-surface section along the San Andreas fault from San Juan Bautista southeastward to Bear Valley, showing relationship between surface creepmeter sites and the fault-plane source areas for moderate earthquakes during the period January, 1960 through June, 1973 (after figure prepared by R. Wesson, 1974).

Figure 9. (Same as Fig. 2b, above) Creepmeter records from sites along profile of Fig. 8 for the period 1968-1975, to illustrate increase in average slip rate from northwest to southeast. Heights of displacement envelopes containing total variations in cumulative aseismic slip at each site range from 9 to 16 mm (approximations), and show minimum values at the Cienega Winery (CWC) and Stone Canyon (SCR) sites, directly above and ~ 18 km SE, respectively, of the end of the "Winery gap" in the 1971-73 earthquake sequence (See Fig. 8).

Figure 10. Residual (detrended) creep-rate plots showing the relations between creep-rate fluctuations and the occurrences of mainshocks in the 1971-73 moderate earthquake sequence.

Figure 11a. Residual creep-rate plot for combined building-offset and instrumental records between 1948 (construction date) and September, 1976. Long-term average slip rate (least-squares fit) is 12.3 mm/yr. Times and local magnitudes of near-by moderate earthquakes are indicated by

discontinuous vertical lines. Measurements of several offset reference lines in the building were begun in 1956 and have continued to date (recent data not included). A nearly continuous instrumental record from about mid-1958 to present is available. This record can be combined with (and/or compared to) data from the occasional remeasurements of the building-slab offset. Note the apparent retardation in creep rate from early 1957 through late 1959, briefly interrupted by a short-term afterslip response to a nearby shock of $M_l=3.7$ early in 1959. The first part of the instrumental record is somewhat suspect owing to possible mechanical hysteresis in the instrument mounts and linkage (last half of 1958)... Unfortunately, there were no direct measurements of the slab offset recorded during late 1958 to check the early part of the instrumental record. The late-1950's creep-rate retardation was terminated Nov. 22, 1959 by an unusually large (~ 6 mm) creep event 56 days prior to the $M_l=5.0$ mainshock of 01/20/60. Afterslip with a characteristic logarithmic or power-law decay in rate following the 1960 mainshock ended with a second unusually large creep event (~ 4.3 mm) 16 days before the double-mainshock event of 04/09/61, $M_l=5.2, 5.3$ (Savage and McNally, unpublished revision of local UCB catalog). The average creep-event amplitude at the Winery for events in the class >1.0 mm is 2.4 ± 0.6 mm (standard deviation), 1968 through 1977. Coseismic slip steps of ~ 3 mm and ~ 11 mm were recorded across the joint between concrete slabs of the Winery floor during the 1960 and 1961 mainshocks, respectively. The cessation of creep for more than a year after the April 1961 mainshocks and the low rate from mid-1962 to mid-1964 are thought to be due to the relatively large surface slip during the 1961 double-mainshock event. The amplitude of the surface response (secondary faulting?) was apparently sufficient to drop the near-surface potential along the creeping zone of the fault plane to below the creep-event threshold. These features of the creep record are also evident in the results of local geodetic measurements conducted at the Winery site (B. K. Meade, 1964). Potential apparently was restored when the long-term, pre-shock average trend was intersected about mid-1964 (See compressed raw record of Fig. 11b). Note the remarkable stability in average creep rate following restoration of near-surface creep-event potential until about mid-1970, the onset time of apparent creep-rate reduction prior to the shock of $M_l=4.0$ (UCB $M_l=3.9$) on 12/29/71 associated with rupture on the adjacent fault section to the southeast (see Fig. 8). The length and stability of the 1964-70 portion of the creep record may serve to heighten the significance of the 1970-71 Winery retardation, thus supporting conditional acceptance of several other apparent creep-retardation onsets in adjacent regions (Fig. 10).

Figure 11b. Plot of cumulative creep for the Winery site, after Nason (1973), emphasizing the rate increase before, and the arrested creep condition after the April 1961 double-mainshock event. The increased creep rate during 1960-61 is *not* independent of the 1960 mainshock of $M_l=5.0$; it is instead more characteristic of afterslip responses documented at several other sites by various types of measurements.

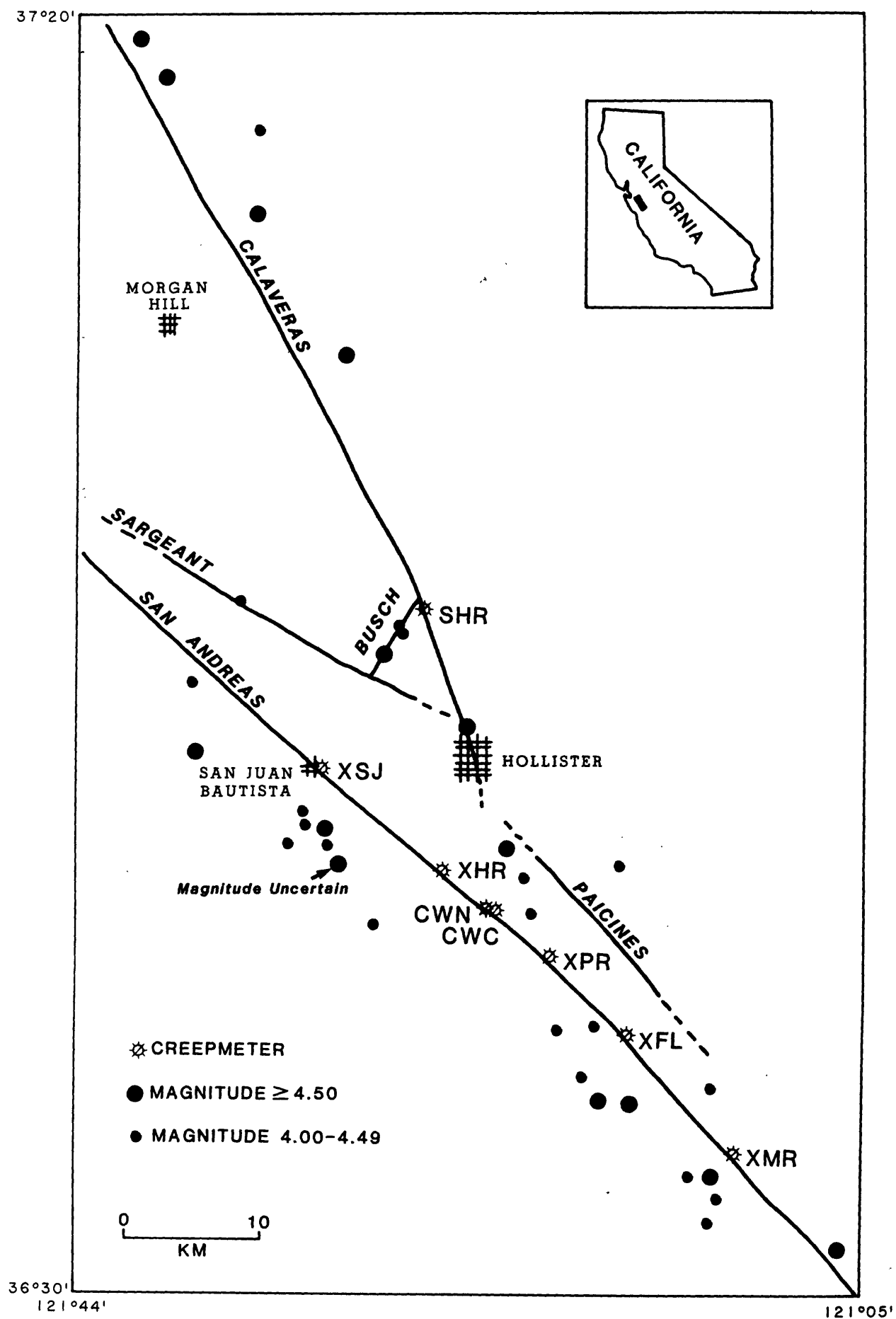


Figure 1.

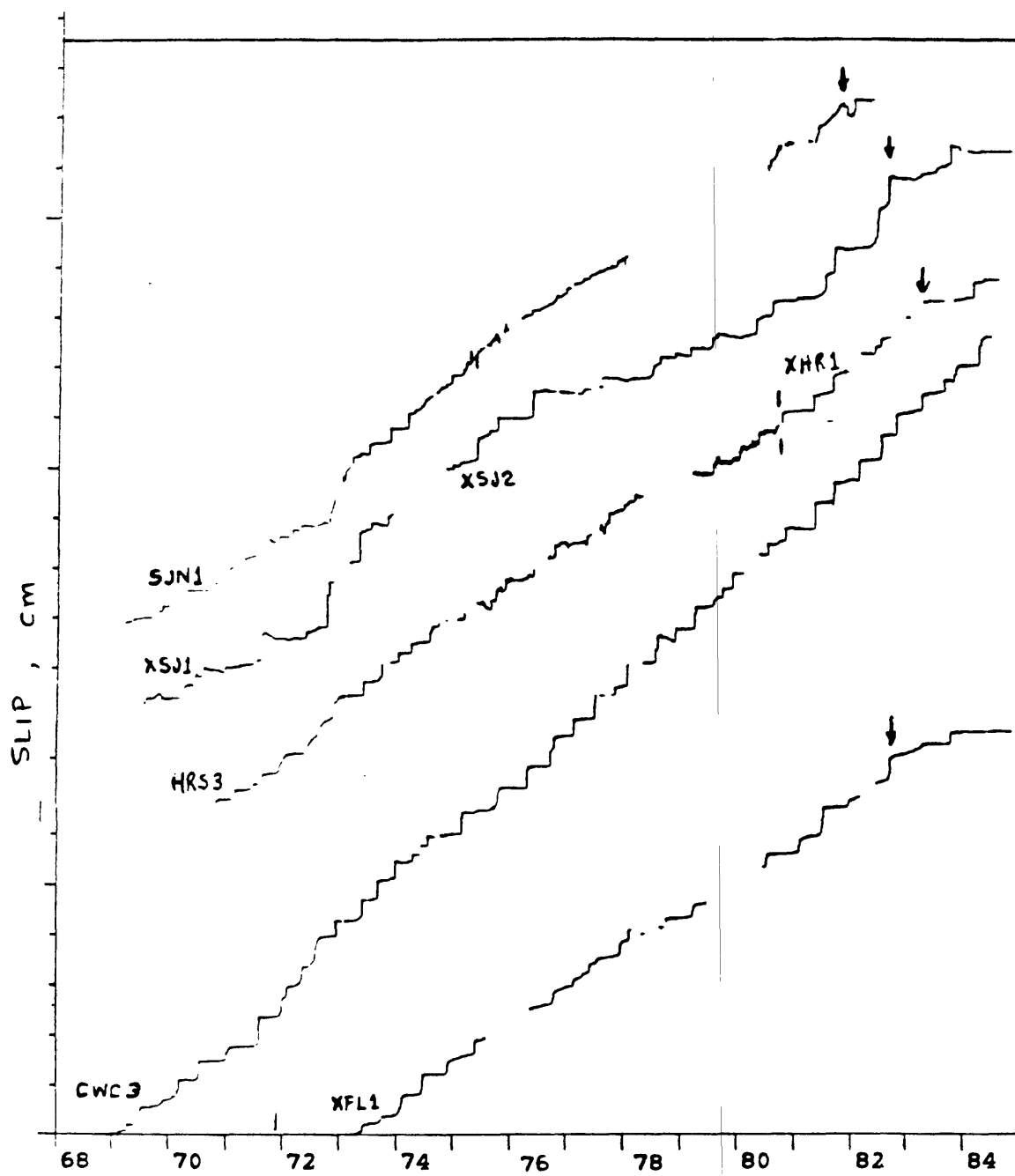


Figure 2. a.

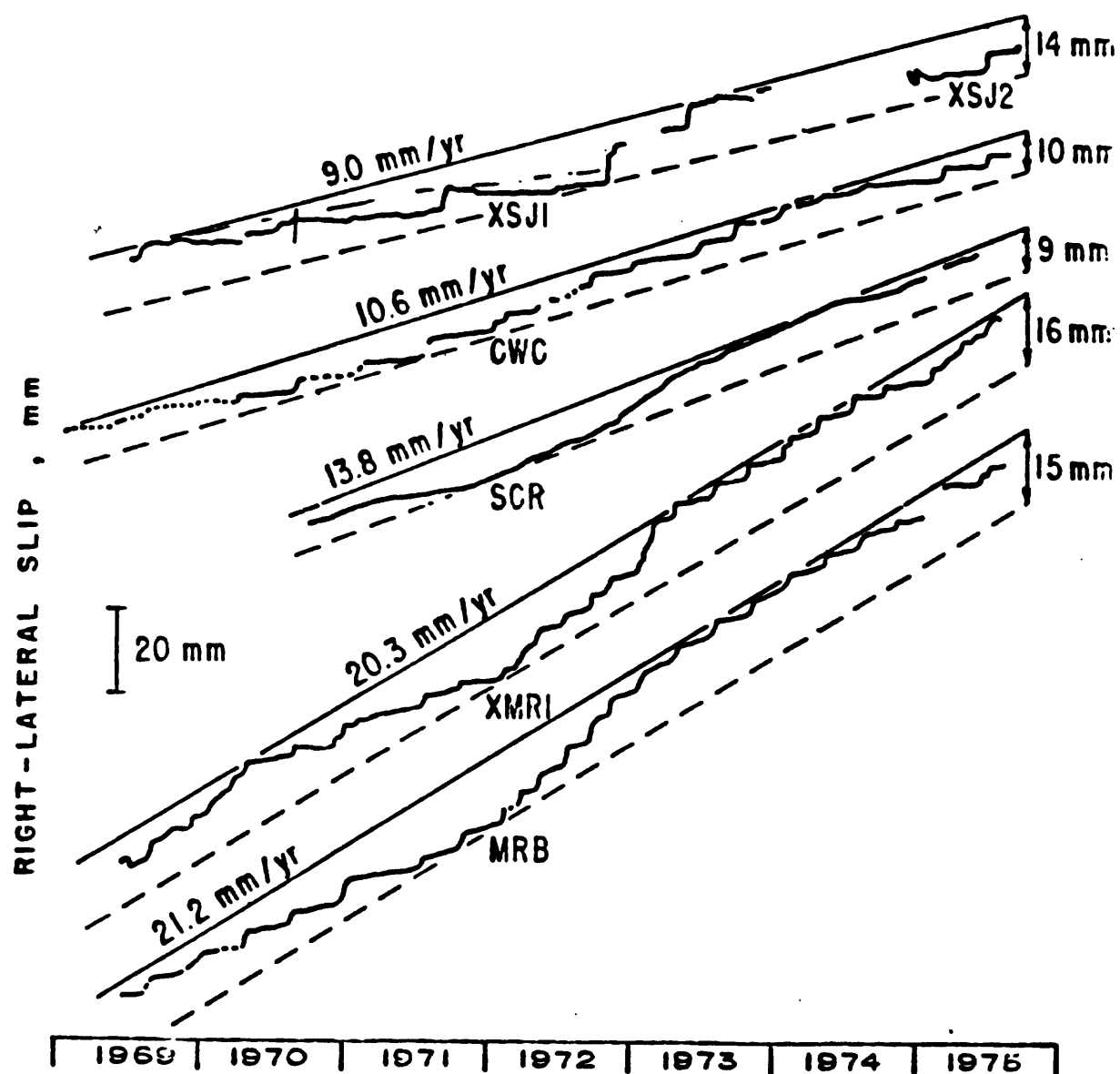


Figure 2b.

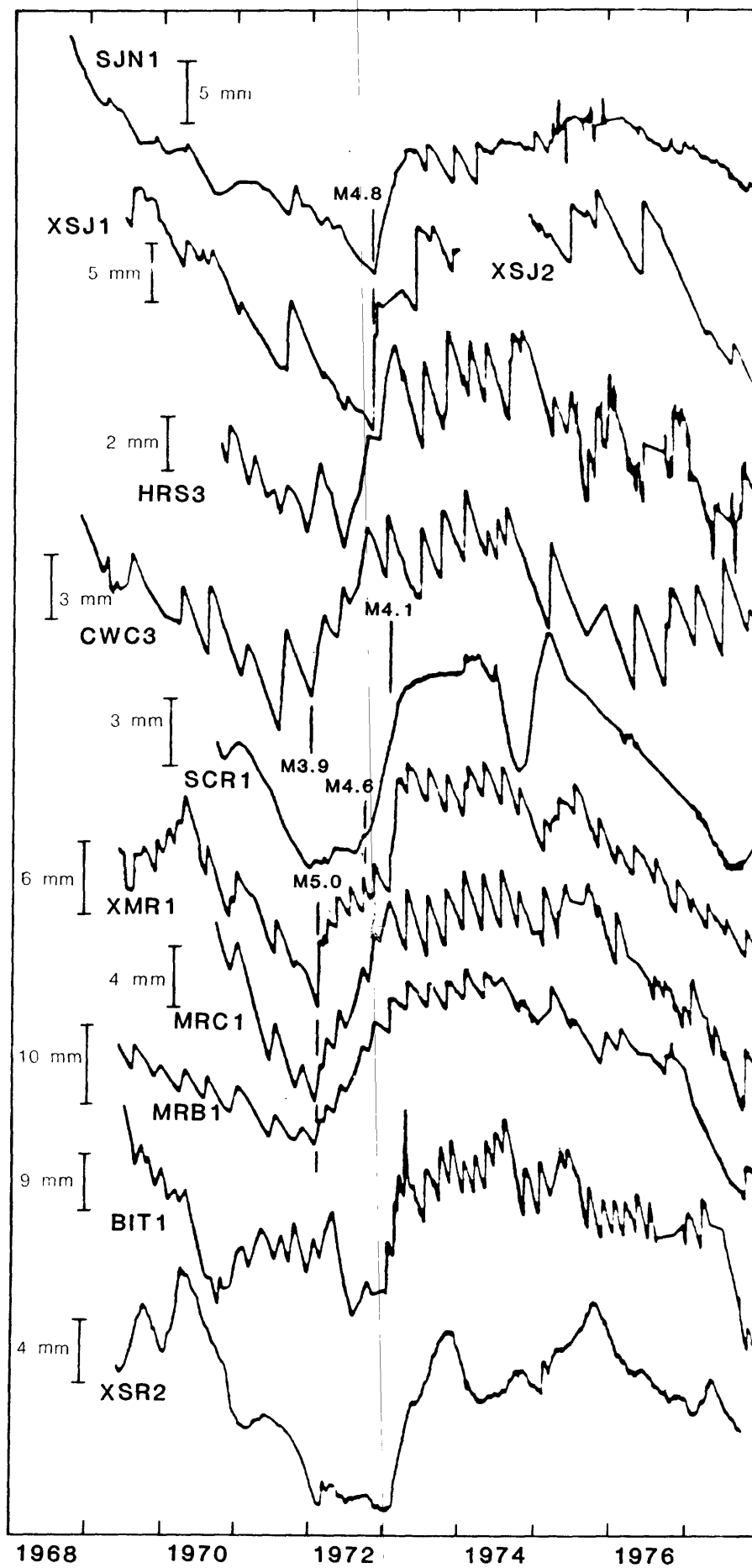


Figure 2c.

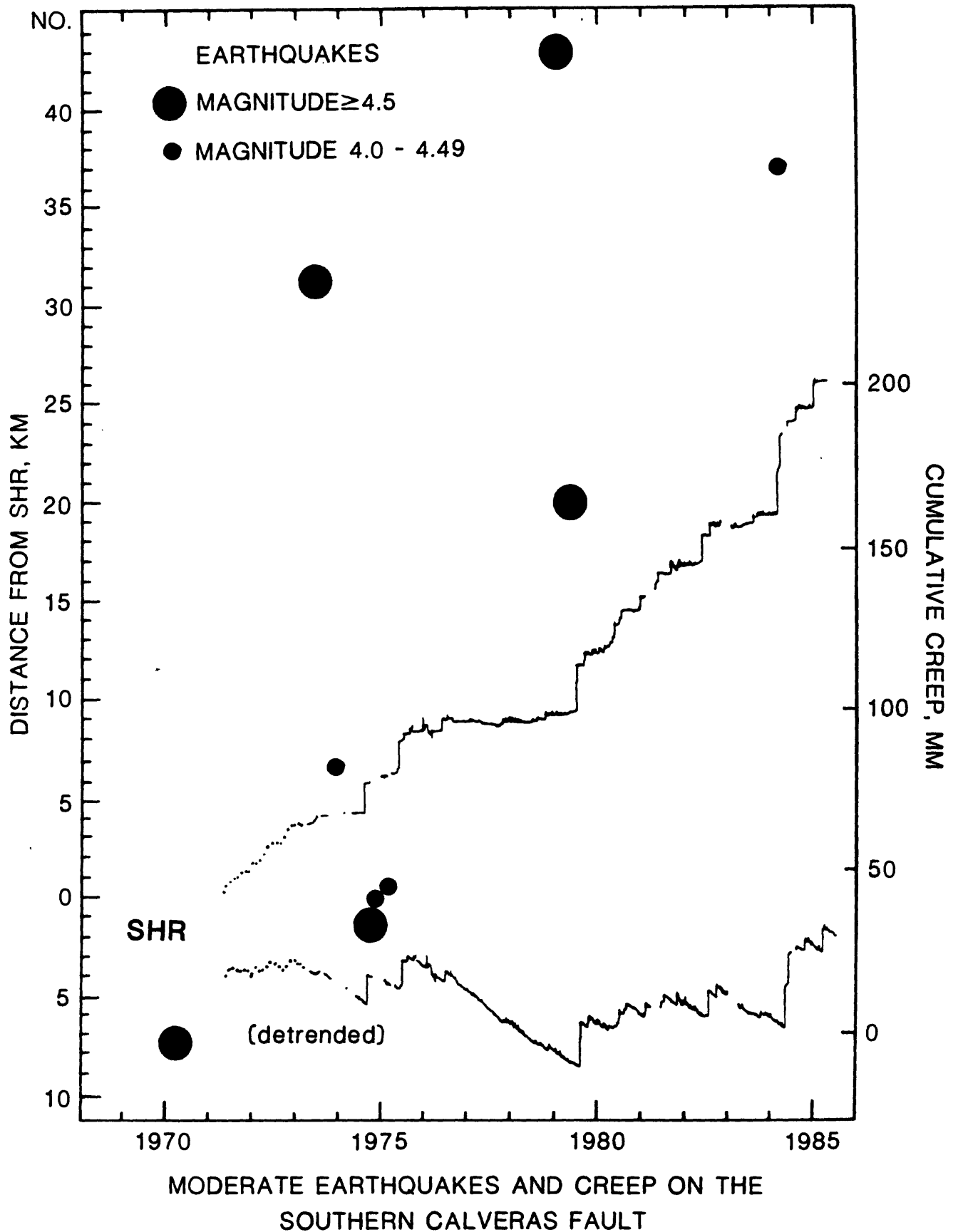


Figure 3.

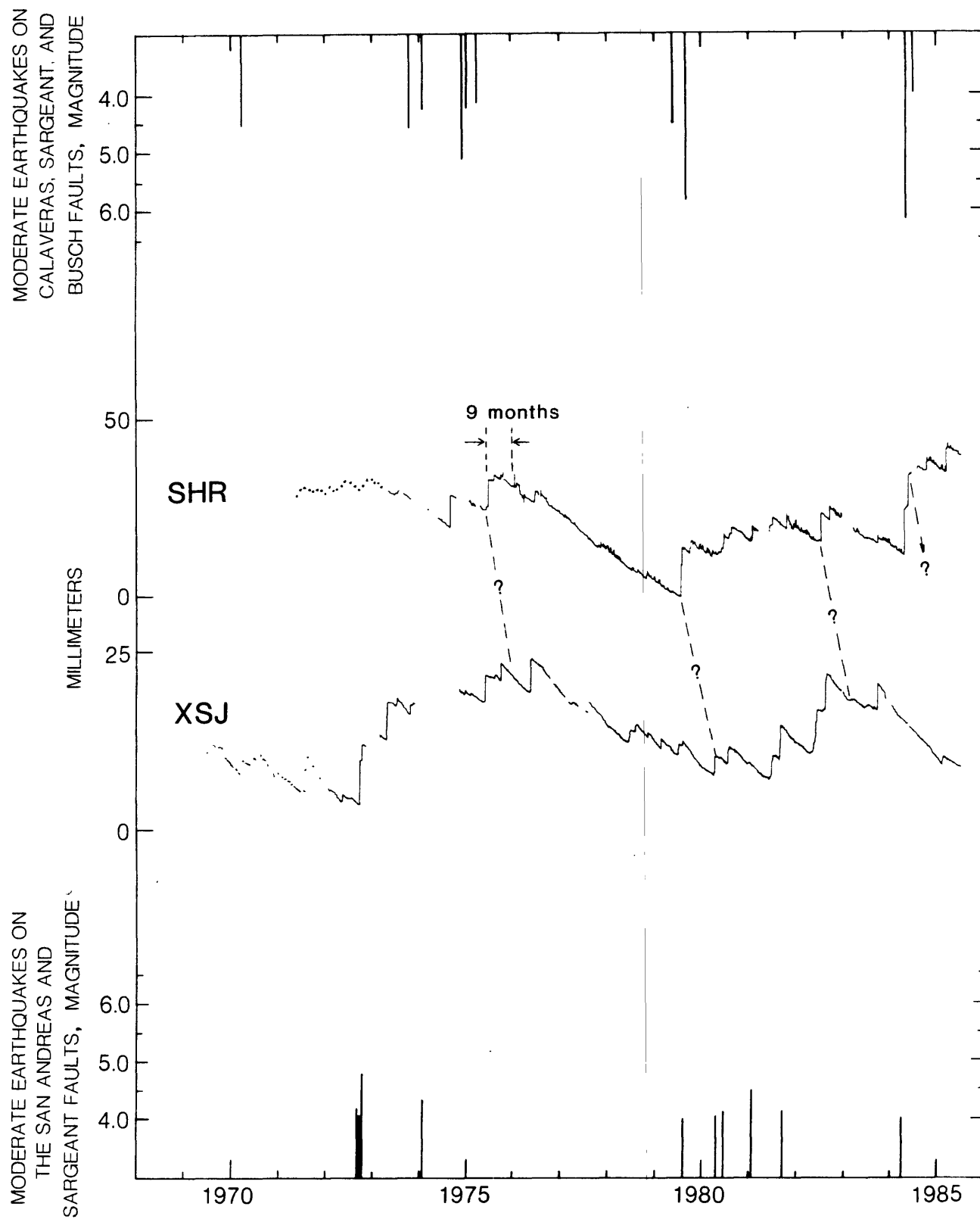


Figure 4.

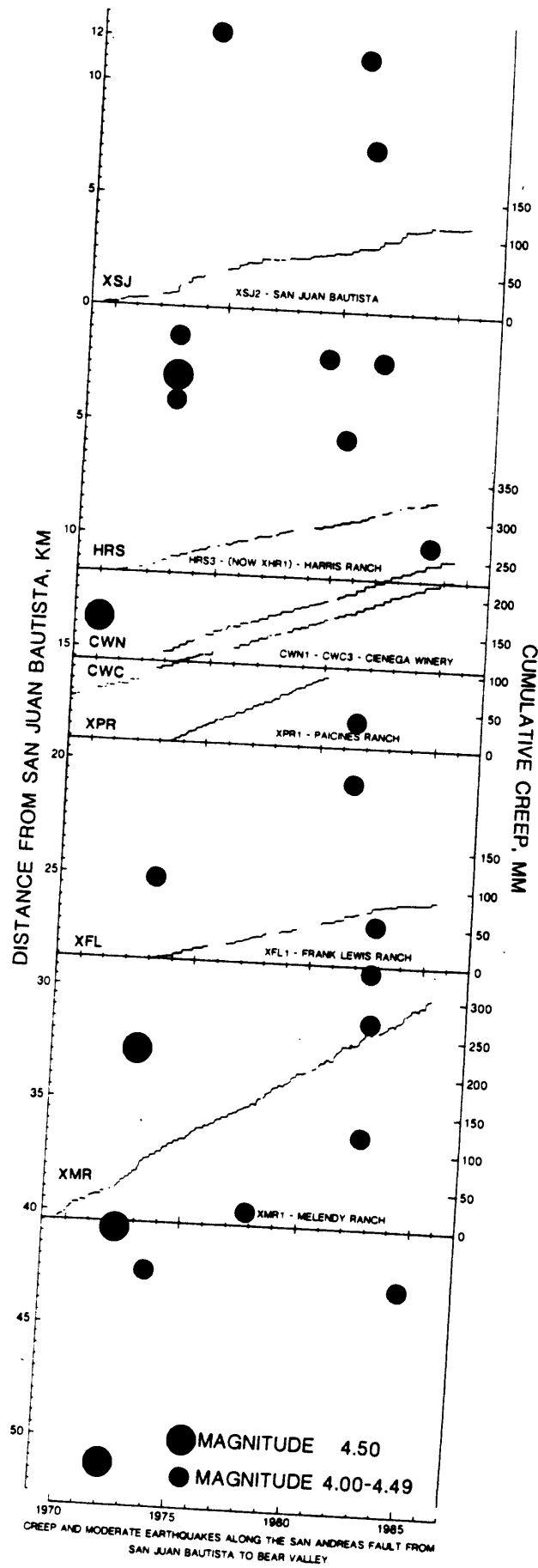


Figure 5a.

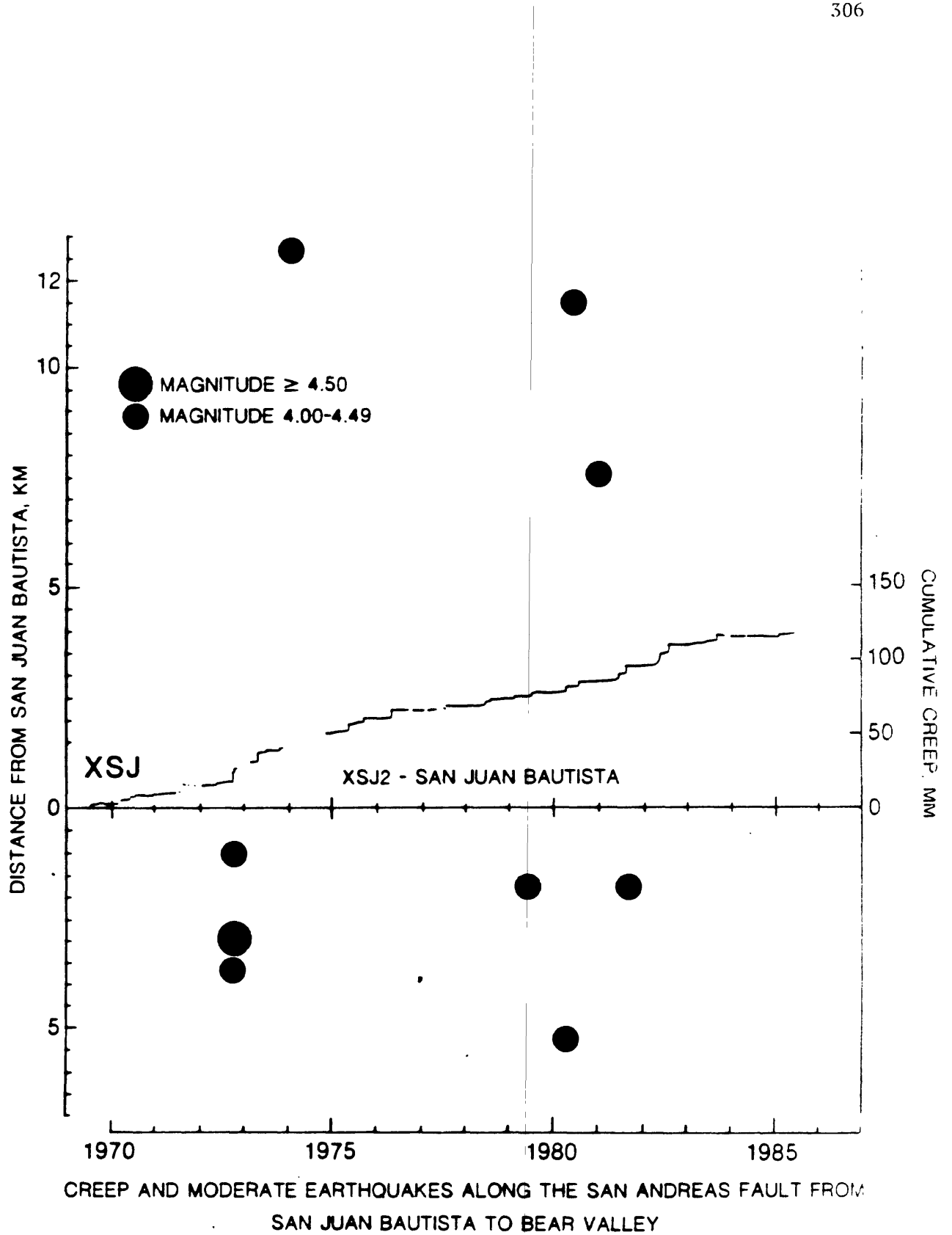


Figure 5b.

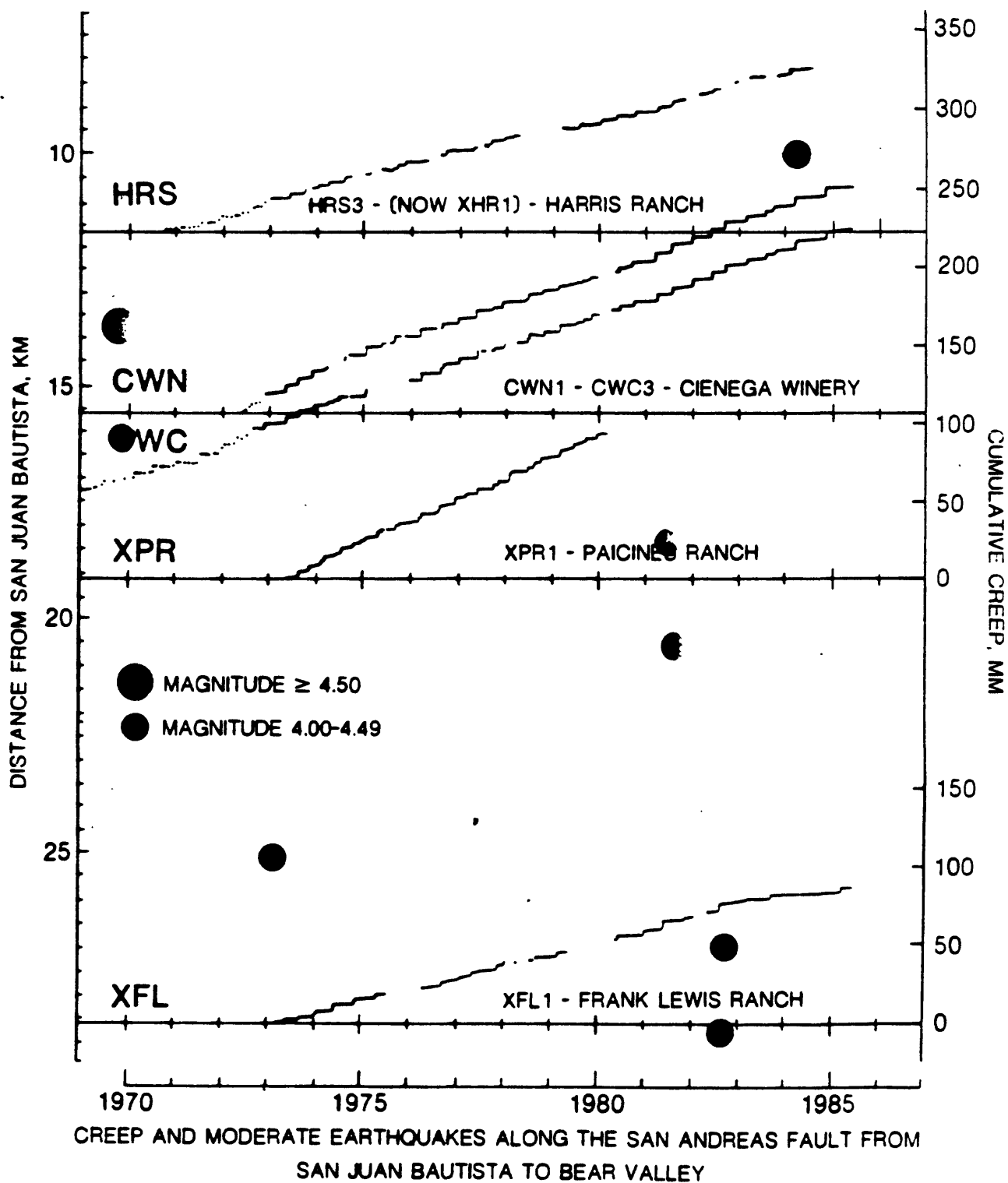


Figure 5c.

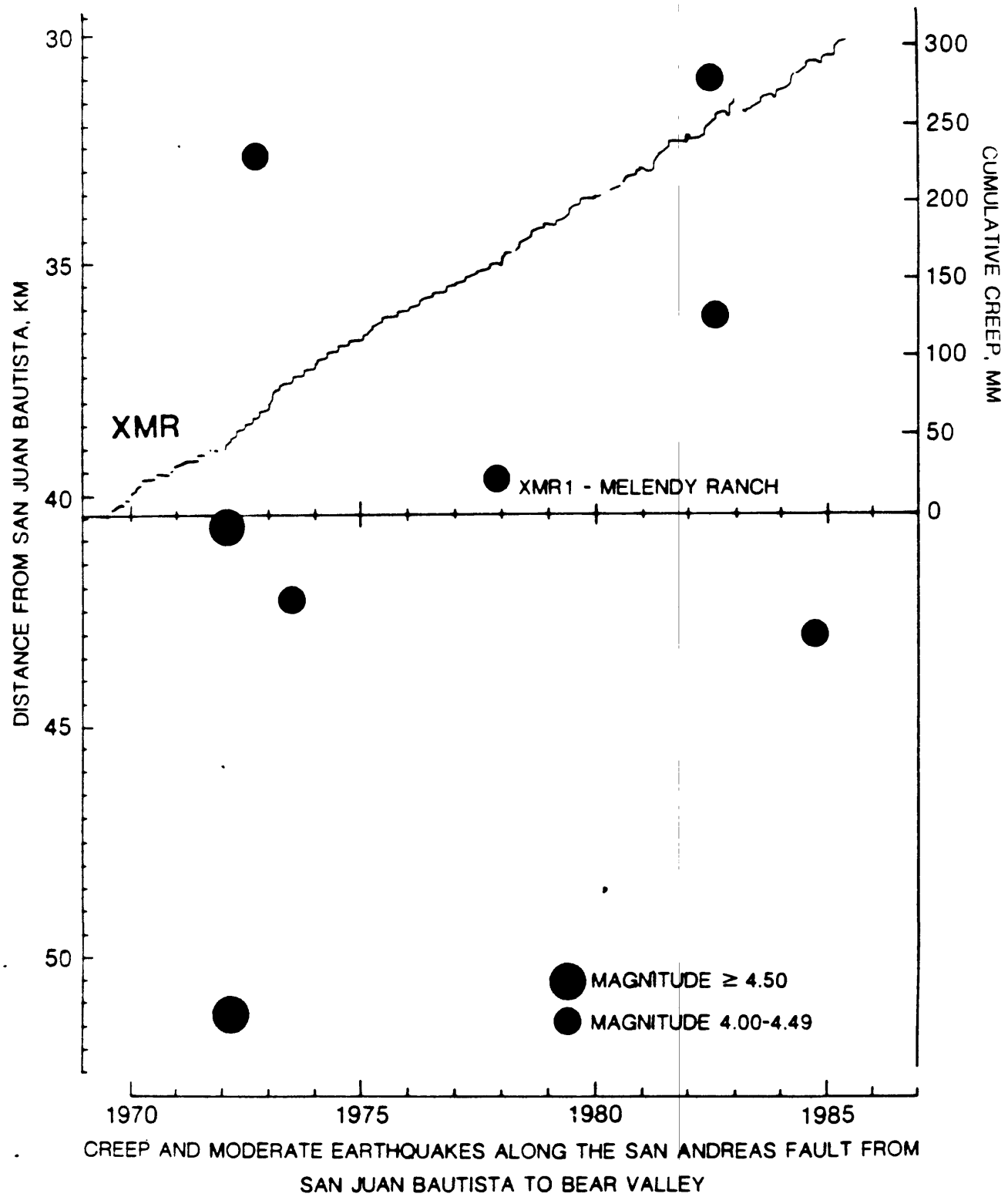


Figure 5d.

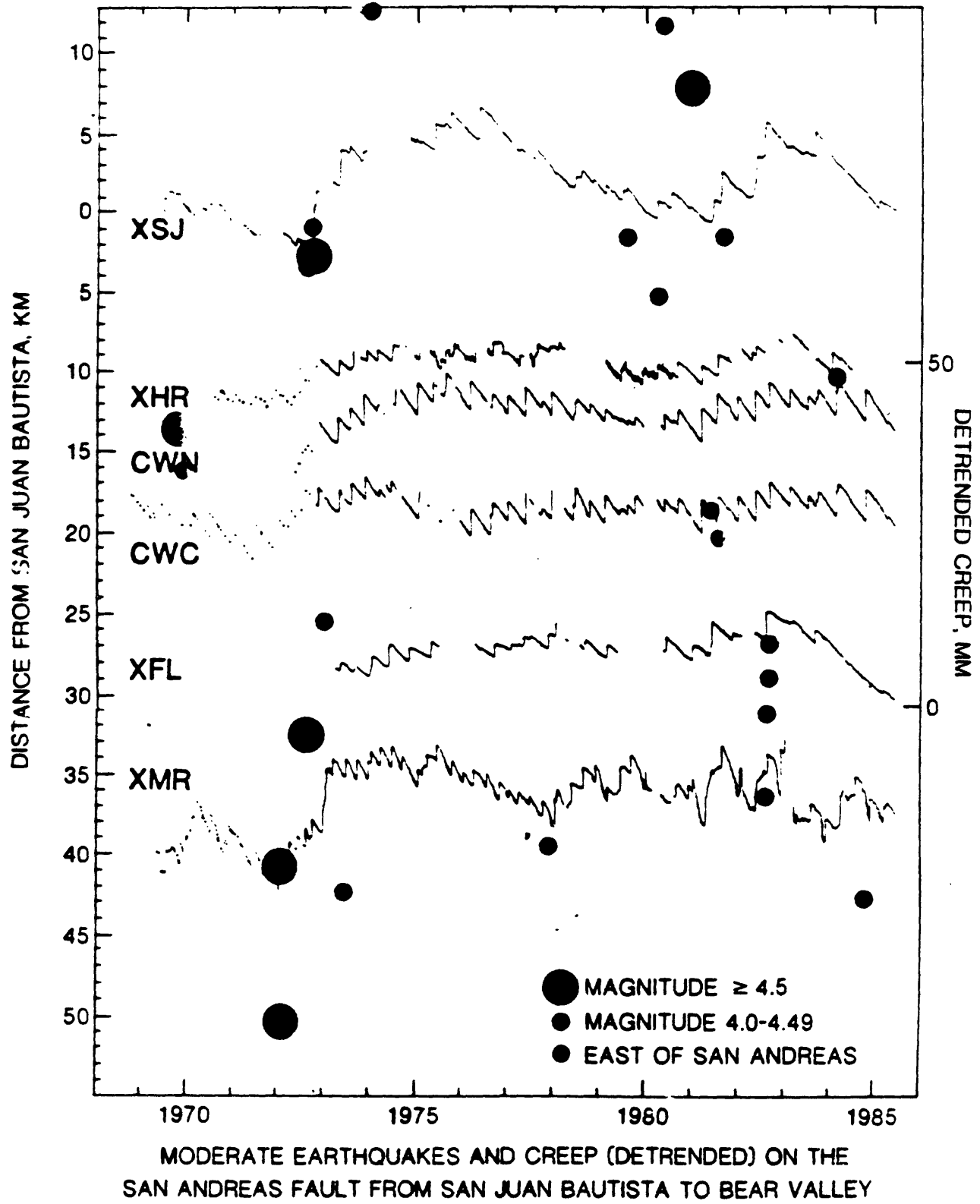


Figure 6.

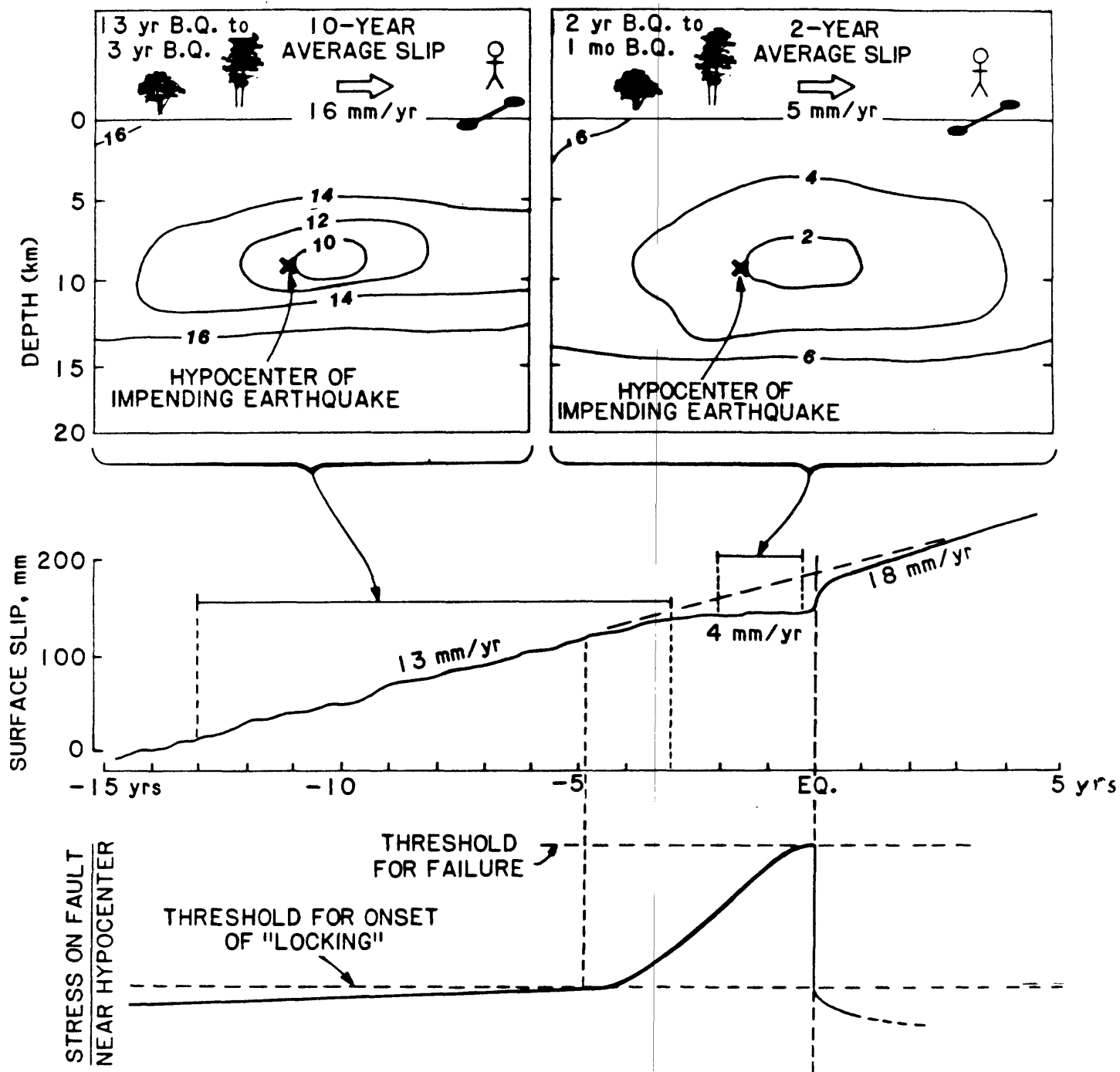


Figure 7.

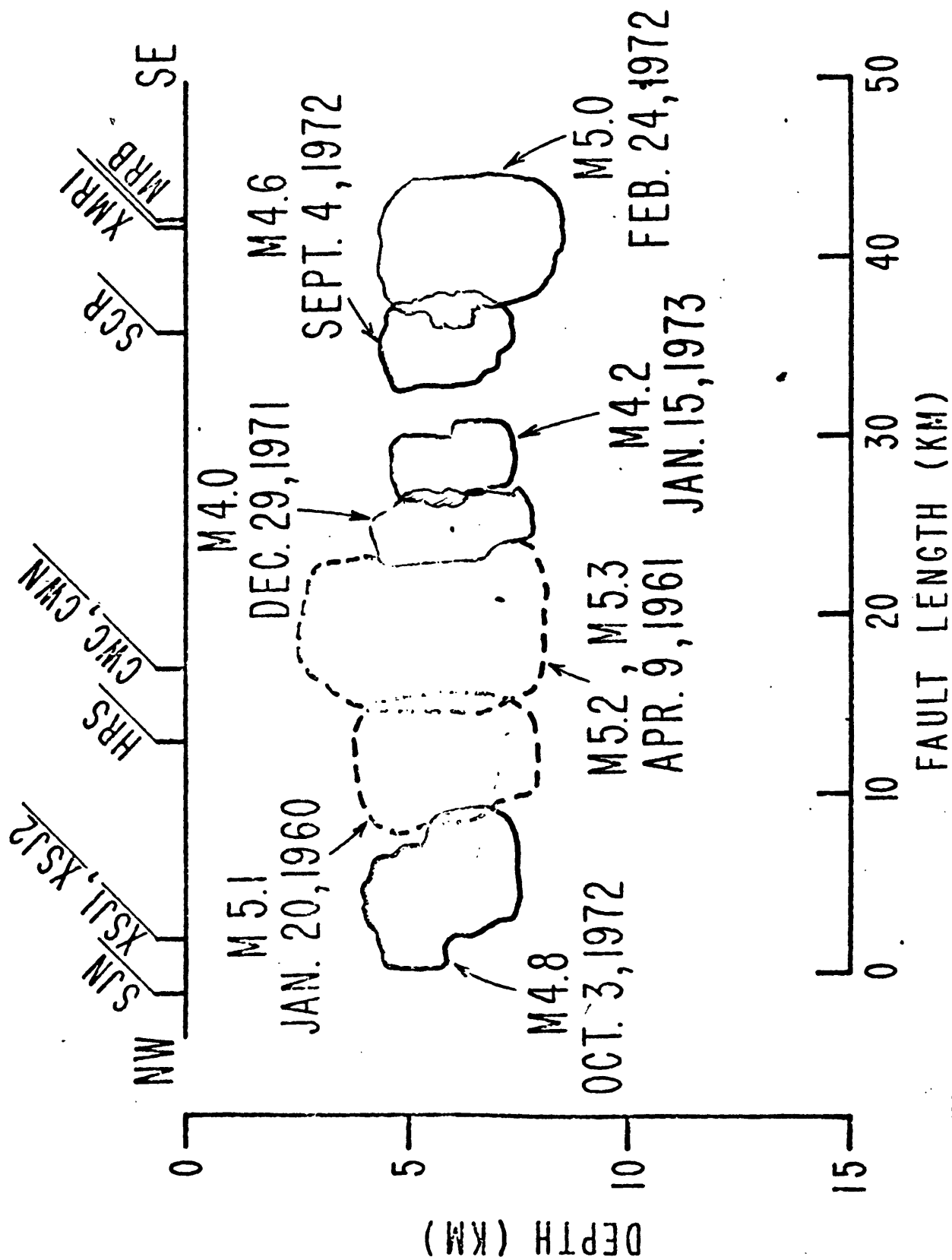


Figure 8.

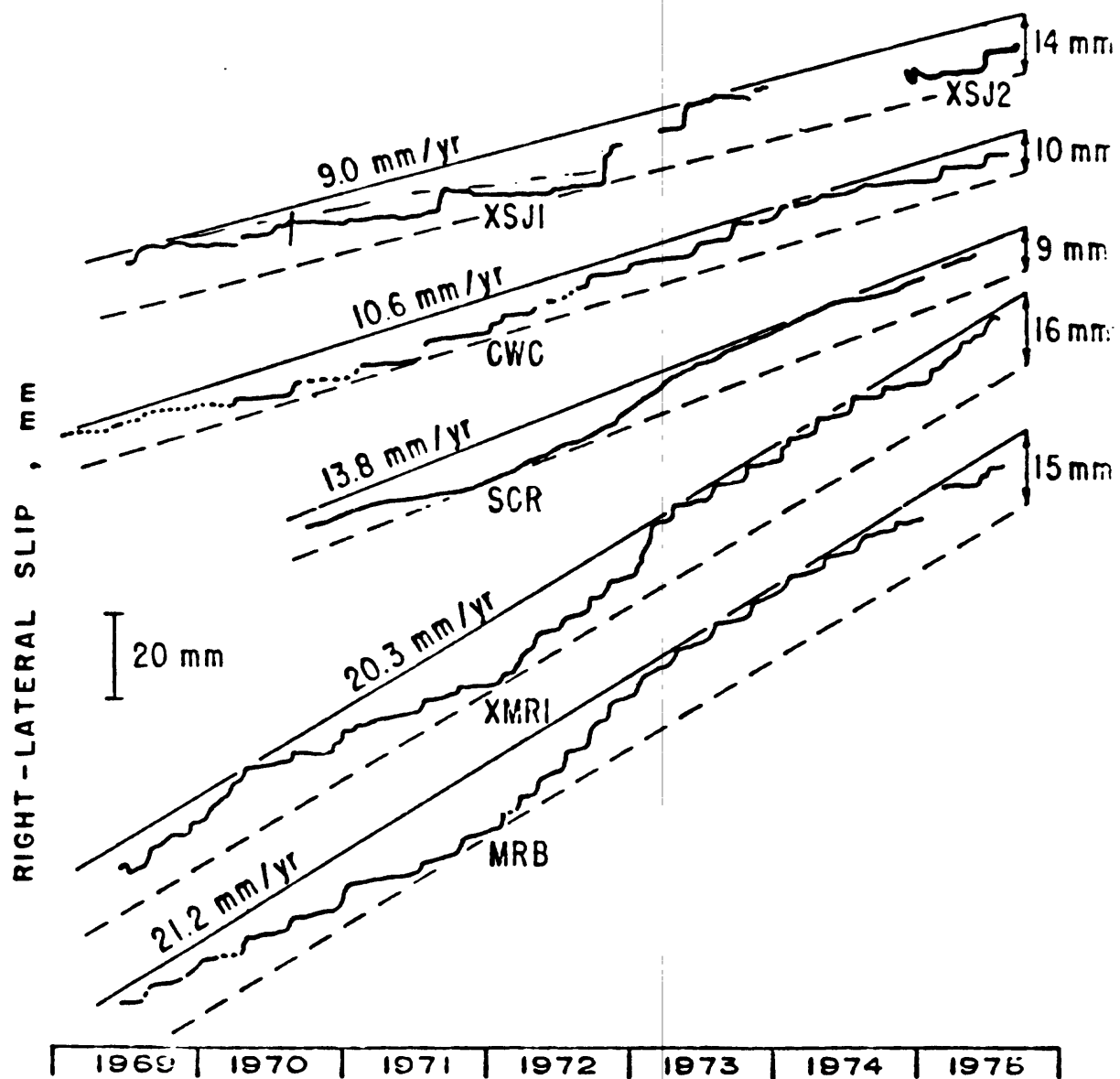


Figure 9.

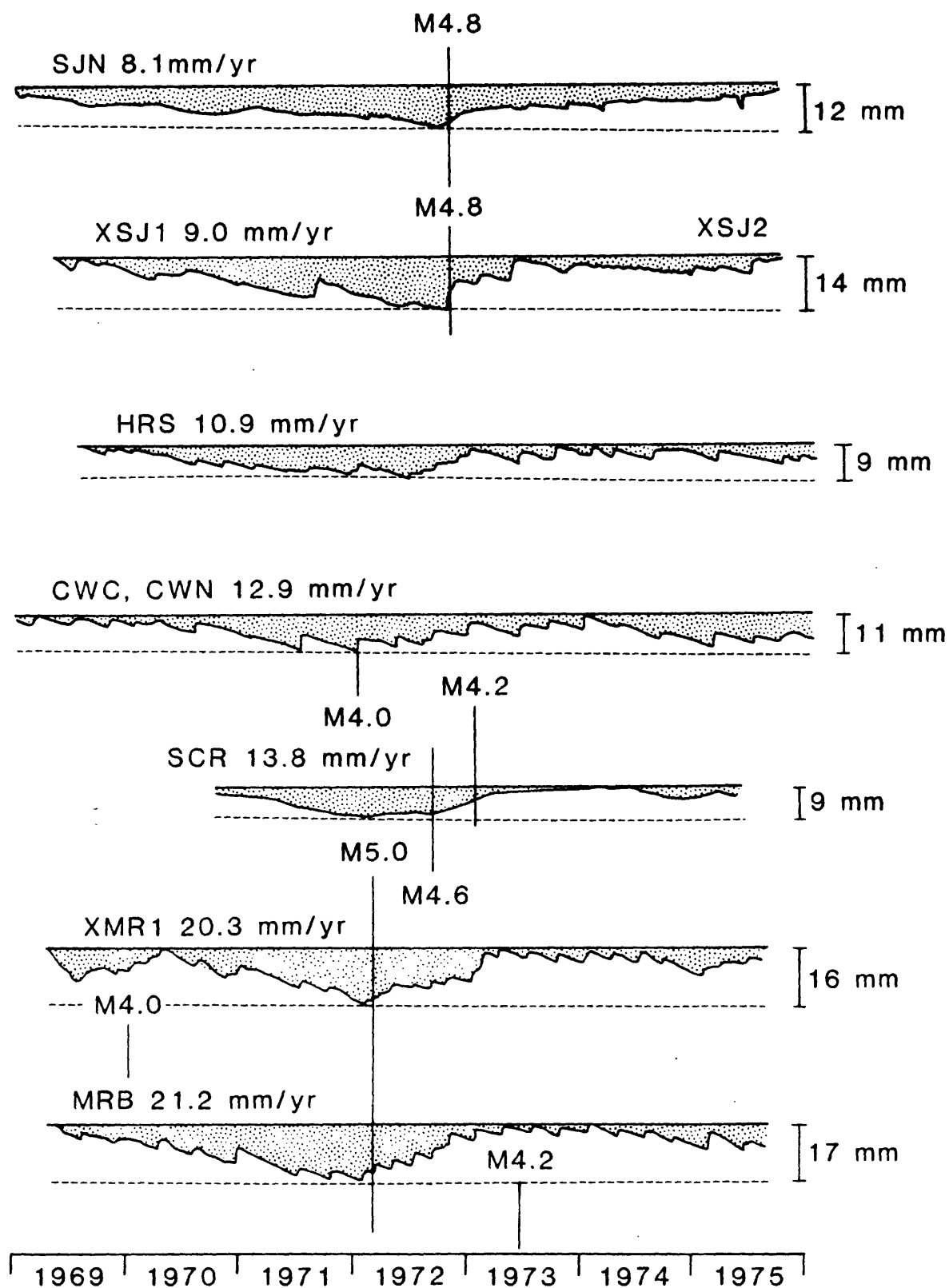


Figure 10.

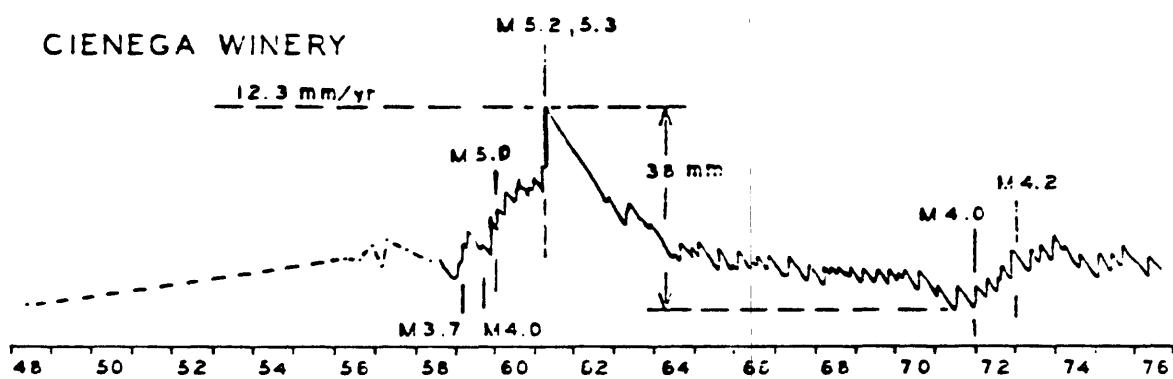


Figure 11a.

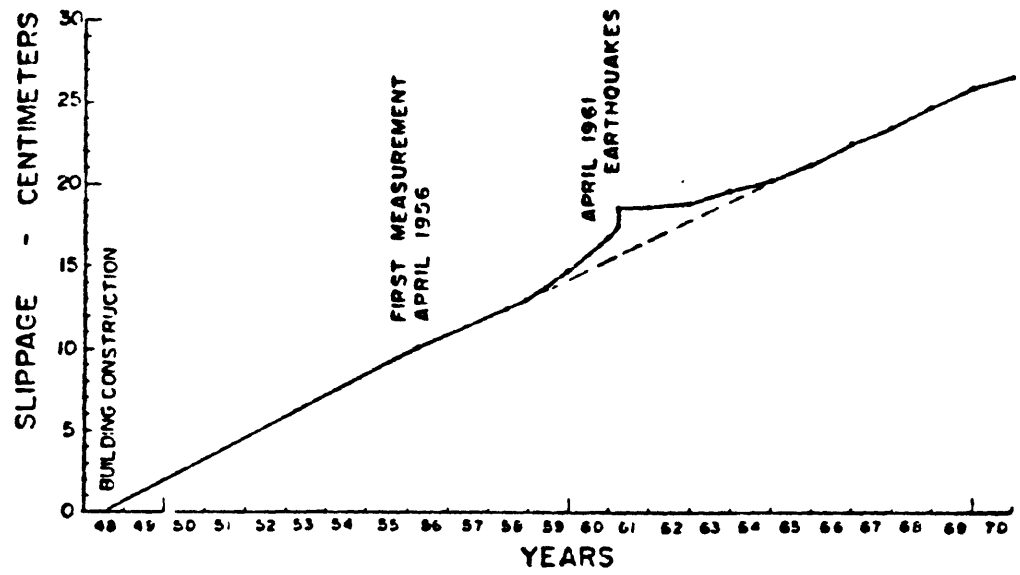


Figure 11b.

(AFTER NASON, 1973)

APPENDIX A. 19.

Seismicity of the San Andreas Fault from Cienega
Winery to the Golden Gate

J. Olson and A. G. Lindh

NEPEC San Francisco Bay Area Workshop, Menlo Park, July 27, 1985.

Seismicity of the San Andreas Fault from Cienega Winery to the Golden Gate
Jean Olson and Allan Lindh

While the 1906 break is generally considered to be locked at present, it produces some low-level microearthquake activity between Corralitos and the latitude of the Golden Gate. In order to further our understanding of the behavior of this part of the fault, we carefully relocated the USGS Central California Microearthquake Network (CALNET) catalog of microearthquakes along the San Francisco Peninsula and analyzed that seismicity in detail.

Figure 1 is a map showing the well-located microearthquake epicenters in the San Francisco Bay area during 1969-80. The epicenters along the Peninsula are from our catalog of relocated earthquakes and the remainder are from routine CALNET locations.

Our relocated epicenters indicate that the San Andreas fault seismicity on the Peninsula occurred in three zones: most of the microearthquakes on the Peninsula occurred in the 1906 epicentral area between Crystal Springs Reservoir and the latitude of the Golden Gate (zone SF in Figure 2). The largest event on the Peninsula since the 1906 aftershocks, the 1957 M5.3 Daly City earthquake (Figure 3), and the largest event on the Peninsula since 1969, a M4.4 event in 1979, occurred within this zone at the same location. A second concentration of activity occurred in the mid-Peninsula near Portola Valley (zone PA in Figure 2). We found that most of this activity is located off the San Andreas fault trace. Many of these events occurred in swarms. A third concentration of microearthquakes occurred at the junction of the San Andreas and Sargent faults (zone SC in Figure 2).

We determined fault-plane solutions for well-recorded events in our relocated catalog of events along the Peninsula, shown in Figure 4. Right-lateral strike-slip solutions in general alignment with the San Andreas fault trace are associated with some events along the San Andreas fault on the northern part of the Peninsula, near Portola Valley, and near the San Andreas-Sargent fault junction. In contrast, many of the events located off the fault are associated with thrust or reverse solutions.

Figure 2 serves as a key to the series of hypocenter cross-sections shown in Figure 5. This map also shows the profuse subsidiary Quaternary faults that have been mapped along the peninsula in the Santa Cruz Mountains. The microearthquake activity east of the San Andreas fault can be associated with small thrust faults, but in the case of the microearthquake swarms that occurred west of the San Andreas fault in the mid-Peninsula for which some thrust/reverse fault-plane solutions were also determined, no clear spatial association with mapped surface faults can be made.

The activity directly beneath the San Andreas fault trace on the Peninsula (zones SF, PA, and SC in Figure 5) is located 5-15km deep and a peak in the focal depth distribution (Figure 6) occurs at 10km depth. In contrast, the dense concentration of activity southeast of San Juan Bautista (25-45km on the longitudinal cross-section for zone SJB in Figure 5) occurred along the entire portion of the fault above 10km depth. A peak in the depth distribution for events in zone SJB (Figure 6) occurs between 4-5km depth. Focal depths increase with increasing distance northwest of the transition zone beneath San Juan Bautista.

Figure Captions

Figure 1. Map showing well-located epicenters of earthquakes in the San Francisco Bay area during 1969-80. USGS Central California Microearthquake Network (CALNET) locations are shown except along the San Francisco Peninsula north of about 37°N latitude (within the polygon shown in Figure 4), where epicenters were relocated with an improved velocity model and station corrections, described in Olson (in press).

Figure 2. Map showing relocated microearthquake epicenters along the southern part of the 1906 break. Those located near San Juan Bautista are from Moths et al. (1981). Faults are reproduced from the Fault Map of California (Jennings, 1975).

Figure 3. Epicenter map of earthquakes ($M \geq 5$) during 1855-1980, after Ellsworth et al. (1981).

Figure 4. Map showing preliminary fault-plane solutions determined from P-wave first-motions for well-observed events along the San Francisco Peninsula during 1969-80. The solutions are lower-hemisphere projections with shaded quadrants indicating compressional first-motions. Larger diameters indicate solutions with better constrained nodal planes.

Figure 5. Cross-sections of hypocenters shown in Figure 4, oriented along, and transverse to, the San Andreas fault; the fault trace is located at 0 km on the transverse sections.

Figure 6. Histograms of focal depths of events in each of the zones delineated in Figure 4.

References

Ellsworth, W. L., Lindh, A. G., Prescott, W. H., and Herd, D. G., 1981: The 1906 San Francisco earthquake and the seismic cycle, In Simpson, D. W., and Richards, P. G. (Editors): Earthquake Prediction: An International Review. Am. Geophys. Union, Maurice Ewing Series 4: 126-140.

Jennings, C. W. (Compiler). 1975: Fault map of California with locations of volcanoes, thermal springs, and thermal wells. California Division of Mines and Geology, California Geologic Data Map Series I, scale 1:750,000.

Moths, B. L., Lindh, A. G., Ellsworth, W. L., and Fluty, L., 1981: Comparison between the seismicity of the San Juan Bautista and Parkfield regions, California (abstr). EOS, Am. Geophys. Union Transactions 62: 958.

Olson, J. A.,: Seismicity of the San Andreas fault zone in the San Francisco peninsula area, California, In Proceedings of the International Symposium on Recent Crustal Movements in the Pacific Region: Bull. Roy. Soc. N.Z., (in press).

SAN FRANCISCO BAY AREA SEISMICITY 1969 - 1980

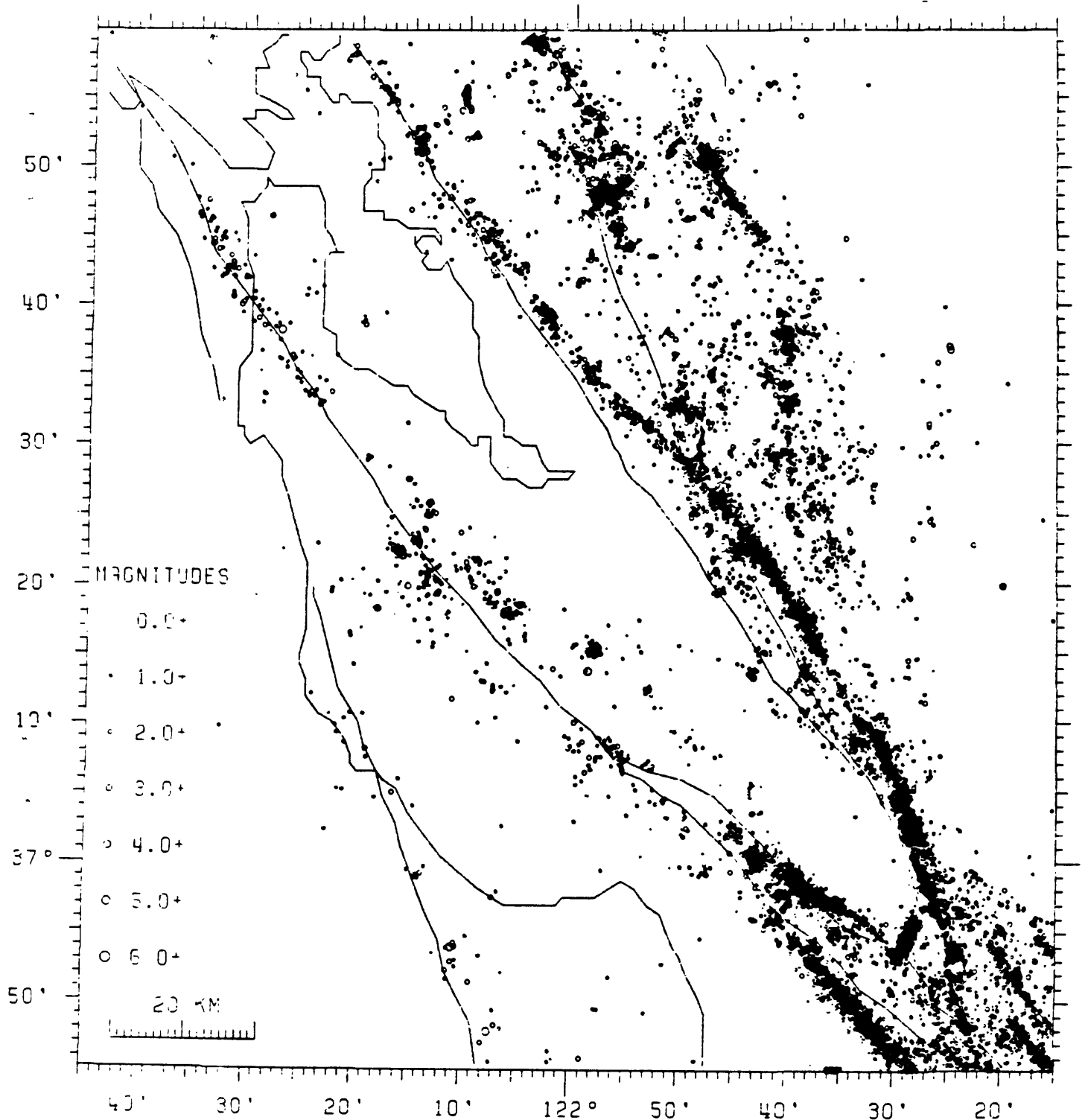


Figure 1.

1969 - 1980

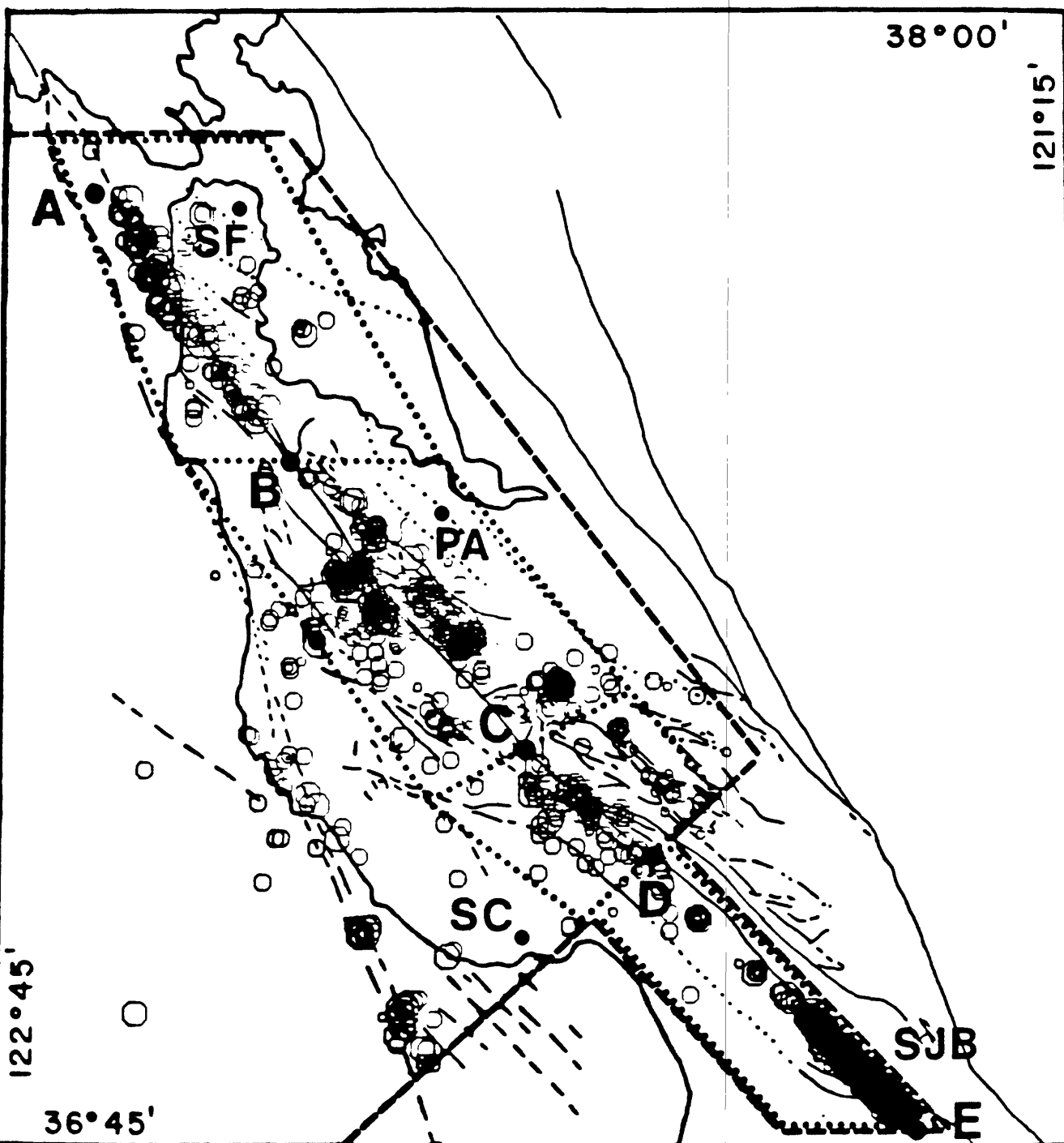


Figure 2.

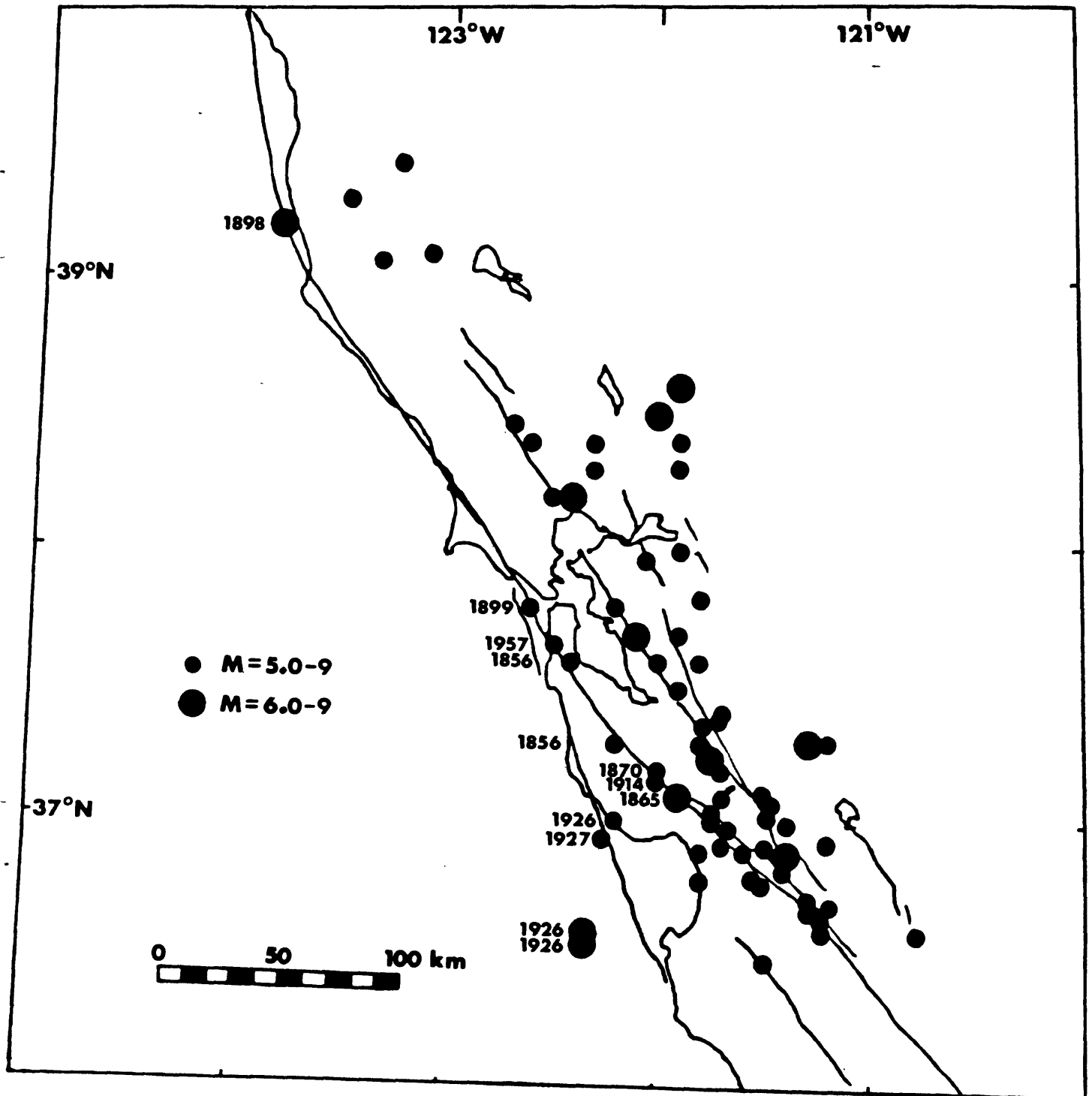


Figure 3.

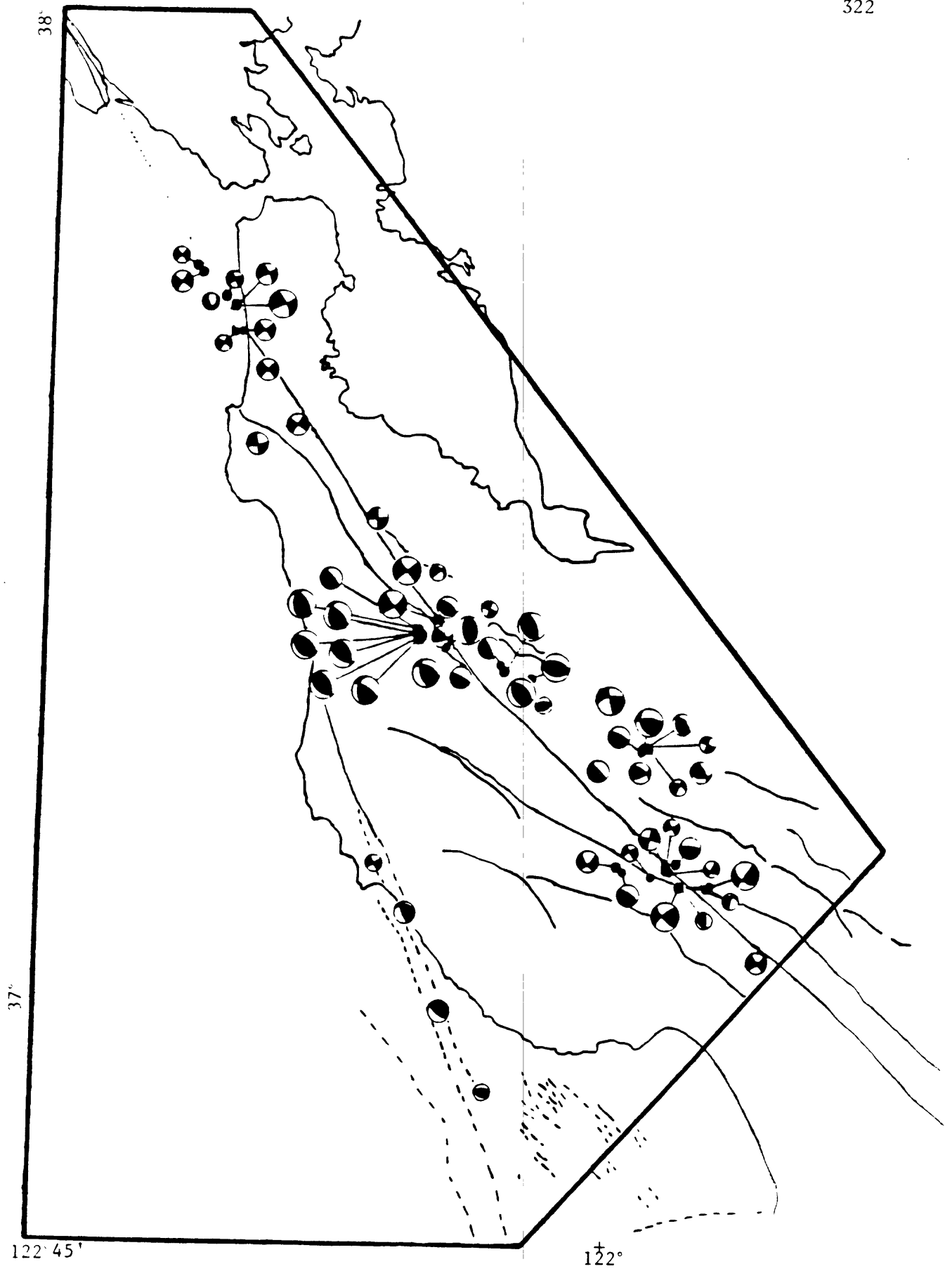


Figure 4.

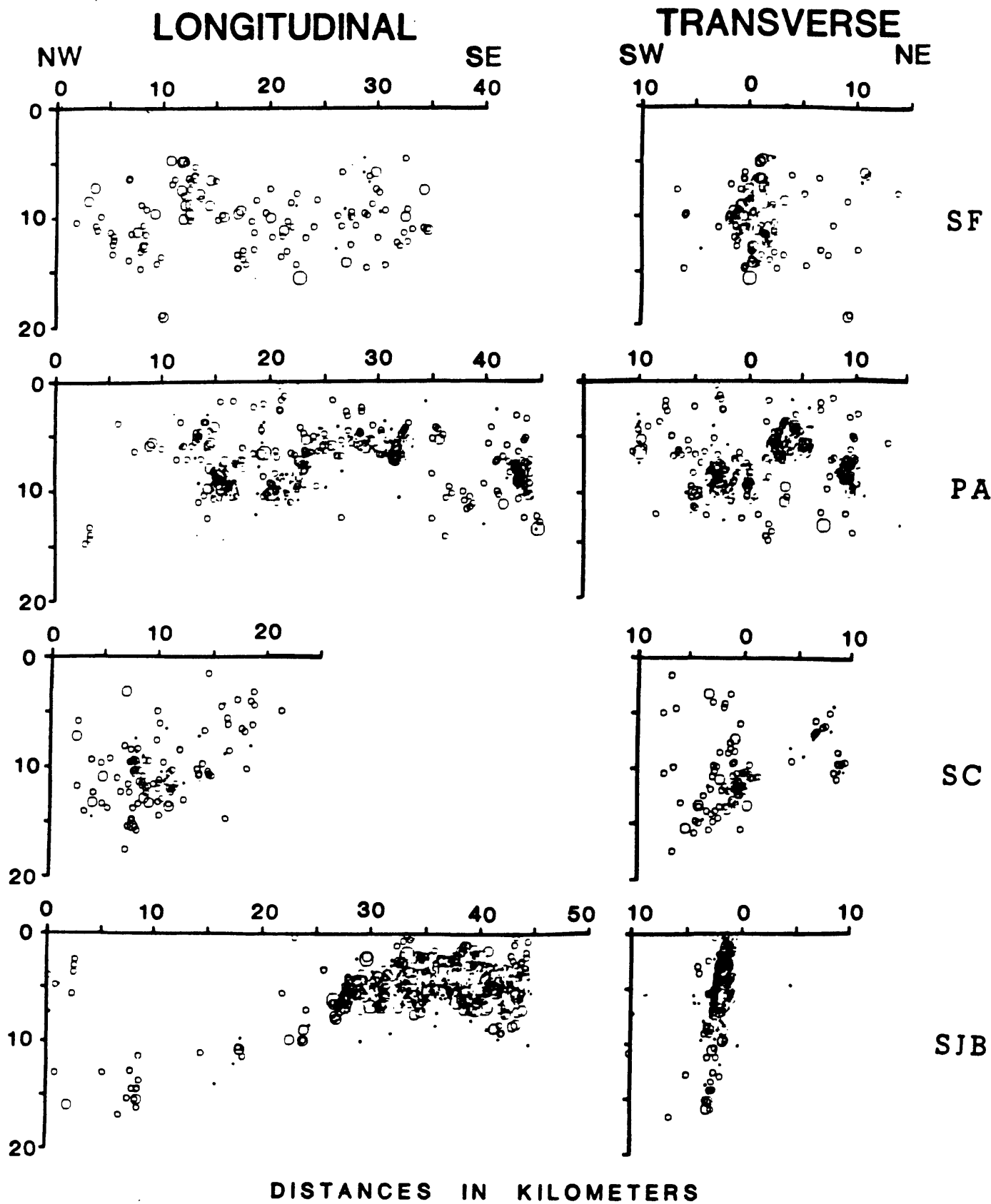


Figure 5.

NUMBER vs DEPTH

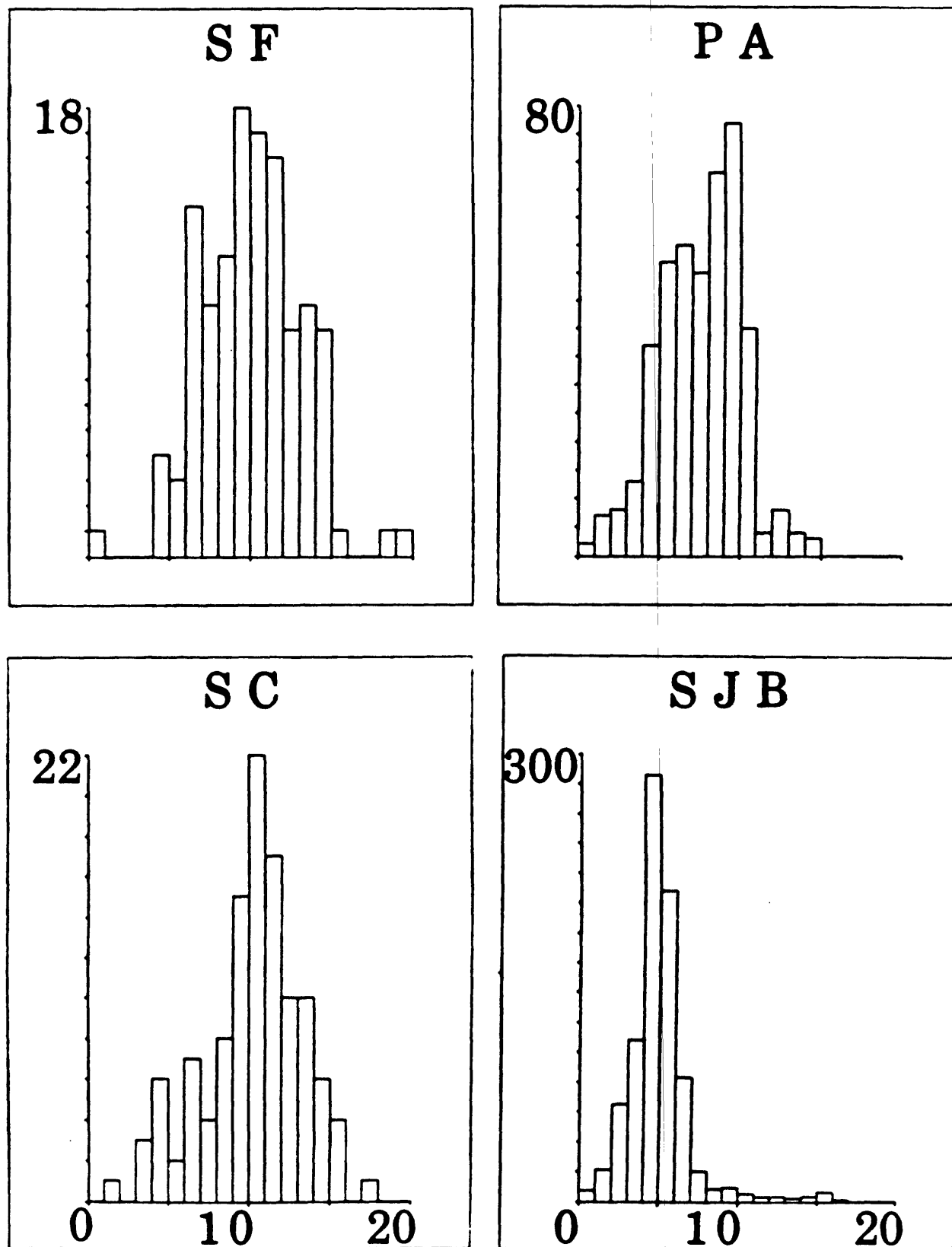


Figure 6.

APPENDIX A. 20.

Seismic Hazard from the Southern Segment of the
1906 Rupture, California

C. H. Scholz

Seismic Hazard from the Southern Segment of the
1906 Rupture, California

C. H. Scholz

Lamont-Doherty Geological Observatory
and Department of Geological Sciences of Columbia University
Palisades, New York 10964

Several workers have independently assessed the seismic hazard expected for the next few decades due to rupture of known seismic gaps of the San Andreas fault system [Lindh, 1983; Sykes and Nishenko, 1984; Scholz 1985]. All concluded that the southern end of the 1906 rupture, which slipped only 1-1.4 m in 1906, has a high conditional probability of rupturing again within the next 20 years.

Lindh [1983], in considering that fault segment, concluded that the most likely part to rupture in a single earthquake was the 45 km segment from Wright, where a railroad tunnel was offset 1.4 m 1906, to San Juan Bautista, which would be expected to rupture in a $M_s = 6.5$ earthquake. Sykes and Nishenko [1984] calculated a 60% conditional probability that this fault segment would rupture in the next 20 years, which is the highest probability estimate they made for any section of the San Andreas fault other than Parkfield. They were less definitive than Lindh concerning the northernmost extent of this potential rupture zone, saying only that it extended to about San Jose, but they pointed out that a more precise determination of the northern extent of this potential rupture was very important from the standpoint of seismic risk. This is because Wright, which is where

the San Andreas fault crosses U.S. Route 17, divides the fault into two distinct risk provinces. To the south of Wright the fault traverses a region of very sparse population, whereas to the north it is adjacent to the highly developed Santa Clara Valley.

Fault offsets produced by the 1906 earthquake in the zone from Crystal Springs Reservoir to San Juan Bautista are shown in Figure 1 (data from Lawson [1908]). The reduction in slip from the 3-4 m typical of the rupture over most of its extent NW of this point occurs abruptly between Alpine Rd. and Page Mill Rd., SW of Palo Alto. Page Mill Rd. is 30 kms NW of Wright, so that if this marks the northern end of the slip deficit region of the 1906 earthquake it would substantially increase the size of an expected earthquake on that section of the fault over that suggested by Lindh [1983] and would greatly increase the expected damage from such an event.

The three data points between Page Mill Rd. and Wright, though consistent with reduced slip on that section, are considered to be of poor quality and hence not definitive. At Page Mill Rd., however, the fault crosses the road in a well defined trough, and fences on both sides of the road were observed to be offset 0.9 m in 1906. The question that remains, however, is how slip could be so drastically reduced between Alpine Rd. and Page Mill Rd., which are only 5 kms apart.

In Fig. 2 is shown a map of the southern part of the 1906 rupture. Alpine Rd. and Page Mill Rd. are at either end of an abrupt bend in the San Andreas fault at Black Mountain (BM) which delineates the northern end of a 100 km segment that strikes 9° more E-W than the fault to the north or south. Since the 1906 rupture propagated toward

this bend from the north, the bend at Black Mt. would act as a compressional restraint on rupture, which often has an inhibiting effect [King and Nabelek, 1985].

The Black Mtn. bend occurs just between Alpine Rd. and Page Mill Rd. (Figure 3). Black Mountain marks a major change in the physiographic expression of the fault, which to the NW follows a well defined linear fault valley on the San Francisco Peninsula and to the SE follows a poorly defined trace that traverses the rugged Santa Cruz Mts. Two faults, the Pilarcitos fault and the Black Mtn. fault splay symmetrically from the fault bend (Fig. 3). According to the Lawson [1908] report, the wedge in the interior of the bend between the Black Mtn. fault and the San Andreas fault was intensively shattered in 1906, with some minor faulting possibly occurring on the Black Mtn. fault. This type of deformation is suggestive that Black Mtn. acted as a major asperity on the fault and produced the major reduction of slip as observed at Page Mill Rd.

We therefore conclude that the slip deficit region in the 1906 earthquake extended from Black Mtn. to San Juan Baustista. If this entire 75 km segment ruptures in a single earthquake we can expect, using a simple scaling law [Scholz, 1982] the following parameters of this earthquake: $u=92$ cm, $M_0=3 \times 10^{26}$ dyne-cm, $M_s=6.9$. This earthquake would then be about 3 times larger than the one proposed by Lindh [1983] and moreover constitute a far greater risk since it would propagate 30 kms to the NW, adjacent to the highly developed Santa Clara Valley.

Since this fault segment slipped 1-1.4 m in 1906, and this section of fault moves at a geological rate of about 12 mm/yr [Hall,

1984] and is presently accumulating strain at about 15 ± 2 mm/yr [Prescott et al., 1985] we can estimate that it would take 60-110 yrs to re-accumulate the strain dropped in 1906. Hence we are presently about midway within a time window in which we can expect this zone to rupture. The conditional probability of this earthquake occurring in the next 20 years is the same as that estimated for the smaller event by Lindh (1983) and Sykes and Nishenko (1984).

References

- Hall, N.T., Holocene history of the San Andreas fault between Crystal Springs Reservoir and San Andreas Dam, San Mateo Co., Calif., Bull Seismol. Soc., Amer., 79, 281-299, 1984.
- King, G.C.P. and J. Nabelec, Role of fault bends in the initiation and termination of earthquake rupture, Science, 228, 984-987, 1985.
- Lawson, A.C., The California Earthquake of April 18, 1906 Carnegie Inst., Wash., D.C., 1908.
- Lindh, A.G., Preliminary assessment of long-term probabilities for large earthquakes along selected segments of the San Andreas fault system in California, U.S. Geol. Surv. Open File Report, 83-63, 1-15, 1983.
- Prescott, W.H., N.E. King, M. Lisowski, J.C. Savage, Deformation of the Pacific Plate Near San Francisco, California, subm. Science, 1985.
- Scholz, C.H., Scaling laws for large earthquakes: consequences for physical models, Bull Seismol. Soc., Am., 72, 1-14, 1982.
- Scholz, C.H., Earthquake Prediction and Seismic Hazard, Earthquake Pred. Res., 3, 11-25, 1985.

Sykes, L.R. and S. Nishenko, Probabilities of occurrence of large plate rupturing earthquakes for the San Andreas, San Jacinto, and Imperial Faults, California, 1983-2003, J. Geophys Res., 89, 5905-5927, 1984.

Fig. 1 Fault offset data for the 1906 earthquake: Crystal Springs to San Juan Bautista (from Lawson, 1908). Less reliable data are shown as half-filled circles.

Fig. 2 Map of the southern part of the 1906 rupture on the San Andreas fault. The region discussed in the text is from Black Mountain (BM) through Wright (W) to San Juan Bautista (SJB). Star denotes epicenter of the 1906 earthquake.

Fig. 3 Map of the region of the Black Mountain asperity, showing deformation and slip reported in 1906. Circled numbers are slip (in meters) reported in 1906.

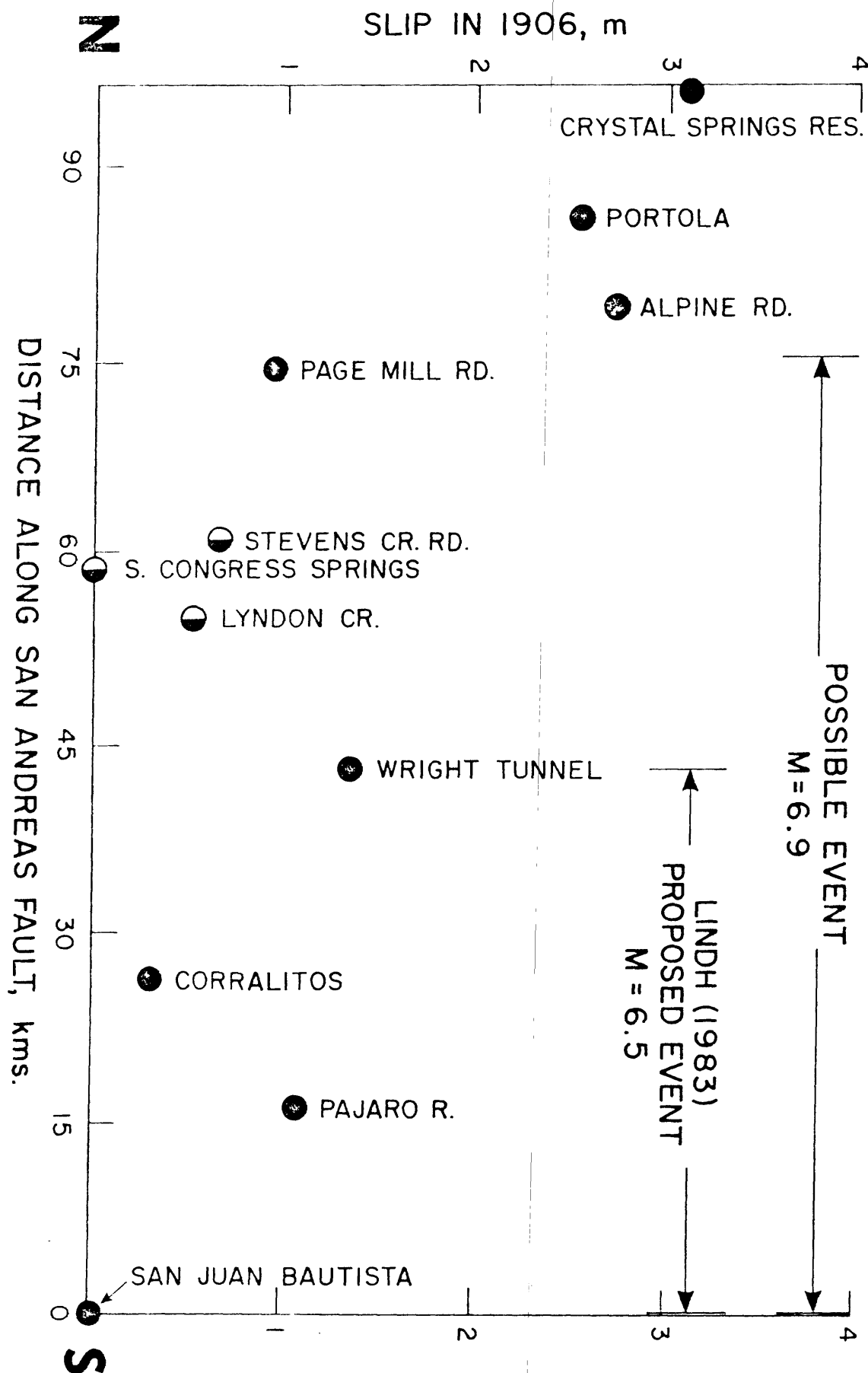


Figure 1.

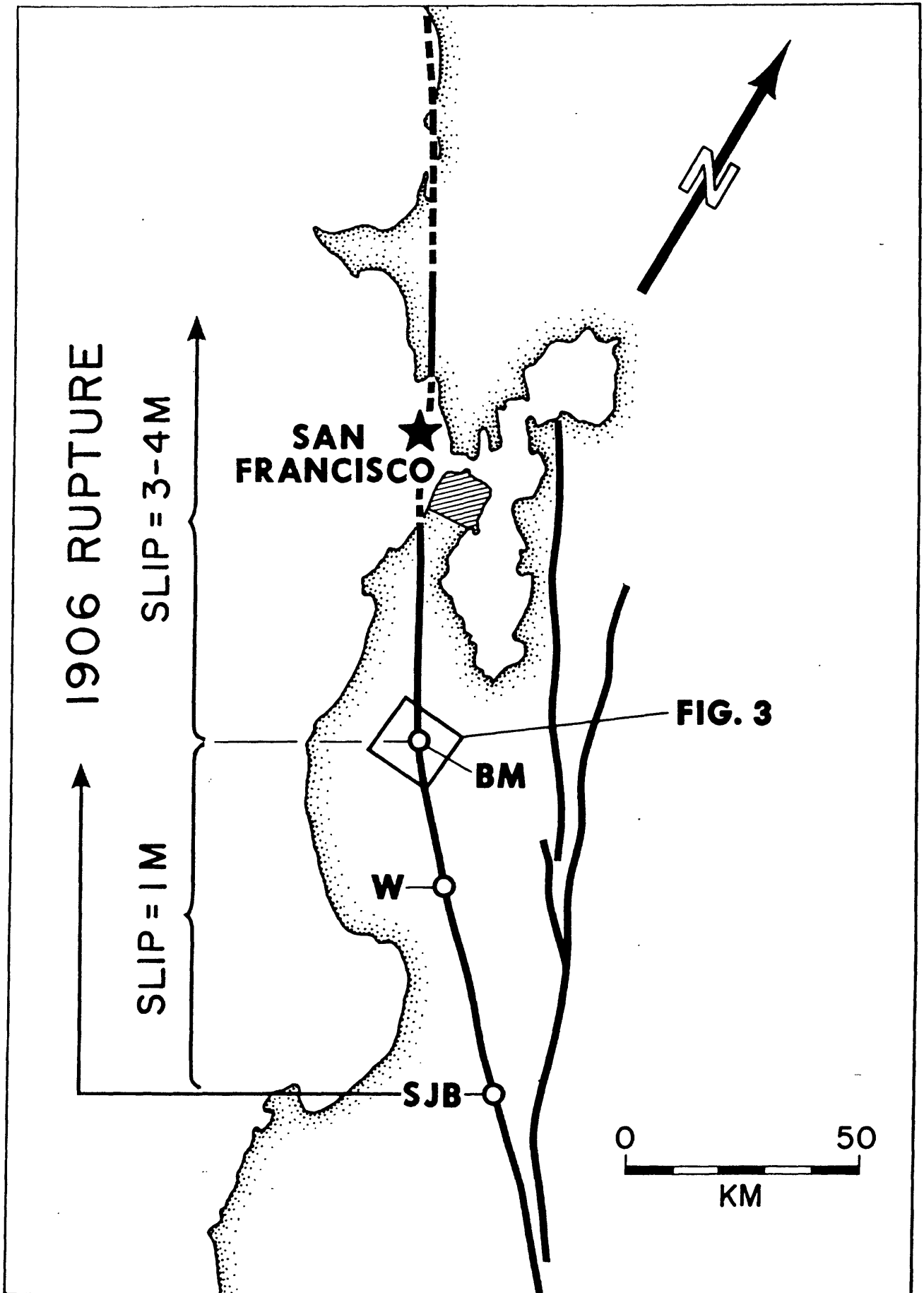


Figure 2.

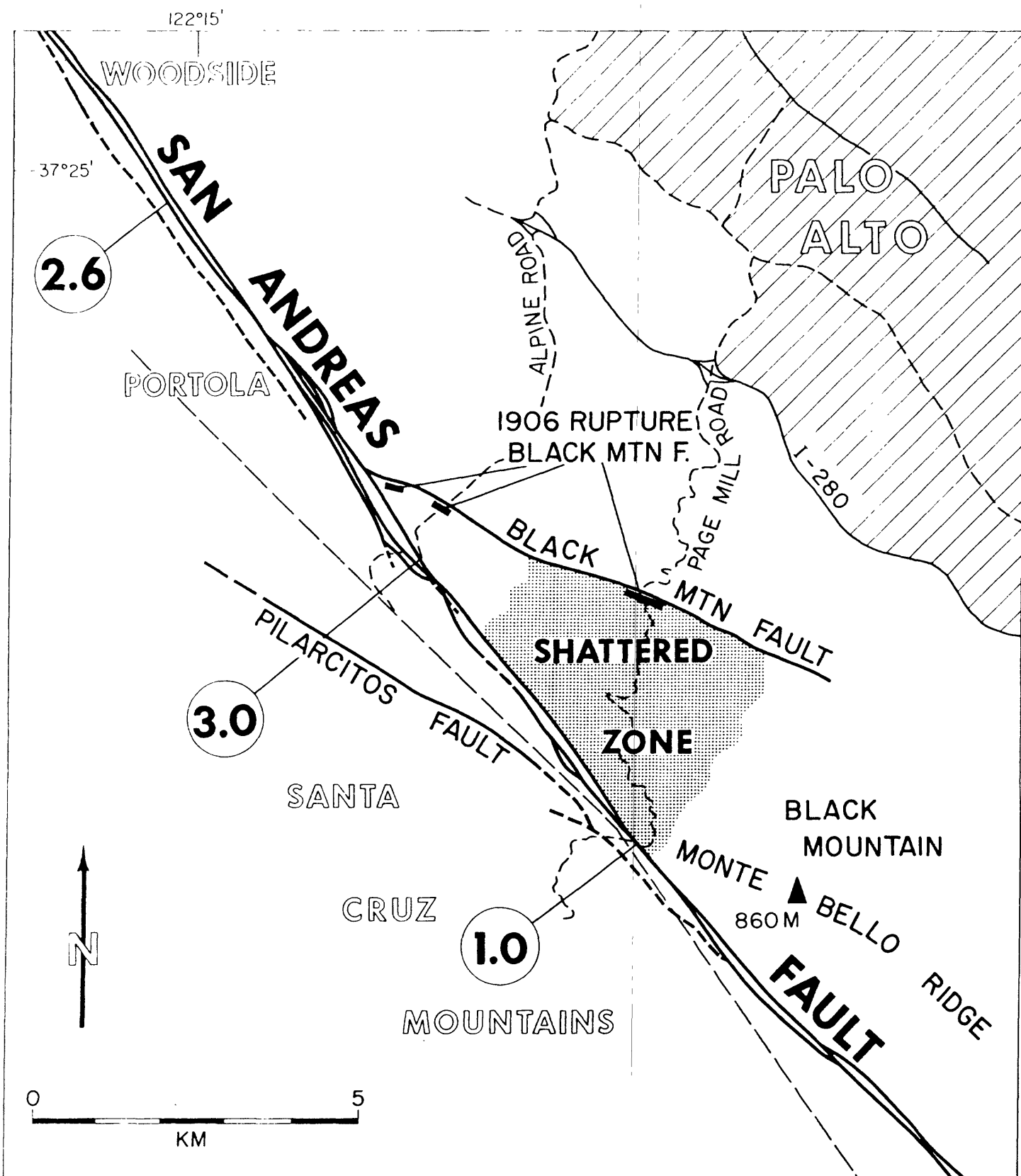


Figure 3.

APPENDIX A. 21.

San Andreas Fault, Central California

K. McNally



CHARLES F. RICHTER SEISMOLOGICAL LABORATORY
EARTH SCIENCES

SANTA CRUZ, CALIFORNIA 95064
(408) 429-4137

27 July 1985

SAN ANDREAS FAULT, CENTRAL CALIFORNIA

(EARTHQUAKE PREDICTION RESEARCH REPORT FOR CEPEC/NEPEC)

KAREN C. McNALLY

Summary of structural and seismicity analyses.

1. Historic data indicate a moderate earthquake, M_L 5.0-5.6, is now ^{*} overdue for the Stone Canyon-Bear Valley region.
2. A Parkfield earthquake, M_L 5.0-5.6 should follow this event by 3.83 ± 2.14 years (range: 1-6 years).
3. Anomalous clustering of seismicity ($M_L = 2.5$), statistically detected, indicates a location for (1) between latitudes $36^\circ 36' - 41^\circ N$, along the San Andreas fault. The last moderate earthquake at this location occurred in 1938, M_L 5.0.
4. Since 1978, an increase in lateral refraction of seismic waves (at the fault plane) is observed at the same location as the clustering. This suggests a time-dependent change in velocity contrast at the fault interface. This refraction was not indicated between 1969 and 1977, at the same location.

* by May, 1984, 1 std dev
by May, 1985, 2 std dev
by May, 1986, 3 std dev

FIGURE 1

CINTRAI SAN ANDRIAS FAULT

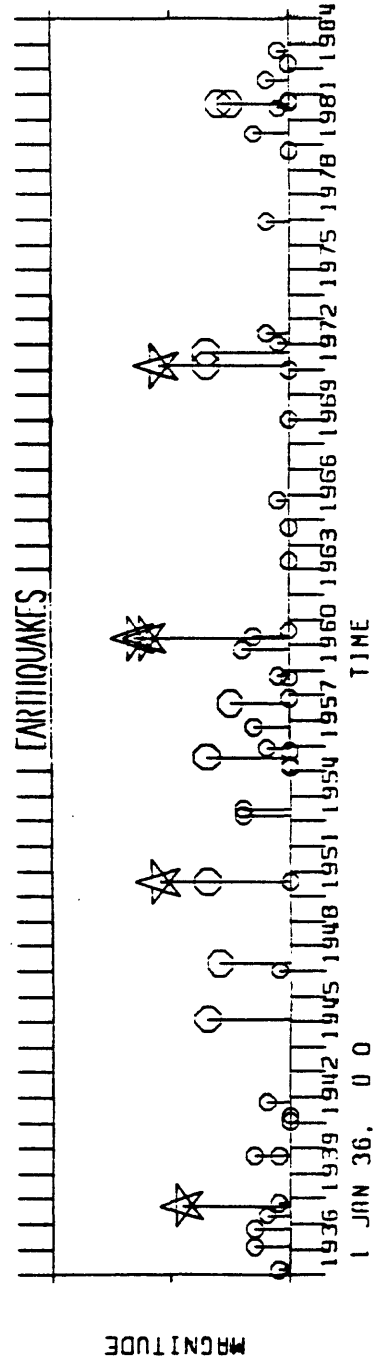
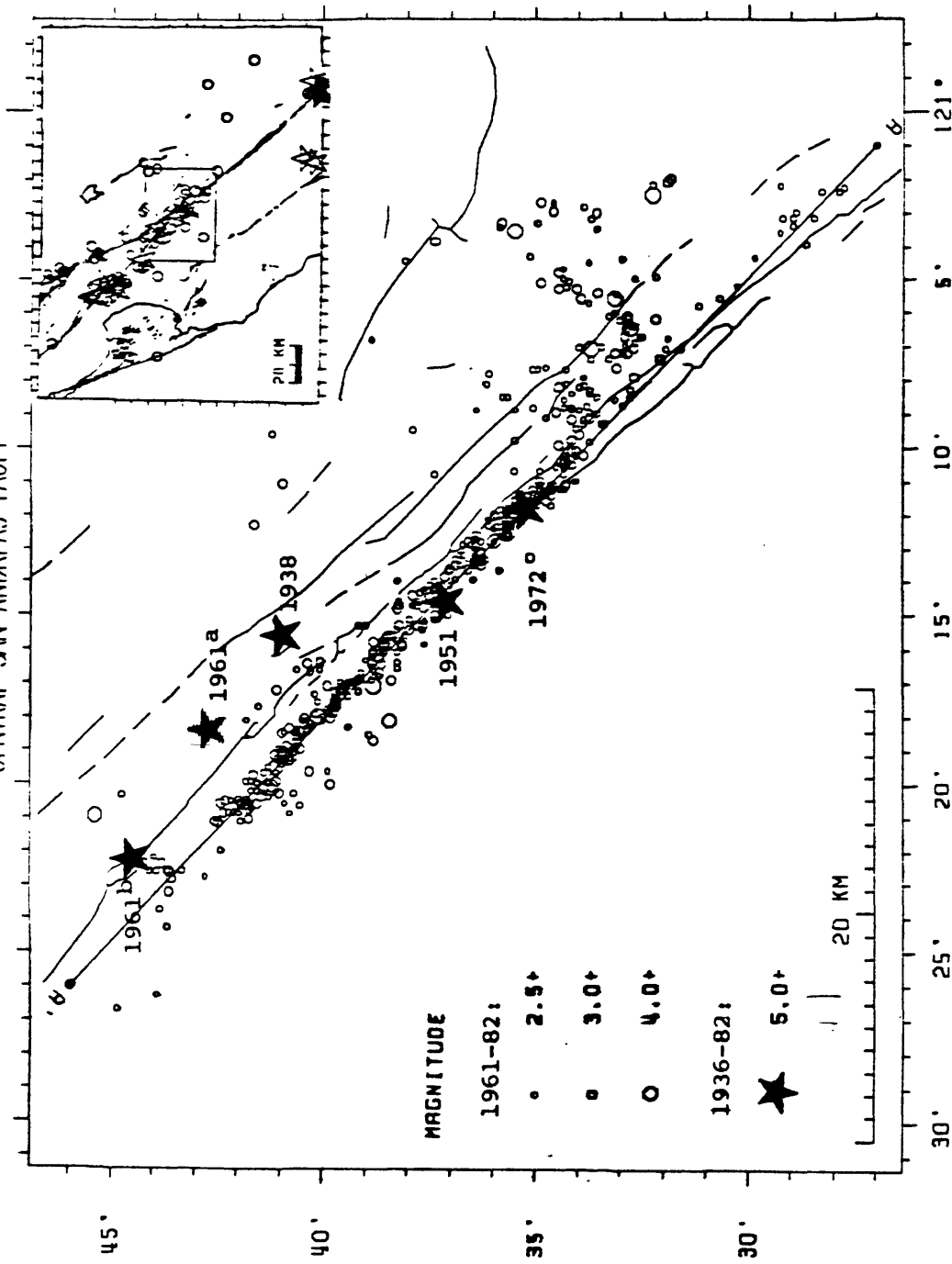
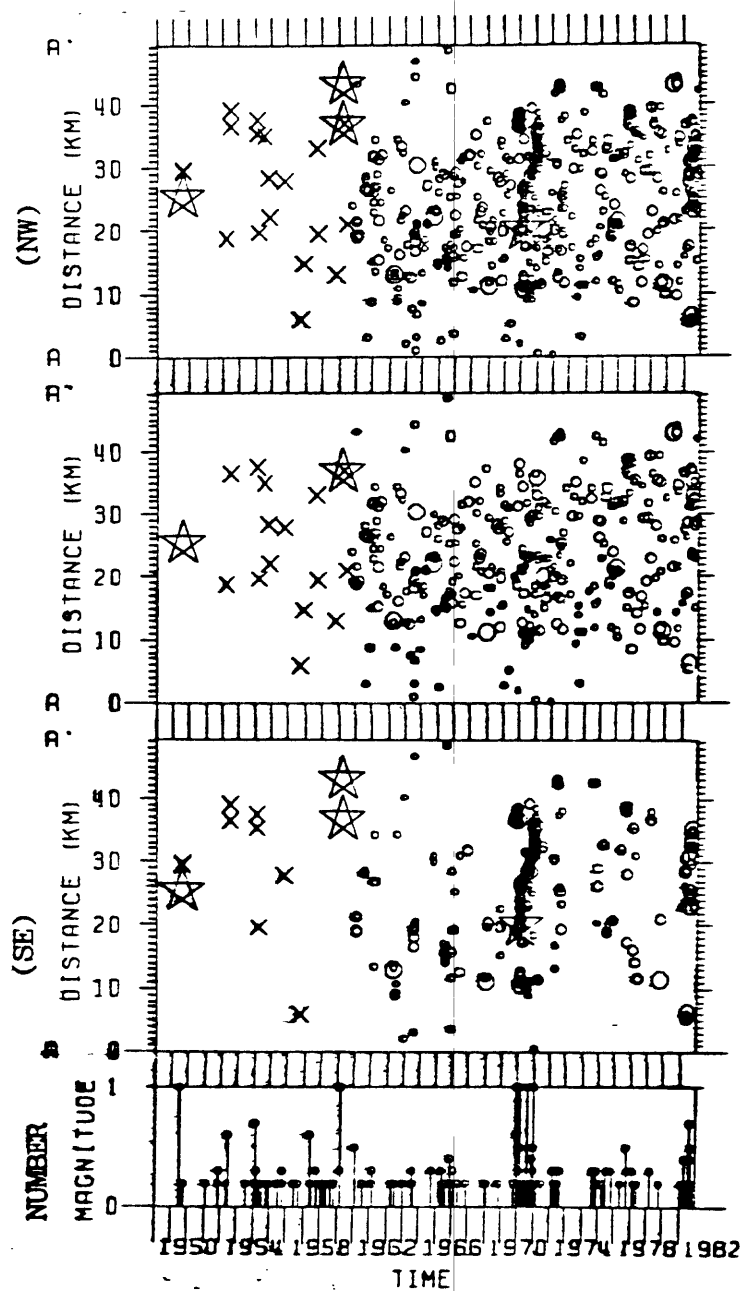


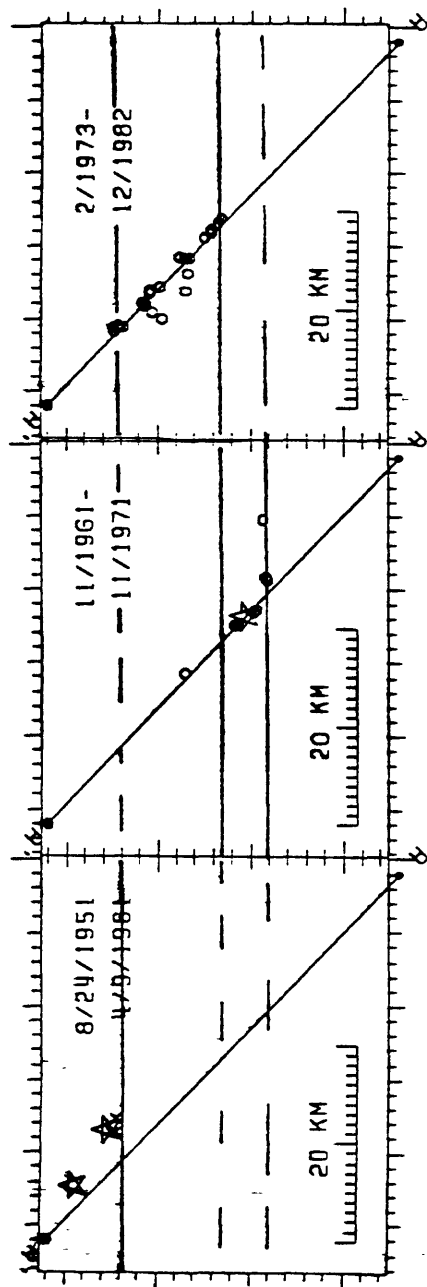
FIGURE 2

SEISMICITY SEPARATED STATISTICALLY

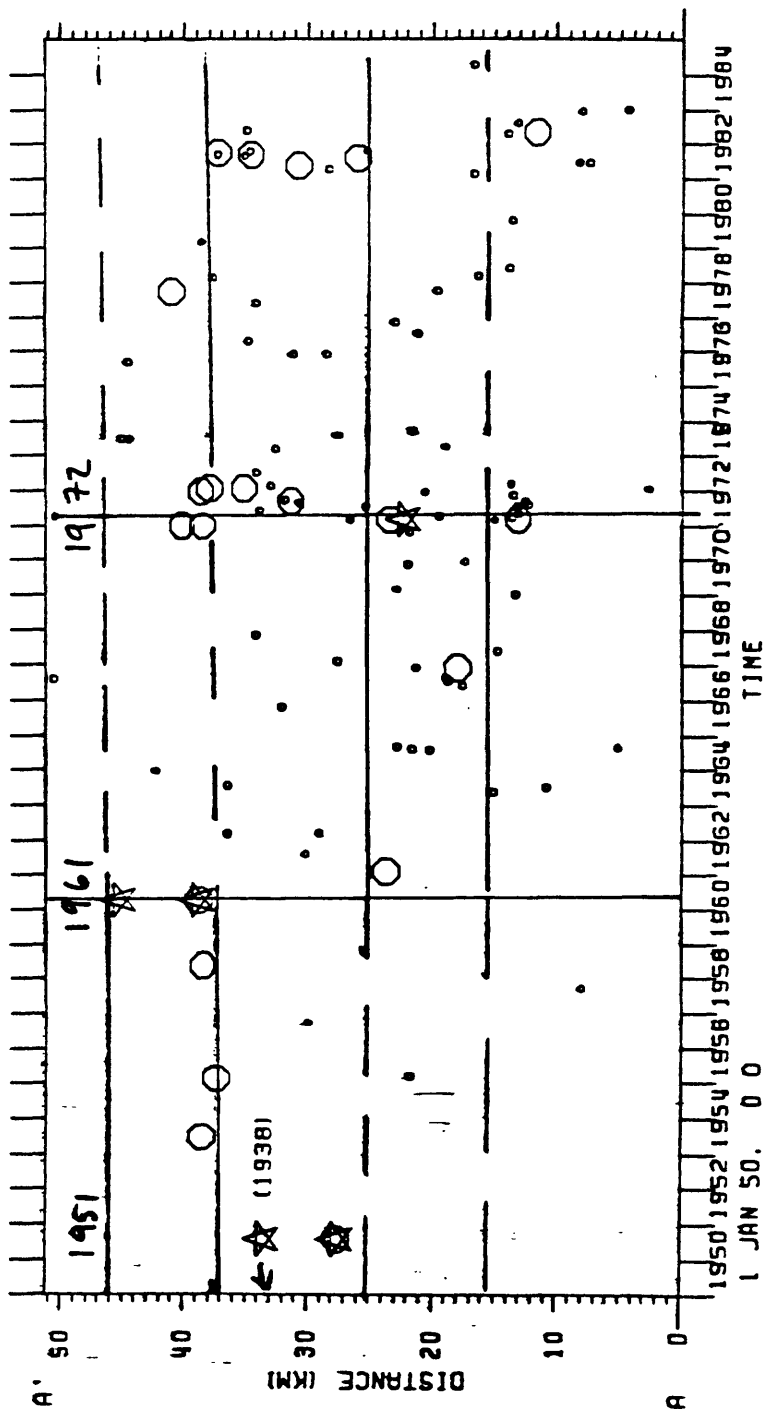


LARGE SEISMICITY CLUSTERS AND MAINSHOCKS

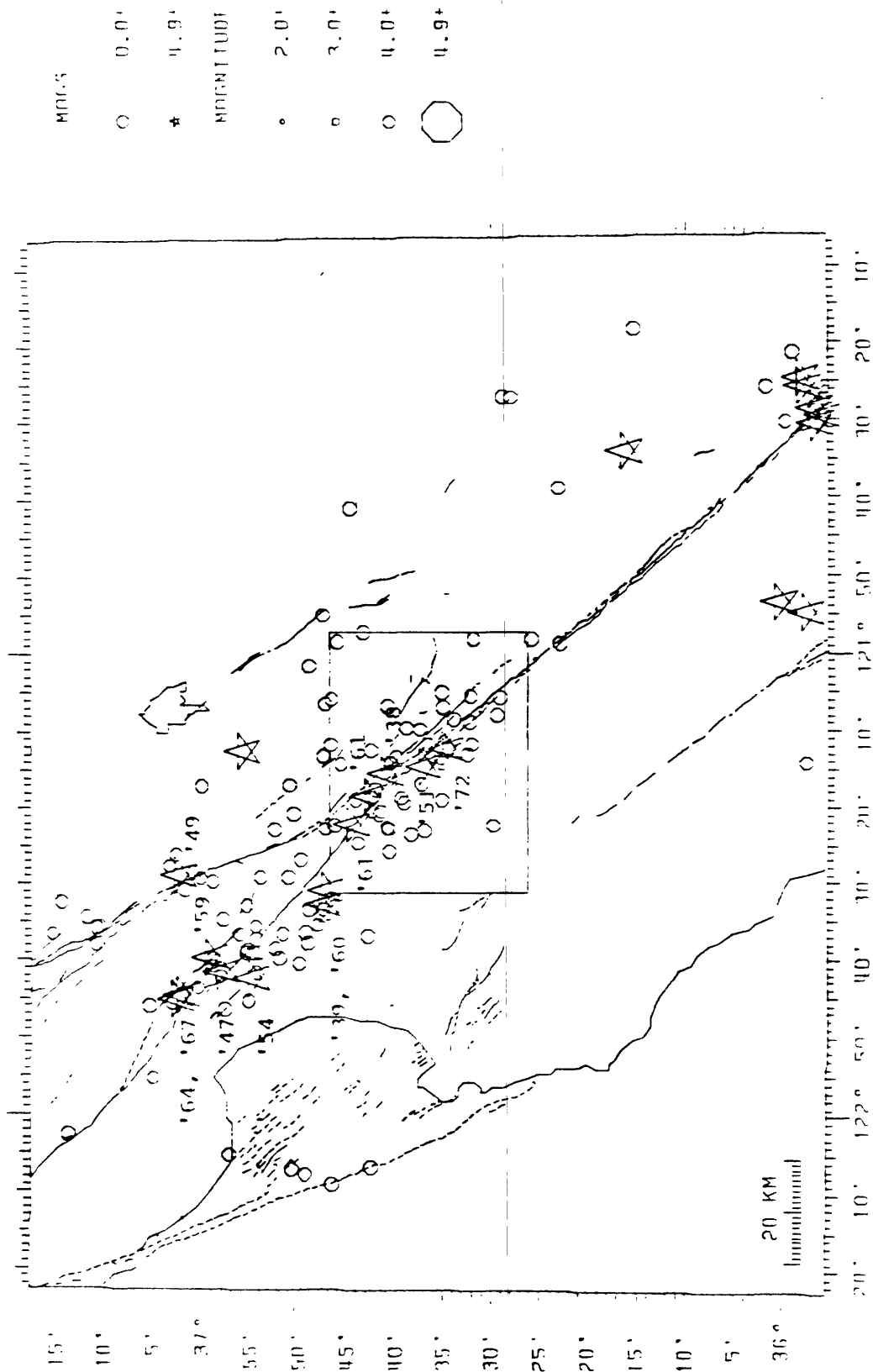
A) LOCATIONS



B) TIMES & POSITIONS



CENTRAL CALIFORNIA EARTHQUAKES



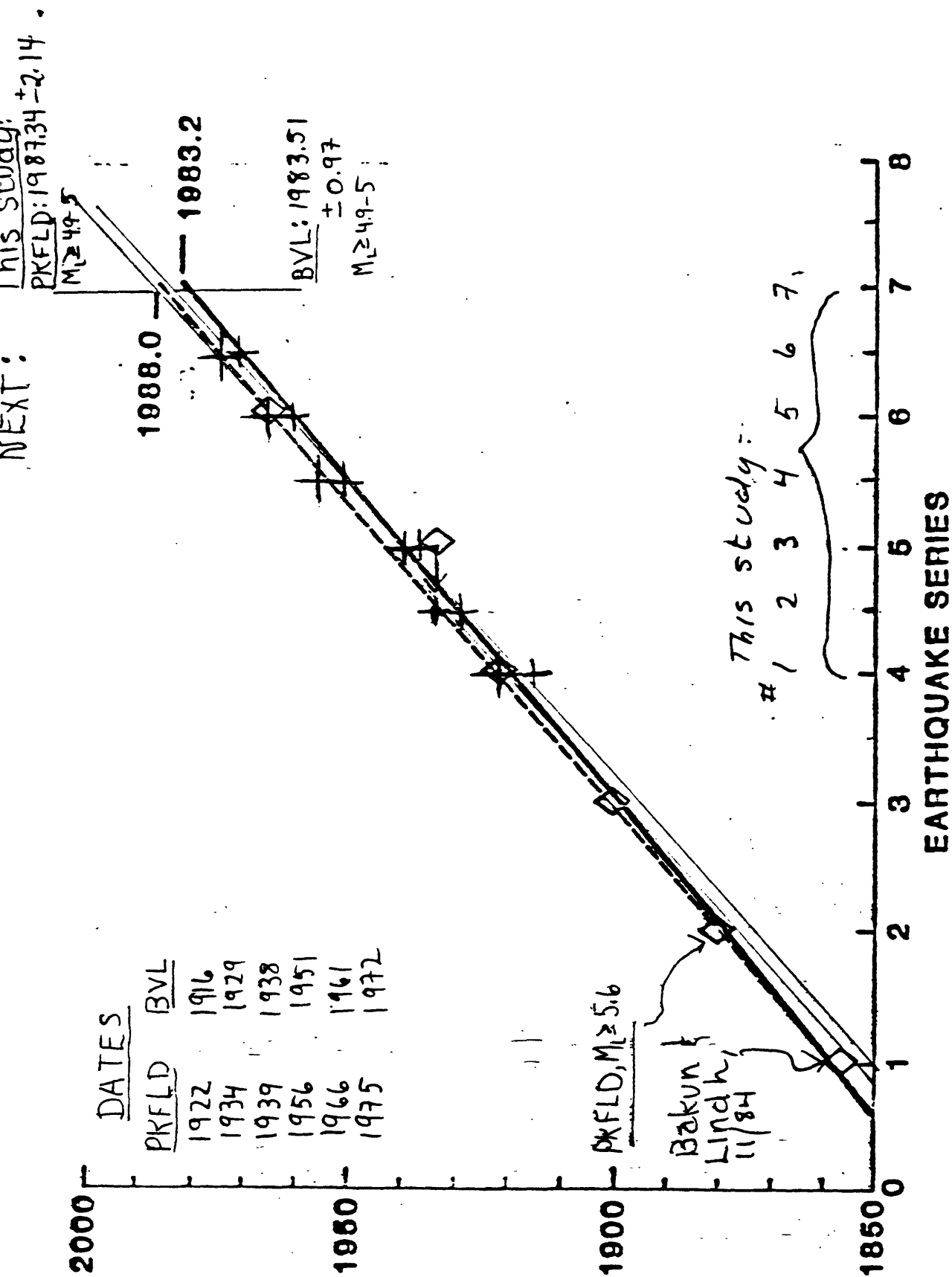
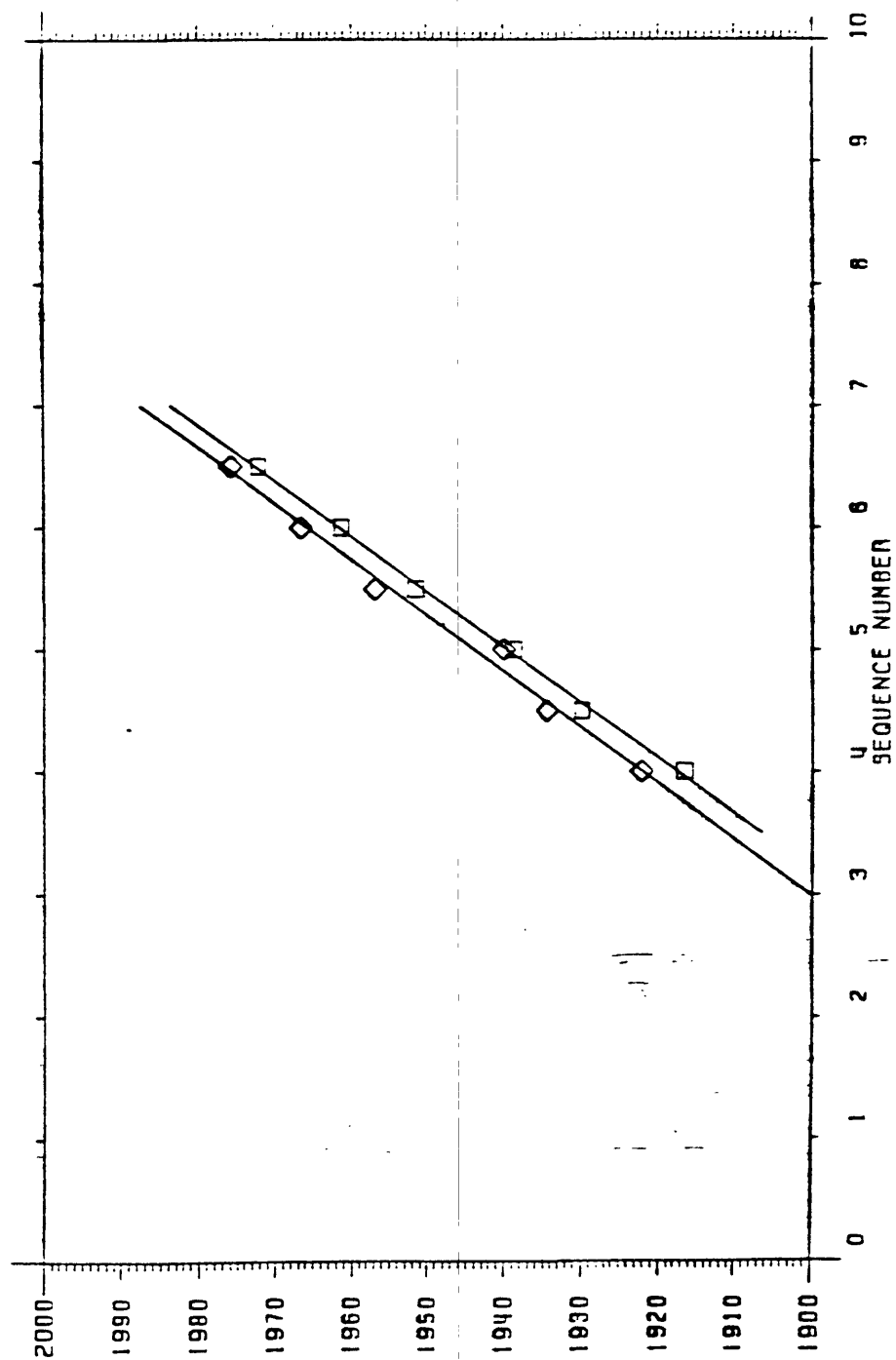


Figure 2

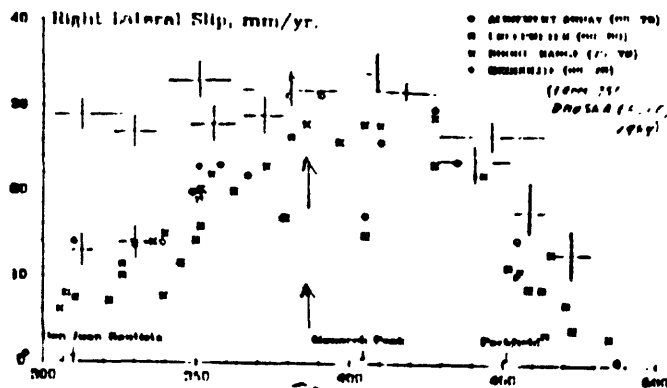
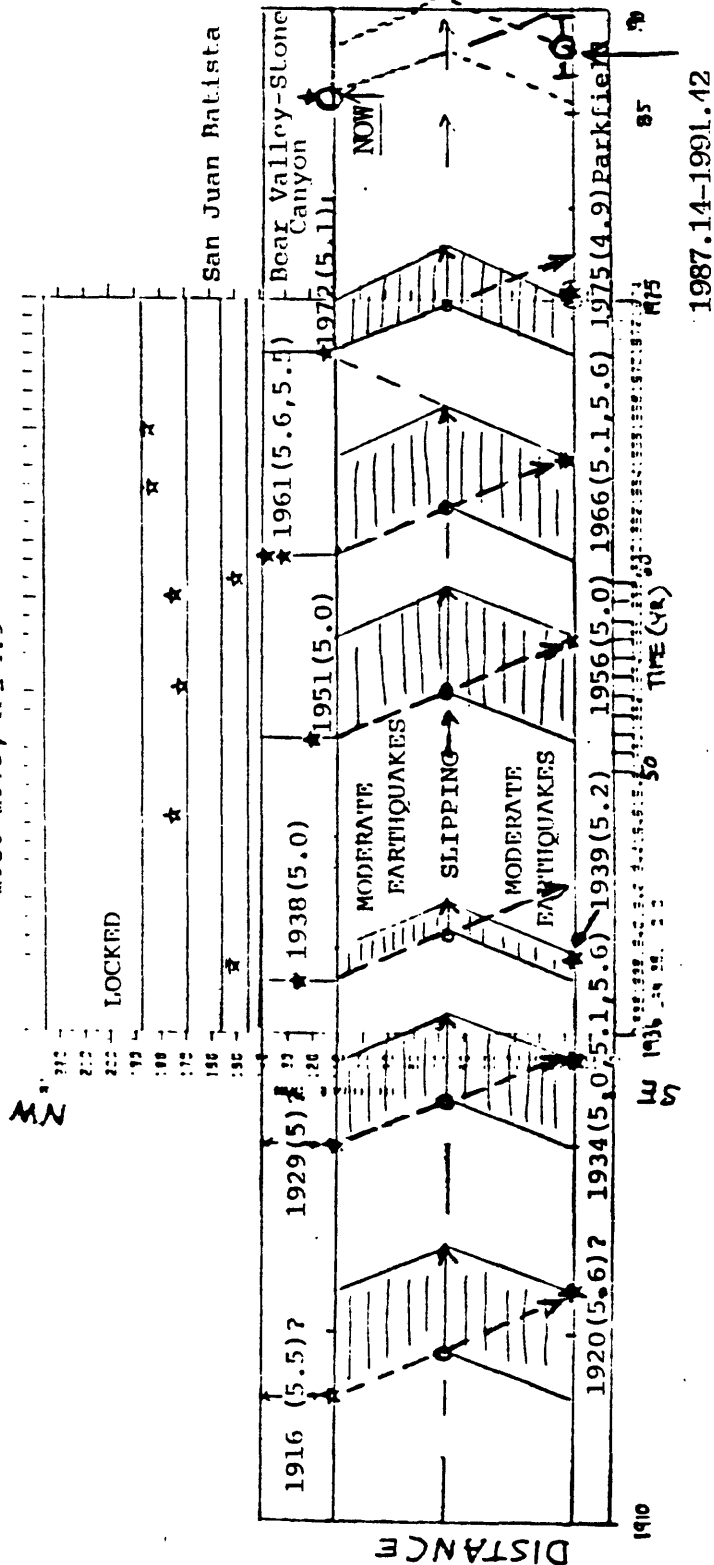
BEAR VALLEY AND PARKFIELD

APPROX. $M > 4.9$

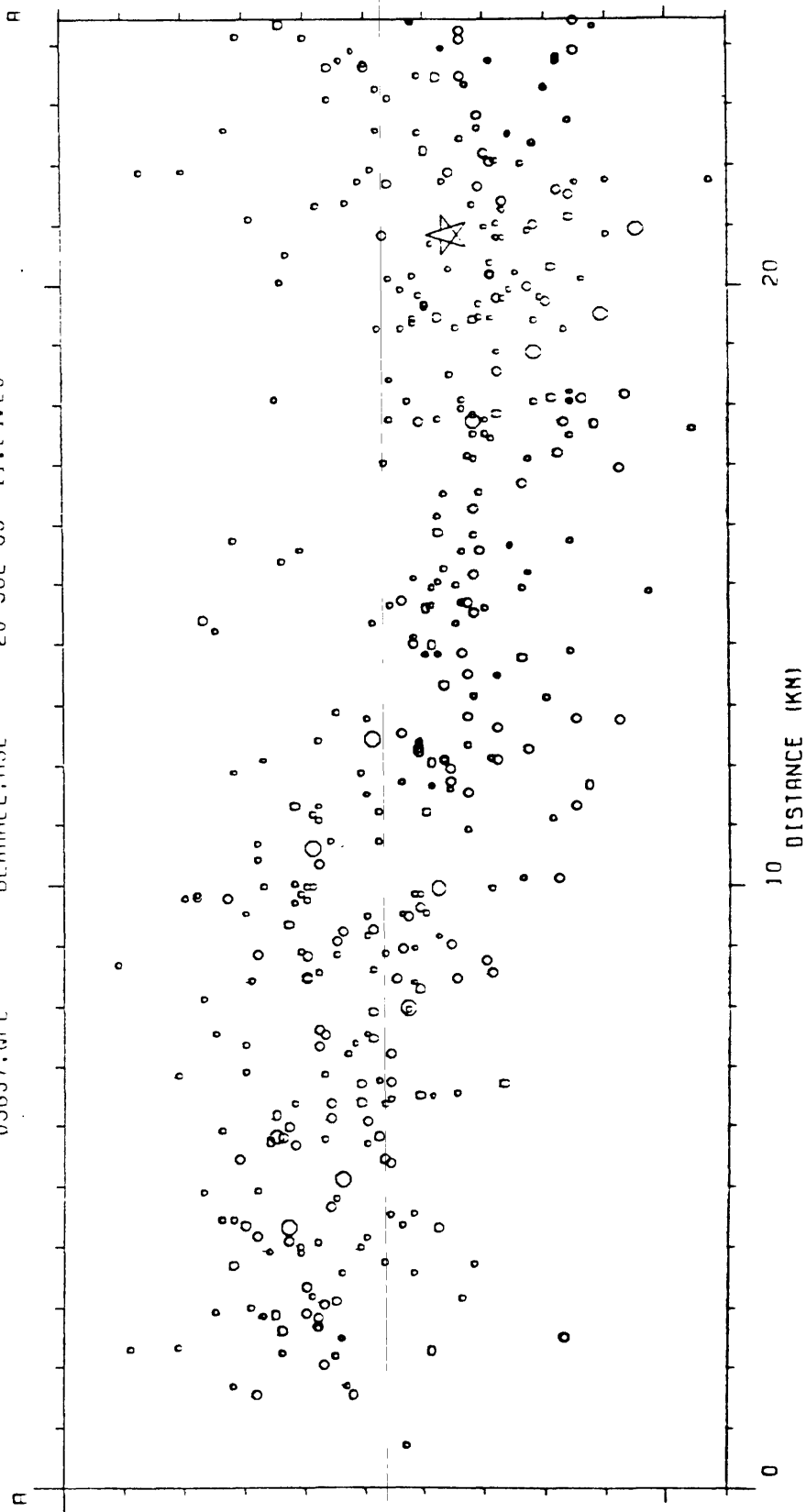
TIMES.OPL BV_XY.DAT 28-JUL-85 10:57:22



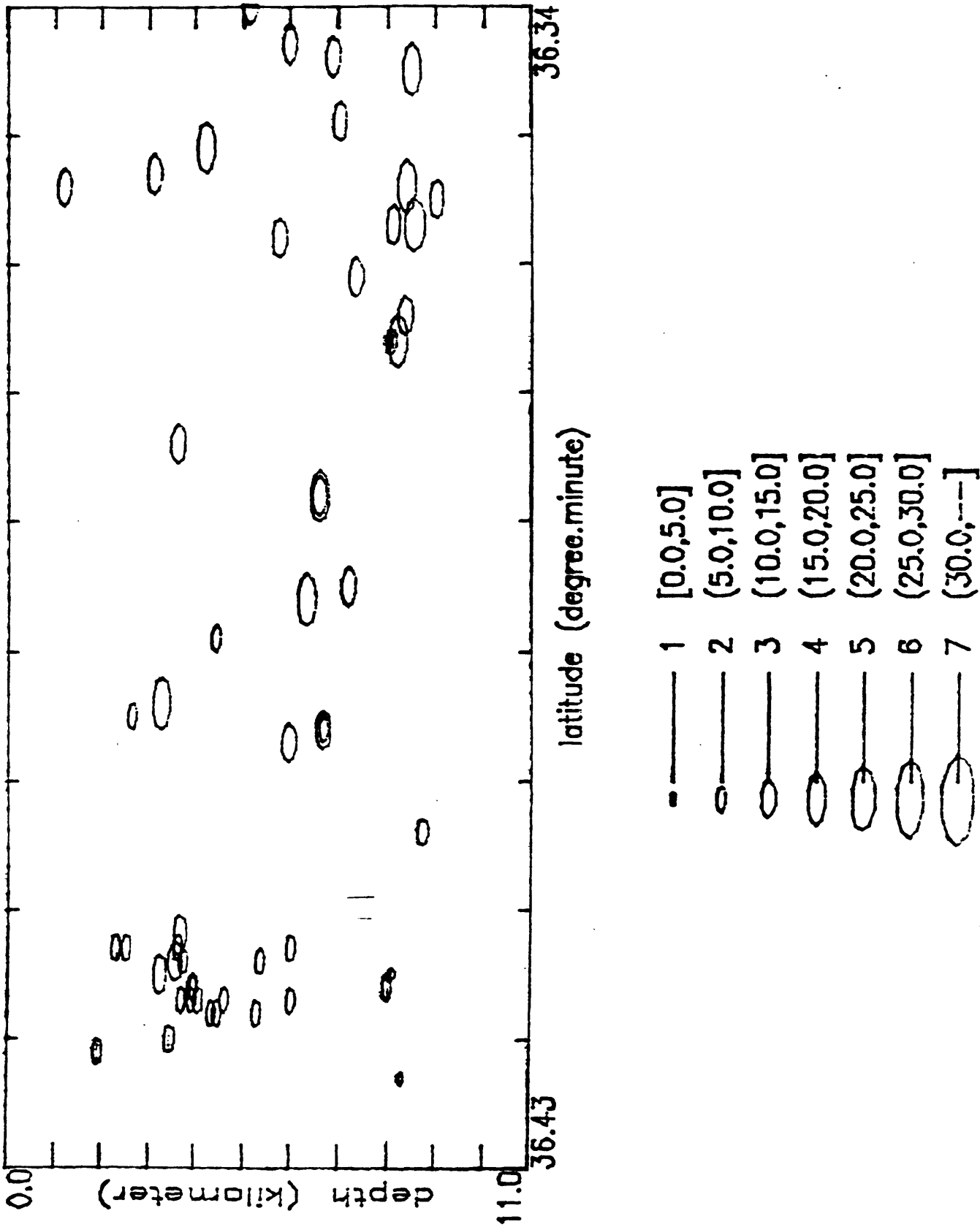
1936-1975, $M \geq 4.9$



11/1/61 THRU 12/31/82
ALL EVENTS
US657.0PL BERRILL.NSL 26-JUL-85 11:24:25



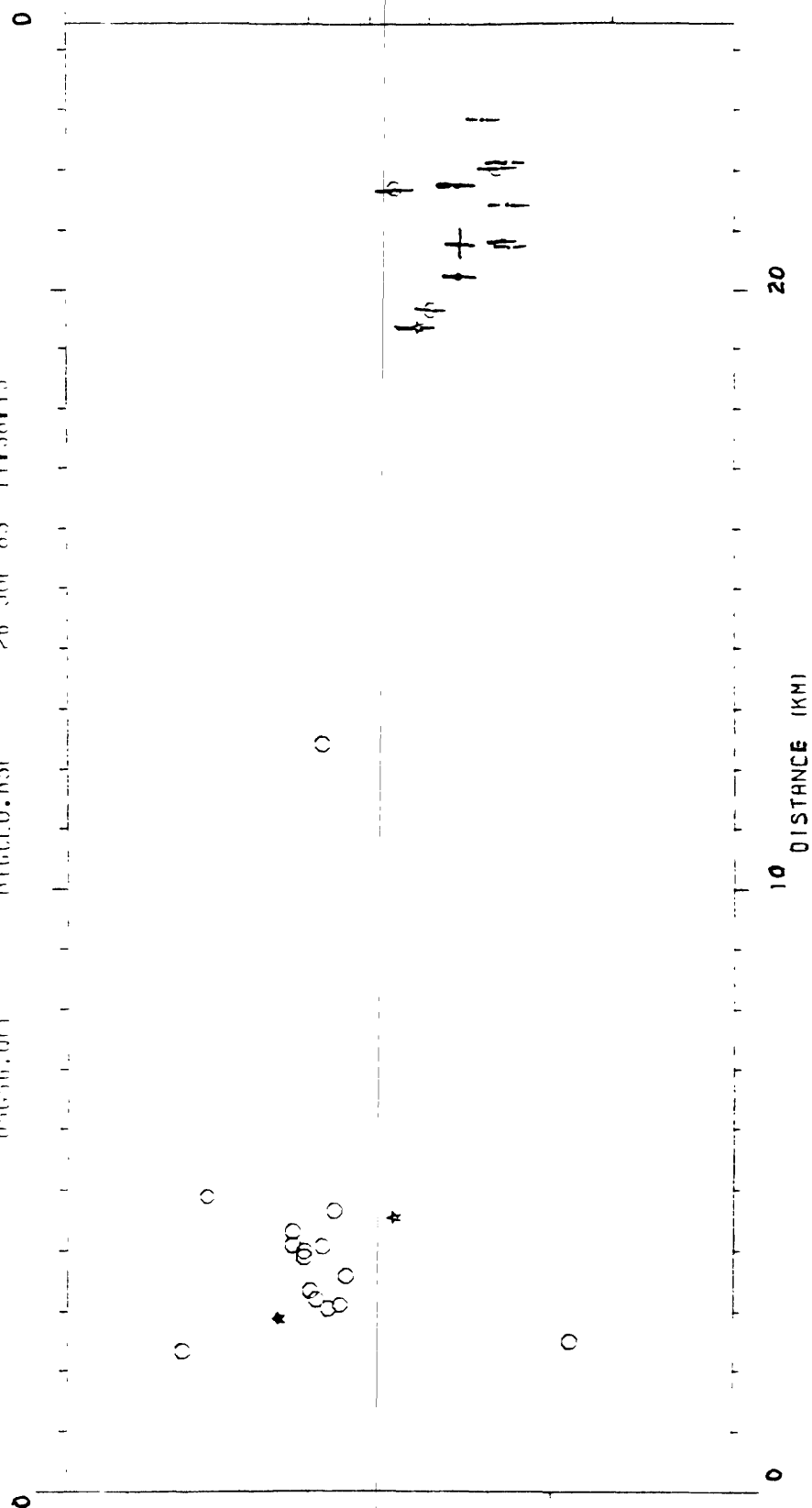
05/16/69---02/23/72



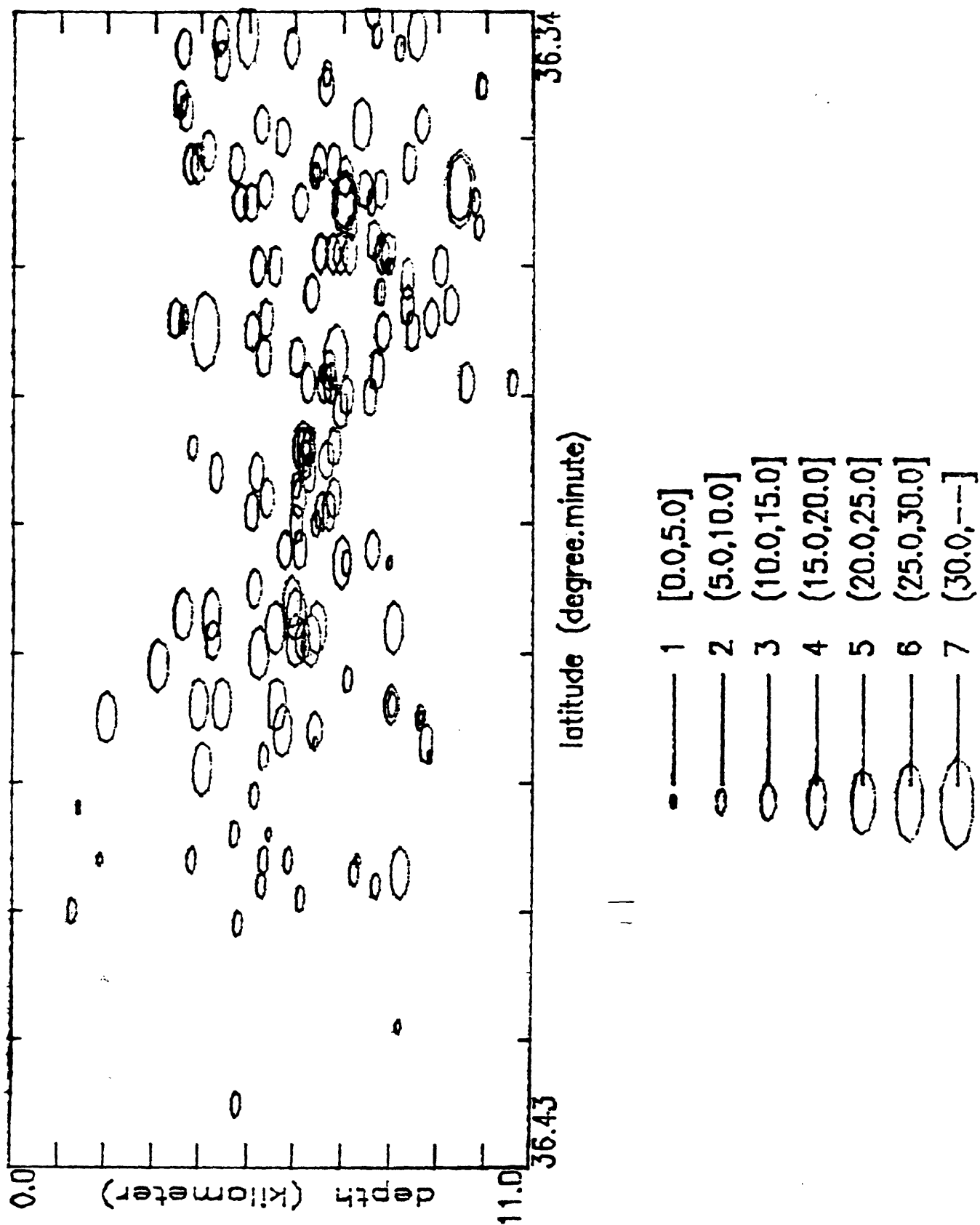
11/1/61 THRU 2/23/72

LARGE CLUSTER EVENTS

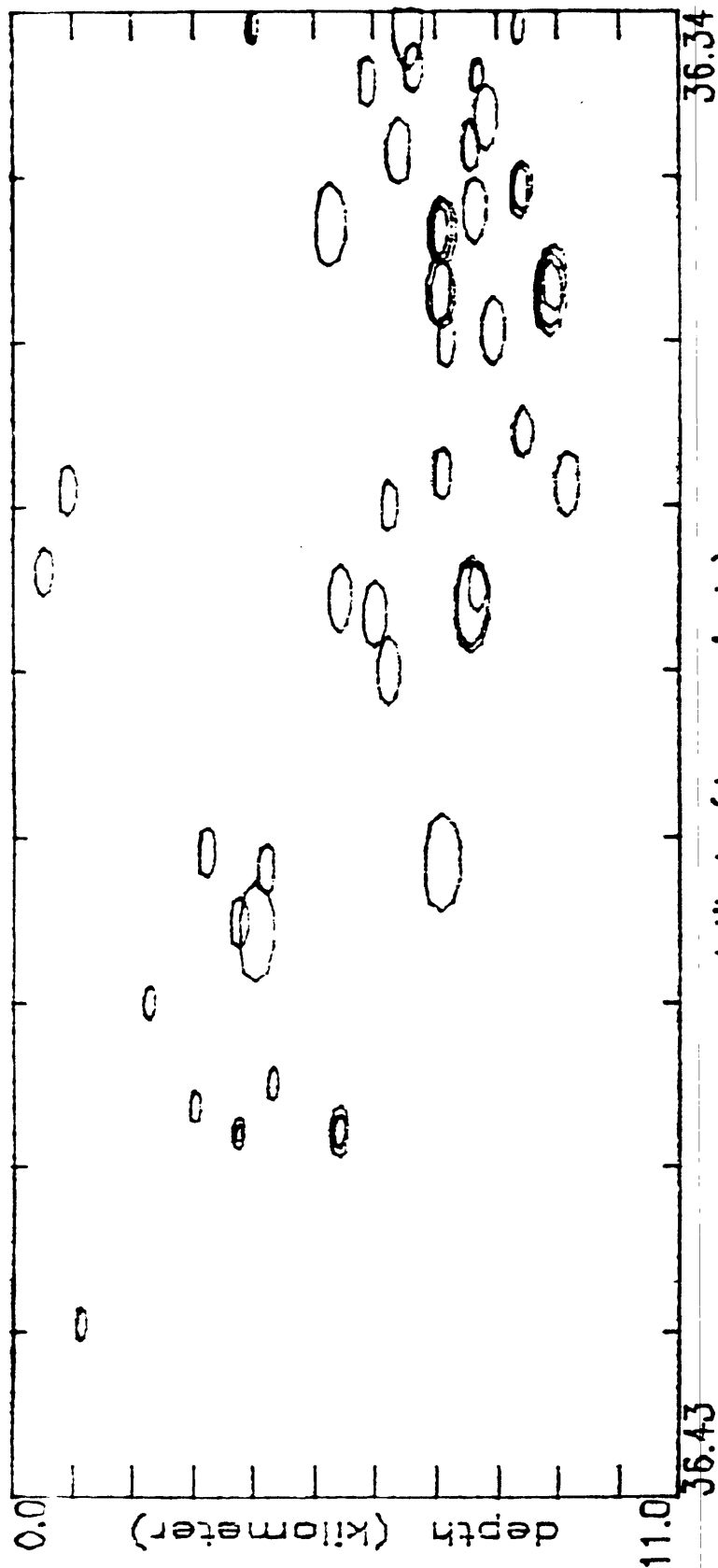
USC-16, 001 REC'D. RSF 26 JUL 85 11:58.15



02/24/72-----12/31/73



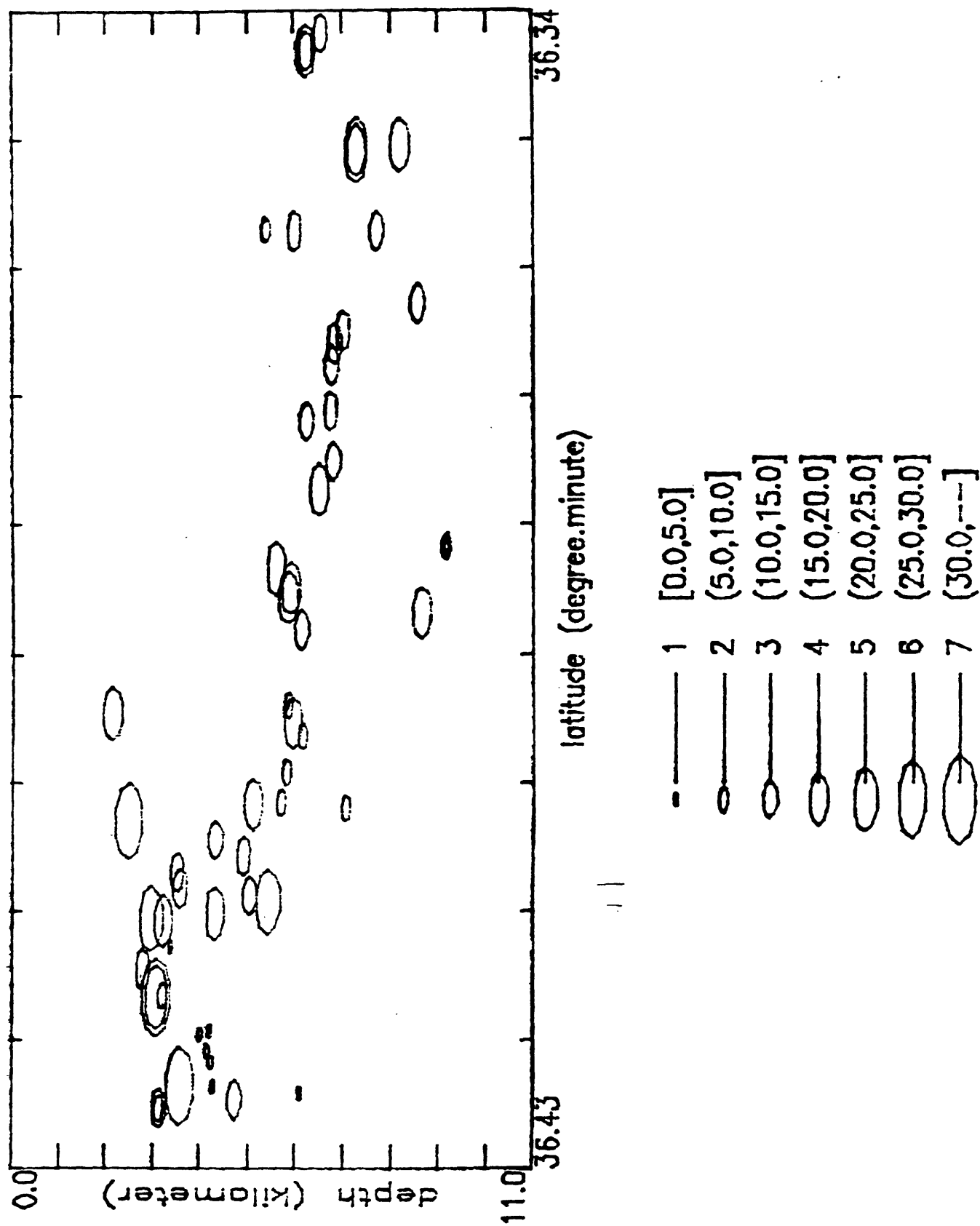
minimum retraction angle
01/01/74-----05/31/78



latitude (degree.minute)

- 1 [0.0,5.0]
- 2 [5.0,10.0]
- 3 [10.0,15.0]
- 4 [15.0,20.0]
- 5 [20.0,25.0]
- 6 [25.0,30.0]
- 7 [30.0,--]

minimum refraction angle
06/01/78---12/31/82



APPENDIX A. 22.

Seismic Hazard Estimate for the San Jose-San Juan
Segment of the San Andreas Fault: 1985-2005

S. P. Nishenko and P. L. Williams

Seismic Hazard Estimate for the San Jose - San Juan segment of the San Andreas fault: 1985-2005

Stuart P. Nishenko

National Earthquake Information Center, U.S. Geological Survey, Denver, CO
80225

Patrick L. Williams

Lamont-Doherty Geological Observatory, Palisades, NY, 10964 and Dept. of
Geological Sciences, Columbia University, N.Y.

ABSTRACT

Various lines of evidence suggest that the segment of the San Andreas fault between San Jose and San Juan Bautista should be regarded as a likely candidate for a M 6-7 earthquake within the next 1 to 2 decades. Analysis of the fault geometry in this area indicates a number of segments that may be capable of breaking independently in events of M near 6, while the extent of the low slip zone from Black Mountain to San Juan Bautista may produce an event of M near 7. In both scenarios, damage to critical facilities in the southern San Francisco bay region should be considered highly likely and appropriate mitigation measures taken.

Introduction

This summary of earthquake hazards along the San Jose - San Juan Bautista segment of the San Andreas fault is divided in 3 sections: Recurrence Probabilities, Regional Tectonics and Models for Future Events.

Recurrence Probabilities

This section updates the probability estimates and discussions presented by Sykes and Nishenko (1984) for the San Juan - San Jose segment (see pages A1

and A2 and Figure 1) for the time period 1985-2005. The two data sets which have been used to formulate recurrence estimates for this segment of the fault are 1] the occurrence of a large earthquake in 1838 and 2] the direct calculation of a recurrence time based on dividing the coseismic displacement in 1906 by the rate of fault motion.

1838 Earthquake

Descriptions for the June, 1838 earthquake (M 7.3 ?) however, poor and incomplete, are suggestive of a large earthquake on the San Andreas which may have extended from San Francisco to San Juan Bautista (see intensity descriptions of 1838 and comparisons with the 1906 shock on page A3). If the 68 year time interval (1838-1906) is a reasonable estimate of a recurrence time for large shocks along this segment, the conditional probability for the next 20 years (1985-2005) ranges from 51% to 73% [Note: these estimates are computed assuming a simple time- dependent recurrence model as described in Sykes and Nishenko (1984). We have expanded this approach by allowing the width of the Gaussian or normal distribution function to vary between 33% and 50% of the estimated recurrence time].

Direct Calculation

Sykes and Nishenko (1984) suggested that the region of low coseismic displacement in 1906 between San Jose and San Juan Bautista had a intermediate to high probability for recurrence based on relatively short recurrence time estimates (see pages A1 and A2). The discussion by Scholz (this meeting) constrains the northern limit of the low slip zone in 1906 to the vicinity of Black Mountain. Using this point and the southern limit at San Juan Bautista, the

estimated length of the low slip zone is 75 km. The largest, well surveyed offset along this segment of the fault occurred at Wright Station (1.4 m). Dividing this offset by the rate of strain accumulation (1.5 cm/yr, Prescott et al., 1985), the estimated recurrence time is 93 years, and the conditional probability ranges from 27% to 37% for the next 20 years [note: again allowing the standard deviation to vary between 33% and 50%].

As seen in Figure 1, the probabilities associated with both estimates (68 and 93 years) are significantly higher than those estimates for the remaining 1906 break. For comparison, estimates of conditional probability based on the above repeat times and a Poisson model of recurrence are also shown. In contrast to the time-dependent models, Poisson based conditional probabilities are time-invariant or static (see Figure 1 in Sykes and Nishenko, 1984). Note that in Figure 1, both sets of time-dependent estimates are higher than the Poisson estimates.

Regional Tectonics

In this section, we examine changes in strike of the San Andreas fault between Bear Valley, San Francisco and the southern Point Reyes peninsula. A number of structures which are well expressed geologically, appear to partition the fault zone between Bear Valley and San Francisco into segments that may be capable of breaking independently.

Between Bear Valley and the southern end of Point Reyes peninsula, the fault trace makes a pronounced westward turn. In map view, the fault traces an arc (concave to the NE and centered at approximately San Jose, see Figure 2).

This bend is about 200 km in length and has a maximum deflection of approximately 12 km.

This large scale deflection is composed in part by a number of abrupt changes in strike at the ends of 20 to 60 km long fault segments. In particular, 4 bends of $\sim 8^\circ$ appear to dominate the changes in strike which make up an "S" shaped bend in the fault between San Francisco and Bear Valley. The segments bounded by these abrupt bends also have shorter wavelength complexities, but do not have major changes in strike which persist for more than about 5 km.

Looking from the south to the north (see Figure 3), the fault first bends to the left $\sim 8^\circ$ rather gradually. 60 km farther north, the fault bends abruptly left 8° more at the southern end of the Loma Preita segment. 20 km further north, the fault bends abruptly back to the right in a bend of about 10° . The last bend to the right ($\sim 9^\circ$) occurs at Black Mountain, 40 km further north. North of Black Mountain, on the San Francisco peninsula, the fault trace is very straight. Overall, a net change of strike of about 5 degrees occurs between the Parkfield-Bear Valley segment and the San Francisco peninsula, and a maximum step over of 12 km occurs between these segments at the northern bend near Black Mountain. (see Figure 2A).

The restraining bend geometry between San Francisco and Bear Valley is expressed in the strong deformation of Franciscan rocks. This deformation is closely correlated with changes in strike of the San Andreas fault (see Figure 3). Reverse slip along the Black Mountain fault is described by Scholz (this meeting). Reverse slip on an extensive set of faults striking N 60 W to N 70 W has caused uplift of the Franciscan rocks and associated Cenozoic rocks in the Santa

Cruz Mountains. The maximum width of this uplifted, deformed zone to the NE of the San Andreas fault is centered at the Loma Prieta segment where the San Andreas fault strikes 16 to 20 degrees oblique to its average central California trend. Although shortening of Franciscan rocks on the North American side of the fault is expressed on the north at Black Mountain (Scholz, this meeting), the greatest development of shortened structures is at Loma Prieta.

Abrupt bends in faults are candidate sites for the initiation and stopping of fault rupture. We suggest that the bends bounding the Loma Prieta segment, and the bend at Black Mountain effectively partition the San Andreas between Bear Valley and San Francisco into segments that can break independently.

Models for Future Events

Descriptions of previous earthquakes (1838, 1865 and 1890) that have occurred along or near this segment of the San Andreas (summarized and annotated on pages A3 and A4) provide a set of examples or models for possible future ruptures in this area.

The fact that large ($M 7$) events can occur in this area is supported by the the June, 1838 earthquake. The endpoints are poorly constrained, and it is not known if the rupture stopped to the south in the vicinity of Santa Clara (Black Mountain ?, Loma Prieta ?) or if it continued farther south to San Juan Bautista (as is suggested by the intensity data at Monterey).

At present, one possible candidate for a future earthquake would involve the entire low slip zone (from Black Mountain to San Juan Bautista) in an event

of $M \sim 6.9$ (see Scholz, this meeting).

Intermediate sized events in this area include the 8 October 1865 (M 6.3, location uncertain) and the 24 April 1890 (M 6.5) events. The data for the 1890 event (summarized on page A4) clearly documents it as a San Andreas earthquake. The northern end of the rupture appears to have stopped by complexities in the fault geometry, where the fault takes 2 sharp bends of about 8, near Loma Preita (see Figure 3). Figure 4 shows isoseismals for the 1865 and 1890 events. While the area of high intensity is not as widespread as that estimated for the 1838 event (and by inference for the postulated Black Mountain to San Juan Bautista event), it is clear that intensities of MM VI to VII could be expected in the southern Bay area for smaller shocks originating from this zone as well.

References

Louderback, G.D., BSSA, 37, 33-74, 1947.

Lawson, A.C., The California earthquake of April 18, 1906, Report of the State Earthquake Investigation Commission, Carnegie Inst., Washington, D.C., 1908.

Prescott, W.H. et al., Deformation of the Pacific plate near San Francisco, submitted Science, 1985.

Scholz, C., The Black Mountain asperity: Seismic hazard of the southern

San Francisco peninsula, California. This meeting.

Sykes L.R. and S.P. Nishenko, JGR, 89, 5905-5927, 1984.

Topozada T.R. et al., Calif. Div. Mines Geol. Open File Rpt.81-11 SAC
1981.

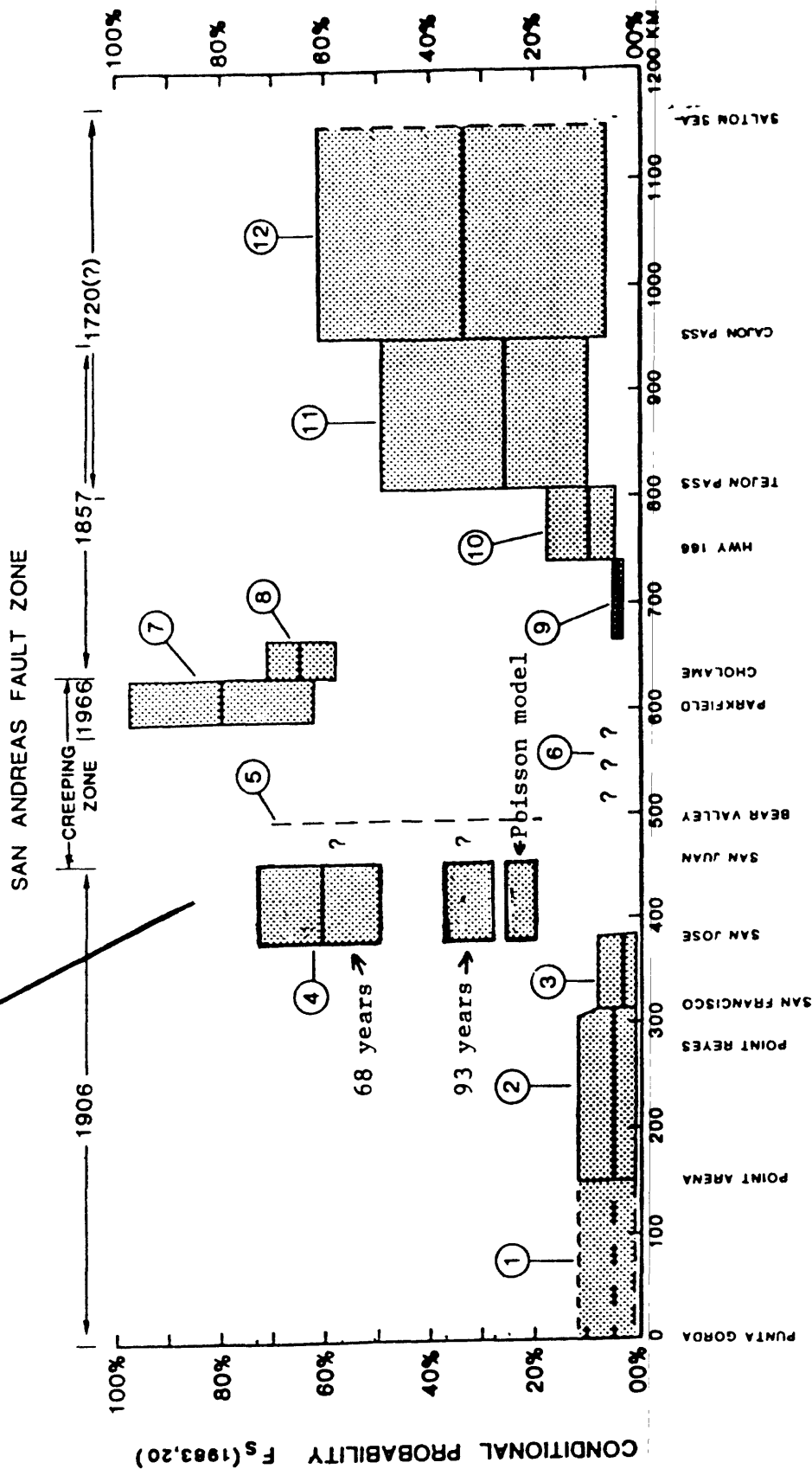


FIGURE 1.

Fig. 3. Conditional probabilities for plate rupturing events along (a) San Andreas fault during the time period 1983 to 2003. Entircled numbers refer to the fault segments discussed in the text and listed in Tables 1 and 2. For each segment the height of the stippled box is the range of probabilities based on our data set. Heavy horizontal line for each segment denotes either the average or our preferred value of probability. Along the San Andreas, two areas (segments 4, 5, 7, and 8) that have the highest chance for recurrence during the next 20 years are situated at or near the two ends of the creeping zone. Segments 11 and 12 along the southern San Andreas fault may be preparing in phase for a future earthquake of magnitude near 8. Segment 6 is assumed to have a low probability since most or all of the fault motion is taken up by aseismic creep.

GEOLOGIC SETTING OF THE SAN ANDREAS FAULT, SOUTHERN COAST RANGES

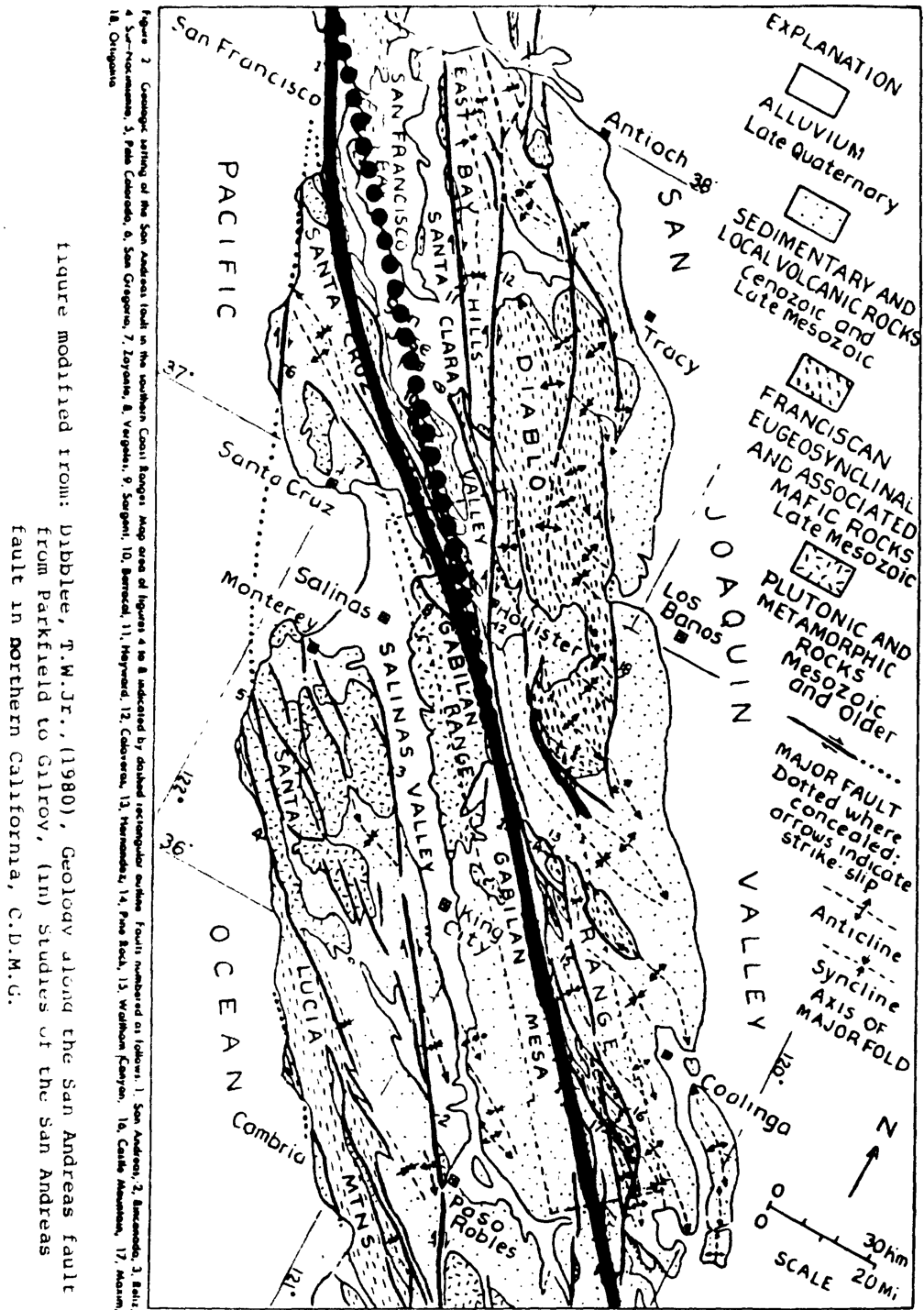


FIGURE 2.

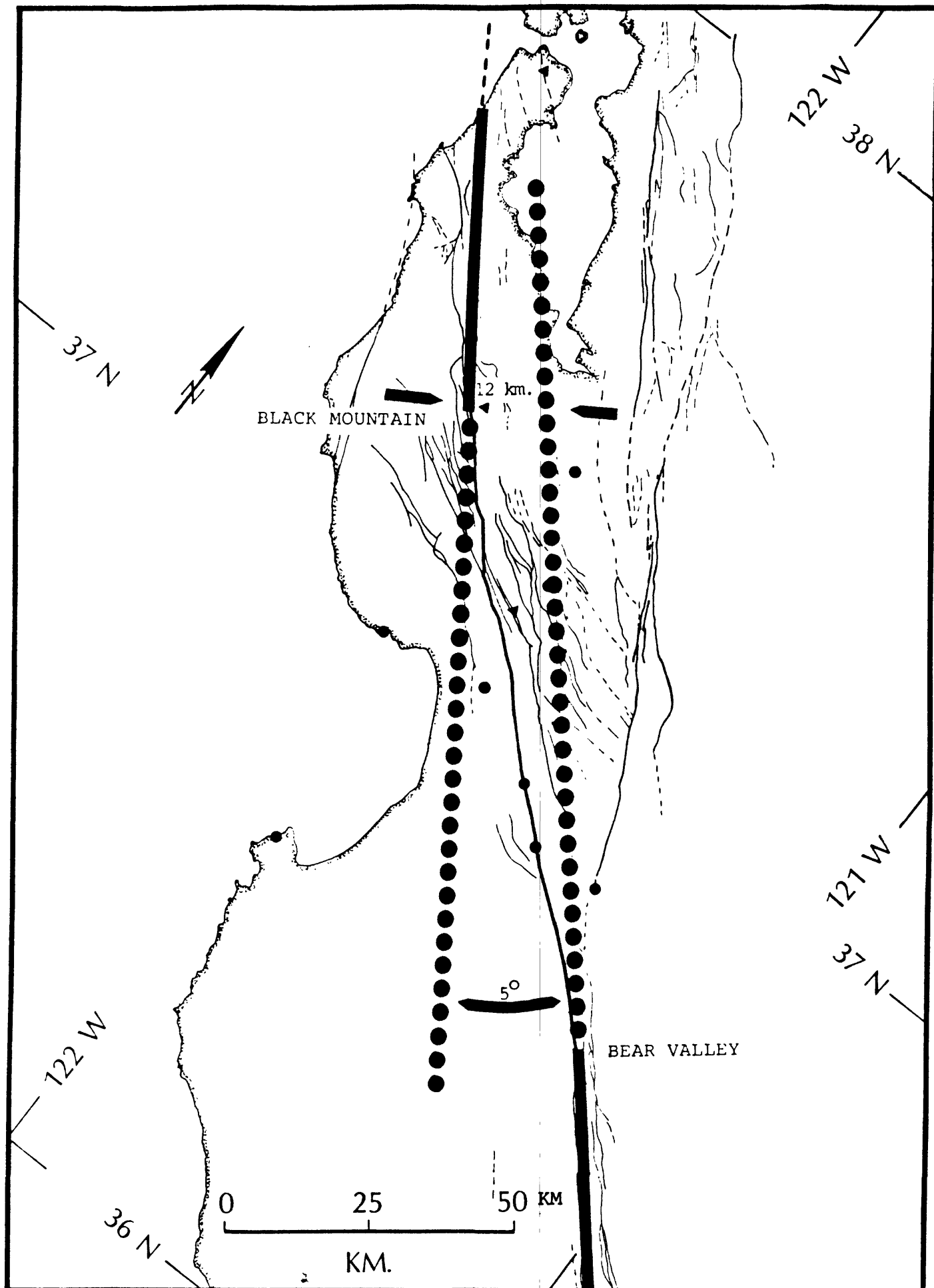
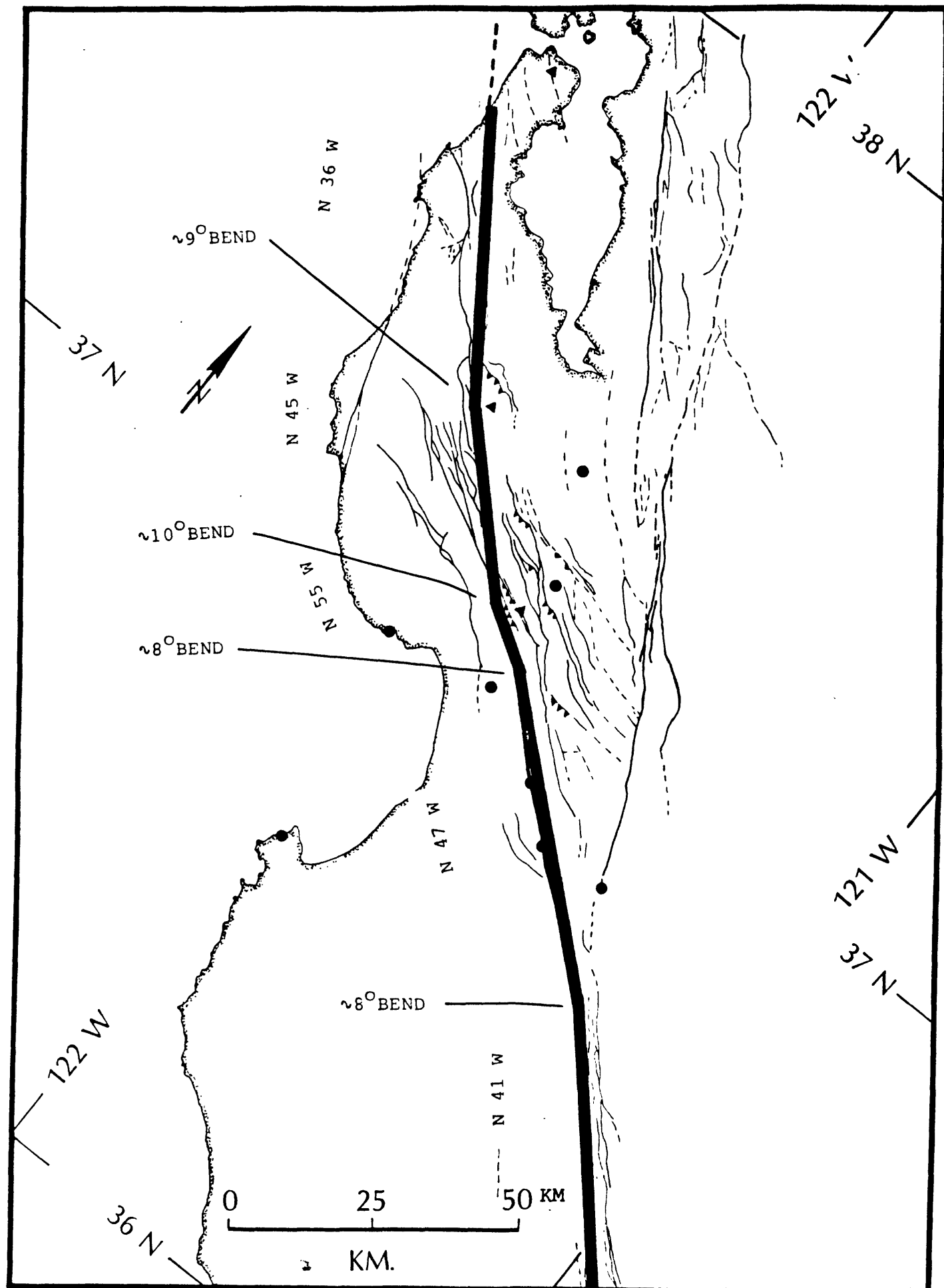
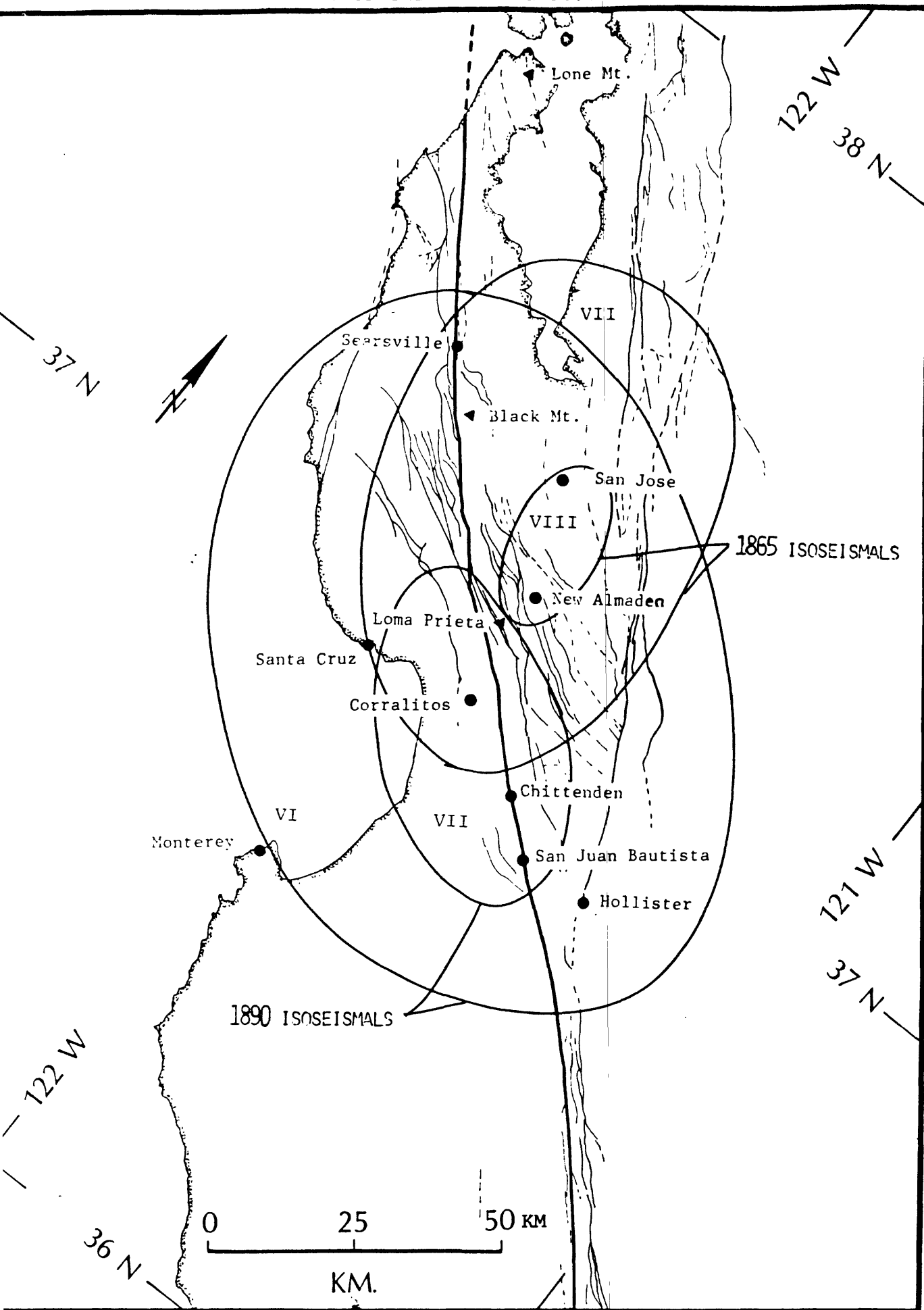


FIGURE 2A.

FAULT SEGMENTS BOUNDED BY ≥ 8 DEGREE BENDS IN THE SAN ANDREAS



The distribution of coseismic offsets in the 1906 shock along the San Francisco peninsula decrease southward from 4.5 m at Mussel Rock at San Francisco to 2.5 m at San Mateo, a distance of about 30 km [Lawson, 1908; Thatcher, 1975]. As in zone 2 the phenomenon of displacement distributed over a wider zone than the actual fault break is evident wherever detailed surveys were conducted. It is not clear from geologic and geodetic data if slip rates along this part of the San Andreas fault itself are significantly smaller than those in zone 2. Plate motion in this part of California is distributed among the San Andreas, Hayward, Calaveras, and San Gregorio faults. The San Francisco peninsula is well instrumented and a number of determinations of slip and strain rates are available for comparison with the longer-term geologic data. Prescott et al. [1981] determined a slip rate of $12.2 \pm 3.9 \text{ mm yr}^{-1}$ and a strain rate of $0.6 \pm 0.1 \text{ } \mu\text{strain yr}^{-1}$ near the San Andreas fault for the time period 1970 to 1980. The long-term geologic rate of offset for the San Andreas in zone 3 is 6 to 22 mm yr^{-1} , based on displaced Pliocene rocks, 1.8 to 5 Ma old [Addicott, 1969], and 10 to 30 mm yr^{-1} from offsets of materials 1 to 3 Ma old [Cummings, 1968].

Dividing the coseismic offsets in 1906 (3 to 4 m) by the above slip rates yields recurrence intervals that range from 150 to 330 years. Thatcher [1975] determined a strain drop of about $115 \text{ } \mu\text{strain}$ for the 1906 event in the peninsular region from geodetic data. Dividing by the present strain rate of $0.6 \text{ } \mu\text{strain yr}^{-1}$ gives an estimated recurrence time of 190 years. For comparison, Hall et al. [1982] estimate the average recurrence interval as determined from trenching at a site between San Andreas Lake and Crystal Springs Reservoir (SAL-CSR in Figure 2) to be 232 ± 32 years. Based on these estimates of recurrence time, the conditional probability for zone 3 is 0.6 to 8.0%.

The 1838 earthquake, which we think may have broken zone 4, also ruptured much of this zone as well. Since the displacements associated with the 1906 shock in much or all of segment 3 are large, we conclude that it still has a low probability of rupturing during the next 20 years.

Zone 4: San Jose to San Juan Bautista

Surface faulting associated with the 1906 shock was dramatically less, 0.2 to 0.6 m, along this segment than it was farther north. At Wright Station an underground tunnel was offset 1.4 m in 1906 [Lawson, 1908]. Using the same slip rate as for zone 3 and a coseismic displacement of 0.6 to 1.4 m, which we think is a better estimate of the slip at depth and which is clearly less than that in the other segments that broke to the north during the 1906 shock, we obtain a recurrence time of 50 to 115 years. The case for zones 3 and 4 being distinct comes entirely from differences in coseismic offset in 1906. The boundary we picked between the two zones is somewhat arbitrary since offset in 1906 does vary along zone 3. Obviously, more work is needed to better define segments that may rupture in individual shocks in zones 3 and 4 since the amount of damage from a future earthquake in zone 4 is very sensitive to the northwestern extent of rupture.

Prior to the 1906 event, segment 4 may have ruptured during a shock of M 7 or greater in 1838. It was also the locus of a shock of magnitude 6.0 in 1890 and may have ruptured in a shock of M 6.3 in 1865 [Lawson, 1908; Topozada et al., 1981]. Ground breakage was noted in 1838 from Lone Mountain south of San Francisco to Santa Clara (near San Jose) and may have continued farther south. The reported felt effects for the 1838 shock at Monterey, San Jose, and Santa Clara indicate greater intensities in 1838 than in 1906 [Loudnerback, 1947]. Hence we suggest that the 1838 event ruptured at least as far south as San Juan Bautista and may have continued into zone 5. Both the 1865 and 1890 shocks may have ruptured the southern portion of segment 4; their inferred sizes, however, indicate that they could not have broken all of zone 4. If the 1838 shock ruptured zone 4, a 68 year repeat time (1906 to 1838) is obtained. The broad range of estimated recurrence intervals, 50 to 115 years, for segment 4 translates into an equally broad range of conditional probabilities, 19 to 95%. In any case, these estimates are higher than those for other parts of the 1906 rupture zone. A part of segment 4 could also rupture in a moderate size event like that of 1865.

The southern boundary of this zone is defined by a number of features including the termination of the 1906 rupture zone [Lawson, 1908], the intersection of the Calaveras fault and a change in the frequency of occurrence of the deepest shocks [Moths et al., 1981].

Zone 5: San Juan Bautista to Bear Valley

This zone is transitional between the section of the San Andreas fault that is accommodating most or all of the long-term fault motion by aseismic creep (zone 6) and the noncreeping or locked segments to the north. With the exception of a shock of M 6.2, which may have broken this segment in 1885, no shocks of M > 6.0 are known to have occurred [Topozada et al., 1981].

Approximately 60% of the fault motion in this segment is not relieved by aseismic creep [Wesson et al., 1973] and could eventually be released in a single shock of magnitude near 6 1/2. It is not clear if strains in this segment are relieved significantly by shocks of smaller magnitude, i.e., like the two events of magnitude near 5.5 in 1961. The amount of aseismic slip in segment 5 is similar to that near Parkfield, zone 7. Zone 5 may also rupture in conjunction with segment 4, as it may have previously done in 1838.

Zone 6: Bear Valley to North of Parkfield

This segment of the San Andreas fault is characterized by all or most of the fault motion being accommodated by aseismic slip [Wesson et al., 1973]. Hence, the rate of long-term strain accumulation appears to be negligible and the probability for a large shock almost nil.

Intensity data from: Topozada et al., 1981

June 1838 $M \geq 7.0$ **

Probable rupture on the San Andreas fault was reported from near Santa Clara to San Francisco, about 60 km. This suggests a magnitude of about 7, which is a minimum estimate because no reports were available north of San Francisco or south of Santa Clara, except at Monterey. Walls were cracked at Mission Dolores (San Francisco) in the 1838 earthquake, which is comparable to the effects of the 1906 earthquake. In Monterey, crockery and glassware were broken and some adobe walls were reportedly cracked in 1838, compared to 1906 when the only damage reported was of some glassware and some furniture moved. Louderback (1947) states that "The fault rupture may have occurred throughout all or most of the line active in 1906, but north and south beyond the limits indicated...it lay under water or in wild country uninhabited by whites (except at Fort Ross, from which we have no report). The evidence of greater intensity at Monterey than in 1906 may mean that the fault rupture extended farther south in 1838 than in 1906."

- 1] Comparison of intensity data for the 1838 and 1906 earthquakes (data from Lawson, 1908 and Louderback, 1947).

<u>Location</u>	<u>1838</u>	<u>1906</u>
San Francisco	RF \geq VIII	RF VII - VIII
Monterey	RF \geq VII	RF VI

- 2] Mission walls also cracked at Santa Clara, San Jose as well as Mission Dolores. At San Francisco, there was damage to the buildings at the Presido and observations of a sand body shifting in 1838 shock. Near Searsville, adobe walls were cracked and trees knocked down. At San Juan, a house was knocked down (Louderback, 1947).
- 3] In summary, the primary reason for extending the 1838 rupture south of Santa Clara is the higher intensities at Monterey in 1838 compared to 1906.
- 4] Using an estimated rupture length of 125 km (San Francisco to San Juan Bautista) and scaling laws, the estimated M_0 is 9×10^{26} dyne-cm (160 cm of displacement) and M_s 7.3.

Intensity data from: Topozada et al., 1981

8 October 1865 M6.3

Several houses were thrown down (IX MM) at New Almaden. In Santa Cruz, brick walls were cracked and many chimneys were thrown down (VII-VIII MM). Brick walls were thrown down in San Jose (VIII MM). The earthquake was damaging from San Juan Bautista on the south to Napa on the north. Ground cracking was reported at Mountain Charlie's near the San Andreas fault; This cracking might be fault rupture or secondary failure due to shaking.

1) Where is Mountain Charlie's ??

24 April 1890 M6.0

Extensive damage was done to chimneys and some damage was reported in brick and frame buildings from San Juan Bautista, San Benito County, to Green Valley, Santa Cruz County (VIII MM). At Corralitos, most chimneys were thrown down and buildings were "twisted half around" (IX MM). Probable fault rupture occurred along the San Andreas fault where it crosses the Pajaro River. Cracking was reported on or near the San Andreas, and a railroad bridge across the Pajaro River, near the San Andreas fault, shifted one and a half feet out of line.

- 1) Pajaro River at Chittenden: Railroad bridge abutment shifted 1.5 feet in 1890 and 3.5 feet in 1906.
- 2) Ground cracks 0.5 mile west of Canfields house (approx. 1 mile north of San Juan) Cracks in 1906 similar to those that formed 16 years earlier (i.e. 1890)
- 3) The above descriptions for the 1890 event constrain the rupture zone to the San Andreas fault, and provide an estimate for rupture extending from San Juan north to or near Loma Preita (estimated length ³⁰ - 38 km). Estimated M_0 based on this length and scaling laws is $5 - 8.5 \times 10^{25}$ dyne-cm (slip: 40-50 cm) and M_s 6.5-6.6.

APPENDIX A. 23.

Current Episodes of Seismic Quiescence along the San Andreas Fault
between San Juan Bautista and Stone Canyon, California: Possible
Precursors to Local Moderate Mainshocks?

M. Wyss and R. O. Burford

DRAFT, MAY 1985

Current Episodes of Seismic Quiescence along the San Andreas Fault
between San Juan Bautista and Stone Canyon, California:
Possible Precursors to Local Moderate Mainshocks?

by Max Wyss¹ and Robert O. Burford²

ABSTRACT

A quantitative evaluation of the seismicity rates along a 100-km segment (36.36° to 37.0° N) of the San Andreas fault for the period August 1973 through December 1984 has established that three separate subsegments of the fault are quiescent at the present. For earthquakes of $M_L \geq 1.7$ and $M_L \geq 2.0$ seismicity rates show highly significant average decreases of 66%, 65% and 71% below the background rate in the Cienega Winery seismic gap, the San Juan Bautista seismic gap and the Stone Canyon section, respectively. These anomalies began in June 1982, February 1983 and June 1983. Although these anomalously quiet fault segments are separated by approximately 10-km long segments where the current seismicity rates are normal, there is a possibility that all three are related to a common mechanism. All three anomalies are unique in the data set, surpassing in significance by far any other rate changes, with z values calculated by AS(t) of 4.9 and 7.7 (San Juan and Stone Canyon, respectively for $M_L \geq 2.0$). In addition, two precursory quiescence anomalies were discovered for past mainshocks in the study area: the $M_L=4.0$ (2 August 1979) and $M_L=4.2$ (11 August 1982) mainshocks were preceded by decreases in seismicity rates of 80% and 60% respectively, with the anomalies starting 15 and 19 months before the respective mainshocks. Based on these observations, it is proposed that the present-day quiescence anomalies are probably precursors to one or several future earthquakes. The interpretation that the present quiescences might have been caused artificially by a change of data acquisition or analysis procedures is made unlikely by the observation that six 10-km fault segments in the area show no significant seismicity-rate changes in the last 5 to 11 years. The lengths of the anomalous segments are small, 5 to 10 km, suggesting that the expected mainshocks should be in the range $4 \leq M_L \leq 5$. However, the anomaly durations range from 2.8 to 1.9 years, suggesting that these magnitude estimates may be too low by approximately one unit. This invites the interpretation that the three quiescence anomalies jointly outline the rupture length of one mainshock of $M_s=6.2 \pm 0.3$ centered near 36.75° N and 121.4° W. All magnitude estimates presented are based on the assumption that the expected rupture(s) will occur within the next 12 months. If the quiescence anomalies persist without mainshocks for another year the magnitude estimate should be increased. The probability for an individual quiescence to be a false alarm (no mainshock follows) is estimated from observations in other areas to be approximately 30%.

¹ CIRES, University of Colorado/NOAA, Boulder, CO 80309.

² US Geological Survey, 345 Middlefield Road, Menlo Park, CA 94025.

INTRODUCTION

The hypothesis that seismic quiescence precedes mainshocks has been strengthened over the last few years by several quantitative documentations of the phenomenon (e.g. Habermann, 1981; Wyss et al., 1981; Wyss et al., 1984; Wyss and Koyanagi, 1985). It is now well established that some mainshocks are preceded in their source volume (or parts of it) by statistically highly significant decreases of the background rate of seismicity and that the rate during the precursor time ranges from 10% to 60% of normal (e.g. Wyss, 1985). Most of these data concern fairly large mainshocks ($M > 6$) located outside of California. Two important questions are raised: (1) Does the quiescence hypothesis apply to San Andreas fault mainshocks? (2) Will seismic quiescence also precede events of moderate magnitudes ($4.0 \leq M_L \leq 6$)?

Precursory seismic quiescence has recently been documented along the Imperial and the Calaveras faults in California. The segment of the Imperial fault which ruptured in a $M_L=6.6$ mainshock on 15 October, 1979 showed a decreased seismicity rate during 15 weeks before the mainshock (Johnson and Hutton, 1982; Habermann and Wyss, 1984a). Along the Calaveras fault both the 6 August 1979 Coyote Lake ($M_L=5.8$) and the 24 April 1984 Morgan Hill ($M_L=6.2$) earthquakes were preceded by periods of significant seismic quiescence (Habermann and Wyss, 1984b). Duration of these quiescence precursors were 2.4 and 2.7 years, respectively. However, questions have been raised about the validity of the Coyote Lake observation because changes in network instrumentation and procedures may have affected determination of coda magnitudes beginning in April 1977, approximately at the onset time of the apparent rate decrease (Reasonberg and Ellsworth, 1982). These three cases are the only known quiescence precursors along the San Andreas fault system. In the present paper further evidence is presented to support the hypothesis that seismic quiescence precedes moderate mainshocks along the San Andreas

fault.

The choice of the study area (Figure 1) was based on several factors: Records of fault creep observations have been obtained along this part of the fault for several years (Mayko et al., 198[?]₁). By comparing seismicity-rate changes with fault creep records, clues might be discovered for understanding the mechanism of quiescence, especially since in Hawaii the 1975 precursory quiescence correlated with geodetically observed strain relaxation (Wyss et al., 1981). A 14-km seismic gap at the Cienega Winery (Figure 4) is defined by aftershock sequences for mainshocks ($4 \leq M_L \leq 5$) since December, 1971. Additionally, the local catalog of seismicity is expected to be of high quality, because the area is located near the center of the US Geological Survey seismometer network in central California.

Our initial aim was to further confirm the quiescence hypothesis by searching the study segment of the San Andreas fault for periods of seismicity-rate changes which might be associated with recent mainshocks or creep-rate changes. In the process we have found that seismic quiescence *exists at present* in parts of the study area. Consequently, the aim of the study was redirected toward answering the following questions: (1) What are the spatial extents of the presently quiet segments? (2) How long has quiescence lasted and with what confidence level can it be said to exist? (3) Has precursory quiescence occurred before previous mainshocks along this fault segment and are false alarms likely to be observed? (4) Is it probable that the recent continuing periods of quiescence were introduced artificially by changes in the data acquisition or analysis procedures upon which the seismicity catalog is based?

The reporting of events in earthquake catalogs is generally expected to improve with time as network densities are increased and analysis procedures are strengthened. In some cases, however, changes in organizational policy or priorities may result in

decreases in reporting of events. For meaningful studies of seismicity rate as a function of time, it is therefore necessary to disregard events of small magnitudes for which reporting is most likely to have been nonuniform. Surprising artificial decreases in reporting rates for all magnitudes are contained in some catalogs. For example, the reporting for the Tonga trench was diminished at the time of the world-wide decrease of reporting in the PDE listings (Habermann, 1982), while the Kermadec trench area was not affected. This contrast might have been interpreted as evidence for the tectonic origin of the seismicity-rate decline. However, it was discovered that the closing of seismograph arrays in the U.S., located at a distance greater than 95° from Kermadec, was the chief cause of change in reporting (Habermann, 1982; Wyss et al., 1984). The southern California catalog also contains some strong artificial changes in reporting. For example, the beginning and ending of a period of apparent decreased seismicity for $M \geq 2.5$ events coincided with enhanced reporting of small events and with changes in the network operation (Habermann and Wyss, 1984a). Systematic shifts in routine determinations of magnitudes also appear to be an important cause of artificial changes in seismicity rate. Reasonberg and Ellsworth (1982) proposed that magnitudes in central California were systematically decreased by about 0.1 as a consequence of changes in the recording systems introduced around 27 April 1977. For a study of seismicity rate of events with $M \geq X$, this will mean that after April 1977 the earthquakes in the $M=X$ class will be dropped from consideration, because they then will be assigned the value $M=X-0.1$, and they will be replaced with those events which before the change used to be assigned $M=X+0.1$ (e.g. Habermann and Wyss, 1984b). Although small, such a magnitude shift can introduce apparent rate changes that are nevertheless statistically highly significant. It is not known at this time for which period and which areas the central California catalog may contain other magnitude shifts. Therefore, great care must be taken in

interpreting apparent seismicity-rate changes as potential precursors. However, it is proposed that a rate change which takes place in a small area only (radius approximately 10 km) is not likely to be due to an artificial magnitude shift, because changes in reporting would normally affect larger portions of the seismometer network.

The method employed for seismicity-rate analysis has been described previously (e.g. Habermann, 1981a,b; Habermann and Wyss, 1984a). We define quiescence as a statistically significant decrease of seismicity rate (as a function of time) within a given crustal volume. Rates in neighboring volumes are not compared, as would be done to identify doughnut patterns (Mogi, 1969), because it has been previously noted that different fault segments often have permanent (or very long lasting) differences in rate (e.g. Habermann, 1984; Wyss et al., 1984). Thus, in order to identify a quiescent period within a certain volume, it is necessary to define the normal background rate in the same volume. For the evaluation of the statistical significance of any rate change, the standard deviate z-test is useful. In this study, algorithms developed for z-tests developed by Habermann are used (e.g. Habermann, 1981a,b; Habermann and Wyss, 1984a).

DATA

The data for this study consisted of the U.S. Geological Survey earthquake catalog for central California. Since Reasonberg and Ellsworth (1982) proposed that the magnitudes in the catalog are too low by about 0.1 units after 27 April 1977, we have added 0.1 to the magnitudes of all events which occurred after this date. Otherwise, the existing data are used without modification except for identifying dependent events.

Our preliminary investigation of the catalog homogeneity for the data set at hand is presented in the Appendix. The magnitude signature method (Habermann, 1982, 1983) was used to investigate rate changes in several magnitude bands, focusing on times of significant overall reporting change ($M_L \geq 0$). The most dramatic increase in the

number of events ($M_L \geq 0$) reported per unit time took place in late 1980, and coincided with an apparent rate decrease for $M_L \geq 1.5$ (Appendix A). A change of the same nature was found in the Southern California seismicity catalog to coincide with a change in analysis procedure (Habermann and Wyss, 1984). The 1980 changes in the Central California data also coincides with analysis procedure changes (J. Eaton, personal communication). Therefore, the apparent decrease of $M \geq 1.5$ events in 1980 is interpreted as caused by a magnitude shift of at least -0.1 units (Appendix A).

The April 1977 changes of analysis procedures caused a decrease of reporting rate for small earthquakes (Appendix A). However, in the present study area there is no compelling evidence for a magnitude shift as proposed by Reasonberg and Ellsworth (1982). Based on the analysis contained in Appendix A the data set should be corrected for a magnitude shift in 1980 but not in 1977. However, the correction made in this study is the one proposed by Reasonberg and Ellsworth (1982) and none for 1980, because the analysis in Appendix A is preliminary. It is important to note that none of the conclusions depend on the choice of correction. The current quiescence anomalies are highly significant in the uncorrected as well as either corrected data sets ($M_L + 0.1$ after April 1977, or $M_L = M_L + 0.1$ after October 1980).

The last year of the data available (1984) shows increased reporting for small events but a decrease for larger ones ($M_L \geq 2$). It is not clear at the present whether these changes are localized and real, or whether they may be artificial (perhaps these recent data may be reevaluated for final corrections).

From the homogeneity analysis in the Appendix it is concluded that between 1974 and 1984 earthquakes of $M_L \geq 1.5$ can be used to define quiescence. Because the reporting of small earthquakes may be more open to question, we have taken a conservative

approach by considering only events of $M_L \geq 1.7$ in the analysis, and by confirming important anomalies in addition by analysis of the subset of events of $M_L \geq 2.0$. Rate changes in 1980 discounted because they appear to be caused by changes in the analysis procedure.

Aftershocks and swarm events are first removed from the data set because it is desired to measure changes in background rate alone. Along this particular segment of the fault even relatively small earthquakes ($M \approx 3-4$) are often accompanied by extended aftershock sequences. Because the activity rate is very high along most of the studied fault segment, McNally's (1976) algorithm to identify dependent events was not used. This algorithm contains no provision for evaluation of spatial separation, and consequently shocks occurring at opposite ends of an active segment but close together in time would be judged dependent. Instead, aftershocks and foreshocks were identified and labeled one at a time by plotting events sequentially and by evaluating their spatial and temporal separation from each mainshock ($M_L \geq 3$) in the catalog. Several episodes of diffusely increased seismicity rate were left in the record, and they appear as steep portions, almost step-like features, in the cumulative seismicity curves (e.g. Figures 2, 9). It is recognized that this method leaves somewhat undesirable noise in the data sets, but this cannot be avoided until more sophisticated and appropriate techniques are developed to recognize dependent events.

Reliable assessment of changes in seismicity rate requires that the background rate be well established for as long an observation period as possible. Thus a study of the seismicity rate during the period 1969 through 1984 was attempted. The beginning of the data set was first chosen as 1969, because at that time the central California seismograph network was greatly expanded and smaller magnitude events were reported with improved reliability. However, the data set was subsequently shortened to 11.4 years

(August 1973 through December 1984) because the extraordinary sequence of mainshocks and aftershocks that occurred in 1971-73 (Ellsworth, 1975) greatly influenced the seismicity rates along most of the fault segment selected for study. Before the 1972 earthquake sequence the rates were generally lower than after it. This may suggest that the 1972 sequence was preceded by seismic quiescence. However, this suggestion cannot be substantiated because it is not possible to reliably define the occurrence rate of small earthquakes before 1969. As the pre-1973 data do not in general help in the definition of background rate, mid-1973 was chosen as the beginning of the period for study. By that time, the disturbance of seismicity rates related to the 1971-1973 moderate-earthquake sequence appeared to be over along most of the fault segments examined.

The seismicity data set was not limited in depth, because most of the activity is restricted to an approximately 7-km thick section of the crust centered at about a 6-km depth (e.g. Wesson et al., 1973). The horizontal distance out to which data were included perpendicular to the fault (approximately 5 km) is defined by the polygons shown in Figure 1. These polygons were centered on the zones of epicenters for earthquake activity along the main fault, and their width perpendicular to the fault was chosen such that the dense seismic activity of the immediate main San Andreas fault trace was included, but not much more. This was done in an attempt to exclude diffuse off-fault activity, as well as activity along faults other than the main San Andreas strand.

EXAMPLES OF PRECURSORY QUIESCENCE ALONG THE SAN ANDREAS FAULT

A period of reduced seismicity rate lasted from the beginning of 1981 to the middle of 1982 in volume 361 (Figure 2). During that time the rate was reduced by 59% and 77% of the normal background rate for the data subsets of $M_L \geq 1.7$ and $M_L \geq 2.0$, respectively. This period of seismic quiescence was followed by an increase in seismicity

about three months before the occurrence of several mainshocks in the area during August 1982. The largest of these occurred in volume 361 and had a magnitude of $M_L = 4.2$. Because these mainshock-aftershock sequences were distributed along a longer segment of the fault than that covered by polygon 361, the quiescence anomaly can also be seen clearly in volumes 402 and 386 (Figures 9 and 10). This anomaly does not exist in other fault segments defined in Figure 1 this anomaly does not exist (e.g. volumes 403, 404, 406, and 407; Figures 7 and 8). Thus the spatial and temporal correlation of the quiescence with the mainshocks of August 1982 indicates that this anomaly was a precursor.

The statistical function $AS(t)$ (for details see Habermann and Wyss, 1984a) shows that the 1981-82 quiescence in volume 361 is significant above the 99% level (at its maximum the AS function reaches a value of 4.1 ($M_L \geq 1.7$) for the standard deviate z). The statistical function shown in Figure 2 is derived from the $M_L \geq 1.7$ data, and peaks during December 1980. The function measuring the significance of the $M_L \geq 2.0$ events results in a value of 5.1 for the standard deviate z , and peaks at the same time (not shown in Figure 2). The parameters describing this precursor are summarized in Table 1.

Three $M_L \approx 4$ mainshocks occurred in volume 401. The first of these (August 1979) was preceded by quiescence which lasted 1.3 years (Figure 3, Table 1). This quiescence, as in the example from volume 371, did not continue up to the time of the mainshock. Instead, a 3-month period of high rate (similar to the β -phase of Ohtake et al., 1979) separated the mainshock and its quiescence precursor.

The April 1980 $M_L = 4.1$ mainshock in volume 401 was not preceded by quiescence (Figure 3). We take this to be a failure of the hypothesis that small mainshocks are pre-

ceded by quiescence. Volume 401 also contained strong candidates for false alarms: Periods of 9 and 5 months during 1982 and 1984, respectively, showed low seismicity rates (Figure 3). Depending on what period is used for the background rate against which these rate decreases are measured we can obtain large z -values (in the range $2.6 < z < 3.0$) for these anomalies. Thus we conclude that short periods (less than a year) of quiescence are not always followed by mainshocks. The 1984 period of quiescence in volume 401 is particularly noticeable in the $M_L \geq 2.0$ data. However, a few previous periods of low activity also exist in the $M_L \geq 2.0$ data, and background rates are not as well defined. The $M_L \geq 1.7$ data do not show a significant rate decrease in 1984. Therefore the seismicity rate in volume 401 is considered to have been normal during the period 1982 through 1984.

It is concluded that even moderate-size earthquakes along the San Andreas fault can have clearly measurable precursory quiescence, and it is therefore proposed that the quiescence hypothesis holds for the study area. Rate decreases which are judged highly significant but which are not followed by mainshocks also exist. The number of false alarms generated by such episodes is reduced by defining false alarms as those rate decreases for which both the AS z -value and duration exceed or equal those of the weakest known precursor. In the present study it is postulated that $z \geq 3.0$ and duration ≥ 1 year may serve as minimum threshold constraints for an alarm to be issued. Using these constraints, the quiet periods of 1982 and 1984 in volume 401 ($M_L \geq 2.0$; Figure 3) do not qualify as false alarms.

THE CIENEGA WINERY SEISMIC GAP

The 14-km segment of the San Andreas fault at the Cienega Winery has shown a lower seismicity rate than the segments north and south of it during the period of

detailed monitoring (1969-present) (Burford and Harsh, 1980). The measured fault-creep rate is about 1 cm/year (Burford and Harsh, 1980). This fault segment (Volume 372, Figure 1) may have special properties because the Calaveras fault projects onto the San Andreas fault within this segment. Activity along the Paicines fault nearby to the northeast is locally increased opposite the Winery segment. Instead of assuming that the low rate near the Winery represents a doughnut pattern as defined by Mogi (1969), we interpret it to be a permanent feature related to the unique location near a prominent bifurcation of the fault system.

Aftershock sequences that have occurred in the area since 1969 define the Cienega Winery segment (Figure 4) as a seismic gap of about 14-km length (seismic gap of the first kind, Mogi, 1979). An additional seismic gap near San Juan Bautista is also evident (Figure 4). These two quiet segments will be referred to in the remaining text as the Cienega and the San Juan gaps. Since seismic gaps mark fault segments where future mainshocks are more likely than along the rest of the fault, we have examined the seismicity rate within these gaps in order to determine whether seismic quiescence exists there at the present. If a quiescence anomaly does exist at the present, a gap may be said to be mature, that is, in the precursory stage for a future mainshock (Habermann, 1981a).

The cumulative number of earthquakes is shown as a function of time for the Cienega gap in Figure 5. Although the total number of earthquakes (79) is not large, a highly significant seismic quiescence period lasting from early 1982 to December 1984 can be defined. The rate decrease amounts to approximately 50 to 80% below the background, and is judged significant above the 99% level for all data sets with $M_L \geq 1.5$ (only those for $M_L \geq 1.7$ and $M_L \geq 2.0$ are shown). The volume for which we have presented data in Figure 5 (polygon 372 defined in Figures 1 and 4) does not cover the

entire Cienega gap. It is the volume that optimizes the quiescence anomaly. In the data set covering the entire extent of the gap the anomaly also exists and is judged significant, but slightly less so than the data presented in Figure 5. This period of quiescence just barely qualifies as an alarm because the average of $z=3.05$ (Table 2). Since the anomaly started in June 1982, it will have persisted for over 2.8 years by the time of release of this report assuming that the yet-unavailable data of 1985 will not show a return to normal rates.

THE SAN JUAN SEISMIC GAP

The San Juan seismic gap (volume 382, Figure 1) has a length of only about 6 km. Nevertheless the number of earthquakes within the data set for volume 382 exceeds 100. The cumulative number curves (Figure 6) show a comparatively low variance and a clear seismic quiescence at the end of the data set. This quiescence has lasted from February 1983 to the present. The rate decrease is 56 to 75%. The z -values calculated by the $AS(t)$ algorithm are 2.8 and 4.9 ($M_L \geq 1.7$ and $M_L \geq 2.0$ respectively) and thus the changes are judged significant above the 99% confidence level and the quiescence qualifies both by duration and by z -value as an alarm (Table 2). The exact onset time of the anomaly is less sharply defined than in Figures 2 and 5, where the $AS(t)$ function peaks rapidly and at one value only. In Figure 6 the February 1983 peak in $AS(t)$ is surpassed by a later peak in the same year. In general anomaly onset times are defined as the time of the maximum value of $AS(t)$. However, in the case of volume 382 (Figure 6), where two peaks of similar value exist, the first peak is chosen for defining the onset time.

The San Juan seismic gap is situated near the southern terminus of the 1906 San Francisco great earthquake rupture, and it is separated from the Cienega gap by approximately 10 km (Figure 1).

COMPARISON OF SEISMICITY RATES BETWEEN GAPS AND NON-GAPS

Changes of seismicity rates contained in earthquake catalogs can be due to unexpected artificial causes (Habermann, 1982; Wyss et al., 1984; Habermann and Wyss, 1984a). Therefore, the possibility that current quiescences in the San Juan and Cienega seismic gaps (Figures 5 and 6) may have been due to a reporting procedure change must be tested. For this purpose, seismicity rates during 1982-84 within neighboring fault segments will be compared to background rates in these same segments. If adjacent segments show constant seismicity rates up through the present, the hypothesis that the gap quiescences may have been introduced artificially will be rejected.

In volumes 406 and 407, the seismicity rates slightly decrease with time but are fairly constant (Figure 7). This rate decrease disappears if a magnitude correction of +0.1 is made for the post 1980 data. The important point of this figure is that in both volumes, the rates during 1982-84 are not anomalous, which contrasts with the rate reductions reported for the seismic gaps and suggests that anomalous rates were not artificially introduced. Fault segments with constant seismicity rate during the last several years are not shaded in Figure 1.

The seismicity rates within volumes 403 and 404 (Figure 8) are not as constant as those in volumes 406 and 407. In volume 404 the rate of seismicity was increased markedly during several months of 1978, and in volume 403 a still-current, highly significant rate decrease started in 1980. The analysis presented in the Appendix strongly suggests that a magnitude shift took place at the end of 1980. The seismicity rate in volume 403 is constant throughout the data period if 0.1 is added to all magnitudes after October 1980. The important point for this study is that in both data sets the seismicity rate has been fairly constant during the last 5 to 6 years. Thus these data also support the conclusion that strong rate decreases in 1982/83 in other adjacent volumes were

probably not artificial.

The cumulative seismicity curve within volume 402 shows a larger variance than in other volumes because of the occurrence of the mainshock of August 1982 and its preceding quiescence. The quiescence precursor to this earthquake was best defined in volume 361, but it is clearly evident in all of volume 402 (Figure 9). In addition, a 5-month period of low rate is evident in late 1977-early 1978 in this volume. This decrease in rate is judged significant by the $AS(t)$ function but just barely above the 99% confidence level (not shown in Figure 9), and it was not immediately followed by a mainshock. Instead, a large number of small events followed it and an $M_L=3.8$ shock occurred 3 months after the termination of this quiescence. The 1977-78 quiescence in volume 402 is not classified as a false alarm because swarm activity and a subsequent mainshock followed it, and the significance of the anomaly ($z < 3$) was inferior to that of the precursors listed in Table 1.

The rate during the last year of the data is significantly low in volume 402, especially for larger events ($M \geq 2.0$). Whether this may represent an expansion of the quiet volumes cannot be decided, because an analysis procedure change may have occurred in January 1984 (Appendix A).

Volume 386 is the only volume other than those within the seismic gaps that shows onset of a clear seismic quiescence for the period 1983/84. The rate decrease is approximately 70% and is judged highly significant with $z > 6$ calculated by the $AS(t)$ function (Figure 10, Table 2). This fault segment also showed evidence of quiescence prior to the August 1982 earthquakes, some of which occurred within volume 386. The decrease of seismicity rate during 1983/84 in volume 386 is interpreted to have the same meaning as the decrease in the gaps. The hypothesis that this quiescence may be due to inhomogeneous reporting is rejected because five other fault segments in the area (401, 403, 404,

406 and 407) show nearly constant rates during the critical 1983-84 period.

UNIQUENESS OF QUIESCENCE ANOMALIES

The evaluation of anomaly uniqueness is important for estimating the probability that an anomaly may be a false alarm. Therefore the data set was searched systematically for periods of quiescence which had similar (or longer) durations than those identified as anomalies, and which might equal or surpass the latter in significance. The search was performed in the 10 volumes listed in Appendix B. This list includes the anomaly volumes themselves, the comparison volumes discussed and two additional volumes (459, 458) randomly chosen to include half each of the combined volumes 407/406 and 403/406. three time window lengths corresponding to periods of anomalous data in polygons 386, 382 and 372 were 65, 99 and 130 weeks, respectively. Windows of these lengths were moved through each data set, at one week steps, calculating at each step the z-value resulting from the comparison of the rate within the window with the rate of all preceding data within the volume in question. This test uses the RTZ(t) function (e.g. Habermann and Wyss, 1984b; Wyss and Koyanagi, 1985) to evaluate the significance of seismicity-rate changes in approximately 400 overlapping time windows within the 10 volumes tested. This procedure resulted in approximately 4000 uniqueness evaluations for each window length.

The results of these tests are as follows: The present-day anomalies (Table 2) and the precursor anomalies are completely unique. In this test it was not counted as a failure when one identified anomaly eclipsed in significance another one. The two weakest anomalies (Cienega Gap and $M_L=4.0$ August 1979) would have been surpassed by the 1980 rate decrease as defined by the uncorrected data in volume 403. However, the 1980 rate decrease was interpreted as due to a magnitude shift (Appendix A) and therefore it was discounted.

The absence of false alarms in the study area suggests that the false alarm rate estimated to be about 30% elsewhere (Wyss and Habermann, 1984) may be lower in the area of study. Thus a conservative estimate of the false alarm rate is 30%.

DISCUSSION

The hypothesis that fault segments may be characterized by fairly constant rates of seismicity over long periods of time (years to decades) is supported by most of the data analyzed. Although some volumes contained rate changes which are not understood, thereby making the quantification of background rate more difficult, in general the variances of the rates are small enough so that we can hope to identify precursory quiescences if they last longer than a year.

Within the 100-km segment of the San Andreas fault studied (Figure 1), two small mainshocks were preceded by seismicity-rate decreases of 60-85%. These anomalies were confined to volumes within 10 km of the respective mainshock locations. In both cases the anomalies did not last until the times of the mainshocks. Instead, the rates returned to normal, or even higher, values for some three or so months before the mainshock occurrence. Because this type of pattern has been observed in several other cases (e.g. Ohtake et al., 1979; Ryall and Ryall, 1982; Wyss et al., 1984) it is interpreted as a precursor. These observations are important because they help further establish the validity of the quiescence-anomaly hypothesis for the San Andreas fault system. They are also important for defining the precursor time versus magnitude relationship for quiescence anomalies. Most existing high-quality data sets apply to mainshocks in the range $6 \leq M \leq 8$ (Wyss, 1985). For the range $6 \leq M \leq 7$, the precursor times of quiescence tend to be in the range of 1.5 to 3.5 years, and for $7 \leq M \leq 8$ mainshocks they range from 2 to 6 years. From observations reported here (Table 1), and from those of Habermann and Wyss (1984b), it is concluded that, in the study area, mainshocks in the range

$4 \leq M_L \leq 6.5$ can be expected to have quiescence precursor times between 0.5 and 3 years. Of course, exceptions to this guideline and mainshocks without precursory quiescence are possible in the study area.

The segment of the San Andreas fault between 36.36° and 37° N shows a complex pattern of seismicity rates as a function of time: While three segments contain seismic quiescence from 1982/83 to the present (Table 2), the seismicity rate in five other segments continued at nearly constant rates. Rate decreases in the quiet volumes averaged about 70%, a highly significant result based on the standard deviate z-test. Also, all three of these quiescence anomalies are unique within the data period studied (August 1973-December 1984). The fact that volumes of 10 km dimensions with constant seismicity rates are intermixed with volumes of quiescence (Figure 1) suggests that the present quiescence anomalies should not be dismissed as artificial changes due to changes in reporting. It is herein proposed that the observed quiescences are more likely due to an underlying tectonic process, in which case there are three options for interpretation: (1) The periods of quiescences are false alarms and no mainshocks are to be expected. (2) Some or all of the anomalies are precursors, and separate mainshocks are expected in each volume of quiescence. (3) The anomalies are precursors which are related to each other, or to a more regional tectonic process, and one large rupture may be expected to include all three quiescent segments, as well as the segments between them. The merits and implications of these options are examined below.

(1) *False Alarms* can be defined as quiescence periods that are not followed by mainshocks, but are nevertheless of greater or equal significance and duration in comparison with precursory periods of quiescence. From areas other than the San Andreas fault it has been estimated that the probability for a significant quiescence to be a precursor is approximately 70% (Wyss and Habermann, 1984). In the data set at hand,

other quiescences equaling the 1982 to 1984 anomalies in volumes 372, 382 and 386 have not been found. However, this does not guarantee that the currently observed anomalies are definitely precursors. Assuming that the ratio of actual precursors to false alarms estimated for other regions also holds here, it would be most likely that two of the three anomalies are precursors. The alternative that all three anomalies will turn out to be false alarms is less likely.

(2) *If separate mainshocks* are expected to terminate quiescences in the individual segments, the mainshock parameters may be estimated based on the anomaly dimensions and durations. In examples from Hawaii, where many details regarding seismicity patterns were available, it was found that only parts of the ultimate rupture volume had turned quiet. Significantly, the mainshock initiation points of the ruptures were located within volumes that continued to be seismically active at constant rates (Wyss et al., 1981; Wyss and Koyanagi, 1985). This suggests the possibility that the expected ruptures may be somewhat larger than the quiet segments, and that the ruptures may initiate outside the quiet volumes. However, the seismic history of the study area suggests a pattern of isolated mainshocks of $4 \leq M_L \leq 5.7$ perhaps occurring as part of a related sequence. In the separate mainshock hypothesis it is assumed that the length of each separate quiescent segment will be the length of the expected rupture.

(2a) The Cienega Winery event may thus have a source length between 13 and 18 km, which corresponds approximately to a magnitude $M_L = 5.1 \pm 0.5$ mainshock. However, the quiescence started in mid-1982 which makes it almost three years long at the time of this writing. Along the Calaveras fault and in Hawaii, quiescences of 2.4-year durations were terminated by $M_L = 6.0$ and $M_L = 6.6$ mainshocks (Habermann and Wyss, 1984b; Wyss and Koyanagi, 1985). Based on the precursor length alone one might therefore expect a mainshock of $M_L \approx 6.5 \pm 0.5$, provided that it happens soon. The

choice of ± 0.5 for an uncertainty estimate is derived from the variance with which the precursor-time versus magnitude relationship is defined. If more time elapses without a mainshock the anomaly time will become larger and the magnitude estimate will further rise. The discrepancy between magnitude estimates based on the dimension and the duration of the anomaly suggests that the single-rupture hypothesis (option 3) may be more likely than the separate rupture scenario. Averaging the two magnitude estimates above would lead to an estimate of $M_L = 5.75 \pm 0.5$. However, if more weight is given to the estimate based on segment length, the preferred magnitude range would be $4.6 \leq M_L \leq 5.6$. The statistical significance of the Cienega anomaly estimated by $AS(t)$ is lower than that of the San Juan and Stone Canyon anomalies. Also, if the test volume is decreased, seismicity-rate changes can no longer be defined within the Cienega gap owing to paucity of events. For these reasons the Cienega quiescence is not as clearly defined in space and time as the other anomalies. Consequently, the Cienega anomaly may represent a false alarm.

(2b) The San Juan quiescence extends over about 5 km, but the entire gap is approximately 7 km long. These dimensions would be appropriate for an $M_L = 4.0 \pm 0.5$ mainshock. However, the duration of the quiescence is 2.2 years at the time of release of this report, suggesting a mainshock which would possibly be as high as $M \approx 6$. The average of these estimates is $M_L = 5.0 \pm 1.0$. Because the magnitude-versus-precursor time criteria are much more uncertain than the magnitude-versus-rupture length relationship, more weight is given to the latter, arriving at a preferred estimate of $M_L = 4.7 \pm 0.5$.

(2c) The Stone Canyon quiescence also has lasted for almost 2 years. This duration period agrees with the anomaly (segment) length of about 7 km in the sense that an event of $M_L \approx 5.0 \pm 0.5$ happening immediately would satisfy both constraints. As the anomaly shows very large z-values (Table 2) one may argue that the probability of a

future mainshock within segment 386 is higher than anywhere else along the 100-km segment of the San Andreas fault studied here. But the anomaly onset is later than in the two other cases, making the definition of quiescence more dependent on the suspect 1984 data. For these reasons the expectation for a mainshock here are not larger than in segment 382.

(3) *The single rupture hypothesis*, is suggested by the fact that the three anomalies all developed within a 1-year period. One could thus assume that they are interrelated with a common starting time of 1982.9 ± 0.5 . Also, the fact that the combined anomaly duration is too long for the dimensions of two of the gaps, suggests that a single process may be governing all three anomalies. In addition, the pattern of quiet and non-quiet fault segments (Figure 1) is strikingly similar to the pattern observed in the source area of the 1975 Hawaii $M_s=7.2$ earthquake. Figure 11 compares the San Andreas seismicity pattern defined here with the precursor pattern to the 1975 Hawaii earthquake. The dimensions of the quiet segments, their spacing and the overall dimensions in the two cases are almost identical.

The Hawaii $M=7.2$ rupture was a multiple event consisting of several $M \approx 6$ shocks including a foreshock 70 minutes ahead of the main rupture. The foreshock and mainshock were located in one of the non-quiet segments (Wyss and et al., 1981). Based on these and other facts, the hypothesis was proposed that the non-quiet segments in Hawaii represented asperities (Wyss et al., 1981). Quiescence was interpreted in that case as being due to strain softening (Stuart, 1974) because geodetic observations suggesting strain release were made during the precursory anomaly time (Wyss et al., 1981). The 1983 Kaoiki $M_L=6.6$ earthquake showed precursory seismicity patterns which exactly conformed to the hypothesis developed on the basis of the 1975 mainshock data (Wyss and Koyanagi, 1985). Both of these mainshock ruptures started in a central

volume of non-quiescence, then spread into the surrounding quiet areas. Based on these facts, the following scenario for termination of the current San Andreas fault quiescences may be proposed: It is postulated that a multiple rupture may start in one of the non-quiet segments adjoining any of the quiet segments (shaded dark in Figures 1 and 11), i.e. volumes 401, 402, 403 or 404. The total rupture length, L , might be expected to be 45 ± 5 km if all three quiet segments join in a multiple-event rupture.

Combining the seismic data of these anomalous fault segments, the cumulative number of events was plotted as a function of time (Figure 12). Since volume 386 is the seismically most active one, it dominates this figure. Using the $AS(t)$ function, we find that the quiescence is highly significant with a peak of $z=6$. In comparison the rest of the study area shows a constant seismicity rate during the entire time (Figure 12). The onset of the anomaly is placed at the beginning of 1983 defined by the first $z > 3$ peak of the AS function. If the joint anomaly is evaluated by the RTZ function (Wyss and Koyanagi, 1985), it is found that the alarm could have been issued in the first half of 1984, because at that time enough information was available to define the quiescence anomaly with a standard deviate $z > 3$, the requirement for issuing an alarm.

The seismic moment for the combined sources, $M_o = \mu LWD$, may be estimated using the following assumptions: The rupture width, W , is assumed to be approximately 6 km, similar to values estimated for the $M_L = 6.2$ Morgan Hill 1984 (Bakun et al., 1984) and $M_s = 6.4$ Parkfield 1966 (Scholz et al., 1969) earthquakes. The possible dislocation, D , is more difficult to estimate. Slip accumulated by plate motion in this region is partly distributed on various fault branches, and occurs partly as aseismic slip. No significant fault creep has been observed north of the San Juan gap since about 1968. Within the source area of the expected earthquake the creep rate ranges from about 0.8 to 1.5 cm/year (Burford and Harsh, 1980). A conservative estimate is that

approximately 1 cm of potential slip is accumulated per year which will be available for relaxation during a future mainshock rupture along the San Andreas fault segment in question. The last mainshocks in the Cienega gap occurred on 20 January 1960 ($M_L=5.0$) and on 9 April 1961 ($M_L=5.7$ and 5.5). The latter sequence caused a 1.3 cm slip at the Cienega Winery (Nason, 1973) and the rupture apparently extended to some distance on both sides of the Cienega Winery site (D. Tocher, personal communication, 1974). Making the conservative assumption that the strain available for seismic rupture in the Cienega gap was completely released at the time of the 1961 shock, we estimate that a minimum slip of $D=24$ cm is now available for the expected mainshock. Thus a seismic moment of $M_0 \approx 2 \cdot 10^{25}$ dyne.cm can be estimated for the combined sources (assuming the shear modulus $\mu=3 \cdot 10^{11}$ dyne/cm²). This seismic moment is approximately equal to that of the 1966 Parkfield earthquake (e.g., Scholz et al., 1969). With an average stress drop, the magnitude from such an event would be approximately $M_s=6.2$ (Kanamori and Anderson, 1975).

The occurrence time of the combined-source rupture is more difficult to estimate than its magnitude because the quiescence precursor time versus magnitude relationship is poorly known. Along the Calaveras fault two earthquakes ($M_L=6 \pm 0.2$) were preceded by quiescences which lasted 2.4 and 2.7 years (Habermann and Wyss, 1985). The 1977 Imperial Valley ($M_n=6.5$) mainshock showed a precursor lasting for only 0.3 years, and the 1983 Koaiki ($M_{Nubs}=6.6$) shock was preceded by 2.5 years of quiescence. Based on these limited data one would expect that the present quiescence in the Cienega and the San Juan gaps is indicative of a future mainshock with $M_s \approx 6.5$. The precursory quiescence to the $M_s=7.2$ Hawaii earthquake (1975) lasted 3.8 years. Thus, if the expected event does not rupture the identified quiet segments (Figure 1) within the next

12 months, it could be argued that the magnitude estimate should be raised to $M_s \approx 7$. Considering the absence of historical records of earthquakes of this size along the fault segment in question (the 1890 earthquake may be an exception), it may be argued that the estimate of $M_s > 6$ is unreasonably large. In that case the proposed combined-source mainshock should occur within the next 12 months, in order to conform to the presently known relationship between magnitude and quiescence length. Although no event of this magnitude is known during the short history of the area, Sykes and Nishenko (1984) estimated that this fault segment may be capable of $M_s = 6.5$ ruptures. Therefore we find our estimate of the magnitude for imminent rupture of combined source areas in agreement with the maximum magnitude expected for this area based on other independent evidence. However, the entire single rupture interpretation may be regarded as unlikely if one heavily weighs the fact that no historic rupture of such a large size is known to have occurred along the fault segment in question.

It should be emphasized at this point that all of the above reasoning is based on a poorly consolidated hypothesis. All estimates of the proposed rupture characteristics could be considerably in error. Some of the major problems and shortcomings affecting the several proposed scenarios are briefly discussed below.

(1) The homogeneity of the catalog may not be continuous. Since the reporting of small events is most easily affected by procedure changes, we have conservatively used only $M_L \geq 1.7$ and $M_L \geq 2.0$ data sets, although the $M_L \geq 1.5$ data are probably acceptable for the period in question. However, procedure changes which affect the magnitudes assigned to the events can cause apparent rate changes in all magnitude classes. Magnitude shifts exist in the central California catalog (Reasonberg and Ellsworth, 1982; W. Bakun, personal communication; R.E. Habermann, personal communication) and they may have varied in amplitude in different parts of central California. A preliminary

study of the homogeneity problem showed that changes in analysis procedures in 1977 and 1980 influenced the reporting rate of events. However, the validity of the conclusions reached were not affected by these changes or the corrections one may chose for canceling these effects. The last year of the seismicity catalog, however, may not be fully compatible with the rest of the data, and if this is so than the significance of the current quiescence anomalies may be overestimated.

(2) False alarms (tectonic quiescences not followed by mainshocks) are known to have occurred. Thus it is possible that all of the identified anomalies are false alarms. This is not likely, however, because the ratio of real to false alarms from previous examples is estimated at 2:1.

(3) There exist only a few cases of detailed quantitative analysis of abundant seismicity-pattern data. Thus, our knowledge of the "typical quiescence pattern" and its variance is extremely limited. This problem is likely to introduce unknown errors into any predictions, but it does not necessarily invalidate the conclusions presented here.

(4) The variance of most tectonic processes is large. Different tectonic settings may cause differences in all aspects of the phenomenon of seismic quiescence. The Hawaii examples cited above include a horizontal thrust (1975) and a near-vertical strike-slip event (1983), both of which occurred within a brittle crust and were caused by stresses due to magnetic intrusions at 10- to 15-km distance. One may question the relevance of the Hawaii data for the San Andreas region. Nevertheless, the Calaveras examples are more similar in tectonic style to the Cienega setting and they agree very closely with the Hawaii data. Therefore, it is concluded as being likely that the existing quiescence hypothesis is valid for the study area.

(5) The known seismic history of the area is very short. The great 1906 San Francisco earthquake rupture extended to the vicinity of the San Juan seismic gap, but

displacements along its southern faulting extent were smaller than further north by a factor of 4 (e.g., Sykes and Nishenko, 1984). In 1838 the San Andreas fault north of the study area ruptured in an event of $M \approx 7$, and the rupture may have extended into the fault segments studied here (Sykes and Nishenko, 1984). In 1885 an $M \approx 6.2$ shock may have broken the fault segment studied, and in 1890 an $M \approx 6.0$ rupture appears to have extended northward from the San Juan seismic gap (Sykes and Nishenko, 1984). Therefore, it may be speculated that between repeats of the great ruptures ($M > 8$, San Francisco 1906), lesser magnitude earthquakes, perhaps of the $M=7$ class, could add the slip in the San Juan Bautista area that is necessary to equal the slip further north. As an outside chance, it is not inconceivable that the expected rupture may trigger a runaway event extending an unknown distance to the north of San Juan Bautista. Along the fault segment north of volume 404 (Figure 1) the seismicity rate is too low for an analysis of the type presented here, so there this tool is unable to furnish information for this area. The above speculation is similar to the idea that the next (or some subsequent) Parkfield earthquake may escalate into a larger rupture to the south of Cholame. The fault segment studied here is similar to the Parkfield segment in the following ways: Both areas are located at ends of the creeping part of the San Andreas fault where creep rates decrease rapidly towards the non-creeping adjoining fault segments, which in both cases have ruptured in great historic earthquakes (Burford and Harsh, 1980).

(6) The complexity of the quiescence pattern suggests that the state of stress along the fault also varies strongly on the 10-km scale. Since the details of the stress distribution are unknown it is impossible to assess in advance whether the entire 45-km segment will break in a multiple rupture or whether the individual quiet segments each will host smaller mainshocks. The latter scenario would more or less duplicate sequences of moderate earthquakes like the 1971-73 sequence, whereas the combined-sources,

multiple-rupture scenario is not supported by historic precedents in the study area.

Considering the facts, the interpretations and the speculations outlined above one may ask what types of observations might help in refining the hypothesis and the predictions put forth. The model explaining the 1975 Hawaii quiescence precursor postulates that fault-creep activity may have caused seismic quiescences by de-stressing the source volume where the seismicity rate decreased. The chief support for this model came from the observation of strain relaxation measured geodetically above the source area (Wyss et al., 1981). A preliminary examination of the creep records for the San Andreas fault segments in question shows instead that the rate of fault creep has also decreased to lower-than-average values at most monitoring sites in the study area since 1982. A detailed analysis of these records is in progress. If slip-rate changes along deeper portions of the fault are associated with quiescence anomalies some of the concurrent geodetic data may contain information that could be pertinent for understanding the processes at work.

A possible means of refining the specification of occurrence time(s) for the mainshock(s) may be the real-time monitoring of the seismicity rate in the now-quiet fault segments. It may be speculated that renewed higher seismicity rates could indicate that the expected mainshocks are near, because the two previous examples of precursory quiescence (Figures 2, 3) showed renewed activity before the mainshocks. If, however, normal rates return and persist over a long period (e.g. longer than one year) the anomalies would have to be reclassified as false alarms.

CONCLUSIONS

The seismicity rate along the San Andreas fault between 36.36° and 37° N latitude showed the following pattern: Within three separate segments, 5- to 10-km long, the seismicity rates are presently lower than average by approximately 70%. These periods

of quiescence started around 1982.9 ± 5 years, and the quiet segments are separated from one another by volumes of more nearly constant rate. Two previous periods of quiescence (1.3 to 1.6 years) were followed by mainshocks of $M_L = 4.0$ and 4.2 within the respective quiet fault segments. These precursor anomalies and the presently existing anomalies are unique in statistical significance.

In the interpretation of these observations two hypotheses emerge: (1) The three quiescence anomalies are not interrelated, but one or several of them will lead to separate mainshocks with $M_L = 5.4 \pm 0.5$ (Cienega gap), $M_L = 4.7 \pm 0.5$ (San Juan gap) and $M_L = 5.0 \pm 0.5$ (Stone Canyon). The shocks are expected to happen within the next 12 months. It is estimated that the probability for at least one of these events to occur is at least about 70%. (2) A second hypothesis, which is not supported by the recent seismic history, is that the three quiescence anomalies may be related to the preparation process for a single, fairly large rupture involving all three quiet segments as well as the intervening segments. In this case the seismic moment of the expected event can be estimated at about $2 \pm 1 \cdot 10^{25}$ dyne.cm, corresponding to a mainshock of $M_s \approx 6.2 \pm 0.3$. The rupture would be centered in the Cienega gap (36.75° N and 121.4° W) and extend roughly from San Juan Bautista to Stone Canyon. If this event is to occur at all, it should occur within the next 12 months.

Other interpretations of the observations are possible but less likely in our opinion. Included among the possibilities are that all quiescences are false alarms, or that a larger rupture towards the north past San Juan Bautista may be triggered by the expected events within the study area.

Acknowledgments: We thank R.E. Habermann for the software for statistical analysis. R.E. Wallace, J. Savage, R. E. Habermann, W. Bakun and J.R. Bowman made helpful comments for the improvement of the manuscript. This work was supported in

part by NSF grant EAR-8417014.

REFERENCES

- Bakun, W.H., M.M. Clark, R.S. Cockerham, W.L. Ellsworth, A.G. Lindh, W.H. Prescott, A.F. Shakal, P. Spudich, The 1984 Morgan hill, California, earthquake, *Science*, **225**, 288-291, 1984.
- Burford, R.O. and P.W. Harsh, Slip on the San Andreas fault in Central California from alignment array surveys, *Bull. Seismol. Soc. Amer.*, **70**, 1233-1262, 1980.
- Ellsworth, W. L., Bear Valley, California, earthquake sequence of February-March 1972, *Bull. Seismol. Soc. Amer.*, **65**, 483-506, 1975.
- Habermann, R.E., Precursory seismicity patterns: Stalking the mature seismic gap, in Earthquake Prediction, Maurice Ewing Series, Amer. Geophys. Union, **4**, 29-42, 1981a.
- Habermann, R.E., The quantitative recognition and evaluation of seismic quiescence: Application to earthquake prediction and subduction zone tectonics, Ph.D. thesis. Univ. of Colorado, Boulder, 1981b.
- Habermann, R.E., Consistency of teleseismic reporting since 1963, *Bull. Seismol. Soc. Amer.*, **72**, 93-112, 1982.
- Habermann, R. E., Seismicity rates in the Kuriles Island Arc, *Earthquake Prediction Research 1*, 73-94, 1982.
- Habermann, R. E., Teleseismic detection in the Aleutian Island Arc, *J. Geophys. Res.*, **88**, 5056-5064, 1983.
- Habermann, R.E., Spatial seismicity variations and asperities in the New Hebrides seismic zone, *J. Geophys. Res.*, **89**, 5891-5904, 1984.
- Habermann, R.E. and M. Wyss, Background seismicity rates and precursory seismic quiescence: Imperial Valley, California, *Bull. Seismol. Soc. Amer.*, **74**, 1743-1755, 1984a.

- Habermann, R.E. and M. Wyss, Seismic quiescence and earthquake prediction on the Calaveras fault, Californian, Abstract, *EOS*, 65, 988, 1984b.
- Johnson, C.E. and L.K. Hutton, Aftershocks and preearthquake seismicity, in The Imperial Valley, California, earthquake of October 15, 1979; U.S. Geol. Survey, Prof. Paper, 1254, 59-76, 1982.
- Kanamori, H. and D.L. Anderson, Theoretical basis of some empirical relations in seismology, *Bull. Seismol. Soc. Amer.*, 65, 1073-1096, 1975.
- McNally, K., Spatial, temporal and mechanistic character in earthquake occurrence, Ph.D. Thesis, Univ. of California, Berkeley, CA, 1976.
- McNally, K., Plate subduction and prediction of earthquakes along the middle America trench, in Earthquake Prediction, Maurice Ewing Series, eds. D.W. Simpson and P.G. Richards, Amer. Geophys. Union, 4, 63-72, 1981.
- Mogi, K., Some features of recent seismic activity in and near Japan (2), Activity before and after great earthquakes, *Bull. Earthq. Res. Inst., Univ. Tokyo*, 47, 395-417, 1969.
- Mogi, K., Two kinds of seismic gaps, *Pure Appl. Geophys.*, 115, 1172-1186, 1979.
- Nason, R.D., Fault creep and earthquakes on the San Andreas fault, in Proceedings of the Conference on Tectonic Problems of the San Andreas Fault System, Stanford Univ. Geol. Sci., 13, 275-285, 1973.
- Ohtake, M., T. Matumoto and G.V. Latham, Seismicity gap near Oaxaca, Southern Mexico as a probable precursor to a large earthquake, *Pure Appl. Geophys.*, 115, 375-378, 1977.
- Reasonberg, P. and W.L. Ellsworth, Aftershocks of the Coyote Lake, California, earthquake of August 6, 1979: A detailed study, *J. Geophys. Res.*, 87, 10637-10655, 1982.

- Ryall, A. and F. Ryall, Spatial-temporal variations in seismicity preceding the May 1980, Mammoth lakes, California earthquakes, *Bull. Seismol. Soc. Amer.*, **71**, 747-760, 1981.
- Scholz, C.H., M. Wyss and S.W. Smith, Seismic and aseismic slip on the San Andreas fault, *J. Geophys. Res.*, **74**, 2049-2069, 1969.
- Stuart, W.D., Diffusionless dilatancy model for earthquake precursors, *Geophys. Res. Lett.*, **1**, 261, 1974.
- Sykes, L., and S. P. Nishenko, Probabilities of occurrence of large plate rupturing earthquakes for the San Andreas, San Jacinto, and Imperial faults, California, 1983-2003, *J. Geophys. Res.*, **89**, 5905-5928, 1984.
- Wesson, R. L., R. O. Burford, and W. L. Ellsworth, Relationship between seismicity, fault creep and crustal loading along the central San Andreas fault, in *Proced. of the Conf. on Tectonic Problems of the San Andreas fault system*, eds. R. L. Kovach and A. Nur, Stanford Univ., Geol. Sci., **13**, 303-321, 1973.
- Wyss, M., F.W. Klein and A.C. Johnston, Precursors to the Kalapana M=7.2 earthquake, *J. Geophys. Res.*, **86**, 3881-3900, 1981.
- Wyss, M. and R.E. Habermann, Precursory seismic quiescence shows similar patterns for thrust, normal and strikeslip earthquakes along plate boundaries and elsewhere, *EOS*, **65**, 987, 1984.
- Wyss, M., R.E. Habermann and J.-C. Griesser, Seismic quiescence and asperities in the Tonga-Kermadec arc, *J. Geophys. Res.*, **89**, 9293-9304, 1984.
- Wyss, M. and R. Koyanagi, Seismic quiescence precursor to the 1983 Katoiki (M=6.6). Hawaii, earthquake, *Bull. Seismol. Soc. Amer.*, submitted, 1985.
- Wyss, M., Precursors to large earthquakes, *Earthq. Pred. Res.*, in press, 1985.
- Wyss, M. and D. Harvey, Comparison of a complex rupture model with the precursor

asperities of the 1975 Hawaii $M=7.2$ earthquake, *Bull. Seismol. Soc. Amer.*, submitted, 1985.

TABLE 1

Seismic Quiescence Precursor Parameters to Two Small Mainshocks

Dates (start-end of anomaly)	Precursor Time [years]	M_L	Mainshock Date	Location		Rate Decrease %		Z_{max}	
				Lat ° N	Long ° W	$M_L = 1.7+$	$M_L = 2.0+$	$M_L = 1.7+$	$M_L = 2.0+$
Dec 80-Oct 81	1.6	4.2	11 Aug 82	36.63	121.30	59	77	4.1	5.1
Jul 78-May 79	1.3	4.0	02 Aug 79	36.81	121.54	80	85	3.4	3.3

TABLE 2

Seismic Quiescence Anomaly Parameters for the Present

Dates	Anomaly Duration [years]	Anomaly Length [km]	M_L expected	Volume No.	Location	Rate Decrease %		Z_{max}	
						$M_L = 1.7+$	$M_L = 2.0+$	$M_L = 1.7+$	$M_L = 2.0+$
Jun 82-present	2.8	10	4.6-5.6	372	Cienega Gap	53	80	2.8	3.3
Feb 83-present	2.2	5	4.2-5.2	382	San Juan Gap	56	75	2.8	4.9
Jun 83-present	1.9	7	4.5-5.5	386	Stone Canyon	70	72	6.1	7.7

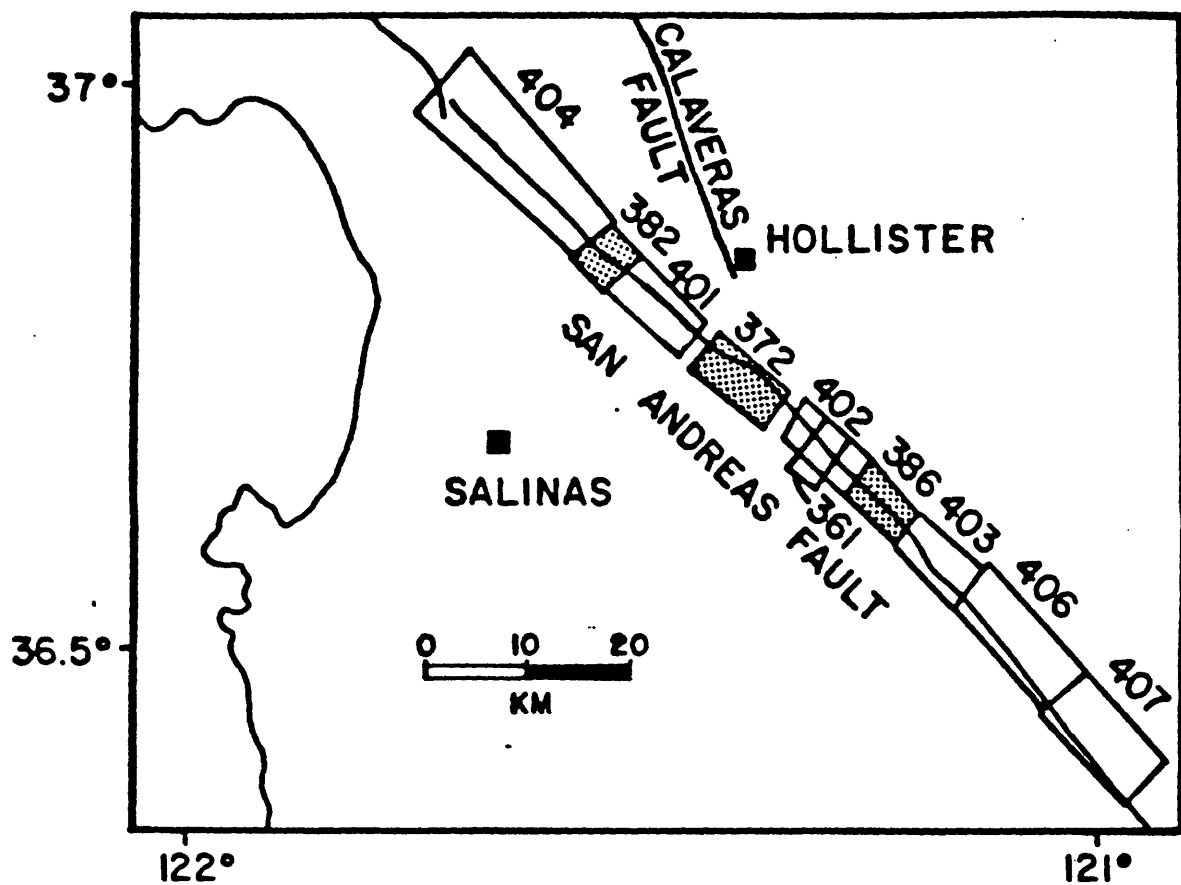


Figure 1: Map of the San Andreas fault segment selected for study in this paper. Seismicity rates within each volume, as defined by surface polygons, are studied separately. Seismic quiescence exists at the present only within the fault volumes indicated by stippled polygons.

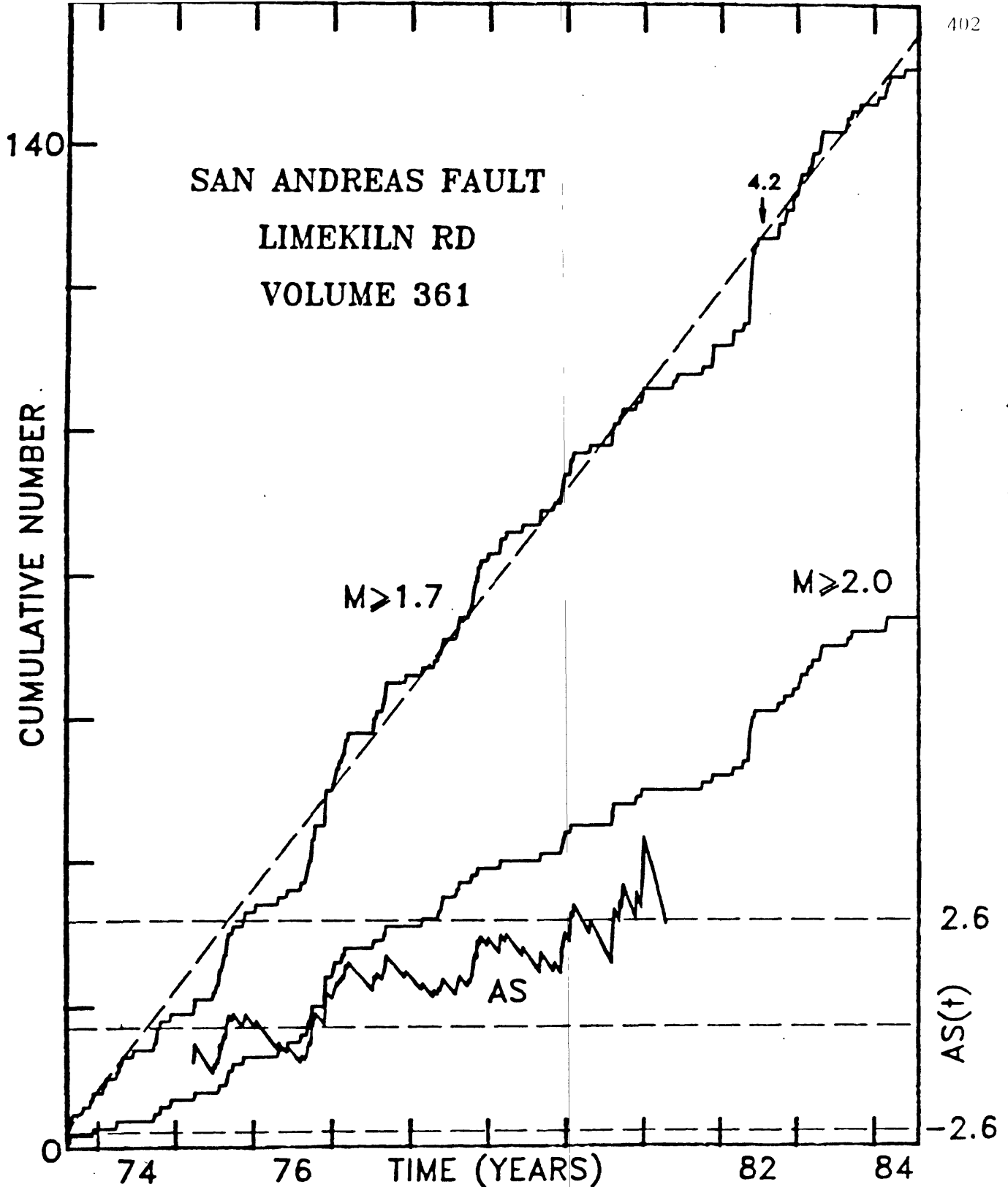


Figure 2: Example for a seismic quiescence precursor to an $M_L = 4.2$ mainshock which occurred on August 11, 1982 near Limekiln Road. Cumulative number of earthquakes in polygon 361 (defined in Figure 1) are shown. This polygon defines one of several neighboring volumes that show the anomaly. The top curve is for earthquakes with $M_L \geq 1.7$, the middle one for $M_L \geq 2.0$. The statistical function $AS(t)$ (bottom curve) is derived from the $M_L \geq 1.7$ data. When this function exceeds the upper dashed-line level, the significance of the seismic-rate decrease exceeds 99%. The quiescence anomaly lasted for about 1.6 years (Table 1).

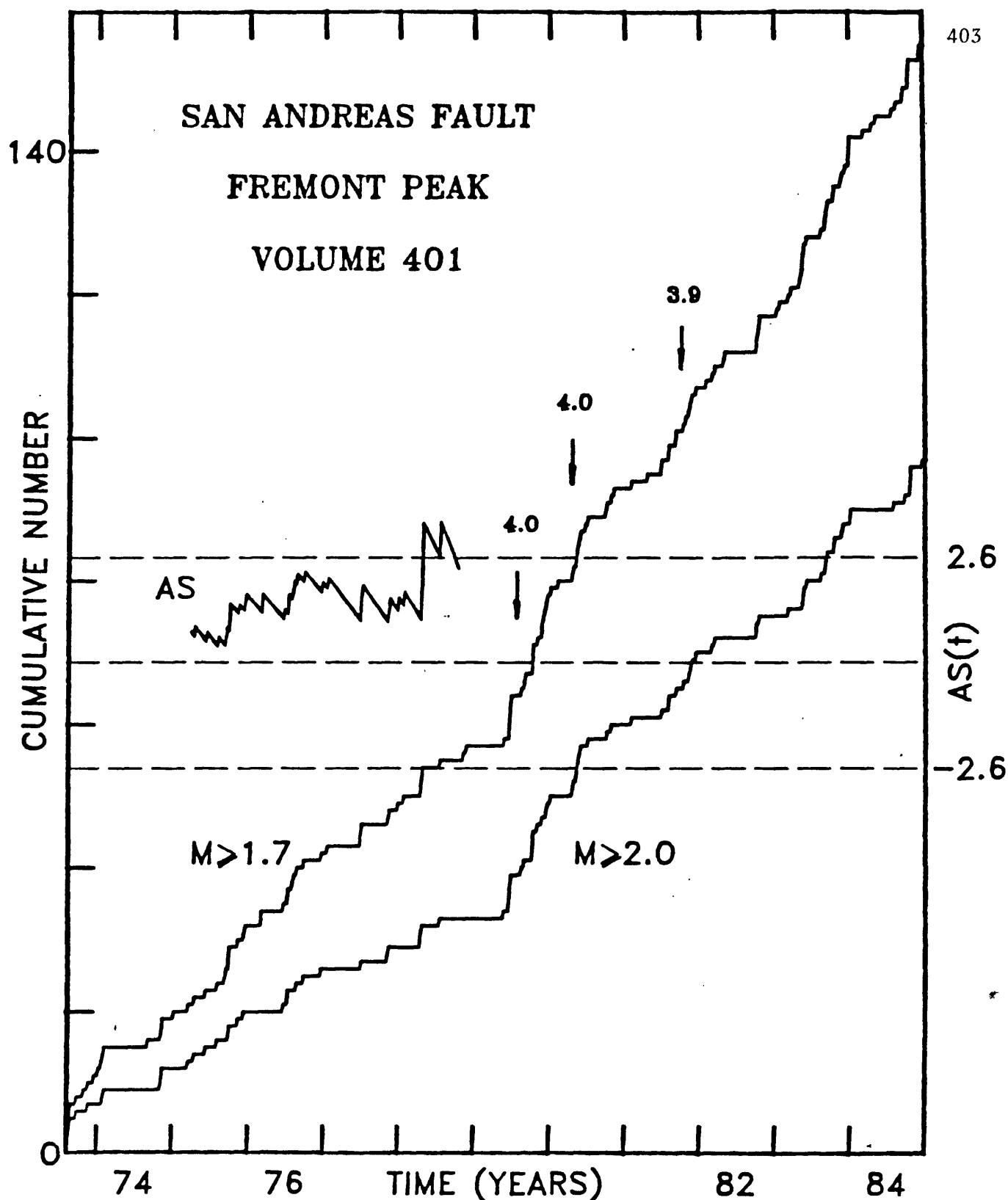


Figure 3: Cumulative number of earthquakes as a function of time within the San Andreas fault volume defined by polygon 401 in Figure 1. A mainshock of $M_L = 4.0$ was preceded by significant seismic quiescence (Table 1), while a $M_L = 4.1$ shock which followed a year later was not.

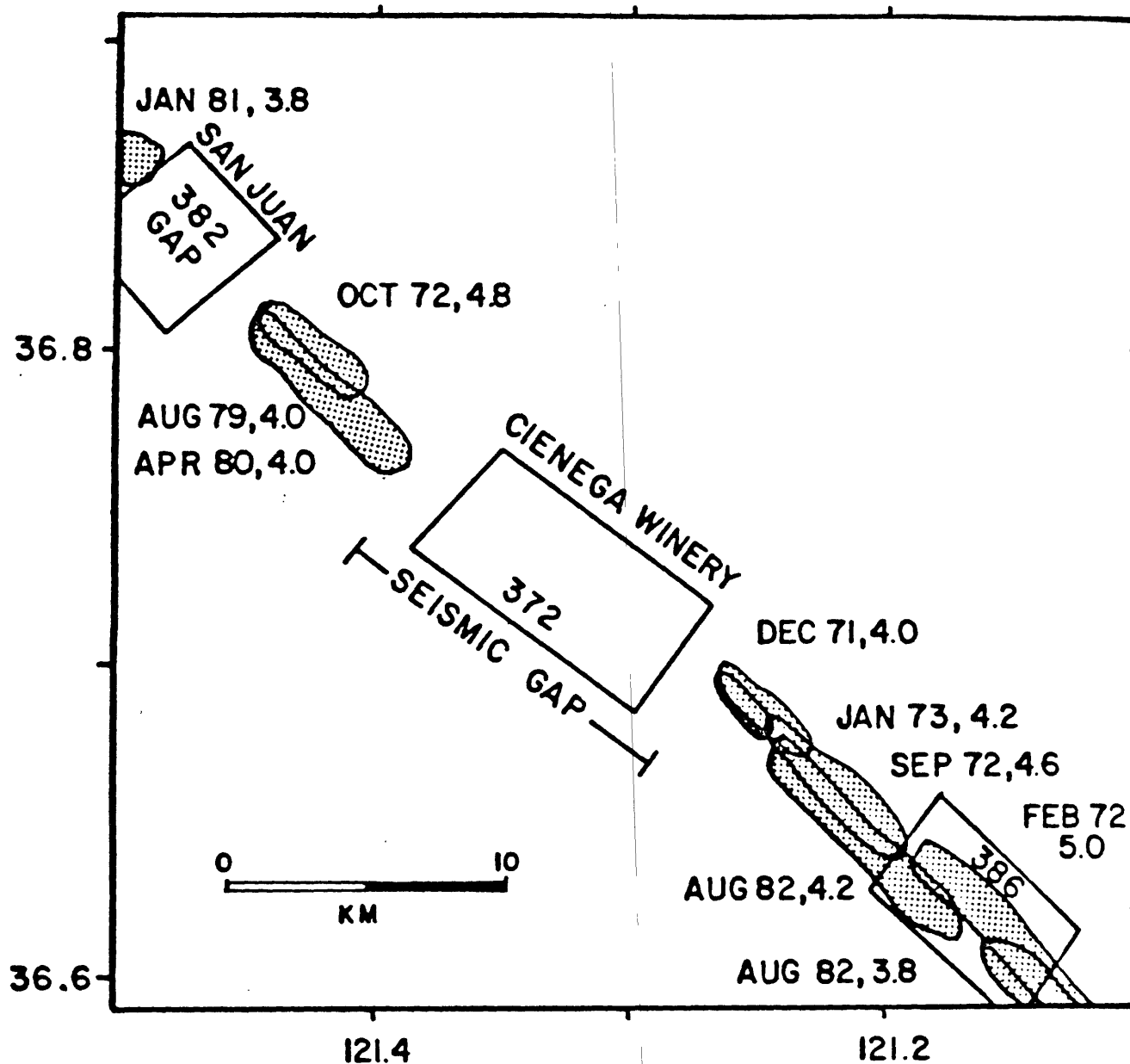


Figure 4: Map of the Cienega Winery section of the San Andreas fault showing aftershock areas of mainshocks which occurred between January 1969 and July 1984. These aftershock areas define a seismic gap of approximately 14-km length centered near the Winery. Another smaller gap of about 7-km length exists near San Juan Bautista. Polygons 372, 382 and 386 define crustal volumes extending to 15-km depth within which statistically significant seismic quiescence exists at the present.

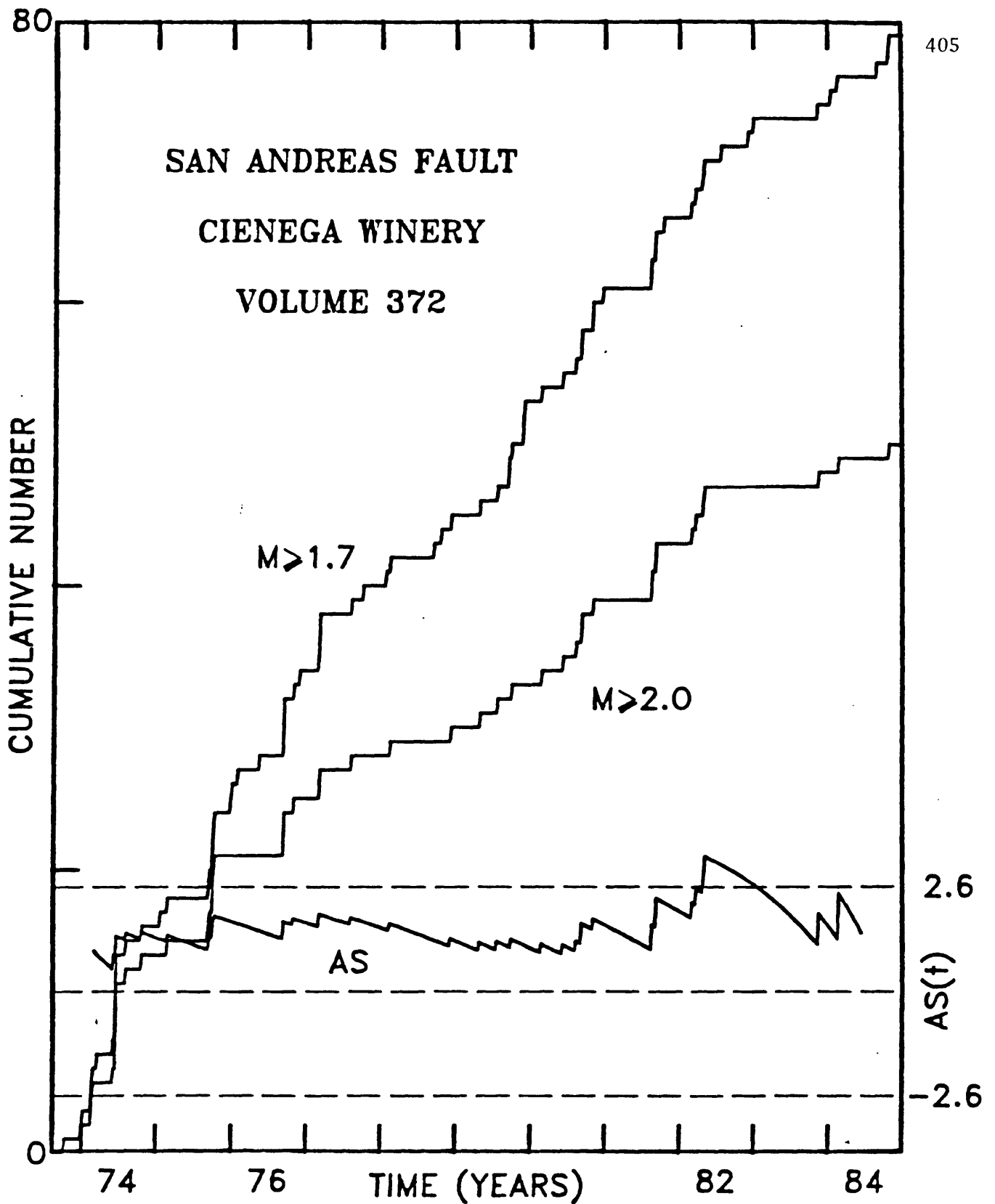


Figure 5: Cumulative number of earthquakes as a function of time for the Cienega Winery seismic gap. Volume 372 is defined in Figures 1 and 3. The upper curve is for earthquakes of $M_L \geq 1.7$, the lower one for $M_L \geq 2.0$. The statistical function $AS(t)$, derived from the $M_L \geq 1.7$ data, indicates that the present seismic quiescence is statistically significant above the 99% confidence level.

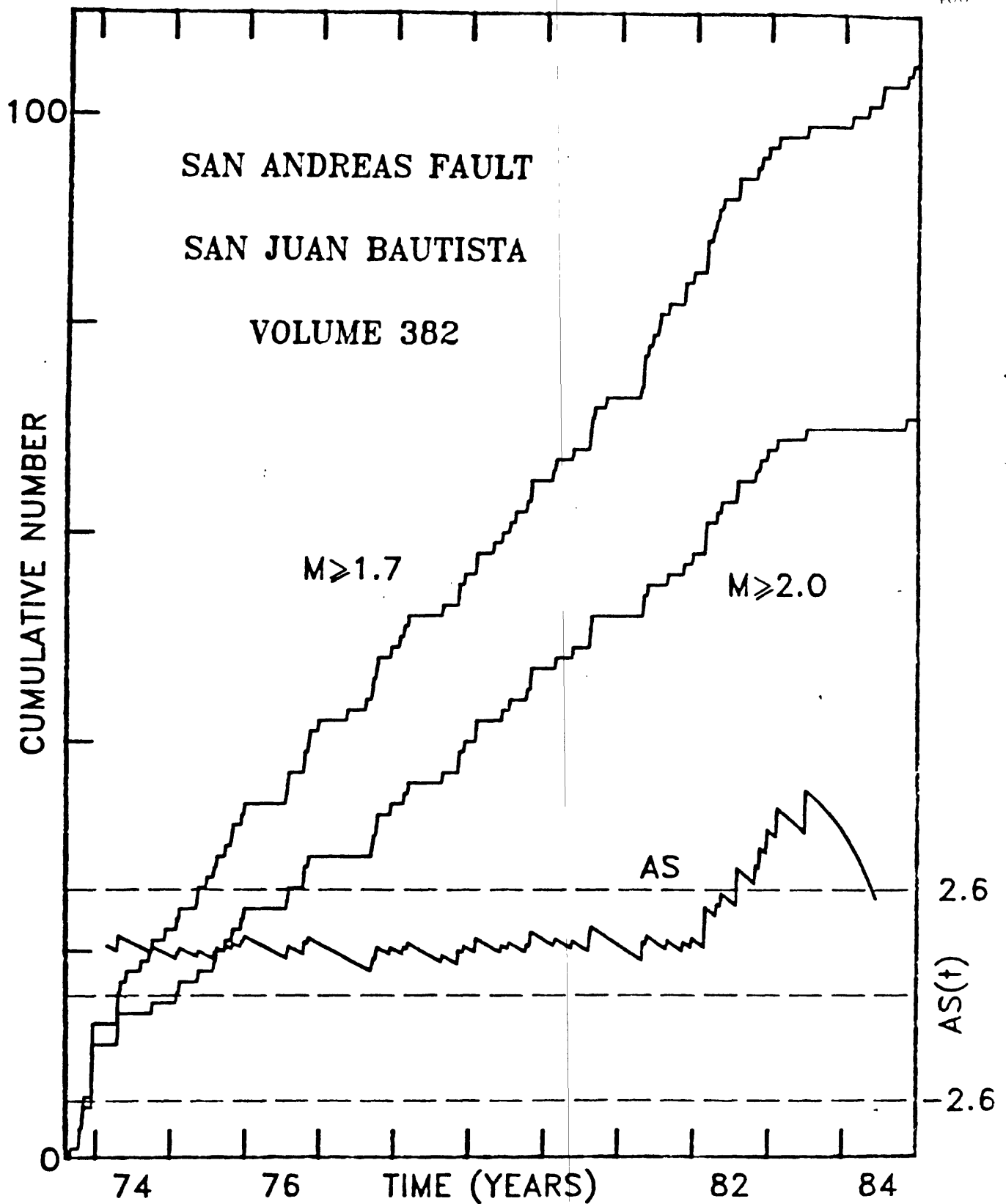


Figure 6: Cumulative number of earthquakes as a function of time for the San Juan Bautista seismic gap (volume 382, Figures 1 and 3). After a constant rate of seismicity during 1973 to 1982, the rate from early 1983 to present is significantly lower than average. The $AS(t)$ function was derived from the $M_L \geq 2.0$ data (lower cumulative curve). The $M_L \geq 1.7$ data (upper curve) show a statistical significance barely exceeding the 99% confidence level (not illustrated) because of renewed low-magnitude activity in 1984.

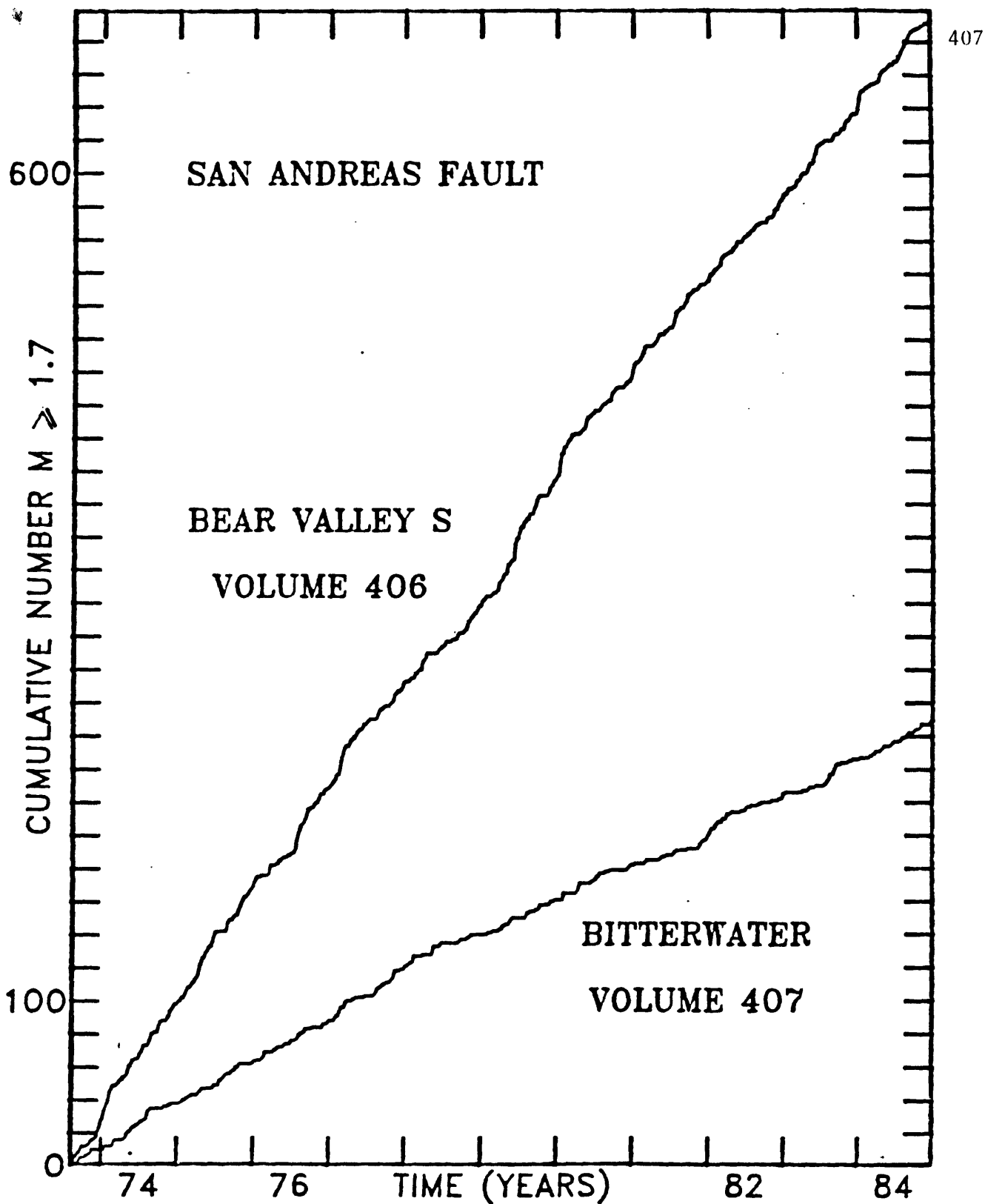


Figure 7: Cumulative number of earthquakes as a function of time within two volumes along the San Andreas fault defined by polygons 406 and 407 in Figure 1. The rates are essentially constant as a function of time in these volumes, especially during the past several years.

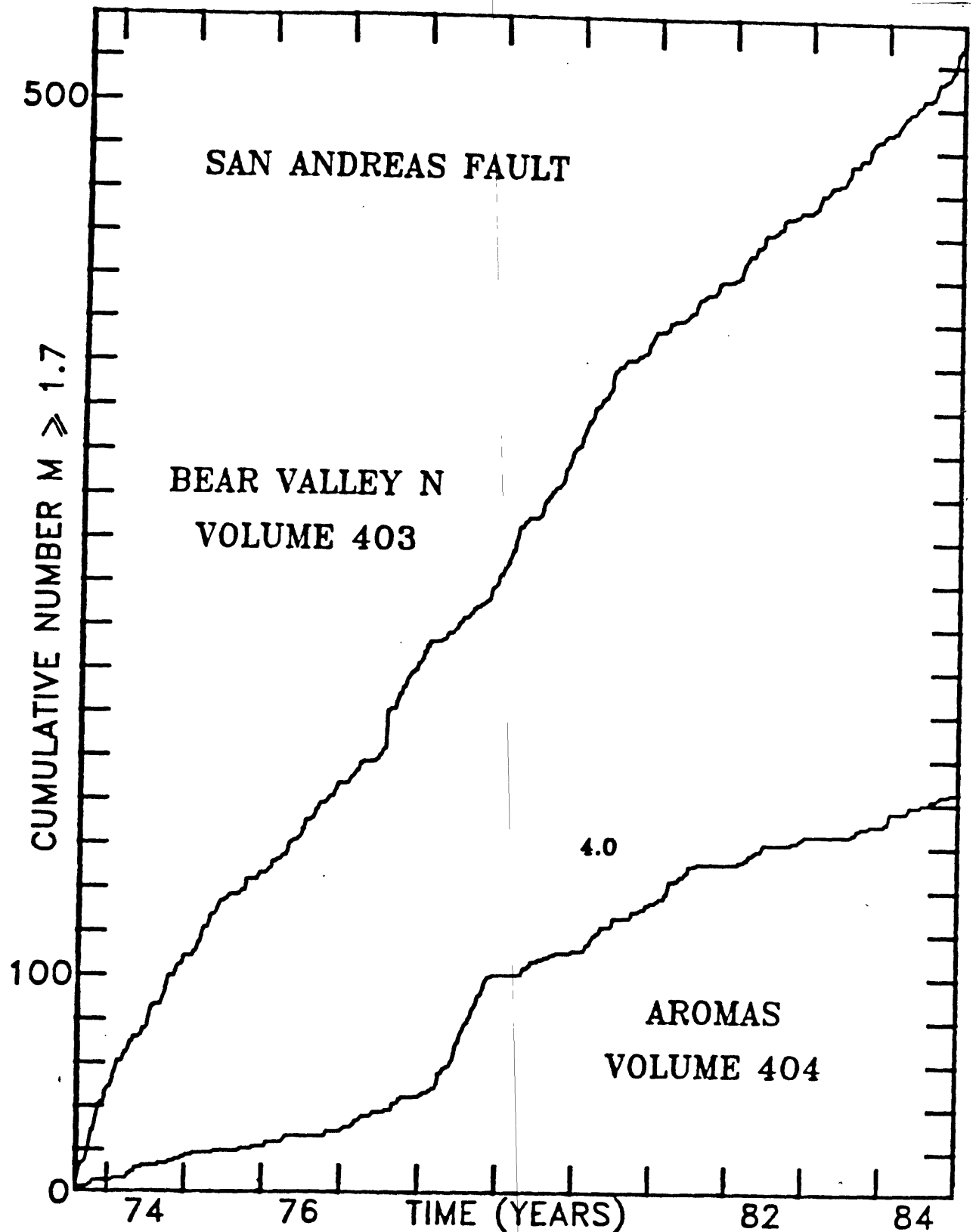


Figure 8: Cumulative number of earthquakes as a function of time within two volumes along the San Andreas fault defined by polygons 403 and 404 in Figure 1. In the last 4 and 6 years, respectively, the rates in 403 and 404 show no significant change. The reason for the high seismicity rate during 1978 in volume 404 is not known. The seismicity-rate decrease beginning in 1980 in volume 403 represents a possible false alarm which is more significant than the current Cienega quiescence anomaly and the 1978-79 quiescence precursor near Fremont Park (Figures 5 and 3 respectively).

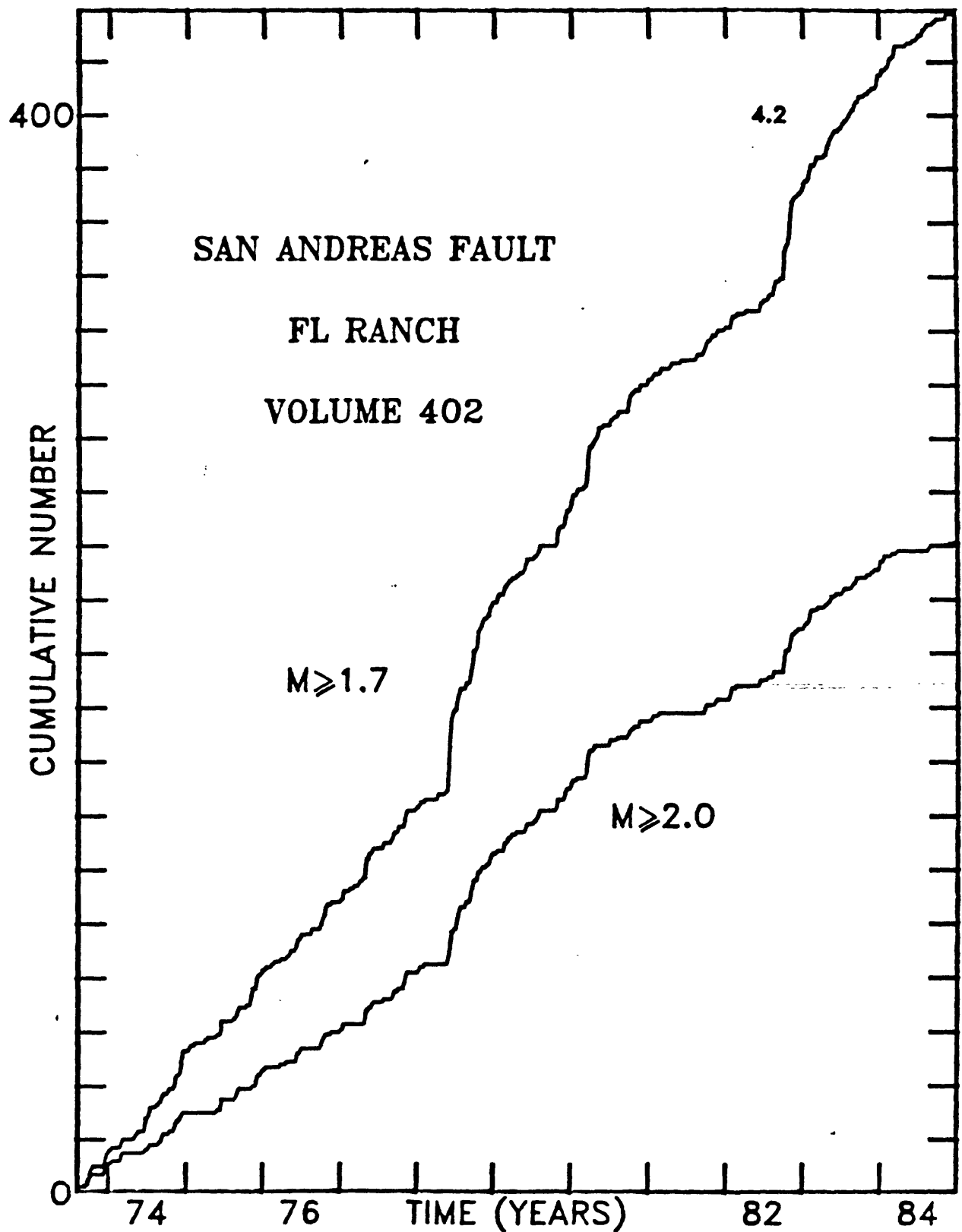


Figure 9: Cumulative number of earthquakes as a function of time within the volume along the San Andreas fault defined by polygon 402 in Figure 1. This volume contains the 1982 mainshock near Limekiln Road (Figure 2) and shows the precursory quiescence related to that event. This volume also contains a 6-month period of significantly reduced seismicity rate in 1977/78, which was followed by a large number of small earthquakes but not by a mainshock.

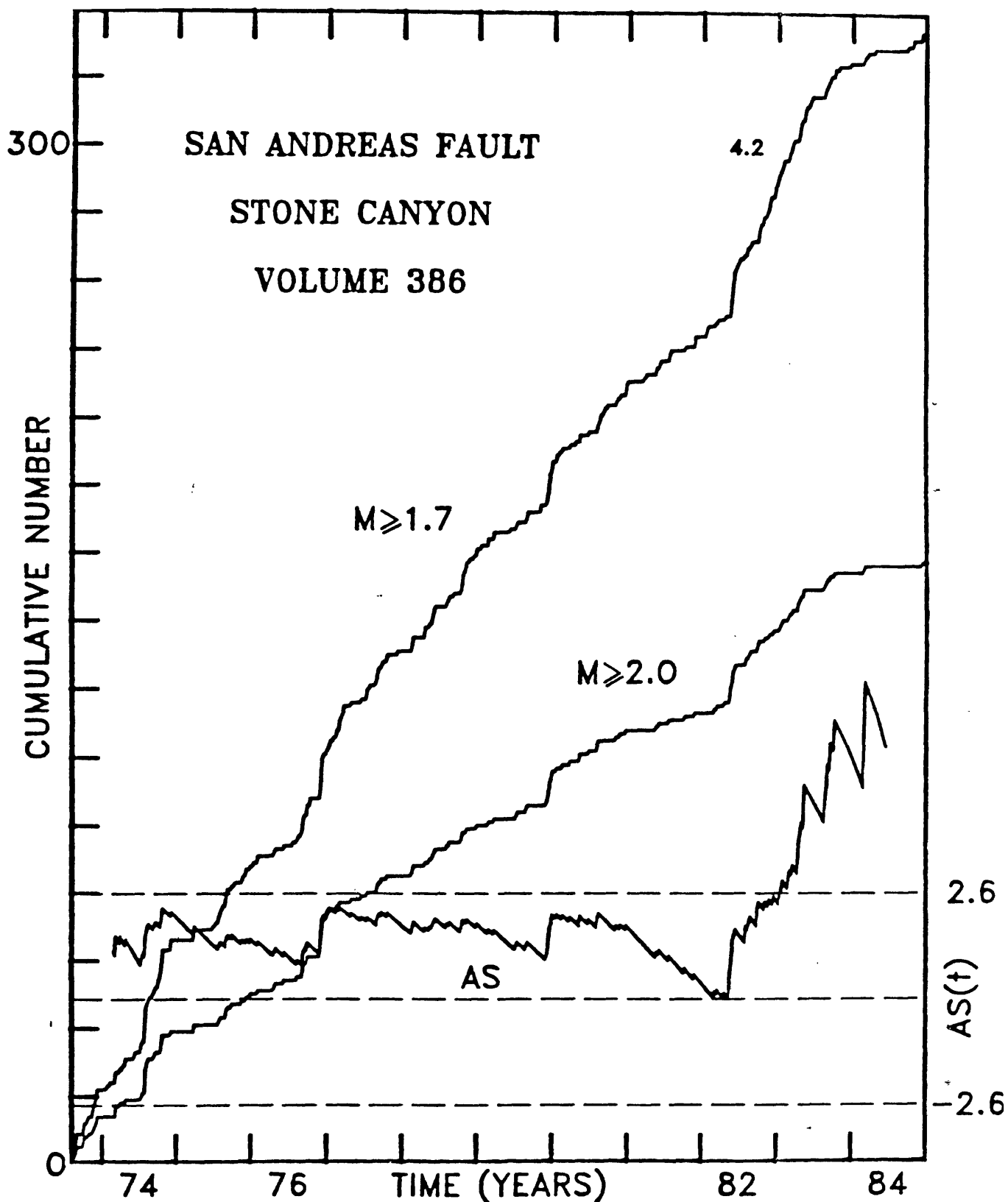


Figure 10: Cumulative number of earthquakes as a function of time along the Stone Canyon segment (polygon 386, Figure 1) of the San Andreas fault (upper curve $M_L \geq 1.7$, lower curve $M_L \geq 2.0$). The 1982 fluctuations in seismicity rate which were evident in volumes 361 and 402 (Figures 2 and 9) are also reflected here because the aftershocks of the August 1982 $M_L = 4.2$ event extended into volume 386 (Figure 4). The $AS(t)$ function shown by the lower curve is derived from the $M_L \geq 2$ data. The present significantly quiet period has persisted here since about mid-1983. The exact onset time of the anomaly may be debated because the $AS(t)$ function shows increasing peaks in 1983 and 1984. The first highly significant peak in $AS(t)$ is selected for defining the onset of quiescence.

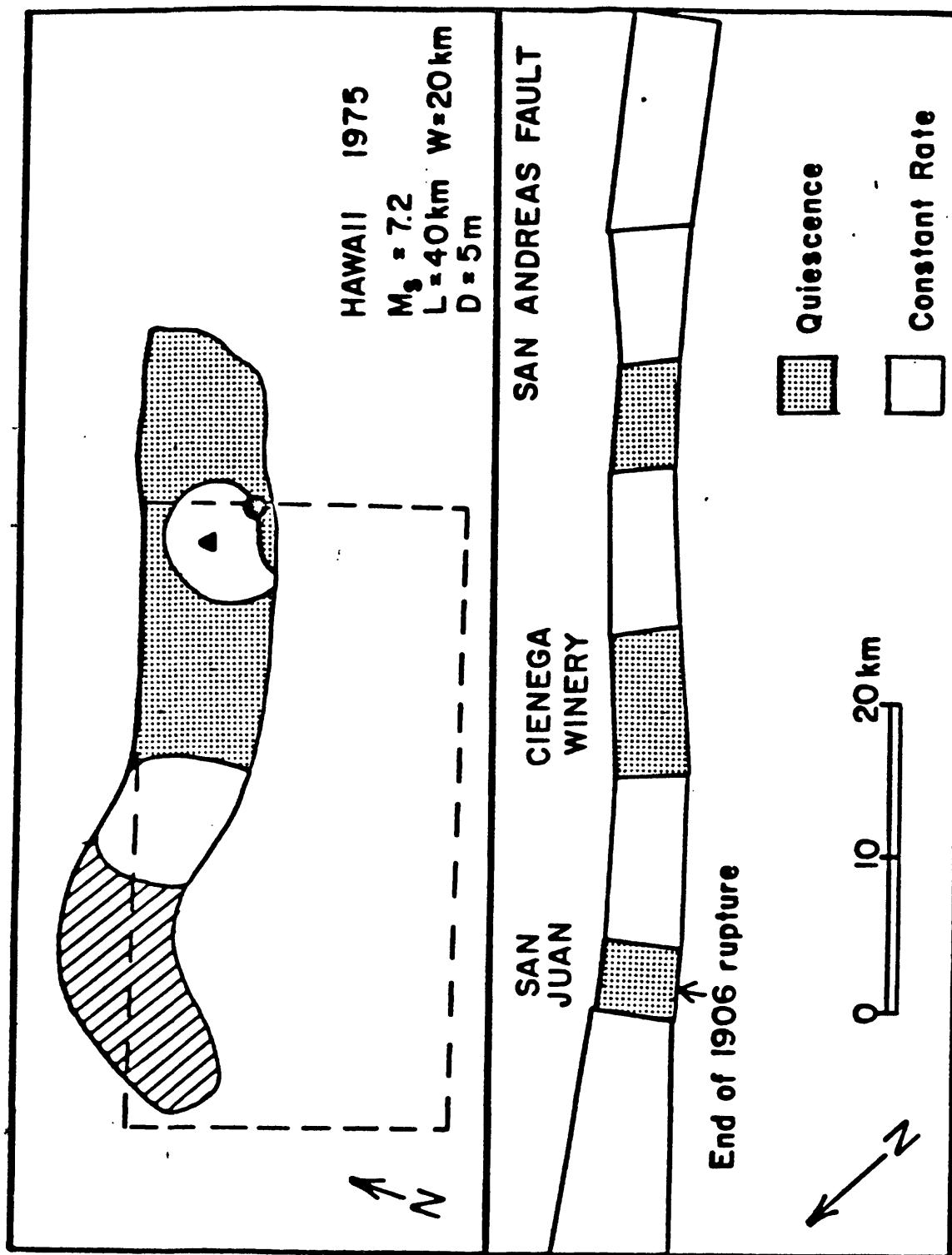


Figure 11: Schematic maps comparing the distribution of quiet and non-quiet segments along the San Andreas fault with the distribution of precursory quiescence before the 1975 Hawaii $M=7.2$ earthquake (Wyss et al., 1981). Volumes containing decreased seismicity rates at present along the San Andreas fault and before the Hawaii mainshock respectively are shaded. The same scale applies to both maps. The end of the 1906 rupture is only known approximately. The shaded volume in the Hawaii case did not have a high enough seismicity rate to permit a study of seismicity patterns.

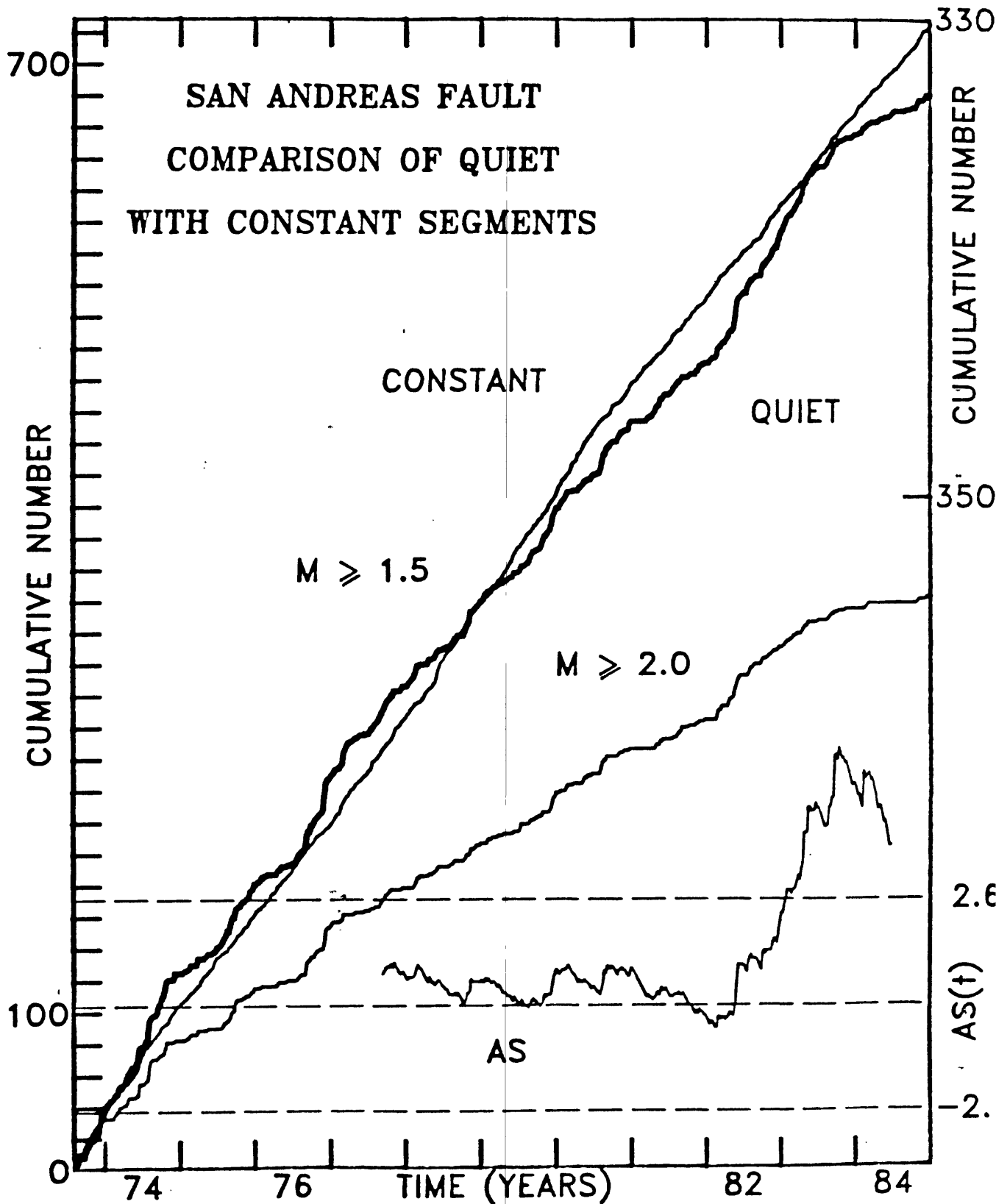


Figure 12: The cumulative number of earthquakes as a function of time for combined anomalous volumes (heavy solid curve) along the San Andreas fault at Cienega Winery, San Juan Bautista and Stone Canyon (polygons 372, 382, and 386) is compared to the cumulative number in the combined other volumes defined in Figure 1 for $M_L \geq 1.5$. The scale for the quiet volume data (heavy line) is on the left side, the scale for the normal volume $M_L \geq 1.5$ data ranges from zero to 3300. The scale for the $M \geq 2.0$ data is indicated at the right side by the number 350. The $AD(t)$ function is derived from the $M_L \geq 2.0$ data.

FIGURE CAPTIONS

Figure 1: Map of the San Andreas fault segment selected for study in this paper. Seismicity rates within each volume, as defined by surface polygons, are studied separately. Seismic quiescence exists at the present only within the fault volumes indicated by stippled polygons.

Figure 2: Example for a seismic quiescence precursor to an $M_L=4.2$ mainshock which occurred on August 11, 1982 near Limekiln Road. Cumulative number of earthquakes in polygon 361 (defined in Figure 1) are shown. This polygon defines one of several neighboring volumes that show the anomaly. The top curve is for earthquakes with $M_L \geq 1.7$, the middle one for $M_L \geq 2.0$. The statistical function $AS(t)$ (bottom curve) is derived from the $M_L \geq 1.7$ data. When this function exceeds the upper dashed-line level, the significance of the seismic-rate decrease exceeds 99%. The quiescence anomaly lasted for about 1.6 years (Table 1).

Figure 3: Cumulative number of earthquakes as a function of time within the San Andreas fault volume defined by polygon 401 in Figure 1. A mainshock of $M_L=4.0$ was preceded by significant seismic quiescence (Table 1), while a $M_L=4.1$ shock which followed a year later was not.

Figure 4: Map of the Cienega Winery section of the San Andreas fault showing aftershock areas of mainshocks which occurred between January 1969 and July 1984. These aftershock areas define a seismic gap of approximately 14-km length centered near the Winery. Another smaller gap of about 7-km length exists near San Juan Bautista. Polygons 372, 382 and 386 define crustal volumes extending to 15-km depth within which statistically significant seismic quiescence exists at the present.

Figure 5: Cumulative number of earthquakes as a function of time for the Cienega

Winery seismic gap. Volume 372 is defined in Figures 1 and 3. The upper curve is for earthquakes of $M_L \geq 1.7$, the lower one for $M_L \geq 2.0$. The statistical function $AS(t)$, derived from the $M_L \geq 1.7$ data, indicates that the present seismic quiescence is statistically significant above the 99% confidence level.

Figure 6: Cumulative number of earthquakes as a function of time for the San Juan Bautista seismic gap (volume 382, Figures 1 and 3). After a constant rate of seismicity during 1973 to 1982, the rate from early 1983 to present is significantly lower than average. The $AS(t)$ function was derived from the $M_L \geq 2.0$ data (lower cumulative curve). The $M_L \geq 1.7$ data (upper curve) show a statistical significance barely exceeding the 99% confidence level (not illustrated) because of renewed low-magnitude activity in 1984.

Figure 7: Cumulative number of earthquakes as a function of time within two volumes along the San Andreas fault defined by polygons 406 and 407 in Figure 1. The rates are essentially constant as a function of time in these volumes, especially during the past several years.

Figure 8: Cumulative number of earthquakes as a function of time within two volumes along the San Andreas fault defined by polygons 403 and 404 in Figure 1. In the last 4 and 6 years, respectively, the rates in 403 and 404 show no significant change. The reason for the high seismicity rate during 1978 in volume 404 is not known. The seismicity-rate decrease beginning in 1980 in volume 403 represents a possible false alarm which is more significant than the current Cienega quiescence anomaly and the 1978-79 quiescence precursor near Fremont Park (Figures 5 and 3 respectively).

Figure 9: Cumulative number of earthquakes as a function of time within the volume along the San Andreas fault defined by polygon 402 in Figure 1. This volume

contains the 1982 mainshock near Limekiln Road (Figure 2) and shows the precursory quiescence related to that event. This volume also contains a 6-month period of significantly reduced seismicity rate in 1977/78, which was followed by a large number of small earthquakes but not by a mainshock.

Figure 10: Cumulative number of earthquakes as a function of time along the Stone Canyon segment (polygon 386, Figure 1) of the San Andreas fault (upper curve $M_L \geq 1.7$, lower curve $M_L \geq 2.0$). The 1982 fluctuations in seismicity rate which were evident in volumes 361 and 402 (Figures 2 and 9) are also reflected here because the aftershocks of the August 1982 $M_L = 4.2$ event extended into volume 386 (Figure 4). The $AS(t)$ function shown by the lower curve is derived from the $M_L \geq x$ data. The present significantly quiet period has persisted here since about mid-1983. The exact onset time of the anomaly may be debated because the $AS(t)$ function shows increasing peaks in 1983 and 1984. The first highly significant peak in $AS(t)$ is selected for defining the onset of quiescence.

Figure 11: Schematic maps comparing the distribution of quiet and non-quiet segments along the San Andreas fault with the distribution of precursory quiescence before the 1975 Hawaii $M=7.2$ earthquake (Wyss et al., 1981). Volumes containing decreased seismicity rates at present along the San Andreas fault and before the Hawaii mainshock respectively are shaded. The same scale applies to both maps. The end of the 1906 rupture is only known approximately. The shaded volume in the Hawaii case did not have a high enough seismicity rate to permit a study of seismicity patterns.

Figure 12: The cumulative number of earthquakes as a function of time for combined anomalous volumes (heavy solid curve) along the San Andreas fault at Cienega Winery, San Juan Bautista and Stone Canyon (polygons 372, 382, and 386) is

compared to the cumulative number in the combined other volumes defined in Figure 1 for $M_L \geq 1.5$. The scale for the quiet volume data (heavy line) is on the left side, the scale for the normal volume $M_L \geq 1.5$ data ranges from zero to 3300. The scale for the $M \geq 2.0$ data is indicated at the right side by the number 350. The AD(t) function is derived from the $M_L \geq 2.0$ data.

APPENDIX A

Artificial changes in the report-rate of earthquakes cannot be avoided, because of many factors. Expansion of seismograph networks and increase of funding for analysis leads to more complete reporting especially for small earthquakes, while decreases of funding can have the opposite effect. Changes in the analysis procedure are introduced occasionally, often in response to announcements in seismological research. Even though more sophisticated analysis techniques may improve seismicity catalogs in some way, they also can introduce heterogeneity of the reporting. For example it is possible that changes in the procedure to estimate magnitude can lead to new magnitudes which are slightly smaller (or larger) in the average. Such artificial magnitude shifts of ΔM_L can cause an apparent reporting change for events with $M_L \geq M_{\min}$. If ΔM_L is negative then the smallest class of events which was counted before the change $M_L = M_{\min}$, will no longer be counted for the rate estimates after the change, because $M_L = M_{\min} - \Delta M < M_{\min}$ is outside of the range studied. A cut-off at M_{\min} is necessary, however, to avoid the fluctuations (usually increases) of reporting of small events. It is not easy to detect and correctly interpret artificial reporting rate changes, but a systematic analysis of this problem is underway (R. E. Habermann, personal communication). Below we will present some preliminary clues regarding the homogeneity of the Central California Seismicity Catalog.

Changes of the total reporting-rate (Figure A1) suggest that changes of the analysis procedure were made in approximately April 1977, October 1980 and January 1984. The most profound change took place in 1980/81 when the total rate of earthquake reports was dramatically increased. The z-value reads -11 for this change. A less profound but still highly significant ($z=4$) decrease of reporting took place in April 1977. A less significant increase of reporting ($z=-2.6$) can be noticed in January 1984. These changes are

usually most pronounced for the small magnitude events, and this makes necessary a cut of some M_{\min} .

Magnitude signatures (Habermann, 1982, 1983) provide a tool for investigating the nature of a reporting change. In this method the data set is divided into two periods of approximately constant seismicity rate before and after the change, and then the rates in these two periods are compared for magnitude classes with $M \leq M_i$ and with $M \geq M_i$. For example the strong rate change of 1980 (Figure A1) is evaluated by the z-test for each magnitude class shown along the abscissa of Figure A2. This figure shows that an extraordinarily strong increase of reports exists in the data, but for small magnitudes only. The larger events (eg. $M_L \leq 2.0$) do not show a rate change, and medium magnitude events ($M \geq 1.5$) event show a highly significant decrease in rate. This rate decrease is noticeable in several of the cumulative curves presented in this paper, especially in those for volumes 403 and 406 (Figures 8 and 7 respectively). Without the magnitude signature analysis one might interpret the 1980 rate decreases in volumes 403 and 406 as false alarms. However, these changes must be interpreted as artificial, because the rate *decrease* for $M_L \geq 1.5$ events clearly coincides with the strong reporting *increase* for $M_L < 1.5$ quakes. The southern California catalog was also found to contain changes with these characteristics which were identified as artificial (Habermann and Wyss, 1984).

The rate decrease which peaks in significance for $M_L \geq 1.5$ events (Figure A2) can be understood by assuming that a new definition for the procedure to estimate magnitude which was introduced in 1980 (J. Eaton, personal communication), may have had the effect of reducing the magnitudes by approximately 0.1 units in the average, compared to the magnitude estimates during the 1977-1980 period. The new procedure to estimate magnitude was implemented at the same time as a general change in analysis

procedure (J. Eaton, personal communication) evidently lead to a sharp increase in total events reported (Figure A1). In order to examine the hypothesis that the M_L estimates after 1980 may have been lower by 0.1 units compared to before the corrected data set (for pre-Oct. 1980 assume $M_L(\text{corr}) = M_L(\text{orig}) - 0.1$) was also plotted in the magnitude signature curve (Figure A2). After the correction the peak in the magnitude signature at $M_L = 1.5$ is lowered but not quite eliminated, suggesting that the ΔM_L might have been larger than 0.1.

From the evidence presented in Figures A1 and A2 it is concluded that the apparent seismicity rate decrease for $M_L \geq 1.7$ (Figures 7 and 8) was introduced artificially by a change in data gathering procedures. While the reporting of seismic events was improved strongly, the catalog gave the appearance that the rate of larger magnitude events had decreased.

The magnitude signature of the April 1977 rate decrease (Figure A1) shows a pattern different from the one seen in the example above. The rate decrease in 1977 resides mostly in the smaller events, with larger "and above" categories showing little or no decrease (Figure A3a). Reasonberg and Ellsworth (1982) stated that a magnitude shift of +0.1 after April 1977 was introduced by procedure changes at this time for the Calaveras fault region. Because unpublished data support the assumption that a similar change may have occurred in the area studied in this paper (W. Bakun, personal communication) the data set used was corrected by +0.1 for events after April 1977. However, the magnitude signature of the 1977 rate change suggests that no significant magnitude shift occurred at this time (Figure 3A) in the area studied here.

The current quiescence anomaly was tested by the magnitude signature method for the possibility that it might have been introduced artificially. Figure A3b contains the separate rate comparisons for the quiet volumes (triangles) and the constant rate

volumes (dots). The data set for the quiet volumes consists of all earthquakes located in the stippled part of the study area (Figure 1) and the "constant" data set consists of the rest of all events. Figure A3b shows clearly that the rates the joint data of those volumes previously judged constant individually (e.g. Figures 3, 7, 8) are indeed constant, except for the very smallest events ($M_L \leq 1.3$) for which the rate was *increasing*. At the same time 1982/83 the rates of all magnitude bands decrease in the "quiet volumes" (triangles in Figure A3b). Also the absence of any peaks in the magnitude signatures of both data sets in Figure A3b, indicates that no magnitude shift took place at the beginning of 1983. Thus it is concluded that the seismicity rate decreases in parts of the studied area were most likely not caused artificially by reporting procedure changes.

Although these results seem solid, we wish to emphasize that they are preliminary. Artificially introduced rate changes are a complex problem, and they are not well understood at the present. Further studies, perhaps using several methods, are needed to reach a final solution for the question of catalog homogeneity.

The least resolved pressing question is whether the 1984 data set may be different from the rest because it is new and may see further improvement through reanalysis of epicenter and magnitude calculations. The overall rate of reporting increased in January 1984, and there is evidence that the number of larger events decreased (eg. in volume 402, Figure 9). It is difficult to judge reliably with the available data what the status of the 1984 catalog is. The observed increase in reporting rate for small events may downgrade the definition of the current quiescence anomalies, but an artificial reduction of larger event reporting (i.e. a magnitude shift) would cause an overestimate of the significance of the current quiescence anomalies. In the anomalous volumes 372 and 382 the quiescence is well defined by the 1983 data, but the significance of the anomaly in volume 386 would be overestimated if a magnitude shift is present in the 1984 data set.

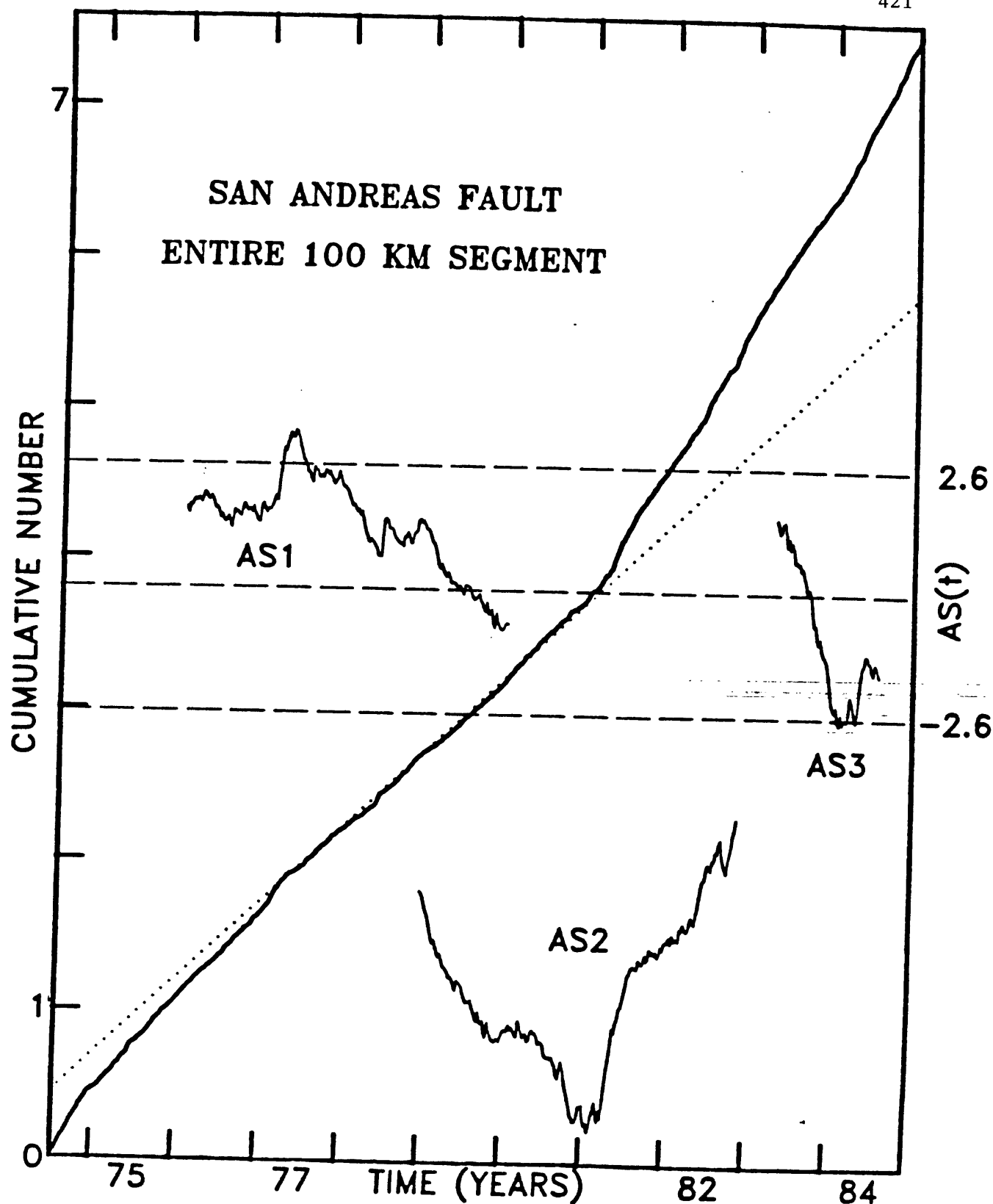


Figure A1: Cumulative numbers of earthquakes ($M \geq 0$) as a function of time for the 100 km segment of the San Andreas fault between 36.36° and 37.0° N latitude. The average reporting rate for the period between early 1977 and late 1980 is extrapolated by a dotted line for comparison with the rates during other periods. The significance of the reporting rate changes are evaluated by three separate AS(t) functions, which were calculated for the periods January 1975-October 1980, April 1977-December 1983 and January 1981-December 1984 respectively. The cumulative number scale is in units of thousands.

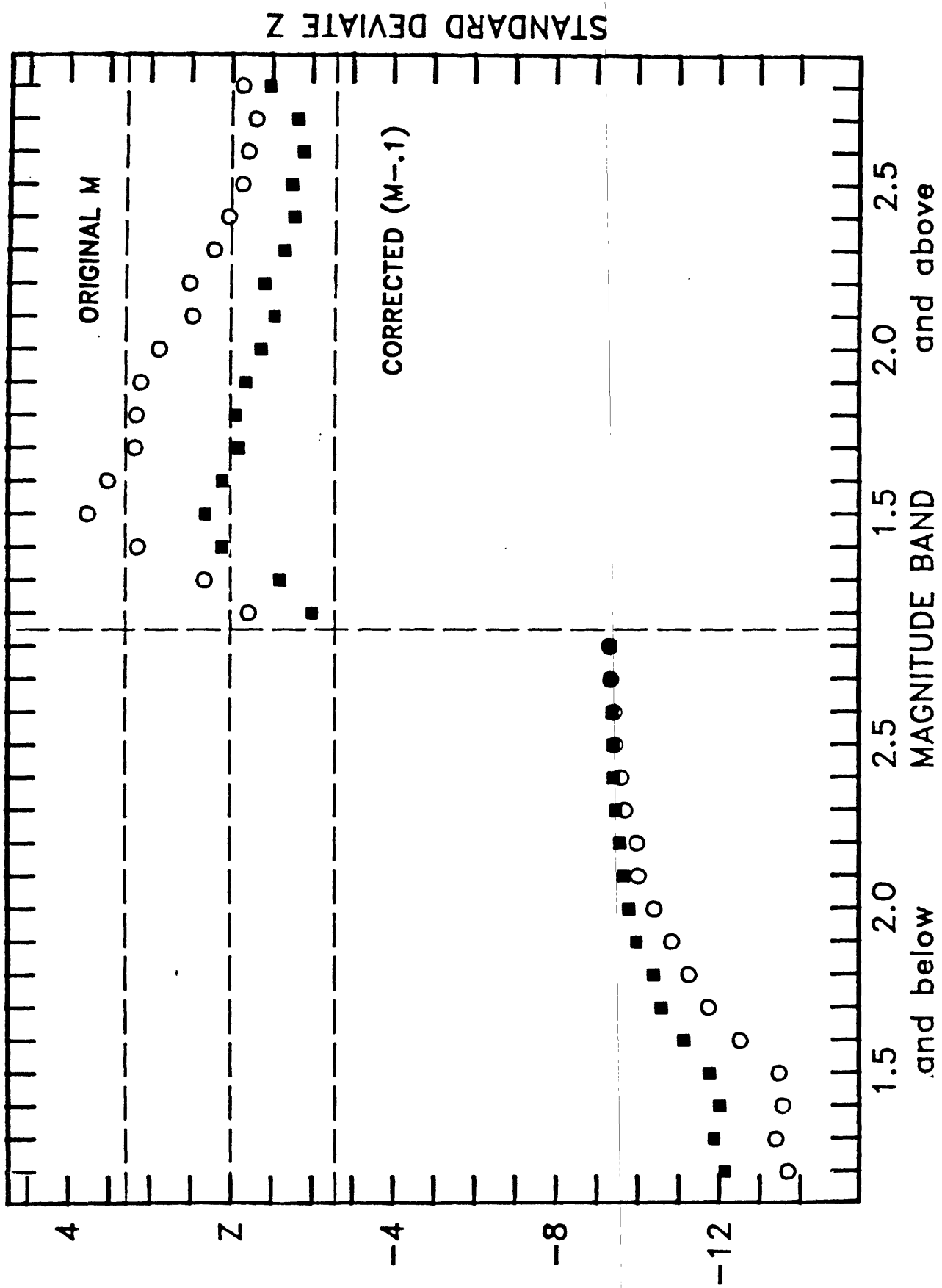


Figure A2: Magnitude signature for the seismicity rate change of late 1980. The standard deviate z is plotted as a function of magnitude-band ranging from "1.2 and below" ($M_L \leq 1.2$) to "2.8 and above" ($M_L \geq 2.8$). For all magnitude bands the average rate for the period April 1977-October 1980 is compared to the rate during October 1980-December 1982. Dots show the original seismicity catalog data, squares show the results after 0.1 units have been subtracted from magnitudes for

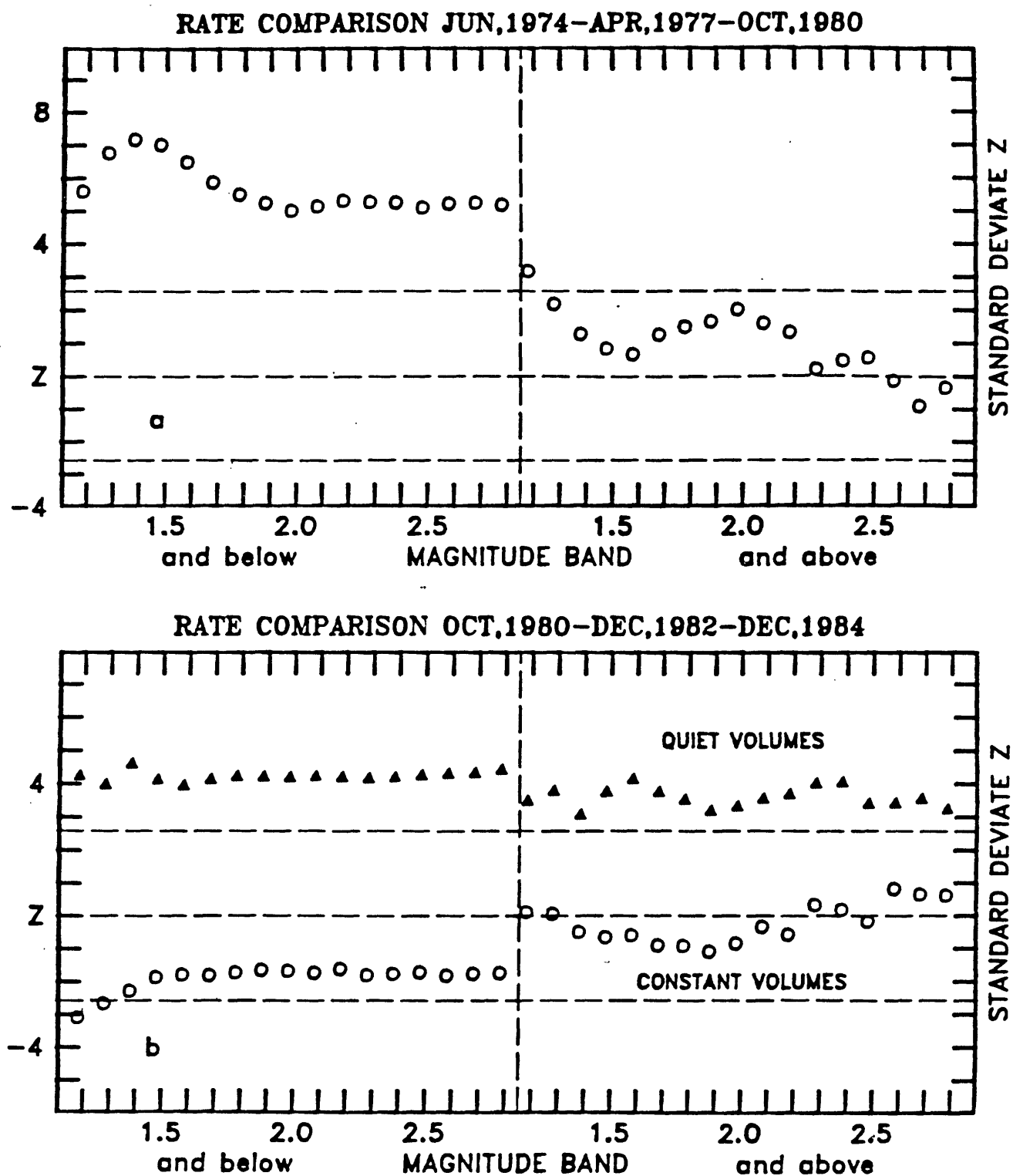


Figure A3: Magnitude signatures for the seismicity rate change of April 1977 (a), and for the present quiescence anomaly period assuming the average change took place in December 1982 (b). In Figure 3b the dots show that now rate change took place in the combined normal volumes (not stippled in Figure 1), while the triangles show that a highly significant rate change took place in all magnitude bands within the combined quiet volumes (stippled in Figure 1).

FIGURE CAPTIONS

Figure A1: Cumulative numbers of earthquakes ($M \geq 0$) as a function of time for the 100 km segment of the San Andreas fault between 36.36° and 37.0° N latitude. The average reporting rate for the period between early 1977 and late 1980 is extrapolated by a dotted line for comparison with the rates during other periods. The significance of the reporting rate changes are evaluated by three separate $AS(t)$ functions, which were calculated for the periods January 1975-October 1980, April 1977-December 1983 and January 1981-December 1984 respectively. The cumulative number scale is in units of thousands.

Figure A2: Magnitude signature for the seismicity rate change of late 1980. The standard deviate z is plotted as a function of magnitude-band ranging from "1.2 and below" ($M_L \leq 1.2$) to "2.8 and above" ($M_L \geq 2.8$). For all magnitude bands the average rate for the period April 1977-October 1980 is compared to the rate during October 1980-December 1982. Dots show the original seismicity catalog data, squares show the results after 0.1 units have been subtracted from magnitudes for events which occurred before October 1980. Positive z measure rate decreases, negative z signify increases.

Figure A3: Magnitude signatures for the seismicity rate change of April 1977 (a), and for the present quiescence anomaly period assuming the average change took place in December 1982 (b). In Figure 3b the dots show that now rate change took place in the combined normal volumes (not stippled in Figure 1), while the triangles show that a highly significant rate change took place in all magnitude bands within the combined quiet volumes (stippled in Figure 1).

APPENDIX B

Geographical definition of polygons used to
subdivide the seismicity data

Polygon Number	Coordinates	
	Latitude	Longitude
361	36.626	-121.337
	36.672	-121.293
	36.691	-121.317
	36.646	-121.365
372	36.770	-121.450
	36.737	-121.485
	36.684	-121.397
	36.718	-121.368
382	36.837	-121.536
	36.868	-121.571
	36.837	-121.615
	36.807	-121.579
386	36.657	-121.278
	36.626	-121.307
	36.583	-121.249
	36.612	-121.223
401	36.837	-121.538
	36.806	-121.576
	36.746	-121.493
	36.777	-121.463
402	36.712	-121.352
	36.676	-121.376
	36.626	-121.304
	36.657	-121.274
403	36.612	-121.220
	36.580	-121.250
	36.525	-121.181
	36.561	-121.145
404	36.837	-121.612
	36.868	-121.567
	37.024	-121.732
	36.964	-121.792
406	36.566	-121.142
	36.526	-121.180
	36.435	-121.079
	36.468	-121.030
407	36.470	-121.030
	36.433	-121.085
	36.352	-120.987
	36.389	-120.941
458	36.515	-121.084

	36.589	-121.183
	36.552	-121.214
	36.473	-121.124
459	36.433	-120.989
	36.515	-121.084
	36.475	-121.124
	36.388	-121.031

APPENDIX B. 1.

Review of Wyss and Burford Paper "Current Episodes of Seismic
Quiescence along the San Andreas Fault between San Juan Bautista
and Stone Canyon, California: Possible Precursors
to Local Moderate Mainshocks?"

CAMPUS BOX 349

UNIVERSITY OF COLORADO AT BOULDER
BOULDER, COLORADO 80309UNIVERSITY OF COLORADO
TELEPHONE (303) 492-8028NATIONAL OCEANIC AND
ATMOSPHERIC ADMINISTRATION

May 14, 1985

Dr. L. Sykes
Chairman, Earthquake Prediction
Evaluation Council
Lamont-Doherty Geol. Obs.
Palisades, NY

Dear Lynn:

This regards our paper "Current episodes of seismic quiescence may be precursors to mainshocks along the San Andreas fault between San Juan Bautista and Stone Canyon, California", a copy of which was sent to you.

The status of this paper is the following: We have sent copies to a few seismologists knowledgeable about the subject, especially those within the USGS. A slightly improved version of the manuscript will be submitted formally for internal review within the USGS.

We plan to submit the manuscript for publication in the near future to the BSSA, but we also think it may be useful if your council would review our work. We are interested in criticism and exchanges of ideas between scientists, with a minimum of public attention.

If the council should find merit in our analysis we think that some kind of discussion should be initiated to define a research program designed to further test the hypothesis put forth by us, and to refine the prediction if possible.

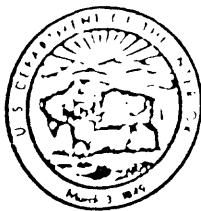
Unfortunately, I am just about to depart for a leave of one year, which I will spend at the Grafenberg array. I am leaving the US on May 30th, and I can be reached starting on June 10th at

Seismologisches Zentralobservatorium
Krankenhausstr. 1
Erlangen 8520
(49) (09131) 25900
Federal Republic of Germany

If you have any criticism of our work, suggestions of how to proceed, or requests for further information, please let us know.

With best wishes,

Max Wyss



United States Department of the Interior

429

GEOLOGICAL SURVEY

OFFICE OF EARTHQUAKES, VOLCANOES & ENGINEERING
Branch of Tectonophysics
345 Middlefield Road, MS/977
Menlo Park, California 94025

July 16, 1985

- Professor Max Wyss
Seismologisches Zentralobservatorium Graffenberg
Der Bundesanstalt für Geowissenschaften und Rohstoffe (BGR)
Krankenhausstraße 1-3, D-8520 Erlangen
West Germany

Dear Max,

Reviews by Allan Lindh, Bill Bakun, and Mark Matthews of your draft manuscript "Current episodes of seismic quiescence along the San Andreas fault ..." are enclosed. I believe that some brief comments on your draft by Jim Savage have already reached you. We had asked Lindh and Savage for internal USGS technical reviews and requested informal written comments from Bakun. We also invited Mark Matthews, a graduate student in statistics working with us this summer, to examine the statistical methods used in your paper.

Everyone seems agreed that you are addressing an important problem and both of us certainly encourage you to continue your work. In particular, the relationship between seismicity and creep which initially motivated your collaborative work is a topic of keen interest here in Menlo Park. In addition, the apparently static distribution of seismicity during 1973-84 shown in your Figure 2 deserves to be documented more completely.

However, as you can see your analysis of seismicity rate variations has come in for some heavy criticism. First of all, a subjective removal of aftershocks of events greater than magnitude 3 does not seem sufficient to extract all true aftershocks--it is impossible "by eye" to get them all, and mainshock-aftershock sequences persist down to very small magnitudes. Whether or not a more systematic method (see enclosed reprint by Reasonberg, JGR, 90, 5479-5495, 1985, for example) will change the main characteristics of cumulative numbers versus time that you show cannot be determined until it is actually done. If you wish, a number of Menlo Park scientists are available to help out on this.

Nonetheless, even if we provisionally accept the validity of your culled catalogue, substantial criticisms remain. Your methodology seems to be rather biased towards enhancing "interesting looking" quiescences. Just the statistical test itself will preferentially emphasize rate changes at the beginning and end of the record over those occurring towards the middle of the time series. Furthermore, very subjective adjustments of free parameters are employed to boost the statistical significance of favored anomalies - region size is adjusted, magnitude thresholds for samples tested are not consistent

Professor Max Wyss
 July 16, 1985
 Page Two

($M > 1.5$, 1.7 and 2.0 are all used at one time or another), and particular quiescence intervals (> 1 year?) are arbitrarily chosen as more significant than others. In view of these adjustments the quoted levels of statistical significance can have scarcely any objective validity.

Even were these objections refuted the paper would still be remiss in failing to estimate the probability that the predicted events would occur by chance. Based on the past seismic history of the region, events as small as $M = 4$ certainly have a non-negligible probability of occurring at any time, quiescence or not. This issue is not unrelated to the estimation of a false alarm rate, which the reviewers rightly criticize as inadequate.

We have emphasized here only the main points of criticism and commend to your attention the attached reviews, which we found to be uniformly thorough and thoughtful. Our feeling is that this work is a promising beginning but the objections raised are substantial and the manuscript requires considerable reworking before it is ready to be submitted for publication.

We hope these collected comments are constructive and useful to you and hope for further discussion with you of this work. Your presentation will make a positive contribution to the NEPEC workshop and we look forward to your participation.

Sincerely,



Wayne Thatcher



Bill Ellsworth

Enclosures

cc. L.R. Sykes
 R.E. Haberman
 A. Lindh
 B. Bakun
 M. Matthews
 J. Savage



United States Department of the Interior

431

GEOLOGICAL SURVEY
OFFICE OF EARTHQUAKES, VOLCANOES AND ENGINEERING
Branch of Seismology
345 Middlefield Road - Mail Stop 977
Menlo Park, California 94025

July 15, 1985

MEMO

TO: W. Thatcher & B. Ellsworth

FROM: Al Lindh

SUBJECT: Review of "Current Episodes of Seismic Quiescence...." by Wyss and Burford

Statement of problem

The hypothesis proposed is not clearly defined, but I infer that the authors mean to assert that there is a non-random association between periods of quiescence and subsequent larger earthquakes. (I assume the authors realize that the significance of this association will have to be judged against the likelihood of the "predicted" earthquake occurring by chance, but I can find no mention of this essential aspect of the problem.)

To establish this hypothesis it is clearly not sufficient to show that some earthquakes are preceded by some kind of quiescence some of the time; this is of course well known in seismology, and discussed widely in the literature, although curiously almost none of that work is cited here. What is required is a carefully documented demonstration that the association of periods of quiescence is non-randomly associated with larger events. In its present form this work does not contribute to that task, nor does the earlier work by Habermann/Wyss so far as I can tell. Thus the premise they start from, that periods of quiescence have significant predictive value:

1. Is not established in this paper,
2. Is not demonstrated in the earlier work they cite,
3. And is generally regarded as not demonstrated by most workers in the field.

Since the initial premise is unsubstantiated, I regard all references to prediction in this paper as inappropriate; this is simply a bad paper area whose demonstratable implications for the occurrence of future large earthquakes is nil.

The problem they are actually doing

Apart from the problem of establishing a significant relationship between periods of quiescence and earthquakes, there still remains the problem of recognizing significant periods of quiescence. In practice this divides into two parts:

1. Given an earthquake time-series which is demonstrably non-Poissonian, can one remove the non-Poissonian component in such a way that what remains is "close enough" to Poissonian that it's properties can be tested against the Poisson model, and
2. Assuming that you succeed at 1), can you then identify significant rate changes in the "pseudo-Poisson" residuum.

Concerning 2), I defer to the careful work of Mark Matthews on this problem, of which I believe you have a copy.

This paper, however, should also be rejected on the basis of the authors treatment of 1), the removal of dependent events. The authors tell us nothing about the algorithm used, nor do they demonstrate via before and after plots what the effects of their algorithm were. Since the thirties, Jefferys and many others have pointed out the self-similar, or fractal-like character of earthquake time series. This makes "Poissonizing" them very difficult. To my knowledge no one has yet demonstrated a final solution to this problem (although Reasenber (JGR, 90, 5479 (1985) appears to have made significant progress); however this does not permit one to pretend that the problem does not exist. In particular the remaining non-Poissonian remnant in Wyss and Burford's declustered time-series (which they acknowledge on p.7), renders meaningless assertions concerning significance based on a Poisson model.

Lack of adequate description of method

In a paper of this length it is totally unacceptable that there is not even a brief summary of the statistical techniques used, particularly in light of the dozen odd pages at the end of the paper devoted to a rambling speculative discourse on the size of the hypothetical earthquake. The paper is replete with undefined jargon such as $AS(t)$, $AD(t)$ (typo?) and RTZ . Although the heart of the presentation is the purported significance of the z values derived from the $AS(t)$ function, the only mention I can find of how the significance varies with z is a brief reference in the caption of Figure 2. Even if the scientific case presented were sound, which it is not, such inadequacies in the presentation should preclude publication in its present form.

Duration of quiescence vs magnitude

Although no relation is stated explicitly relating the duration of the purported anomaly to the magnitude of the expected earthquake, the authors refer in the abstract and the discussion to some such implied relationship.

Unfortunately the only references they cite (pages 17, 22) are an abstract (Habermann and Wyss, 1984b), an unpublished manuscript (Wyss, 1985), and their own Table 1. Table 1 only contains 2 events -- a M4.2 and a M4.0 with precursor times of about 1 1/2 years -- hardly much basis for establishing a magnitude-precursor relationship. Moreover, although they refer repeatedly to the anomaly of Johnson and Hutton (1982) preceding the M6.6 Imperial Valley earthquake, it was preceded by a possible quiescence of only 15 weeks; clearly not consistent with their implied relationship. In addition if we assign any reasonable uncertainties to the quiescence periods listed in Table 1, the quiescence period for a M4 overlaps the range listed for a M7-8 on page 22. The lack of a significant correlation between magnitude and length of quiescence is, of course, what one would expect if the purported associations on which it is based were in fact largely random. It is my conclusion that from the data presented there is no basis for any assertion concerning the magnitude of the expected earthquake, even if one took the evidence for quiescence at face value.

The authors should summarize in a single table all the published evidence for premonitory quiescence and let the readers judge for themselves the quality and consistency. Their selective disjointed presentation amounts to no more than telling us what their opinion is on the matter.

Seismicity figures

The data presentation is confusing and disjointed, and the figures do not adequately present the data. The major deficiencies are:

1. Although there are repeated references to seismic gaps in the microseismicity -- they play a major part in the presentation -- there is no mention of how they were identified, and not a single figure of the pattern of micro-earthquakes.
2. The central point in the paper is the purported temporal and spatial relation between the "quiescences" and the larger earthquakes which supposedly followed them, yet trying to figure out which earthquakes relate to which anomalies is left as an exercise for the reader. If you don't want to take my word for this, try deciphering the first paragraph of the "Examples of Precursory Quiescence" section starting on page 8. This is the only presentation of one of the two observations of quiescence which supposedly justify this work, yet the paragraphs and figures which describe it are almost incomprehensible.

A minimum presentation for each anomaly would be a clear set of figures showing the spatial relation of the box used for calculating rates to the microseismicity, the location of any larger events purportedly "predicted", and the locations of other nearby events not "predicted".

Recommendations

For all the reasons cited above, plus the disproportionate length of the manuscript relative to the substance of the material presented, I strongly recommend that it not be published in its present form. If it is published

in this form, I will feel compelled to forward these comments to BSSA as a comment on the work.

My recommendation for what to do with the manuscript would be to remove all the ill-posed arm-waving concerning earthquake prediction, and tighten up the presentation of the seismicity data, preferably in conjunction with the creep data, as I believe Bob originally intended.



United States Department of the Interior

435

GEOLOGICAL SURVEY

OFFICE OF EARTHQUAKES, VOLCANOES AND ENGINEERING

Branch of Seismology

345 Middlefield Road - Mail Stop 977

Menlo Park, California 94025

July 5, 1985

Wayne Thatcher
Chief, Branch of Tectonophysics
USGS

Dear Wayne:

Bill Ellsworth has asked me to formally convey to you my informal comments to Bob Burford regarding "Current episodes of seismic quiescence along the San Andreas fault between San Juan Bautista and Stone Canyon, California: Possible precursors to local moderate mainshocks?" by Max Wyss and Robert O. Burford. It is my understanding that Bob transmitted these comments to Max by phone before Max left for Europe.

The San Juan Bautista section of the San Andreas fault is near, or at the top, of most lists of plausible sites for future damaging shocks in central and northern California. A change in the creep rate (suggested by Burford in a recent monthly data review meeting) and changes in the seismicity rate (suggested by Wyss and Burford in the above mentioned manuscript) are only some of the evidence that can be focused on the San Juan Bautista question. The suggestion by Burford that creep and seismicity changes are correlated at San Juan Bautista is interesting in itself, and, if properly documented, should not be ignored in light of other evidence that identifies the San Juan Bautista section of the San Andreas fault as a likely candidate for the location of a future damaging shock.

First, there is no written description of the creep rate changes so that the seismicity rate evidence must be evaluated independently. This is a serious shortcoming. The identification of earthquake precursors has proved difficult so that prediction strategies in recent years have stressed the desirability for simultaneous precursor observations of different kinds. The availability of collaborative deformation measurements would clearly give confidence that the seismicity evidence advanced by Wyss and Burford has not been misread.


Second, the analysis of the seismicity data described in Wyss and Burford's manuscript is compromised by their reliance on subjective data analysis procedures that are impossible for me to evaluate with the available information:

1. Wyss and Burford subjectively cull the catalog to remove aftershocks and swarm events. Aftershock and swarm events are only loosely

defined so that this culling process is troublesome even when accomplished by an algorithm defined before, and independent of, the data analysis. When the culling process is subjective and part of the analysis process, there is every reason to worry that expectations of the people doing the analysis has subconsciously influenced the culling decisions. Although there is no complete defense against this criticism, Wyss and Burford can (and must) argue in their paper that their culling procedure has not manufactured their results. They could easily show in illustrations the change in the seismicity rate as a function of location along the fault for the sequence of data analysis steps. It would be helpful to me to see if the effects of their procedures are spatially uniform, what portion of the seismicity is removed in the culling, etc. While these demonstrations might not answer these questions, they would at least address them.

2. Wyss and Burford subjectively select the spatial extent of their fault segments. Would a minor change in the position and/or extent of the segments change the character of the seismicity patterns? Why not let the data select the spatial extent of seismic quiescence? For example, use a moving window, perhaps 10-kilometers long, and perform the analysis for incremental steps of perhaps 1 kilometer. If Wyss and Burford are correct, their segments will come out of the analysis.

Given the results of these demonstrations, it should be possible to evaluate the manuscript for scientific content. Without this additional information, I am unable to evaluate whether this work meets the standards of the U.S. Geological Survey.


William H. Bakun

cc: R. O. Burford
W. Ellsworth



United States Department of the Interior

437

GEOLOGICAL SURVEY
OFFICE OF EARTHQUAKES, VOLCANOES AND ENGINEERING
Branch of Seismology
345 Middlefield Road - Mail Stop 977
Menlo Park, California 94025

July 15, 1985

MEMORANDUM

TO: Wayne Thatcher and Bill Ellsworth

FROM: Mark Matthews

Subject: "Current episodes of seismic quiescence along the San Andreas Fault between San Juan Batista and Stone Canyon, California: Possible precursors to local moderate mainshocks?" by M. Wyss and R. O. Burford

Through statistical analysis of local seismicity rates along a section of the San Andreas fault, Wyss and Burford claim to have detected three presently quiescent segments. Examination of the historical seismic record in the region under study leads the authors to conclude that precursory quiescence is a demonstrable feature of earthquakes along the San Andreas fault, and, therefore, that moderate mainshocks in the near future are likely along the quiescent segments.

A careful look at the statistical techniques employed by Wyss and Burford finds them inappropriate and unsupportive of the stated conclusions. The contention that mainshocks are imminent at various points on the San Andreas fault is without sound statistical basis in this paper. Since statistical arguments concerning seismicity rates are central to the earthquake predictions of Wyss and Burford, those predictions must be seriously questioned.

Following is a discussion of the statistical methods used by Wyss and Burford. The discussion includes a brief description of the methods, general comments on their shortcomings and mistaken assumptions, and, finally, remarks directed specifically at their use in this paper.

The Model and Methods

Wyss and Burford base their analysis of seismicity rates on a method proposed by Habermann (1981b) (references are the same as in the paper under discussion) and described in Habermann (1983) and Habermann and Wyss (1984a). Surprisingly, this method has been used by Habermann and others in numerous analyses, but there appears nowhere in the published literature a precise

specification of the model for which it's supposed to be appropriate. By piecing together the implications of several vague statements, one may infer that Habermann intends the model specified below.

Suppose we are interested in the seismicity in a given region from some specified time onward. Let the starting time be the origin of the time axis and define the seismicity process $S(.)$ on $[0, \infty)$ by

$S(t) \triangleq$ cumulative number of seismic events (above threshold magnitude) detected by time t .

The seismicity process may be decomposed into the sum of two processes which will be called N and D . In the decomposition

$$S(t) = N(t) + D(t)$$

$D(.)$ is the "dependent events" process and $N(.)$ is the underlying, possibly inhomogeneous, Poisson process in which we are interested.

The dependent events process consists of those seismic events which are attributed to a common physical cause on the basis of spatio-temporal relationships. These events might be, for example, aftershock sequences from a common mainshock. Whatever their cause, these events are not to be considered as stochastically independent and are not of interest here. It is necessary, in order to look at the interesting process N , to subtract D from the observed seismicity process.

Having subtracted out D (supposedly) we are left with the process N . Now if it is a homogeneous Poisson process, then it is completely specified by some value $\lambda > 0$ called the "intensity". We are interested in the possibility that the process is inhomogeneous, meaning that its intensity, rather than being constant, is a function of time. Specifically, we may have $\lambda(t)$ of the form

$$\lambda(t) = \begin{cases} \lambda_1 & \text{if } 0 \leq t < T_c \\ \lambda_2 & \text{if } t > T_c \end{cases}$$

Where λ_1 and λ_2 are unknown positive constants and T_c is a fixed, unknown "change point" on the time axis.

The problem under consideration may then be characterized as that of deciding whether there is actually a change point in the process and assigning some confidence to that decision.

Habermann proposes the following solution to this problem.

Suppose the process $N(.)$ has been observed for a period of n weeks. Break up the time axis into week-long intervals. Let t_j be the time at which the

i^{th} week ends and X_i the random variable representing the number of events observed in the i^{th} week. For a given t , let

$$l(t) = \#\{j: \tilde{t}_j < t\}, \quad r(t) = n - l(t)$$

and take

$$\bar{X}_{l(t)} = \sum_{j=1}^{l(t)} \frac{X_j}{l(t)}, \quad \bar{X}_{r(t)} = \sum_{j=l(t)+1}^n \frac{X_j}{r(t)}$$

and

$$\sigma^2(t) = \sum_{j=1}^{l(t)} \frac{(X_j - \bar{X}_{l(t)})^2}{l(t)(l(t)-1)} + \sum_{j=l(t)+1}^n \frac{(X_j - \bar{X}_{r(t)})^2}{r(t)(r(t)-1)}$$

Now define the "anomaly start" function by

$$AS(t) = \frac{\bar{X}_{l(t)} - \bar{X}_{r(t)}}{\sigma(t)}$$

and base a test for an anomaly on the value $AS(\hat{T}_c)$, where

$$\hat{T}_c = \max_t^{-1} |AS(t)|$$

Habermann contends that if there is no anomaly then $AS(\hat{T}_c)$ has a standard normal distribution, so the resulting test requires looking at the amount by which $AS(\hat{T}_c)$ differs from zero.

Critique of Habermann's Proposal

Allowing, for the moment, the questionable assumption that the process N can be successfully isolated by accurate removal of dependent events, one finds serious problems with Habermann's treatment of the resulting data.

First of all, the definition of and distributional assumptions about $AS(t)$ for any fixed t are technically inappropriate. Since technical objections will be seen to be relatively minor, however, they are simply listed and not discussed.

- ° Since the mean and variance are equal for the Poisson distribution, the definition of $AS(t)$ should assume equal variances.
- ° When variances must be estimated, the resulting test statistic has a t -distribution, not a normal distribution.
- ° Data are observed in the form of continuous-time stochastic processes, not finite random samples from well-defined populations. Tests for differences in means are not called for.
- ° The decision to discretize the data by weeks is arbitrary.

- Most of the useful properties of Poisson processes on which tests could be based are ignored.

The most serious objection to Habermann's method is that it simply cannot be used to obtain meaningful significance test for the hypotheses in question. If we state the null hypothesis.

H_0 : The process $N(\cdot)$ is a homogeneous Poisson process and the alternative

H_1 : $N(\cdot)$ is a Poisson process with a change point then we might reasonably accept the claim that for any fixed t , the approximate null distribution of $AS(t)$ is the standard normal distribution. But now what if $AS(\cdot)$ is evaluated at several values of t , say at t_1, t_2, \dots, t_k , for instance, and the maximum of $|AS(t_1)|, \dots, |AS(t_k)|$ is taken as the test statistic. It is clear then that this statistic does NOT have a standard normal distribution under H_0 . Habermann apparently assumes, erroneously, that if X_1 and X_2 are identically distributed random variables and $Y = \max(X_1, X_2)$ then Y has the same distribution as X_1 .

Although it's not possible to specify the null distribution of $AS(\hat{T}_c^{(k)})$ where

$$\hat{T}_c^{(k)} = \max_{1 \leq i \leq k} \{ |AS(t_i)| : i = 1, 2, \dots, k \}$$

because of the dependencies of $AS(t_i)$ and $AS(t_j)$ for each i, j , we can surely say that the distribution is not standard normal and is dependent on k . Intuitively we know that the expected value of $AS(\hat{T}_c^{(k)})$ will increase with k . This intuition is borne out in the results of applying Habermann's technique to synthetic data sets. One thousand homogeneous Poisson processes of length 26 weeks ($\sim 1/2$ year) and one thousand of length 52 weeks (~ 1 year) were simulated and Habermann's AS statistic was calculated for each. The number of processes in which $AS(\hat{T}_c)$ exceeded the $1-\alpha/2$ percentage point of the standard normal distribution for $\alpha = .05$ and $\alpha = .01$ were counted with these results:

Length of process	26 weeks	Exceedances of	
		97.5 percent point	99.5 percent point
		271 (50)	117 (10)
	52 weeks	410 (50)	153 (10)

The expected number of exceedances under Habermann's assumption is shown in parentheses below each number in the table.

marks specific to Wyss and Burford paper

In addition to general objections concerning basic statistical technique, one may raise the following relevant points:

° The method for removing dependent events, described on p.7 seems ad hoc and unsophisticated. The authors concede that there is no satisfactory technique for accurately removing aftershock sequences, yet the possible effects of inaccurate event removal are never discussed. It would appear imprudent to make sweeping conclusions and predictions based on data which have been filtered through a poorly understood algorithm which lacks solid objective footing.

° The "Z-values" from which claims of statistically significant quiescence are drawn are quite low in some cases (e.g., $Z = 2.8$ for Cienega and San Juan at $M_L > 1.7$) and, as we saw above, even in instances where higher Z-values are observed significance statements are impossible.

° The sheer number of comparisons made in the catalogues under study (comparisons in 10 crustal volumes over a period of over 10 years) makes it quite likely that Habermann's method will find "significant" anomalies even if none are present.

° The discussion of "false alarms" and how they are dealt with is unconvincing. The authors note (on p.10, for instance) that they sometimes detect quiescence in periods which do not precede mainshocks. The decision to discount significant periods of quiescence if they have duration less than one year is unjustified. It is made simply because it apparently strengthens the evidence in favor of the authors' hypothesis.

° On p. 16 the false alarm rate is estimated to be about 30 percent. It is claimed, based on that rate, that with high probability at least one of their detected anomalies is a true precursor to a main shock. The relevant question may not be, "What's the chance that at least one of three detected anomalies is real?" But rather, "If there are no real anomalies and we search 10 volumes with a misdetection probability of .3, then what's the chance that we find at least 3 significant anomalies?" (The answer is $p = .62$).

° In addition to the various problems with the AS(.) function already noted, it appears that this function might not detect anomalies, depending how these are defined. Since AS(t) compares events to the left of t with events to the right, the function would be useful only in situations where the intensity parameter is as stated above in the change point model, i.e., some rate up until time T_c and then some other rate thenceforth.

Wyss and Burford suggest that they sometimes detect "short periods of quiescence". If their assumptions about the AS function were correct, then they shouldn't detect these periods very often because these small inhomogeneities should be offset by the relatively long periods of uniform seismicity rate on either side of them.

In summary, the earthquake predictions of Wyss and Burford rest on unsound statistical methods derived from an unspecified model and partially justified by arbitrary a posteriori adjustment. These methodological shortcomings must render their predictions highly questionable in their present form.

J.C. Savage

Although the draft that I reviewed requires extensive rewriting, I believe that the observations and ideas presented are of major interest and merit publication. It is unfortunate that this paper cannot be simply presented as "a test of the hypothesis of seismic quiescence as an earthquake precursor", but I suppose it will have to go forward as an earthquake prediction. That being the case, I recommend that a copy be sent to Lynn Sykes to see whether NEPAC (or whatever it is called) is interested in considering the prediction. The review given by that committee should be much more thorough than the usual reviews. Moreover, it would get the prediction on record but at the same time allow NEPAC to qualify the prediction as they see fit. That, after all, is the job that NEPAC is supposed to do.

My own opinion is that periods of seismic quiescence have been demonstrated as convincingly as they are likely to be, the objections of Ellsworth and Reasonberg effectively refuted, and the question of quiescence as a precursor discussed in a reasonable way. I am not convinced that the prediction is valid, but I think the anomaly is interesting and bears watching (i.e., I would not be surprised if the authors are right).

I think it might be worthwhile to include the creep data in the paper. There is a demand for independent corroborative evidence in prediction and the creep data might provide that. I also believe Malcolm Johnston has an interesting change in shear rate from the down-hole strainmeter at San Juan that might be pertinent.

Minor comments are written directly on the manuscript.

APPENDIX B. 2.

Council letter to Director, USGS, regarding its review
of a prediction for the San Andreas fault near
San Juan Bautista, California

Lamont-Doherty Geological Observatory
of Columbia University

Camp - LAMONTGEO

61 Rte 9000 New York 51 11

TX 2-710 570-2051

Telephone 609 612 1111

7 August 1985

Dr. Dallas Peck
Director
U.S. Geological Survey
MS106 National Center
12201 Sunrise Valley Drive
Reston, Virginia 22092

Dear Dallas,

The National Earthquake Prediction Evaluation Council (NEPEC) met in Menlo Park on July 26 and 27, 1985. The Council examined the Parkfield region, the San Andreas fault from the middle of the San Francisco Peninsula to Bear Valley and the Calaveras fault. The minutes of the meeting and summaries of papers presented will be mailed to you separately by Clem Shearer, the Executive Secretary.

A prediction was brought to the Council in the form of a preprint by Wyss and Burford concerning the San Andreas fault in the vicinity of San Juan Bautista, California. The following is a written statement that the Council prepared on July 27 and read to Wyss and Burford.

Wyss and Burford have presented data and interpretations indicating a period of seismic quiescence in three zones along the San Andreas fault between San Juan Bautista and Bear Valley. They interpret this quiescence to indicate the imminence of one or more earthquakes of magnitude 4-5 or larger in one or more of these three areas. Alternatively, they suggest that if these three zones and the intervening portions of the fault were to rupture at once, an earthquake of magnitude 6.2 might be produced.

The area in question is one of the most active areas of seismicity in Central California. The chance of an earthquake of magnitude 5 or larger within this zone is about 1 in 10 per year based on historical seismicity alone. The chance of an earthquake of magnitude 4 or larger is substantially greater.

The Council believes that the methods upon which this prediction is based warrant substantial further investigation and that the area of observed seismic quiescence bears watching. However, the Council identifies the following concerns with the prediction at the present time:

1. Members of the Council and others have raised questions about methodology, data, and interpretations -- many of which the authors have agreed to investigate further.
2. The probability of an earthquake in the magnitude 4-5 range, occurring in the area and time specified is sufficiently high, based solely on the historical seismicity of the area, as to render this prediction of earthquakes in the magnitude 4-5 range of questionable utility.
3. The Council is not convinced that a adequate predictive relation applicable to this situation has been established between periods of seismic quiescence and subsequent earthquakes nor does it believe that adequate study has been made of false alarm probability.

In view of the above reservations the Council is of the opinion that no public action is warranted with respect to the prediction of a magnitude 6.2 earthquake at this time.

Yours sincerely,

Lynn R. Sykes
Chairman, National Earthquake Prediction
Evaluation Council

LRS/llm

cc: J. Filson
C. Shearer
M. Wyss
R. Burford